

Sheet Metal Forming

FUNDAMENTALS

Edited
by
Taylan Altan and A. Erman Tekkaya



ASM International®
Materials Park, Ohio 44073-0002
www.asminternational.org

Copyright © 2012
by
ASM International®
All rights reserved

No part of this book may be reproduced, stored in a retrieval system, or transmitted, in any form or by any means, electronic, mechanical, photocopying, recording, or otherwise, without the written permission of the copyright owner.

First printing, August 2012

Great care is taken in the compilation and production of this book, but it should be made clear that NO WARRANTIES, EXPRESS OR IMPLIED, INCLUDING, WITHOUT LIMITATION, WARRANTIES OF MERCHANTABILITY OR FITNESS FOR A PARTICULAR PURPOSE, ARE GIVEN IN CONNECTION WITH THIS PUBLICATION. Although this information is believed to be accurate by ASM, ASM cannot guarantee that favorable results will be obtained from the use of this publication alone. This publication is intended for use by persons having technical skill, at their sole discretion and risk. Since the conditions of product or material use are outside of ASM's control, ASM assumes no liability or obligation in connection with any use of this information. No claim of any kind, whether as to products or information in this publication, and whether or not based on negligence, shall be greater in amount than the purchase price of this product or publication in respect of which damages are claimed. THE REMEDY HEREBY PROVIDED SHALL BE THE EXCLUSIVE AND SOLE REMEDY OF BUYER, AND IN NO EVENT SHALL EITHER PARTY BE LIABLE FOR SPECIAL, INDIRECT OR CONSEQUENTIAL DAMAGES WHETHER OR NOT CAUSED BY OR RESULTING FROM THE NEGLIGENCE OF SUCH PARTY. As with any material, evaluation of the material under end-use conditions prior to specification is essential. Therefore, specific testing under actual conditions is recommended.

Nothing contained in this book shall be construed as a grant of any right of manufacture, sale, use, or reproduction, in connection with any method, process, apparatus, product, composition, or system, whether or not covered by letters patent, copyright, or trademark, and nothing contained in this book shall be construed as a defense against any alleged infringement of letters patent, copyright, or trademark, or as a defense against liability for such infringement.

Comments, criticisms, and suggestions are invited, and should be forwarded to ASM International.

Prepared under the direction of the ASM International Technical Book Committee (2011–2012), Bradley J. Diak, Chair.

ASM International staff who worked on this project include Scott Henry, Senior Manager, Content Development and Publishing; Karen Marken, Senior Managing Editor; Steven L. Lampman, Content Developer; Sue Sellers, Editorial Assistant; Bonnie Sanders, Manager of Production; Madrid Tramble, Senior Production Coordinator; and Diane Whitelaw, Production Coordinator.

Library of Congress Control Number: 2011945709
ISBN-13: 978-1-61503-842-8
ISBN-10: 0-61503-842-6
SAN: 204-7586

ASM International®
Materials Park, OH 44073-0002
www.asminternational.org

Printed in the United States of America

Preface

In sheet metal forming, a sheet blank that has a simple shape is plastically formed between tools (or dies) to obtain a part with relatively complex geometry with desired tolerances and properties. Sheet metal forming processes usually produce little scrap and generate the final part geometry in a very short time, usually in one stroke or a few strokes of a press. As a result, sheet forming offers potential savings in energy and material, especially in medium and large production quantities, where tool costs can be easily amortized.

The ever-increasing costs of material, energy and manpower require that sheet metal forming processes and tooling be designed and developed with minimum amount of trial and error with shortest possible lead times. Therefore, to remain competitive, the cost-effective application of computer-aided technologies, i.e. CAD, CAM, CAE, and especially finite element analysis (FEA), computer-based simulation is an absolute necessity. Thus, process modeling using FEA has been discussed in all appropriate chapters.

The practical and efficient use of these technologies requires a thorough knowledge of the principle variables of the sheet metal forming processes and their interactions. These variables include:

1. the flow behavior and formability of the formed sheet material under processing conditions;
2. die geometry, materials and coatings;
3. friction and lubrication;
4. the mechanics of deformation, i.e. strains, stresses and forces;
5. characteristics of the sheet metal forming presses and tooling;
6. geometry, tolerances, surface finish and mechanical properties of the formed parts, and
7. the effects of the process on the environment.

These topics are addressed in two companion volumes *Sheet Metal Forming—Fundamentals* and *Sheet Metal Forming—Processes and Applications*. Principles are described, and major emphasis is placed on the latest developments on the design of sheet forming operations, equipment and tooling.

In *Sheet Metal Forming—Fundamentals*, the role of sheet metal forming in manufacturing has been introduced in Chapter 1. Chapter 2 gives the classification and description of sheet metal forming operations. The fundamentals of plastic deformation, i.e. metal flow, flow stress of materials, testing methods to determine flow stress and formability are discussed in Chapters 3, 4, and 5. Chapters 6 and 7 cover the significant process variables materials and friction. The introduction to deep drawing is discussed in Chapter 8. Chapters 9, 10, 11, and 12 discuss the characteristics and operations of various sheet metal forming presses (hydraulic, mechanical, servo-drive) and cushion systems.

In *Sheet Metal Forming—Processes and Applications*, Chapters 1 and 2 cover blanking, and bending. Process modeling and its applications are discussed in Chapter 3 as well as in several other chapters, where appropriate. Chapter 4 reviews progressive and transfer die forming. Relatively new technologies, i.e. warm forming, forming of advanced high strength steels (AHSS) and hot stamping are discussed in Chapters 5, 6, and 7, respectively. Processes that are related to sheet forming such as sheet and tube hydroforming, roll forming, and high velocity forming are covered in Chapters 8, 9, 10, and 11. Special sheet forming operations spinning, incremental forming and mechanical joining are discussed in Chapters 12, 13, and 14. Sensors and die materials are critical for practical application of sheet forming technology and they are discussed in Chapters 15 and 16.

The preparation of this book was possible through extensive efforts by many friends, associates and students of the editors who authored and co-authored many of the chapters. We would like to thank them all for their very valuable contributions.

We would like to thank Ms. Linda Anastasi, Administrative Assistant of the Center for Precision Forming (CPF – www.cpforming.org), who revised the chapters several times, Mr. Xi Yang and Manan Shah at CPF who assisted in the editing of some chapters and Mr. Doug Dragoo of Cincinnati Inc. who reviewed Chapter 15 on Bending and made valuable suggestions. We would also like to thank our families, who offered us enormous support and encouragement throughout the preparation of this book.

Finally, we would like to gratefully acknowledge the financial support from member companies of CPF and especially from the National Science Foundation (NSF) that helped us summarize the results of sheet metal forming research, conducted over the years at The Ohio State University.

Taylan Altan
Center for Precision Forming (CPF)
The Ohio State University

A. Erman Tekkaya
Institut für Umformtechnik und Leichtbau
(IUL)
Technische Universität Dortmund, Germany

Contents

Preface.....	vii
Abbreviations and Symbols.....	ix
Chapter 1 Metal Forming Processes in Manufacturing.....	1
1.1 Classification of Manufacturing Processes.....	1
1.2 Characteristics of Manufacturing Processes.....	1
1.3 Metal Forming Processes in Manufacturing.....	2
1.4 Classification of Metal Forming Processes.....	3
Chapter 2 Classification and Description of Sheet Metal Forming Operations	5
2.1 Process Variables	5
2.2 Sheet Metal Forming as a System.....	6
2.3 Classification of Geometries	10
2.4 Bending and Flanging.....	11
2.5 Blank Preparation	14
2.6 Deep Drawing.....	15
2.7 Stretch Forming.....	18
2.8 Incremental Forming.....	22
2.9 Hybrid Forming Processes.....	23
Chapter 3 Plastic Deformation—Strain and Strain Rate	27
3.1 Homogeneous or Uniform Deformation	27
3.2 Volume Constancy during Plastic Deformation	29
3.3 Infinitesimal True Strains and Strain Rates	29
3.4 Principal Strains and Strain Paths	31
3.5 Equivalent Strain Rate and Equivalent Strain	32
Chapter 4 Plastic Deformation—Flow Stress, Anisotropy, and Formability	33
4.1 Tensile Test.....	33
4.2 Flow Stress Curves	37
4.3 Methods to Determine Flow Stress of Sheet Materials.....	39
4.4 Formability	44
4.5 Forming Limit Curves (FLCs)	48

Chapter 5	Plastic Deformation—State of Stress, Yield Criteria Flow Rule, and Hardening Rules	53
5.1	General State of Stress	53
5.2	Principal Stresses	54
5.3	Volumetric Stress or Hydrostatic Pressure	54
5.4	Deviatoric Stress	55
5.5	Isotropic Yield Criteria (Flow Criteria)	56
5.6	Tresca Yield Criterion	56
5.7	Von Mises Yield Criterion	57
5.8	Comparison of Tresca and von Mises Criteria	58
5.9	Anisotropic Yield Criteria	58
5.10	Flow Rules	63
5.11	Power and Energy of Deformation	64
5.12	Effective Strain and Effective Strain Rate	65
5.13	Hardening Laws	66
Chapter 6	Materials for Sheet Forming	73
6.1	Low-Carbon Sheet Steels	73
6.2	Coated Sheet Steels	78
6.3	Stainless Steels	79
6.4	Aluminum Alloys	82
6.5	Magnesium Alloys	86
Chapter 7	Friction and Lubrication	89
7.1	Lubrication Mechanisms and Friction Laws	89
7.2	Lubricants for Sheet Metal Forming	91
7.3	Tribological Tests for Evaluation of Lubricants in Sheet Metal Forming	94
7.4	Tribological Tests for Warm and Hot Stamping	98
7.5	Tribological Tests for Punching and Blanking	100
Chapter 8	Deep Drawing of Round and Rectangular Cups	105
8.1	Deformation during Deep Drawing	105
8.2	Deep Drawing of Rectangular Cups	121
8.3	Prediction of Punch Force and BHF—Case Study	123
Chapter 9	Principles of Sheet Forming Presses	129
9.1	Components of Presses	129
9.2	Characteristics of Presses	131
9.3	Quick Die Change Systems	139
Chapter 10	Mechanical Presses	145
10.1	Mechanical Press Designs	145
10.2	Characteristics of Mechanical Presses	150
10.3	Other Features of Mechanical Presses	155
Chapter 11	Electromechanical Servo-Drive Presses	161
11.1	Servo-Press Drives Versus Conventional Press Drives	161
11.2	Servo-Press Drives	163

11.3	Applications.....	167
11.4	Cushions/Die Cushions.....	173
11.5	Comparison of Mechanical and Servo Presses	174
11.6	New Process Development Using Servo-Press Characteristics	176
11.7	Summary	178
Chapter 12	Hydraulic Presses.....	181
12.1	Components of Hydraulic Presses.....	182
12.2	Drive Systems	188
12.3	Characteristics of Hydraulic Presses.....	190
12.4	Hydraulic Press Designs	196
Chapter 13	Cushion Systems for Sheet Metal Forming.....	203
13.1	Blank holder Systems in Double-Action Presses	203
13.2	Single-Action Presses with Cushion System	206
13.3	Multipoint Cushion (MPC) Systems.....	211
Appendix A	Flow Stress Curves	221
Appendix B	Glossary.....	233
Index.....		267

CHAPTER 1

Metal Forming Processes in Manufacturing

Taylan Altan, The Ohio State University

A. Erman Tekkaya, Technische Universität Dortmund, Germany

IN A MANUFACTURING process, a given material is transformed into a useful part having a **complex geometry with well-defined** (a) shape, (b) size, (c) accuracy and tolerances, (d) appearance, and (e) properties (Ref 1.1). The material usually begins in a shapeless form (such as liquid metal in casting) or of a simple geometry (such as a blank sheet metal forming). The various manufacturing processes have advantages and limitations in achieving the desired shape, size, tolerances, appearance, and properties of a part.

1.1 Classification of Manufacturing Processes

Manufacturing processes can be divided, in a simplified manner, into five general areas (Ref 1.2):

1. *Primary shaping* processes, such as casting, melt extrusion, die casting, and pressing of metal powder. In all these processes, the material initially has no shape but obtains a **well-defined geometry through the process**. Here the first shape is given to the material.
2. *Forming* processes, such as rolling, extrusion, cold and hot forging, bending, and deep drawing, where metal is formed by plastic deformation, without destroying the cohesion of the material.
3. *Material removal* processes, in which excess material is removed from the starting workpiece in order to obtain the desired ge-

ometry. Some important processes in this category are turning, milling, drilling, sawing, and electrodischarge machining.

4. *Material treatment* processes aim to change the properties and appearance of the part without changing its shape. Heat treating, anodizing, and surface treatment are commonly used material treatment processes.
5. *Joining* processes, in which two or more parts are joined to form a new component or subassembly. Metallurgical joining processes, such as welding, brazing, and soldering, form a permanent and robust joint between components. Mechanical joining processes, such as riveting and mechanical assembly, bring two or more parts together to build a subassembly that can be disassembled conveniently.

1.2 Characteristics of Manufacturing Processes

There are four main characteristics of any manufacturing process: achievable geometry, tolerances, production rate, and environmental factors.

1. **Geometry.** Each manufacturing process is well suited for producing a particular type of geometry. Other geometries may be produced in some cases, but usually not without considerable expense. For example, manufacturing processes using dies and molds can produce parts that are easily removed from a mold made from two halves.

However, by using a “split-die” design, it is possible to manufacture forgings, castings, or injection moldings with undercuts and more complex shapes.

2. **Tolerances.** When fabricating a given component, it is nearly impossible and very costly to make the part to the exact dimensions specified by the designer. Therefore, dimensions should be associated with a tolerance. By using more sophisticated variations of the process and by means of new developments, the quality of the tolerance, that is, precision, can always be improved. For example, it is possible to control sheet metal flow and obtain better parts with more uniform thickness distribution and tighter tolerances with multipoint binder pressure control systems than with the conventional uniform pressure distribution obtained with die cushion. Dimensional tolerances serve a dual purpose. First, they allow proper functioning of the manufactured part; for example, an automotive brake drum must be round, within specified acceptable limits, to avoid vibrations and to ensure proper functioning of the brakes. Second, dimensional tolerances provide interchangeability. Modern mass production would be unthinkable without interchangeability—the ability to replace a defective part or component (a bearing, for example) with a new one, manufactured by a different supplier.
3. **Production rate.** The rate of production, that is, number of parts produced per unit time, that can be attained with a given manufacturing operation is probably the most significant feature of that operation, because it indicates the economics of and the achievable productivity with that manufacturing operation. In industrialized countries, manufacturing industries represent 15 to 25% of gross national product. Consequently, manufacturing productivity, that is, production of discrete parts, assemblies, and products per unit time, is one of the most important factors influencing the standard of living in a country, as well as that country’s competitive position in international trade in manufactured goods.

The rate of production or manufacturing productivity can be increased by improving existing manufacturing processes and by introducing new machines and new

processes, all of which require new investments. However, the most important ingredient for improving productivity lies in human and managerial resources, because good decisions regarding investments (when, how much, and in what) are made by people who are well trained and well motivated. As a result, the present and future manufacturing productivity in a plant, an industry, or a nation depends not only on the level of investment in new plants and machinery but also on the level of training and availability of manufacturing engineers and specialists in that plant, industry, or nation.

4. **Environmental factors.** Every manufacturing process must be examined in view of (a) its effects on the environment, that is, in terms of air, water, and noise pollution; (b) its interfacing with human resources, that is, in terms of human safety, physiological effects, and psychological effects, and (c) its use of energy and material resources, particularly in view of the changing world conditions concerning scarcity of energy and materials. Consequently, the introduction and use of a manufacturing process must also be preceded by a consideration of these environmental factors.

1.3 Metal Forming Processes in Manufacturing

Metal forming includes (a) bulk forming processes such as forging, extrusion, rolling, and drawing and (b) sheet forming processes such as brake forming, deep drawing, and stretch forming. Among the group of manufacturing processes discussed earlier, metalforming represents a highly significant group of processes for producing industrial and military components and consumer goods (Ref 1.3).

A common way of classifying metal forming processes is to consider cold (before the crystallization temperature) and hot (above the recrystallization temperature) forming. Most materials behave differently under different temperature conditions. Usually, the yield stress of a metal increases with increasing strain (or deformation) during cold forming and with increasing strain rate (or deformation rate) during hot forming. However, the general principles governing the forming of metals at various temper-

atures are basically the same. Therefore, **classification of forming processes based on initial material temperature does not contribute a great deal to the understanding and improvement of these processes.** In fact, tool design, machinery, automation, part handling, and lubrication concepts can be best considered by means of a **classification based not on temperature but rather on specific input and output geometries and material and production rate conditions.**

Complex geometries, in both massive and sheet forming processes, can be obtained equally well by hot or cold forming. Of course, because of the lower yield strength of the deforming material at elevated temperatures, tool stresses and machine loads are, in a relative sense, lower in hot forming than in cold forming. However, part accuracy is usually higher in cold-formed parts.

Forming is especially attractive in cases where (a) the part geometry is of moderate complexity and the production volumes are large, so that tooling costs per unit product can be kept low—for example, in automotive or appliance applications; and (b) the part properties and metallurgical integrity are extremely important, in examples such as load-carrying aircraft and jet engine and turbine components.

The design, analysis and optimization of forming processes require (a) analytical knowledge regarding metal flow, stresses and heat transfer as well as (b) technological information related to lubrication, heating and cooling techniques, material handling, die design and manufacture, and forming equipment.

1.4 Classification of Metal Forming Processes

Metal forming processes can be classified as:

1. Bulk deformation processes, such as forging, extrusion, rolling, and drawing
2. Sheet-metal forming processes, such as brake forming, deep drawing, and stretch forming
3. Hybrid forming processes such as drawing and ironing and bending and coining

Bulk deformation (massive forming) processes are **generally characterized by significant deformation and massive shape change and consider-**

able increase in the area-to-volume ratio occurring in the formed part. The term *bulk* indicates the low area-to-volume ratio in the starting material. The starting material is in billet, rod, or slab form.

Bulk forming processes have the following characteristics:

- The workpiece undergoes large plastic deformation, resulting in an appreciable change in shape or cross section.
- The portion of the workpiece undergoing permanent (plastic) deformation is generally much larger than the portion undergoing elastic deformation, so elastic recovery after deformation is usually negligible.

In sheet forming, sheet blanks are plastically deformed into a complex three-dimensional geometry, **usually without any significant change in sheet thickness and surface characteristics.** The surface area-to-volume of the starting metal is high; therefore, this ratio is a useful means to distinguish bulk deformation from sheet metal processes.

Sheet metal operations are nearly always performed as cold working processes and are accomplished using a tool set consisting of a *punch* and a *die*, which are the positive (male) and negative (female) portion of the tool set, respectively.

The characteristics of sheet metal forming processes are:

- The workpiece is a sheet or a part fabricated from a sheet.
- The deformation usually has the objective to **cause significant changes in shape, but not in cross section, of the sheet.** Reduction in sheet thickness is usually not desirable, but it is an unavoidable consequence of the process.
- In some cases, the magnitudes of permanent (plastic) and recoverable (elastic) deformations are comparable; thus, **elastic recovery or springback may be significant.**

Examples of sheet-metal forming processes are **discussed in Chapter 2, “Classification and Description of Sheet Metal Forming Operations,”** of this book.

Some processes, known as hybrid forming processes, can fall under both sheet metal and bulk forming categories according to the work-

piece geometry. For example, a deep draw cup can be ironed in the same die set to reduce the cup wall thickness. In this case, deep drawing is a sheet forming process while ironing can be considered as a bulk forming process. Another example for hybrid forming processes is coining. Bottoming in brake bending is a type of coining where bottoming pressure causes reduction in thickness at the bending area as well as springback. In some cases, relatively thick sheet (or plate) is used as a blank. The cross section of the part, formed from this blank, may

be subsequently reduced by a bulk forming process.

REFERENCES

- 1.1 T. Altan, S. Oh, and H.L. Gegel, *Metal Forming: Fundamentals and Applications*, American Society for Metals, 1983
- 1.2 K. Lange, *Handbook of Metal Forming*, McGraw-Hill, 2000
- 1.3 E. Tekkaya, Metal Forming, *Handbook of Mechanical Engineering*, Springer, 2005

CHAPTER 2

Classification and Description of Sheet Metal Forming Operations

Taylan Altan, The Ohio State University

A. Erman Tekkaya, Technische Universität Dortmund, Germany

IN SHEET METAL forming, an initially simple part—a sheet blank, for example—is plastically deformed between tools (or dies) to obtain the desired final configuration. Thus, a simple part geometry is transformed into a complex one, whereby the tools “store” the desired geometry and impart pressure on the deforming material through the tool/material interface. Sheet metal forming processes usually produce little or no scrap and generate the final part geometry in a very short time, usually in one or a few strokes of a press. As a result, sheet metal forming offers potential savings in energy and material—especially in medium and large production quantities, where tool costs can be easily amortized. In addition, for a given geometry, parts produced by sheet metal forming exhibit better mechanical and metallurgical properties and reliability than do those manufactured by casting or machining.

Until recently, sheet metal forming was basically an experience-oriented technology. Throughout the years, a great deal of know-how and experience have been accumulated in this field, largely by trial-and-error methods. During the last two decades, computer-aided finite element analysis has allowed quantitative design of sheet forming processes and dies. Thus, the sheet metal forming industry is capable of supplying sophisticated products manufactured to very rigid requirements from newly developed, difficult-to-form alloys, as in the case of aerospace applications.

2.1 Process Variables

To design reliable sheet forming processes and the necessary dies, it is essential to understand the physical phenomena governing sheet metal forming and the process variables that must be controlled and optimized. The boundary conditions describing a sheet metal forming operation such as heat transfer or friction coefficients are difficult to define quantitatively. For a given material and shape, the surface transformations occurring in the plastic deformation zone are controlled by the equipment, tooling, and work piece/tool interface. The metal flow, the friction at the tool/material interface, and the relationship between process conditions are difficult to predict and analyze. Therefore, thorough knowledge of complex interactions between the process components and the work piece material is important for effective process design. The process components and key technologies that enable the correct design and operation of sheet metal forming processes are depicted schematically in Fig. 2.1.

In sheet metal forming, a blank is plastically deformed into a complex three-dimensional geometry, usually without any intended significant change in sheet thickness and surface characteristics. Sheet metal forming operations are usually performed as cold working processes, which means that they are performed at a temperature that is below the recrystallization temperature of the materials being formed. How-

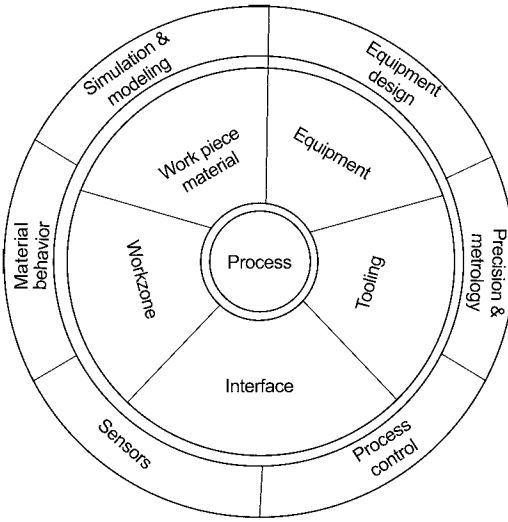


Fig. 2.1 Sheet metal forming process components. Source: Ref 2.1

ever, some sheet forming operations are conducted at elevated temperatures, for example, warm forming of aluminum, titanium, or nickel alloy sheets or hot stamping of special steels to obtain specific part properties. These processes are accomplished using a tool set consisting of a *punch* and a *die*, which are the positive (male) and negative (female) portion of the tool set respectively. Often, these components are also referred to as “upper” and “lower” dies.

Often, in producing discrete sheet metal parts, several successive forming operations are required to transform the initial “simple” geometry into a “complex” geometry, without causing material failure and degradation of material properties. Consequently, one of the most significant objectives of any method of analysis is to assist the forming engineer in the design of optimal forming sequence. For a given operation, the design process essentially consists of the following steps:

1. Predicting metal flow by establishing the geometric process parameters such as shape, velocities, strain rates, and strain
2. Establishing the formability limits, that is, determining whether it is possible to form the part without failure such as fracture and wrinkling
3. Designing the tooling (e.g., dies) and selecting the equipment based on the prediction of the force and energy necessary to perform the forming operation

For the understanding and design of sheet metal forming operations, it is useful to consider these processes as a system and classify them in a systematic way.

2.2 Sheet Metal Forming as a System

A sheet metal forming system is composed of all the input variables such as the blank (geometry and material), the tooling (geometry and material), the conditions at the tool/material interface, the mechanics of plastic deformation, the equipment used, the characteristic of the final product, and finally the plant environment where the process is being conducted. The application of the system approach to sheet metal forming is illustrated in Fig. 2.2, as applied to deep drawing, and allows the study of the input/output relationships and the effects of process variables on product quality and process economics.

To obtain the desired shape and properties in the product, the metal flow should be well understood and controlled. The direction of flow, the magnitude of deformation, and the temperature involved greatly influence the properties of formed products. Process variables affecting the metal flow are given in Table 2.1.

Material Characterization

In analyzing and optimizing a sheet metal forming process for a given material, the most important variables are the blank properties (e.g., composition, temperature, deformation history, and prestrain), the flow stress of the blank material for various strain values, stress states and strain rates, the formability (or ductility) in various directions (i.e., anisotropy), and the surface conditions. Reliable estimation of tool stresses and the equipment loading, as well as prediction of metal flow and elimination of forming defects, depends on the accurate determination of the flow properties of the starting material.

The flow curves (Eq 2.1) for sheet materials are usually determined based on load versus elongation data obtained from tensile tests. For a given microstructure and material flow direction, the flow stress (equivalent stress in plastic state), $\bar{\sigma}$, is expressed as a function of equivalent strain, $\bar{\epsilon}$; equivalent strain rate, $\dot{\bar{\epsilon}}$ and temperature, T :

$$\bar{\sigma} = f(\bar{\epsilon}, \dot{\bar{\epsilon}}, T) \quad (\text{Eq 2.1})$$

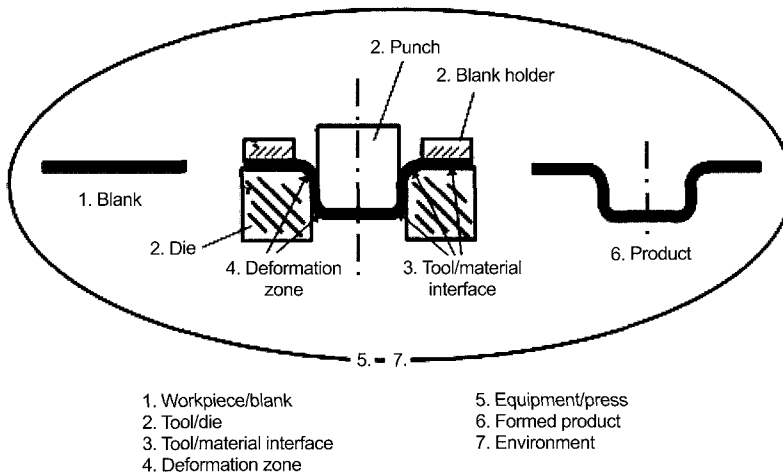


Fig. 2.2 Schematic of system approach in metal forming (using deep drawing as an example)

Table 2.1 Significant variables in sheet metal forming

Sheet material or blank	Deformation zone
Flow stress as a function of strain, strain rate, temperature, and microstructure	Deformation mechanics
Formability as a function of strain, strain rate, temperature, strain path, and microstructure (forming limit curves)	Metal flow, velocities, strain, strain rate (kinematics)
Surface texture	Stresses (variation during deformation)
Thermal/physical properties (density, melting point, specific heat, thermal conductivity and expansions, resistance to corrosion and oxidation)	Temperatures (heat generation and transfer)
Initial conditions (composition, temperature, strain history/prestrain)	Damage accumulation
Geometric anisotropy	Equipment used
Hardening anisotropy	Speed/production rate
Blank size, location, and thickness	Binder design and capabilities
Tooling	Force/energy capacity
Tool geometry and forces	Rigidity and accuracy
Surface conditions	Flexibility
Material/heat treatment/hardness	Product
Temperature	Geometry
Condition at tool/material interface	Dimensional accuracy/tolerances
Lubricant type and temperature	Surface finish
Insulation and cooling characteristics of the interface layer	Microstructure, metallurgical, and mechanical properties
Lubricity and frictional shear stress	Environment
Characteristic related to lubricant application and removal	Available manpower
	Air, noise, and wastewater pollution
	Plant and production facilities and control

Source: Ref 2.2

The material will yield if the equivalent stress is equal to flow stress, $\bar{\sigma}$. At room temperature $\bar{\sigma}$ is primarily dependent on $\bar{\epsilon}$ and to some extent on $\dot{\bar{\epsilon}}$. At higher deformation temperatures, the effect of T and $\bar{\epsilon}$ increases.

Workability or formability is the capability of a material to deform without failure. It depends on: (a) conditions existing during deformation (e.g., temperature, rate of deformation, stresses, and strain history) and (b) material variables (e.g., composition, microstructure, voids, inclusions, anisotropy, flow stress, ductility). Other

important parameters are the size, location, thickness, and geometric characteristics of incoming material (i.e., tolerances, quality of sheared edge, and surface finish). Material thickness affects die pressure, tendency to wrinkling, and deformation forces. It becomes necessary to use harder and more wear-resistant die materials to form very thick sheets.

As material thickness decreases, its load-carrying capacity decreases as well. Consequently, preventing failures during forming becomes more difficult with decreasing sheet

thickness. The uniformity of thickness also has an effect on strain localization.

Plastic anisotropy (e.g., difference in deformation behavior of the material when stressed in various directions) is a very crucial factor in sheet forming. It is the tendency of sheet materials to deform differently in different directions. The average plastic anisotropy is a good measure of the drawability of a material but has very little effect on its stretchability or bendability.

Beside geometric anisotropy, hardening anisotropy is also important in sheet metal forming. Hardening anisotropy is the generalization of the well known Bauschinger effect (Ref 2.3).

The location of the blank in the die has a significant effect on the strain state in the sheet during deformation. Shifting the blank location increases the amount of flange material on some edges and decreases it on others. Areas with increased flange material experience more resistance to flow, while areas of decreased flange material experience less resistance. Changing the blank size has a similar effect. Blank flatness is also another important variable. A blank, which is excessively out of flat, will not nest into the die correctly and cause problems in obtaining proper blank location. Leveling processes are used to obtain flat blanks. While leveling effectively flattens the coil, it also leaves some residual strains in the blanks.

Tooling and Equipment

Design and manufacturing of tooling are essential factors determining the performance of deformation processes. The key to successful deformation processing is tool design, which was based, until recently, on experience. However, to design and fabricate forming tools today, we use “virtual prototyping,” such as computer-aided engineering and computer-aided manufacturing using numerical simulation.

The productivity and reliability of equipment used in sheet forming are also very important factors in determining the practical application of a given process. The stroking rate of the forming press determines the production rate. The use of sensors for process monitoring and control assists in improving and maintaining part quality.

Flexibility of tooling and equipment is gaining importance because of the increased variability of products and reduction in batch sizes. Tooling concepts that allow the manufacturing

of various product geometries in one tool setup represent a preferred strategy today.

Variations in tool performance are caused by: (a) changes in setup and (b) continuous wear through normal usage. Sensors can also be used to continuously monitor the condition of the tooling, improving part quality as well production rates. This is achieved by greatly reducing unscheduled breakdowns of expensive production equipment and increasing the tool life.

During the setup of tooling in a press, care must be taken to properly align the tooling. Misalignment may lead to significant changes in the process and to defects in formed parts. In deep drawing, for example (Fig. 2.2), binder (or blank holder) forces play a major role in the formability of sheet material. The magnitude of binder force should be controlled so that neither fracture nor wrinkling will occur in the formed part. Deep drawability can be increased by varying binder pressure throughout the punch stroke or around the periphery of the flange in more complicated operations.

Draw beads are used when material flow needs to be restrained more than what can be provided by a flat binder plate using blank holder pressure only (Fig. 2.3, 2.4). Punch and die radii are other important variables affecting the flow and stretch of sheet material (Ref 2.4).

Shut height is the distance between the ram, at its bottom dead center position, and the lower platen or bolster (see Chapter 9 in this volume). Variations in shut height affect the final part geometry as well as the strain patterns in deep drawing. A slight increase in shut height or ram stroke position can increase the draw or stretch of a part and cause increased straining, leading to excessive thinning or fracture. Increasing punch speed has the effect of increasing the impact of the punch on the sheet, which leads to

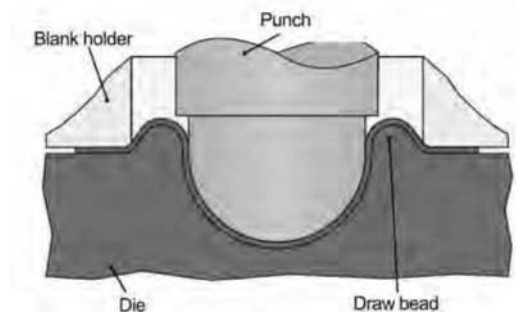


Fig. 2.3 Draw bead located inside the die. Source: Ref 2.4

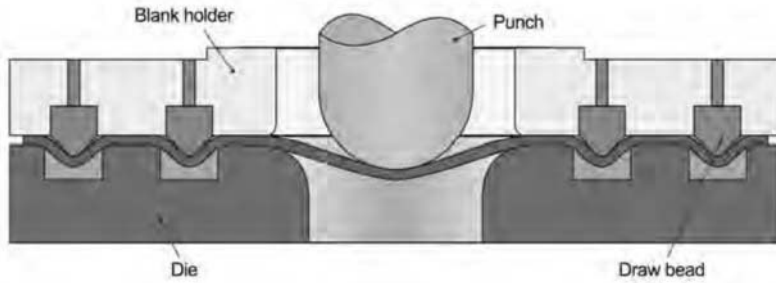


Fig. 2.4 Draw beads located in the blank holder. Source: Ref 2.4

the creation of shock lines on the sheet. High impact speed also tends to cause breakdown of the lubricant layer.

The selection of a machine for a given process is influenced by the time, accuracy, and load-energy characteristics of that machine. Optimum equipment selection requires consideration of the entire forming system, including lot size, conditions at the plant, environmental effects, and maintenance requirements, as well as the requirements of the specific part and process under consideration.

The tooling variables include: (a) design and geometry, (b) surface finish, (c) stiffness, and (d) mechanical and thermal properties under processing conditions.

Friction and Lubrication at the Tool/Work Piece Interface

Knowledge of friction and heat transfer at the tool-material interface should be expressed quantitatively in order to develop an adequate design of the process. The mechanics of interface friction is very complex. One way expressing friction quantitatively is through a friction coefficient, μ , or a friction shear factor, m . Thus, the frictional shear stress, τ_f , is

$$\tau = \sigma_n \mu = p \mu \quad (\text{Eq 2.2})$$

where $0 < \mu < 0.577$,
or

$$\tau = m \bar{\sigma} / \sqrt{3} = f \bar{\sigma}, \quad 0 \leq m \leq 1 \quad (\text{Eq 2.3})$$

where σ_n or p is the normal stress or pressure at the interface, $\bar{\sigma}$ is the flow stress of the deforming material, and f is the friction factor ($= m/\sqrt{3}$).

For small values of pressure, which is usually the case in sheet forming, friction force increases with increasing pressure. In this case, friction conditions are best characterized by Coulomb's law (Eq 2.2). With increasing pressure, friction force cannot increase indefinitely. It approaches a finite value for very high pressures. At this time, sticking friction conditions occur when $\mu p \geq k$, where k is shear strength, equal to $2\bar{\sigma}/\sqrt{3}$, according to von Mises criterion of plastic flow. This condition occurs often in bulk forming operations where $p \gg k$. At this high pressure, since there is no relative motion between tool and the work piece at the interface, the coefficient of friction, μ , becomes meaningless. In this case, the friction factor, m (Eq 2.3), is used to model friction conditions.

Recent studies in forming mechanics indicate that Eq 2.2 adequately represents the frictional shear stress in sheet metal forming. There are various methods of evaluating friction, that is, estimating the value of μ or m . Tests most commonly used for evaluating friction are discussed in Chapter 7 of this volume.

Die temperature increases at high stroking rates due to friction and deformation. This affects the stamping process by causing heat transfer between the warmer die and cooler sheet and by reducing the effectiveness of the lubricant used. Cooling/heating of sheet also tends to increase/decrease its flow stress. Thus, die temperature may also affect the sheet forming process.

Deformation Zone and Mechanics of Deformation

When material is deformed plastically, metal flow is influenced mainly by: (a) tool geometry, (b) friction conditions, (c) mechanical properties of the initial work piece material, and (d)

thermal condition existing in the deformation zone. Detailed understanding of metal flow enables prediction of the quality and properties of the formed product and the force and energy requirements of the process. This leads to forming high-quality products with a minimum of trial and error by optimizing the tool design and process conditions. The mechanics of deformation (i.e., the metal flow, strains, strain rates, and stresses) can be investigated using appropriate methods of analysis such as the finite element method.

Product Geometry and Properties

The two main characteristics of a deformed product are its geometry (e.g., dimensions, tolerances, thickness distribution, and surface finish) and its mechanical properties. As in all manufactured parts, the design of the deformed part—that is, the consideration of manufacturing feasibility during the design stage—determines the magnitude of the effort necessary for process and tool development. For example, geometric features that satisfy various functional requirements such as stiffness and strength should be evaluated regarding their formability.

Product geometry and its mechanical properties are influenced by process variables. For example, the process conditions (temperature, strain, and strain rate) have an effect on final product properties by determining the microstructural variations taking place during deformation. Therefore, in a realistic system approach, the relationship between mechanical properties and microstructure of the final product and the quantitative effect of process conditions and heat treatment schedules on microstructural variations must be considered.

Safety and Environmental Factors

Safety and environmental effects are important matters in forming process. The importance of safety increases with increasing machine speeds and forces. Adverse environmental effects of lubrication, cooling and heating fluids, noise, smoke, and waste material must be considered in process development, and efforts should be made to minimize or eliminate adverse environmental effects.

The components of the sheet metal forming system, illustrated in Fig. 2.2 and discussed above, must be integrated by the metal forming specialist in designing a sheet metal forming operation. Thus, for a given material and its me-

chanical properties, the forming machine, tooling, and lubrication must be selected for a robust production process to achieve the desired production rates with minimum use of energy and damage to the environment.

2.3 Classification of Geometries

A shape classification system should cover the entire range of possible shape of parts formed from sheet and strip. The basis of such a classification is the geometry of the finished parts. Various representative sections of the part and the curvatures in each section must be known in order to classify sheet metal parts based on geometry.

Most sheet metal parts fit readily into a system of classification. However, sometimes different part types appear to be similar. They are distinguished in a quantitative manner rather than in a qualitative manner. A variety of geometries are required in sheet metal components used in automotive and aircraft industries (Ref 2.5, 2.6). Major sheet forming processes used in manufacturing these components are summarized in Table 2.2. These commonly used sheet metal forming operations are briefly described

Table 2.2 Commonly used sheet forming processes

Bending and straight flanging processes (Section 2.4)	
Brake bending	Tube Bending
Hemming	Flanging
Roll Forming	Hole Flanging
Roll Bending	Jogging
Blank Preparation (Section 2.5)	
Sheet leveling and straightening	
Shearing, blanking, and piercing	
Deep Drawing (Section 2.6)	
Deep drawing (using hard dies)	Marform process
Sheet hydroforming with punch	Drop hammer forming
Sheet hydroforming with die	Hot stamping
Fluid bladder (diaphragm) forming	
Stretch Forming (Section 2.7)	
Stretch forming asymmetric parts	Tube hydroforming
Linear stretch forming	Expanding
Creep forming	Dimpling
Age forming	Electromagnetic forming
Die quench forming	Explosive forming
Bulging	
Incremental Forming (Section 2.8)	
Spinning	Shear forming
Hybrid Forming Processes (Section 2.9)	
Ironing	Nosing
Coining	

Source: Modified from Ref 2.7

in Sections 2.4–2.9 for the basic types of operations.

2.4 Bending and Flanging

Brake bending is a forming operation widely used for forming flat sheets into linear sections, such as angles, channels, and hats. Bending produces little or no change in the thickness of the sheet metal. The general objectives in bending are obtaining rigidity and producing a part of required curved shape. There are several brake-forming setups: air bending, die bending, and edge bending. In air bending (Fig. 2.5a), the work piece is supported only at the outer edges so that the length of the ram stroke determines the bend angle of the part. In die bending (Fig. 2.5b), the sheet is forced into a female die cavity of the required part angle. In edge bending (Fig. 2.5c), the base of the sheet is held between a pressure pad and a die while the sheet is forced to yield and bend over the edge of the die.

- *Equipment:* mechanical press brakes, hydraulic press brakes
- *Materials:* carbon and alloy steels; aluminum alloys; titanium alloys; iron-, nickel-, and cobalt-base superalloys; molybdenum alloys; beryllium; tungsten

- *Process Variations:* brake forming with elastic (urethane) dies, folding (bending of sheet held on one side only)
- *Application:* production of straight shapes from sheet and plate

Hemming. In the hemming process, the edge of the sheet is folded over itself (180° or more) to remove the burred edge. Hemming operations are usually done in three stages: bending or flanging to 90° , prehemming to approximately 135° , and hemming to 180° or more. They are not as rigid or accurate as a flange, but they very effectively remove a dangerous sheared edge (Fig. 2.6):

- *Equipment:* mechanical and hydraulic presses, tabletop hammer
- *Materials:* carbon and alloy steels, (in sheet form)
- *Process Variations:* rotary hemming, robot hemming
- *Applications:* in automobiles to join inner and outer doors and truck lid stampings; appliances; used for appearance or for attachment of one sheet metal part to another

Roll Forming. The process of roll forming is a continuous bending process that is used to produce long components of uniform cross sections. The sheet metal is formed by passing it through a succession of progressively shaped, power-driven, contoured rolls (Fig. 2.7). The material thickness is not changed except for a slight thinning at bend radii. In this process, in contrast to regular bending, longitudinal strains are introduced:

- *Equipment:* roll forming machines
- *Materials:* carbon and alloy steels aluminum alloys; titanium alloys; iron-, nickel-, cobalt-base superalloys; molybdenum alloys; niobium alloys
- *Process Variations:* edge rolling
- *Application:* production of large quantities of complex structural shapes from sheet; channels, gutters, welded pipes, and tubing.

Roll bending gives a curvature to a sheet, bar or shaped section by bending it between two or three cylindrical rolls (Fig. 2.8) that can be adjusted. Flattened cylinders and elliptical cylinders can also be formed:

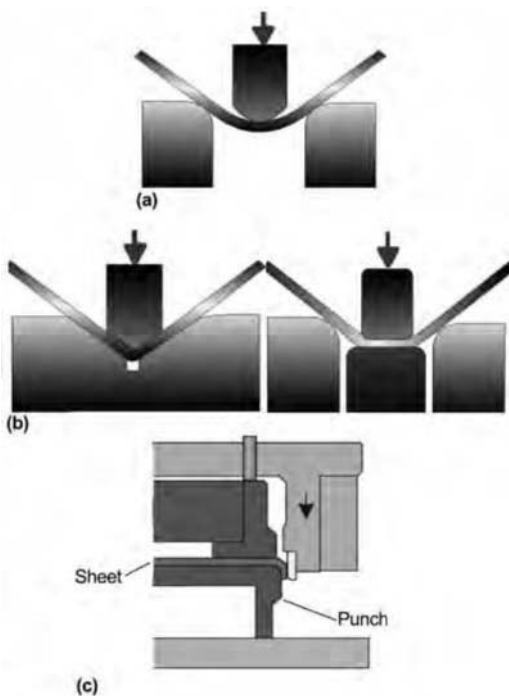


Fig. 2.5 Bending: (a) air bending; (b) die bending; (c) edge bending. Source: Ref 2.4

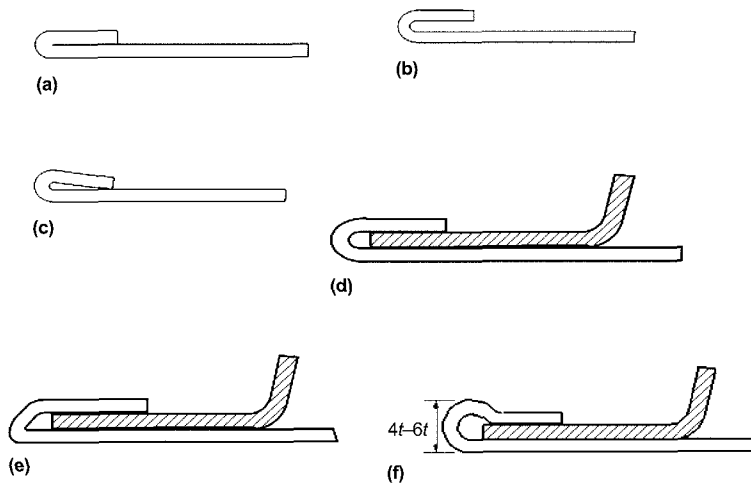


Fig. 2.6 Hemming: (a) flattened hem; (b) open hem; (c) teardrop hem; (d) radius flat hem; (e) modified flat hem; (f) rope hem

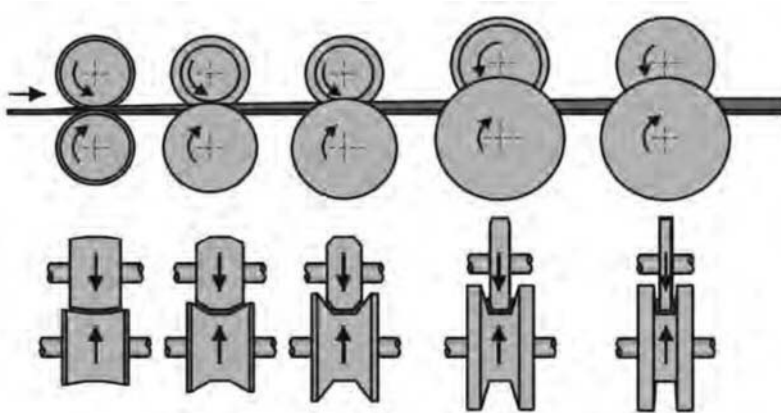


Fig. 2.7 Roll forming (contour roll forming). Source: Ref 2.4

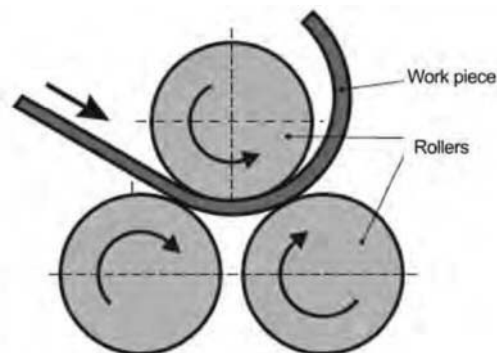


Fig. 2.8 Roll bending. Source: Ref 2.4

- *Equipment:* roll-bending machines, pinch-roll-type machines, pyramid-roll-type machines
- *Materials:* carbon and alloy steels, aluminum alloys, titanium alloys
- *Process Variations:* roller leveling
- *Applications:* cylinders for pressure tanks; boilers; corrugated pipe; cones; hoppers; regular and irregular shapes from structural sections for submarines, aircraft, and nuclear reactors

Tube bending is a method for obtaining tubes with one or several curvatures (Fig. 2.9). During bending, the tube wall will tend to move toward the centerline of the tube. As a result, the

circular tube may tend to become oval. Therefore, many tube bending techniques use mandrels to maintain the original cross section of the tube during bending:

- *Equipment:* special tooling, rotary draw of compression bending machines
- *Materials:* all ductile materials
- *Process Variations:* rotary draw bending, compression bending, ram bending, press bending
- *Applications:* manufacturing of furniture, performing for tube hydroforming, various structural hardware applications

Flanging is essentially a bending operation around the curved edge. Due to the nature of the curvature, the process is called either *stretch flanging* (concave edge curvature) or *shrink flanging* (convex edge curvature). Flanges help to achieve stiffness in a formed part and can be used to facilitate assembly or as a preforming operation as in hemming. Various examples of flanging are illustrated in Fig. 2.10.

- *Equipment:* press and appropriate tooling
- *Materials:* all sheet materials
- *Process Variations:* hole flanging, reverse flanging, jogged flange

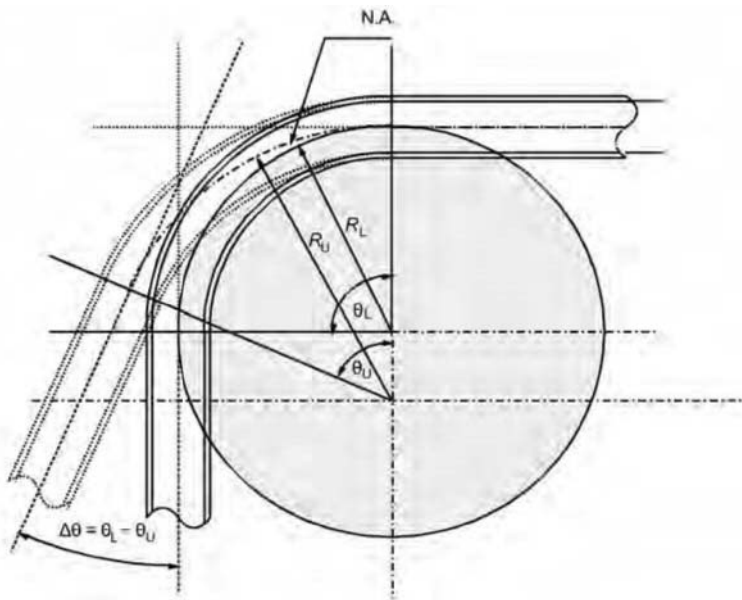


Fig. 2.9 Typical tube bending operation; thickness distribution around and along the cross-section of the bent tube; springback

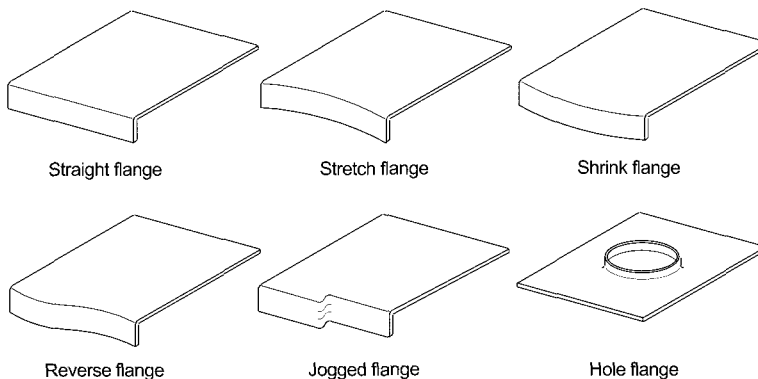


Fig. 2.10 Various types of flanges

- *Applications:* preforming operation in hemming, to provide ease in assembly

Hole flanging is a method of forming under combined compressive and tensile conditions using a punch and die to raise closed rims (flanges) on cut-out orifices (Fig. 2.11). The orifice can be on the flat or in the curved surfaces. Flanges are often provided with female threads for the purpose of connecting sheet metal parts:

- *Equipment:* press
- *Materials:* all sheet materials
- *Process Variations:* flanging
- *Applications:* used for appearance and assembly ease

Hole flanging involves stretch flanging of a hole in the product. Higher hole flanges require a smaller punched hole diameter to provide the required additional material.

Jogging is the process of making an offset in a flat plane by two parallel bends in opposite directions at the same angle (Fig. 2.12). Jog-

ging permits flush connections to be made between sheets, plates, or structural sections.

- *Equipment:* mechanical presses, hydraulic presses
- *Materials:* alloy steels; aluminum alloys; titanium alloys; iron-, nickel-, and cobalt-base superalloys; molybdenum alloys; niobium alloys; beryllium; tungsten
- *Applications:* forming of aerospace parts

2.5 Blank Preparation

Sheet Leveling/Roll Strengthening. Roll straightening is used to eliminate undesirable deformations in sheet metal, wire, rods, or pipes. Each roll is usually driven separately with individual electric motors. The material is flexed in opposite directions as it passes through the sets of rollers (Fig. 2.13).

- *Equipment:* rotary-roll leveling equipment, parallel leveling equipment, automatic press straighteners, epicyclic straighteners

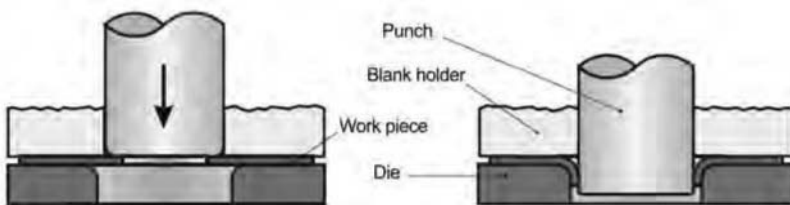


Fig. 2.11 Hole flanging. Source: Ref 2.4

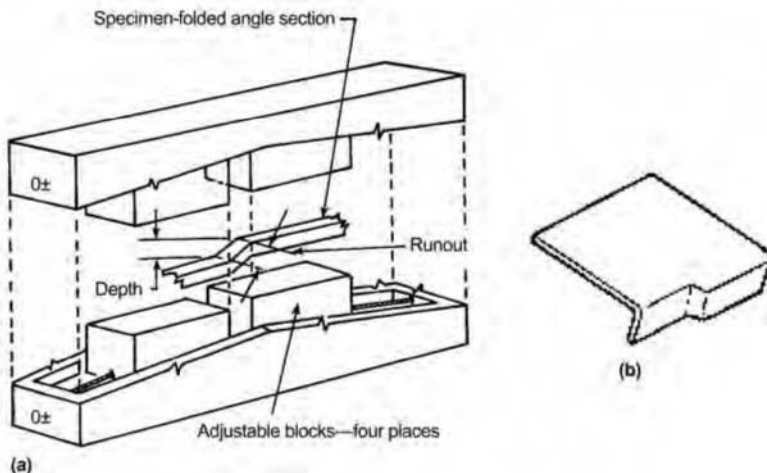


Fig. 2.12 Jogging: (a) universal joggle die; (b) jogged flange

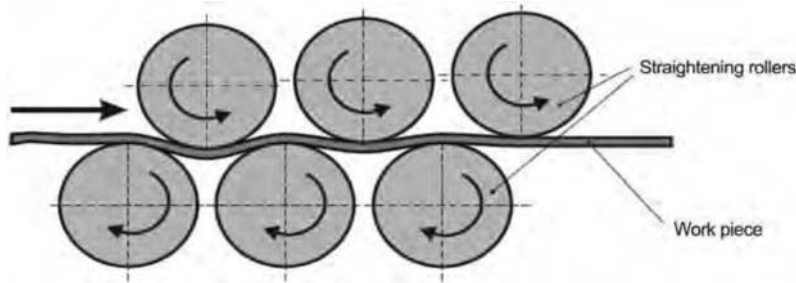


Fig. 2.13 Roll straightening. Source: Ref 2.4

- *Process Variations:* parallel roll straightening, automatic press straightening, rotary-roll straightening, parallel-rail straightening, epicyclic straightening, moving-insert straightening
- *Applications:* eliminating residual stresses, twist, face, and edge camber

Shearing and Blanking/Piercing. The process of shearing is the cutting action along a straight line to separate metal by two moving blades. In shearing, a narrow strip of metal is plastically deformed to the point where it fractures at the surfaces in contact with the blades. The fracture then propagates inward to provide complete separation. It is used for production blanks:

- *Equipment:* squaring shears
- *Materials:* all metals, plastics
- *Process Variations:* fine blanking, nibbling, notching, punching, piercing (Fig. 2.14)
- *Applications:* in producing blanks for subsequent operations, trimming of flanges, preparation of holes

Blanking involves shearing a piece out of stock (strip of sheet metal) to a predetermined contour. It results in excessive waste of metal compared to cutoff and parting. However, the blank shape makes the use of blanking a necessity in most cases. It is performed in a die operated by a press.

2.6 Deep Drawing

Deep Drawing Using Hard Dies. In deep drawing (Fig. 2.15a), a sheet blank (hot or cold), usually subjected to a peripheral restraining force, is forced by a punch into and through a die to form a deep recessed part having a wall thickness essentially the same as that of the

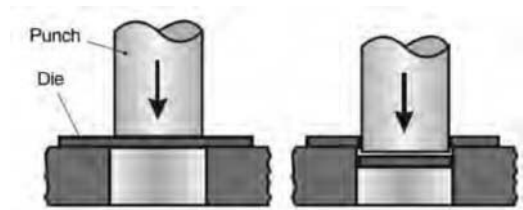


Fig. 2.14 Blanking. Source: Ref 2.4

blank. If the amount of shape change required in deep drawing is too severe, then more than one drawing operation is required to form the part completely. The second step and any further steps, if needed, are referred to as redrawing (Fig. 2.15b). In reverse drawing (Fig. 2.15c), which is another related operation, an initially drawn part is positioned face down on the die so that the second drawing operation produces an inversely drawn part:

- *Equipment:* hydraulic presses, mechanical presses, transfer presses
- *Materials:* carbon and alloy steels, aluminum alloys, titanium alloys, high-temperature alloy
- *Process Variations:* deep drawing with multiple acting punch, deep drawing with rigid contour punch, rubber forming without blank holder, rubber forming with blank order (Marform process), drawing against liquid (Aquadraw process), explosive forming, hydroforming
- *Applications:* drawing of deep and shallow cups, ammunition sheets, cartridge cases, beverage cans, sinks, cooling pots; drawing of irregular curved forms as in automotive body panels

Sheet Hydroforming with Punch. In sheet hydroforming, one of the die halves is replaced

with fluid under pressure. In sheet hydroforming with punch, the punch is pushed against the fluid pressure (Fig. 2.16):

- *Equipment:* double-action hydraulic presses, special machines

- *Materials:* carbon and alloy steels, aluminum alloys
- *Process Variations:* high-draw technique, Marform process, rubber forming, bladder forming

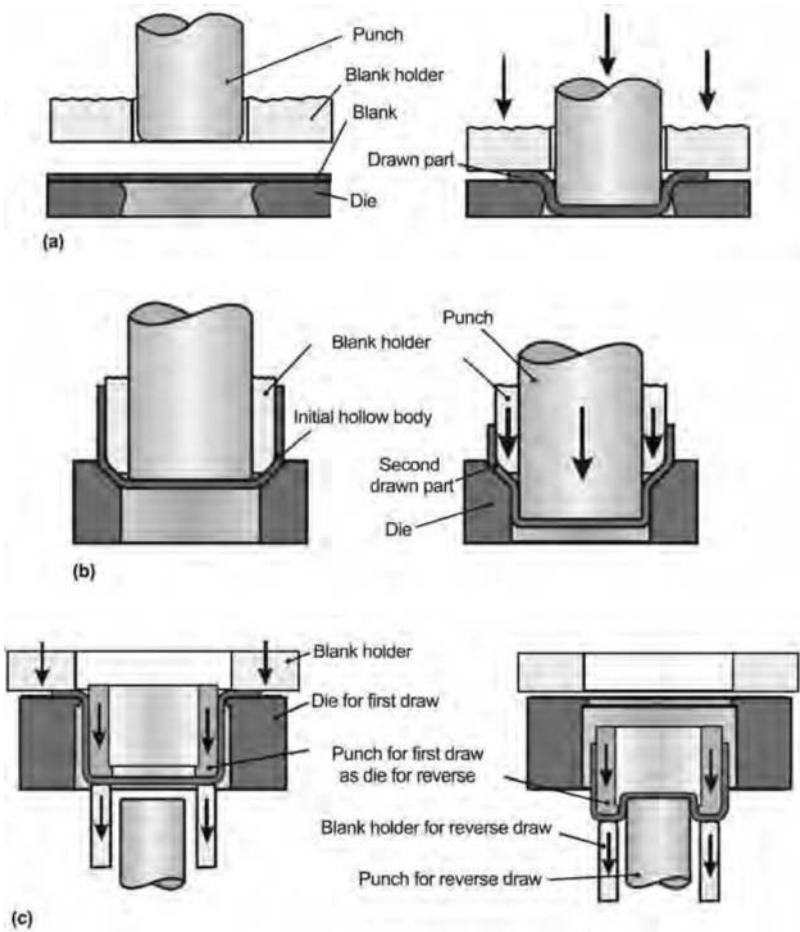


Fig. 2.15 Drawing operations: (a) single deep drawing with blank holder; (b) redrawing; (c) reverse drawing. Source: Ref 2.4

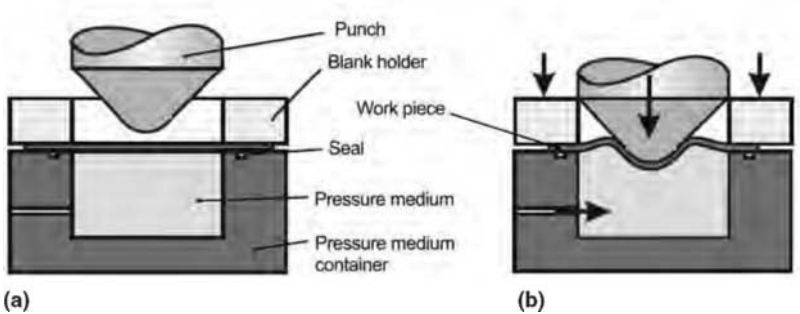


Fig. 2.16 Sheet hydroforming with punch: (a) before deformation; (b) during deformation. Source: Ref 2.4

- *Application:* deeply recessed parts with or without flanges, produced in relatively small batches

Sheet hydroforming with die is an alternative to the deep drawing process where the punch is replaced by hydraulic medium that generates the pressure and forms the part (Fig. 2.17). The forming operation in this process can be divided into two phases. Phase I involves the free forming operation where the sheet bulges freely in the die cavity until it contacts the die surface. Free bulging ensures uniform deformation in the sheet, which improves the dent resistance of the hydroformed part compared to parts formed in hard dies, that is, with a female die and a male punch. However, after a large portion of the sheet leans against the die wall, the flow of sheet metal is restricted because of friction at the sheet-die interface. Phase II involves calibrating the sheet against the die cavity to obtain the final desired shape, where a high fluid pressure is required. The level of this fluid pressure depends on the sheet material and

thickness, part complexity, and the smallest corner radius of die geometry:

- *Equipment:* hydraulic press, special machines
- *Materials:* carbon and alloy steels, aluminum alloys
- *Process Variations:* double-blank sheet forming
- *Application:* auto-body panels having without sharp corners, dent-resistant parts, low-production-volume products

Fluid Bladder (Diaphragm) Forming. In this process, the sheet is forced over a forming punch or into a forming die by the pressure exerted on it by a thick rubber pad (Fig. 2.18). The pad, which is soft, is driven by the action of oil filled bladder, which is contained between the pad and the containing structure:

- *Equipment:* Versor-Wheelon and ABB Flexform presses
- *Material:* carbon and alloy steels, aluminum alloys
- *Process Variations:* sheet hydroforming with punch or die
- *Applications:* in aerospace, automotive, electric lightning, and cookware industries; production of parts with reentrant wall profiles and bottom C-flanges

Marform Process (Rubber Pad Forming). In the Marform process, the blank is gripped between a blank holder and a rubber pad contained inside a retainer ring attached to the ram (Fig. 2.19). As the ram moves down, the blank is drawn over the punch (form block) under the

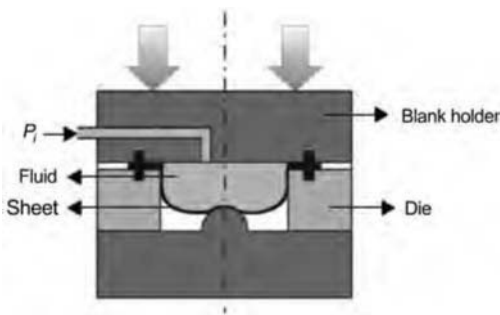


Fig. 2.17 Sheet hydroforming with die

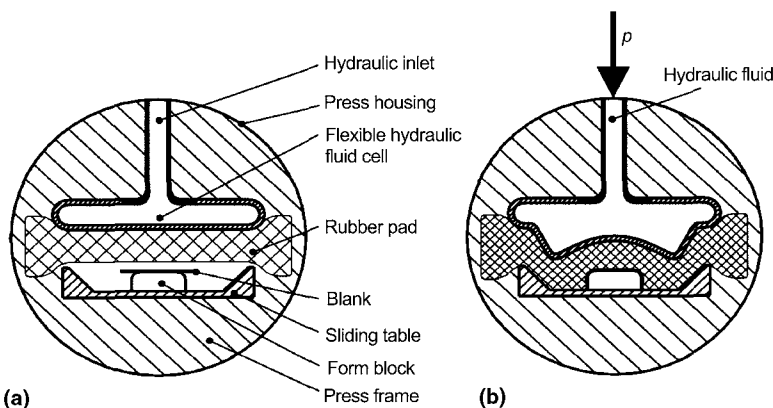


Fig. 2.18 Fluid bladder and diaphragm process: (a) before; (b) during forming. Source: Ref 2.8

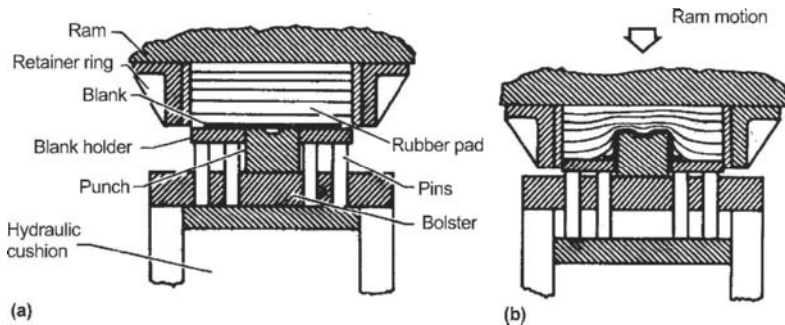


Fig. 2.19 Marform process: (a) die open; (b) die closed. Source: Ref 2.2

hydrostatic pressure exerted on the incompressible but pliable rubber pad:

- *Equipment:* hydraulic presses, special machines
- *Material:* carbon and alloy steels, aluminum alloys
- *Process Variations:* hydroforming process, high-draw technique, rubber-diaphragm forming
- *Applications:* deeply recessed parts with or without flanges

Drop hammer forming is a process for producing shapes by the progressive deformation of sheet metal in matched dies under repetitive blows of a gravity-drop or power-drop hammer (Fig. 2.20):

- *Equipment:* hammers
- *Materials:* carbon and alloy steels, aluminum alloys, titanium alloys
- *Process Variations:* coining, forming to size
- *Applications:* configurations most commonly formed by drop hammer forming include shallow, smoothly contoured, double-curvature parts, shallow-beaded parts, parts with irregular and comparatively deep recesses; used mainly in aircraft industry for low-volume production

Hot stamping is a nonisothermal forming process for manufacturing ultra-high-strength parts (ultimate tensile strength = 1500 MPa) from manganese boron steel (22MnB5). In this process (Fig. 2.21), austenitized sheet metal is formed and quenched in the same operation by using tools with integrated cooling channels. The final part has martensite microstructure that can be tempered to improve ductility. (See the chapter on hot stamping in the companion vol-

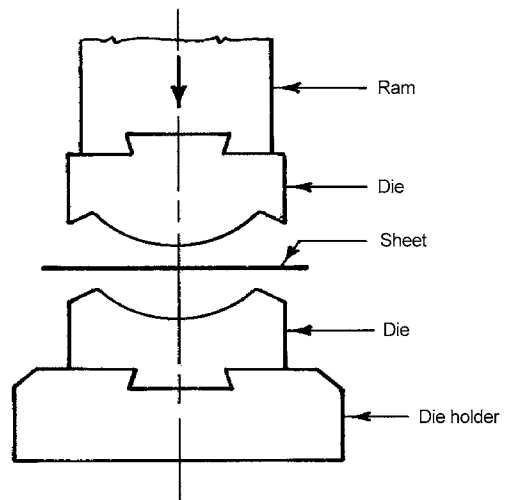


Fig. 2.20 Drop hammer forming

ume, *Sheet Metal Forming Processes and Applications*, for more detailed information):

- *Equipment:* hydraulic press (most common), servo press
- *Materials:* manganese boron steel (MnB5)
- *Applications:* crash-resistant body-in-white components such as B-pillar reinforcement, A-pillar reinforcement, front and rear bumper, door beam, roof rail reinforcement

2.7 Stretch Forming

Stretch Forming Asymmetric Parts. Stretch forming is very similar to deep drawing. It differs from deep drawing in that the material is clamped tightly between the binder and die (Fig. 2.22). Deformation is restricted to the area

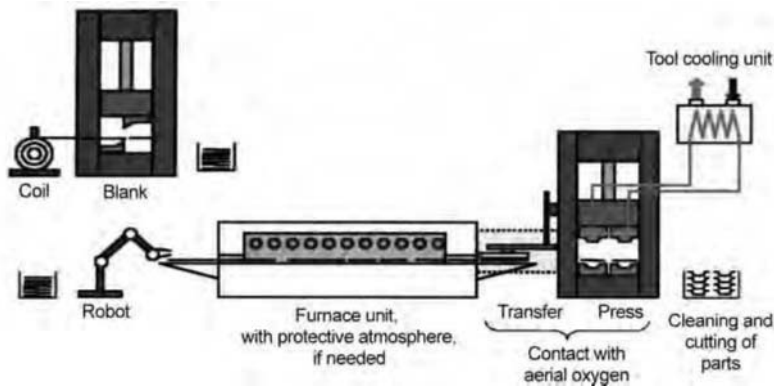


Fig. 2.21 Principles of hot stamping (heating in furnace/forming and quenching in press)

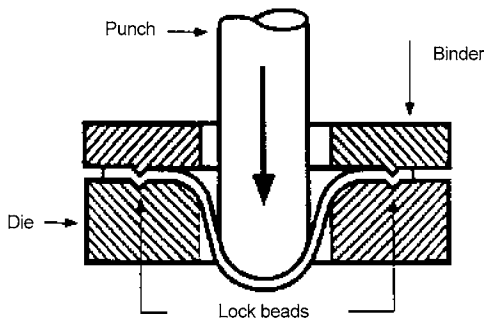


Fig. 2.22 Stretch forming

within the lock beads. Stretch forming is used to form compound curves in sheet stock:

- *Equipment:* hydraulic presses, mechanical presses
- *Materials:* aluminum alloys, stainless steels, low-carbon steels, titanium alloys
- *Applications:* body panels, such as doors, roofs, or fenders for trucks, buses, and special vehicles; prototype parts of large radius of curvature, frequently with double curvature

Linear Stretch Forming. Stretch forming is a method that combines controlled stretching and bending of sheet metal blanks, roll-formed sections, and extrusions around form blocks (dies) to produce accurately countered parts without wrinkles. Usually, two opposite ends of the work piece are gripped in jaws and pulled or wrapped around the form block (Fig. 2.23):

- *Equipment:* stretch forming machines
- *Materials:* aluminum alloys, stainless steels, low-carbon steels, commercially pure titanium

- *Process Variations:* stretch-draw forming
- *Applications:* aircraft and aerospace industries; production of truck bumpers, structural frames for vehicles, monorail guide beams, telecommunication antennas

Creep forming occurs when pressure is applied to the irregularly shaped or preformed part placed against a heated die. In contact with the hot die, the part is heated and assumes the desired shape against the die by slow creep deformation (Fig. 2.24):

- *Equipment:* special creep forming presses
- *Materials:* aluminum and titanium
- *Process Variations:* age forming, hot die forming
- *Application:* forming of parts for the aerospace industry; forming of airplane wing skins

Age Forming. In this process, panels to be shaped are restrained on a fixture of required contour and heat-treated or aged at a specified temperature for a prescribed period of time. During aging of the part, the material yields to the stress introduced by the action of holding it in the fixture, and it retains the contour when removed from the fixture after aging (Fig. 2.25):

- *Equipment:* special age forming fixtures/furnaces
- *Materials:* aluminum and titanium alloys
- *Application:* imparting contours to panels and sheets in small quantities

Die Quench Forming. In die-quench forming, the heated work piece is formed between cold dies under high forming pressure without allowing it to contract during forming (Fig.

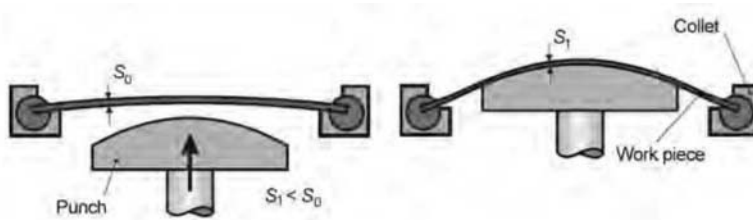


Fig. 2.23 Linear stretch forming. Source: Ref 2.4

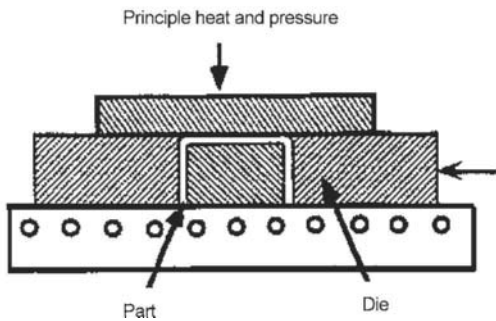


Fig. 2.24 Creep forming

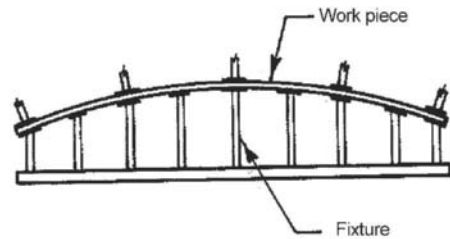


Fig. 2.25 Age forming

2.26). The percentage of stretch introduced in the metal is proportional to the coefficient of thermal expansion of the alloy at the processing temperature:

- *Equipment:* hydraulic presses
- *Materials:* aluminum and titanium alloys
- *Process Variations:* hydrodynamic die-quench forming
- *Application:* forming of complex parts that are to be formed free from warpage and residual stresses; shaping of integrally stiffened skins

Bulging. In bulging, an internal pressure is applied to form a tube to the desired shape (Fig. 2.27). The internal pressure can be delivered by expanding a segmented punch through a fluid, or by using an elastomer:

- *Equipment:* mechanical presses, hydraulic presses
- *Materials:* carbon and alloy steels, aluminum alloys
- *Process Variations:* die forming, free forming, bulging by buckling, bulging with steel balls, bulging with internal fluid pressure, explosive (magnetic/electric) bulging
- *Applications:* contoured tubes and shells for aerospace and automotive chassis applications

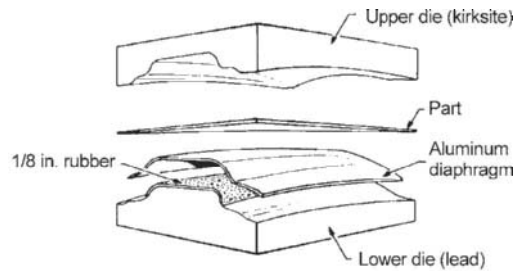


Fig. 2.26 Die-quench die with aluminum diaphragm

Tube Hydroforming. In tube hydroforming, a straight or prebent tubular blank is placed in a closed die set. The ends of the tube are sealed, and the inside is filled and pressurized with a hydraulic fluid (Fig. 2.28). At this point the forming pressures can be supplied through the application of an axial force and/or increasing the internal pressure:

- *Equipment:* tube hydroforming press or hydraulic press with tube hydroforming tooling and pressure system
- *Materials:* stainless steel, low-carbon steel, aluminum 5000-6000, copper, brass
- *Process Variations:* high/low-pressure hydroforming, tube hydroforming by axial force and/or internal pressure
- *Applications:* forming frame rails, cross members, suspension and engine subframes,

cross-car beams, A/B/C pillars, roof rails in automotive industry

Expanding. The process of expanding is a tensile forming with a view to expanding the periphery of a hollow body. As the case with deep drawing, rigid as well as yielding tools,

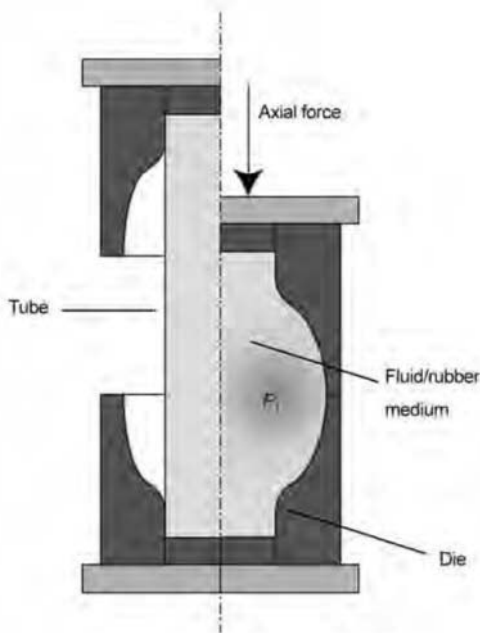


Fig. 2.27 Bulging. Source: Ref 2.4

active media and active energies are also used (Fig. 2.29):

- *Materials:* aluminum alloys, carbon alloys, stainless steel, any material with sufficient ductility
- *Applications:* appliances industry (liners, baskets, tubes, laundry equipment); beads, threads, flanges, bosses, flute; aircraft and aerospace industry (fuel tanks, missile cases, jet engine rings, etc.); automotive industry (wheel rims for cars and trucks, etc.).

Dimpling is a process for producing small conical flanges around holes in sheet metal parts that are to be assembled with flush or flat-headed rivets (Fig. 2.30). Dimpling is most commonly applied to sheets that are too thin for countersinking:

- *Equipment:* special dimpling machines
- *Material:* alloy steels; aluminum alloys; titanium alloys; iron-, nickel-, and cobalt-base superalloys; beryllium; tungsten
- *Process Variations:* radius dimpling, coin dimpling, flanging
- *Applications:* sheet metal parts requiring assembly with flush or flat-headed rivets

Electromagnetic forming (magnetic pulse forming) is a process for forming metal by direct application of an intense, transient magnetic field induced around the work piece by an

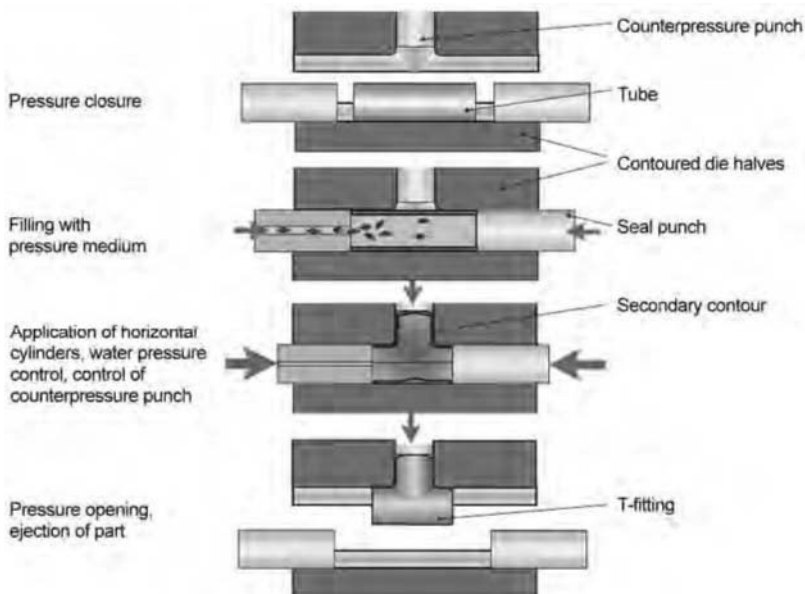


Fig. 2.28 Tube hydroforming with axial feed and internal pressure. Source: Ref 2.4

energized coil (Fig. 2.31). This generates eddy currents in the work piece that produce its own magnetic field. The induced field opposes the primary field, producing an electromagnetic force that deforms the part into the surrounding cavity. The forming process is essentially completed within 80 to 110 μs :

- *Equipment:* special equipment
- *Materials:* aluminum alloys
- *Process Variations:* electric discharge forming, explosive forming
- *Applications:* used primarily for single-step assembly of tubular parts to each other or other components; used to a lesser extent for shaping of tubular parts and shallow forming of flat stock

Explosive forming changes the shape of a metal blank or preform by the instantaneous high pressure that results from the detonation of an explosive (Fig. 2.32). The work piece is clamped and sealed over a die, and the air in the die cavity is evacuated. The work piece is then placed in a tank filled with water. An explosive charge deto-

nated at a certain distance generates a shock wave whose energy is high enough to form the metal. Explosive forming is reserved for large parts, typical of the aerospace industry:

- *Equipment:* special explosive forming equipment
- *Materials:* aluminum alloys, steels, high-temperature alloys
- *Applications:* forming of thin-wall tubing to contours with close tolerances; forming of metal plate; aerospace industry

2.8 Incremental Forming

Spinning is the process of shaping seamless hollow cylinders, cones, hemispheres, or other axially symmetrical metal shapes by the combined forces of rotation and pressure. Spinning does not result in any significant change in thickness (Fig. 2.33). It is a typical incremental forming process:

- *Equipment:* modified lathes, power assisted spinning machines, shear forming machines
- *Materials:* carbon and alloy steels aluminum alloys; titanium alloys; iron-, nickel-, and cobalt-base superalloys; molybdenum alloys; niobium alloys; beryllium; tungsten
- *Process Variations:* manual spinning, power spinning, shear forming, tube spinning, elevated temperature spinning
- *Application:* forming of flanges, rolled rims, cups, cones, and double-curved surfaces of revolution, such as bells; automotive, appliance, air handling, aircraft and aerospace, machinery, ordnance, power generation, and petroleum industries

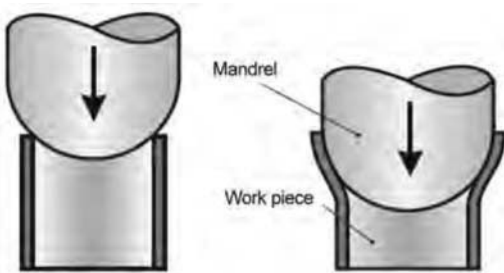


Fig. 2.29 Expanding. Source: Ref 2.4

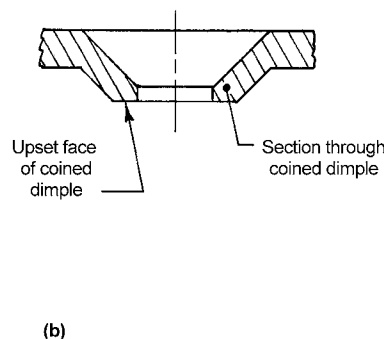
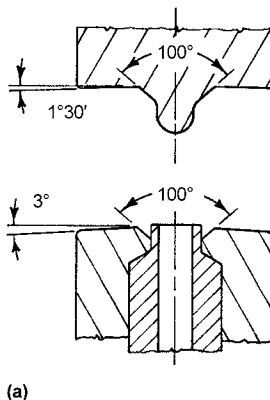


Fig. 2.30 Ram-coin dimpling: (a) tooling setup; (b) dimpled part. Source: Ref 2.2

Shear forming is a process for hot or cold seamless shaping of dished parts by the combined forces of rotation and pressure (Fig. 2.34). This process differs from spinning principally in that it intentionally reduces thickness of the formed part:

- *Equipment:* shear forming machines
- *Materials:* steels, aluminum alloys, copper, titanium alloys
- *Process Variations:* cone shear forming, tube shear forming, roll extrusion
- *Applications:* hardware items such as tumblers; components used in the aerospace industry, such as rocket noses; dish-shaped parts produced in small and moderate quantities

2.9 Hybrid Forming Processes

Ironing is the process of smoothing and thinning the wall of a shell or cup by forcing it through a die with a punch (Fig. 2.35). The working of the metal is severe, and annealing of parts is often necessary between ironing processes. Ironing makes the cylindrical cups more uniform in wall thickness. The ironed part is

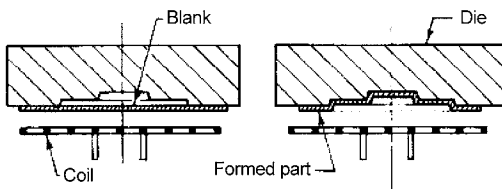


Fig. 2.31 Electromagnetic forming (magnetic pulse forming)

therefore longer and more efficient in terms of material usage:

- *Equipment:* mechanical presses, hydraulic presses
- *Materials:* carbon and alloy steels, aluminum and aluminum alloys, titanium alloys
- *Applications:* shells/cups for various uses (beverage cans and artillery shells)

Coining. In sheet-metal working, coining is used to form indentations and raised sections in the part. During the process metal is intentionally thinned or thickened to achieve the required indentations or raised sections. It is widely used for lettering on sheet metal or components such as coins (Fig. 2.36a). Bottoming (Fig. 2.36b) is a type of coining process where bottoming pressure causes reduction in thickness at the bending area:

- *Equipment:* presses and hammers
- *Materials:* carbon and alloy steels, stainless steels, heat-resisting alloys, aluminum alloys, copper alloys, silver and gold alloys

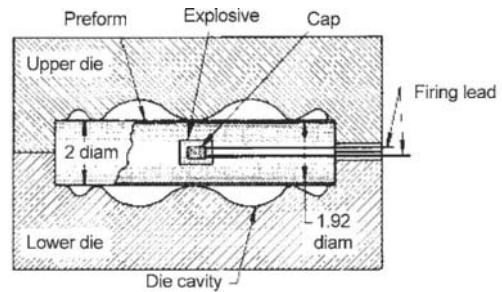


Fig. 2.32 Confined system for explosive forming. Dimensions in inches

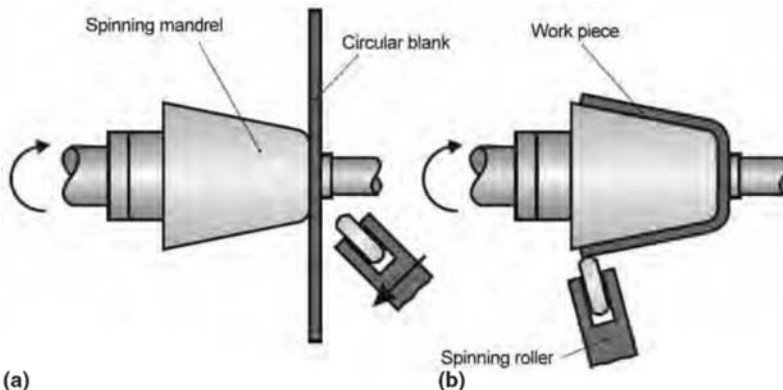


Fig. 2.33 Spinning: (a) before deformation; (b) end of deformation. Source: Ref 2.4

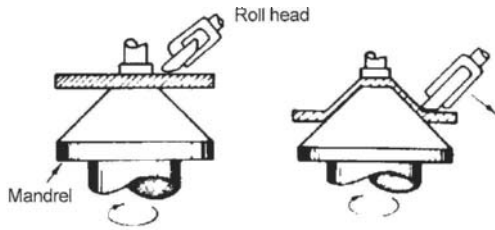


Fig. 2.34 Shear forming

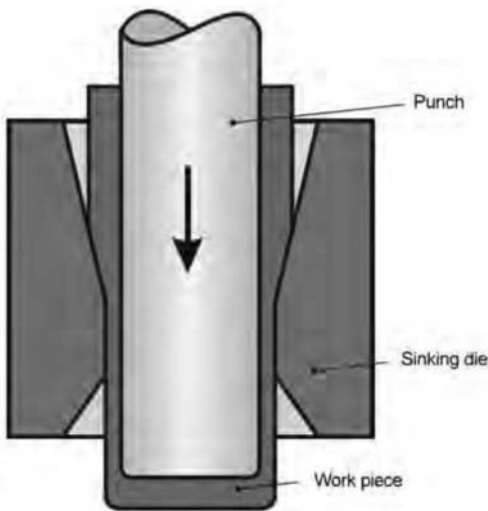


Fig. 2.35 Ironing. Source: Ref 2.4

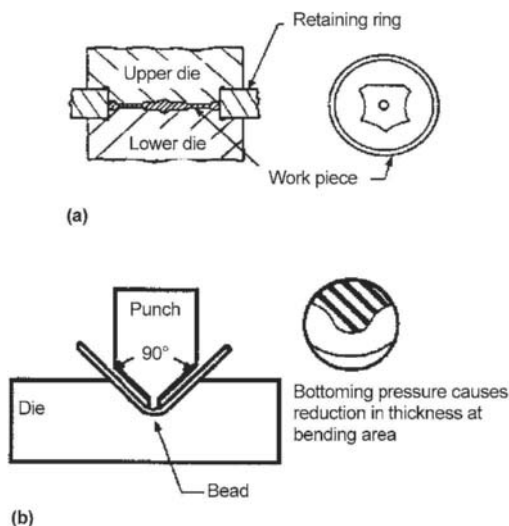


Fig. 2.36 (a) Coining; (b) bottoming

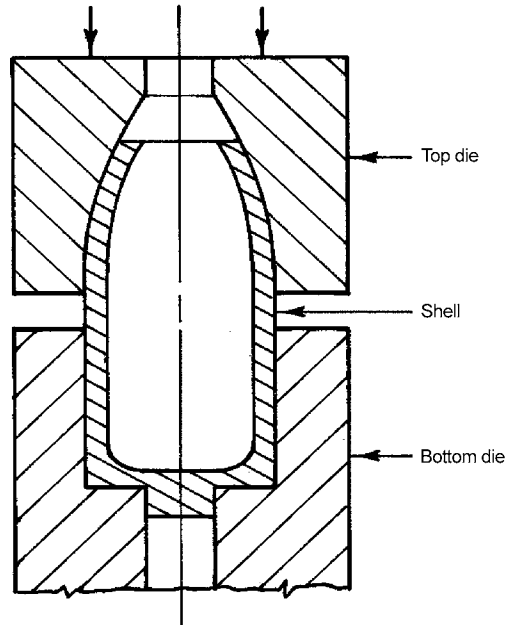


Fig. 2.37 Nosing

- *Process Variations:* coining without flash, coining with flash, coining in closed die, sizing
- *Applications:* metallic coins; decorative items, such as patterned tableware, medallions and metal buttons; sizing of automobile and aircraft engine components

Nosing is a hot or cold forming process in which the open end of a shell (Fig. 2.37) or tubular component is closed by axial pressing with a shaped die:

- *Equipment:* mechanical and hydraulic presses, hammers
- *Materials:* carbon and alloy steels, aluminum alloys, titanium alloys
- *Process Variations:* tube sinking, tube expanding
- *Applications:* forming of open ends of ammunition shells, forming of gas pressure containers

REFERENCES

- 2.1 Unit Manufacturing Process Research Committee, National Research Council, Unit Manufacturing Processes: Issues and Opportunities in Research, National Academy Press, 1995

- 2.2 T. Altan, S. Oh, and H.L. Gegel, Metal Forming: Fundamentals and Applications, American Society for Metals, 1983
- 2.3 E. Tekkaya, Metal Forming, Mechanical Engineering Handbook, Springer, 2005, Chap. 7.2
- 2.4 Schuler, Metal Forming Handbook, Springer, 1998
- 2.5 O.D. Lascoe, Handbook of Fabrication Processes, ASM International, 1988
- 2.6 E.M. Mielnick, Metal Working Science and Engineering, McGraw-Hill, 1991
- 2.7 G. Sachs, Principles and Methods of Sheet-Metal Fabricating, Reinhold, 1951
- 2.8 T. Khandeparkar, Hydroforming Deep Drawing under the Influence of High Pressure, Institut für Umformtechnik, University of Stuttgart, 2007

CHAPTER 3

Plastic Deformation— Strain and Strain Rate

Eren Billur, The Ohio State University

A. Erman Tekkaya, Technische Universität Dortmund, Germany

METAL FORMING requires the controlled change of shape of metals. The shape change has to be quantified mathematically to determine the amount of plastic deformation, which in turn is required to determine the forming loads and possibly the failures during the forming process. The key concept to describe the amount of shape change is the concept of strain. In this chapter, the definitions of various strain measures are given, along with their significance for the sheet forming process.

3.1 Homogeneous or Uniform Deformation

Homogeneous deformation refers to the state in which the magnitude of deformation has the same value for all material points in the sheet metal. A typical example of a homogeneous deformation state is given during the extension of a strip of metal until necking. In this case, the deformation at every point in the strip is identical. Figure 3.1 shows the deformation

of such a strip that is extended under an axial force F .

If the force is smaller than a threshold value, the strip will recover its original length ℓ_0 . This deformation is called *elastic* deformation. If the magnitude of the force is larger than a threshold value, then the deformation will be also plastic, resulting in an extended length after the force is removed. The homogeneous strain for this deformation can now be defined as:

$$e = \frac{\ell - \ell_0}{\ell_0} = \frac{\Delta \ell}{\ell_0} \quad (\text{Eq 3.1})$$

Hence, strain is the change of length relative to the initial length. This strain is called the *engineering* strain. Note two facts for this simple case:

1. The strain value is the same for any point of the strip.
2. The strain under load consists the *elastic strain*, which is the recoverable part of the total strain when the force is removed, and the *plastic strain*, which is unrecoverable.

The latter observation can be expressed mathematically by:

$$e = e_{el} + e_{pl} \quad (\text{Eq 3.2})$$

In sheet metal forming, the elastic strain, ϵ_{el} , is much smaller than the plastic strain, ϵ_{pl} , so we can usually neglect the elastic strains in describing the plastic deformation unless springback is considered. Elastic strains are in the order of 10^{-4} , whereas plastic strains can be in the order

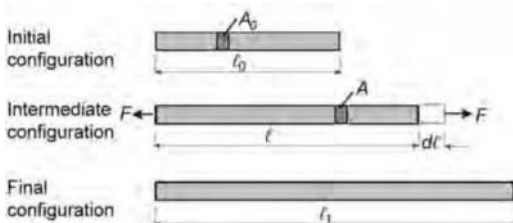


Fig. 3.1 Homogeneous (uniform) deformation of a strip under tensile force (Ref 3.1)

of 10^{-1} to 10^0 (Ref 3.2). As a result, the total strain can be described by:

$$e \approx e_{pl} \quad \text{since} \quad e_{el} \ll e_{pl} \quad (\text{Eq 3.3})$$

Thus, for the final length, ℓ_1 , after removal of the force,

$$e_{pl} = \frac{\ell_1 - \ell_0}{\ell_0} \quad (\text{Eq 3.4})$$

This engineering strain measure is not appropriate for large plastic strains because the engineering strain (a) cannot correctly describe the extension and compression of the strip, and (b) cannot describe sequences of deformations properly. Consider, for example, the following two cases demonstrating the deficiencies.

Case 1: Tension. A strip with length ℓ_0 (state 0) is uniformly extended in tension to a length of $2\ell_0$ (state 1). Using Eq 3.4, the engineering strain (e) would be:

$$e_{01} = 1 \quad (\text{Eq 3.5})$$

Case 2: Compression. If the same strip with length ℓ_0 (state 0) is uniformly compressed of $\ell_0/2$ (state 2), then using Eq 3.4, the engineering strain would be:

$$e_{02} = -5 \quad (\text{Eq 3.6})$$

Thus, the engineering strains, calculated for Case 1 and Case 2, show great asymmetry. Similarly, the use of engineering strain to study plastic deformation in more complex conditions does not describe the plastic deformation adequately.

The deficiencies can be overcome if the natural or true strain measure is introduced. The definition of the engineering strain can be rewritten in terms of the differential change of length $d\ell$:

$$de = \frac{d\ell}{\ell_0} \quad \text{yielding} \quad e = \int_0^e de = \int_{\ell_0}^{\ell_1} \frac{d\ell}{\ell_0} = \frac{\ell_1 - \ell_0}{\ell_0} \quad (\text{Eq 3.7})$$

Hence, the engineering strain is referred to the initial length of the specimen. If, however, this change of length is referred to the current length ℓ , the infinitesimal strain can be written as:

$$d\varepsilon = \frac{d\ell}{\ell} \quad (\text{Eq 3.8})$$

Integration over the whole stretching period yields:

$$\varepsilon = \int_0^\varepsilon d\varepsilon = \int_{\ell_0}^{\ell_1} \frac{d\ell}{\ell} = \ln \left(\frac{\ell_1}{\ell_0} \right) \quad (\text{Eq 3.9})$$

where ε is known as the material or true strain. For deformation in tensile and compression, as discussed in Cases 1 and 2, the relations between true strain, ε , and engineering strain, e , can be illustrated as follows:

	Compression, for $\ell_1 = \frac{\ell_0}{2}$		Tension, for $\ell_1 = 2\ell_0$	
$\varepsilon = \ln \frac{\ell_1}{\ell_0}$	-0.693	+0.693	(Eq 3.10a)	
$e = \ln \frac{\ell_1 - \ell_0}{\ell_0}$	-0.5	+1	(Eq 3.10b)	

The engineering strain and the true strain can be related to each other:

$$\begin{aligned} \varepsilon &= \ln \left(\frac{\ell_1}{\ell_0} \right) = \ln \left(\frac{\ell_0 + \Delta\ell}{\ell_0} \right) \\ &= \ln \left(1 + \frac{\Delta\ell}{\ell_0} \right) = \ln(1 + e) \end{aligned} \quad (\text{Eq 3.11})$$

Expanding the logarithmic function by a Taylor's series gives:

$$\varepsilon = \ln(1 + e) \approx e - \frac{e^2}{2} + \frac{e^3}{3} - \dots \quad (\text{Eq 3.12})$$

Hence, for small strains, the true strain value converges to the engineering strain value as shown in Table 3.1.

Table 3.1 Comparison of engineering strain with true strain for various strain values

e	0.001	0.010	0.02	0.05	0.10	0.20	0.50	1.0
ε	0.0009995	0.00995	0.0198	0.0487	0.0953	0.182	0.405	0.693
ε/e	0.9995	0.995	0.990	0.976	0.953	0.912	0.811	0.693

3.2 Volume Constancy during Plastic Deformation

Plastic deformation is caused microscopically either by the slip or twinning of atomic layers. These operations do not change the volume of the metal, which would require a permanent change of the lattice dimensions. This fact that the volume must remain constant during plastic deformations has also been observed experimentally.

Consider the homogeneous deformation of a workpiece as shown in Fig. 3.2. Volume constancy requires:

$$V_0 = V_1 \quad (\text{Eq 3.13})$$

or, in terms of the dimensions,

$$a_0 \cdot b_0 \cdot c_0 = a_1 \cdot b_1 \cdot c_1 \quad (\text{Eq 3.14})$$

Manipulating this equation by dividing both sides by the left terms yields:

$$1 = \frac{a_1}{a_0} \cdot \frac{b_1}{b_0} \cdot \frac{c_1}{c_0} \quad \text{or} \quad 0 = \underbrace{\ln\left(\frac{a_1}{a_0}\right)}_{\varepsilon_a} \cdot \underbrace{\ln\left(\frac{b_1}{b_0}\right)}_{\varepsilon_b} \cdot \underbrace{\ln\left(\frac{c_1}{c_0}\right)}_{\varepsilon_c} \quad (\text{Eq 3.15})$$

Hence, the condition of volume constancy can be described for homogeneous deformations by the three true strains in the three orthogonal directions as:

$$\varepsilon_a + \varepsilon_b + \varepsilon_c = 0 \quad (\text{Eq 3.16})$$

One important consequence of the volume constancy is the observation that during a simple tension test of a strip or rod, the cross section reduces as the length increases. If the cross

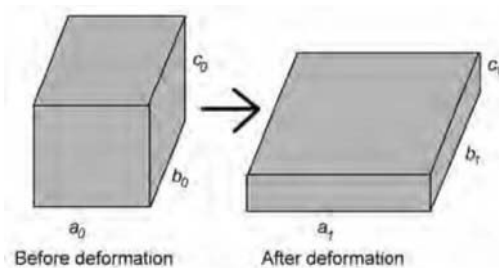


Fig. 3.2 Homogeneous plastic deformation of a workpiece

section reduces uniformly over the principal axes, the material is isotropic in the cross-sectional plane. For anisotropic materials, however, the cross section will reduce nonuniformly, such that for a strip, for instance, the thickness strain will be different from the width strain.

Equation 3.16 is another reason for using true strains in metal forming. Engineering strains would result a complicated relationship to express the simple identity given in Eq 3.16.

3.3 Infinitesimal True Strains and Strain Rates

In sheet metal forming, the strain states are usually nonuniform in space and time. For such complicated deformations, the use of total strain values that are integrated over time has no physical meaning. Also, the use of overall dimensions for computing the strains is no longer applicable. Therefore, for advanced analysis of metal forming processes, the so-called *infinitesimal* strains or strain rates are used for the mathematical description of instantaneous plastic deformation.

To determine the local strain at a material point (instead of the uniform strain value considered in Section 3.2), consider an infinitesimal rectangular material element ABCD on a sheet that deforms within an infinitesimal time dt under the action of internal forces into the rhombus A'B'C'D' as shown in Fig. 3.3. The whole *two-dimensional* deformation consists of three basic items:

1. Change of length of the sides in two orthogonal directions x and y

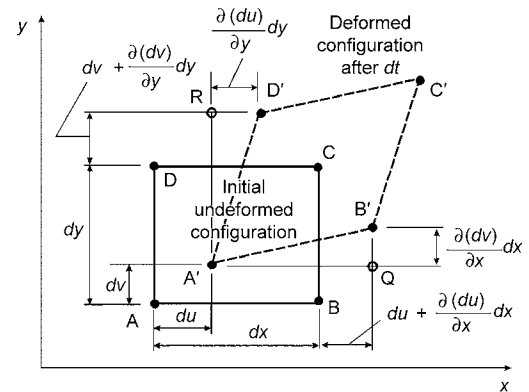


Fig. 3.3 Undeformed and deformed infinitesimal material element

2. Change of the included 90° angle between the sides of the infinitesimal element
3. Rigid body translation and rotation of the whole element

While the changes in length of the sides are described by the infinitesimal *normal* strains, the changes in angles are described by the so-called infinitesimal *shear* strains. The rigid body translations and rotations change the orientation of the infinitesimal element but do not contribute to the change of the shape of that element and are therefore not considered in the analysis of true deformation requiring mechanical energy.

If the displacement field leading to the described deformation can be described by du and dv for point A, the infinitesimal normal strains in the directions x and y can be obtained by:

$$d\epsilon_{xx} = \frac{\overline{A'B'} - \overline{AB}}{\overline{AB}} = \frac{\partial(du)}{\partial x} \quad (\text{Eq 3.17})$$

$$d\epsilon_{yy} = \frac{\overline{A'D'} - \overline{AD}}{\overline{AD}} = \frac{\partial(dv)}{\partial y} \quad (\text{Eq 3.18})$$

The first of the double indices represents the direction of the line element considered, and the second represents the direction of extension of the element. Hence, the index-pair xx in Eq 3.17 means that this strain is the strain of the line element in direction x being extended in the same x -direction (Ref 3.3).

Note that, for the infinitesimal displacements within the infinitesimal time dt , the infinitesimal engineering strain and the infinitesimal natural strain are practically identical, that is,

$$d\epsilon_{xx} \hat{=} de_{xx} \quad \text{and} \quad d\epsilon_{yy} \hat{=} de_{yy} \quad (\text{Eq 3.19})$$

In this two-dimensional deformation state, the only independent change of angle is the change of angle at A:

half of change of $\angle A$: $d\epsilon_{xy}$

$$= \frac{1}{2} (\angle B'A'Q + \angle RA'D') \quad (\text{Eq 3.20})$$

From Fig. 3.3, this change, called the *infinitesimal shear angle*, $d\epsilon_{xy}$, can be expressed in terms of the infinitesimal displacements:

$$d\epsilon_{xy} = \frac{1}{2} \left[\frac{\partial(dv)}{\partial x} + \frac{\partial(du)}{\partial y} \right] \quad (\text{Eq 3.21})$$

The indices x and y here indicate the directions of the sides including the original (undeformed) 90° angle. In contrast to the definitions of true and engineering normal strains, the relation for shear strains is by definition:

$$d\epsilon_{xy} \hat{=} \frac{1}{2} de_{xy} \quad (\text{Eq 3.22})$$

Since the whole deformation occurs in time interval dt , the change of the normal strain in the x -direction per unit time, or the *strain rate*, can be expressed simply by (Ref 3.4):

$$\dot{\epsilon}_{xx} = \frac{d\epsilon_{xx}}{dt} = \frac{\partial(du)/\partial x}{dt} = \frac{\partial(du/dt)}{\partial x} \quad (\text{Eq 3.23})$$

Simplifying this equation yields:

$$\dot{\epsilon}_{xx} = \frac{\partial \dot{u}}{\partial x} \quad (\text{Eq 3.24})$$

Here, \dot{u} is the instantaneous material point velocity in the x -direction. Similarly, in the y -direction:

$$\dot{\epsilon}_{yy} = \frac{d\epsilon_{yy}}{dt} = \frac{\partial(dv)/\partial y}{dt} = \frac{\partial(dv/dt)}{\partial y} \quad (\text{Eq 3.25})$$

resulting in:

$$\dot{\epsilon}_{yy} = \frac{\partial \dot{v}}{\partial y} \quad (\text{Eq 3.26})$$

with \dot{v} the instantaneous material point velocity in the y -direction. The shear strain rate is:

$$\begin{aligned} \dot{\epsilon}_{xy} = \frac{d\epsilon_{xy}}{dt} = \dot{\epsilon}_{yx} &= \frac{\frac{\partial}{\partial t} [(dv)/\partial x + (du)/\partial y]}{dt} \\ &= \frac{1}{2} \left(\frac{\partial \dot{v}}{\partial x} + \frac{\partial \dot{u}}{\partial y} \right) \end{aligned} \quad (\text{Eq 3.27})$$

Note the following:

1. These three strain rate components describe the instantaneous shape change of the material independent of the magnitude of the total strain and the displacements. This means that these strain rates can be used in the description of deformation in metal forming processes.
2. The three strain rate components are the complete set of deformation measures that

describe the whole shape change of the material at a specific point of the sheet metal for plane deformations.

Usually the analysis of deformation in a single plane is not sufficient, and the general three-dimensional case must be considered including the z -direction. For this case, three further strain rate components must be introduced: The normal strain rate in the z -direction:

$$\dot{\epsilon}_{zz} = \frac{\partial \dot{w}}{\partial z} \quad (\text{Eq 3.28})$$

with \dot{w} the instantaneous material point velocity in the z -direction; and the two shear strain rates:

$$\dot{\epsilon}_{xz} = \frac{1}{2} \left(\frac{\partial \dot{w}}{\partial x} + \frac{\partial \dot{u}}{\partial z} \right) \quad (\text{Eq 3.29})$$

and

$$\dot{\epsilon}_{yz} = \frac{1}{2} \left(\frac{\partial \dot{v}}{\partial z} + \frac{\partial \dot{w}}{\partial y} \right) \quad (\text{Eq 3.30})$$

Hence, for the most general three-dimensional deformation case, the complete set of strain rate components consists of three normal strain rate components and three independent shear strain rate components.

In sheet metal forming, axisymmetric deformation problems occur frequently. In these cases, it is useful to use, instead of a Cartesian coordinate system, a cylindrical coordinate system as shown in Fig. 3.4. Here the three independent coordinates of a point P are the radius r , the axial coordinate z , and the circumferential angle θ .

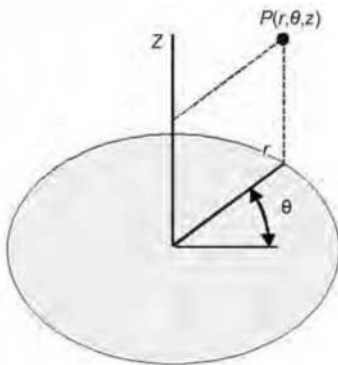


Fig. 3.4 Cylindrical coordinate system for axisymmetric problems

The three normal strain rates are (Ref 3.5):

$$\dot{\epsilon}_{rr} = \frac{\partial \dot{u}_r}{\partial r}, \quad \dot{\epsilon}_{\theta\theta} = \frac{1}{r} \dot{u}_r, \quad \dot{\epsilon}_{zz} = \frac{\partial \dot{u}_z}{\partial z} \quad (\text{Eq 3.31})$$

and the only nonvanishing shear strain rate is:

$$\dot{\epsilon}_{rz} = \frac{1}{2} \left(\frac{\partial \dot{u}_r}{\partial z} + \frac{\partial \dot{u}_z}{\partial r} \right) \quad (\text{Eq 3.32})$$

3.4 Principal Strains and Strain Paths

In the general two-dimensional deformation state, besides the two normal strain components, one shear strain component also exists. For analysis of deformation and mechanics, it is preferred to work in the so-called *principal strain directions*, for which only normal strain components exist.

To introduce the concept of principal directions, consider the sheet strip extended as shown in Fig. 3.5. Consider the two squares drawn on the sheet before applying the tensile force. One of the squares has its edges along the tension direction and normal to this; the other is rotated by 45° to the tension direction. Figure 3.5(b) shows the two squares after the extension of the strip. The larger square deformed into a rectangle and the smaller one deformed into a rhombus. Although both initially square geometries represent the same deformation, one does not show any shearing, that is, change of angles, whereas the other shows shear strains as well as normal strains. For every deformation, it is possible to find a unique orientation of an initially square element that will be deformed after an infinitesimal time step into a rectangular shape. The element in this special unique orientation is named the *principal directions*, and the normal strains (rates) are named *principal strains* or *principal strain rates*. For convenience, the principal strain directions are designated by Arabic numbers 1, 2, and 3. Hence, for the principal strain directions the three normal strains are:

$$\dot{\epsilon}_1, \dot{\epsilon}_2, \dot{\epsilon}_3 \quad \text{or} \quad \epsilon_1, \epsilon_2, \epsilon_3 \quad (\text{Eq 3.33})$$

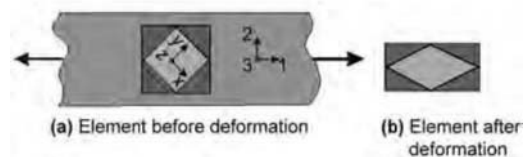


Fig. 3.5 Principal strain directions

A crucial concept in sheet forming for deciding whether total strains or strain rates must be used in the analysis is the strain path concept. For the two-dimensional deformation mode, the **strain rate ratio is defined by:**

$$\alpha = \frac{\dot{\epsilon}_{xx}}{\dot{\epsilon}_{yy}} \quad (\text{Eq 3.34})$$

If this strain ratio is constant over the whole deformation of the material element, and if the shear strain rate is zero or nearly zero, then it is possible to integrate the strain rates, and the total logarithmic strains correctly represent the deformation pattern:

$$\left. \begin{aligned} \epsilon_{xx} &= \int_t \dot{\epsilon}_{xx} dt \\ \epsilon_{yy} &= \int_t \dot{\epsilon}_{yy} dt \end{aligned} \right\} \text{ if and only if } \alpha = \frac{\dot{\epsilon}_{xx}}{\dot{\epsilon}_{yy}} \\ = \text{const. and } \dot{\epsilon}_{xy} = 0 \quad (\text{Eq 3.35})$$

In this case, the total true strains are also the principal strains:

$$\epsilon_1 = \epsilon_{xx} \quad \text{and} \quad \epsilon_2 = \epsilon_{yy} \quad (\text{Eq 3.36})$$

If the deformation is homogeneous over the sheet or portions of the sheet, then for constant strain ratio case, the total true strain can be computed using macroscopic dimensions as given by Eq 3.15, for instance.

These concepts are applied extensively in the experimental measurement of strains by visio-plasticity concepts or also in evaluating the validity of the forming limit diagrams discussed later in this book.

3.5 Equivalent Strain Rate and Equivalent Strain

The complex states of plastic strain in metal forming can be transformed into a single strain value that represents the strain in simple tension

with the equivalent amount of hardening. This single plastic strain (rate) value is called *equivalent strain (rate)*.

The von Mises equivalent plastic strain, $\bar{\epsilon}$, is:

$$\dot{\bar{\epsilon}} = \sqrt{\frac{2}{3} \left[\left(\dot{\epsilon}_{xx}^2 + \dot{\epsilon}_{yy}^2 + \dot{\epsilon}_{zz}^2 \right) + 2 \left(\dot{\epsilon}_{xy}^2 + \dot{\epsilon}_{yz}^2 + \dot{\epsilon}_{xz}^2 \right) \right]} \quad (\text{Eq 3.37})$$

The total equivalent plastic strain can be integrated independently of the constancy of the strain ratios:

$$\bar{\epsilon} = \int_t \dot{\bar{\epsilon}} dt \quad (\text{Eq 3.38})$$

This equivalent strain is the basis of the flow curve characterizing the plastic behavior of metals, as discussed in Chapter 5, “Plastic Deformation—State of Stress, Yield Criteria Flow Rule, and Hardening Rules,” of this book.

If the strain ratio is constant and the shear strains are vanishingly small, the equivalent plastic strain can be also computed from the three principal strains:

$$\bar{\epsilon} = \sqrt{\frac{2}{3} (\epsilon_1^2 + \epsilon_2^2 + \epsilon_3^2)} \quad (\text{Eq 3.39})$$

REFERENCES

- 3.1 S. Kalpakjian and S.R. Schmid, *Manufacturing Engineering and Technology*, Prentice-Hall, 2001
- 3.2 Z. Marciniak and J.L. Duncan, *Mechanics of Sheet Metal Forming*, Edward Arnold, 1992
- 3.3 W.F. Hosford and R.M. Caddell, *Metal Forming. Mechanics and Metallurgy*, 2nd ed., Prentice-Hall, 1993
- 3.4 W. Johnson and P.B. Mellor, *Engineering Plasticity*, Van Nostrand Reinhold, 1973
- 3.5 K. Lange, *Handbook of Metal Forming*, McGraw-Hill, 1985

CHAPTER 4

Plastic Deformation—Flow Stress, Anisotropy, and Formability

Hari Palaniswamy, Altair Engineering, Inc.
Eren Billur, The Ohio State University

WHEN A MATERIAL is deformed, two types of deformation occur: elastic and plastic. The elastic phase is the initial phase, in which the material will change shape as load is applied. However, when the load is removed, the material returns to its original shape. The relationship between load and deformation in the elastic phase is linear. In most metallic materials, when load is increased further, the deformation will enter the plastic phase. In this region, the material deforms permanently. The load-deformation relationship in the plastic region is nonlinear, as a result of phenomena such as strain hardening and area reduction. To understand all these fundamental issues, it is convenient to understand the tensile test.

4.1 Tensile Test

In the tensile test, a standard size specimen, as shown in Fig. 4.1, is cut out from the sheet

metal and pulled slowly until it breaks. The specimen is held by the special fixtures that grip its wider ends without influencing the deformation. These fixtures also ensure that the specimen is held straight during the test. They are attached to the fixed and moving crossheads of the tensile test device as shown in Fig. 4.2. An extensometer is attached to the specimen to measure the elongation over an original gage length, l_0 .

During the test, the moving crosshead that is guided by the columns is moved, extending the specimen along its length, inducing tensile load. Throughout the test, the load applied by the crosshead, the crosshead of displacement, and the elongation of gage length, measured by an extensometer, are recorded in real time. The test is conducted in accordance with the standards specified by the American Society for Testing Materials (Ref 4.1, 4.2).

Engineering Stress-Strain Curves. In order to obtain fundamental material properties, the

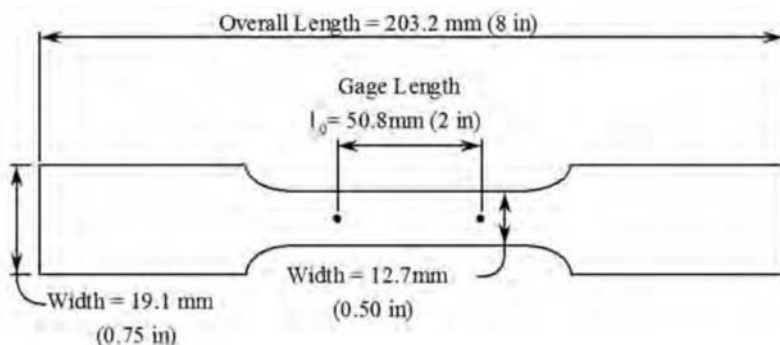


Fig. 4.1 Tensile test specimen, according to ASTM E8 (Ref 4.1)

force-elongation curve, obtained in a tensile test (Fig. 4.3), can be normalized with respect to the geometry to calculate stress and strain. Thus, the curve obtained will be independent of the initial sample dimensions (Ref 4.3). The engineering stress, σ_e is defined as the force, F , divided by the original cross-sectional area of the tensile specimen, A_0 :

$$\sigma_e = \frac{F}{A_0} \quad (\text{Eq 4.1})$$

Similarly, the engineering strain, e , is given by (see also Eq 3.4):

$$e = \frac{\Delta l}{l_0} \times 100\% \quad (\text{Eq 4.2})$$

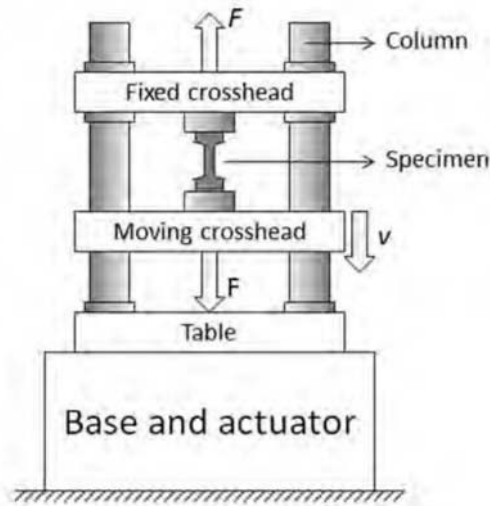


Fig. 4.2 Schematic of a fixture used in a tensile test

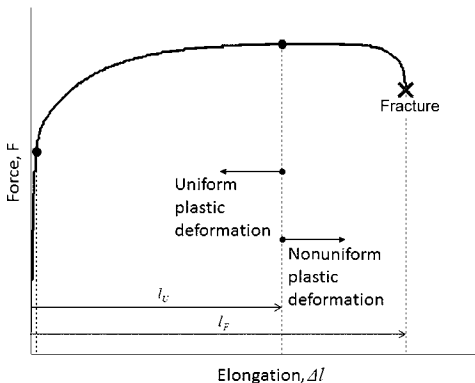


Fig. 4.3 The schematic of the force-elongation curve, obtained from a tensile test (l_u = uniform elongation, l_t = total elongation at fracture)

where e is the engineering strain, l_0 is the original gage length, and Δl is the elongation of l_0 during the test. Engineering strain is usually expressed as percentage. Engineering stress-strain curves are useful for design purposes, that is, when plastic deformation is not desired.

As illustrated in Fig. 4.4, engineering stress-strain curves are useful to determine several basic mechanical material properties:

- **Yield strength** (Y or σ_y) indicates the start of plastic deformation. Yield strength can be determined by any of the three techniques as illustrated in Fig. 4.5.
- **Ultimate tensile strength** (UTS or σ_{UTS}) is the maximum engineering stress in a tensile test and signifies: (1) the end of uniform elongation and (2) start of localized necking, that is, plastic instability, as discussed later.
- **Elastic modulus** (E) (also known as Young's modulus) is the slope of the elastic part of an engineering stress-strain curve.
- **Uniform elongation** (e_u) is the elongation at the maximum load.
- **Total elongation** (e_t) (also known as elongation at break) is the total elongation of the original gage length of a tensile specimen at fracture. This includes both uniform (e_u) and postuniform elongations.
- **Area reduction** (A_r) is the percentage of reduction in the area, and calculated by cross-section area at fracture (A_f) and initial cross-section area (A_0):

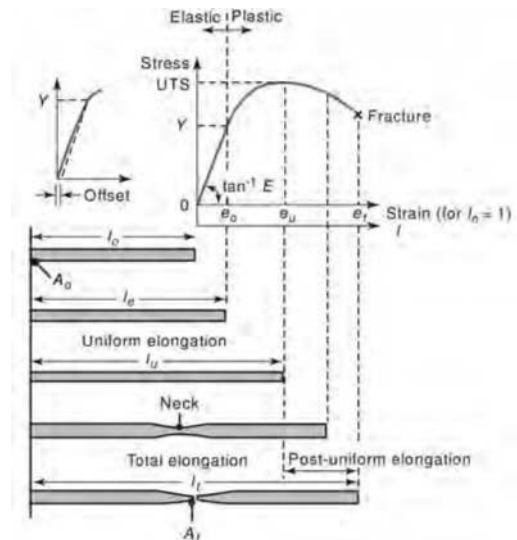


Fig. 4.4 Engineering stress-strain curve; UTS, ultimate tensile strength (Ref 4.4)

$$A_r = \frac{(A_0 - A_f)}{A_0} \times 100\% \quad (\text{Eq 4.3})$$

The total elongation at fracture, e_f , and the total area of reduction at fracture given by Eq 4.3, A_r , are considered to be indications of material ductility. However, the uniform elongation, e_u , better represents the ductility or formability of the specimen material in uniaxial deformation since, for all practical purposes, after necking (i.e., when uniform elongation is exhausted), the material can be considered to have failed.

True Stress-Strain Curves. The stress and strain definitions given above, are based on the original cross-sectional area of the tensile specimen. Hence, they are known as *engineering* stress and strain. *True* stress is based upon the instantaneous cross-sectional area:

$$\sigma = \frac{F}{A} \quad (\text{Eq 4.4})$$

where σ is the true normal stress, F is the applied load, and A is the instantaneous cross-sectional area. True stress values are more accurate measures of stress than engineering values for large deformations (Ref 4.4, 4.6). True stress can be calculated through these equations (Ref 4.3):

$$\sigma = \frac{F}{A} = \frac{F}{A_0} \frac{A_0}{A} = \sigma_e \frac{A_0}{A} = \sigma_e \frac{l}{l_0} = \sigma_e (1 + e) \quad (\text{Eq 4.5})$$

Similarly, true strain is calculated by considering the instantaneous gage length of the speci-

men (l) instead of the initial length (l_0) (compare Eq 3.7):

$$d\varepsilon = \frac{dl}{l} \rightarrow \varepsilon = \ln\left(\frac{l}{l_0}\right) = \ln(1 + e) \quad (\text{Eq 4.6})$$

A true stress-strain curve does not reach a maximum like an engineering curve, as shown in Fig. 4.6, because by definition it can be drawn up to the strain value corresponding to the start of necking; that is, Eq 4.5 is valid in the range of uniform elongation.

Fig. 4.7 shows tensile data for a draw-quality steel (AKDQ), an aluminum alloy (Al 5754), and a high-strength steel (DP600). Force and elongation are the measured values; stress-strain curves are calculated using the equations above.

Stress-Strain Relationships. By using the tensile test and Eq 4.1 to 4.6, it is possible to determine uniaxial stress-strain relationships, both in elastic and in plastic regions. The constitutive equations, such as Hooke's law and Hollomon's (power) law, relate stress and strain or load and deformation. These relations are useful to display the data for practical and design purposes. In the elastic region, Hooke's law can be used to relate stress to strain:

$$\sigma_e = Ee \quad (\text{Eq 4.7})$$

where E is the modulus of elasticity. This is a linear relation, so the modulus of elasticity can be determined from the slope of the engineering stress-strain curve in the elastic region (Ref 4.7). In the plastic region, the relationship be-

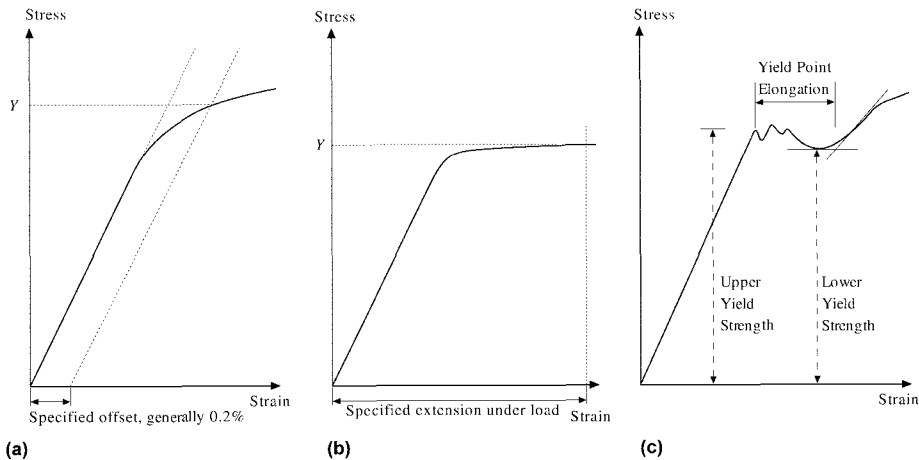


Fig. 4.5 Determination of yield strength: (a) offset method, (b) extension under load method, and (c) autographic diagram method (Ref 4.1, 4.5)

tween stress and strain is nonlinear. In this region, true stress-strain definitions are used. A simple and commonly used empirical stress-strain relationship is Hollomon's (power) law:

$$\sigma = K \epsilon^n \tag{Eq 4.8}$$

where K is the strength coefficient and n is the strain-hardening exponent. Some other equations are listed in Table 4.1.

Anisotropy. In sheet materials, the microstructure may be either uniform in all directions (isotropic) or aligned in a certain direction (anisotropic). Anisotropy is considered in two forms: (1) normal and (2) planar. Normal anisotropy measures the change in material characteristics, which differ through the thickness of the sheet, while planar anisotropy measures material characteristic differences in various directions within the plane of the sheet, as shown in Fig. 4.8.

The microstructure of the metal can have great impact on the ability of the metal to be formed into the desired shape. A prevalent cause for planar anisotropy in sheet metals is the rolling direction (Ref 4.7). During processing of sheet metal, the rolling operation elongates and aligns the grains of the metal's microstructure in the rolling direction and packs

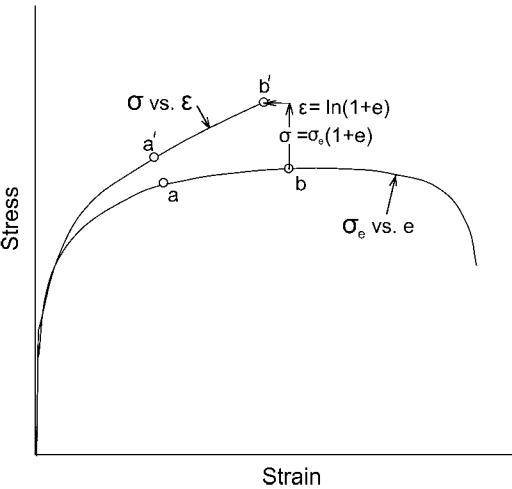


Fig. 4.6 Comparison of engineering and true stress-strain curves (Ref 4.7)

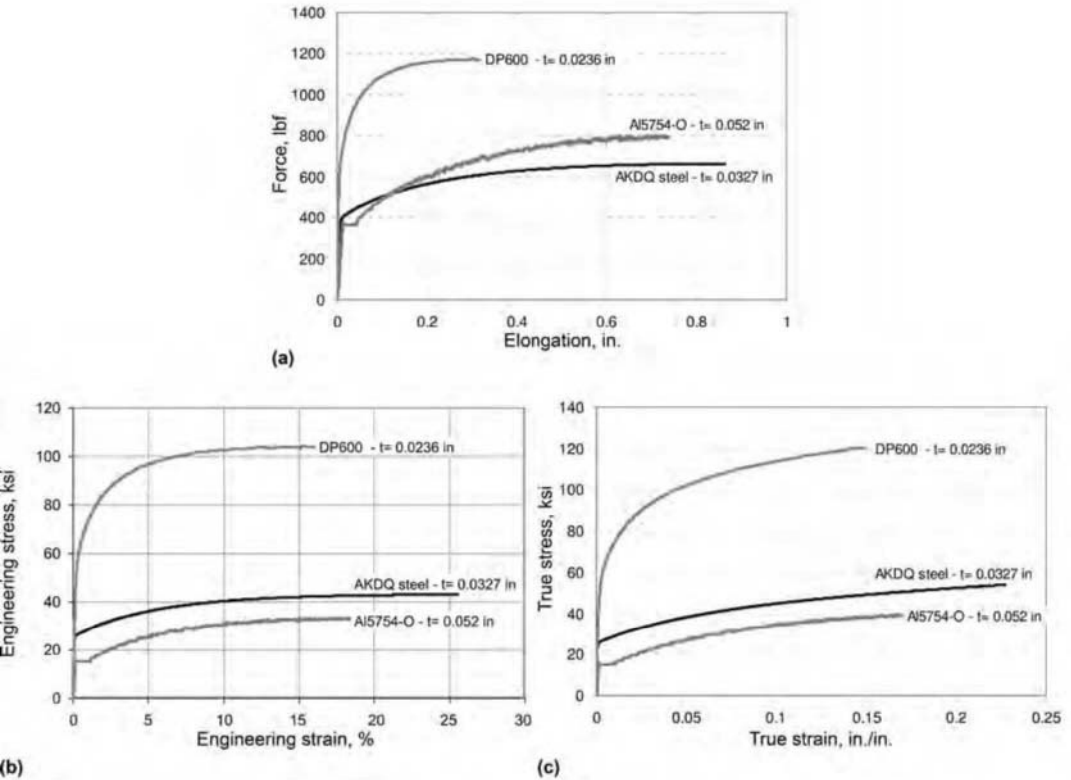
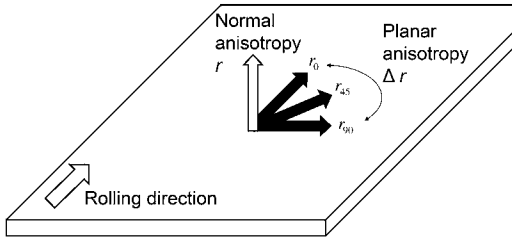


Fig. 4.7 Examples of tensile data: (a) force-elongation, (b) engineering, and (c) true stress-strain curves

Table 4.1 Flow curve equations (Ref 4.3, 4.12, 4.13)

Name	Equation	Comments
Ludwik	$\bar{\sigma} = \sigma_0 + K\bar{\epsilon}^n$	σ_0 is initial yield stress
Linear strain hardening	$\bar{\sigma} = \sigma_0 + P\bar{\epsilon}$	Used for small plastic strains (Fig 4.12c)
Fields and Backofen	$\bar{\sigma} = K\bar{\epsilon}\dot{\bar{\epsilon}}^m$	m is strain rate sensitivity
Vöce	$\bar{\sigma} = a + (b - a)[1 - \exp(-c\bar{\epsilon})]$	

**Fig. 4.8** True stress-strain curve of Al 1100-O, plotted on log-log scale (Ref 4.7)

the grains in the thickness direction, which leads to significantly different strength properties in “rolling” and “transverse or perpendicular to rolling” directions.

The degree of anisotropy in the sheet material between in plane and through thickness is defined using the plastic strain ratio (also known as the Lankford coefficient), r :

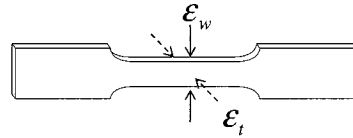
$$r = \frac{\epsilon_w}{\epsilon_t} \quad (\text{Eq 4.9})$$

where ϵ_w is the width strain and ϵ_t is the thickness strain, as depicted in Fig. 4.9. If the ratio is equal to 1, then the material is isotropic. The plastic strain ratio also describes the material's resistance to thinning. Materials with higher r values are desirable for forming due to their resistance to thinning, while a material with lower r values will thin early and possibly rupture during forming.

The plastic strain ratio, r , is determined relative to the rolling direction of the sheet material usually along directions parallel (r_0), diagonal (r_{45}), and transverse (r_{90}) to rolling direction (see Fig. 4.8). The weighted average, r_m , of these strain ratios, referred to as normal anisotropy, is:

$$r_m = \frac{r_0 + 2r_{45} + r_{90}}{4} \quad (\text{Eq 4.10})$$

Anisotropy within the plane of sheet material is referred as **planar anisotropy** and is defined using the strain ratios:

**Fig. 4.9** Sheet orientations relative to normal and planar anisotropy (Ref 4.8)

$$\Delta r = \frac{r_0 - 2r_{45} + r_{90}}{2} \quad (\text{Eq 4.11})$$

where r_0 , r_{45} , and r_{90} are the strain ratios. The planar anisotropy is useful for determining the earing tendency of the material. The “earing tendency” is simply the likelihood that the sheet will draw nonuniformly and form “ears” in the flange of a drawn cup (Fig. 4.10).

List of Material Properties. The material properties useful in sheet metal forming are listed in Table 4.2. These properties are determined using tensile test.

4.2 Flow Stress Curves

Stress Components. In tensile test, the load is uniaxial. However, in an actual metal forming operation (Fig. 4.11), forces may be applied in any number of directions, so the stress must be organized by directional components: σ_{xx} , σ_{yy} , and σ_{zz} . These stresses, known as normal stress components, are dependent on their relative force and the area normal to that force:

$$\sigma_{xx} = \frac{F_x}{A_{yz}}, \quad \sigma_{yy} = \frac{F_y}{A_{xz}}, \quad \sigma_{zz} = \frac{F_z}{A_{xy}} \quad (\text{Eq 4.12})$$

where A_{yz} is the area normal to the x -direction, A_{xz} is the area normal to the y -direction, and A_{xy} is the area normal to the z -direction.

Shear stress components are dependent on areas tangent to the force directions and are defined as:

$$\tau = \frac{F}{A} \tag{Eq 4.13}$$

where τ is the shear stress, F is the applied force, and A is the area tangent to that force. As



Fig. 4.10 Definitions of width and thickness strains in a tensile specimen (Ref 4.9)

with the normal stress, shear stress is also direction dependent, and there are a total of six shear stress components: τ_{xy} , τ_{yx} , τ_{xz} , τ_{zx} , τ_{yz} , and τ_{zy} . However, since there is a static equilibrium of moments, pairs of shear stresses with the same subscripts are always equal (i.e., $\tau_{xy} = \tau_{yx}$). Hence, there are three orthogonal shear stresses:

$$\tau_{xy} = \frac{F_y}{A_{yz}}, \quad \tau_{yz} = \frac{F_z}{A_{xz}}, \quad \tau_{zx} = \frac{F_x}{A_{xy}} \tag{Eq 4.14}$$

Flow Stress. In metal forming processes, the forming loads and material stresses depend on the part geometry, friction, and flow stress of the metal being formed. When the applied stress, in uniaxial tension, without necking, reaches the yield stress (flow stress), the material is considered to begin deforming plastically. Flow stress is simply the yield stress of a material undergoing uniaxial deformation, as a function of strain, strain rate, temperature, and microstructure:

$$\bar{\sigma} = f\left(\theta, \bar{\epsilon}, \dot{\bar{\epsilon}}, S\right) \tag{Eq 4.15}$$

Table 4.2 Material properties useful in metal forming (determined by tensile test) (Ref 4.10)

Material	Young's modulus, 10 ⁶ psi (MPa)	Yield strength, ksi (MPa)	Tensile strength, ksi (MPa)	Uniform elongation, %	Total elongation, %	Average strain ratio (r_{avg})	Planar anisotropy, r	Strength coefficient (K), ksi (MPa)	Strain hardening exponent, n	Strain rate sensitivity (m)
Aluminum-killed drawing-quality steel	30 (207)	28 (193)	43 (296)	24	43	1.8	0.7	77 (529)	0.22	0.013
Interstitial free steel	30 (207)	24 (165)	46 (317)	25	45	1.9	0.5	82 (564)	0.23	0.015
Rimmed steel	30 (207)	31 (214)	44 (303)	22	42	1.1	0.4	...	0.2	0.012
High-strength low-alloy steel	30 (207)	50 (345)	65 (448)	20	31	1.2	0.2	...	0.18	0.007
Dual-phase steel	30 (207)	60 (414)	90 (621)	14	20	1.0	0.1	...	0.16	0.008
Bake-hardened steel	...	33 (225)	51 (350)	86 (591)	0.2	...
Inconel 718 steel	29 (203)	86 (591)
301 stainless steel	28 (193)	40 (276)	100 (690)	58	60	1.0	0.0	...	0.48	0.012
409 stainless steel	30 (207)	38 (262)	68 (469)	23	30	1.2	0.1	...	0.2	0.012
2008 aluminum
3003.O aluminum	10 (69)	7 (48)	16 (110)	23	33	0.6	0.2	...	0.24	0.005
5052.H32 aluminum	9 (60)	25 (175)	33 (230)	54 (371)	0.16	...
5182 aluminum
5454 aluminum
5754 aluminum
6009.T4 aluminum	10 (69)	19 (131)	34 (234)	21	26	0.6	0.1	...	0.23	0.002
6111.T4 aluminum	11 (73)	24 (168)	43 (298)	23	25	0.6	0.1	77 (533)	0.24	...
70.30 brass	16 (110)	16 (110)	48 (331)	54	61	0.9	0.2	...	0.56	0.001

where $\bar{\sigma}$ is the flow stress, θ is the temperature, $\bar{\epsilon}$ is the effective strain (see Section 3.5), $\dot{\bar{\epsilon}}$ is the effective strain rate, and S is the microstructure.

The flow stress of most metals, deformed at room temperature, increases with increasing strain. This phenomenon is known as *strain* or *work hardening*. Strain hardening is the result of interaction of inclusions or dislocations in the crystalline structure of the metal (Ref 4.11).

Flow Curve Equations. Flow stress curves are very important in design of metal forming processes, since they describe the material behavior during deformation. To be useful, flow stress curves must be determined at the specific strain, strain rate, and temperature as the deformation process being studied. Many different methods for mathematically representing the flow stress curves have been developed. For annealed materials experiencing plastic deformation at room temperature, the power law (also known as Hollomon's law) is a good approximation of the flow stress (Fig. 4.12a) (see also Eq 4.8):

$$\bar{\sigma} = K \bar{\epsilon}^n \quad (\text{Eq 4.16})$$

For prestrained materials, the power law must be shifted, as shown in Fig 4.12(b):

$$\bar{\sigma} = K (\epsilon_0 + \bar{\epsilon})^n \quad (\text{Eq 4.17})$$

This equation is known as Swift's law, where ϵ_0 represents prestrain of the material (Ref 4.13).

In addition to Hollomon's and Swift's laws, there are several other flow curve equations, as shown in Fig. 4.12 and tabulated in Table 4.1.

4.3 Methods to Determine Flow Stress of Sheet Materials

In addition to the tensile test, explained in Section 4.1, the hydraulic bulge test (Ref 4.14–4.16), plane strain compression (Ref 4.7), shear test (Ref 4.17, 4.18), and in-plane compression test (Ref 4.19) are used to estimate the flow stress of the sheet materials at room temperature (Table 4.3). Only the tensile and hydraulic bulge tests are described here, because they are most commonly used.

Tensile Test. The tensile test, as explained in Section 4.1, is commonly used for determining the mechanical properties of metals. However, the material properties determined from the tensile test are more useful for designing components than for manufacturing parts by a metal forming process. That is because, in the tensile test, the flow stress data can be obtained only for small amounts of plastic strains due to necking. Tests that provide flow stress data over a large range of strain are more suited to determine flow stress for metal forming analysis and quality control.

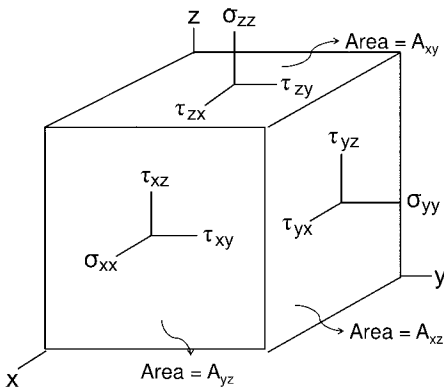


Fig. 4.11 Sheet metal drawn cup that exhibits earing in deep drawing (Ref 4.5)

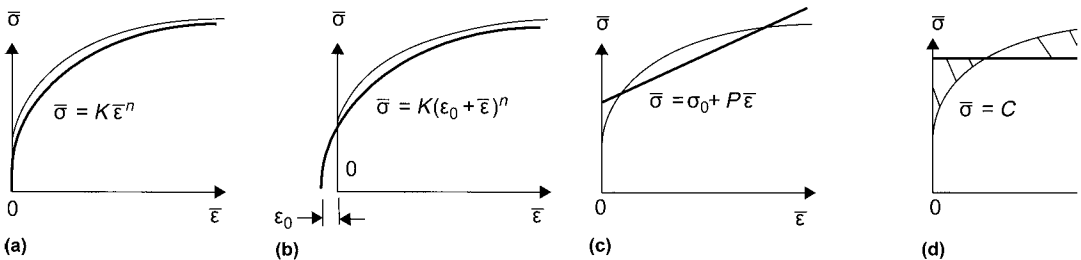


Fig. 4.12 Nine components of stress (Ref 4.7)

At room temperature, the $\bar{\sigma} - \bar{\epsilon}$ relation for most metals can be expressed with the Hollomon's (power) law: $\bar{\sigma} = K\bar{\epsilon}^n$. The strength coefficient, K and strain-hardening exponent, n , can be obtained from the graphical representation of the curve in log-log coordinates, as illustrated in Fig. 4.13. The strain-hardening exponent, n , is given by the slope of the curve, and the strength coefficient is the true stress value when the true strain is equal to 1. It should be noted that at small stresses, an experimentally determined curve may depart from the curve given by Hollomon's law. In that case, other values of n and K may be specified for different ranges of effective strain. In practice, the coefficient n is often used as an indication of material formability because it corresponds to the value of uniform elongation in the engineering stress-strain curve, as illustrated below.

The instantaneous load in tension is given by $F = \bar{\sigma}A$. The criterion for instability in tensile test (necking) can be formulated as the condition that F be maximum, or:

$$\frac{dF}{d\bar{\epsilon}} = 0 \tag{Eq 4.18}$$

Near but slightly before reaching the maximum load, the uniform deformation conditions (i.e., Eq 4.5 and Eq 4.6) are valid. From Eq 4.18:

$$A = A_0 \exp(-\bar{\epsilon}) \rightarrow F = \bar{\sigma}A_0 \exp(-\bar{\epsilon}) \tag{Eq 4.19}$$

Combining Eq 4.18 and 4.19:

$$\frac{dF}{d\bar{\epsilon}} = 0 = A_0 \left(\frac{d\bar{\sigma}}{d\bar{\epsilon}} \exp(-\bar{\epsilon}) - \bar{\sigma} \exp(-\bar{\epsilon}) \right) \tag{Eq 4.20}$$

Table 4.3 Methods used to determine flow stress of sheet metals (Ref 4.12, 4.17–4.19)

Criterion	Tensile test	Hydraulic bulge test	Plane strain compression test	Shear test	In-plane compression test
Sources of error	Dimensional accuracy, necking	Anisotropy	Measurement of height, friction	Friction	Buckling, friction, anisotropy
Limit of sheet thickness	—	≤3 mm	≥5 mm	—	—
Maximum strain	$\bar{\epsilon}_u = n$	≈0.5–0.7	1–2	$\gamma = 1 - 1.5$	>0.15
Anisotropy determination	Yes	—	—	Yes	—
Standard exists	Yes	—	—	—	*

*The standardized compression test is for bulk forming, where the specimen is a round cylinder. the in-plane compression test (for sheet materials) is not standardized.

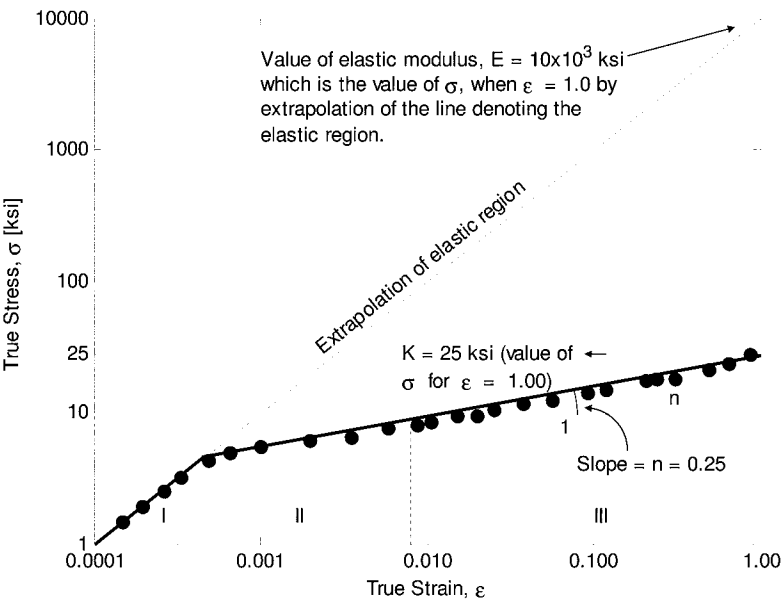


Fig. 4.13 Some of the flow curve equations used in plastic deformation studies (Ref 4.3)

$$\rightarrow \frac{d\bar{\sigma}}{d\bar{\epsilon}} = \bar{\sigma} \quad (\text{Eq 4.21})$$

Using Hollomon's equation, strain level at which tensile instability occurs can be predicted:

$$\frac{d\bar{\sigma}}{d\bar{\epsilon}} = nK\bar{\epsilon}^{n-1} = \bar{\sigma} = K\bar{\epsilon}^n \quad (\text{Eq 4.22})$$

or:

$$\epsilon_{\text{instability}} = n \quad (\text{Eq 4.23})$$

This condition is shown schematically in Fig. 4.14, where the stress and strain at the start of necking in a flow stress curve correspond to point $(\bar{\sigma}, \bar{\epsilon})$ in the curve where Eq 4.21 is satisfied. From this figure and from Eq 4.23, it is evident that at low forming temperatures, where Hollomon's equation $(\bar{\sigma} = K\bar{\epsilon}^n)$ is valid, a mate-

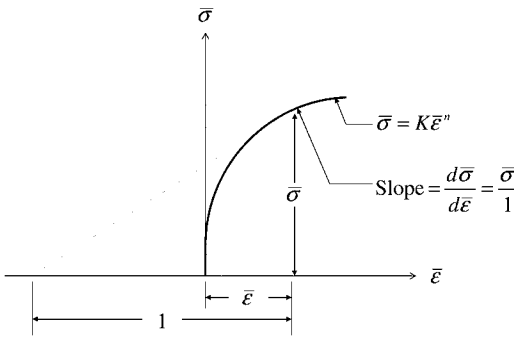


Fig. 4.14 Schematic representation of stress-strain conditions for necking in simple tension (Ref 4.6)

rial with a large n , or strain-hardening coefficient, has greater formability, that is, sustains a larger amount of uniform deformation before necking in tension, than does a material with a smaller n . It should be noted, however, that this statement is not correct for materials and conditions where the flow stress cannot be expressed by Hollomon's equation.

Hydraulic Bulge Test. In the hydraulic bulge test (also known as the viscous pressure bulge test), the sheet metal clamped at its edges is stretched against circular die using oil/viscous fluid as a pressurizing medium, as depicted in Fig. 4.15. The sheet metal bulges into a hemispherical dome, and eventually it bursts, as shown in Fig. 4.16.

The flow stress of the sheet material can be calculated from the bulge test using an analytical closed form solution, assuming sheet metal is a thin membrane (Ref 4.20, 4.21). Considering an infinitesimal element at the apex of the dome (Fig. 4.17), the strain along three different directions (ϕ, θ, δ) is obtained from thickness strain and volume constancy $(\epsilon_1 - \epsilon_2 - \epsilon_3 = 0)$ in plasticity:

$$\epsilon_t = \ln \left(\frac{t}{t_0} \right), \quad \epsilon_\theta = \epsilon_\phi = -\frac{\epsilon_t}{2} \quad (\text{Eq 4.24})$$

where t is the instantaneous thickness at the apex of the dome and t_0 is the initial sheet thickness at the apex of the dome. The stress at the apex of the dome can be obtained from the force equilibrium normal to the infinitesimal element (Fig. 4.17) and assuming that the deformed shape of the sheet along the radius fits to a

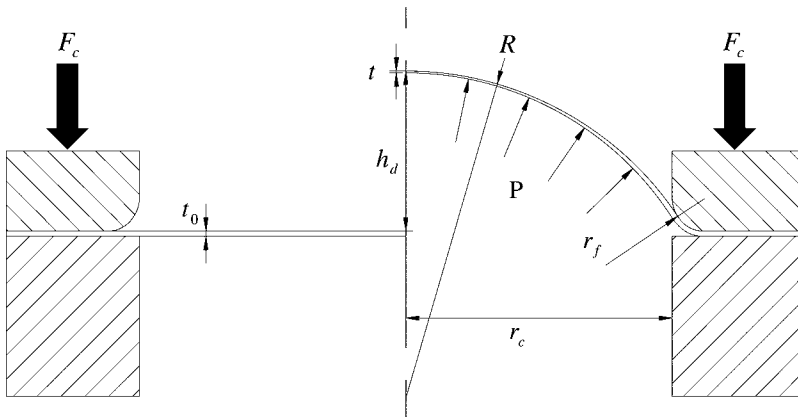


Fig. 4.15 Schematic of hydraulic bulge test (t_0 = original sheet thickness, t = sheet thickness at the apex, h_d = bulge height, P = hydraulic pressure, r_f = die fillet radius, r_c = die cavity radius)

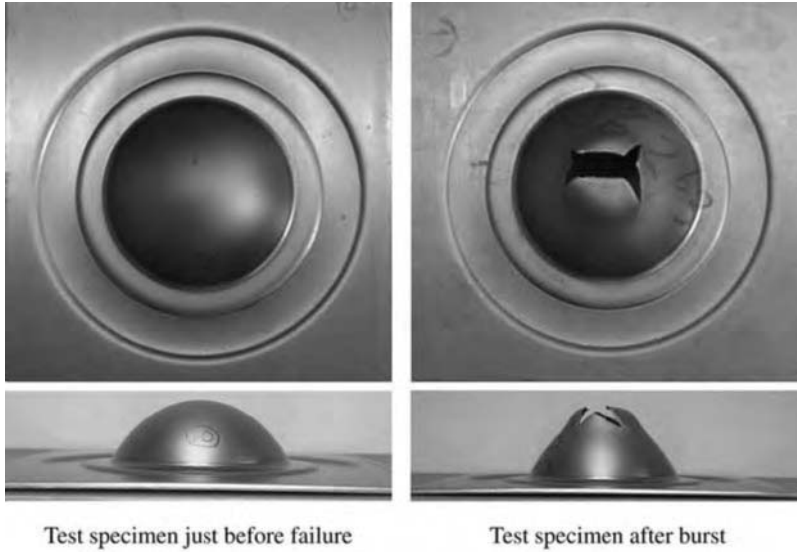


Fig. 4.16 Example test specimens from bulge test

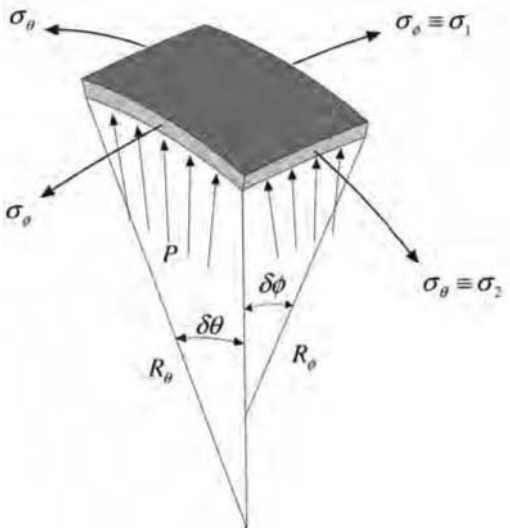


Fig. 4.17 Schematic of infinitesimal element at the apex of the bulge test dome

sphere. The stress along the major and minor axis is given by:

$$\sigma_{\theta} = \frac{PR}{2t}, \quad \sigma_{\phi} = \frac{PR}{2t}, \quad \sigma_t = 0 \quad (\text{Eq 4.25})$$

where R is the radius of curvature at the apex of the dome, t is the instantaneous thickness at the apex of the dome, and P is the forming pressure.

Calculation of the flow stress from the bulge test requires: (1) fluid pressure (P), (2) radius of curvature at the top of the dome (R), and (3) thickness at the top of the dome (t) to be measured real time in the experiment. Different techniques were used with the test to measure or calculate the thickness (t) and radius of curvature (R) using dome height (Ref 4.22–4.24). Because of the practical difficulties in measuring the thickness at the top of the dome and radius of curvature at the top of the dome, the hydraulic bulge test was not commonly used. Recently, the finite element (FE) simulation-based inverse technique was developed to estimate the flow stress from forming pressure and dome height without measuring the thickness and radius of curvature at the top of the dome. Thus, the flow stress estimation process from the bulge test is greatly simplified (Ref 4.16).

The FE simulation-based inverse procedure to estimate the flow stress from the bulge test is valid for sheet materials with flow stress that obeys the power law ($\bar{\sigma} = K\bar{\epsilon}^n$). In this method, the relationship between (1) the dome height (h_d) and radius of curvature at the apex of the dome (R), and (2) the dome height (h_d) and the instantaneous thickness at the apex of the dome (t) are obtained as a function of strain-hardening exponent (n) from FE simulation and stored in a database. The pressure (P) and the dome height (h_d) are measured in real time by experiment. The flow stress is obtained from the measured

data, and the FE is generated from the database using an iterative procedure as shown in Fig. 4.18.

An example curve of pressure versus dome height obtained in real time from experiment for

AKDQ sheet materials is shown in Fig. 4.19. The pressure continuously increases with dome height and reaches a maximum value beyond which necking occurs, resulting in eventual failure of the sheet material in the test (Fig. 4.16).

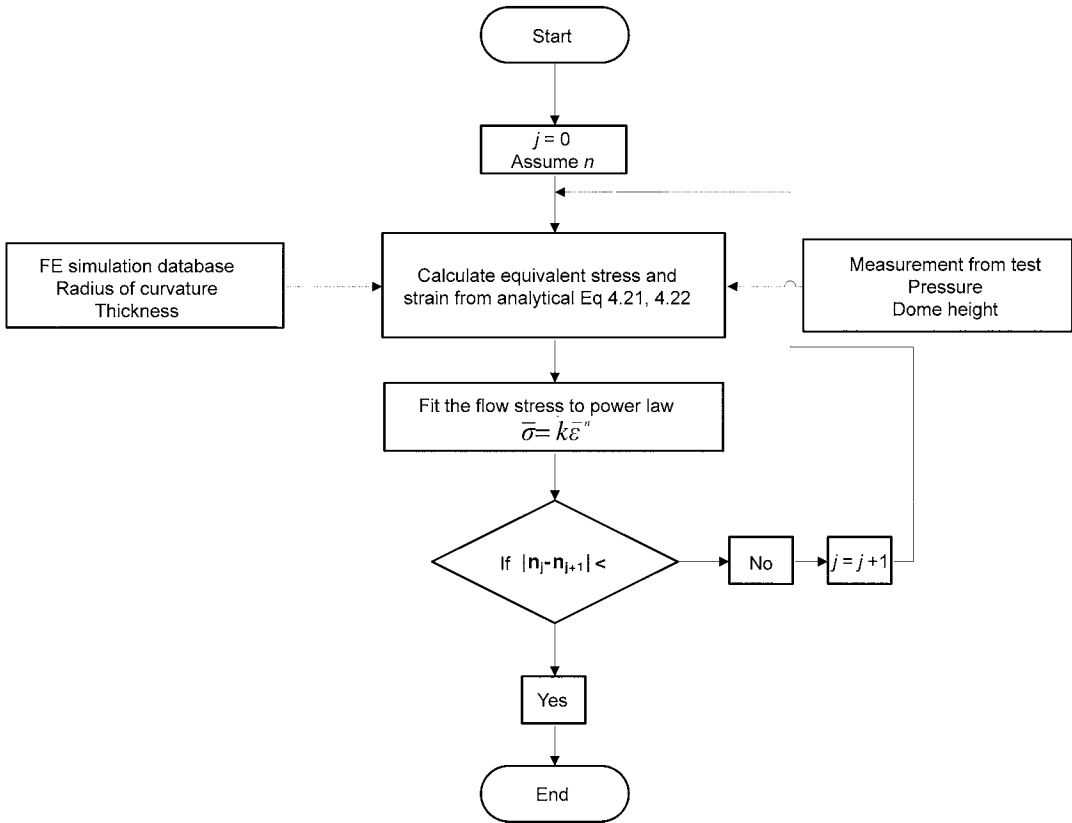


Fig. 4.18 Iterative procedure to estimate flow stress from bulge test (Ref 4.16)

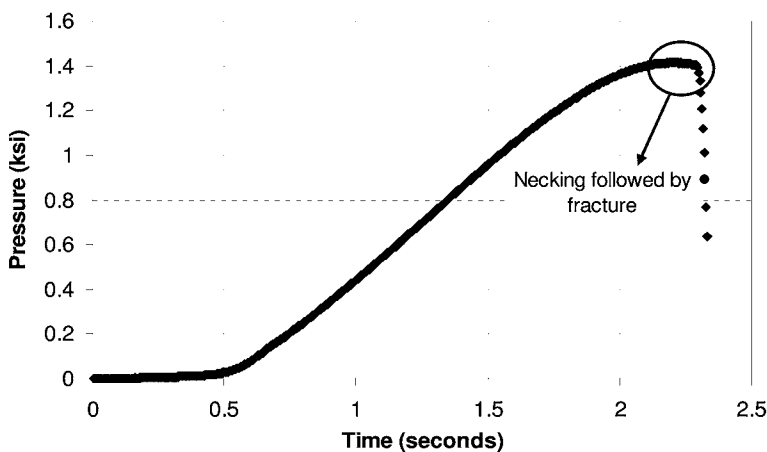


Fig. 4.19 Pressure-time measurement in a hydraulic bulge test for AKDQ sheet material

The pressure versus dome height up to maximum pressure is used to determine the flow stress using the procedure described. The dome height at which failure occurs provides an index for formability of the material that can be used for quality control.

A comparison of the flow stress obtained from the bulge test and tensile test for the same sheet material is shown in Fig. 4.20. Flow stress over very large plastic strain (nearly twice) can be obtained from the bulge test compared to the tensile test. This indicates that flow stress obtained from the bulge test is most appropriate for sheet metal forming analysis where strains are much larger than in the tensile test and can be used without extrapolation, which is needed when using tensile test data. Bulge test data of various sheet materials also are given in Chapter 6 in this volume.

4.4 Formability

In sheet metal forming, the initial blank is a flat sheet and undergoes bending, stretching, or a combination of bending and stretching or drawing to form a complex geometry. The mechanical properties (flow stress and anisotropy) describe the ability of the sheet materials to deform to produce complex parts.

Formability describes the limit to which the sheet materials can undergo deformation before

failure during forming. Several tests have been developed specifically to evaluate the abilities of a sheet material to undergo deformation by:

- Stretching (stretchability)
- Bending (bendability)
- Bending under stretching
- Stretching at the edge
- Deep drawing (drawability)

This information significantly helps process and tool design engineers predict failure during analysis of sheet metal forming processes for tool design. In addition, formability information is also used by sheet metal part design engineers to evaluate manufacturability of the designed part and for material selection based on complexity of parts features and the strength requirements.

Stretchability. Stretchability is the ability of the material to be stretched biaxially without failure. The Erichsen cup test, limiting dome height (LDH) test, and hydraulic bulge test are commonly used tests to evaluate the stretchability.

Erichsen cup test. In Erichsen cup test, the sheet metal clamped at the edges is bulged against the circular cavity die using a ball of diameter of 0.787 in. (20 mm). During the test, the sheet metal is stretched biaxially as it deforms to a hemispherical cup and eventually fractures (Fig. 4.21). The depth of ball travel before failure, called the Erichsen index (IE), is

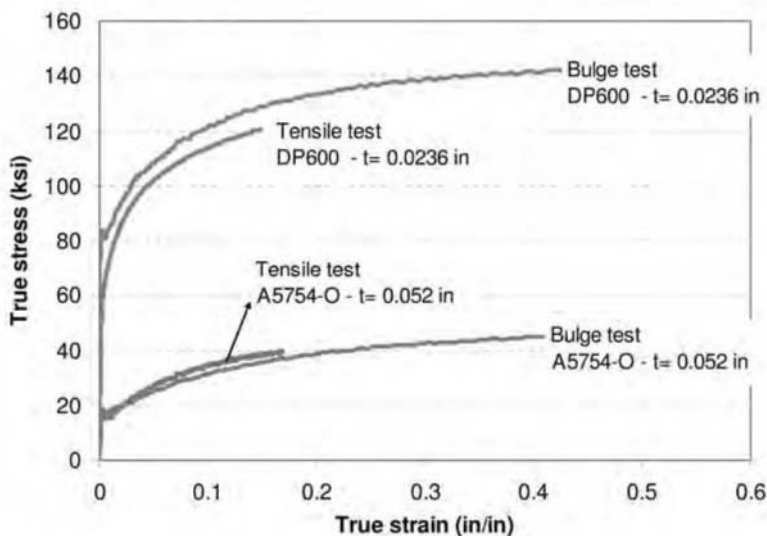


Fig. 4.20 Comparison of flow stress obtained from tensile test and bulge test for sheet materials DP600 and A5754-O

the index of stretchability of the material from this test; the higher the IE, the better the stretchability. The Erichsen test has limited practical application because: (a) a relatively small area of the sheet material is subjected to deformation **in the test, so the sheet thickness significantly influences stretchability limits of the material**; (b) deformation area in the test is too small to represent any industrial sheet forming process; and (c) friction between the sheet sample and the **spherical tool influences the test results**.

Limiting dome height (LDH) test. The LDH test is a larger version of the Erichsen cup test. In the LDH test, the circular sheet material is clamped at the edges using force and a lock bead while it is stretched biaxially at the center using a hemispherical punch against a circular die cavity (Fig. 4.22). The sheet material deforms following the contour of the punch and eventually fractures. The height of the dome or the punch travel and the maximum strain in the dome before failure indicate the stretchability of the material. Friction between the sheet and the punch has significant effect on the test measure-

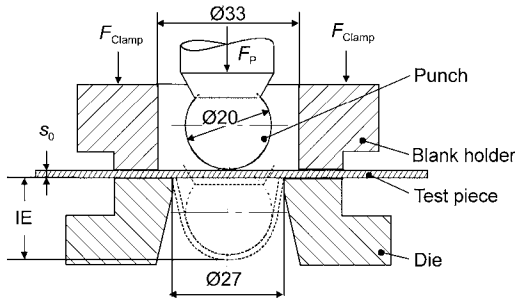


Fig. 4.21 Schematic of the Erichsen cup test (Ref 4.25)

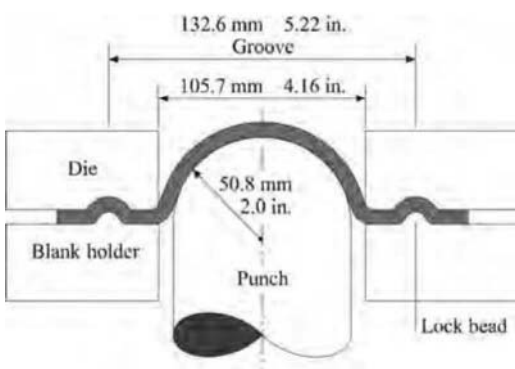


Fig. 4.22 Schematic of limiting dome height tooling (Ref 4.5)

ments: higher friction between the sheet and punch results in earlier failure. Fig. 4.23 shows the LDHs of several steel grades.

Hydraulic bulge test. In the hydraulic bulge test (explained in Section 4.3), the sheet material is stretched biaxially and equally until it bursts. The maximum height of the dome at burst gives an index of the stretchability of the material (Fig. 4.24): higher value of dome height before burst indicates better stretchability. The tests have not been standardized, and therefore test results from two different tooling dimensions/laboratories cannot be compared directly. In the hydraulic bulge test, there is no effect of friction on the deformation of the sheet material, so it accurately evaluates the stretchability of the material. Thus, the hydraulic bulge test has been widely advocated and used to assess the material characteristics of sheet material and quality of sheet materials coming to the stamping plant. An example of results from the bulge test from different coil/heat/suppliers of same-thickness SS304 stainless steel sheet material (Fig. 4.25) indicates that batch G has the highest formability while batch F is more consistent. The same was observed in forming processes, providing a good correlation.

Bendability. Bendability is the ability of the sheet material to be bent around a corner radius along a straight line by 90°. Bendability of sheet material is evaluated using a three-point bending test. During bending, the outer fiber of the material is subjected to tensile stress while the inner fiber is subjected to compressive stress. The sheet material during bending begins to fracture when the maximum tensile stress at the outer fiber exceeds a critical value. The maxi-

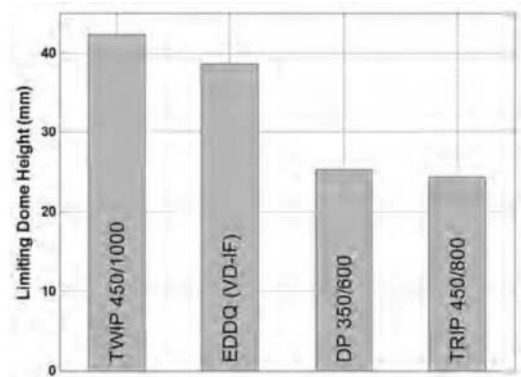


Fig. 4.23 Comparison of stretchability results of different steels from limiting dome height test (Ref 4.26)

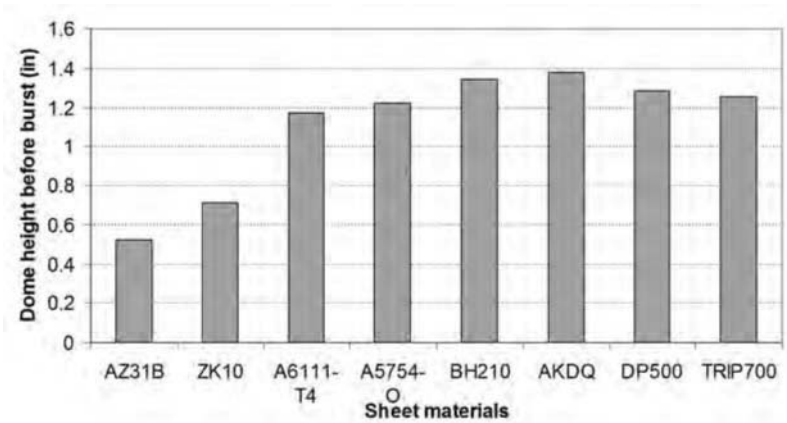


Fig. 4.24 Dome height obtained from the hydraulic bulge test for different sheet materials (die diameter = 4 in.)

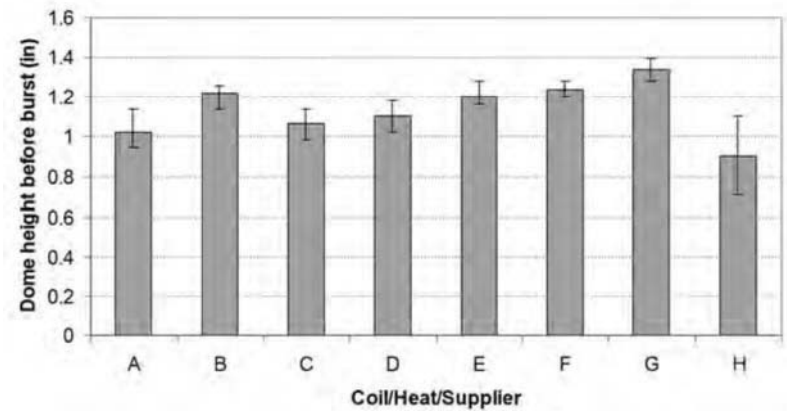


Fig. 4.25 Dome height obtained from the hydraulic bulge test for sheet material SS304 from different sources (die diameter = 4 in.)

num stress in the fiber depends on the bend radius, bending angle, and the sheet thickness. The bendability of the material is defined as a minimum r -to- t (bend radius-to-sheet thickness) ratio, where r is the minimum bending radius the sheet material can be bend over an angle of 90° and t is the thickness of the sheet material. Smaller value of r to t implies better bendability, as the sheet material can be bent over a very small corner radius. Fig. 4.26 shows bendability of various steels. The tests have not been standardized and therefore test results from two different tooling dimensions/laboratories cannot be compared directly.

Combined Bending and Stretching Limits. Combined bending and stretching is a common deformation mode in sheet metal forming. The

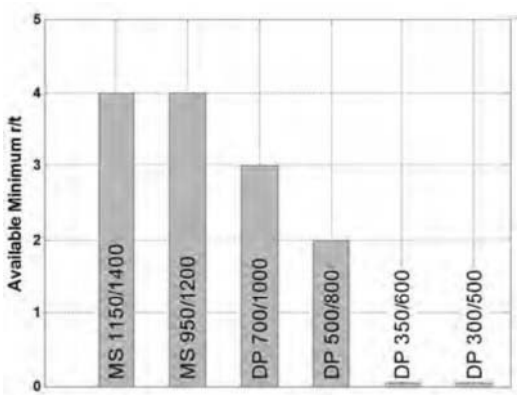


Fig. 4.26 Bendability of several steels under the three-point bending test (Ref 4.26)

stretch bend (SB) test (Fig. 4.27) is used to evaluate the limits of sheet materials under stretching and bending deformation modes. In the SB test, the sheet locked by the draw beads is stretched and bent continuously along a straight line by the moving punch until it fractures. The measure of bending under tension limit is represented by the punch stroke (height) at which failure occurs in the test for different punch corner radius-to-thickness (r -to- t) ratios. In general, height of failure increases with increases in the r -to- t ratio, as a smaller radius induces very high bending stress, resulting in failure at smaller height/punch strokes. Fig. 4.28 shows the height at which failure occurred for different steels in the SB test. For a given r -to- t ratio, the higher the height of failure, the better the sheet material's ability to bend during stretching. The tests have not been standardized, and therefore test results from two different tooling dimensions/laboratories cannot be compared directly.

Drawability. Drawability of the sheet material is defined as the ability of the sheet material to be drawn to a desired shape. The circular-cup

deep-drawing process (Fig. 4.29) is used to evaluate the drawability of the sheet materials. Circular sheet blanks progressively increasing in diameter are drawn to circular cups with **fixed punch diameter** until the sheet material fractures during the drawing process. Drawability of the sheet material is defined as the ratio of the largest blank diameter (D_0) to the punch diameter (D_p) that can be drawn to a circular cup without failure for a given material. It is also called limited drawing ratio (LDR). The higher the LDR, the better the drawability. A comparison of LDR for different steel materials is shown in Fig. 4.30. In the test, sheet material deformation depends on the blank holder force applied, friction conditions between the tool and sheet material, and the tool dimensions. Therefore, LDRs obtained for a material from two different tooling/laboratories cannot be compared.

Edge Stretching Limits. Trimmed/sheared edges in the sheet material fail during the forming process because of excessive tensile stress at the edges. The edge stretchability, or the abil-

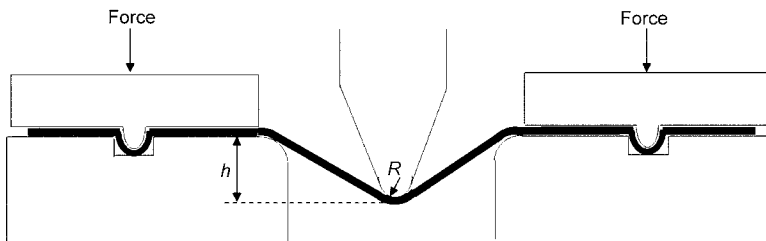


Fig. 4.27 Schematic of the stretch bend test

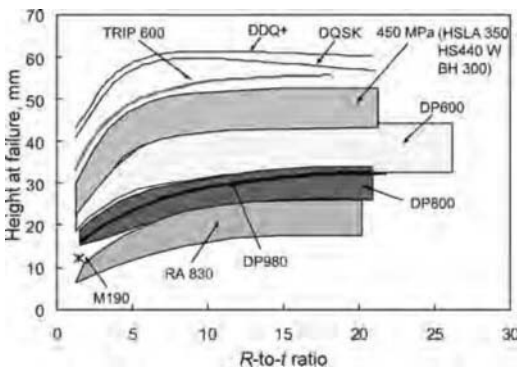


Fig. 4.28 Height of failure versus r -to- t ratio obtained from the stretch bend test for different steel materials (Ref 4.28)

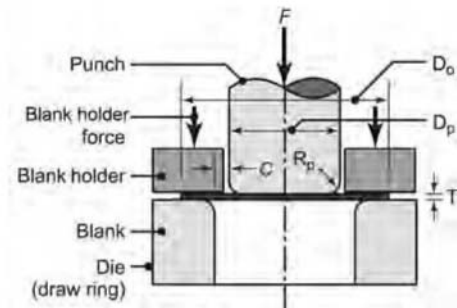


Fig. 4.29 Schematic of the tooling to evaluate the drawability of the sheet materials (Ref 4.4)

ity of sheet material edges to avoid failure, is commonly studied using the hole expansion test. In the hole expansion test, a machined/pierced circular hole is expanded until fracture using a conical or a flat-bottom punch (Fig. 4.31). The ratio of the change in the hole diameter just before failure to the initial hole diameter, commonly known as the percent hole expansion, describes the edge stretchability limit of the material. Fig. 4.32 shows the percent hole expansion (%HE) for different steel materials obtained from a conical punch hole expansion test. In the hole expansion test, the quality of the hole edge in the sheet material significantly influences the onset of failure. Also, the test is not standardized. Therefore, test results from two different tooling dimensions/laboratories cannot be compared directly.

4.5 Forming Limit Curves (FLCs)

In the stamping process, the deformation path of the material is much more complex than just stretching, bending, combination of bending and stretching, and drawing. Also, the deformation mode varies spatially within a component during forming. Hence, forming limits in stretching, bending, and drawing (as discussed in Section 4.4) alone may not be sufficient to predict

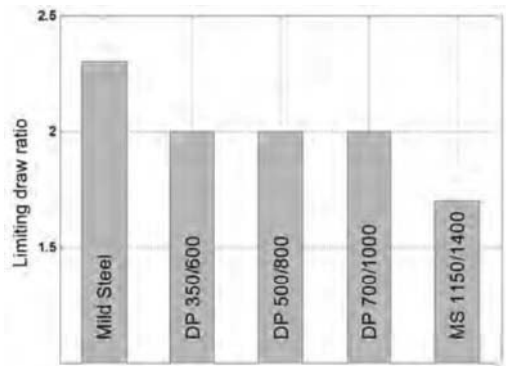


Fig. 4.30 Comparison of limited drawing ratio of mild steel and AHSS steel (Ref 4.26)

Blank

Fig. 4.31 Schematic of hole expansion test $d_0/2$ and $d_f/2$ = hole half diameter before and after deformation, respectively (Ref 4.27)

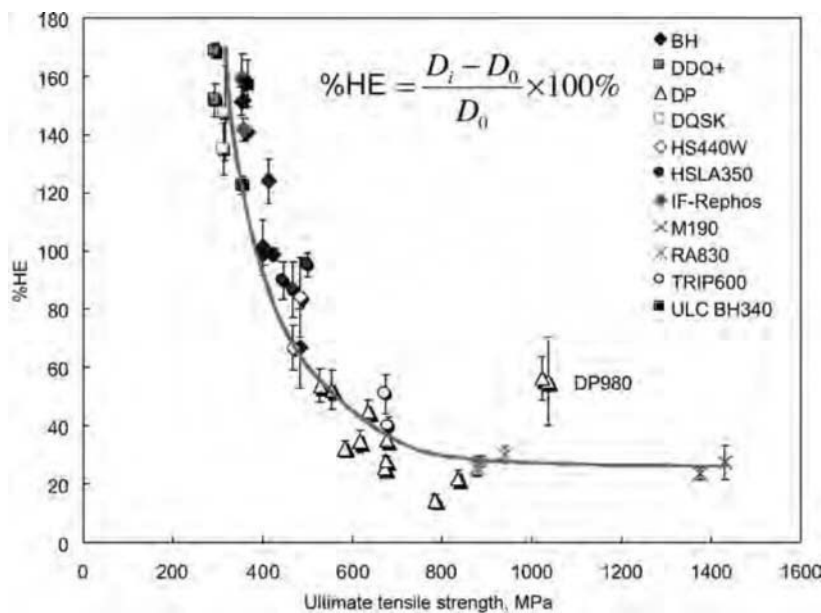


Fig. 4.32 Percentage hole expansion versus ultimate tensile strength for different steel materials in a hole expansion test using conical punch (Ref 4.28)

failure in a sheet forming process. The FLC specifies the limits in terms of in-plane principal strain $\epsilon_1 - \epsilon_2$ that sheet material can withstand before failure during forming for different ratios of in-plane principal strains. The FLC covers failure limits for principal strain ratios/strain paths (Fig. 4.33) from equibiaxial tension/stretch forming ($\epsilon_1 = \epsilon_2$), plane strain ($\epsilon_2 = 0$), uniaxial strain ($\epsilon_1 = -2\epsilon_2$), and pure shear/deep drawing ($\epsilon_1 = -\epsilon_2$) commonly observed in forming a complex part. In addition to the failure limit curve, the FLC also provides the strain limit at which necking starts for different ratios of principal strain. The region between the necking curve and the failure curve corresponds to instability in the sheet material. However, in the FLC, the effect of strain due to bending is not included in establishing the limits. Therefore, the FLC must be used with caution in regions that undergo excessive bending. In technical literatures, FLC is also referred as the forming limit diagram. FLCs are generated using the standard Nakajima test method or Marciniak test method.

Nakajima Test. The Nakajima test is similar to the LDH test for stretchability (described in Section 4.4) except for the blank shape. Circular blanks with different circular recesses on either side, as shown in Fig. 4.34, are used in the Nakajima test to induce different ratios of principal strain/strain paths in the LDH test. Increasing the size of the circular recess in the specimen reduces the principal strain (ϵ_2) encountered by the material, thereby covering strain ranges required to determine the FLC, as shown in Fig. 4.35. The sheet material, electrochemically

etched with circular grids for strain measurements, is clamped at the periphery using a lock bead while the punch deforms the sheet against the circular die cavity until it fails. The dimensions of the circular grids at the failure locations of the sheet are measured after the test to obtain the limiting strains of failure. In addition, using the punch load/displacement curve from the test, the movement of the punch is stopped at the very onset of necking for successive test specimens to obtain the limiting principal strains at which necking begins. In modern test equipments, charge-coupled device cameras combined with optical strain measurement techniques are used to measure the strains in real time to obtain both necking and limiting strains from same specimen (Ref 4.27).

Marciniak Test. The Marciniak test is similar to Nakajima test except that it uses a flat-faced cylindrical punch with the circular hole in the bottom to reduce the effect of friction on the FLC, as shown in Fig. 4.36. A driving blank may be added as well. The Marciniak test also uses blanks with different widths, as explained in the Nakajima tests, to cover entire range of the FLC.

Determination of FLCs. In North America, FLCs for mild steel, HSS steel, and selective AHSS steel have been studied, and the FLC for the sheet material is approximated by the Keeler-Brazier equation based on the initial sheet thickness (t) and the strain-hardening exponent (n) of the material:

$$FLD_0^{\text{True}} = \ln \left[1 + (23.3 + 14.13t) \cdot \frac{n}{0.21} \right] \quad n \leq 0.21$$

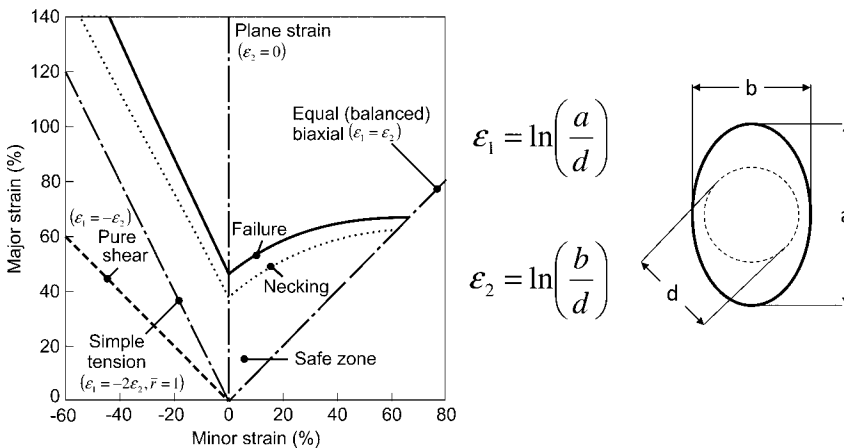


Fig. 4.33 Forming limit curve and grid analysis used to calculate strains

(Eq 4.26)

$$\varepsilon_1 = \text{FLD}_0^{\text{True}} - \varepsilon_2 \quad \varepsilon_2 < 0 \quad (\text{Eq 4.27})$$

$$\varepsilon_1 = \ln \left[0.6 (\exp(\varepsilon_2) - 1) \right] + \exp(\text{FLD}_0^{\text{True}}) \quad \varepsilon_2 > 0 \quad (\text{Eq 4.28})$$



Fig. 4.34 Example specimens used in the limiting dome height test to obtain the forming limit curve (Ref 4.27)

where ε_1 and ε_2 are true major and minor strains, respectively. However, for AHSS steels such as DP steels and TRIP steels, these equations predict more conservative limits, as shown in Fig. 4.37 (Ref 4.28).

Factors affecting the FLCs include sheet thickness, test conditions, and strain path.

Sheet Thickness. This changes the FLC of the material. It was observed that the increase in the sheet thickness postpones the failure. This moves the FLC up along the y - (major strain, ε_1) axis (Ref 4.11).

Tests Conditions. Radius of curvature of the hemispherical punch and the friction conditions influence the deformation of the material in the test. Increase in the friction condition results in earlier failure of the sheet during test, resulting in moving the curve down along the y - (major strain, ε_1) axis. Therefore, test results from two different tooling dimensions/laboratories cannot be compared directly (Ref 4.11).

Strain Path/Deformation History. In the tests used to estimate the FLCs, the sheet material is subjected to constant strain path/deformation history until it fractures (Fig. 4.35). However, in

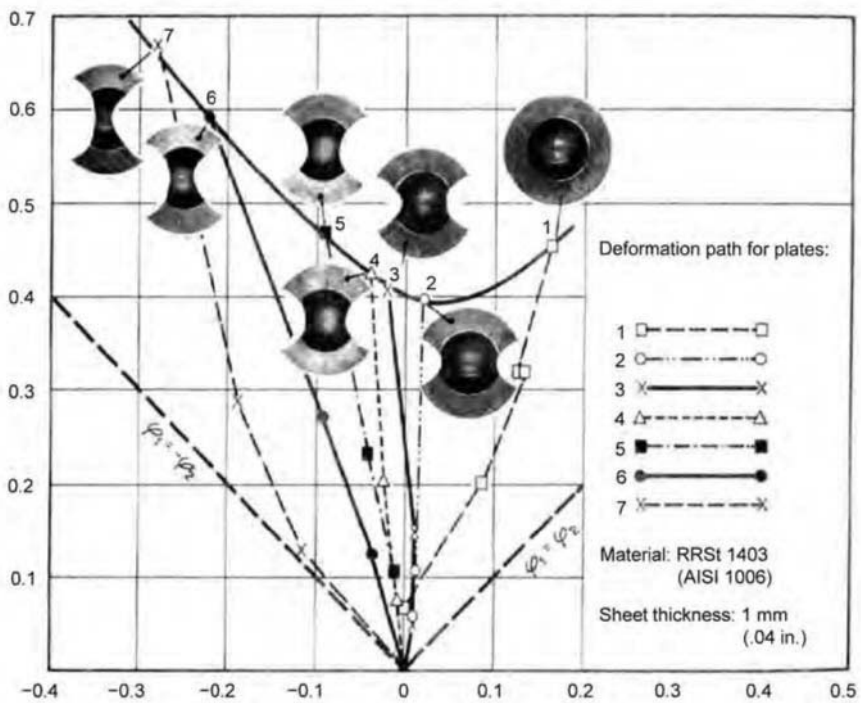


Fig. 4.35 Relationship between the specimen shape, strain path, and fracture limit in the forming limit curve obtained from the limiting dome height test (Ref 4.11)

practical stamping processes, the strain paths are not as constant as in the test. Therefore, the FLCs need to be used with much care in predicting failures in stamping process. It was observed that the FLC decreases (moves down in y -axis) when the sheet materials are initially subjected to positive minor strain (ϵ_2) followed by negative minor strain (ϵ_2) during deformation. FLC increases (moves up in y -axis) when the sheet materials are initially subjected to negative minor strain (ϵ_2) followed by positive minor strain (ϵ_2) during deformation (Ref 4.11).

REFERENCES

- 4.1 “Standard Designation: E8/E8M-09,” American Society for Testing Materials, 2009
- 4.2 N.E. Dowling, *Mechanical Behavior of Materials*, Prentice Hall, 1998
- 4.3 Z. Marciniak, J.L. Duncan, and S.J. Hu, *Mechanics of Sheet Metal Forming*, Butterworth Heinemann, 2002
- 4.4 S. Kalpakjian and S. Schmid, *Manufacturing Processes for Engineering Materials*, 5th ed., Pearson Education, 2008
- 4.5 K.H. Grote and E.K. Antonsson, Eds., *Springer Handbook of Mechanical Engineering*, Springer, 2009.
- 4.6 T. Altan, S. Oh, and H. Gegel, *Metal Forming: Fundamentals and Applications*, American Society for Metals, 1983
- 4.7 W.F. Hosford and R.M. Caddell, *Metal Forming: Mechanics and Metallurgy*, 3rd ed., Cambridge University Press, 2007
- 4.8 G.E. Totten and D.S. MacKenzie, Eds., *Handbook of Aluminum*, Vol 1, *Physical Metallurgy and Process*, Marcel Dekker, 2003
- 4.9 J.R. Davis, *Tensile Testing*, 2nd ed., ASM International, 2004
- 4.10 B. Taylor, Formability Testing of Sheet Metals, *Metals Handbook*, Vol 14, *Forming and Forging*, ASM International, 1988.
- 4.11 K. Lange, Ed., *Handbook of Metal Forming*, McGraw-Hill, 1985
- 4.12 K. Pöhlndt, Materials Testing for the Metal Forming Industry, Springer, 1989
- 4.13 Z. Gronostajski, The Constitutive Equations for FEM Analysis, *Journal of Materials Processing Technology*, Vol 106, 2002, p 40–44.
- 4.14 W. Panknin, “Der hydraulische Tiefungsversuch und die Ermittlung von Fließkurven” (“The Hydraulic Bulge Test and Determination of the Flow Stress Curves”), Ph.D. dissertation, Institute for Metal Forming Technology, University of Stuttgart, 1959

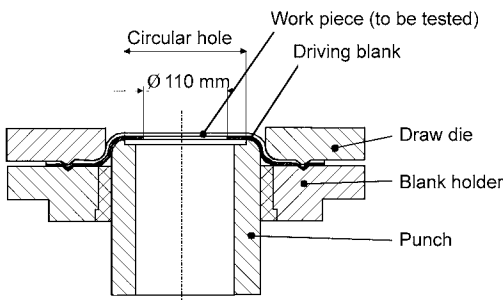


Fig. 4.36 Schematic of the Marciniak test (Ref 4.25, 4.29)

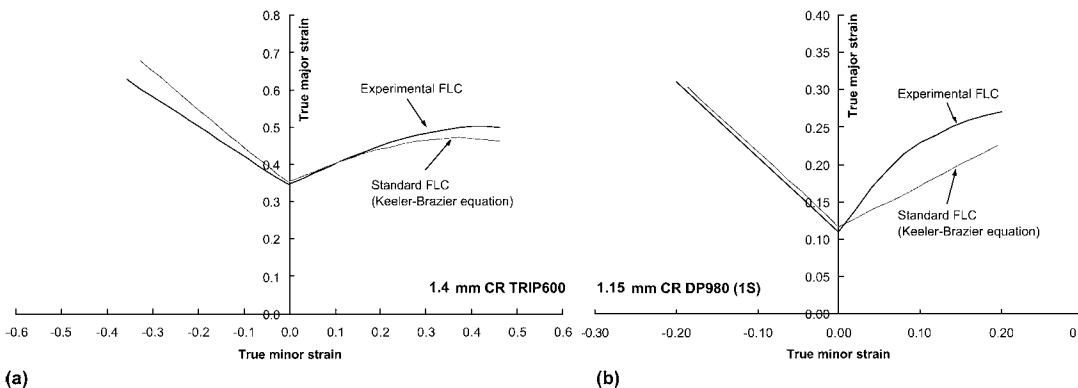


Fig. 4.37 Comparison of experimental forming limit curves (FLCs) with the Keeler-Brazier equation for (a) TRIP 600 and (b) DP980 (Ref 4.28)

- 4.15 F. Gologranc, “Beitrag zur Ermittlung von Fließkurven im kontinuierlichen hydraulischen Tiefungsversuch” (“Evaluation of the Flow Stress Curve with the Continuous Hydraulic Bulge Test”), Ph.D. dissertation, Institute for Metal Forming Technology, University of Stuttgart, 1975
- 4.16 G. Gutscher, H. Wu, G. Ngaile, and T. Altan, Determination of Flow Stress for Sheet Metal Forming using the Viscous Pressure Bulge (VPB) Test, *Journal of Materials Processing Technology*, Vol 146, 2004, p 1–7
- 4.17 E.F. Rauch, Plastic Anisotropy of Sheet Metals Determined by Simple Shear Tests, *Materials Science and Engineering A*, Vol 241, 1998, p 179–183
- 4.18 R.K. Boger, R.H. Wagoner, F. Barlat, M.G. Lee, and K. Chung, Continuous, Large Strain, Tension/Compression Testing of Sheet Material, *International Journal of Plasticity*, Vol 21, 2005, p 2319–2343
- 4.19 S. Bouvier, H. Haddadi, P. Levée, and C. Teodosiu, Simple Shear Tests: Experimental Techniques and Characterization of the Plastic Anisotropy of Rolled Sheets at Large Strains, *Journal of Materials Processing Technology*, Vol 172, 2006, p 96–103
- 4.20 R. Hill, Mathematical Theory of Plasticity, Oxford University Press, 1956
- 4.21 D.W.A. Rees, Plastic Flow in the Elliptical Bulge Test, *International Journal of Mechanical Sciences*, Vol 37, 1995, p 373–389
- 4.22 R. Hill, A Theory of the Plastic Bulging of a Metal Diaphragm by Lateral Pressure, *Philosophical Magazine Series 7*, Vol 41, 1950, p 1133
- 4.23 J. Chakrabarty and J. Alexander, Hydrostatic Bulging of Circular Diaphragms, *Journal of Strain Analysis for Engineering Design*, Vol 5, 1970, p 155–161
- 4.24 J. Bird and J. Duncan, Strain Hardening at High Strain in Aluminum Alloys and Its Effect on Strain Localization, *Metallurgical and Materials Transactions A*, Vol 12, 1981, p 235–241
- 4.25 E. Doege and B.A. Behrens, Eds., *Handbuch Umformtechnik (Metalforming Handbook)*, Springer, 2010
- 4.26 Advanced High Strength Steel (AHSS) Application Guidelines, Version 4.1, World Steel Association.
- 4.27 L. Xu, L. Chen, B. De Cooman, D. Steglich, and F. Barlat, Hole Expansion of Advanced High Strength Steel Sheet Sample, *International Journal of Material Forming*, Vol 3, 2010, p 247–250
- 4.28 S. Sadagopan and D. Urban, *Formability Characterization of a New Generation of High Strength Steels*, American Iron and Steel Institute/U.S. Department of Energy Technology Roadmap Program, 2003
- 4.29 M. Moore, and P. Bate, Microstructural Inhomogeneity and Biaxial Stretching Limits in Aluminium Alloy AA6016, *Journal of Materials Processing Technology*, Vol 125–126, 2002, p 258–266

CHAPTER 5

Plastic Deformation—State of Stress, Yield Criteria Flow Rule, and Hardening Rules

Hari Palaniswamy, Altair Engineering, Inc.

WHEN A MATERIAL is deformed, two types of deformation occur: elastic and plastic. Elastic deformation is always the initial phase of loading, in which the material will change shape as load is applied. However, when the load is removed, the material returns to its original shape. The relationship between stress and strain in the elastic phase is linear. In most metallic materials, when load is increased further, the elastic deformation will be accompanied by plastic deformation. In this load region, the material deforms not only elastically but also permanently. The stress-strain relationship in the elastic-plastic state is nonlinear because phenomena such as irrevers-

ible dislocation motions are the basis of plastic deformations. In metal forming, elastic strains are smaller by several orders of magnitude than plastic strains. Yet, in case of sheet metal forming, they are still very significant since they are the reason for the springback.

5.1 General State of Stress

A typical sheet forming process, deep drawing, is shown in Fig. 5.1. Various stresses are present at distinct points in the work piece during the forming operation. In general, at a mate-

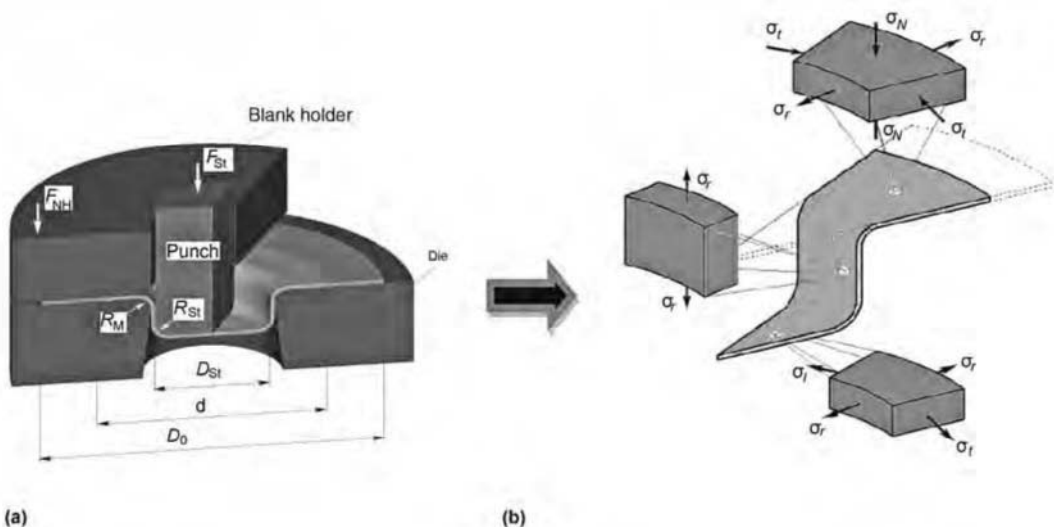


Fig. 5.1 (a) Deep drawing process. (b) Various states of stress in deep drawing

rial point, the whole internal forces can be completely described by stress components acting on three orthogonal planes passing through this point (Fig. 5.2).

These stresses can be described by the components of the true stress (also named Cauchy stress) tensor:

$$\sigma_{ij} = \begin{bmatrix} \sigma_{xx} & \sigma_{xy} & \sigma_{xz} \\ \sigma_{yx} & \sigma_{yy} & \sigma_{yz} \\ \sigma_{zx} & \sigma_{zy} & \sigma_{zz} \end{bmatrix} \quad (\text{Eq 5.1})$$

where σ_{xx} denotes the stress along the x -axis in the plane normal to the x -axis, commonly known as **normal stress**, with simplified notation as σ_x . Similarly, $\sigma_{yy} = \sigma_y$ and $\sigma_{zz} = \sigma_z$. σ_{xy} denotes the stress along the y -axis in the plane normal to x -axis, commonly known as shear stress. Considering moment equilibrium in the discretized element, it can be proved that $\sigma_{xy} = \sigma_{yx}$, $\sigma_{xz} = \sigma_{zx}$, and $\sigma_{yz} = \sigma_{zy}$, reducing the stress components to six to describe the full stress state at a single point:

$$\sigma_{ij} = \begin{bmatrix} \sigma_{xx} & \sigma_{xy} & \sigma_{xz} \\ \sigma_{xy} & \sigma_{yy} & \sigma_{yz} \\ \sigma_{xz} & \sigma_{yz} & \sigma_{zz} \end{bmatrix} = \begin{bmatrix} \sigma_{xx} & \sigma_{xy} & \sigma_{xz} \\ & \sigma_{yy} & \sigma_{yz} \\ & \text{sym} & \sigma_{zz} \end{bmatrix} \quad (\text{Eq 5.2})$$

5.2 Principal Stresses

In any general stress state, there exist three mutually perpendicular planes corresponding to

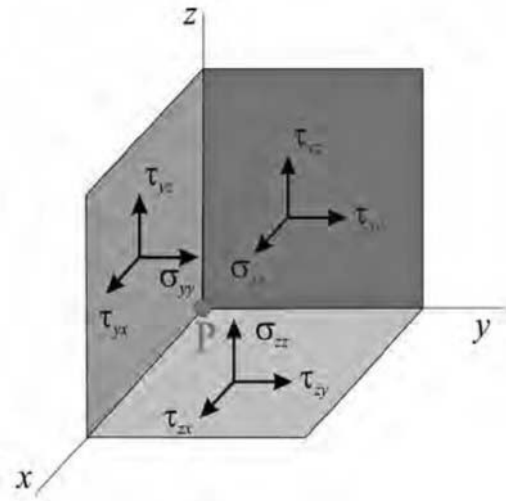


Fig. 5.2 Complete stress components at a material point P

a coordinate system along which the shear stress is zero. The normal stresses in these planes are called *principal stress*, denoted by σ_1 , σ_2 , and σ_3 . They are estimated by setting shear stress along arbitrary plane denoted by normal \vec{n} to zero:

$$\sigma \cdot \vec{n} = \lambda I \cdot \vec{n}$$

$$(\sigma - \lambda I) \cdot \vec{n} = 0 \Rightarrow \begin{bmatrix} \sigma_{xx} - \lambda & \sigma_{xy} & \sigma_{xz} \\ \sigma_{xy} & \sigma_{yy} - \lambda & \sigma_{yz} \\ \sigma_{xz} & \sigma_{yz} & \sigma_{zz} - \lambda \end{bmatrix} = 0 \quad (\text{Eq 5.3})$$

where I is the identity tensor. The resulting characteristics equation is:

$$\lambda^3 - I_1 \lambda^2 - I_2 \lambda - I_3 = 0 \quad (\text{Eq 5.4})$$

where

$$I_1 = \sigma_{xx} + \sigma_{yy} + \sigma_{zz}$$

$$I_2 = (\sigma_{xx}\sigma_{yy} + \sigma_{yy}\sigma_{zz} + \sigma_{zz}\sigma_{xx}) + \sigma_{xy}^2 + \sigma_{yz}^2 + \sigma_{zx}^2$$

$$I_3 = \sigma_{xx}\sigma_{yy}\sigma_{zz} - \sigma_{xx}\sigma_{yz}^2 - \sigma_{zz}\sigma_{xy}^2 + 2\sigma_{xy}\sigma_{yz}\sigma_{xz} - \sigma_{yy}\sigma_{xz}^2 = \det \sigma_{ij}$$

The three principal stresses (σ_1 , σ_2 , and σ_3) can be determined by finding the roots of the cubic Eq 5.4. The coefficients I_1 , I_2 , and I_3 are independent of coordinate system and therefore are called *invariants*. Consequently, the principal stresses for a given stress state is unique. These invariants have physical significance in theory of plasticity. The invariants can also be expressed in terms of principal stresses:

$$I_1 = \sigma_1 + \sigma_2 + \sigma_3$$

$$I_2 = -(\sigma_1\sigma_2 + \sigma_2\sigma_3 + \sigma_3\sigma_1) \quad (\text{Eq 5.5})$$

$$I_3 = \sigma_1\sigma_2\sigma_3$$

5.3 Volumetric Stress or Hydrostatic Pressure

The volumetric stress is the average of the normal stresses:

$$\sigma_m = \frac{(\sigma_{xx} + \sigma_{yy} + \sigma_{zz})}{3} = \frac{(\sigma_1 + \sigma_2 + \sigma_3)}{3} = \frac{1}{3} I_1 \quad (\text{Eq 5.6})$$

The stress quantity σ_m is like three equal components of normal stress acting in all the three directions. This is equivalent to the hydrostatic pressure acting on a structure except that the sign is reversed and can be expressed in terms of hydrostatic pressure:

$$p = -\frac{(\sigma_1 + \sigma_2 + \sigma_3)}{3} = -\frac{(\sigma_{xx} + \sigma_{yy} + \sigma_{zz})}{3} \quad (\text{Eq 5.7})$$

The stress state containing only the hydrostatic stress is called the *hydrostatic stress state*. The important experimental observation is that the hydrostatic stress state does not cause any plastic deformation. This is easily verified by the physical fact that plastic deformation requires shearing of atomic planes, which in turn requires shear stresses. Since no shear stress is given in a hydrostatic stress state, no plastic deformation can be induced. The hydrostatic stress state only introduces an elastic volume change.

5.4 Deviatoric Stress

The stress state that causes plastic deformation is called the *deviatoric stress state*, s_{ij} , which is defined as the normal stress state reduced by the hydrostatic stress state (Fig. 5.3). The tensor equation for the deviatoric stress state is $s_{ij} = \sigma_{ij} - \sigma_m \delta_{ij}$, which can be expanded into its components for the tensor matrix (\mathbf{S}):

$$\mathbf{S} = \begin{bmatrix} s_{xx} & s_{xy} & s_{xz} \\ s_{xy} & s_{yy} & s_{yz} \\ s_{xz} & s_{yz} & s_{zz} \end{bmatrix}$$

where:

$$\mathbf{S} = \begin{bmatrix} \sigma_{xx} - \sigma_m & \sigma_{xy} & \sigma_{xz} \\ \sigma_{xy} & \sigma_{yy} - \sigma_m & \sigma_{yz} \\ \sigma_{xz} & \sigma_{yz} & \sigma_{zz} - \sigma_m \end{bmatrix} \quad (\text{Eq 5.8})$$

The principal deviatoric stresses (s_1 , s_2 , and s_3) can be calculated in a manner similar to that principal stress, as root of the cubic equation:

$$(S - \lambda I) \cdot n = 0 \Rightarrow \begin{bmatrix} s_{xx} - \lambda & s_{xy} & s_{xz} \\ s_{xy} & s_{yy} - \lambda & s_{yz} \\ s_{xz} & s_{yz} & s_{zz} - \lambda \end{bmatrix} = 0$$

$$\lambda^3 - J_1 \lambda^2 - J_2 \lambda - J_3 = 0 \quad (\text{Eq 5.9})$$

where

$$J_1 = s_{xx} + s_{yy} + s_{zz} = 0$$

$$J_2 = -(s_{xx}s_{yy} + s_{yy}s_{zz} + s_{zz}s_{xx}) + s_{xy}^2 + s_{yz}^2 + s_{zx}^2$$

$$= \frac{1}{6} \left((\sigma_x - \sigma_y)^2 + (\sigma_y - \sigma_z)^2 + (\sigma_z - \sigma_x)^2 \right) + \sigma_{xy}^2 + \sigma_{yz}^2 + \sigma_{zx}^2$$

$$= \frac{1}{6} \left((\sigma_1 - \sigma_2)^2 + (\sigma_2 - \sigma_3)^2 + (\sigma_3 - \sigma_1)^2 \right)$$

$$J_3 = \det S_{ij}.$$

The coefficients J_1 , J_2 , and J_3 are the deviatoric stress invariants. Among the invariants, the second invariant, J_2 , is widely used in theory of plasticity to describe yielding of the material.

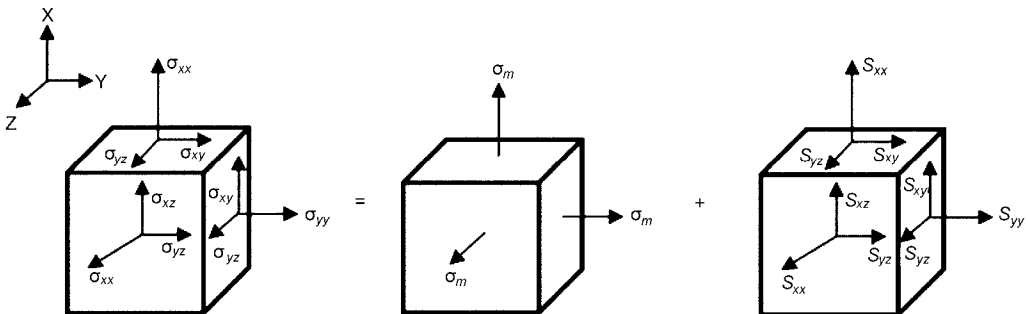


Fig. 5.3 Stress state that can be decomposed to volumetric stress and deviatoric stress

5.5 Isotropic Yield Criteria (Flow Criteria)

Yield criteria define the condition for the limit of elastic behavior or the onset of plastic deformation in a material under multiaxial states of stress. A criterion used for determining the condition of continuing plastic flow is also called the *flow criterion*. In the uniaxial compression or tensile test, the metal starts to flow plastically when the stress in the material reaches the material's yield stress:

$$\sigma = \frac{F}{A} = \bar{\sigma}$$

where F is the instantaneous force, A is the instantaneous area of the test specimen, and $\bar{\sigma}$ is the yield stress of the material. In multiaxial states of stress, the determination of plastic flow is not trivial and depends on a combination of all the stresses in the stress tensor.

The most popular yield criteria for isotropic material and anisotropic material used in numerical modeling of sheet metal forming processes are described in this chapter:

Isotropic yield criteria (Sections 5.6–5.8)

- Tresca or shear stress yield criterion
- Von Mises or distortion energy criterion

Anisotropic yield criteria (Section 5.9):

- Hill's 1947 yield criterion
- Hill's 1990 yield criterion
- Barlat and Lian yield criterion
- Barlat 1996 yield criterion

5.6 Tresca Yield Criterion

The Tresca yield criterion indicates that the plastic flow begins or the material starts to yield when the maximum shear stress reaches the critical value K or when $|\tau_{\max}| = K$, where K is the shear flow stress of the material, which is a function of strain, strain rate, temperature, microstructure, and so on.

The Tresca yield criterion can be easily described by the aid of Mohr's circle. Fig. 5.4 shows the Mohr's circle representation for in-plane stresses whose coordinate axes are shear stress, τ (ordinate), and normal stress, σ (abscissa). The principal stress, σ_1, σ_3 , defines the maximum and minimum principal stress along the direction where the shear stress vanishes and defines limits of Mohr's circle. The sub-

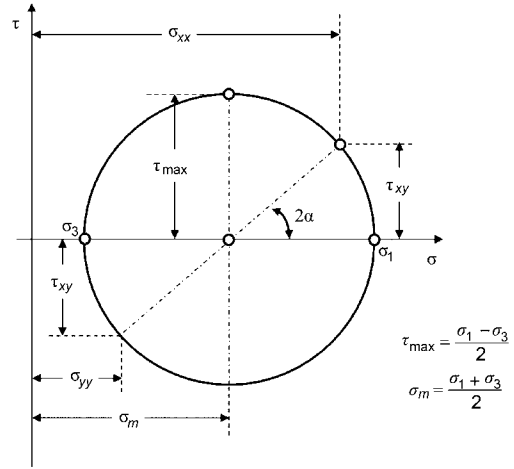


Fig. 5.4 Schematic of Mohr's circle for in-plane stresses

scripts are arbitrary, only indicating that $\sigma_1 \geq \sigma_2 \geq \sigma_3$. As shown in Fig. 5.4, the maximum shear stress is given by the radius of Mohr's circle. Hence, the maximum shear stress can be expressed in terms of principal stress as $\tau_{\max} = (\sigma_1 - \sigma_3)/2$. The Tresca yield criterion in terms of principal stress can be written as:

$$|\tau_{\max}| = \left| \frac{(\sigma_1 - \sigma_3)}{2} \right| = K \quad (\text{Eq 5.10})$$

Fig. 5.5 shows Mohr's circle in the tensile test (no necking) and compression test (no bulging), respectively. In both cases, the deformation is uniaxial; that is, $\sigma_2 = 0, \sigma_3 = 0$. The plastic deformation begins as:

$$\sigma_1 = \frac{F}{A} = \bar{\sigma} = 2K \quad \text{or} \quad k = \frac{\bar{\sigma}}{2} \quad (\text{Eq 5.11})$$

where F is the tensile or compressive force, A is the instantaneous cross-sectional area of the sample, and $\bar{\sigma}$ is the flow stress (or instantaneous yield stress) in the uniaxial stress state.

If the principal stresses are arranged as $\sigma_1 \geq \sigma_2 \geq \sigma_3$, then the Tresca criterion in terms of principal stress can be written as:

$$\bar{\sigma} = \sigma_1 - \sigma_3 \quad (\text{Eq 5.12})$$

Fig. 5.5 also shows that the position of Mohr's circle does not affect the yielding, indicating that the hydrostatic pressure does not affect the yielding.

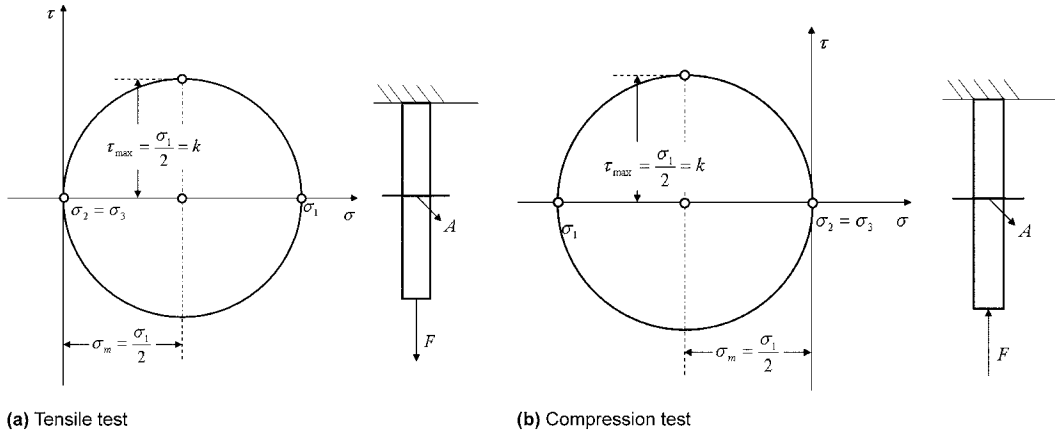


Fig. 5.5 Schematic of Mohr's circle in uniaxial tensile and compression tests (Ref 5.1)

In the general case, the Tresca yield criterion can be expressed in terms of principal stresses:

$$\max \{ |\sigma_1 - \sigma_2|, |\sigma_2 - \sigma_3|, |\sigma_3 - \sigma_1| \} = \bar{\sigma} \quad (\text{Eq 5.13})$$

where $\bar{\sigma}$ is the flow stress (or instantaneous yield stress) in uniaxial stress state.

In three-dimensional stress space, the Tresca criterion results in a hexagonal surface, as shown in Fig. 5.6(a). In sheet metal forming, most analysis is done assuming the plane stress condition along the thickness direction ($\sigma_3 = 0$). The yield surface reduces to a hexagon (Fig. 5.6b).

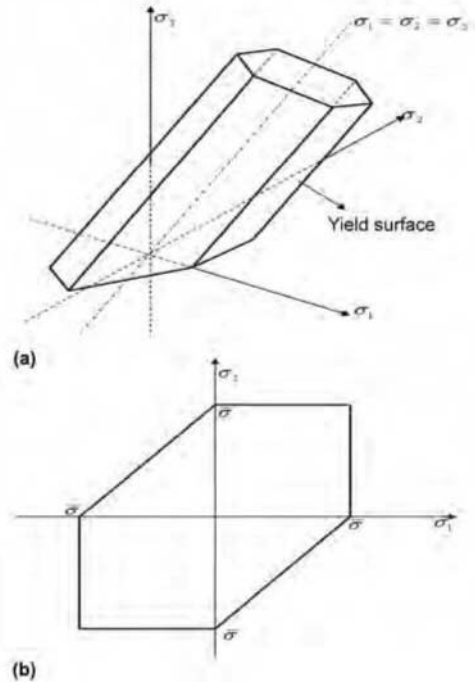


Fig. 5.6 Schematic of Tresca yield criterion in (a) three-dimensional and (b) two-dimensional stress space

5.7 Von Mises Yield Criterion

In contrast to the Tresca flow condition, the von Mises flow condition considers all the principal shear stresses. Accordingly, plastic flow starts if:

$$c' = \sqrt{\frac{1}{3} \left[(\tau_{\max}^1)^2 + (\tau_{\max}^2)^2 + (\tau_{\max}^3)^2 \right]} \quad (\text{Eq 5.14})$$

where c' is a material constant. Again, tuning this equation by the simple tension test supplies:

$$\bar{\sigma} = \sqrt{\frac{1}{2} \left[(\sigma_{xx} - \sigma_{yy})^2 + (\sigma_{yy} - \sigma_{zz})^2 + (\sigma_{zz} - \sigma_{xx})^2 + 6(\tau_{xy}^2 + \tau_{yz}^2 + \tau_{zx}^2) \right]} \quad (\text{Eq 5.15})$$

or, in terms of principal stresses:

$$\bar{\sigma} = \sqrt{\frac{1}{2} \left[(\sigma_1 - \sigma_2)^2 + (\sigma_2 - \sigma_3)^2 + (\sigma_3 - \sigma_1)^2 \right]} \quad (\text{Eq 5.16})$$

The von Mises criterion can also be expressed in terms of deviatoric stress invariant using Eq 5.9:

$$3J_2 = \bar{\sigma}^2 \quad (\text{Eq 5.17})$$

In three-dimensional stress space, the von Mises criterion results in a cylindrical surface, as shown in Fig. 5.7(a). For the plane stress condition commonly used in sheet metal forming analysis, the von Mises yield locus takes the form of an elliptical curve, as shown in Fig. 5.7(b) (Ref 5.2).

5.8 Comparison of Tresca and von Mises Criteria

The Tresca and von Mises yield criteria can be compared by superimposing the plane stress versions of the yield criteria, as shown in Fig. 5.8. The shaded areas show the difference between the two yield criteria (Ref 5.1), and points A, B, C, D, and E are used to describe the similarities and differences of the two yield surfaces:

- In uniaxial tension or compression loading (points A and B, respectively), both von Mises and Tresca yield criteria exhibit the same values for yielding. That is, when $\sigma_2 = 0$, $\sigma_3 = 0$, the von Mises yield criterion gives $\sigma_1 = \bar{\sigma}$, and the same is true for the Tresca yield criterion using Eq 5.11.
- At point C, corresponding to balanced biaxial state ($\sigma_1 = \sigma_2 = \sigma$, $\sigma_3 = 0$), both Tresca

and von Mises yield criteria exhibit the same value for yielding.

- In pure shear (point D), the two criteria exhibit different yield stresses. In pure shear, the stress state is $\sigma_1 = -\sigma_2$, $\sigma_3 = 0$.
 - The von Mises yield criterion reduces to:

$$\bar{\sigma} = \sqrt{\frac{1}{2} \{ (\sigma_1 + \sigma_1)^2 + (-\sigma_1)^2 + (-\sigma_1)^2 \}} = \sqrt{3}\sigma_1$$

$$\tau_{\max} = \sigma_1 = \frac{\bar{\sigma}}{\sqrt{3}}$$

- The Tresca yield criterion gives:

$$\bar{\sigma} = 2\sigma_1 \quad \text{and} \quad \tau_{\max} = \sigma_1 = \frac{\bar{\sigma}}{2}$$

- In the plane strain (point E), the two yield criteria exhibit different yield stresses. With the Tresca yield criterion, the stress required for plastic deformation is $\bar{\sigma}_1$. With the von Mises yield criterion, the stress required for plastic deformation is $1.15\bar{\sigma}_1$

5.9 Anisotropic Yield Criteria

Sheet metals exhibit anisotropic characteristics due to the rolling process used to manufacture sheet metal coil. The rolling process aligns the grains along the rolling direction and packs the grains along the thickness direction. This

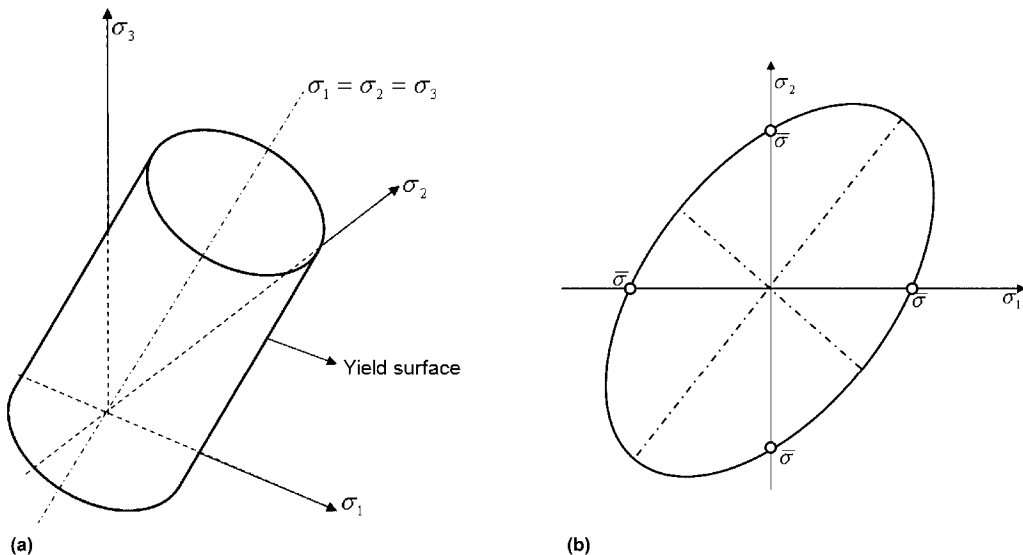


Fig. 5.7 Schematic of von Mises yield criterion in (a) three-dimensional and (b) two-dimensional stress space

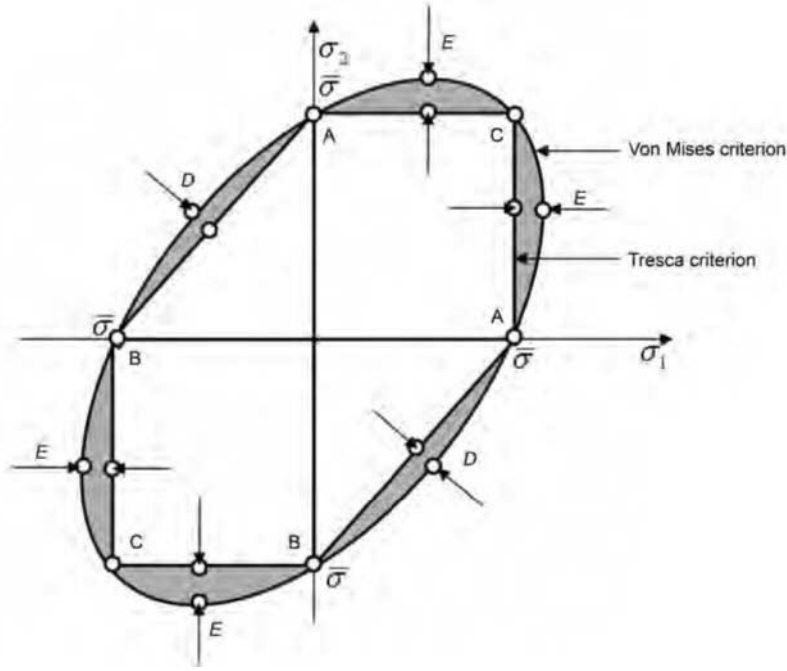


Fig. 5.8 Comparison of von Mises and Tresca yield criteria (Ref 5.1)

causes the sheet material to behave differently along the three orthotropic directions: the rolling, transverse, and thickness directions. To model the orthotropic behavior of sheet metals, several orthotropic yield criteria have been proposed. Among those, the ones commonly used in numerical methods for analysis of sheet metal forming process are described in this section.

Hill's 1948 Yield Criterion

In 1948 Hill proposed a yield criterion based on the von Mises yield criterion for orthotropic material:

$$2f(\sigma_{ij}) = H(\sigma_x - \sigma_y)^2 + G(\sigma_y - \sigma_z)^2 + F(\sigma_z - \sigma_x)^2 + 2N\tau_{xy}^2 + 2M\tau_{yz}^2 + 2L\tau_{xz}^2 = 1 \quad (\text{Eq 5.18})$$

where $\sigma_x, \sigma_y, \sigma_z$ are the normal stress in x, y, z -orthotropic axis, $\tau_{xy}, \tau_{xz}, \tau_{yz}$ are the shear stress, and F, G, H, L, M, N are the anisotropy constants in the yield criterion.

In the case of sheet material, the x, y, z -orthotropic axes are rolling, transverse, and thickness directions. The constants F, G, H can be determined from the uniaxial test along the orthotropic axes.

Let X, Y, Z be the yield stress along the orthotropic axis; then Hill's yield criterion can be reduced to:

$$H + G = \frac{1}{X^2}, H + F = \frac{1}{Y^2}, F + G = \frac{1}{Z^2} \quad (\text{Eq 5.19})$$

From these equations, constants F, G, H can be expressed as a function of yield stress in three orthotropic axes.

Similarly, let R, S, T be the shear yield stresses in orthotropic directions; then Hill's yield criterion can be reduced to:

$$2L = \frac{1}{R^2}, 2M = \frac{1}{S^2}, 2N = \frac{1}{T^2} \quad (\text{Eq 5.20})$$

The coefficients L, M, N can be estimated directly from shear yield stresses. In three-dimensional space, the yield criterion is represented by a surface. Inside the yield surface, the material is in an elastic state, and outside of the yield surface it is in a plastic state.

In analysis of sheet materials, the state of the stress is assumed to be plane stress along the thickness direction ($\sigma_z = \tau_{xz} = \tau_{yz} = 0$). Therefore, Hill's yield criterion reduces to:

$$2f(\sigma_{ij}) = H(\sigma_y - \sigma_x)^2 + G\sigma_x^2 + F\sigma_y^2 + 2N\tau_{xy}^2 = 1 \quad (\text{Eq 5.21})$$

After introducing the yield stress from uniaxial test along the three directions and shear yield stress the Eq 5.21 can be reduced to:

$$2f(\sigma_{ij}) = \frac{1}{X^2}\sigma_x^2 - \left(\frac{1}{X^2} + \frac{1}{Y^2} + \frac{1}{Z^2}\right)\sigma_x\sigma_y + \frac{1}{Y^2}\sigma_y^2 + \frac{1}{T^2}\tau_{xy}^2 = 1 \quad (\text{Eq 5.22})$$

The constants can also be more easily obtained from the plastic strain ratio (r_0 , r_{90} and r_{45}) obtained from the tensile test along rolling and transverse directions and 45° to the rolling direction.

The relationship between the plastic strain ratio in the tensile test and constants in Hill's plane stress yield criterion can be obtained using the flow rule and the yield function:

$$\frac{H}{G} = r_0, \frac{H}{F} = r_{90}, \frac{H}{2N} = \frac{1}{(2r_{45} + 1)\left(\frac{1}{r_0} + \frac{1}{r_{90}}\right)} \quad (\text{Eq 5.23})$$

From Eq 5.21 and 5.23 we get:

$$2f(\sigma_{ij}) = H(\sigma_y - \sigma_x)^2 + \frac{H}{r_0}\sigma_x^2 + \frac{H}{r_{90}}\sigma_y^2 + H(2r_{45} + 1)\left(\frac{1}{r_0} + \frac{1}{r_{90}}\right)\tau_{xy}^2 = 1 \quad (\text{Eq 5.24})$$

Consider a tensile test (before necking) or compression test (before bulging), where the deformation is uniaxial along the rolling direction (i.e. $\sigma_2 = 0$, $\sigma_3 = 0$), so the plastic deformation begins when:

$$\sigma_1 = \frac{F}{A} = \bar{\sigma}_0 \quad (\text{Eq 5.25})$$

where F is the tensile or compressive force, A is the instantaneous cross-sectional area of the sample, and $\bar{\sigma}_0$ is the flow stress (or instantaneous yield stress) in uniaxial stress state along the rolling direction.

Hill's yield function at the start of plastic deformation in uniaxial loading along rolling direction can be obtained from Eq 5.24 as:

$$2f(\sigma_{ij}) = H\left(1 + \frac{1}{r_0}\right)\bar{\sigma}_0^2 \quad (\text{Eq 5.26})$$

Combining Eq 5.24 and 5.26, we get Hill's yield criterion in terms of constants that can be measured from experiments:

$$\bar{\sigma}_0^2 = \frac{r_0 r_{90} (\sigma_y - \sigma_x)^2 + r_{90} \sigma_x^2 + r_0 \sigma_y^2 + (2r_{45} + 1)(r_0 + r_{90}) \tau_{xy}^2}{r_{90}(r_0 + 1)} \quad (\text{Eq 5.27})$$

Therefore, either Eq 5.24 or 5.27 can be used to describe the behavior of sheet material in the finite element (FE) simulations by Hill's 1948 yield criterion.

In the case of principal directions of stress tensors coinciding with the orthotropic axes ($\sigma_x = \sigma_1$, $\sigma_y = \sigma_2$, $\tau_{xy} = 0$), Eq 5.26 can be expressed in terms of principal stress:

$$\frac{r_0 r_{90} (\sigma_1 - \sigma_2)^2 + r_{90} \sigma_1^2 + r_0 \sigma_2^2}{r_{90}(r_0 + 1)} = \bar{\sigma}_0^2 \quad (\text{Eq 5.28})$$

Hill's 1948 yield criterion is very similar to von Mises yield criterion. In three-dimensional stress space, it is represented by an ellipsoid; in two-dimensional space it is an ellipse. The influence of anisotropy values r_0 and r_{90} on the shape of the yield surface is schematically shown in Fig. 5.9.

In case of material exhibiting normal anisotropy ($r_0 = r_{90} = r_{45} = r$), Eq 5.27 can be further reduced to:

$$\sigma_1^2 + \sigma_2^2 - 2\sigma_1\sigma_2 \frac{r}{1+r} = \bar{\sigma}_0^2 \quad (\text{Eq 5.29})$$

In the case of isotropic material ($r_0 = r_{90} = r_{45} = 1$), Eq 5.29 reduces to the von Mises yield criterion in plane stress condition:

$$\frac{(\sigma_y - \sigma_x)^2 + \sigma_x^2 + \sigma_y^2 + 6\tau_{xy}^2}{2} = \bar{\sigma}_0^2 \quad (\text{Eq 5.30})$$

Hill's yield criterion requires, at a minimum, the plastic strain ratio (r_0 , r_{90} , r_{45}) test parameters from the tensile test along three directions to describe this criterion in plane stress conditions. Thus, it is commonly used to describe the behavior of sheet metals. The criterion has few drawbacks, which are described as anomalous behaviors of the materials (Ref 5.3).

First Anomalous Behavior. Consider a balanced biaxial test $\sigma_1 = \sigma_2 = \sigma_b$; then Eq 5.27 of Hill's yield criterion reduces to:

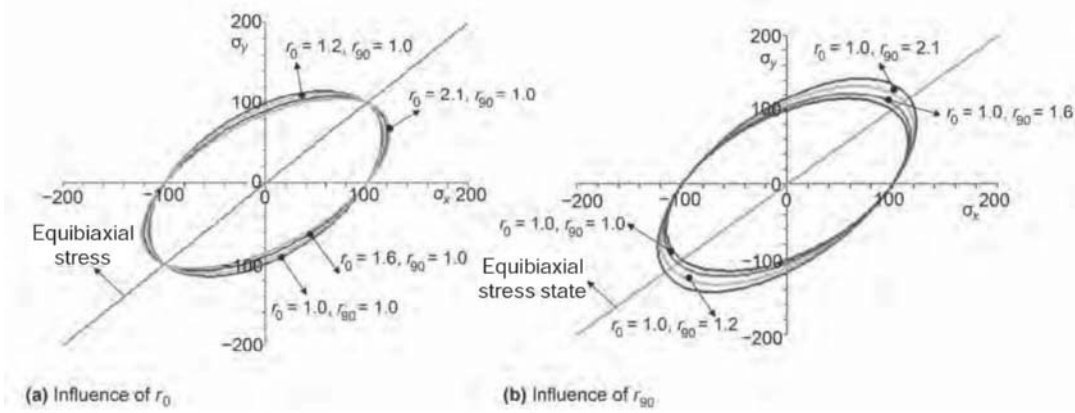


Fig. 5.9 Effect of anisotropy constants on the shape of Hill's 1948 yield criterion in the plane stress condition

$$\sigma_b = \bar{\sigma}_0 \sqrt{\frac{1+r}{2}} \quad \text{or} \quad \frac{\sigma_b}{\bar{\sigma}_0} = \sqrt{\frac{1+r}{2}} \quad (\text{Eq 5.31})$$

This indicates that the yield stress in the balanced biaxial test (bulge test) is proportional to r . If $r > 1$, then $\sigma_b > \bar{\sigma}_0$; if $r < 1$, then $\sigma_b < \bar{\sigma}_0$. However, aluminum alloys have $r < 1$, but the yield stress in the balanced biaxial (bulge test) is greater than the yield stress from the tensile test. Hence, Hill's yield criterion cannot be used for such alloys that exhibit this behavior (Ref 5.2).

Second Anomalous Behavior. Consider a tensile test (before necking) or compression test (before bulging) where the deformation is uniaxial along the transverse direction; that is, $\sigma_x = 0$, $\tau_{xy} = 0$. The plastic deformation begins when:

$$\sigma_y = \frac{F}{A} = \bar{\sigma}_{90} \quad (\text{Eq 5.32})$$

where F is the tensile or compressive force, A is the instantaneous cross-sectional area of the sample, and $\bar{\sigma}_{90}$ is the flow stress (or instantaneous yield stress) in the uniaxial stress state in the transverse direction. Then Eq 5.27 of Hill's yield criterion reduces to:

$$\frac{r_0(r_0+1)\bar{\sigma}_{90}^2}{r_0(r_0+1)} = \bar{\sigma}_0^2 \quad \text{or} \quad \frac{\bar{\sigma}_0}{\bar{\sigma}_{90}} = \sqrt{\frac{r_0(r_0+1)}{r_0(r_0+1)}} \quad (\text{Eq 5.33})$$

This indicates that if $r_0/r_{90} > 1$, then $\bar{\sigma}_0/\bar{\sigma}_{90} < 1$, and vice versa. However, some materials do not exhibit this behavior. Hence, Hill's yield criterion cannot be used for such alloys (Ref 5.2, 5.3).

Hill's 1990 Yield Criterion

Hill's 1990 yield criterion overcomes the limitations of Hill 1948 and Hill 1979. In a generalized orthotropic coordinate system for plane stress condition, it is given by:

$$\begin{aligned} \phi &= |\sigma_x + \sigma_y|^m + \left(\frac{\sigma_b}{\tau} \right)^m \left[(\sigma_x - \sigma_y)^2 + 4\tau_{xy}^2 \right]^{\frac{m}{2}} + \\ & \left| \sigma_x^2 + \sigma_y^2 + 2\tau_{xy}^2 \right|^{\frac{m-1}{2}} \left\{ -2a(\sigma_x^2 - \sigma_y^2) + b(\sigma_x - \sigma_y)^2 \right\} \\ &= (2\sigma_b)^m \end{aligned} \quad (\text{Eq 5.34})$$

Here x, y are the orthotropic directions, σ_b is the yield stress in balanced biaxial state ($\sigma_x = \sigma_y$), τ is the yield stress in pure shear ($\sigma_x = -\sigma_y$), and a, b , and m are constants.

The constants a and b can be estimated from the yield stress due to uniaxial loading along the rolling and transverse directions and 45° to the rolling direction. Let σ_0 , σ_{90} , and σ_{45} be the yield stresses along the rolling, transverse, and 45° to rolling directions, respectively, in the uniaxial tensile test. Then, constants a and b are obtained as:

$$a = \frac{1}{4} \left[\left(\frac{2\sigma_b}{\sigma_{90}} \right)^m - \left(\frac{2\sigma_b}{\sigma_0} \right)^m \right] \quad (\text{Eq 5.35})$$

$$b = \frac{1}{2} \left[\left(\frac{2\sigma_b}{\sigma_0} \right)^m + \left(\frac{2\sigma_b}{\sigma_{90}} \right)^m \right] - \left(\frac{2\sigma_b}{\sigma_{45}} \right)^m \quad (\text{Eq 5.36})$$

$$\left(\frac{\sigma_b}{\tau} \right)^m = \left(\frac{2\sigma_b}{\sigma_{45}} \right)^m - 1 \quad (\text{Eq 5.37})$$

Using the flow rule, the plastic strain ratio r_{45} in tensile test can be related to m as:

$$r_{45} = \frac{1}{2} \left[\left(\frac{\sigma_b}{\tau} \right)^m - 1 \right] \quad (\text{Eq 5.38})$$

Combining Eq 5.40 in Eq 5.41:

$$r_{45} = \frac{1}{2} \left[\left(\frac{2\sigma_b}{\sigma_{45}} \right)^m - 2 \right] \quad (\text{Eq 5.39})$$

The constants can also be obtained from the plastic strain ratio in the tensile tests that is used to characterize anisotropy in sheet metals:

$$a = \frac{(r_0 - r_{90}) \left[1 - r_{45} \frac{m-2}{2} \right]}{r_0 + r_{90} - (m-2)r_0 r_{90}},$$

$$b = \frac{m \left[2r_0 r_{90} - r_{45} (r_0 + r_{90}) \right]}{r_0 + r_{90} - (m-2)r_0 r_{90}} \quad (\text{Eq 5.40})$$

where r_0 and r_{90} are the plastic strain ratios in the rolling and transverse direction obtained from the tensile test.

Using Mohr's circle, the yield stress can be expressed in terms of principal stress:

$$\phi = |\sigma_1 + \sigma_2|^m + \left(\frac{\sigma_b}{\tau} \right)^m |(\sigma_1 - \sigma_2)|^m + |\sigma_1^2 + \sigma_2^2|^{\frac{m-1}{2}}$$

$$\left\{ -2a(\sigma_x^2 - \sigma_y^2) + b(\sigma_x - \sigma_y)^2 \cos 2\alpha \right\}$$

$$\cos 2\alpha = (2\sigma_b)^m \quad (\text{Eq 5.41})$$

where σ_1 and σ_2 are the principal stresses and α is the angle between the principal axis corresponding to the rolling direction.

Hill's 1990 yield criterion requires estimation of five constants: σ_b , τ , a , b , and m . σ_b must be estimated from the balanced biaxial test; the other four parameters can be estimated from the tensile test results, σ_0 , σ_{90} , σ_{45} , and r_{45} or r_0 , r_{90} , r_{45} , and σ_{45} , as explained above (Ref 5.2, 5.4).

Barlat and Lian Yield Criterion (Ref 5.5)

Logan and Hosford proposed a generalized yield criterion in terms of the principal deviatoric stress condition considering plastic yielding to be independent of mean stress, σ_m :

$$f = |S_1 - S_3|^m + |S_2 - S_3|^m + |S_2 - S_1|^m = 2\bar{\sigma}^m \quad (\text{Eq 5.42})$$

where S_1 , S_2 , and S_3 are the principal deviatoric stresses, $\bar{\sigma}$ is the yield stress in the uniaxial tensile test, and m is the material constant. This is a generalized form of the yield criterion: when $m = 2$, Eq 5.42 reduces to the von Mises yield criterion. Also, when $m = 1$ or ∞ , Eq 5.42 reduces to the Tresca yield criterion, as shown in Fig. 5.10. Hosford and Hill found that the proposed yield criterion represents the yield surface of bcc and fcc sheet material calculated by the Bishop Hill model when $m = 6$ and 8, respectively (Ref 5.2).

The yield criterion in the generalized reference frame x , y , z (orthotropic axis) for plane stress condition is:

$$f = |K_1 + K_2|^m + |K_1 - K_2|^m + |2K_2|^m = 2\bar{\sigma}^m$$

$$K_1 = \frac{\sigma_x + \sigma_y}{2}$$

$$K_2 = \sqrt{\frac{(\sigma_x - \sigma_y)^2}{2} + \sigma_{xy}^2} \quad (\text{Eq 5.43})$$

where σ_x , σ_y , and σ_{xy} are the normal stress and shear stress in plane.

Barlat and Lian extended the Hosford formulation to orthotropic materials for plane stress condition by introducing anisotropy constants a , c , h , and p as

$$f = a|K_1 + K_2|^m + a|K_1 - K_2|^m + c|2K_2|^m = 2\bar{\sigma}^m,$$

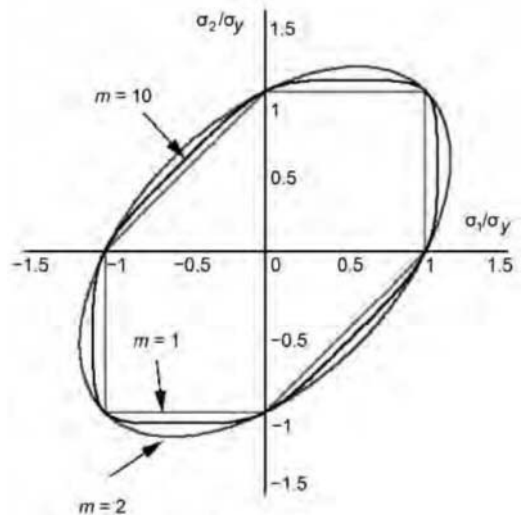


Fig. 5.10 Influence of parameter m on the shape of the Logan and Hosford yield surface (Ref 5.2)

$$K_1 = \frac{\sigma_x + h\sigma_y}{2},$$

$$K_2 = \sqrt{\frac{(\sigma_x - h\sigma_y)^2}{2} + p^2\sigma_{xy}^2}. \quad (\text{Eq 5.44})$$

The material constants a , c , h , p , can be obtained from the yield stress in the tensile test along the rolling direction (σ_0), from yield stress along the rolling transverse direction (σ_{90}), and from yield stress in the shear test ($\sigma_x = -\sigma_y = \tau_{s1}$, $\sigma_{xy} = 0$, and $\sigma_x = \sigma_y = 0$, $\sigma_{xy} = \tau_{s2}$):

$$a = 2 - c = \frac{2\left(\frac{\sigma_0}{\tau_{s2}}\right)^m - 2\left(1 + \frac{\sigma_0}{\sigma_{90}}\right)^m}{1 + \left(\frac{\sigma_0}{\sigma_{90}}\right)^m - \left(1 + \frac{\sigma_0}{\sigma_{90}}\right)^m}$$

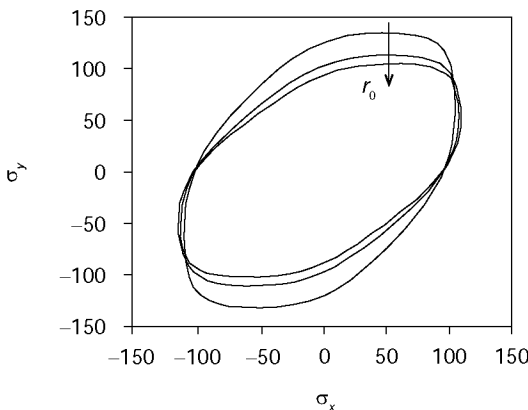
$$h = \frac{\sigma_0}{\sigma_{90}}$$

$$p = \frac{\sigma_0}{\tau_{s1}} \left(\frac{2}{2a + 2^m c} \right)^{\frac{1}{m}} \quad (\text{Eq 5.45})$$

Also, the parameters a , c , and h can be obtained from the plastic strain ratio r_0 , r_{45} , and r_{90} . The relationship between plastic strain ratio and the constant is obtained using the associated flow rule:

$$a = 2 - c = 2 - 2\sqrt{\frac{r_0}{1+r_0} \frac{r_{90}}{1+r_{90}}}$$

$$h = \sqrt{\frac{r_0}{1+r_0} \frac{1+r_{90}}{r_{90}}} \quad (\text{Eq 5.46})$$



(a) Influence of r_0

Influence of the plastic strain ratio on the shape of the yield surface is shown in Fig. 5.11 (Ref 5.5). The Barlat and Lian yield criterion could overcome the anomalous behavior exhibited by Hill's 1948 yield criterion. However, it is limited to plane stress condition, and it could not exactly capture the variation of plastic strain and yield stress along different in-plane directions in aluminum alloys obtained from the tensile test (Ref 5.5–5.7). Barlat and colleagues (Ref 5.8) proposed yield criteria to better describe the behavior of aluminum alloys that are commonly used in numerical analysis of sheet metal forming using aluminum alloys, described in the following section.

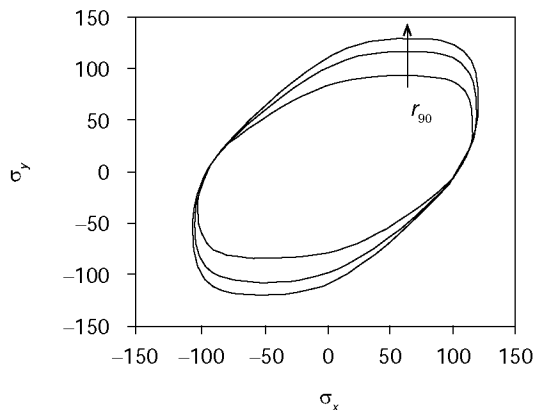
Barlat 1996 Yield Criterion

A more generalized anisotropy yield criterion that applies to aluminum alloys was proposed by Barlat and colleagues (Ref 5.8). The material constants necessary to describe this criterion are obtained from: (a) the yield stress and plastic strain ratio measured in a tensile test, along rolling and transverse directions, and (b) the yield stress measured in a balanced biaxial test.

It has been shown that the Barlat 1996 yield criterion captures the variation of the yield stress and plastic strain ration across different angles to the rolling direction in an aluminum alloy, as shown in Fig. 5.12.

5.10 Flow Rules

When the stress at any point in the metal reaches the level specified by the yield criterion,



(b) Influence of r_{90}

Fig. 5.11 Influence of the plastic strain ratio r_0 and r_{90} on the shape of the Barlat and Lian yield surface

further loading will result in plastic deformation. Hooke's law describes the stress-strain relationships in the elastic range. Analysis of plastic deformation requires a similar relationship. The flow rule describes such a relationship between the principal stress and the plastic strain increments. Based on the experimental observations, the hypothesis postulates that the ratio of plastic strain increment is the same as the ratio of the principal deviatoric stress. This is commonly known as the Levy-Mises flow rule. In other words, the axis of principal deviatoric stress coincides with the principal strain increments. It can be expressed as:

$$\frac{d\varepsilon_1}{S_1} = \frac{d\varepsilon_2}{S_2} = \frac{d\varepsilon_3}{S_3} = d\lambda$$

or

$$\frac{d\varepsilon_{ij}}{S_{ij}} = d\lambda \quad (\text{Eq 5.47})$$

where $d\lambda$ is the constant.

In the case of the von Mises yield criterion, where the yield function is given by second invariant of deviatoric stress J_2 (Eq 5.17), the deviatoric stress can be expressed as:

$$\frac{df}{d\sigma_{ij}} = S_{ij} \quad (\text{Eq 5.48})$$

Therefore, Eq 5.47 reduces to:

$$d\varepsilon_{ij} = d\lambda \frac{df}{d\sigma_{ij}} \quad (\text{Eq 5.49})$$

In the case of the plane stress condition, the flow rule can be demonstrated schematically for different stress conditions (Fig. 5.13). The slope of strain increments is normal to the yield surface at the yield stress. This normality rule is commonly used in estimating the material parameters of the yield functions based on the plastic strain ratios in different directions obtained from uniaxial tensile tests (Ref 5.9, 5.10).

In the case of the von Mises yield function under proportional loading, the constant $d\lambda$ can be determined as:

$$d\lambda = \frac{3}{2} \frac{d\bar{\varepsilon}}{\bar{\sigma}} \quad (\text{Eq 5.50})$$

The expression of plastic strain increment can also be given as

$$d\varepsilon_{ij} = \frac{3}{2} \frac{d\bar{\varepsilon}}{\bar{\sigma}} S_{ij} \quad (\text{Eq 5.51})$$

5.11 Power and Energy of Deformation

The plastic deformation process is irreversible. The mechanical energy consumed during deformation is largely released as heat. When we consider a homogeneous block (original

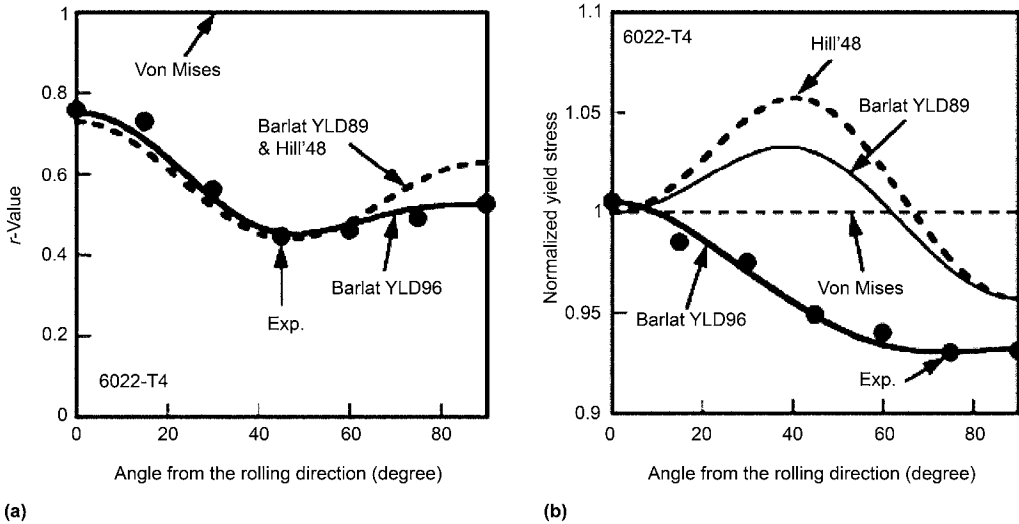


Fig. 5.12 (a) Plastic strain ratio and (b) yield stress along the different directions calculated from von Mises, Hill 1948, Barlat YLD89, and Barlat 1996 yield criterion (Barlat YLD96) and from experiments (Exp.) for aluminum alloy 6022-T4 (Ref 5.8)

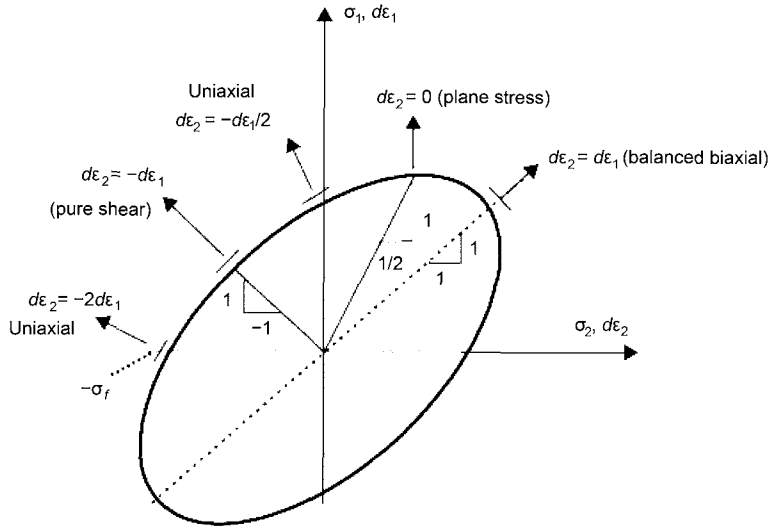


Fig. 5.13 Strain increments based on the Levy-Mises flow rule at different stress states for the in-plane von Mises yield criterion (Ref 5.9)

height, h_o ; original width, W_o ; original length, l_o deformed at velocities V_h , V_w , and V_l (Fig. 5.14), the principal strains are given by:

$$\begin{aligned}\epsilon_1 &= \ln \frac{h}{h_o}; \dot{\epsilon}_1 = \frac{V_h}{h}, \\ \epsilon_2 &= \ln \frac{w}{w_o}; \dot{\epsilon}_2 = \frac{V_w}{w}, \\ \epsilon_3 &= \ln \frac{l}{l_o}; \dot{\epsilon}_3 = \frac{V_l}{l}.\end{aligned}\quad (\text{Eq 5.52})$$

Following Fig. 5.14, the instantaneous power of deformation (force times velocity) is given by:

$$\begin{aligned}P &= \sigma_1 w l v_h + \sigma_2 h l v_w + \sigma_3 w h v_l \\ &= \sigma_1 w l \dot{\epsilon}_1 + \sigma_2 w l \dot{\epsilon}_2 + \sigma_3 w l \dot{\epsilon}_3 \\ &= (\sigma_1 \dot{\epsilon}_1 + \sigma_2 \dot{\epsilon}_2 + \sigma_3 \dot{\epsilon}_3) V\end{aligned}\quad (\text{Eq 5.53})$$

where V is the volume of the deforming block. The energy of deformation, E , is given by:

$$E = V \int_{t_o}^t (\sigma_1 \dot{\epsilon}_1 + \sigma_2 \dot{\epsilon}_2 + \sigma_3 \dot{\epsilon}_3) dt \quad (\text{Eq 5.54})$$

With $\dot{\epsilon} dt = d\epsilon$, Eq 5.54 also can be written as:

$$E = V \left(\int_{t_o}^t \sigma_1 d\epsilon_1 + \int_{t_o}^t \sigma_2 d\epsilon_2 + \int_{t_o}^t \sigma_3 d\epsilon_3 \right) \quad (\text{Eq 5.55})$$

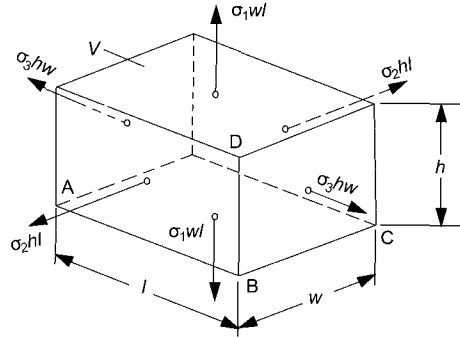


Fig. 5.14 Homogeneous deformation of a block (Ref 5.1)

5.12 Effective Strain and Effective Strain Rate

The flows stress $\bar{\sigma}$ is determined from tests such as tensile or compression under uniaxial deformation condition. However, in sheet metal forming the stress are multiaxial. The yield criterion discussed previously relates the multiaxial stress states to the uniaxial conditions to predict the onset of plastic deformation. The stress calculated using the yield criterion under multiaxial stress conditions is equivalent to stress under the uniaxial condition and is commonly referred as *equivalent* or *effective stress*. The

corresponding effective strain and effective strain rate can be estimated by equating the power and energy of deformation in multiaxial stress state to uniaxial stress state (Ref 5.1).

The deformation energy in multiaxial state over time Δt is:

$$dW = V(\sigma_1 d\varepsilon_1 + \sigma_2 d\varepsilon_2 + \sigma_3 d\varepsilon_3) \quad (\text{Eq 5.56})$$

or, divided by dt , the deformation power, P , is:

$$P = \frac{dW}{dt} = V(\sigma_1 \dot{\varepsilon}_1 + \sigma_2 \dot{\varepsilon}_2 + \sigma_3 \dot{\varepsilon}_3) \quad (\text{Eq 5.57})$$

Let $\bar{\varepsilon}$ be the effective strain, and let $\dot{\bar{\varepsilon}}$ be the effective strain rate; then the deformation energy and power in the uniaxial condition are given by:

$$dW = \bar{\sigma} d\bar{\varepsilon} V, \text{ or } P = \bar{\sigma} \dot{\bar{\varepsilon}} V \quad (\text{Eq 5.58})$$

Equating multiaxial power Eq 5.57 and uniaxial power Eq 5.58:

$$\bar{\sigma} \dot{\bar{\varepsilon}} = \sigma_1 \dot{\varepsilon}_1 + \sigma_2 \dot{\varepsilon}_2 + \sigma_3 \dot{\varepsilon}_3 \quad (\text{Eq 5.59})$$

For volume constancy it can be shown that:

$$\dot{\varepsilon}_1 + \dot{\varepsilon}_2 + \dot{\varepsilon}_3 = 0 \quad (\text{Eq 5.60})$$

or,

$$\sigma_m (\dot{\varepsilon}_1 + \dot{\varepsilon}_2 + \dot{\varepsilon}_3) = 0$$

Combining Eq 5.59 and 5.60, we obtain:

$$\dot{\bar{\varepsilon}} = \frac{(\sigma_1 - \sigma_m) \dot{\varepsilon}_1 + (\sigma_2 - \sigma_m) \dot{\varepsilon}_2 + (\sigma_3 - \sigma_m) \dot{\varepsilon}_3}{\bar{\sigma}} \quad (\text{Eq 5.61})$$

For the von Mises yield criterion, using flow rule Eq 5.51, the strain increment is given by:

$$\dot{\varepsilon}_1 = \frac{3}{2} \frac{\dot{\bar{\varepsilon}}}{\bar{\sigma}} S_1 = \frac{3}{2} \frac{\dot{\bar{\varepsilon}}}{\bar{\sigma}} (\sigma_1 - \sigma_m) \quad (\text{Eq 5.62})$$

Substituting Eq 5.62 into Eq 5.61, the effective strain rate in terms of strain rates in principal direction for the von Mises yield criterion can be obtained as:

$$\dot{\bar{\varepsilon}} = \sqrt{\frac{2}{3} (\dot{\varepsilon}_1^2 + \dot{\varepsilon}_2^2 + \dot{\varepsilon}_3^2)} \quad (\text{Eq 5.63})$$

Effective strain is obtained by integrating strain over time as:

$$\bar{\varepsilon} = \int_{t_0}^t \dot{\bar{\varepsilon}} dt \quad (\text{Eq 5.64})$$

5.13 Hardening Laws

The yield surface defines the criterion that specifies the start of the plastic deformation. As explained in Chapter 4 of this volume, after the start of plastic deformation and further loading in the tensile or balanced biaxial tests, the material deforms plastically and shows increase in strength with further increased plastic strain until failure. This phenomenon is commonly referred to as *strain-hardening behavior* of the materials. In the case of multiaxial loading as in sheet metal forming, which also involves loading and unloading, the strain-hardening behavior can be expressed using the yield criterion described in previous sections and the hardening laws that are explained below.

Isotropic Hardening Law. With the isotropic hardening law, the metal continues to yield plastically with further loading when the equivalent stress calculated using the yield criterion exceeds the flow stress at the current plastic strain. It can be expressed as:

$$f = f_Y(\sigma_{ij}) - \bar{\sigma}_Y(\varepsilon_p) \quad (\text{Eq 5.65})$$

where f_Y is the expression for yielding proposed by different yield criteria discussed in preceding sections, and $\bar{\sigma}_Y(\varepsilon_p)$ is the expression of flow stress as a function of plastic strain obtained from tensile or biaxial tests. In describing the strain-hardening behavior, the isotropic hardening rule results in the initial yield surface proposed by various yield criteria to expand uniformly without any change to the location or shape, as shown in Fig. 5.15 for von Mises yield criterion (Ref 5.10).

Although the isotropic hardening rule is very simple to represent, it does not model the Bauschinger effect commonly observed in the metals during reverse loading. During reverse loading, isotropic yielding predicts higher stress for yielding compared to experimental observations (Fig. 5.16). Capturing this behavior is essential in sheet metal forming, especially for spring-

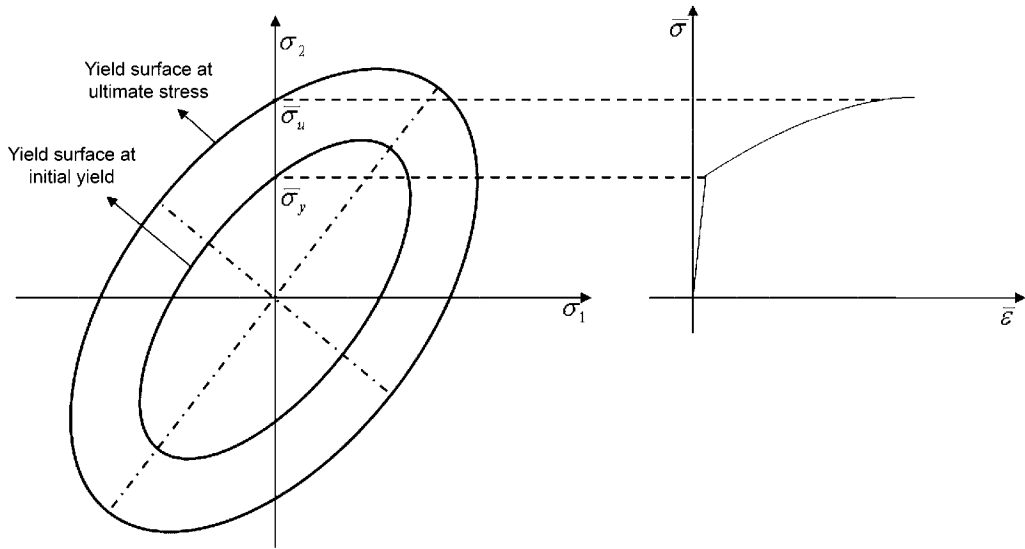


Fig. 5.15 Isotropic hardening for the von Mises yield criterion

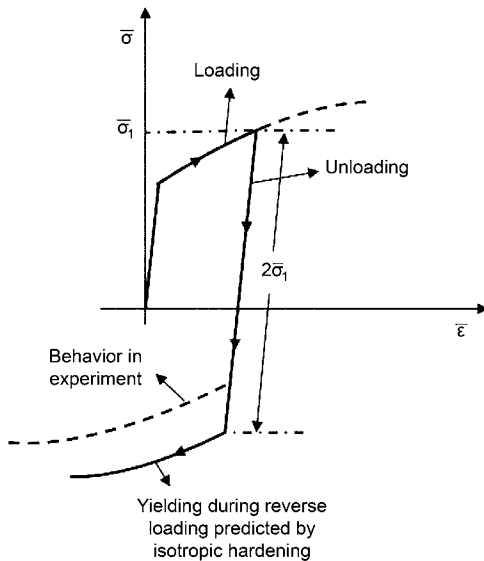


Fig. 5.16 The Bauschinger effect in metals and the yielding predicted during reverse loading by isotropic hardening

back prediction as the sheet material undergoes reverse loading during bending and unbending when it flows over a radius and eventually springs back after forming.

Kinematic Hardening Law. The kinematic hardening law states that the initial yield surface translates in the stress space with further loading without changing its size to model the

strain-hardening behavior in the multiaxial stress state. This can be expressed as:

$$f = f_Y(\sigma_{ij} - \alpha_{ij}) - k^2 \quad (\text{Eq 5.66})$$

where f_Y is the expression for yielding proposed by different yield criteria discussed for Eq 5.65, k is the constant equal to initial yield stress, and α_{ij} represents the translation in the stress space, commonly referred as *back stress*.

Prager's kinematic hardening rule states that the direction of the yield surface translation is proportional to the plastic strain increments:

$$d\alpha_{ij} = C d\epsilon_{ij}^p \quad (\text{Eq 5.67})$$

where C is a material constant. Prager's kinematic hardening rule results in the initial yield surface moving along the direction of the plastic strain increment, as shown in Fig. 5.17.

Ziegler's kinematic hardening rule states that the direction of the yield surface translation is proportional to the line joining the center of the yield surface to the current stress point on the yield surface. It can be expressed as:

$$d\alpha_{ij} = (\sigma_{ij} - \alpha_{ij}) d\mu \quad (\text{Eq 5.68})$$

where $d\mu$ is a positive scalar that can be obtained from the condition that the stress point

remains on the yield surface after translation. The translation of the yield surface based on Ziegler's kinematic condition is shown in Fig. 5.18.

Both Ziegler's and Prager's kinematic hardening laws result in yielding at very low stress during reverse loading compared with that observed in experiments, as shown in Fig. 5.19. Therefore, kinematic hardening is not sufficient enough to model the materials behavior during reverse loading (Ref 5.10).

Mixed Hardening Law. The mixed hardening law combines the isotropic and Prager's kinematic hardening laws to better address the Bauschinger effect. With the mixed hardening law, the yield surface expands in shape uniformly and translates in the stress space. It is expressed as:

$$f = f_Y(\sigma_{ij} - \alpha_{ij}) - \bar{\sigma}_Y(\epsilon^p) \quad (\text{Eq 5.69})$$

where f_Y is the expression for yielding proposed by different yield criteria discussed in preceding sections, $\bar{\sigma}(\epsilon^p)$ is the stress strain relationship from uniaxial or biaxial test, and α_{ij} represents the translation in the stress space. It is commonly referred as *back stress*.

The plastic strain is represented in two parts, isotropic and kinematic contribution:

$$d\epsilon^p = d\epsilon^{pi} + d\epsilon^{pk} = M d\epsilon^p + (1-M) d\epsilon^p \quad (\text{Eq 5.70})$$

where $d\epsilon^{pi}$ is the plastic strain increment for isotropic hardening part, $d\epsilon^{pk}$ is the plastic strain increment for kinematic hardening part, and M is the constant, where $M = 1$ corresponds to iso-

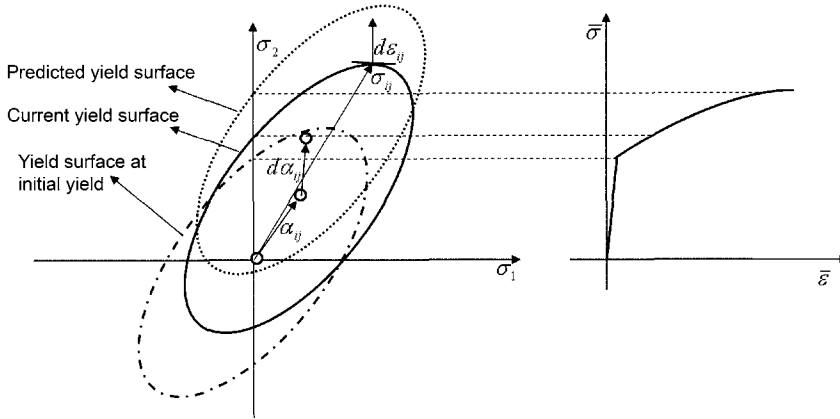


Fig. 5.17 Prager's kinematic hardening for the von Mises yield criterion

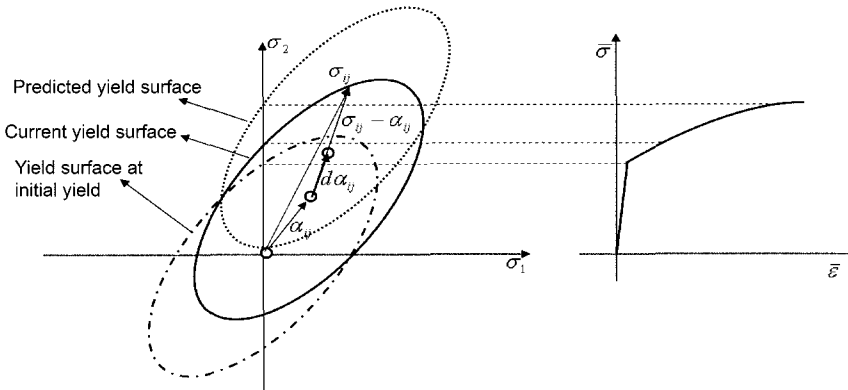


Fig. 5.18 Ziegler's kinematic hardening for the von Mises yield criterion

tropic hardening and $M=0$ corresponds to kinematic hardening.

The back-stress increment for kinematic hardening part is given by Prager's kinematic model as:

$$d\alpha_{ij} = C(1-M)d\epsilon_{ij}^p \quad (\text{Eq 5.71})$$

The rate of expansion of the yield surface is given by:

$$d\bar{\sigma}_y = \frac{d\bar{\sigma}_y}{d\bar{\epsilon}^{pi}} M d\bar{\epsilon}^p \quad (\text{Eq 5.72})$$

where $d\bar{\sigma}_y/d\bar{\epsilon}^{pi}$ is the tangent modulus at the equivalent isotropic plastic strain of $\bar{\epsilon}^{pi}$.

The constant C can be estimated using consistency condition that yield stress lie on the yield surface as:

$$C = \frac{2 \frac{d\bar{\sigma}_y}{d\bar{\epsilon}^p} - M \frac{d\bar{\sigma}_y}{d\bar{\epsilon}^{pi}}}{1 - M} \quad (\text{Eq 5.73})$$

where $d\bar{\sigma}_y/d\bar{\epsilon}^p$ is the tangent modulus at the equivalent isotropic plastic strain of $\bar{\epsilon}^p$.

Alternatively, the rate of translation of yield surface and rate of expansion can also be obtained:

$$d\alpha_{ij} = \frac{2}{3} \frac{d\bar{\sigma}_y}{d\bar{\epsilon}^p} (1-M) d\epsilon_{ij}^p \quad (\text{Eq 5.74})$$

$$d\bar{\sigma}_y = \frac{d\bar{\sigma}_y}{d\bar{\epsilon}^p} M d\bar{\epsilon}^p \quad (\text{Eq 5.75})$$

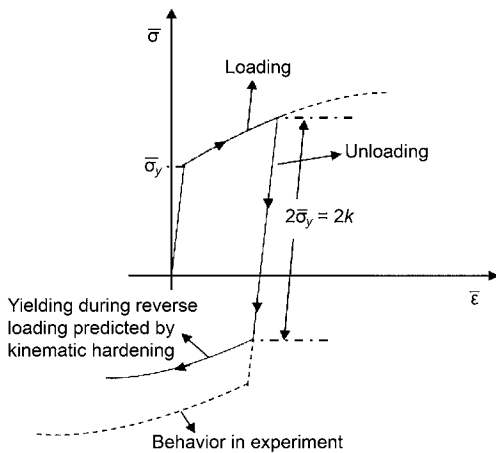


Fig. 5.19 The Bauschinger effect in metals and the yielding predicted during reverse loading by kinematic hardening

where M is a constant: $M = 1$ corresponds to isotropic hardening, and $M = 0$ corresponds to kinematic hardening (Ref 5.11).

Nonlinear Hardening Models. Mixed hardening models can predict the Bauschinger effect. However, they cannot model exactly the nonlinear transient behavior at the start of plastic deformation during reversal loading. Fredrick and Armstrong introduced a nonlinear hardening model based on Prager's kinematic hardening model with a nonlinear term to express the back stress. Chaubocche further refined this model, which can be expressed as:

$$d\alpha_{ij} = \frac{2}{3} C d\epsilon_{ij}^p - \gamma \alpha_{ij} d\bar{\epsilon}^p \quad (\text{Eq 5.76})$$

where C and γ are constants and $d\bar{\epsilon}^p$ is the effective plastic strain increment expressed by Eq 5.63. This kinematic hardening model can be used in mixed hardening models to model the translation of the yield surfaces (Ref 5.12).

Yoshida-Uemori Model. Material behavior during cyclic loading and unloading is quite complex, as shown in Fig. 5.20. During unloading, the path is not linear, and there is an early plastification, followed by a transient Bauschinger effect, where the material starts to yield during reverse loading, followed by work-hardening stagnation, where the yield stress remains constant with increased strain, followed by strain hardening (Ref 5.14).

Yoshida and Uemori proposed a nonlinear hardening model based on two surface models

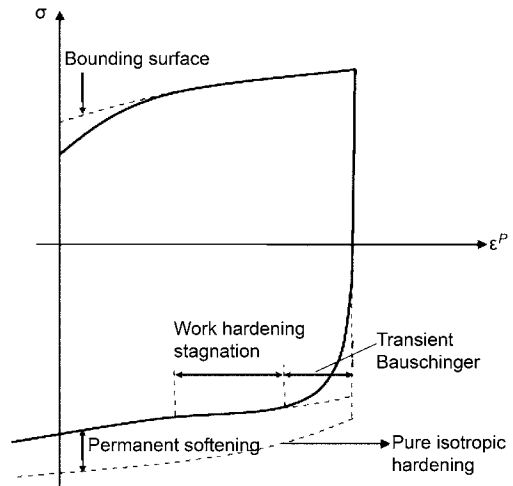


Fig. 5.20 Hardening behavior during unloading and reverse loading observed in experiments (Ref 5.13)

to better capture the unloading and reverse loading behavior. This model involves two surfaces: the yield surface and the bounding surface. Yield surface f of size Y translates within the bounding surface with back stress α , while bounding surface F translates with back stress β and expands uniformly in shape by R , as shown in Fig. 5.21.

In high-strength steels, during unloading the unloading modulus is observed to change with the plastic strain. This plays a significant role in springback predictions. In the Yoshida-Uemori model this variation of unloading modulus is represented using the exponential function:

$$E = E_0 - (E_0 - E_a) \left(1 - \exp(-\zeta \bar{\epsilon}^p) \right) \quad (\text{Eq 5.77})$$

where E_0 , E_a , and ζ are material constants to be estimated from the material test, and $\bar{\epsilon}^p$ is the plastic strain.

To model sheet materials using the Yoshida-Uemori model, the constants Y , B , m , b , R_{sat} , C , h , E_0 , E_a , and ζ need to be estimated from tests (Ref 5.15). Ghaei and colleagues (Ref 5.13) compared the springback predicted using isotropic hardening, mixed hardening, and the Yoshida-Uemori model for U-channel parts with experiments for DP600 material and found that the Yoshida-Uemori model predictions were close to the experimental measurements.

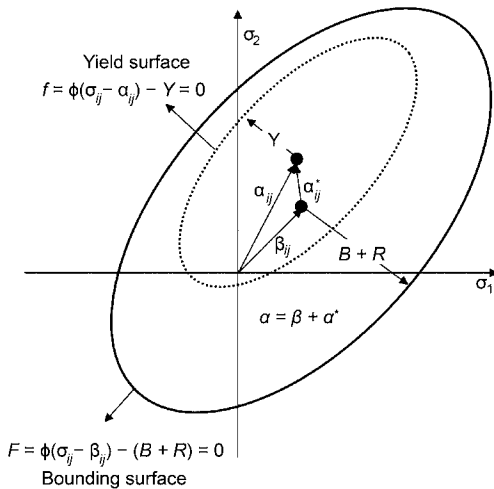


Fig. 5.21 The Yoshida-Uemori model illustrating the bounding surface and yield surface (Ref 5.14, 5.15)

REFERENCES

- 5.1 T. Altan, G. Ngaile, and G. Shen, *Cold and Hot Forging: Fundamentals and Applications*, ASM International, 2005
- 5.2 D. Banabic, H.J. Bunge, K. Pohlandt, and A.E. Tekkaya, *Formability of Metallic Materials—Plastic Anisotropy, Formability Testing, Forming Limits*, Springer, 2000.
- 5.3 R. Hill, *Mathematical Theory of Plasticity*, Oxford University Press, 1956
- 5.4 R. Hill, Constitutive Modelling of Orthotropic Plasticity in Sheet Metals, *Journal of the Mechanics and Physics of Solids*, Vol 38, 1990, p 405–417
- 5.5 F. Barlat and J. Lian, Plastic Behavior and Stretchability of Sheet Metals. Part I: A Yield Function for Orthotropic Sheets under Plane Stress Conditions, *International Journal of Plasticity*, Vol 5, 1989, p 51–66
- 5.6 F. Barlat, D.J. Lege, and J.C. Brem, A Six-Component Yield Function for Anisotropic Materials, *International Journal of Plasticity*, Vol 7, 1991, p 693–712
- 5.7 F. Barlat, R.C. Becker, Y. Hayashida, Y. Maeda, M. Yanagawa, K. Chung, J.C. Brem, D.J. Lege, K. Matsui, S.J. Murtha, and S. Hattori, Yielding Description of Solution Strengthened Aluminum Alloys, *International Journal of Plasticity*, Vol 13, 1997, p 385–401
- 5.8 F. Barlat, Y. Maeda, K. Chung, M. Yanagawa, J.C. Brem, Y. Hayashida, D.J. Lege, K. Matsui, S.J. Murtha, S. Hattori, R.C. Becker, and S. Makosey, Yield Function Development for Aluminum Alloy Sheets, *Journal of the Mechanics and Physics of Solids*, Vol 45, 1997, p 1727–1763
- 5.9 Z. Marciniak, J.L. Duncan, and S.J. Hu, *The Mechanics of Sheet Metal Forming*, Butterworth-Heinemann, 2002
- 5.10 A.S. Khan, and S. Huang, *Continuum Theory of Plasticity*, John Wiley and Sons, 1995
- 5.11 K.J. Bathe, and F.J. Montans, On Modeling Mixed Hardening in Computational Plasticity, *Computers and Structures*, Vol 82, 2004, p 535–539
- 5.12 J. Lemaitre and J.-L. Chaboche, *Mechanics of Solid Materials*, Cambridge University Press, 1990

- 5.13 A. Ghaei, D.E. Green, and A. Taherizadeh, Semi-implicit Numerical Integration of Yoshida-Uemori Two Surface Plasticity Model, *International Journal of Mechanical Sciences*, Vol 52, 2010, p 531–540
- 5.14 F. Yoshida and T. Uemori, A Model of Large Strain Cyclic Plasticity Describing the Bauschinger Effect and Work Hardening Stagnation, *International Journal of Plasticity*, Vol 18, 2002, p 661–686
- 5.15 F. Yoshida and T. Uemori, A Model of Large-Strain Cyclic Plasticity and Its Application to Springback Simulation, *International Journal of Mechanical Sciences*, Vol 45, 2003, p 1687–1702

CHAPTER 6

Materials for Sheet Forming

Soumya Subramonian and Nimet Kardes, The Ohio State University

FORMING APPLICATIONS may range from simple bending to stamping and deep drawing of complex shapes. To produce good quality parts, it is essential to know the forming characteristics or formability of the sheet material under the conditions in which it is formed. Formability refers to the ability of a sheet metal to be deformed into a desired shape while maintaining structural integrity without tearing, buckling and wrinkling, excessive thinning, and so on. Various criteria of formability—as described in Chapter 4, “Plastic Deformation—Flow Stress, Anisotropy, and Formability,” in this book—also have been developed, depending on the nature of the forming operation and the applied forces.

The most common materials for sheet forming include various types of sheet steels, stainless steels, aluminum and its alloys, and magnesium alloys. This chapter gives an overview of the classification, designation, and properties relevant to forming of low-carbon steels, stainless steels, and aluminum and magnesium alloys. Advanced high-strength steels (AHSSs), which are an important category of sheet steels for weight reduction in the automotive industry, are discussed in Chapter 6, “Forming of Advanced High Strength Steels,” of the companion book, *Sheet Metal Forming—Processes and Applications* (Ref 6.1).

In addition, this chapter gives flow stress data of various sheet metal alloys under biaxial loading based on viscous pressure bulge (VPB) tests, also referred to as the hydraulic bulge test (see Chapter 4). The tests were conducted at Engineering Research Center for Net Shape Manufacturing in order to obtain the flow stress characteristics of various sheet materials, such as

steels, stainless steels, and aluminum and magnesium alloys. These flow curves are better suited for analysis of forming operations when compared to flow stress obtained from tensile tests. For some of the sheet materials, flow stress curves obtained by tensile tests also are provided.

6.1 Low-Carbon Sheet Steels

Steels are the most widely used sheet materials because of their relative strength, good formability, and moderate cost. They also provide a wide range of mechanical properties, from moderate yield strength levels of 200 to 300 MPa (29 to 43 ksi) with excellent ductility to yield strengths exceeding 1400 MPa (203 ksi) for some types of high-strength low-alloy (HSLA) steels.

Sheet steels are supplied over a wide range of chemical compositions, but the vast majority are unalloyed, low-carbon steels selected for stamping applications, such as automobile bodies and appliances. For these major applications, typical compositions are 0.03 to 0.10% C, 0.15 to 0.50% Mn, 0.035% P (max), and 0.04% S (max). Low-carbon steels with carbon content from 0.05% to 0.2% are used for stamping, but high-formability steels contain less than 0.1% C. They are generally cold rolled and annealed. They are used in automotive body panels and appliances. Aluminum-killed steels are also preferred for deep-drawing applications.

In the past, rimmed (or capped) ingot cast steel has been used because of its lower price. More recently, however, rimmed steels have been largely replaced by killed steels produced

by the continuous casting process. Continuous casting is inherently suited to the production of killed steels, but killed steels are also produced by ingot metallurgy. Regardless of the method of casting or manufacture, killed steels are preferred because they have better formability and are not subject to aging or strain aging (that is, mechanical properties do not change with time).

Classification of sheet steels can be based on various descriptors, such as:

- Chemical compositions (plain carbon, low alloy, stainless steel, etc.)
- Required strength level (as specified in ASTM standards)
- Finishing method (hot rolling, cold rolling, etc.)
- Quality descriptors (commercial quality, draw quality, etc.)

Low-carbon steels are the most commonly used sheet metal because of their low cost and good formability. However, ordinary low-strength, low-carbon sheet steel are being replaced by a number of HSLA steels and advanced high strength steels (AHSSs). Also, coated steels and stainless steels are produced for corrosion protection of sheet products. This section describes the classification and forming characteristics of low-carbon and HSLA sheet steels. Coated steel sheet and stainless steels are discussed in separate sections, while AHSS forming is detailed in Chapter 6, “Forming of Advanced High Strength Steels,” of the companion book, *Sheet Metal Forming—Processes and Applications* (Ref 6.1).

Forming Grades and Properties

Low-carbon steels, coated and uncoated, are generally supplied as commercial-quality, drawing-quality, and drawing-quality special-

killed grades. AISI designations of some of the draw quality steels are given in Table 6.1. The compositions of steels commonly used in stamping are given in Table 6.2.

Drawing quality (DQ) materials are suitable for deep drawing of parts and formed components that require severe deformation. For very severe deformations, drawing quality special killed (DQSK) is specified. Generally, DQ or DQSK material is not ordered to a specific chemical composition and does not need any other mechanical requirements.

Typical mechanical properties of low-carbon sheet steels are given in Table 6.3. Materials with high plastic-strain ratio, r , have better deep-drawing characteristics. Materials with

Table 6.1 Specifications and designations of some of the steels used in stamping

Quality/temper	AISI-SAE grade designation
Hot rolled and cold rolled sheets	
Commercial quality	1008–1012
Drawing quality	1006–1008
Drawing quality, special killed	1006–1008

Source: Ref 6.2

Table 6.2 Composition ranges and limits for low-carbon sheet steels

ASTM specification	Description(a)	Composition, %			
		C	Mn	P	S
A 619	CR DQ	0.10	0.50	0.025	0.035
A 620	CR DQSK	0.10	0.50	0.025	0.035
A 569	HR CQ	0.15	0.60	0.035	0.040
A 621	HR DQ	0.10	0.50	0.025	0.035
A 622	HR DQSK	0.10	0.50	0.025	0.035

(a) CQ, commercial quality; CR, cold rolled; DQ, drawing quality; DQSK, drawing quality special killed; HR, hot rolled. Source: Ref 6.2

Table 6.3 Typical mechanical properties of low-carbon sheet steels

Quality level	Tensile strength		Yield strength		Elongation in 50 mm (2 in.), %	Plastic-strain ratio (r)	Strain-hardening exponent (n)	Hardness (HRB)
	MPa	ksi	MPa	ksi				
Hot rolled								
Commercial quality	358	52	234	34	35	1.0	0.18	58
Drawing quality	345	50	220	32	39	1.0	0.19	52
Drawing quality, aluminum killed	358	52	234	34	38	1.0	0.19	54
Cold rolled, box annealed								
Commercial quality	331	48	234	34	36	1.2	0.20	50
Drawing quality	317	46	207	30	40	1.2	0.21	42
Drawing quality, aluminum killed	303	44	193	28	42	1.5	0.22	42
Interstitial free	310	45	179	26	45	2.0	0.23	44
Source: Ref 6.3								

Source: Ref 6.3

high values of n , mean good formability in stretching operations because they promote uniform strain distribution but have little effect on drawability. Table 6.4 compares forming features of some cold rolled sheet steels.

Figures 6.1 and 6.2 show the flow stress curves of aluminum-killed draw quality steel and deep-draw quality steel, respectively. The flow stress curves are obtained using uniaxial tensile test and the biaxial VPB (viscous pressure bulge) test. The flow stress data given by the biaxial VPB tests is obtained under conditions similar to those present in forming operations like stamping. It can also be noted that VPB tests give a larger range of strain values because of the biaxial nature of strain. The flow stress curves of other carbon steels are given in appendix A of this book.

Some steel mills also offer specialized grades, such as interstitial-free deep-drawing steels and enameling steels. Grade designations of common formable grades include:

- Commercial-quality (CQ) steel
- Drawing steel (DS)
- Extra-deep-drawing steel (EDDS)
- Extra-deep-drawing steel plus (EDDS+)
- Structural steel (SS)
- High-strength low-alloy (HSLA) steel
- Dent-resistant (DR) steel
- Bake-hardenable (BH) steel
- Inclusion-shape-controlled steel

Modified Low-Carbon Steel Sheet. In addition to the low-carbon steel sheet and strip products, there are numerous low-carbon steels with slightly modified chemical compositions to satisfy specific customer requirements. For example, in structural-quality (SQ) steels, alloying additions of manganese and phosphorus are used to increase strength by substitutional solid-solution strengthening: approximately 3 MPa (0.4 ksi) per 0.1% Mn, and 7 MPa (1 ksi) per 0.0 1% P. Hot rolled SQ steels contain 0.90 to

Table 6.4 Cold rolled steel sheet forming features and typical mechanical properties determined using tensile test

Type or quality	Special feature	Yield strength		Tensile strength		Elongation in 50 mm (2 in.), %	Hardness (HRB)	Strain-hardening exponent (n)	Plastic-strain ratio (r)
		MPa	ksi	MPa	ksi				
Commercial	Standard properties	234	34	317	46	35	45	0.18	1.0
Drawing (rimmed)	Stretchable	207	30	310	45	42	40	0.22	1.2
Drawing (special killed)	Deep drawing	178	25	296	43	42	40	0.22	1.6
Interstitial free	Extra deep drawing	152	22	317	46	42	45	0.24	2.0
Medium strength	Formable	414	60	483	70	25	85	0.20	1.2
High strength	Moderately formable	689	100	724	105	10	25 ^(HRC)

Source: Ref 6.2

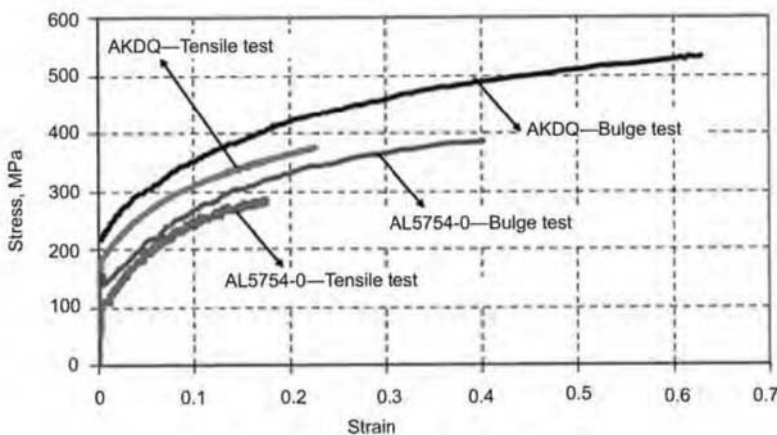


Fig. 6.1 Flow stress curves obtained from the bulge test and the tensile test for (a) aluminum killed draw quality (AKDQ steel (0.83 mm) and AL5754-O (1.3 mm). Experimental strain range for AKDQ steel: tensile, 0 to 0.24; bulge, 0 to 0.64; for AL5754-O: tensile, 0 to 0.18; bulge, 0 to 0.4.

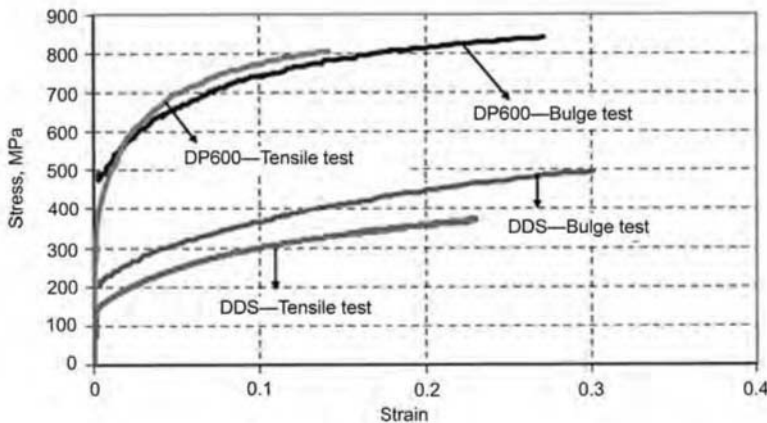


Fig. 6.2 Flow stress curves obtained from the bulge test and the tensile test for DP600 high-strength steel (0.6 mm thickness) and deep drawing steel (DDS; 0.77 mm thickness). Experimental strain range for DP600: tensile, 0 to 0.14; bulge, 0 to 0.27; for DDS: tensile, 0 to 0.23; bulge, 0 to 0.3.

1.35% max Mn and 0.035% max P. Cold rolled SQ steels contain 0.60 to 0.90% max Mn and 0.035 to 0.20% P. Carbon contents for SQ steels are generally 0.20 to 0.25%.

Interstitial-Free Steels. In interstitial-free (IF) steels, which are also referred to as extra-deep-drawing quality, the elimination of interstitials (carbon and nitrogen) is accomplished by adding sufficient amounts of carbide/nitride-forming elements (generally titanium and/or niobium) to tie up carbon and nitrogen completely, the levels of which can be reduced to less than 50 ppm by modern steelmaking/casting practices, including vacuum degassing.

Steels with very low interstitial content exhibit excellent formability with low yield strength (138 to 165 MPa, or 20 to 24 ksi), high elongation (41 to 45%), and good deep drawability. With the addition of carbonitride-forming elements, the deep drawability and the nonaging properties are further improved.

Bake-hardening (BH) steels are characterized by their ability to exhibit an increase in yield strength because of carbon strain aging during paint-baking operations at moderate temperature (125 to 180 °C, or 260 to 355 °F). Bake hardening has little effect on tensile strength. **Bake-hardening steels are finding increased use** in automotive outer-body applications (hoods, doors, fenders) to achieve an improvement in dent resistance and, in some cases, a sheet thickness reduction as well.

The bake-hardening behavior is dependent on steel chemistry and processing, in addition to the

amount of forming strain and paint-baking conditions (temperature and time). Steels that exhibit bake-hardening behavior include plain low-carbon steels (continuously annealed or batch annealed), IF steels (continuously annealed), and dual-phase steels (continuously annealed).

Automotive specifications for BH steels can be categorized according to those that specify a minimum yield strength level or a minimum bake-hardening increment, in the formed (strained) plus baked condition. The conventional test for determining bake hardenability characteristics involves a 2% tensile prestrain, followed by baking at 175 ± 5 °C (345 ± 10 °F). The resulting increase in yield strength measures the bake hardenability of the material.

While all the specifications call for a minimum yield strength level in the as-received (that is, prior to forming) condition, some also require a minimum yield strength after baking the as-received material in the absence of any tensile prestrain. The as-received yield strength is in the range of 210 to 310 MPa (30 to 45 ksi) (compared with approximately 175 MPa, or 25 ksi, for DQSK), while the final yield strength, that is, after 2% prestrain plus bake, ranges between 280 and 365 MPa (40 to 53 ksi) (compared with approximately 225 MPa, or 33 ksi, for DQSK).

The HSLA steels are generally formed at room temperature using conventional equipment. Cold forming should not be done at temperatures below 10 °C (50 °F). As a class, high-strength steels are inherently less formable than

low-carbon steels because of their greater strength and lower ductility. This reduces their ability to distribute strain. The greater strength makes it necessary to use greater forming pressure and to allow for more springback compared to low-carbon steels. However, high-strength steels have good formability, and straight bends can be made to relatively tight bend radii, especially with the grades having lower strengths and greater ductility. Further, high-strength steels can be stamped to relatively severe shapes, such as automotive bumper facings, wheel spiders, and engine-mounting brackets.

High-strength low-alloy steels can be hot formed. However, hot forming usually alters mechanical properties, and a particular problem that arises in many applications is that some of the more recent thermomechanical processing techniques (such as controlled rolling), used for plates in particular, are not suitable where hot forming is used during fabrication. This problem can be circumvented by the use of a rolling finishing temperature that coincides with the hot forming temperature (900 to 930 °C, or 1650 to 1700 °F). Subsequent hot forming therefore simply repeats this operation, and deterioration in properties is then small or even absent, provided that grain growth does not occur. Producers should be consulted for recommendations of specific hot forming temperatures and for comments on their effects on mechanical properties.

General Forming Characteristics

General forming characteristics of the more commonly used formable grades are:

- *Commercial-Quality (CQ) Steel:* Available in hot rolled, cold rolled, and coated grades; the least expensive grade of sheet steel; subject to aging (mechanical properties may deteriorate with time); **not intended for difficult-to-form shapes**
- *Drawing Steel (DS):* Available in hot rolled, cold rolled, and coated grades; exhibits better ductility than CQ-grade steels but has low plastic-strain ratio (r) values; subject to aging (mechanical properties may deteriorate with time); has excellent base metal surface quality
- *Drawing-Quality Special-Killed (DQSK) Steel:* Available in hot rolled, cold rolled, and coated grades, with good forming capabilities; not subject to aging (mechanical properties do not change with time)
- *Interstitial-Free Steels:* Available in cold rolled and coated grades, with excellent forming capabilities for deep drawing (as EDDS or EDDS+ grades)
- *Enameling Steels:* Available in cold-rolled grades. Various types of processing are used to make a product that is satisfactory for porcelain enameling. All grades have good forming capabilities.
- *Structural Steels:* When higher strength is required, structural-quality sheet, also called **physical-quality sheet**, can be specified, although at some sacrifice in ductility.
- *Higher-Strength Steel Sheets:* Available in hot rolled, cold rolled, and coated grades. Various types of processing are used to obtain the desired strength levels. In general, the formability of these grades decreases as yield strength increases. Springback may be a problem at lower sheet thicknesses.
- *Inclusion-Shape-Controlled Steels:* Cold formability has been substantially improved by inclusion-shape-controlled steels, which enables steel to be formed to nearly the same extent in both the longitudinal and transverse directions. Any grade produced with inclusion shape control can be more severely formed than a grade of the same strength level produced without inclusion shape control. Inclusion-shape-controlled steels are responsible for the moderately good formability of the higher-strength HSLA steels, such as the grades having 550 MPa (80 ksi) yield strengths.

Effect of Composition on Formability. An increase in carbon content increases the strength of steel and reduces formability. Phosphorus and sulfur increase the likelihood of cracking or splitting and are not desirable for forming, drawing, or bending operations. Silicon increases the strength of steel and hence reduces formability. Copper is added to improve corrosion resistance but has no significant effect on strength. Titanium helps in developing high normal anisotropy values. Boron is added to improve hardenability and is most effective in low-carbon steels.

Effect of Steelmaking Methods on Formability. Cold rolled steels generally have a better surface finish than hot rolled steels and are preferred for forming operations. Draw quality rimmed steels, which are available as both hot rolled and cold rolled have excellent formabil-

ity, and they are more suitable for stretch-type forming operations than for deep drawing. Aluminum-killed steels are generally recommended for deep drawing. Interstitial-free steels especially coated ones, deep draw better than other grades of steels with less breakage.

Effect of Microstructure on Formability.

Coarse-grained steels are better formable than fine-grained steels, which are stronger. Grain shape also affects formability. Aluminum-killed steels have good formability and have equiaxed grains. Micro constituents affect the formability by influencing the strength of steel. Alloying elements that dissolve in ferrite increase the strength of steel, and nonmetallic inclusions induce cracking at the edge of the part while forming and hence affect formability.

6.2 Coated Sheet Steels

Nearly every type of sheet steel commonly used in the automotive, appliance, or building industries is available coated, from high-strength steels used for automotive structural members, steel roofing, and architectural framing to vacuum-degassed interstitial-free steels used in applications demanding the highest available formability.

Common steel coatings include zinc, aluminum, tin, lead, nickel, and various alloys of these metals, as well as a range of organic coatings. Coatings such as porcelain enamels and electroplated copper or chromium are also commonly found on sheet steel parts, but these are typically applied after forming and are not discussed here. Most coatings commonly used on sheet steel substrates have corrosion resistance as their primary function, although appearance is often important as well, especially for the organic coatings. Application methods vary widely and include dipping in a molten bath (zinc, aluminum, tin, and terne—a lead-tin alloy), electroplating (zinc and tin), and spraying or roll coating (paints or organics).

Coated flat rolled steels are formed using the same general equipment, tooling, and lubrication used to form uncoated steels. While the properties of the base steel remain the primary determinants of the formability of a coated product, coatings do have an effect on the forming process and must be taken into account when designing parts, dies, and forming strategies. Coatings have frictional effects that may affect formability of the material. In some cases,

the coating process may affect the substrate. For example, galvannealing affects the material properties and formability of the base metal and leads to lower formability compared to uncoated low-carbon steels.

Zinc Coatings. Steel sheets are protected from rust by using a process called galvanizing by applying a zinc coating. During galvanizing, the zinc metallurgically bonds to the steel and creates a zinc-iron alloy layer topped by a layer of impact-resistant pure zinc. The resulting coated steel can be used in much the same way as uncoated steel. A large amount of galvanized steel is used by the automotive industry for exposed and unexposed panels.

Galvannealed steels are those that are given a secondary heat treatment after the hot dip galvanization. The galvannealed steels have advantages with respect to welding and paint adhesion. The coating is harder than pure zinc and is more prone to peeling during forming. It is not easily scratched while handling.

Aluminum Coatings. Aluminum-coated steel sheets are used in applications where heat resistance, heat reflectivity, or corrosion resistance is required. Aluminum-coated steel sheets combine the desirable properties of both steel and aluminum. Only moderate forming of aluminumized steel sheets is recommended. The protective value of aluminum coating depends on coating thickness. They are used in automotive mufflers and related components, household appliances, industrial heating equipment, and so forth.

Aluminum-Zinc Alloy Coatings. Aluminum-zinc alloy coatings have improved corrosion resistance of galvanized parts. One type consists of about 55% Al and 45% Zn; the other type, zinc plus 5% Al. These coatings give improved coating ductility compared to hot dip galvanized coatings. Sheets coated with aluminum-zinc alloy are also good for deep drawing.

Phosphate Coatings. Phosphate coating consists of treatment of the sheet metal with a dilute solution of phosphoric acid and other chemicals. This makes the top layer of the sheet less reactive than the metal surface and also more absorbent of lubricants and paints. Two types of phosphate coatings in general use are zinc phosphate and iron phosphate. Phosphate coating beneath a paint film helps prevent moisture and other corrosives that may penetrate the paint from reaching the metal.

Terne Coatings. Terne coatings are applied to carbon steel sheets to increase corrosion re-

sistance and formability and have excellent solderability and paintability. They are widely used in automobile gasoline tanks and are very good for applications demanding high formability. Terne is mostly lead with a small percentage of tin.

Prepainted Sheets. Prepainted sheets are those that have been painted before being manufactured into parts or finished products. The painting operation in any plant takes up costly space and requires energy, labor, raw materials, and time. This can be avoided by using prepainted sheets. The paints for coil coating are modified for flexibility, hardness, and adhesion. They adhere for flexing and can endure most forming operations from simple bending to drawing. However, a few changes are needed to form precoated sheets. Prepainted sheets are more prone to scratches, and extreme care should be taken to avoid deterioration of the painted surface. Prepainted steel can be breakpress formed, roll formed, stamped, and drawn by using padded tables and handling devices with appropriate tooling.

6.3 Stainless Steels

Stainless steels contain at least 10.5% chromium, which prevents rust because of the formation of an invisible layer of a chromium-rich oxide layer. In addition to good corrosion resistance, some stainless steels also have the ability to withstand high heat. In general, stainless steels have the following characteristics compared to carbon steels:

- Greater strength
- Greater susceptibility to work hardening

- Higher yield strength and work hardening, which results in greater springback compared to carbon steels
- Higher propensity to gall to tooling
- Lower heat conductivity, which reduces dissipation of heat from deformation and friction

However, the different types of stainless steels have more variability in properties and formability than do low-carbon sheet steels.

The different types of stainless steels include five basic categories based on microstructure: austenitic, ferritic, duplex, precipitation-hardening, and martensitic. The austenitic alloys, which have a very ductile face-centered cubic (fcc) crystal structure, are the most formable, but are the most expensive (because alloying with nickel is needed to stabilize the fcc phase). Ferritic stainless steels, which are the least alloyed and least expensive type, are less formable due their body-centered cubic (bcc) crystal structure. Formability of duplex stainless steels, which have a mixed microstructure of fcc (austenitic) and bcc (ferritic) phases, is between that of austenitic and ferritic stainless steels.

If precipitation-hardened and martensitic stainless sheet steels require forming, the forming is done in soft condition prior to hardening. The most common type of martensitic stainless steel is 420. Precipitation hardened stainless steels are designated as dead soft, quarter-hard, half-hard, three-quarters hard, and full hard.

Mechanical tensile properties of commonly used stainless steels are given in Table 6.5 Most stainless steels exhibit large strain hardening (large *n*-value), as shown in Fig. 6.3. Some stainless steels are used at elevated temperatures because they can provide superior corro-

Table 6.5 Properties of stainless steels

Type	Condition	Tensile strength, MPa	0.2% yield strength, MPa	Elongation, %	Hardness (HRB)
Austenitic stainless steel					
304	Annealed	515	205	40	92 max
304L	Annealed	480	170	40	88 max
316	Annealed	515	205	40	95 max
316L	Annealed	485	170	40	95 max
Ferritic steels					
409	Annealed	380	205	20	80 max
430	Annealed	450	205	20	88 max
439	Annealed	450	205	22	88 max
Martensitic steels					
420	Annealed	690	—	15	96 max

Source: Ref 6.2

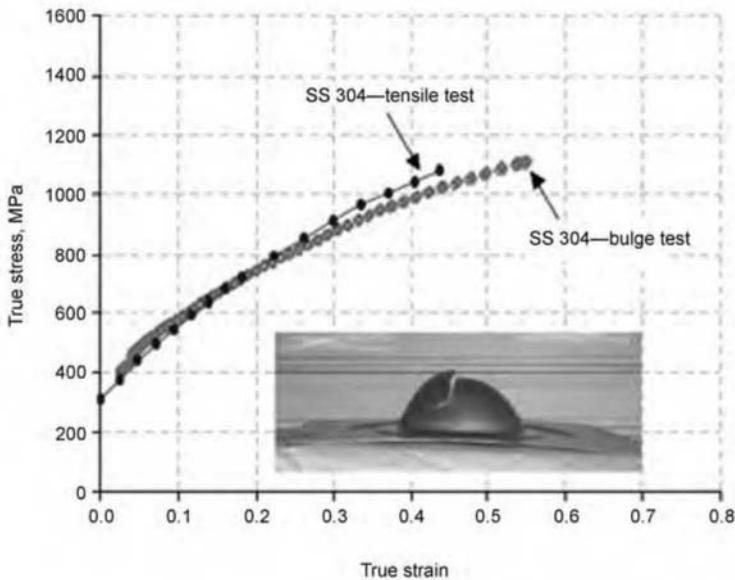


Fig. 6.3 Flow stress at room temperature for type 304 stainless steel (1 mm) obtained by viscous pressure bulge test and tensile test. Experimental strain range: tensile test, 0 to 0.44; bulge test, 0.03 to 0.56.

sion resistance and/or sufficient strengths compared to carbon steels/low alloy steels. The H-version types of stainless steels are used in high-temperature applications where temperature levels exceed 370 °C. Austenitic stainless steels offer the highest strengths at higher temperatures. However, the advantage of using ferritic stainless steels is that they offer good oxidation resistance at higher temperatures. Martensitic and precipitate hardening steels are not suitable for high-temperature applications. Stainless steels are also used in elevated temperature application that require good creep and rupture resistance.

Table 6.6 summarizes relative suitability ratings of some common stainless steels for different forming operations. These ratings are based on comparison of the steels within any one class (austenitic, ferritic, etc.). For example, a ferritic steel with an A rating is not more formable than an austenitic steel with a C rating for a particular method.

Austenitic Steels

Austenitic stainless steels are designated as 200 and 300 series. Austenitic stainless steels are the most common type of stainless steel and have greatest formability among all grades of stainless steels. Types 304, 304L, 316, and 316L are the most widely used of the austenitic group.

Austenitic steels are hardened by cold working with a wide range of strength levels obtained by cold working. Yield strength can vary from about 200 MPa in the soft (annealed) condition to more than 2000 MPa (290 ksi) in the cold-worked condition. The degree of work hardening depends on nickel content (Ref 6.2).

Formability of Austenitic Types. Type 301 steel has an extremely high rate of work hardening that results in appreciable increase in tensile strength and yield strength with increasing amount of cold working. The n -value for this alloy can be typically 0.45 or higher. For deep drawing, a lower n -value is preferred, which can be obtained by having additional nickel content—types 304, 304L, and 305, which have n -values 0.38 to 0.42, are generally used for this. The more alloying elements that are added to a 300-series alloy, the lower its work hardening and drawability. Conversion of the microstructure from austenite to martensite also increases work hardening during forming. Temperature, strain, and strain rate play important roles in controlling the change in microstructure.

Warm forming improves formability of austenitic stainless steels. When austenitic stainless steels are formed at room temperatures, the austenitic phase, being unstable, is transformed into martensite as a function of strain, strain rate, and temperature. Martensite enhances strain harden-

Table 6.6 Relative suitability of stainless steels for various methods of forming

Steel	0.2% yield strength, 6.89 MPa (1 ksi)	Suitability for:							
		Blanking	Piercing	Press-brake forming	Deep drawing	Spinning	Roll forming	Coining	Embossing
Austenitic steels									
201	55	B	C	B	A–B	C–D	B	B–C	B–C
202	55	B	B	A	A	B–C	A	B	B
301	40	B	C	B	A–B	C–D	B	B–C	B–C
302	37	B	B	A	A	B–C	A	B	B
302B	40	B	B	B	B–C	C	...	C	B–C
303, 303(Se)	35	B	B	D(a)	D	D	D	C–D	C
304	35	B	B	A	A	B	A	B	B
304L	30	B	B	A	A	B	A	B	B
305	37	B	B	A	B	A	A	A–B	A–B
308	35	B	...	B(a)	D	D	...	D	D
309, 309S	40	B	B	A(a)	B	C	B	B	B
310, 310S	40	B	B	A(a)	B	B	A	B	B
314	50	B	B	A(a)	B–C	C	B	B	B–C
316	35	B	B	A(a)	B	B	A	B	B
316L	30	B	B	A(a)	B	B	A	B	B
317	40	B	B	A(a)	B	B–C	B	B	B
321, 347, 348	35	B	B	A	B	B–C	B	B	B
Martensitic steels									
403, 410	40	A	A–B	A	A	A	A	A	A
414	95	A	B	A(a)	B	C	C	B	C
416, 416(Se)	40	B	A–B	C(a)	D	D	D	D	C
420	50	B	B–C	C(a)	C–D	D	C–D	C–D	C
431	95	C–D	C–D	C(a)	C–D	D	C–D	C–D	C–D
440A	60	B–C	...	C(a)	C–D	D	C–D	D	C
440B	62	D	...	D	D
440C	65	D	...	D	D
Ferritic steels									
405	40	A	A–B	A(a)	A	A	A	A	A
409	38	A	A–B	A	A	A	A	A	A
430	45	A	A–B	A(a)	A–B	A	A	A	A
430F, 430F(Se)	55	B	A–B	B–C(a)	D	D	D	C–D	C
442	...	A	A–B	A(a)	B	B–C	A	B	B
446	50	A	B	A(a)	B–C	C	B	B	B

Suitability ratings are based on comparison of the steels within any one class; therefore, it should not be inferred that a ferritic steel with an A rating is more formable than an austenitic steel with a C rating for a particular method. A, excellent; B, good; C, fair; D, not generally recommended. (a) Severe sharp bends should be avoided.

ing, thus delaying the onset of necking in sheet metal. While delayed necking is desirable for high formability and drawability, the martensitic phase raises forming loads, reduces formability, and decreases corrosion resistance. For further **deformation after the first forming operation**, annealing is required. However, each intermediate annealing operation slows down production and increases costs. To eliminate or reduce the intermediate annealing operations and avoid martensitic transformation, warm forming of stainless steel is an option.

In warm forming, the die and blank holder are heated (by either built-in heaters or heating

coils) to a higher temperature. For stainless steels, they are heated to 100 to 200 °C. The punch is cooled by circulating water under 10 °C. The schematic of warm forming tooling for deep drawing SS304 cups is shown in Fig. 6.4.

Experiments conducted in warm forming SS304 cups have shown that drawing at higher **temperatures gives a significantly higher limiting draw ratio, which signifies better drawability** at elevated temperatures. Figure 6.5 shows how temperature affects drawability of austenitic steel SS304. Lower velocities and higher **temperatures enable a significant increase in drawability**.

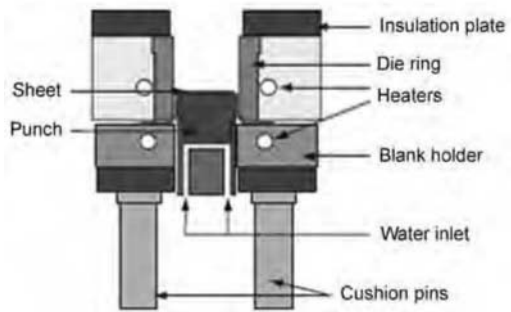


Fig. 6.4 Schematic of experimental setup for warm forming cylindrical cups of SS304 steel. Source: Ref 6.4

Ferritic Stainless Steels

Ferritic steels are designated the 400 series. They cannot be hardened by heat treatment and only moderately by cold working. This grade of steel is more popular in the automotive industry. It provides resistance to both corrosion and heat, and some 400 series steels are suitable for drawing. The common types are 409, 439, and 430.

Formability of Ferritic Types. The n -value, or work-hardening rate, of ferritic steels is 0.18 to 0.22, which is almost the same as that for low carbon steels. The r -value, or plastic strain ratio, for 409 or 430 stainless steels is about 1.1 to 1.8. A problem frequently seen in cold working of thicker (greater than 2.5 mm) ferritic steels is that at cooler temperatures and higher strain rates they fail in a brittle manner. This is because the material cannot absorb energy and deform in a ductile way below some temperatures and above some strain rates. Moderate warming (20 to 60 °C) or reduced rate of forming could be used to avoid brittle failure. When ferritic alloys are being formed in multiple stages, the alloy is warmed by deformation, although it is cold worked. The partially formed part cools before the subsequent steps and leads to brittle failure when the cycle commences again. This is because the ductile-to-brittle transition temperature, which was lower before the first stage of forming, is now increased to a higher temperature, which might be the room temperature or higher.

The strain hardening characteristics of common stainless steels are shown in Fig. 6.6. Type 409, a ferritic stainless steel, is mostly used in automotive exhaust systems. Austenitic types 304 and 304L are also used in exhaust systems, fuel tanks, chassis for buses and trucks, struc-

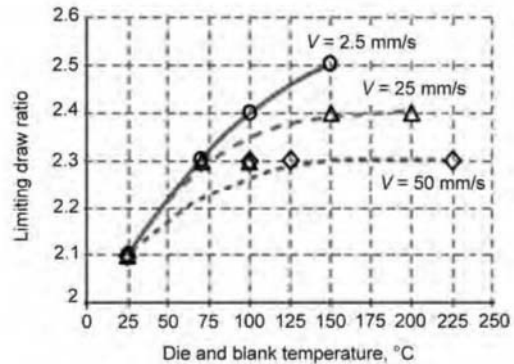


Fig. 6.5 Effect of temperature on drawability of type 304 austenitic stainless steel. Source: Ref 6.5

tural parts, and turbochargers. Types 304 and 304L are also widely used railway applications, such as carriage chassis, and in structural applications and exhaust systems. Ferritic type 430 and austenitic types 316 and 316L are used as beading for windows, doors, and handles for railways. 22Cr duplex stainless steel is used in building roofing because of its high corrosion resistance. Type 304 is used in a wide variety of applications such as the food industry because of its resistance to corrosion. It is also used in home appliances, such as sinks, stoves, and refrigerators, and in utensils and cooking appliances.

6.4 Aluminum Alloys

Aluminum alloys with a wide range of properties are used in engineering structures. Alloy systems are classified by the ANSI number system or by names indicating their main alloying constituents. Aluminum is used extensively in modern aircraft and to a significant extent in the automobile industry because of its high strength-to-weight ratio. The aluminum alloys commonly used in aircraft and other aerospace structures are 7075, 6061, 6063, 2024, and 5052. 6111, A6022, and AA6016 are commonly used in automotive body panels. The mechanical properties and chemical composition of some of the commonly used aluminum alloys in automotive applications are listed in Tables 6.7 and 6.8 for structural and body sheet applications, respectively.

Designations and Tempers. Wrought and cast aluminum alloys use different identification systems. Wrought aluminum is identified with a

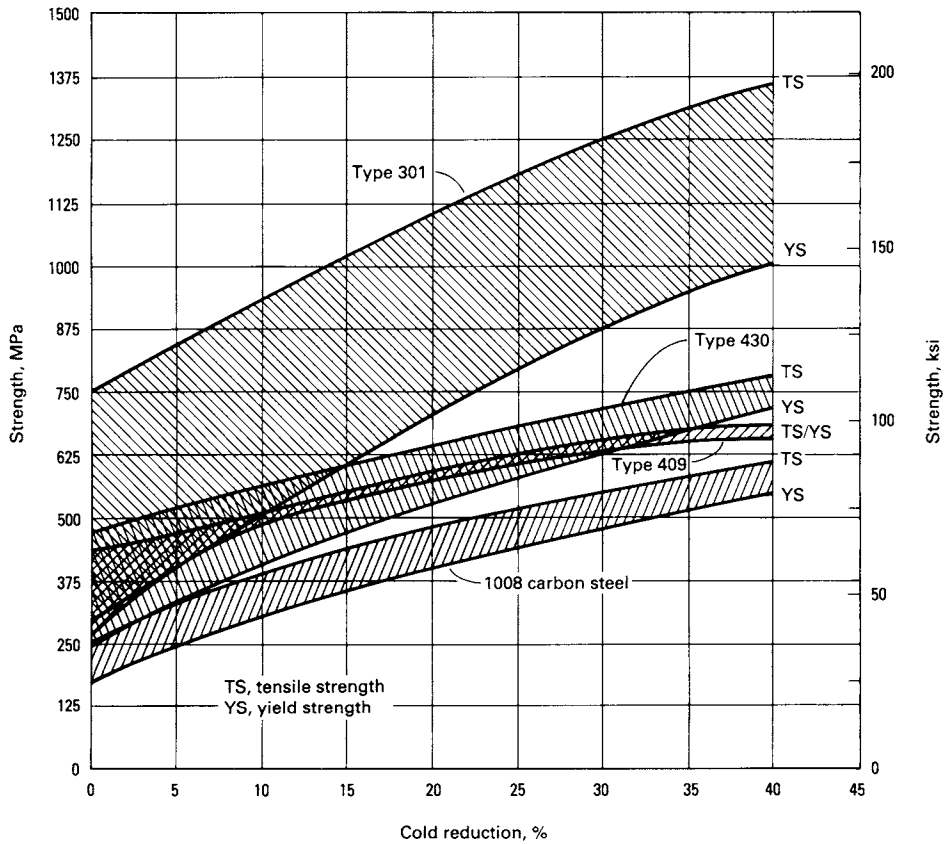


Fig. 6.6 Work-hardening qualities of type 301 austenitic stainless steel, types 409 and 430 ferritic stainless steels, and 1008 low-carbon steel. Source: Ref 6.2

Table 6.7 Chemical composition and mechanical properties of some aluminum alloys used in automotive structural parts

Alloy	Chemical composition, wt%								Mechanical properties(a)		
	Si	Fe	Cu	Mn	Mg	Cr	Zn	Ti	TS, MPa	YS, MPa	EL, %
5000 series											
AA5052	0.25	0.25	0.1	0.1	2.2–2.8	0.15–0.35	0.1	—	190	90	26
AA5182	0.25	0.35	0.15	0.2–0.5	4.0–5.0	0.1	0.25	0.1	275	125	28
AA5454	0.25	0.4	0.1	0.5–1.0	2.4–3.0	0.05–0.2	0.25	0.2	110	110	24
AA5154	0.5	0.5	0.1	0.5	3.1–3.9	0.25	0.2	0.2	105	105	27
AA5754	0.4	0.4	0.1	0.5	2.6–3.6	0.3	0.2	—	—	—	—
6000 series											
AA6061	0.4–0.8	0.7	0.15–0.4	0.15	0.8–1.2	0.04–0.35	0.25	0.15	315	275	12

(a) EL, elongation; TS, tensile strength; YS, yield strength. Source: Ref 6.6

four-digit number that identifies the alloying elements, followed by a dash, a letter identifying the type of heat treatment, and a one- to four-digit number identifying the specific temper. For example, for 6061-T6, the most common

general engineering alloy, the T denotes strength gained from thermal heat treatment; for 5083-O/H111, the next common general engineering alloy, O denotes strength gained from work hardening (Ref 6.2).

Table 6.8 Chemical composition and mechanical properties of some aluminum alloys used in automotive body sheets

Alloy	Chemical composition, wt%								Mechanical properties				
	Si	Fe	Cu	Mn	Mg	Cr	Zn	Ti	TS, MPa	YS, MPa	EL, %	<i>n</i> -Value	<i>r</i> -Value
5000 series													
AA5022	0.25	0.4	0.2–0.5	0.2	3.5–4.9	0.1	0.3	0.1	275	135	30	0.3	0.67
AA5023	0.25	0.4	0.2–0.5	0.2	5.0–6.2	0.1	0.3	0.1	285	135	33	—	—
AA5182	0.25	0.35	0.15	0.2–0.5	4.0–5.0	0.1	0.3	0.1	265	125	28	0.33	0.8
AA5052	0.25	0.25	0.1	0.1	2.2–2.8	0.15–0.35	0.1	—	190	90	26	0.26	0.66
6000 series													
AA6022	0.8–1.5	0.05–0.2	0.01–0.11	0.02–0.1	0.45–0.7	0.1	0.3	0.2	275	155	31	0.25	0.6
AA6016	1.0–1.5	0.5	0.2	0.2	0.25–0.6	0.1	0.2	0.2	235	130	28	0.23	0.7
AA6111	0.7–1.1	0.4	0.5–0.9	0.15–0.45	0.5–1.0	0.1	0.2	0.1	290	160	28	0.26	0.6

(a) EL, elongation; TS, tensile strength; YS, yield strength. Source: Ref. 6.6

Naming Scheme for Wrought Alloys

- 1xxx: controlled unalloyed (pure) compositions
- 2xxx: alloys in which copper is the principal alloying element, although other elements, notably magnesium, may be specified
- 3xxx: alloys in which manganese is the principal alloying element
- 4xxx: alloys in which silicon is the principal alloying element
- 5xxx: alloys in which magnesium is the principal alloying element
- 6xxx: alloys in which magnesium and silicon are principal alloying elements
- 7xxx: alloys in which zinc is the principal alloying element, but other elements such as copper, magnesium, chromium, and zirconium may be specified
- 8xxx: alloys including tin and some lithium compositions characterizing miscellaneous compositions
- 9xxx: reserved for future use

Basic Temper Designations

- F: as fabricated
- O: annealed
- H: strain hardened (wrought products only)
- W: heat treated
- T: solution heat treated

Some of Commonly Used T Tempers

- T3: solution heat treated and then cold worked
- T4: solution heat treated and naturally aged
- T5: cooled from an elevated temperature shaping process and then artificially aged
- T6: solution heat treated and then artificially aged

Aluminum Designations for Strain-Hardened Products

- H1: strain hardened only
- H2: strain hardened and partially annealed
- H3: strain hardened and stabilized

Heat Treatment of Aluminum Alloys. Some aluminum alloys are heat treated in order to increase the strength and hardness by precipitation hardening. The term *heat treatable* serves to distinguish the heat-treatable alloys from those alloys in which no significant strength improvement can be achieved by heating and cooling. 2xxx, 6xxx and 7xxx are heat treatable aluminum alloys. Heat treatment to increase strength of aluminum alloys is a three-step process:

1. Solution heat treatment: dissolution of soluble phases
2. Quenching: development of super saturation
3. Age hardening: precipitation of solute atoms either at room temperature (natural aging) or elevated temperature (artificial aging or precipitation heat treatment)

Solution Heat Treatment. This involves a heat treatment process in which the alloying constituents are taken into solution and retained by rapid quenching. Subsequent heat treatment at lower temperatures (age hardening) at room temperature allows for a controlled precipitation of the constituents, thereby achieving increased hardness and strength. In solution heat treatment, a solid solution of the alloying constituents is obtained. The alloy is soaked for a temperature high enough and time period long enough to obtain a fairly homogeneous solid solution.

Quenching. The objective of quenching is to preserve the solid solution formed at the solution heat-treating temperature, by rapidly cooling to some lower temperature, usually near room temperature. In order to avoid the types of precipitation that are detrimental to mechanical properties or to corrosion resistance, the solid solution formed during solution heat treatment must be quenched rapidly enough (and without interruption) to produce supersaturated solution at room temperature—the optimum condition for precipitation hardening. Quenching is mostly done by immersing in or spraying cold water over the sheet.

Age Hardening. Aging is allowing precipitation of the solid solution of the alloying elements. When this is done at room temperatures, it is called natural aging. 2xxx alloys are generally naturally aged. The time period involved is

generally 5 to 30 days. Artificial aging involves precipitation at temperatures from 115 to 190 °C. The time period involved is 5 to 48 h. The objective is to select the cycle that gives the required precipitate size and distribution that in turn affects the mechanical properties.

Flow Stress. The flow stress data of aluminum alloy AA5754-O is given in Fig. 6.7. The flow stress data of other aluminum alloys are given in Appendix A. These are flow stress data at room temperature unless specified otherwise.

The formability of aluminum alloys improves with increase in temperature from room temperature upward (Fig. 6.8). At elevated temperatures, yield strength changes little, but tensile strength decreases considerably.

Warm Forming of Aluminum Alloys. Aluminum alloy sheets have lower elongations, n -values, r -value, and moduli of elasticity com-

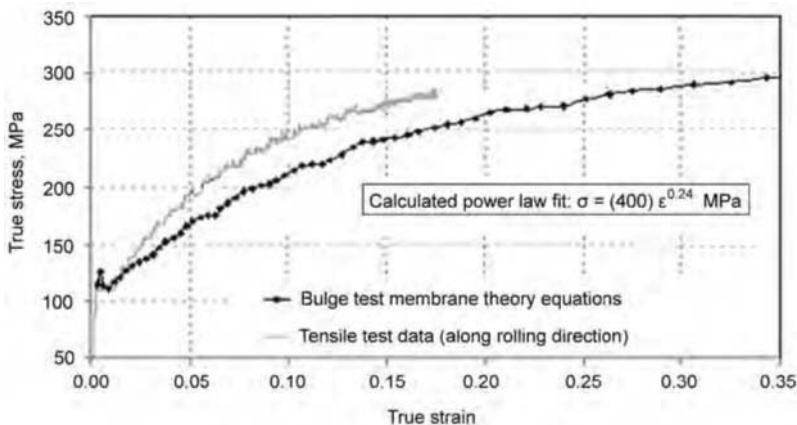


Fig. 6.7 Comparison of the flow stress of aluminum alloy AA5754-O (1.3 mm) obtained by the tensile test and the bulge test. Experimental strain range: tensile data, 0 to 0.157; bulge test membrane theory, 0.01 to 0.0.35.

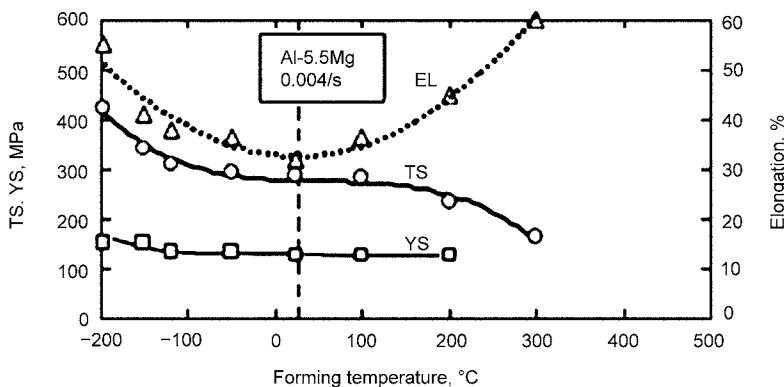


Fig. 6.8 Effect of forming temperature on mechanical properties of 5000 series aluminum alloys. EL, elongation; TS, tensile strength; YS, yield strength. Source: Ref 6.8

pared to steel. Hence, aluminum alloys have low formability at room temperature, which restricts the shapes that can be formed. This can be overcome by warm forming.

In warm forming, the dies and blank holders are heated to a temperature of 200 to 300 °C through electrical heating rods. Solid lubricants are more effective in warm forming. Significant improvements in formability at elevated temperatures can be noted in such alloys as 5xxx and 6xxx. Aluminum that contains 6% magnesium could give a 300% total elongation at about 250 °C, which finds more application in industry. Experimental analyses of rectangular conical cups from an aluminum alloy (5754-O) drawn at room temperature (20 °C), 100 °C, 175 °C, and 250 °C were conducted and maximum cup heights, obtained without fracture, were compared (Ref 6.7). These cup heights were 35 mm, 38 mm, 38 mm, and 60 mm for temperatures of 20 °C, 100 °C, 175 °C, and 250 °C, respectively. The forming velocity and the drawing ratio increase as the forming temperature increases to around 275 °C. Higher temperatures around 300 °C are best suited for drawing deep cups. Fig. 6.8 shows how the elongation and tensile strength vary with forming temperature. The elongation is close to 60% at 300 °C, compared to 35% elongation at room temperature.

Quick-plastic forming was developed by General Motors to primarily form parts of Al5083 because it has higher uniform elongation at higher strain rates (10^{-3} s $^{-1}$ to 10^{-1} s $^{-1}$) and higher temperatures (450 °C). It is similar to sheet hydroforming process. The heated sheet metal is formed against the die using a pneumatic pressurizing medium. It is used for auto body production (Ref 6.9).

Applications of Aluminum Alloys. Aluminum sheets are widely used automotive panels and structural parts. They are also used in heat insulators and fuel tank protectors, which insulate heat and noise and protect bodies from dirt, and in exhaust manifold covers in engine compartments. 1000- and 3000-series aluminum alloys are used for these parts. 2000-, 7000-, and 8000-series aluminums, which are very strong, are used in aircrafts. 7000-series aluminums are also used in military vehicles because they have good ballistic properties. The food packaging industry uses 1000-series alloys in such products as beverage cans. 1000-, 3000-, 5000-, and 6000-series aluminums are used in building and architecture for roofing, window panes, and other applications.

6.5 Magnesium Alloys

Magnesium alloys are important candidates for lightweight structural materials. They are used in selected applications by the automotive and aerospace industries and for industrial machinery. Magnesium sheet alloys are difficult to form at room temperature. However, they possess excellent forming behavior at elevated temperatures (Ref 6.10).

Designations and Properties of Some Magnesium Alloys. There is a standardized system for naming of magnesium alloys. It can be divided into four parts. For example, in the alloy AZ91E-T6, the first part indicates the alloying elements—in this case aluminum and zinc. The second part indicates the percentage of alloying elements: 9% Al and 1% Zn. In the third part, “E” indicates that this is the fifth magnesium alloy with 9% Al and 1% Zn. The fourth part, “T6,” denotes that it is solution treated and artificially aged (Ref 6.6).

Temperature plays a significant part in determining the mechanical properties, especially tensile and yield strength of magnesium alloys. These properties deteriorate noticeably with increases in temperature, while elongation increases significantly with temperature up to 315°C (Table 6.9).

There is a remarkable increase in the strains achievable at higher temperatures with increase in temperature of even 40 °C (Fig. 6.9). There is nearly a 300% increase in the strain range obtained at forming at 145 °C and 221 °C.

Table 6.9 Properties of some magnesium alloys

Magnesium alloy	Testing temperature, °C	Tensile strength, MPa	Yield strength, MPa	Elongation in 50 mm, %
AZ31B-H24				
	21	290	221	15
	100	207	145	30
	200	103	59	55
	315	41	21	125
HK31A-H242				
	21	260	205	8
	150	180	165	20
	200	165	145	21
	260	140	115	19
	315	89	48	70
HM21A-T8				
	21	235	170	8
	200	125	115	30
	260	110	105	25
	315	97	83	12
	370	76	55	50

Source: Ref 6.6

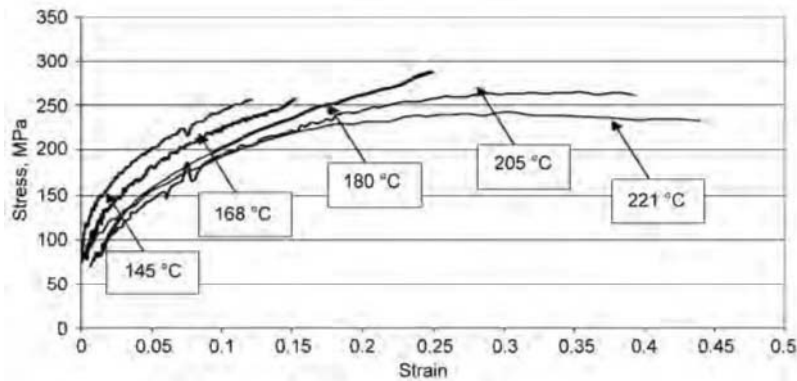


Fig. 6.9 True stress/true strain curve for the flow stress of AZ31B-O obtained using the hydraulic bulge test at a strain rate of approximately 0.25 s^{-1} and a temperature range of 145 to 221 °C. Experimental strain range at 145 °C, 0 to 0.12; 168 °C, 0 to 0.16; 180 °C, 0.02 to 0. Source: Ref 6.11

Factors Influencing Formability of Magnesium Alloys. Flow stresses are influenced by the forming temperature (Fig. 6.9). Stresses and strains strongly depend on the forming temperature. Elevated temperatures contribute to improved ductility and hence forming capability, and this strategy can help reduce the yield point of the material and hence the forming forces and pressures required. Magnesium alloys show good formability at elevated temperatures compared to room temperatures. The maximum stretching heights of magnesium alloys increase with increasing temperature. Hot stretch forming also results in lower springback.

The influence of strain rate becomes more significant with increasing forming temperature. Increases strain rate result in considerable increases in flow stress. Increases in strain rate also decrease the maximum elongation of the material regardless of the forming temperature.

For more details on factors influencing formability of magnesium alloys, see “Influences of Formability, Formability of Magnesium Alloys” in Ref 6.3.

ACKNOWLEDGMENTS

Portions of this chapter were adapted from:

- *Properties and Selection: Irons, Steels, and High Performance Alloys*, Vol 1, ASM Handbook, ASM International, 1990
- *Properties and Selection: Nonferrous Alloys and Special-Purpose Materials*, Vol 2, ASM Handbook, ASM International, 1991

- *Metalworking: Sheet Forming*, Vol 14B, ASM Handbook, ASM International, 2006
- The section “6.1 Low-Carbon Sheet Steels,” was adapted from Mahmoud Y. Demeri, Forming of Carbon Steels, *Metalworking: Sheet Forming*, Vol 14B, ASM Handbook, ASM International, 2006, p 495–529; and *Properties and Selection: Irons, Steels, and High Performance Alloys*, Vol 1, ASM Handbook, 1990.

REFERENCES

- 6.1 T. Altan and E. Tekkaya, Ed., Forming of Advanced High Strength Steels, *Sheet Metal Forming: Processes and Applications*, ASM International, 2012
- 6.2 *Properties and Selection: Irons, Steels, and High Performance Alloys*, Vol 1, ASM Handbook, ASM International, 1990
- 6.3 *Metalworking: Sheet Forming*, Vol 14B, ASM Handbook, ASM International, 2006
- 6.4 A. Yadav, T. Altan, and G. Spampinato, Warm Forming of Stainless Steels—Part I, *Stamping Journal*, July 2006, p 36
- 6.5 A. Yadav, T. Altan, and G. Spampinato, Warm Forming of Stainless Steels—Part II, *Stamping Journal*, August 2006, p 28
- 6.6 *Properties and Selection: Nonferrous Alloys and Special-Purpose Materials*, Vol 2, ASM Handbook, ASM International, 1991.
- 6.7 P.J. Bolt, N.A.M.P. Lamboo, and P.J.C.M. Rozier, Feasibility of Warm Drawing of Aluminum Products, *Journal of Material*

- Processing Technology*, Vol 115, 2001, p 118–121
- 6.8 T. Sakurai, The Latest Trends in Aluminum Alloy Sheets for Automotive Body Panels, *Kobelco Technology Review*, 2008, p 22–28
- 6.9 J. Carsley, P. Krajewski, J. Schroth, and T. Lee, “Aluminum Forming Technologies: Status and Research Opportunities,” presented at New Developments in Sheet Metal Forming conference (IFU, Stuttgart), 2006
- 6.10 E. Doege and K. Dröder, Sheet Metal Forming of Magnesium Wrought Alloys and Process Technology, *Journal of Materials Processing Technology*, Vol 115, 2001, p 14–19
- 6.11 S. Kaya and T. Altan, Warm Forming of Al and Mg: Part II, Determination of Magnesium Sheet Properties at Elevated Temperatures, *Stamping Journal*, 2006, p 32
- S. Kaya and T. Altan, Warm Forming Aluminum and Magnesium, Part I: Forming a Round Cup, *Stamping Journal*, Vol. 17 (No. 12), 2005, p 36

SELECTED REFERENCES

CHAPTER 7

Friction and Lubrication

Hyunok Kim, Edison Welding Institute
Nimet Kardes, The Ohio State University

FRICION AND LUBRICATION in sheet metal forming are influenced by such parameters as material properties, surface finish, temperature, sliding velocity, contact pressure, and lubricant characteristics. The parameters that affect friction and lubrication are schematically shown in Fig. 7.1. Depending on these parameters, the performance of a lubricant and the coefficient of friction (COF) vary.

Material flow in the die cavity is influenced by frictional conditions at the die/work piece interface. Therefore, a good understanding of the parameters that affect friction is essential for

selecting lubricants and producing good-quality sheet metal parts. In sheet metal forming, the magnitude and distribution of friction affect metal flow, part defects, and quality, as well as tool wear and production costs.

7.1 Lubrication Mechanisms and Friction Laws

In metal forming, different lubrication mechanisms may be present:

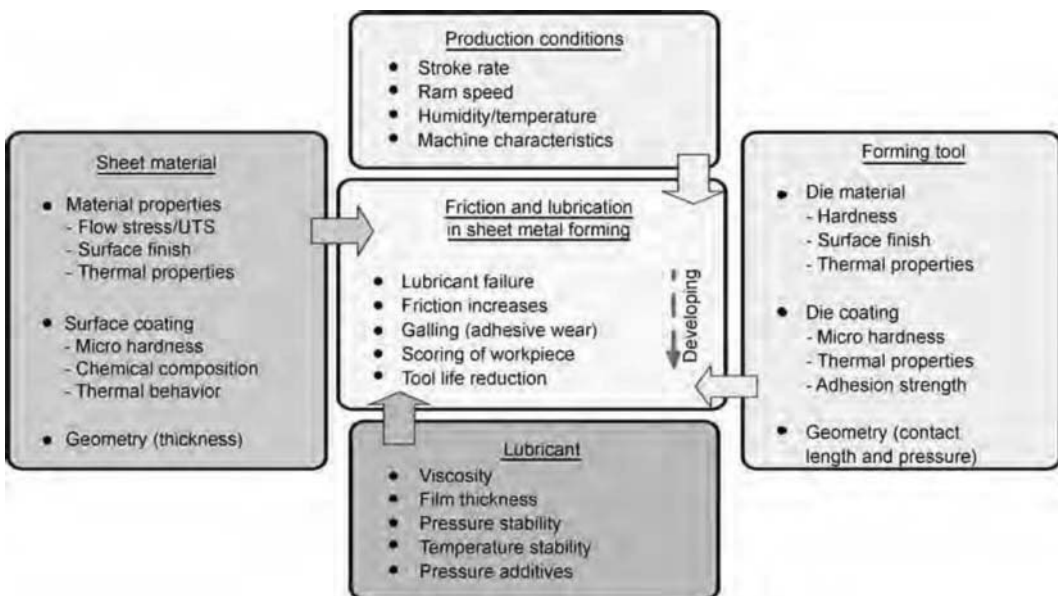


Fig. 7.1 Factors that affect friction and lubrication in sheet metal forming. Ultimate tensile strength (UTS)

- Dry condition
- Boundary lubrication
- Mixed-film lubrication
- Hydrodynamic lubrication

As shown in Fig. 7.2, the Stribeck curve illustrates schematically the onset of various types of lubrication mechanisms as a function of lubricant viscosity, η , sliding velocity, v , and normal pressure, p (Ref 7.1).

A dry condition (Fig. 7.2) means no lubrication is present at the mating surfaces; thus, friction is high. This condition is often used when the material formability is large enough to form a part with simple geometry without lubricants or when the frictional condition does not significantly influence the part quality, for instance, air bending, V-die bending, and U-die bending without stretching. A dry condition is desirable in only a few selected forming operations, such as hot rolling of plates or slabs and nonlubricated extrusion of aluminum alloys.

Boundary lubrication (Fig. 7.2) is defined as a condition where the solid surfaces are so close together that surface interaction between single or multimolecular films of lubricants and the solid asperities dominates the contact (Ref 7.2).

Boundary lubrication is the most widely encountered lubrication condition in metal forming.

Mixed-layer lubrication (Fig. 7.2) is also frequently encountered in sheet metal forming. In this case, the micropeaks of the metal surface experience boundary lubrication conditions and the microvalleys of the metal surface become filled with the lubricant. Hydrodynamic lubrication (Fig. 7.2) is experienced in a few sheet metal forming processes, such as high-speed sheet rolling operations, where large velocities at the material-tool interface create hydrodynamic conditions.

Coulomb, Tresca, and Modified Shear Friction Models. Two friction models are commonly used to describe the frictional condition in metal forming processes: Coulomb's friction model (Eq 7.1) and the shear friction model (Eq 7.2). Both models quantify interface friction by lumping all of the interface phenomena, which are illustrated in Fig. 7.1 into a nondimensional coefficient or factor:

$$\tau_f = \mu p \quad (\text{Eq 7.1})$$

where μ is the coefficient of friction (COF), p is the normal pressure, and τ_f is the frictional shear

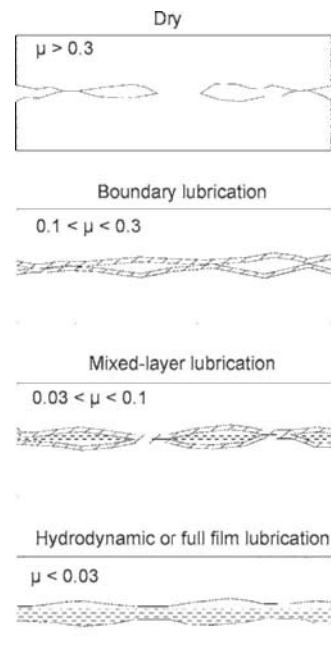
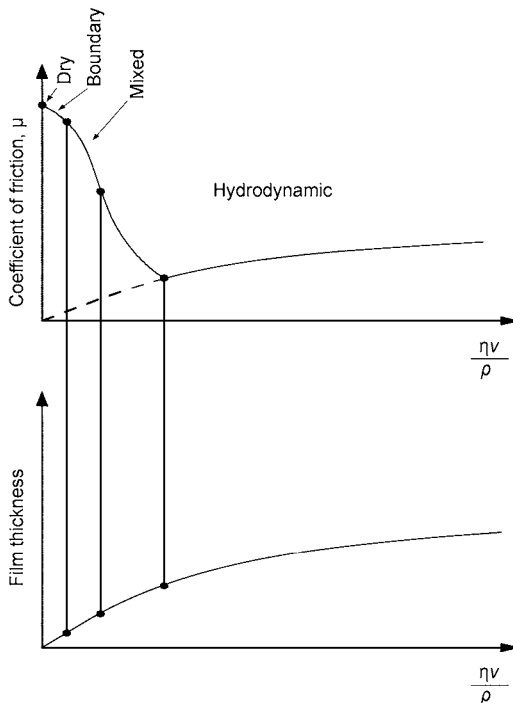


Fig. 7.2 Stribeck curve showing onset of various lubrication mechanisms. η , lubricant viscosity; v , sliding velocity; p , normal pressure; μ , coefficient of friction.

stress. In many metal forming processes, the interface pressure, p , can reach a multiple of the yield strength of the material. Thus, the linear relationship between τ_f and p , as described by Eq 7.1, may not be valid at high contact pressure levels because the shear stress, τ_r , cannot exceed the shear strength, k , of the deformed work piece material. Therefore, the COF becomes meaningless when μp exceeds τ_r . Thus, to avoid this limitation of Coulomb's model, the shear friction model (Eq 7.2) was proposed by Orowan (Ref 7.3):

$$\tau_f = f \bar{\sigma} = m \frac{\bar{\sigma}}{\sqrt{3}} = mk \quad (\text{Eq 7.2})$$

where f is the friction factor; m is the shear factor, $0 \leq m \leq 1$; k is the shear strength; and $\bar{\sigma}$ is the flow stress of the deforming material. In this model, as shown in Fig. 7.3, the frictional shear stress, τ_r , at low pressure is proportional to the normal pressure given by Coulomb's model. However, it equals the shear strength, k , at high interface pressure, p .

In Eq 7.2, m equals to zero for no friction, and m equals to unity for a sticking friction condition, which is the case where sliding at the interface is preempted by shearing of the base material (Ref 7.1). When two nominally flat surfaces are placed in contact, surface roughness causes discrete contact spots. The total area of all these discrete contact spots constitutes the real contact area, A_r , and in most cases this will be only a fraction of the apparent contact area, A_a . The ratio of the real contact area, A_r , to the apparent contact area, A_a , is known as the real contact area ratio, α . To consider the effect of real contact area ratio, α , on friction, Wanheim, Bay, and colleagues (Ref 7.4, 7.5) proposed a general friction model:

$$\tau_f = f' \alpha k = m_r \frac{\bar{\sigma}}{\sqrt{3}} \quad (\text{Eq 7.3})$$

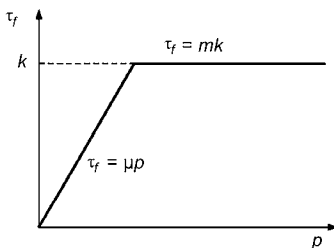


Fig. 7.3 Relationship between contact pressure and frictional shear stress

where f' is the modified friction factor, m_r is the modified shear factor (as a function of real contact area), $\bar{\sigma}$ is the flow stress, and α is the real contact area ratio, A_r/A_a . In this model, the friction shear stress, τ_r , is a function of the real contact area ratio, α .

Wanheim and Bay's model did not consider the effects of lubricant behavior (Ref 7.6). To take lubricant effects into account, a complex model for friction was proposed for boundary and mixed-film lubrication regimes at the tool/work piece interface by Bowden and Tabor (Ref 7.7). In this model the frictional shear stress, τ_r , is given by:

$$\tau_f = \alpha \tau_a + (1 - \alpha) \tau_b \quad (\text{Eq 7.4})$$

where α is the real contact area ratio, τ_a is the average shear stress at contacting asperity peaks, and τ_b is the average shear stress (lower stress) at the lubricant pockets. This model explicitly formulates the real contact area ratio, α , related to τ_a and the lubricant behavior related to τ_b that is influenced by viscosity, pressure, sliding speed, and film thickness.

If there is no lubricant at the tool/work piece interface, τ_b will be zero and the frictional shear stress, τ_r , will be a function of real contact area ratio, as expressed in Eq 7.3. To take into account the lubricant behavior on friction, an artificial lubricant film was assumed to exist at the tool/work piece interface, and the variation of film thickness was calculated to characterize the variation of friction using the Reynolds equation in the fluid mechanics theory (Ref 7.6). Although this approach includes more detailed considerations to express the lubricant behavior, the model is very difficult to apply to practical metal forming problems.

7.2 Lubricants for Sheet Metal Forming

In selecting lubricants for sheet metal forming process, the following factors should be considered (Ref 7.8):

- Methods of lubricant application
- Types of additives
- Corrosion control
- Cleanliness and removal methods
- Compatibility with prelubricants and preapplied oils

- Post-metal forming operations (e.g., welding and adhesive joining)
- Environmental safety and recycling

Types of Lubricants (Ref 7.8)

- *Oils*: Petroleum-based oils are widely used as lubricants for light-duty stamping, blanking, and coining operations. The use of oil can increase the production rate. Paraffinic oils and naphthenic oils are examples of these lubricants.
- *Soluble Oils*: Soluble oils contain emulsifiers that allow the dilution of the oils into water. These oils are referred as preformed emulsions. These oils are normally mixed with water at a dilution ratio of 10 to 50%.
- *Semisynthetics*: These lubricants are more easily mixed with water than soluble oils, because they contain a smaller amount of mineral oil, usually less than 30% of the total concentrate volume.
- *Synthetics*: Synthetic fluids are categorized by two types: water based and hydrocarbon based. The color of this lubricant normally is hazy or milky.
- *Dry-Film Lubricants*: Dry-film lubricants are divided into water-soluble and water-free (“hot melt”) categories. Water-soluble dry-film lubricants are applied in amounts of 0.5 to 1.5 g/m² at the rolling mill (Ref 7.9). They stick to the surface of the sheet metal and offer sufficient corrosion protection but are not compatible with most adhesives used in automotive body construction (Ref 7.10). The water-free dry-film lubricants are also applied on the sheet material in small amounts at the rolling mill. Besides their better drawing performance compared with oil-based lubricants, the most important advantage of water-free dry-film lubricants is their compatibility with almost all commonly used adhesives.

Application of Lubricants (Ref 7.8). The proper application of lubricants is important for good lubricant performance and reduction of lubricant waste and environmental hazards. The most commonly used application methods are:

- *Drip Method*: The simplest and the cheapest method to apply the lubricant, by dripping it on the panel or sheet blank, but applying the desirable amount of lubricant is very difficult
- *Roll Coating*: Lubricant applied on the blank moving between two rollers under con-

trolled pressure, allowing precise control of the amount of lubricant applied

- *Electro-Deposition*: Lubricant deposited on the panel surface using electric charge; used for high-speed applications without any waste of lubricant, but requires high capital investment for small stamping shops
- *Airless Spraying*: Applies precise amounts of lubricant to local areas, with minimal waste of lubricant in this method, but does not work with the high-viscosity lubricants
- *Mops and Sponges*: Low-cost method still used in a lot of small stamping shops to apply lubricants on the panels, which can result in excessive waste of lubricants, poor control of the amount of lubricant, and sloppy work environment

Types of Additives. Various types of additives enhance the performance of lubricants. The extreme pressure (EP) additives are commonly used in heavy-duty metal stamping operations (Ref 7.8). They are categorized as temperature activated and nontemperature activated. The temperature-activated EP additives, such as chlorine, phosphorus, and sulfur, react as the interface temperature increases and generate a film by a chemical reaction with the metal surface. This chemical film helps prevent metal-to-metal contact in stamping operations.

EP additives have different levels of effectiveness in particular temperature ranges:

- Phosphorus is effective up to 205 °C (400 °F).
- Chlorine is effective between 205 to 700 °C (1100 °F).
- Sulfur is effective between 700 to 960 °C (1800 °F).

As the tool and work piece temperatures increase during deformation, lubricants with EP additives become thinner (low viscosity) and may burn. On the other hand, the lubricants with extreme temperature (ET) additives become thicker (high viscosity) with increasing temperature. As a result, at elevated temperatures, the lubricants with ET additives is more effective and stick to the warm workpiece and create a friction-reducing film barrier between the tool and the workpiece. Additives such as phosphorus, chlorine and sulfur, as previously discussed, are also used as ET additives to enhance the effectiveness of lubricants at elevated temperatures.

Corrosion Control. Lubricants often have to provide a thin surface film on the stamped parts

to prevent oxidation and corrosion, because stamping parts may be transferred or stored for postprocessing without cleaning the part. Therefore, the ASTM D130 standard corrosion test is usually conducted to evaluate the performance of stamping lubricants: the sheet sample is dipped into the lubricant for a particular period, usually 1 or 2 weeks.

Cleanliness and Removal Methods. The lubricant needs to be thoroughly removed from the stamped part before painting and electrocathodic coating (E-coating) with primers, because surface contamination can result in poor-quality painting and E-coating.

Straight oils can be removed using vapor degreasers, which are types of solvent. However, this method is not widely used because of environmental and safety problems. Alkaline cleaners are alternatives to vapor degreasers (Ref 7.8). These cleaners can be applied on the part by dipping into a bath or by impingement spray. This method is also effective in water-diluted lubricants that contain oil. Multistage washers are widely used to remove lubricant residues.

Compatibility with Prelubricants and Other Oils. In today's stamping process, various lubricants and washer oils are often applied in different stages. A thin film of prelubricant is usually applied on sheet metal at the rolling mill. This prelubricant exists as a liquid state or as dry-film on the coil.

Post-Metal Forming Operations. Most lubricants are applied on sheet metals before press forming. Lubricants also affect post-metal forming operations such as welding, adhesive bonding, and painting. In addition to their good lubricity, lubricants must be easily removable from the formed panels, because the stamped part has to be completely oil-free for painting. Therefore, in selection/evaluation of stamping lubricants, it is necessary to consider advantages and disadvantages of lubricants not only for deep drawing but also for assembly and painting operations. Fig. 7.4 shows how two stamping processes, one with wet lubricant and one with dry-film lubricant, can change the required operations for stamping and post-metal forming operations.

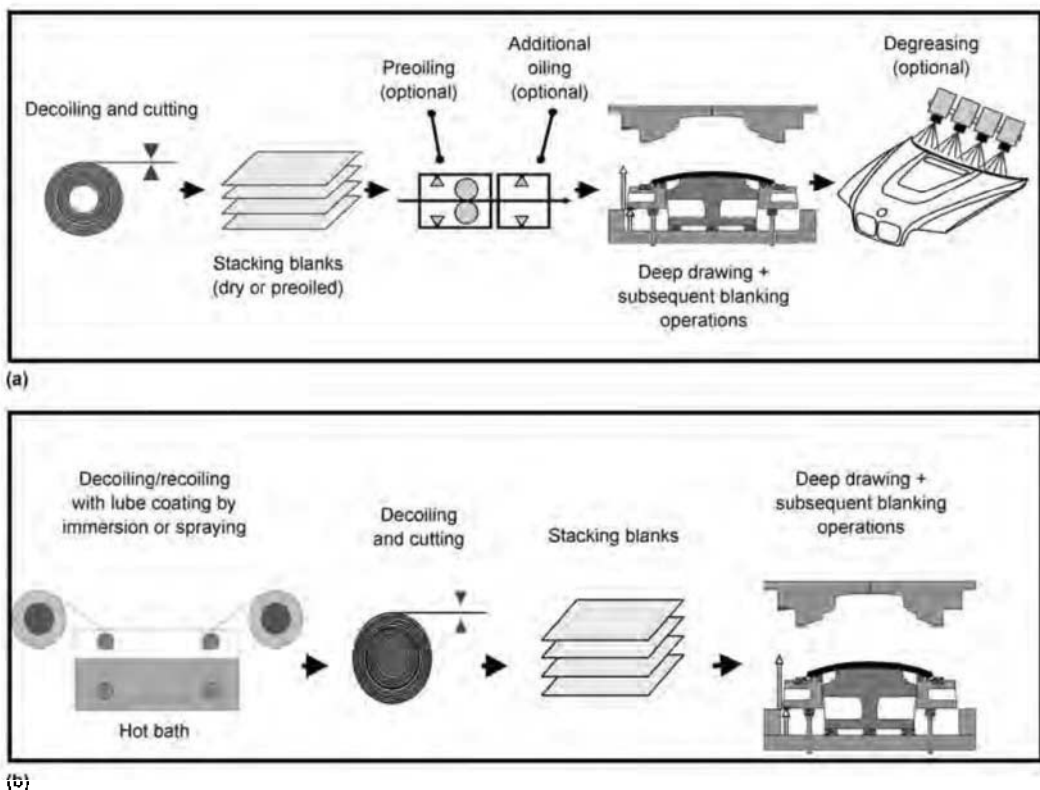


Fig. 7.4 Comparison of stamping processes with (a) wet lubricants and (b) dry-film lubricants. Source: Ref 7.11

7.3 Tribological Tests for Evaluation of Lubricants in Sheet Metal Forming

Laboratory-Scale Tribological Tests. Various tribological tests developed over the years are used to evaluate the performance of lubricants under laboratory conditions. These include the strip drawing test (SDT) and draw bead test (Fig. 7.5) (Ref 7.13, 14). The limiting dome height (LDH) test is also used to evaluate lubricants for stamping (Ref 7.1). In the LDH test, the location of the fracture point depends on the frictional condition between the punch and the sheet. The material is primarily stretched with a small sliding motion; therefore, the test emulates the friction on the die or punch shoulders as shown in Fig. 7.5. The strip reduction test was introduced by Andreasen et al. Ref 7.15 and is extensively used to evaluate lubricants for the ironing operation of stainless steels (Ref 7.16). In this test, the thickness of the metal strip was significantly reduced when it is pulled through a roller element (Fig. 7.6). This test is very useful to test stamping lubricants and tool materials/coatings by quantifying the amount of galling on the roller or the strip.

The twist compression test (TCT) is widely used in laboratories for quick evaluation of lubricants and additives. It is frequently used to estimate the COF for stamping lubricants for different tool coatings and zinc-coated sheet materials as a function of time (Ref 7.17). In the TCT, a rotating annular tool is pressed against a fixed sheet metal specimen while pressure and torque are measured (Fig. 7.7). The COF between the tool and the specimen is calculated by:

$$\mu = \frac{T}{r \times P \times A} \quad (\text{Eq 7.5})$$

where μ is the COF, T is applied torque, r is the mean radius of the tool, P is the pressure applied on the tool, and A is the area of contact between tool and sample.

The strip drawing test (SDT) was developed to test the higher grades of advanced high-strength steels (DP 780, TRIP 780, and DP 980) by considering the effects of different die radii, materials/coatings, and lubricants (Ref 7.18). The SDT (Fig. 7.8) is a simplified version of a round cup deep drawing test (Fig. 7.9).

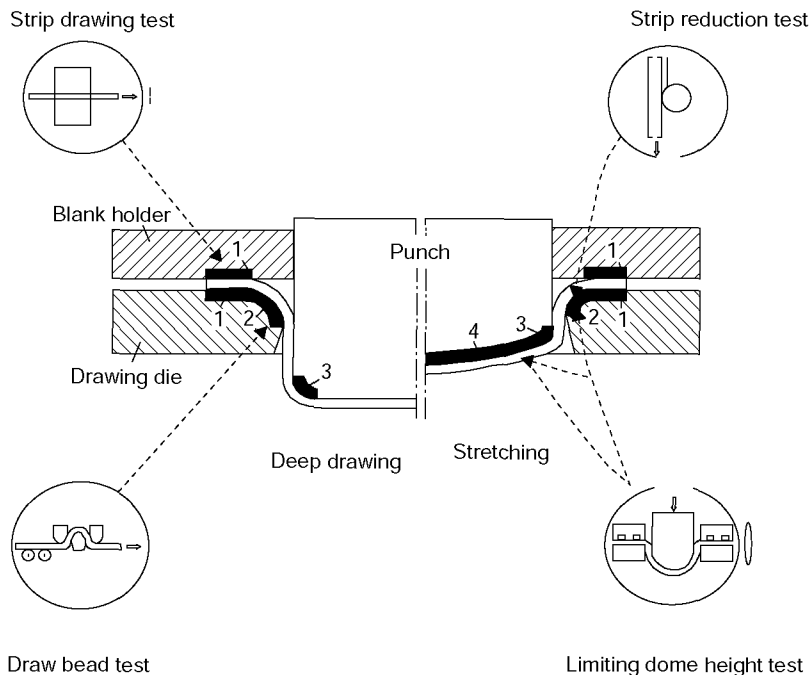


Fig. 7.5 Various Tribotests used for evaluating stamping lubricants; Region 1, flange deformation; Region 2, bending and unbending; Region 3, bending and stretching; Region 4, large friction with little deformation.

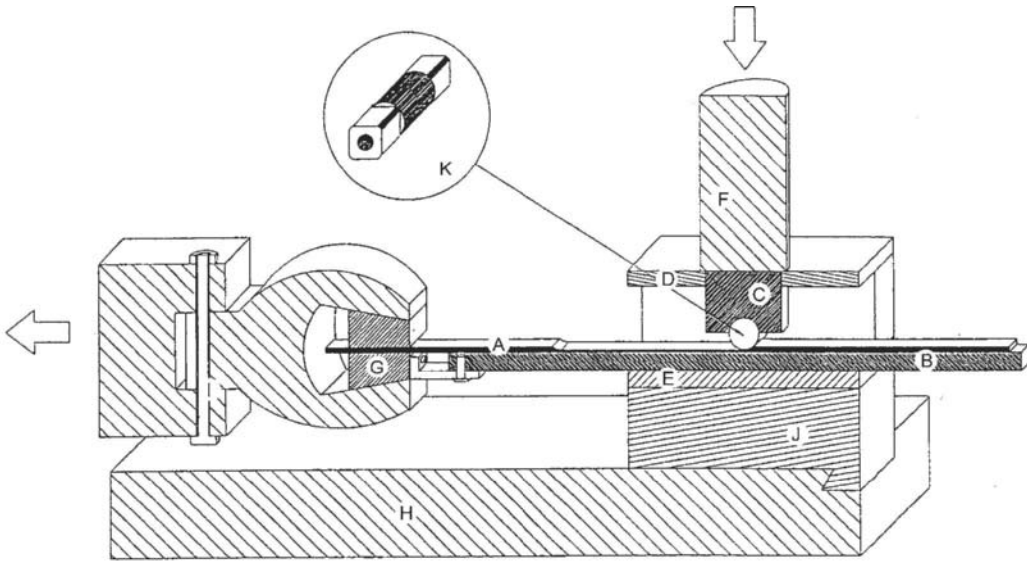


Fig. 7.6 Setup for strip reduction. A, strip; B, hardened steel rod; C, pressing block; D, distance sheet; E, vertical piston; F, horizontal piston with claw; G, tools. Source: Ref 7.12

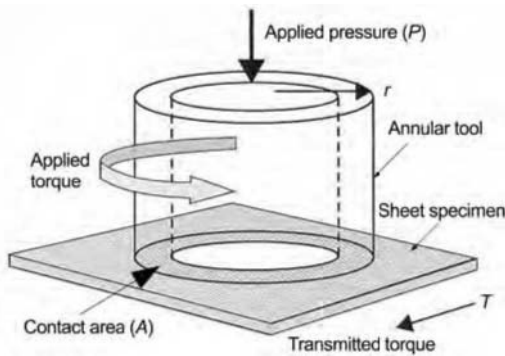


Fig. 7.7 Schematic of the twist compression test. T , applied torque; r , mean radius of the tool. Source: Ref 7.17

These laboratory-scale tests are helpful in evaluating the performance of a lubricant at different locations in the die where the deformed sheet is under different states of stress and strain (Fig. 7.5). The stresses and strains that exist at various locations in the deforming sheet may differ, which may be one of the reasons that we obtain different values for the COF while conducting different tests with the same sheet material and lubricant. Furthermore, laboratory tests have limitations in emulating process conditions (e.g., temperature, contact pressure, and speed) that exist in real stamping operations. Evaluating lubricants in real production condi-

tions is difficult and expensive. Therefore, a good laboratory tribological test that can emulate the conditions found in stamping operations is very useful and practical.

Production-Type Tests—Deep Drawing and Ironing Tests. The deep drawing test (Fig. 7.9) can emulate production conditions and was successfully used for evaluation of lubricants by various European automotive manufacturers (Ref 7.11, 20). The deep drawing tests were conducted under process conditions that are present in practical stamping operations. Major emphasis is put on emulating (a) sheet-die interface pressure levels occurring in production, by adjusting the blank holder force (BHF), and (b) punch speeds found in mechanical stamping presses.

In deep drawing, the most severe friction usually takes place at the die shoulder and flange area, as shown in Figure 7.9. The lubrication condition in these areas influences (a) the thinning or possible failure of the sidewall in the drawn cup and (b) the draw-in length, L_d , in the flange (Figure 7.9). As the blank holder pressure, P_b , increases, the frictional stress, τ , also increases based on Coulomb's law, as shown in Eq 7.1. Therefore, lubricants can be evaluated in deep drawing by determining the maximum applicable BHF without fracture in the cup wall.

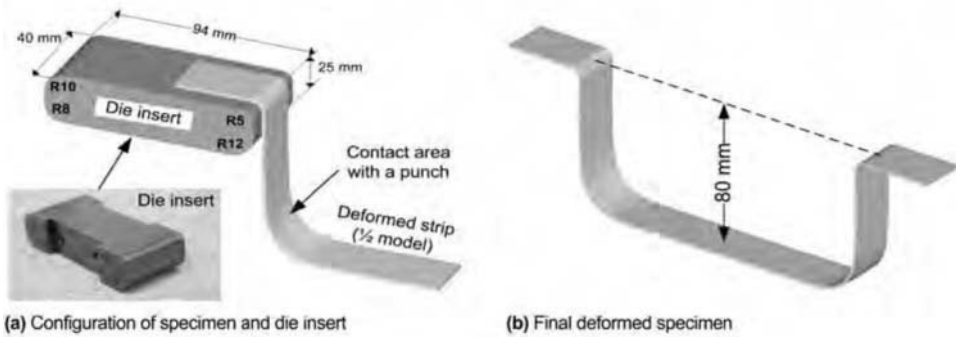


Fig. 7.8 Schematic of strip drawing test. R5, R8, R10 and R12 are radii at the corresponding edges of the insert. Source: Ref 7.18

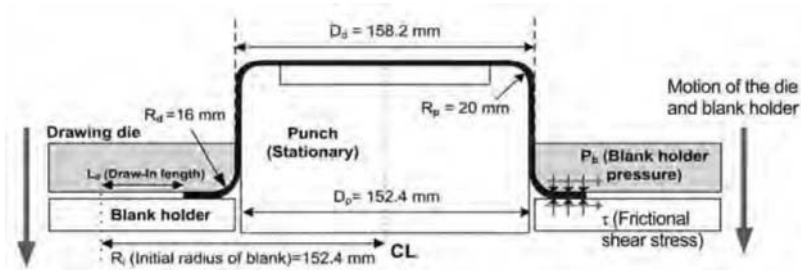


Fig. 7.9 Schematic of deep drawing test and tool dimensions. D_p and D_d = punch and die diameter, respectively. R_d and R_p = die and punch radius, respectively. Source: Ref 7.19

In using the deep drawing test, qualitative and quantitative analyses can be made to determine the effectiveness of lubricants, based on the following criteria:

- Maximum punch force (the lower the force, the better the lubricant)
- Maximum applicable BHF (the higher BHF applied without causing fracture in the drawn cup, the better the lubricant)
- Visual inspection of galling and zinc powdering
- Measurement of draw-in length, L_d , in the flange (the larger the draw-in length, the better the lubrication)
- Measurement of the perimeter in flange area (the smaller the perimeter, the better the lubrication)

This deep drawing test has been successfully used to evaluate various stamping lubricants with DP600 (Ref 7.17). Fig. 7.10 compares load-stroke curves of fully drawn cups and fractured cups at a BHF of 70 tons. This fracture is caused by the breakdown of lubricant film at high contact pressure, while the most of lubri-

cants performed well in a low contact pressure of 30 tons BHF.

In the automotive stamping operation, the sheet panels carry various oils, such as mill oil, washer oil, and press lubricant. As a result, the lubrication system becomes more complicated, and the stamping lubricant may perform very poorly because of the mixture of oils and lubricants. Therefore, the results of a laboratory test with a single lubricant may be unrealistic. To investigate the effects of a mixed lubrication system on stamping performance, the deep drawing test was used to evaluate the performance of these complex lubrication systems for production applications (Ref 7.21). Fig. 7.11 gives the flange perimeters and punch forces recorded for the different lubrication conditions at different BHFs. Lubricants that sustained higher BHFs are classified as “good” lubricants. For the same BHF, the lubricants that give lower flange perimeters are considered to be good lubricants.

The ironing test has been used to evaluate the stamping lubricants under severe conditions of plastic deformation and temperature. The ironing test provides higher pressures (up to 650

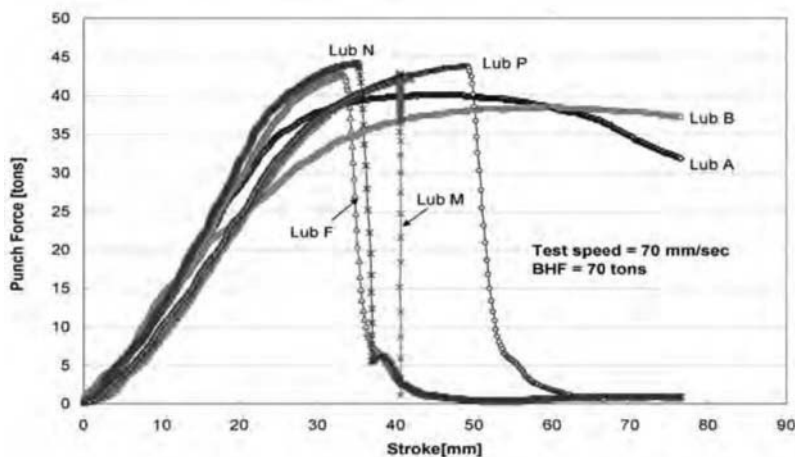


Fig. 7.10 Load-stroke curves obtained for various lubricants (Lub) tested at a high blank holder force (BHF). Source: Ref 7.19

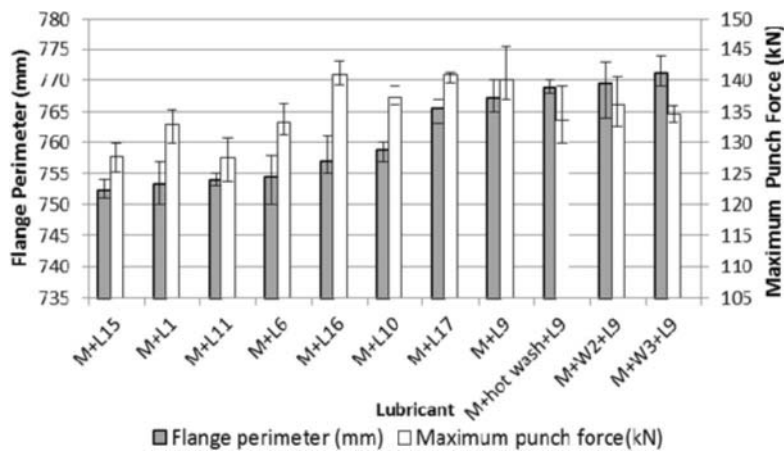


Fig. 7.11 Flange perimeters and punch forces recorded for 11 lubrication conditions at a BHF of 20 tons. M, mill oil; W, washer oil; L, press lube. Source: Ref 7.21

MPa), as illustrated in Fig. 7.12, and higher temperatures at the tool/work piece interface than does the deep drawing test (Ref 7.22). In this test, the maximum punch force and the change in sidewall thinning depend on the interface friction between ironing die and work piece, because the friction increases the tensile stress of the sidewall during ironing. Thus, thinning is reduced with good lubrication. The thinning ratio is calculated by measuring the sidewall thickness of the ironed cup before and after the test.

Ironing tests were conducted to evaluate various stamping lubricants with DP 590 material (Ref 7.17). Average values of thinning ratio

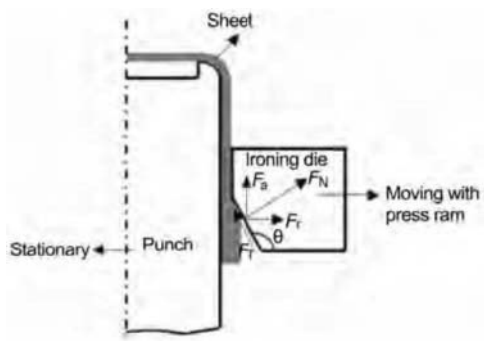


Fig. 7.12 Schematic of ironing test. F_a , F_r , F_t , F_n = forces in axial, radial, tangential to die surface, and normal to surface directions, respectively. Source: Ref 7.19

were plotted along the sidewall of ironed cup, as shown in Fig. 7.13. Lubricants A and B showed smaller thinning distribution than did the other lubricants. No severe galling was observed in this specific test.

7.4 Tribological Tests for Warm and Hot Stamping

Lightweight materials such as boron alloyed steels and aluminum and magnesium alloys are difficult to form at room temperature. Thus, these alloys are formed at elevated temperatures. In order to evaluate lubricants that are used in warm and hot stamping, a tribological test that can emulate the production conditions needs to be selected. The ironing test described in section 7.3 is also used to evaluate the stamping lubricants at elevated temperatures. The ironing die shown in Fig. 7.12 was heated by using a band heater, and ironing tests were conducted to determine the relative performance of five different lubricants in warm forming of AISI 1008 CR steel at 100 °C (210 °F), as shown in Fig. 7.14. Lubricant B performed the best, and lubricants C and D performed the worst (Ref 7.22).

For hot stamping, two methods are used to evaluate lubricants: (a) the hot flat drawing test (similar to strip drawing test shown in Fig. 7.5) (Ref 7.23, 7.24) and (b) the modified cup drawing test (Ref 7.25).

In hot flat drawing test (Fig. 7.15), sheet material is heated in the infrared image furnace to its austenitization temperature under inert gas

atmosphere. It is possible to obtain various scale thicknesses on the sheet material by adjusting the furnace temperature. One end of the strip is clamped with the chuck of the tension device, and it is pulled at constant speed, U_d . Once the heated zone of the strip reaches the entrance of the die, a constant compression force, C_p , is applied. The COF, μ , is calculated from compression force, C_p , and tension force, T_F :

$$\mu = \frac{T_F}{2 \times C_p} \quad (\text{Eq 7.6})$$

In this experimental work, effect of furnace temperature, die pressure, lubrication, and scale thickness on the COF was studied. The experiments were conducted with and without lubricant, and the lubricants were applied to the die surfaces after the dies were heated to 200 °C (390 °F). Two hot forging lubricants (water-based white type with and without solid lubricant) were tested with two sheet materials: 22MnB5 (austenitization temperature: 720 °C (1330 °F)) with Al-Si coating, and SPHC (austenitization temperature: 800 °C (1470 °F)) steel. The compression force, C_p , increased during the experiment for the dry condition, although it was controlled at a constant value. The tension force, T_F , and COF, μ , also increased during sliding for dry and lubricated conditions. Thus, the mean COF, μ_m , is obtained by integrating the COF over sliding distance, L , which is 60 mm:

$$\mu_m = \frac{1}{L_s} \int_{L_o}^{L_s} \mu dL \quad (\text{Eq 7.7})$$

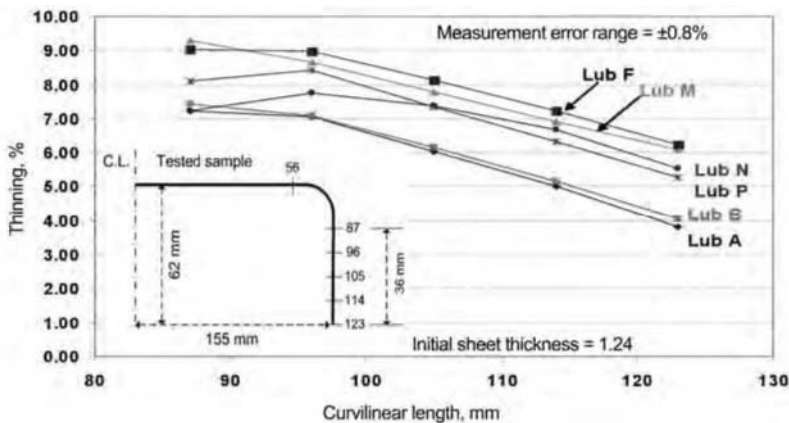


Fig. 7.13 Comparison of sidewall thinning distributions obtained from the ironing tests with different lubricants (Lub); curvilinear length (C.L.). Source: Ref 7.19

Die pressure does not have an effect on the mean COF, μ_m , under the dry condition for SPHC steel tested at 800 °C (Fig. 7.16).

The effect of furnace temperature and lubrication on the mean COF, μ_m , for both SPHC and 22MnB5 steel is shown in Fig. 7.17. Under the dry condition, with an increase in the temperature the mean COF, μ_m , increases for 22MnB5 steel; the effect is smaller for SPHC steel, because of the scale thickness generated during preheating—scale thickness increases as furnace temperature increases. Applying lubricant decreases the mean COF, μ_m (Fig. 7.16); the effect is less significant for 22MnB5 steel due to the Al-Si coating.

The effect of scale thickness on the mean COF, μ_m , was investigated on SPHC steel at 800 °C. Three different scale thicknesses were obtained by adjusting the gas pressure and adding shield pipe between the furnace and the flat dies to avoid oxidation. The mean COF, μ_m , is smaller for thicker scales (50 μm and 150 μm) than for the thinner scale (10 μm), as shown in Fig. 7.18. The flat dies peeled off the scale, and the peeled scale behaved like a lubricant (Ref 7.24).

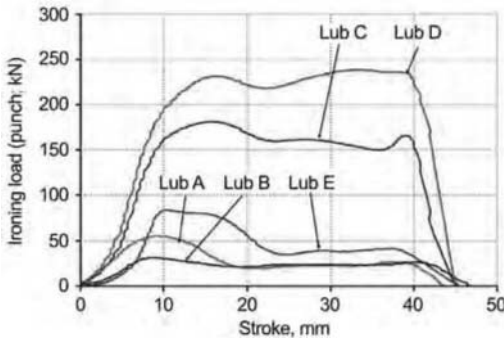


Fig. 7.14 Load-stroke curves obtained for various lubricants (Lub) tested at 100 °C

Geiger et al. (Ref 7.25) modified the cup drawing test as shown in Fig. 7.19 to emulate the process conditions in hot stamping. Punch and die diameters are 50 and 59 mm, and the punch and die corner radii are 10 mm. Punch force and BHF can be measured during the cup drawing test by using load cells. Individual heating cartridges and cooling units are used for controlling the temperature of the tools. It is possible to heat the tools up to 650 °C (1200 °F). In order to increase the formability of the blank, the temperature of the punch was held at room temperature, whereas the temperature of the die and blank holder was varied to investigate the effect of tool temperature on friction in the cup drawing test. BHF is not applied to prevent the cooling/quenching of the blank before forming, and a distance plate is placed between die and blank holder to ensure stable process condition. The 22MnB5 blanks are heated to their austenitization temperature, which is 900 °C (1650 °F) and 950 °C (1740 °F), by a K1150-3 furnace located next to the press. A Variotherm thermal imaging camera measured the blank temperature until the tools were closed. The time between the end of heating the blank and the time the tools are closed was approximately 10 sec, and the punch velocity was 10 mm/sec.

Geiger et al. (Ref 7.25) used the equation by Siebel et al. (Ref 7.26) for estimating the maximum drawing force ($F_{\text{draw,max}}$) to evaluate the COF:

$$F_{\text{draw,max}} = \pi d_m t_0 \left[e^{\mu_s \frac{\pi}{2} 1.1 \sigma_{\text{fmi}} \ln \frac{d_p}{d_m} + \frac{(\mu_1 + \mu_2) F_{\text{BH}}}{\pi d_p t_0}} + \sigma_{\text{fmi}} \frac{t_0}{2r_R} \right] \quad (\text{Eq 7.8})$$

where d_m is the diameter of the cup wall at maximum drawing force ($F_{\text{draw,max}}$), d_p is the external cup diameter at $F_{\text{draw,max}}$, r_R is the die corner ra-

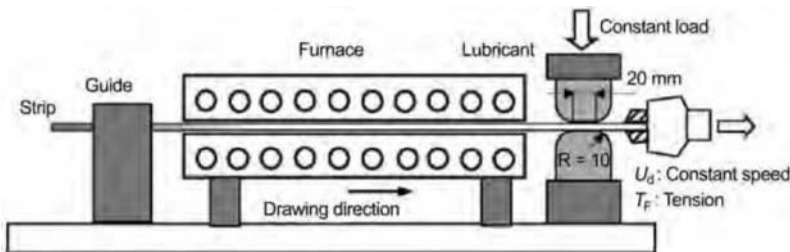


Fig. 7.15 Schematic of tribosimulator. Source: Ref 7.23

dius, t_0 is the initial sheet thickness, σ_{fm1} is the mean true stress in the flange at $F_{draw,max}$, σ_{fm2} is the mean true stress at the drawing radius at $F_{draw,max}$, F_{BH} is the BHF (≈ 0 , no BHF during the test), μ_3 is the COF in the area between blank and the die radius (to be determined), and μ_1 and μ_2 are the COF between the sheet and blank holder/die ($= 0$, since there is a clearance between the sheet and die/blank holder). Except μ_3 , all the values can be determined from experiment and using finite element analysis software. External cup diameter at maximum drawing force, d_p , increases with increase in tool temperature. σ_{fm1} and σ_{fm2} are dependent on the temperature evolution during the test and can be determined from the formulas given by Geiger et al. (Ref 7.25) or using finite element analysis.

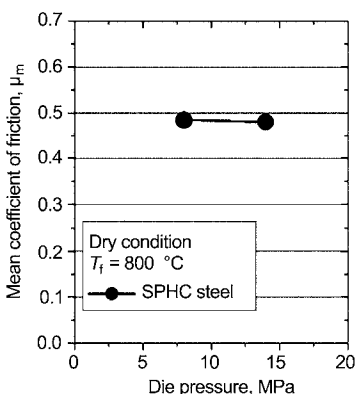


Fig. 7.16 Effect of die pressure on mean coefficient of friction, μ_m . Source: Ref 7.23

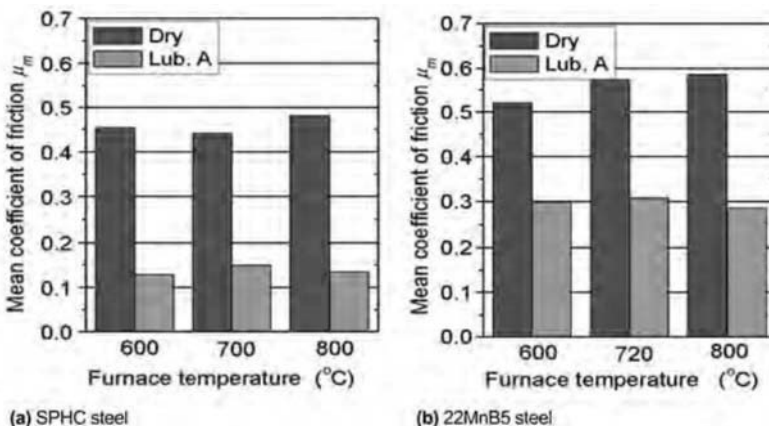


Fig. 7.17 Effect of furnace temperature on mean coefficient of friction, μ_m , both under the dry condition and with a lubricant (Lub.), for two types of steel. Source: Ref 7.23

Fig. 7.20 and 7.21 show the influence of tool temperature on the COF, μ_3 , for two initial blank diameters, 85 and 90 mm. With an increase in the temperature of the die and the blank holder, the COF decreases. The significant temperature-dependent plastic softening of 22MnB5 steel leads to reduced normal forces transferred from the bulk sheet material to the interacting surfaces at the die. This causes reduction in COF with increase in temperature.

7.5 Tribological Tests for Punching and Blanking

In punching and blanking (including fine blanking), contact pressure and temperature at the tool/work piece interface are much higher than with other sheet metal forming processes. As the shearing proceeds, the punch is in contact with fresh surface, and it is difficult to keep the tool/work piece interface lubricated during punching and blanking. In addition, the torn sheet particles can stick to the punch surface and become hard particles due to the presence of oxygen, which leads to galling (Ref 7.9). Fine blanking experiments were conducted (Ref 7.28) with 16MnCr5 steel (AISI 5115) in order to compare the performance of chlorinated (widely used and environmentally hazardous) and nonchlorinated paraffin oils. The punch surface was coated with TiCN and three lubricants, including chlorinated paraffin oil, were evaluated. One of the nonchlorinated paraffin oils resulted in severe galling. Punching tests were

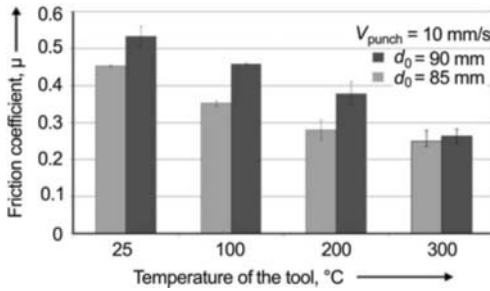


Fig. 7.20 Evolution of COF, μ_3 , with different tool temperatures: 22 MnB5 steel, initial sheet thickness $t_0 = 1.75$ mm, sheet temperature $T_s = 950$ °C, time at temperature $t_t = 5$ min, punch temperature $T_{\text{punch}} = \text{room temperature}$, $d_0 = \text{initial blank diameter}$, $V_{\text{punch}} = \text{punch velocity}$. Source: Ref 7.25

- 7.12 H. Kim, J. Sung, R. Sivakumar, and T. Altan, Evaluation of Stamping Lubricants using the Deep Drawing Test, *International Journal of Machine Tools and Manufacture*, Vol 47/17, 2007, p 2120–2132
- 7.13 G.M. Dalton and J.A. Schey, “Effect of Bead Finish Orientation on Friction and Galling in Drawbead Test,” SAE Technical Paper 920632, Society of Automobile Engineers, 1992
- 7.14 M. Vermeulen and J. Scheers, Micro-Hydrodynamic Effects in EBT Textured Steel Sheet, *International Journal for Machine Tools and Manufacture*, Vol 41, 2001, p 1941–1951

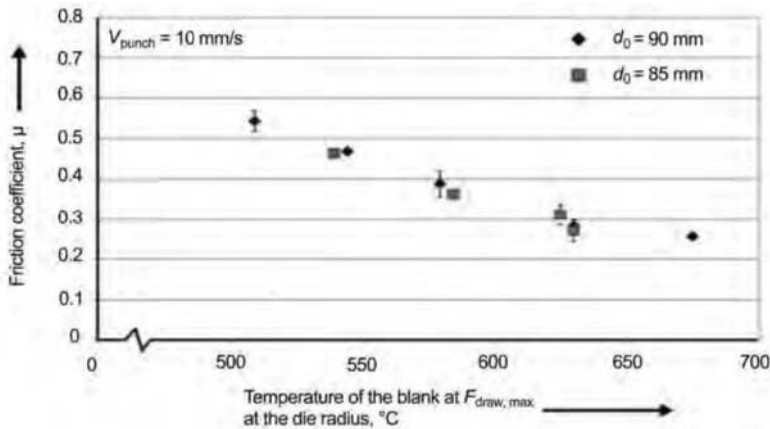


Fig. 7.21 COF, μ_3 , as a function of the blank temperature in the contact area at the die corner radius for maximum drawing force: 22 MnB5 steel, initial sheet thickness $t_0 = 1.75$ mm, sheet temperature $T_s = 950$ °C, time at temperature $t_t = 5$ min, $d_0 = \text{initial blank diameter}$, punch velocity $V_{\text{punch}} = 10$ mm/s punch at room temperature. Source: Ref 7.25

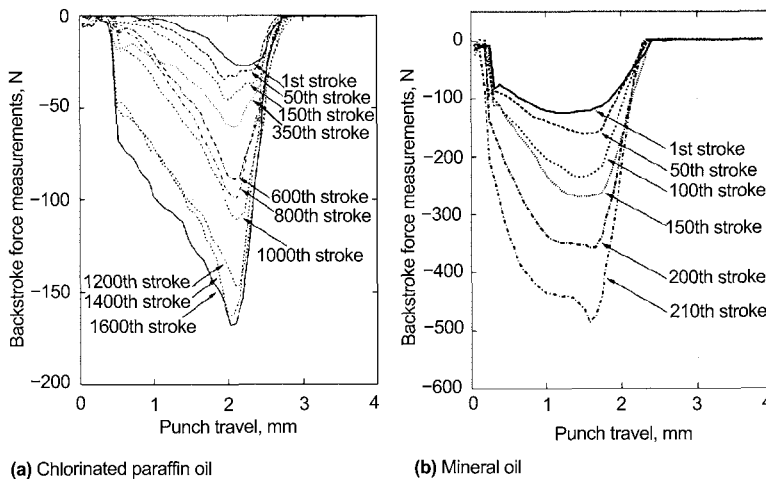


Fig. 7.22 Backstroke force versus punch travel for chlorinated paraffin oil and mineral oil. Source: Ref 7.29

- 7.15 J.L. Andreasen, N. Bay, and L. De Chiffre, **Quantification of Galling in Sheet Metal Forming by Surface Topography Characterization**, *International Journal of Machine Tools and Manufacture*, Vol 38, 1998, p 503–510
- 7.16 D.D. Olsson, N. Bay, and J.L. Andreasen, **Prediction of Limits of Lubrication in Strip Reduction Testing**, *Annals of CIRP*, Vol 53/1, 2004, p 231–234
- 7.17 H. Kim, J. Sung, F.E. Goodwin, and T. Altan, **Investigation of Galling in Forming Galvanized Advanced High Strength Steels (AHSS) using the Twist Compression Test (TCT)**, *Journal of Materials Processing Technology*, Vol 205, 2008, p 459–468
- 7.18 H. Kim, S. Han, F.E. Goodwin, K. Kim, and T. Altan, **“Evaluation of Die Coatings and Stamping Lubricants in Forming Galvanized Advanced/Ultra High Strength Steels using the Strip Drawing Test (SDT),”** presented at the International Deep Drawing Research Group (IDDRG) International Conference (Golden, CO), June 2009
- 7.19 H. Kim, T. Altan, and Q. Yan, **Evaluation of Stamping Lubricants in Forming Advanced High Strength Steels (AHSS) using Deep Drawing and Ironing Tests**, *Journal of Materials Processing Technology*, Vol 209/8, 2009, p 4122–4133
- 7.20 S. Wagner, H. Kleinert, and R. Zimmermann, **Dry Film Lubricants for Sheet Metal Forming**, *Proceedings of the International Conference of New Developments in Sheet Forming*, University of Stuttgart, 2002, p 451–472
- 7.21 S. Subramonian, N. Kardes, Y. Demiralp, M. Jurich, and T. Altan, **Evaluation of Stamping Lubricants in Forming Galvanized Steels in Industrial Environment**, *Journal of Manufacturing Science and Engineering*, in press.
- 7.22 S. Chandrasekharan, H. Palaniswamy, N. Jain, G. Ngaile, and T. Altan, **Evaluation of Stamping Lubricants at Various Temperature Levels using the Ironing Test**, *International Journal of Machine Tools and Manufacture*, Vol 45, 2005, p 379–388
- 7.23 A. Yanagida and A. Azushima, **Evaluation of Coefficients of Friction in Hot Stamping by Hot Flat Drawing Test**, *Annals of CIRP*, Vol 58/1, 2009, p 247–250
- 7.24 A. Yanagida and A. Azushima, **“Evaluation of Coefficients of Friction for Hot Stamping by Newly Developed Tribosimulator,”** presented at the International Deep Drawing Research Group (IDDRG) International Conference (Golden, CO), June 2009
- 7.25 M. Geiger, M. Merklein, and J. Lechler, **Determination of Tribological Conditions within Hot Stamping**, *Production Engineering Research and Development*, Vol 2/3, 2008, p 269–276
- 7.26 E. Siebel and H. Beisswanger, *Deep Drawing*, Carl Hanser Verlag, 1955
- 7.28 F. Klocke, T. Massmann, C. Zeppenfeld, R.A. Schmidt, J. Schulz, and F. Mumme, **Fineblanking of Non-chlorinated Lubricants**, *Tribologie und Schmierungstechnik*, Vol 55/4, 2008, p 33–38
- 7.29 D.D. Olsson, N. Bay, and J.L. Andreasen, **Analysis of Pick-up Development in Punching**, *Annals of CIRP*, Vol 51/1, 2002, p 185–190

CHAPTER 8

Deep Drawing of Round and Rectangular Cups

Nimet Kardes, The Ohio State University

IN DEEP DRAWING, a hollow cup is formed by forcing a flat, circular blank into or through a die using a punch. The blank is constrained by a blank holder while the central portion of the sheet is pushed into a die opening with a punch to draw the metal into the desired shape without causing wrinkles or splits in the drawn part. The term *deep drawing* implies that some drawing in of the flange metal occurs and that the formed parts are deeper than could be obtained by simply stretching the metal over a die (Ref 8.1). The thickness is assumed to be constant during the process (Ref 8.2). The process is capable of forming beverage cans, sinks, cooking pots, ammunition shell containers, pressure vessels, and auto body panels and parts.

Deep drawing involves the use of presses having a double action for hold-down force and punch force. The most critical region of a deep-drawn part is the flange, which is under circumferential compressive and radial tension stresses. In order to prevent wrinkling and to control the process, a blank holder (also referred to as the draw pad or binder) is used (Fig. 8.1). The blank

holder's main function is to apply a blank holder force (BHF) onto the cup flange to suppress wrinkling. If a blank holder is not used or if insufficient BHF is applied, then the cup may wrinkle (Fig. 8.2c, d). A secondary function of the blank holder is to restrain the material flow into the die by increased friction at the flange. This increased friction causes radial tension stresses in the flange, which must be supported by the cup wall. If too much BHF is applied, fracture may result before the desired cup height is attained (Fig. 8.2b). Only with the application of correct BHF can a good cup be drawn (Fig. 8.2a).

In deep drawing, the load required to form the cup is indirectly applied by the punch on the bottom of the cup (Fig. 8.1). The cup wall transmits the load to the deforming zones of the blank (Fig. 8.3). As a result, the cup wall is under tensile stresses that may lead to fracture, usually just above the punch corner radius (Ref 8.2).

8.1 Deformation during Deep Drawing

Deep drawing involves many types of forces and deformation modes, such as tension in the wall and the bottom, compression and friction in the flange, bending at the die radius, and straightening in the die wall. In a typical deep drawing of a round cup, various deformation zones can be identified (see Fig. 8.3):

- Zone A-C: the flange (axial compression, radial tension, circumferential compression)
- Zone C-D: the die corner radius (bending and friction)

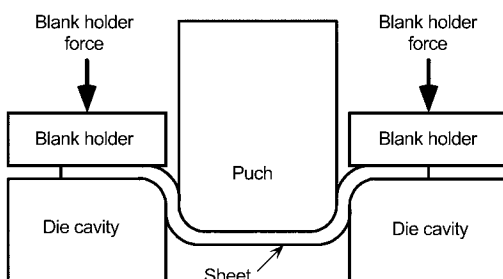


Fig. 8.1 Schematic of the deep drawing process

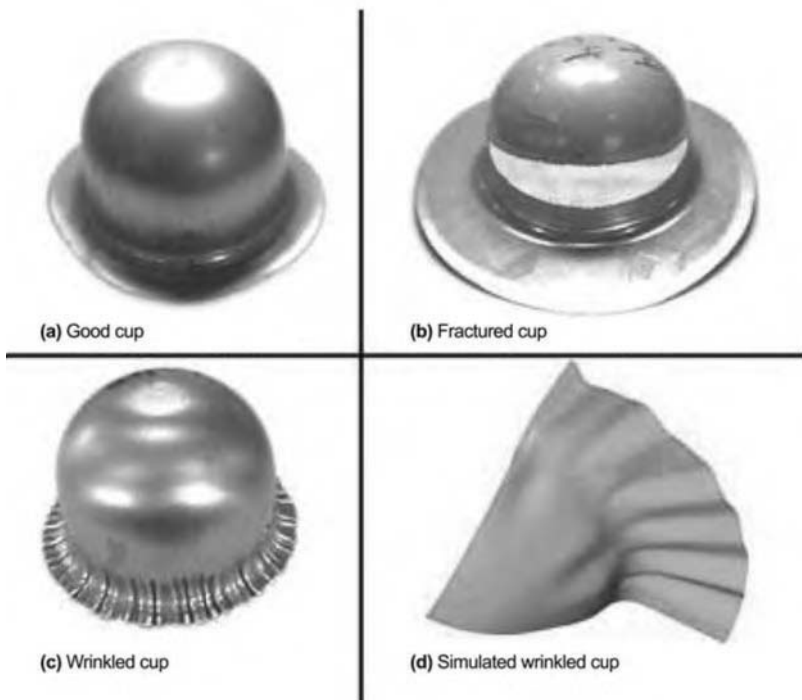


Fig. 8.2 Experimental (a, b, c) and simulated (d) deep-drawn cups

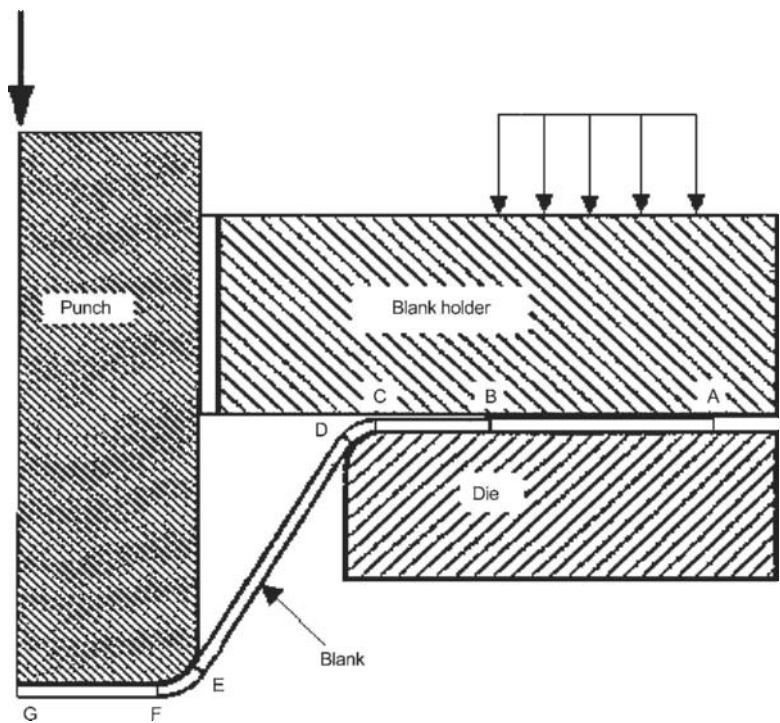


Fig. 8.3 Five deformation zones in deep drawing; Zone A-C: the flange (axial compression, radial tension, circumferential compression); Zone C-D: The die corner radius (bending and friction); Zone D-E: The wall of the cup (tension and potential fracture); Zone E-F: The punch corner radius (bending and friction); Zone F-G: The flat circular bottom (friction and near zero strain)

- Zone D-E: the wall of the cup (tension and potential fracture)
- Zone E-F: the punch corner radius (bending and friction)
- Zone F-G: the flat circular bottom (friction and near zero strain)

Zone A-C. The majority of deformation occurs in the flange of the cup, which undergoes radial elongation and circumferential compression. As the punch draws the sheet into the die cavity, the perimeter of the sheet is forced into a smaller diameter, resulting in flange thickening (zone A-B). Also, because of drawing by the punch, the sheet material close to the die corner undergoes some reduction in thickness (zone B-C). As a result, this portion of the flange may not contact the blank holder surface entirely.

Zone C-D. Once the material overcomes the compression of drawing through the flange, it must bend and unbend over the die radius. The state of stress in this zone is that of radial elongation and bending over the die radius. If the radius is too small, the sheet may fracture at this location. If it is too large, then the draw depth is reduced and the formability of the material is not fully utilized. Hence, certain guidelines are established for the proper selection of the die radius.

Zone D-E. The state of stress in this zone is that of radial and circumferential tension. If the punch die clearance is large, the unsupported regions of the cup wall may experience a form of out-of-plane deformation (similar to wrinkling) called *puckering*. The punch force is transmitted from the bottom of the cup to the deformation zone (flange) through tension on the wall of the cup. The tension must not cause the wall to deform plastically; otherwise, fracture may occur.

Zone E-F. In this zone, the sheet material undergoes bending over the punch corner radius and the state of stress is again that of radial tension. As the material bends over the die radius, it undergoes strain hardening. Hence, the flowing material, which forms the cup wall, becomes strengthened. The material at the punch corner radius is the most common failure site: the cup wall is weakest here because the portion of the sheet in this region has the least strain hardening.

Zone F-G. In this region, because of greater friction between the punch surface and the bottom of the cup, the material does not undergo much plastic deformation.

The deformation of the blank during deep drawing of a cup typically has three main consequences:

- Metal in the periphery of the blank area thickens slightly. The flange, while moving inward, is reduced in diameter and therefore tends to increase slightly in thickness (see Fig. 8.4).
- Metal in the periphery of the blank area moves toward the die under combined compressive and tensile forces that result from punch pressure.
- Metal in the area adjacent to the punch corner becomes thinner because of the stress imposed upon it by the resistance that the metal in the flange area encounters in overcoming compression and friction forces (see Fig. 8.5).

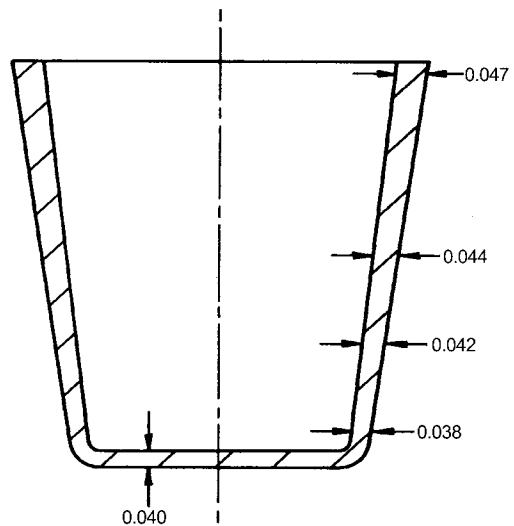


Fig. 8.4 Thickness variation along the cup wall. Source: Ref 8.3

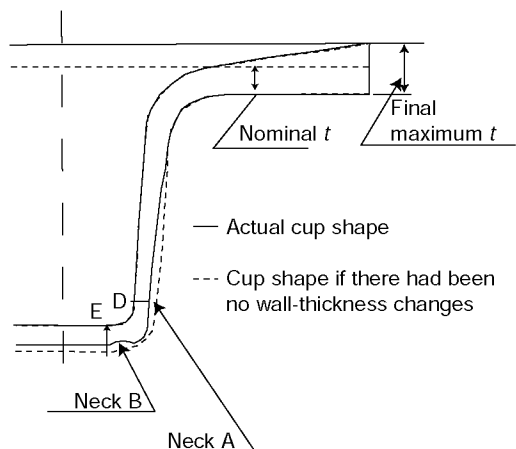


Fig. 8.5 Thinning and thickening of the cup. Source: Ref 8.4

Limiting Draw Ratio (LDR)

The draw ratio (DR) of a deep drawing operation is:

$$DR = \frac{\text{Blank diameter, } d_0}{\text{Cup diameter, } d_1} \quad (\text{Eq 8.1})$$

The limiting draw ratio (LDR) is defined as the maximum DR that can be obtained while drawing a cup without fracture:

$$LDR = \frac{\text{Maximum blank diameter (without fracture)}}{\text{Cup diameter}} \quad (\text{Eq 8.2})$$

The LDR for some common materials is given in Table 8.1. LDR is considered a good measure of drawability of a material. However, it depends on the material properties, the blank thickness, the punch and die geometry, and the lubrication conditions.

LDR is influenced by many factors and can be increased by:

- Decreasing blank holder-sheet friction
- Decreasing sheet-die friction
- Increasing sheet-punch friction
- Increasing relative ratio of blank thickness to diameter (s_0/d_0)
- Increasing ratio of punch corner radius to punch diameter (r_p/d_p)
- Decreasing relative punch diameter (ratio of punch diameter to thickness)
- Using a material with high strain-hardening exponent, n ($\bar{\sigma} = K\bar{\epsilon}^n$)
- Increasing normal anisotropy (\bar{r} -value)
- Decreasing planar anisotropy (Δr -value)

In progressive and transfer die applications, several consecutive draw operations are used, and the practical LDRs are much lower than those given in Table 8.1.

Parameters Affecting the Deep Drawing Process

Deep drawing is affected by a large number of parameters such as material properties, blank

configurations, die and press design and setup, and complex interactions among the sheet, die, and lubrication. The major parameters of the deep drawing process are:

Material Properties

- Strength coefficient, K
- Strain-hardening coefficient, n
- Normal anisotropy, r
- Planar anisotropy, Δr

Geometry (see Fig. 8.6)

- Punch corner radius, r_p
- Die radius, r_D
- Punch-die clearance, u_D
- Blank diameter, d_0
- Blank thickness, s_0

Interface conditions

- Lubrication/friction conditions

Equipment and tooling

- Press speed
- Blank holder

Material Properties and Their Influence on Formability

The plastic behavior of materials is usually described by the strength coefficient, K , and the strain-hardening coefficient, n , when the flow stress of the material is expressed as $\bar{\sigma} = K\bar{\epsilon}^n$. These two material properties significantly influence the deep drawing operation. The normal anisotropy, r , also plays an important role in the drawing process.

Effect of Strength Coefficient, K . The strength coefficient has little influence on formability but affects punch force. During a drawing operation, the metal in the flange must be drawn in easily without causing fracture in the wall. A high K -value means a strong wall, which is beneficial, but also a strong flange, which makes it

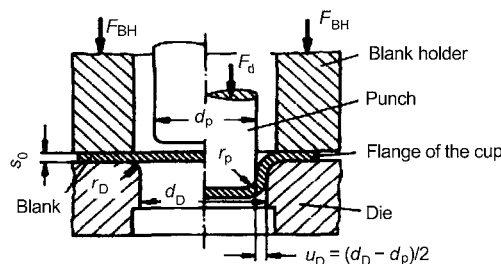


Fig. 8.6 Tool geometry in the deep drawing process. Source: Ref 8.2

Table 8.1 Maximum limiting draw ratio values (approximate) for some common materials

Material	LDR _{max}
Steel sheet, depending on quality	1.8–2.2
Aluminum, copper, Al-Cu-Mg sheets	2.1
Brass sheet, depending on prestrain	1.7–2.2

Source: Ref 8.2

harder to draw in. Therefore, for a successful drawing operation, the K -value should be sufficiently large to assure a reasonable strength of the product, but not be so high as to require excessive punch force to complete the draw.

Effect of Strain Hardening. The strain-hardening exponent, n , is an indicator of material formability and plays a crucial role in sheet metal forming. A higher n -value strengthens the cup wall, but it also strengthens the flange so that more force is needed to deform it. Nevertheless, the LDR tends to increase with increasing n -value.

Effect of Anisotropy. The r -value is a measure of plastic anisotropy in sheet materials and is defined as the instantaneous ratio of width strain to thickness strain during the plastic deformation in a tensile test (see “Plastic Deformation—Flow Stress, Anisotropy, and Formability” in this volume):

$$r = \frac{d\epsilon_{\text{width}}}{d\epsilon_{\text{thickness}}} \quad (\text{Eq 8.3})$$

An average or normal plastic anisotropy, \bar{r} , is defined as:

$$\bar{r} = \frac{r_0 + 2r_{45} + r_{90}}{4} \quad (\text{Eq 8.4})$$

where r_0 , r_{90} , and r_{45} are the r -values at 0° , 90° , and 45° from the rolling direction. Increasing r -values decrease the force to deform the flange while increasing the strength of the cup wall. The planar anisotropy Δr and affects the “earring” of a drawn cup, as shown in Fig. 8.7, and is defined as:

$$\Delta r = \frac{r_0 - 2r_{45} + r_{90}}{2} \quad (\text{Eq 8.5})$$

The r -value indicates the ability of the material to resist thinning. A high r -value means that the material gets narrower rather than thinner. A good drawing material has a high r -value ($r > 1$), which means that it flows easily in the plane of the sheet but not in the thickness direction. A material that flows easily in the thickness direction ($r < 1$) has an undesirable tendency to thin under the influence of wall tension during drawing. This excessive thinning ($> 20\%$) may lead to cup failure by tearing. Typical r -values exceed 1.0 for various steels and are usually less than 1.0 for aluminum. High r -values result in improved LDR (Ref 8.6), as shown by:

$$\ln(\text{LDR}) = \eta \sqrt{(r+1)/2} \quad (\text{Eq 8.6})$$

where η is the deformation efficiency (typically around 0.74 to 0.79 (Ref 8.7)).

Planar anisotropy, Δr , has a minor but important effect on drawability. The higher the Δr , the more earring occurs. Earring typically must be trimmed; therefore, an increase in Δr increases trimming and reduces the total depth of draw (Ref 8.7).

Geometric Parameters and Their Influence

Punch and die geometry affect metal flow and friction in deep drawing.

Die Radius. The die radius should be selected based on the blank thickness and diameter. If the die radius is too small, fracture can occur. Therefore, large die radius is preferred for decreasing the drawing load and increasing the LDR (Fig. 8.6). However, the contact area between the blank holder and the flange becomes smaller with increasing die radius, which may result in wrinkles in the die radius region (Ref 8.2). The recommended values of die radii

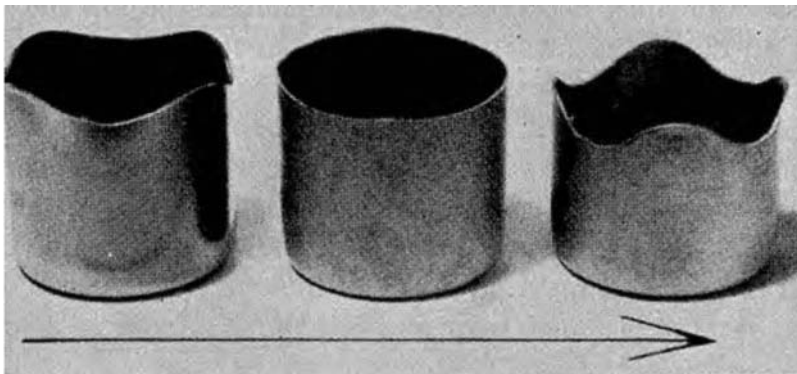


Fig. 8.7 Earring in cup drawing. The arrow indicates the rolling direction. Source: Ref 8.5

for aluminum alloys are about 4 to 8 blank thickness, s_0 , and for stainless steel they are about 5 to 10 s_0 (Ref 8.8).

Punch Corner Radius. Fracture normally occurs at the bottom of the cup wall (where the punch radius meets the cup wall; see Fig. 8.6). The cup is weakest at the bottom because it does not undergo as much work hardening as do the sides of the wall. The walls are strengthened by work hardening due to bending and unbending of the sheet over the die radius. As the punch corner radius is increased, the failure site moves upward into the material (cup walls) that has been strengthened by prior work hardening. A generous corner radius also results in a gradual increase of the punch load with stroke (Ref 8.7). The recommended values of punch radii for aluminum alloys are about 10 s_0 , while for stainless steel they are about 5 to 10 s_0 (Ref 8.9).

- Punch corner radius, r_p , should be three to five times larger than the die radius, r_D (Ref 8.2).
- Die radius, r_D , greater than 10 times the blank thickness, s_0 , may cause wrinkling (Ref 8.10).

Punch-Die Clearance. If the clearance between the punch and the die is smaller than the

thickness of the upper portion of the cup, this portion of the cup will be reduced in thickness due to ironing. During the ironing process, the gap between the die and the punch is larger than the initial blank thickness but smaller than the expected thickness at the top of the cup. As a result, the top of the cup (where the cup is thickened the most) is squeezed between the die and the punch, and a cup with more uniform wall thickness is produced (see Fig. 8.8). This ironing process requires a considerable punch force, and if the cup is nearly formed before ironing occurs, the punch load/punch stroke diagram exhibits a second maximum (see Fig. 8.9).

Empirical equations are used to determine the punch-die clearance for deep drawing of round cups without ironing (Ref 8.2). Suggested values of die clearance, U_D , as a function of blank thickness, s_0 , for common materials are shown in Table 8.2.

Effect of Friction

In the deep drawing, friction exists at three interfaces:

- Between the blank holder and the flange
- Between the flange and the die
- Between the blank and the punch

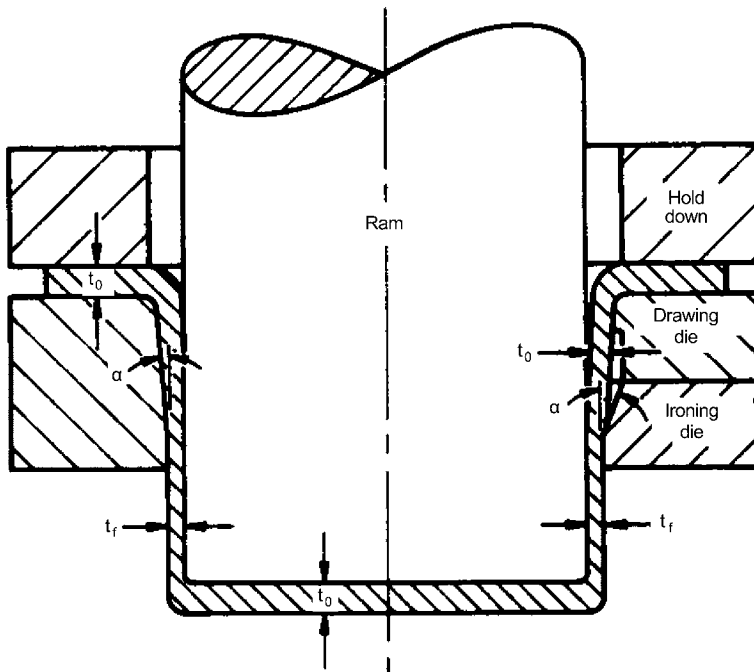


Fig. 8.8 Schematic of the ironing process. Source: Ref 8.4

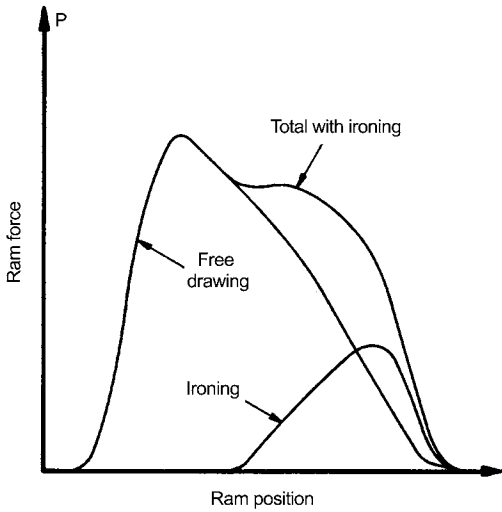


Fig. 8.9 Punch force/punch stroke diagram: ironing process combined with forming. Source: Ref 8.3

Table 8.2 Empirical equations for die clearance, U_D , for various materials

$U_D = s_0 + 0.07 \sqrt{10} s_0$	Steel
$U_D = s_0 + 0.02 \sqrt{10} s_0$	Aluminum
$U_D = s_0 + 0.04 \sqrt{10} s_0$	Other nonferrous alloys
$U_D = s_0 + 0.20 \sqrt{10} s_0$	High-temperature alloys

Source: Ref 8.11

Friction depends not only on lubrication but also on the materials of the tool and the blank, their surface conditions, and the BHF. Low friction at the die/blank holder interface and high friction at the punch and cup interface lead to larger achievable LDRs. Values for coefficients of friction (COFs) in deep drawing are typically in the range of 0.04 to 0.10.

Equipment and Tooling

Ram Speed. Ram speed affects friction at the material-tool interface. As a result, it may determine whether the wall of a drawn part will rupture, particularly at the moment when drawing begins. Ram speed should be adjusted to the complexity of the die geometry and the performance of the lubricant. Such adjustment is possible in hydraulic and servo-drive presses that allow the adjustment of the ram speed during the stroke. In mechanical presses, various link drives are used to achieve high approach, low impact, low deformation, and high return speeds of the ram. Typical drawing speeds for various materials are given in Table 8.3.

Table 8.3 Typical drawing speeds for various materials

Material	Drawing speed	
	fpm	mm/s
Steel	18–50	91–254
Stainless steel	30–40	152–203
Copper	125–150	635–762
Zinc	125–150	635–762
Aluminum	150–175	762–889
Brass	175–200	889–1016

Source: Ref 8.12

Blank holder. The blank holder force (BHF) is applied to prevent wrinkling in the flange as well as in the wall of the drawn cup. Excessive BHF leads to fracture in the cup wall (Fig. 8.10). The maximum draw depth corresponds to simultaneous failure by wrinkling and failure. For any depth of cup less than the corresponding BHF value, there is a “window” of allowable BHF (Fig. 8.10).

“The BHF necessary to avoid wrinkling depends on the drawing ratio, sheet material and the relative blank thickness” (Ref 8.2). As the relative blank thickness (s_0/d_0) decreases, the tendency to wrinkle increases, which necessitates more BHF to control the flow and prevent wrinkling. The blank holder pressure required to prevent wrinkling of the sheet can be estimated as (Ref 8.13):

$$p_{BH} = 10^{-3} c \left[(DR - 1)^3 + \frac{0.005 d_0}{s_0} \right] S_u \quad (\text{Eq 8.7})$$

$$F_{BH} = p_{BH} \times A_{BH} \quad (\text{Eq 8.8})$$

where

s_0 is the blank thickness

d_0 is the blank diameter

p_{BH} is the blank holder pressure

F_{BH} is the blank holder force, BHF

A_{BH} is the area of the blank under the blank holder

c is the empirical factor, ranging from 2 to 3

S_u is the ultimate tensile strength of the sheet material

DR is the draw ratio (blank diameter/cup diameter)

Different modes of failure are important at different stroke positions. At the start of deformation, the flange is relatively large and may

require a relatively large BHF to prevent wrinkling. However, as the punch stroke increases, the drawn cup is deeper and the remaining flange under the blank holder is smaller. Consequently, the BHF can be reduced with punch stroke or draw depth (see, e.g., Fig. 8.11). Thus, the tensile stresses in the cup wall and the probability of premature fracture are also reduced.

The effect of BHF and how it can be adjusted in deep drawing of complex parts are discussed in Chapter 13, “Cushion Systems for Sheet Metal Forming,” in this book, where cushion systems are reviewed.

Prediction of Stresses, Strains, and Punch Force using the Slab Method

Prediction of Stresses. It is possible to analyze the metal flow in round cup drawing by using the slab method (Ref 8.2). In this method, the drawn cup is divided into three different regions: flange, die corner radius, and cup wall (zones A-B, C-D, and D-E, respectively; see Fig. 8.3). The symbols used in the analysis are shown in Fig. 8.12.

The blank is divided into finite number of slabs, and one of these slabs is studied as it is

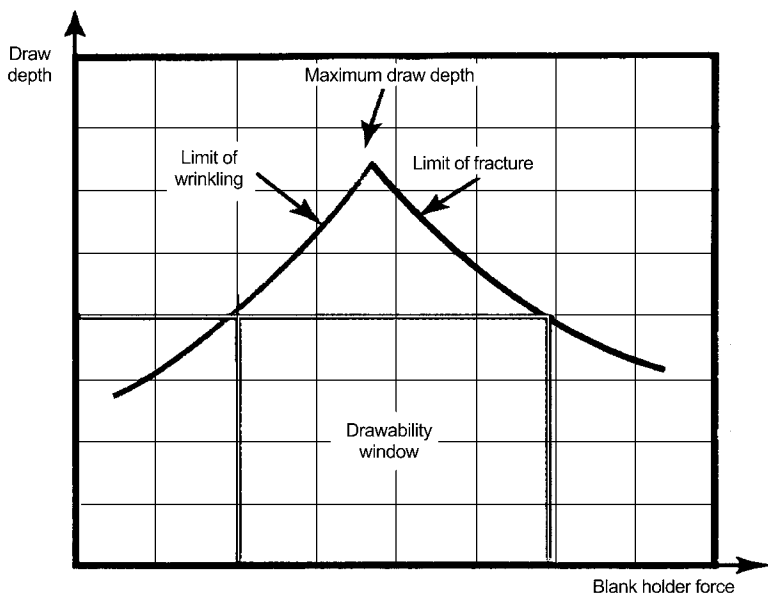


Fig. 8.10 Window showing the allowable blank holder force that can be applied

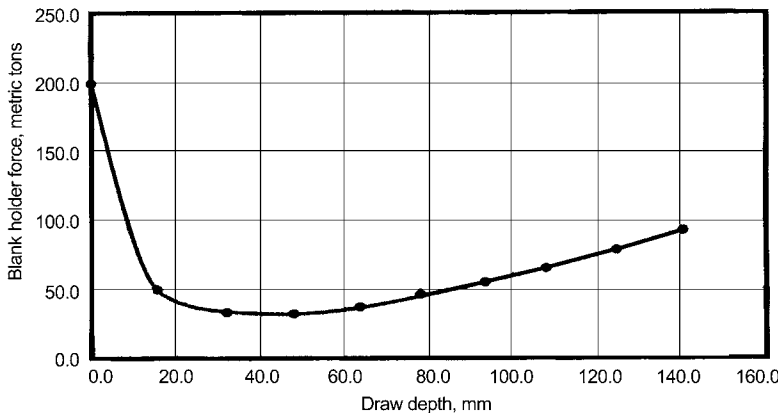


Fig. 8.11 Example optimal blank holder force/time profile for obtaining larger draw depth

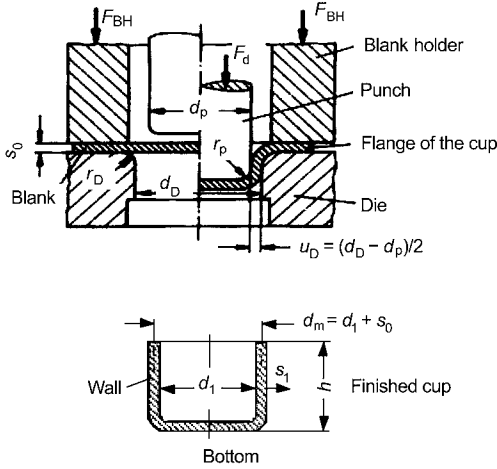


Fig. 8.12 Symbols used in the analysis of cup drawing. Source: Ref 8.2

forced to move from the flange to the cup wall during the process. The stress state in the slab is different in each region. The forces acting on the slab are balanced within each region by considering the different stress states. Consequently, the required drawing force and BHF are determined in terms of these stresses.

Initially the slab is under no stress (position I in Fig. 8.13a). As the punch moves down, the slab moves in the flange region. In this position, the slab is under tension radially and compression tangentially (position II in Fig. 8.13b).

Considering the friction between flange and die and between flange and blank holder, the force balance in the radial direction at position II is given by:

$$(\sigma_r + d\sigma_r)(r + dr) \cdot d\alpha \cdot s - \sigma_r \cdot r \cdot d\alpha \cdot s + 2|\sigma_t|s \cdot dr \cdot \sin\left(\frac{d\alpha}{2}\right) + 2\mu \cdot dr \cdot r \cdot d\alpha \cdot p_{BH} = 0 \quad (\text{Eq 8.9})$$

where

- α is the angle of the slab under consideration
- μ is the coefficient of friction, COF
- r is the instantaneous radius
- σ_r is the stress in radial direction
- σ_t is the stress in tangential direction
- s is the instantaneous sheet flange thickness

In this case, α is assumed to be small, so $\sin(d\alpha/2) = d\alpha/2$ and Eq 8.9, after dividing both sides by $(r d\alpha s)$, becomes:

$$d\sigma_r = -\left[\left(\frac{\sigma_r + |\sigma_t|}{r}\right) + \left(\frac{2\mu p_{BH}}{s}\right)\right] dr \quad (\text{Eq 8.10})$$

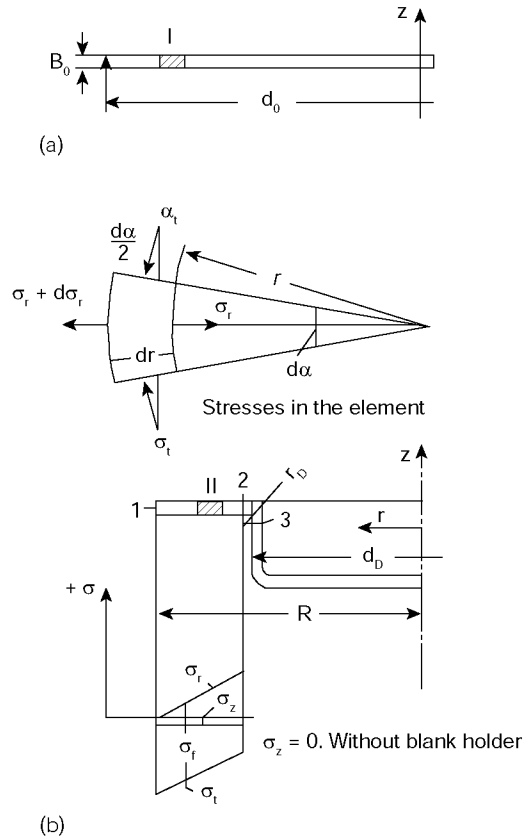


Fig. 8.13 (a) Position I-II of the slab and (b) stress state in position II. Source: Ref 8.2

Using the Tresca yield criterion, $\sigma_1 - \sigma_3 = \sigma_f$, in the analysis and considering that the predicted stress value by using this criterion is about 10% smaller than the actual value, we obtain:

$$\sigma_r + |\sigma_t| = 1.1 \sigma_f \quad (\text{Eq 8.11})$$

where $\sigma_1 = \sigma_r$ is the stress in the first principal direction, $\sigma_3 = \sigma_t$ is the stress in the third principal direction, and σ_f is the flow stress.

The stresses in the radial direction are evaluated by substituting Eq 8.11 into Eq 8.10 and by integrating Eq 8.10 through the flange region:

$$\sigma_r(r) = 1.1 \sigma_{f,m,I} \ln\left(\frac{R}{r}\right) + 2\mu(R-r) \frac{p_{BH}}{s} \quad (\text{Eq 8.12})$$

where $\sigma_{f,m,I}$ is the mean flow stress in the flange region between positions I and II and R is the instantaneous outside radius of the flange.

When the slab is at position III (see Fig. 8.14), the stress in the axial direction, σ_z , at position III is the same as the stress in the radial direction, σ_r , at position II, excluding the effect of friction and bending at the die corner radius region:

$$\sigma_z = \sigma_r \quad (\text{Eq 8.13})$$

When the effect of friction at the die corner radius is taken into account, the stress in the axial direction, σ_z , can be redefined as a function of the COF, μ , and the stress in the radial direction, σ_r :

$$\sigma_z = \sigma_r e^{\mu s/2} \quad (\text{Eq 8.14})$$

Prediction of Strains. In the slab analysis, the effect of bending on the strains in the tangential, radial, and axial directions is neglected. The strains in the tangential (ε_t), axial (ε_z), and radial (ε_r) directions are approximated:

$$\varepsilon_t = \ln\left(\frac{d_1}{d_0}\right), \varepsilon_z = \ln\left(\frac{s_1}{s_0}\right), \varepsilon_r = \ln\left(\frac{s_0 d_0}{s_1 d_1}\right) \quad (\text{Eq 8.15})$$

where d_1 is the inner cup diameter and s_1 is the instantaneous sheet wall thickness.

Prediction of Punch Force. The required force for drawing exerted by the punch is the sum of the forces required to deform the blank and to overcome friction between flange and die and between flange and blank holder. In addition, the effect of bending at the die corner radius region has to be included. Thus, the required

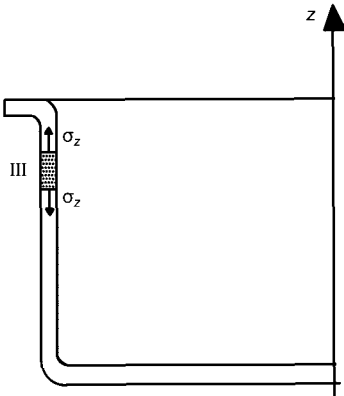


Fig. 8.14 Slab in position III. Source: Ref 8.2

maximum punch force, $F_{d,max}$, can be represented as (Ref 8.13):

$$F_{d,max} = \pi d_m s_0 \left[\underbrace{e^{\mu\pi/2} 1.1 \sigma_{f,m,I} \ln \frac{d_{F,max}}{d_m}}_{\text{Deformation}} + \underbrace{\frac{2\mu F_N}{\pi d_{F,max} s_0}}_{\text{Friction}} + \underbrace{\sigma_{f,m,II} \frac{s_0}{2r_D}}_{\text{Bending}} \right] \quad (\text{Eq 8.16})$$

where

$d_m = d_1 + s_0$ is the mean cup wall diameter

d_1 is the inner cup diameter

$d_{F,max}$ is the outside diameter of the flange when the drawing load is maximum

$\sigma_{f,m,II}$ is the mean flow stress in the die corner radius region between positions II and III

r_D is the die corner radius

F_N is the normal force

The friction at the die corner radius region is included in the deformation term.

Finite Element Method (FEM)

Numerous commercial FEM programs are available for analyzing the mechanics of sheet forming operations. Most of these programs can consider the effect of strain, strain rate, and temperature upon flow stress. Furthermore, they have a database for considering various material models and yield criteria. The main advantages of the FEM are: (a) the ability to obtain detailed information in the deforming sheet material (velocities, strain rates, strains, stresses, temperatures, and pressures) and (b) the fact that the same computer code can be used for a large variety of problems by simply changing the input data (Ref 8.14). These data consist of (a) geometric information (die and blank dimensions), (b) material properties (flow stress in function of strain, strain rate, and temperature), and (c) an average value of the COF at the interface of sheet and tool components. In certain cases it is possible to use a COF that is a function of interface pressure or interface conditions.

For practical application of finite element (FE) simulation in general, the following steps are carried out:

1. A geometric model is created, either in a CAD program, such as IDEAS, Pro-E, or Unigraphics, or in the preprocessor of

an FE program, such as IDEAS, ANSYS, DEFORM, AUTOFORM, LS-DYNA, or PAMSTAMP.

2. The geometric model is imported into one of the FE programs.
3. The physical and material properties of the model are defined.
4. The geometric model is meshed.
5. The boundary conditions such as loading and displacements are applied.
6. The solution is obtained by starting the FE simulation.

FE Model of Round Cup Drawing and Comparison with Experiments. Round cup drawing was simulated with PAMSTAMP, a commercially available FEM code. ASTM A1011 DS type-B material was used in both the simulations and the experiments (Ref 8.15). The geometric model was created in one of the CAD programs, HyperMesh. The quarter model, given in Fig. 8.15, was used because the problem involved symmetry in geometry and loading. The model was meshed in the same CAD program and then imported into the FE code. Shell elements were used in the mesh. Punch, die, and blank holder were assumed to be rigid, and the sheet was assumed to be elastic-plastic. In order to obtain the material properties (see Table 8.4), biaxial (Ref 8.16) and elliptical bulge tests were conducted. Strength and strain-hardening coefficients were obtained by biaxial bulge test, and normal anisotropy was obtained by elliptical bulge test.

The process parameters and tool geometry used in the FE simulations and experiments are given in Table 8.5 and Fig. 8.16.

Prediction of Stress and Strain by FEM.

The stress and strain distributions throughout the process are among the outputs of the FE simulation. The predicted equivalent strain distributions at the last step of the simulation are shown in Fig. 8.17.

Prediction of Punch Force. One of the outputs of the FE simulation is the punch force/punch stroke curve. FE simulations can also be used to determine the COF of a lubricant by comparing the punch force/punch stroke curves obtained from simulations and experiments. Two simulations were done in which the COFs, μ , were 0.07 and 0.09. According to Fig. 8.18, the COF of the lubricant was between 0.07 and 0.09.

Effect of Process Variables on Simulation Results. The process variables that affect the FE simulation results of round cup drawing are:

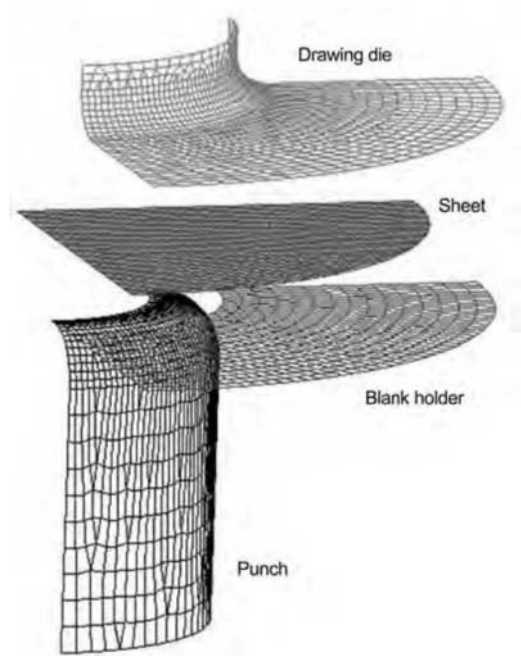


Fig. 8.15 The quarter finite element model of round cup drawing. Source: Ref 8.15

Table 8.4 Material properties of ASTM A1011 DS type-B (for $\bar{\sigma} = K\bar{\epsilon}^n$)

Young's Modulus, E	210 GPa
Poisson's Ratio, ν	0.3
Strength coefficient, K	498.8 MPa
Strain hardening coefficient, n	0.131
Normal anisotropy	1.5

Source: Ref 8.15

Table 8.5 Process parameters

Coefficient of friction, μ	0.07–0.09
Blank holder force, BHF	50 tons
Test speed	15 mm/sec

Source: Ref 8.15

- Material properties: strength coefficient (K) and strain-hardening coefficient (n) (for $\bar{\sigma} = K\bar{\epsilon}^n$)
- Blank diameter
- Blank thickness
- Coefficient of friction, COF (μ)
- Blank holder force, BHF

Several simulations were conducted to investigate the influence of the process variables on the simulation results. The effects were investigated by varying only one process parameter at

a time and keeping all the others constant in the simulations in order to eliminate the interaction between various process parameters and to study the individual effects. The predictions were then compared with experimental results. Certain parameters were chosen among the outputs of the FE simulation for comparison with experimental data:

- Draw-in of the sheet (flange draw and cup depth) (Fig. 8.16)
- Maximum punch force
- Maximum thinning (%)

The tool dimensions used in the simulations and experiments were:

- Punch diameter (mm/in.) = 152.40/6.00
- Punch corner radius (mm/in.) = 20.07/0.79
- Die opening diameter (mm/in.) = 158.24/6.23

- Die corner radius (mm/in.) = 16.00/0.63

Effect of Strength Coefficient (K). Three different simulations shown in Table 8.6 were conducted in order to investigate the influence of K . In these simulations, all the process parameters (see Table 8.7), excluding K , were kept constant.

The influence of K on the FE simulation results is shown in Table 8.8. As K increases, the required punch load increases and thinning (%) decreases. The effect of K on the punch force/punch stroke curve is shown in Fig. 8.19.

Effect of Strain-Hardening Coefficient (n). Three different simulations (Table 8.9) were conducted in order to investigate the influence of n , using the process parameters given in Table 8.10.

As the strain-hardening coefficient (n) increases, the required punch load decreases, and

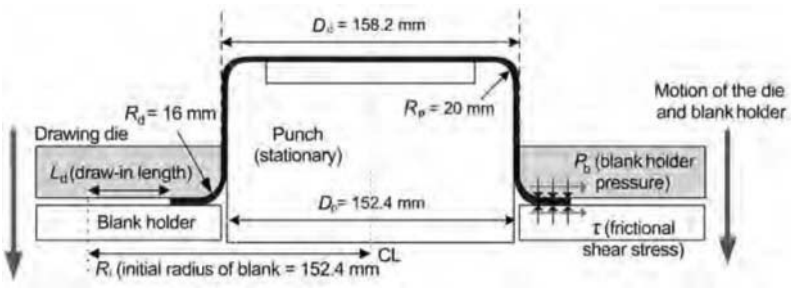


Fig. 8.16 Tool geometry used in the finite element simulations and experiments. Source: Ref 8.15

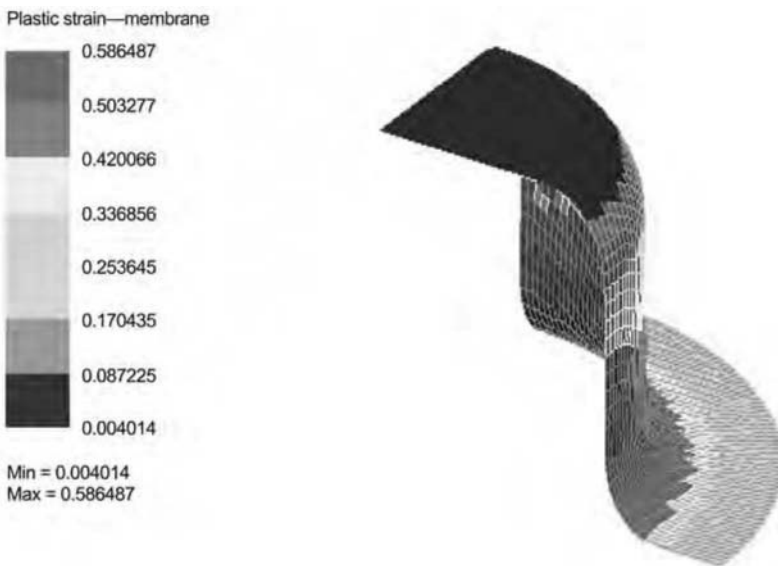


Fig. 8.17 The equivalent strain distribution in the last step (coefficient of friction = 0.07). Source: Ref 8.15

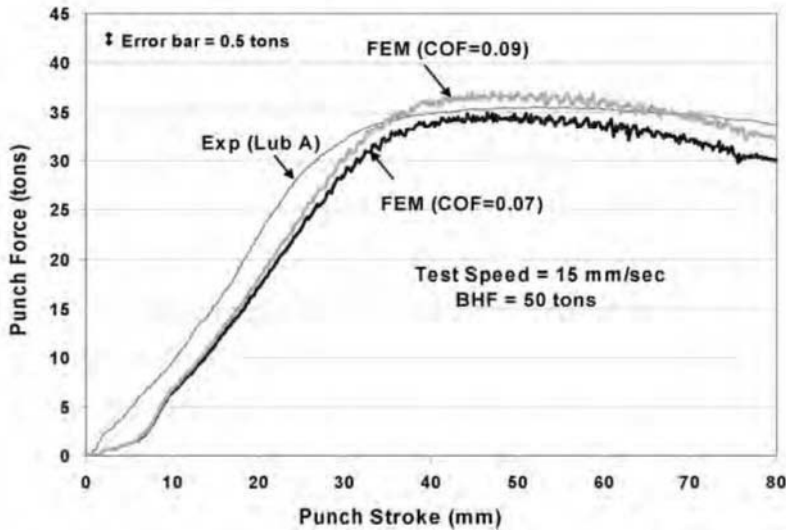


Fig. 8.18 Punch force/punch stroke curves obtained from finite element model (FEM) simulations and experiment (Exp) with lubricant (Lub A). COF, coefficient of friction. Source: Ref 8.15

Table 8.6 Strength coefficient (K) values used in each simulation

Simulation name	K1	K2	K3
Strength coefficient, MPa/ksi	200/29	500/72.5	800/116

Table 8.7 The process parameters used in the simulations

Material	Unknown, $n = 0.3$
Blank thickness, t , mm/in.	0.889/0.035
Blank diameter, d , mm/in.	304.8/12.0
Blank holder force, BHF, kN	117.0
Coefficient of friction, μ	0.08

Table 8.8 The influence of K on the simulation results

Simulation	Draw, mm	Draw, mm	Max. punch force, kN	Thinning, %
	Flange	Cup height		
K1, 200 MPa	9.3	46.8	50.0	20.3
K2, 500 MPa	56.9	107.4	114.0	13.9
K3, 800 MPa	56.7	104.1	170.0	10.6

thinning (%) and draw depth increase (see Table 8.11). The effect of n on punch force versus punch stroke curve is shown in Fig. 8.20.

Effects of Tool Geometry and Friction. The effects of tool geometry and friction on the simulation results were investigated using the mate-

rials listed below. The flow stress data (K and n) were determined by tensile tests.

- Aluminum alloy AA-2024-O: $K = 266.15$ MPa, $n = 0.134$
- High-strength steel: $K = 603.83$ MPa, $n = 0.143$
- Interstitial free steel: $K = 622.38$ MPa, $n = 0.263$

Effect of Blank Thickness. Two different simulations were conducted to investigate the effect of blank thickness (see Table 8.12). All the process parameters are given in Table 8.13.

As blank thickness increases, the punch load and draw depth increase (see Table 8.14). The effect of blank thickness on punch force versus punch stroke curve is shown in Fig. 8.21.

Effect of Blank Diameter. Three different simulations were conducted to investigate the effect of blank diameter (Table 8.15). The rest of the process parameters are given in Table 8.16.

As the blank diameter increases, the required punch load, thinning (%), and draw depth increase (Table 8.17). The effect of blank diameter on punch force/punch stroke curve is shown in Fig. 8.22.

Effect of Coefficient of Friction, COF (μ). Simulations were conducted with three different COFs (Table 8.18). The rest of the process parameters are given in Table 8.19.

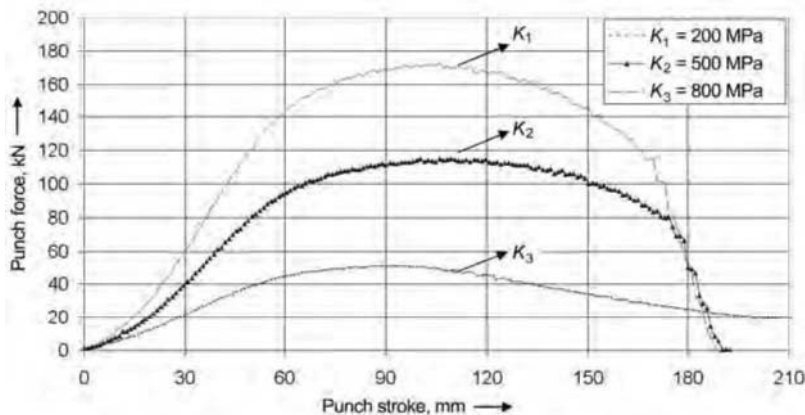


Fig. 8.19 Punch force/punch stroke curves for different K -values

Table 8.9 Values of the strain-hardening coefficient, n , of each simulation

Simulation name	n1	n2	n3
Strain hardening coefficient	0.1	0.3	0.5

Table 8.10 The process parameters used in the simulations

Material	Unknown, $K = 500$ MPa
Blank thickness, t , mm/in.	0.889/0.035
Blank diameter, d , mm/in.	304.8/12.0
Blank holder force, BHF, kN	117.0
Coefficient of friction, μ	0.08

Table 8.11 The influence of the strain-hardening coefficient, n , on the simulation results

Simulation	Draw, mm	Draw, mm	Max. punch force, kN	Thinning, %
	Flange	Cup Height		
N(1) $n = 0.1$	55.5	100.7	146.0	6.8
N(2) $n = 0.3$	56.9	107.4	114.0	13.9
N(3) $n = 0.5$	56.4	114.1	94.0	22.9

As the COF increases, the required punch load and thinning (%) increase, and draw depth remains unchanged (Table 8.20). The effect of COF on punch force/punch stroke curve is shown in Fig. 8.23; the COF of the lubricant used in the experiment was 0.04.

Effect of BHF. Three different simulations were conducted to investigate the effect of BHF

(Tables 8.21 and 8.22). The rest of the process parameters are given in Table 8.23.

According to the simulations and the experiments, high BHF causes fracture, and low BHF causes wrinkling. When a variable BHF (with appropriate values) was used throughout the punch stroke, both fracture and wrinkling were avoided (see Table 8.24)

8.2 Deep Drawing of Rectangular Cups

Various modes of deformation that occur in deep drawing rectangular cups are illustrated in Fig. 8.24. The metal flow at the corners of the cup is similar to an axisymmetric deep drawing operation, whereas the sides undergo a bending and unbending operation. Fracture typically occurs in the corner wall region of the cup (Fig. 8.25). Higher BHF is required to overcome the compressive stresses in the corners than to overcome the bending forces in the sides. Thus, the corner wall regions experience higher stresses than the sidewalls. Furthermore, the corner flange area tends to thicken more than the side flange area. As a result, the blank holder pressure is concentrated on the corner flange areas, and the severity of the corner wall stresses is further increased.

Decreasing the pressure on the flange corners allows the corners to draw in more freely, thereby decreasing stress in the cup wall. Increasing the pressure on the flange sides restrains the flow of material and reduces the ex-

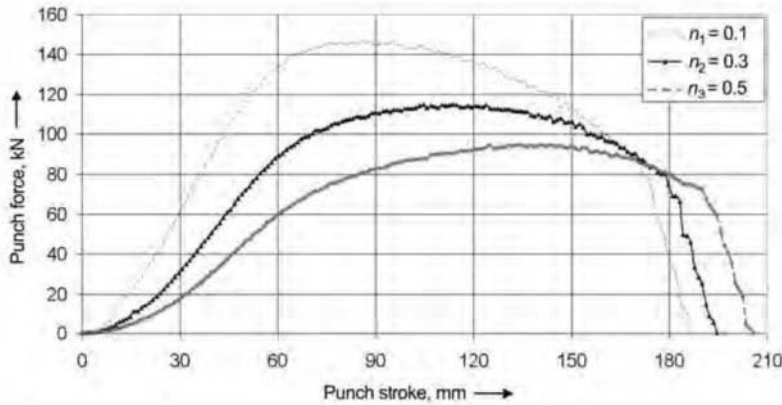


Fig. 8.20 Punch force/punch stroke curves for different n -values

Table 8.12 Blank thickness values used in each simulation

Simulation name	T1	T2
Blank thickness, mm/in.	1.016/0.04	1.60/0.063

Table 8.13 The process parameters used in the simulations

Material	AA 2024 – O
Blank diameter, mm/in.	304.8 /12.0
Blank holder force, BHF, kN	60.0
Coefficient of friction, μ	0.04

Table 8.14 The influence of blank thickness on the simulation results

Simulation	Draw, mm		Max. punch force, kN	Thinning, %
	Flange	Cup height		
T1 = 1.016 mm	55.7	99.2	80.0	7.43
T2 = 1.60 mm	61.0	104.7	124.0	7.31

cess material that causes oil canning and other shape problems in rectangular drawn cups. Thus, it is desirable to have a BHF that varies over the flange area in order to deflect the blank holder elastically in a way that promotes drawing and increases part quality. More BHF is needed in the corners than in the sides, in order to suppress the wrinkling that tends to occur in the corners because of circumferential compressive stresses.

Major Defects in Deep Drawing of Rectangular Cups

A defect in deep drawing generally consists of a final undesirable geometry or surface finish of the cup. Frequent defects encountered in deep drawing of rectangular cups are wrinkling, puckering, tearing, orange peel, and scratches. The two common modes of failure are tearing and wrinkling (Fig. 8.26).

Fracture and Thinning. Fracture may be observed as a split or tear (excessive stretching), a surface crack (excessive bending), or an edge failure (caused by an imperfection in the blanked edge).

Wrinkling or buckling is caused by compressive stresses and typically occurs on the flange of the part. Often it may not be a concern if the flange is trimmed, as with many automotive parts. Puckering is when wrinkling occurs in the sidewall of the rectangular part. Unlike flange wrinkling, puckering is of major concern. It can be avoided by increasing the tensile stretching in the cup wall by using deeper draw beads or greater BHF.

Residual stresses may also cause geometric distortions in the part. Large-scale distortions may take the form of highs or lows in the part surface or appear as oil canning (elastic instabilities). Undesirable surface textures, such as orange peel or stretcher strain markings, may also occur during deformation. Orange peel consists of a rough surface appearance typically caused by the variation of flow stress properties of the various grains contained in the material.

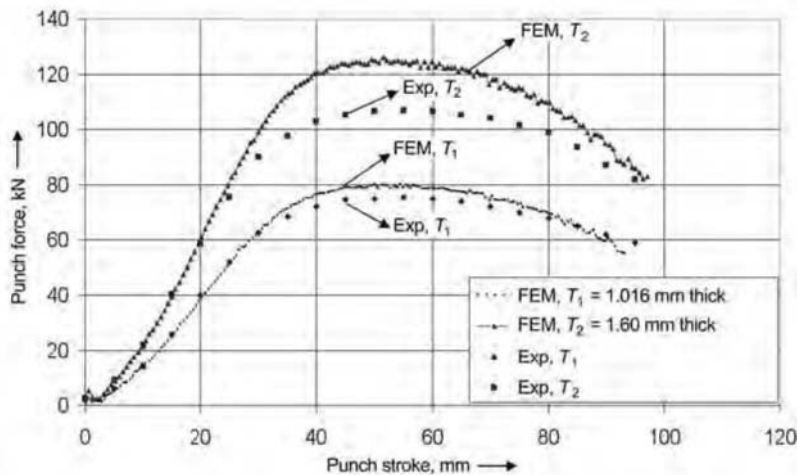


Fig. 8.21 Punch force/punch stroke curves for different blank thickness values obtained in experiment (Exp) and finite element model (FEM) simulations

Table 8.15 Blank diameter values used in each simulation

Simulation name	D1	D2	D3
Blank diameter, mm/in.	254.0/10.0	279.4/11.0	304.8/12

Table 8.16 The process parameters used in the simulations

Material	IF Steel
Blank thickness, mm/in.	0.7874/0.031
Blank holder force, BHF, kN	158.0
Coefficient of friction, μ	0.16

Table 8.17 The influence of blank diameter on the simulation results

Simulation	Draw, mm	Draw, mm	Max. punch force, kN	Thinning, %
	Flange	Cup height		
D1 = 254.0 mm	36.6	66.7	120.0	5.14
D2 = 279.4 mm	38.7	79.4	140.0	6.90
D3 = 304.8 mm	51.9	105.1	158.0	9.23

Current finite element analysis (FEA) techniques allow the prediction of wrinkles and, to some extent, of the tendency to fracture. The maximum thinning in the drawn part has traditionally been used in practice to estimate proximity to failure. This is an approximate method, because the limit of thinning can vary with strain path. Prediction of biaxial strain has been pro-

posed (Ref 8.17) to estimate failure in the form of a forming limit diagram. The determination of a forming limit diagram requires extensive and laborious experimentation for a given material. However, this technique coupled with FEA is widely used for predicting fracture.

From a practical perspective, wall thinning that leads to fracture is due to tensile stresses that occur in the cup wall during deep drawing. For a given material and part geometry, the tendency to wall thinning can be reduced by improving lubrication, reducing the draw velocity (which improves the effectiveness of lubrication), and reducing the BHF, provided the formation of wrinkles is avoided.

Wrinkling

Wrinkling is a phenomenon of compressive instability at the presence of excessive in-plane compression. It is caused by excessive compressive stresses in the flange of the sheet. For example, in a drawing operation, wrinkling can be initiated either under the binder (flange wrinkling; Fig. 8.26a) or in the side wall (puckering; Fig. 8.26b), when the restraining force provided by the blank holder and/or draw beads is not sufficient to prevent excessive material draw-in.

The initiation of wrinkling is a local phenomenon that depends on material properties, stress state, and blank thickness of the material in the region under compression. The state of stress is that of in-plane compression in one direction,

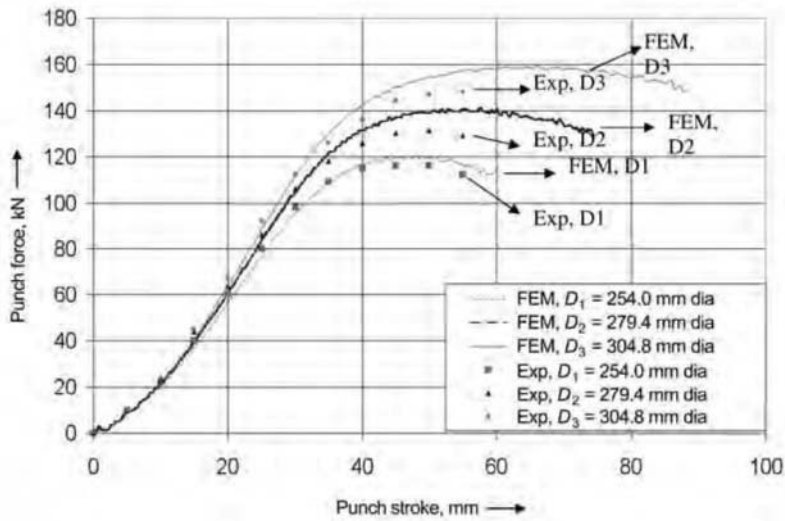


Fig. 8.22 Punch force/punch stroke curves for different blank diameters in experiment (Exp) and finite element model (FEM) simulations

Table 8.18 Coefficient of friction values used in each simulation

Simulation name	Nu1	Nu2	Nu3
Coefficient of friction	0.04	0.08	0.12

Table 8.19 The process parameters used in the simulations

Material	HSS
Blank thickness, mm/in.	0.889/0.035
Blank diameter, mm/in.	254.0/10.0
Blank holder force, BHF, kN	117.0

Table 8.20 The influence of coefficient of friction on the simulation results

Simulation	Draw, mm Flange	Draw, mm Cup height	Max. punch force, kN	Thinning, %
Nu1 = 0.04	37.2	66.7	92.0	2.08
Nu2 = 0.08	36.7	66.7	104.0	2.35
Nu3 = 0.12	36.1	66.6	120.0	2.88

in-plane tension in another direction, and normal constraint by the binder (or blank holder) in the third direction.

To avoid wrinkling, the metal should be kept in tension. Wrinkling is prevented by applying a force on the periphery of the blank with the help of a blank holder or a draw bead that restrains

metal flow. The applied BHF induces friction necessary to convert the compression in the edge of the material of the blank into the desired tension needed for drawing. However, there is a limit to the applied BHF. If BHF is increased until the tension in the blank exceeds the strength of the material, the metal will tear at the mouth of the die or at the bottom of the cup (Fig. 8.25a).

8.3 Prediction of Punch Force and BHF—Case Study

A first approximation to predict forces in deep drawing rectangular cups is to approximate the rectangular cup geometry with that of an axisymmetric/round cup having equal perimeter and width of flange. Thus, the simple equations discussed for deep drawing of round cups can be used. However, the practical state-of-the-art calculation method is to use finite element analysis (FEA). The prediction and control of the BHF are more important in the deep drawing of rectangular cups than in the deep drawing of round cups since it is possible to vary the BHF in position (along the flange) as well as in time (during the punch stroke). The selection of BHF and the use of multiple point cushions are discussed in detail in Chapter 13, “Cushion Systems for Sheet Metal Forming,” in this book.

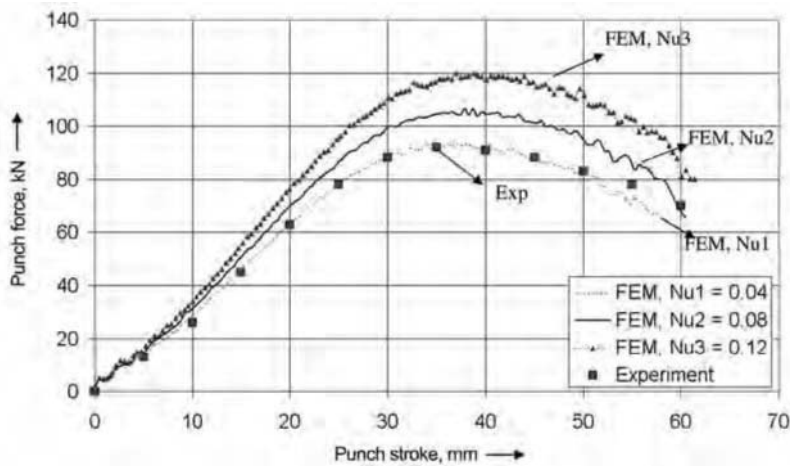


Fig. 8.23 Punch force/punch stroke curves for different coefficients of friction, μ , obtained in experiment (Exp) and finite element model (FEM) simulations

Table 8.21 BHF values used in each simulation

Simulation name	BHF1	BHF2	BHF3
Blank holder force, kN	151.0	70.0	Variable BHF

Table 8.22 Variable BHF values used in BHF3 simulation

Punch stroke, mm	0	10	20	65	95
Blank holder force, kN	147.0	142.1	98.0	68.6	68.6

Table 8.23 The process parameters used in the simulations

Material	IF Steel
Blank thickness, mm/in.	0.889/0.035
Blank diameter, mm/in.	330.2/13.0
Coefficient of friction, μ	0.08

Table 8.24 The influence of blank holder force on the simulation results

Simulation	Simulation results	Experiment results	Thinning, %
BHF1 = 151 kN	Fracture at 58.0 mm	Fracture at 53.5 mm	22.87
BHF2 = 70 kN	Wrinkled at 28.9 mm	Wrinkling observed	...
BHF3 = Variable BHF	108.5 mm	Good part High draw depth	15.4

In the deep drawing of rectangular cups, the prediction of the blank shape and BHF is critical for achieving a successful forming operation. A case study with a rectangular cup geometry and an aluminum alloy (AA 2008-T4) is

discussed here because it is helpful to explain the methodology used for evaluating and improving part quality (Ref 8.18).

Press and Tooling

The deep drawing experiments were performed in a 160-ton hydraulic press installed at the Engineering Research Center for Net Shape Manufacturing laboratory at The Ohio State University. The clamping pressure was applied by a hydraulic die cushion. Die cushion force could be kept constant or varied (by computer numerical control) as a function of stroke, with a maximum load of 100 tons. The geometry of the rectangular cup formed in the experiments is shown in Fig. 8.27. The cross section of the tooling to form this part is shown in Fig. 8.28. The tooling was instrumented to measure the load and stroke during the deformation. As shown in Fig. 8.28, the punch (11) load was measured by an in-line load cell (12). The blank holder support plate (7) was supported by 28 cushion pins (16) that transferred the load from the die cushion to the blank holder support plate. The BHF was measured using eight 15-ton button load cells (20) located at the corners and in the middle of the sides of the rectangular blank holder (6).

Material and Lubrication

The material properties of aluminum alloy AA-2008-T4 used in this experiment are given in Table 8.25. Three different blank geometries (rectangular, oblong, and oval; see Fig. 8.29)

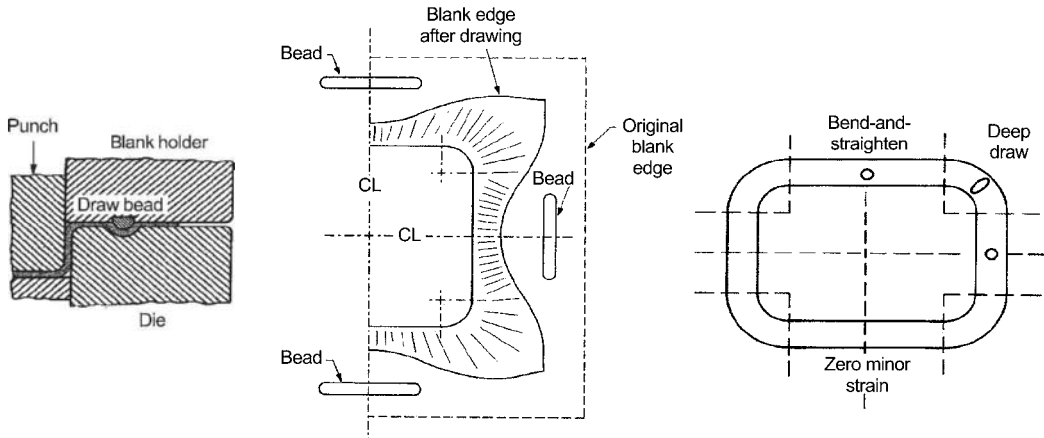


Fig. 8.24 An example of a drawn rectangular cup: corners are similar to deep drawing, and the sides undergo bending and straightening

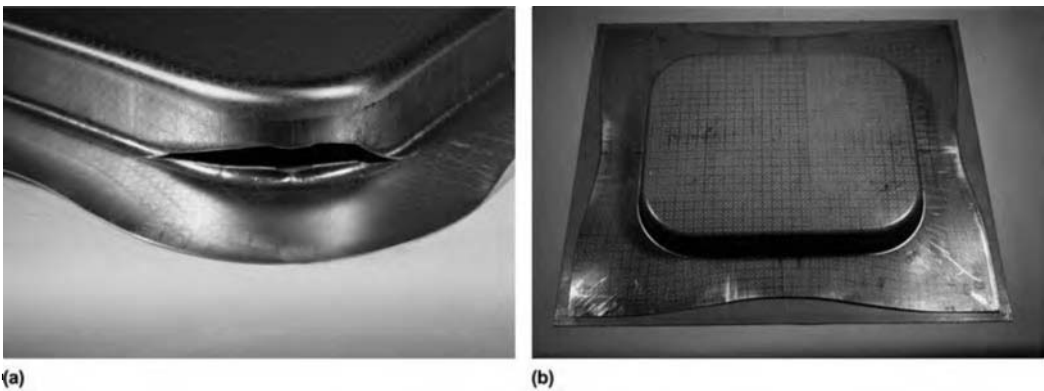


Fig. 8.25 Fracture in experimental rectangular cups

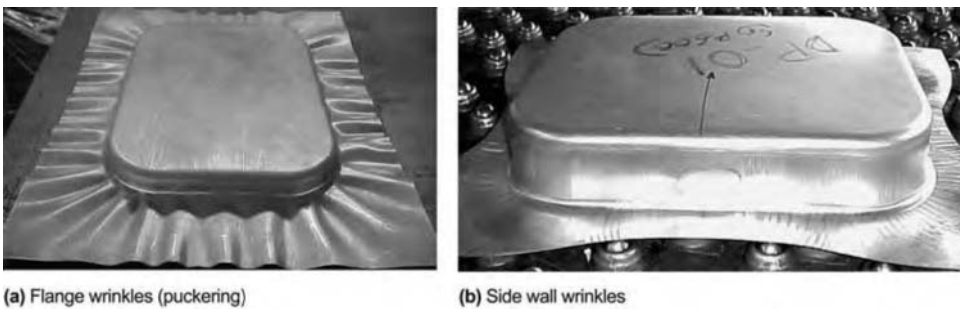


Fig. 8.26 Wrinkles that may occur in deep drawing rectangular cups when blank holder force is too low: (a) flange wrinkles, (b) side wall wrinkles

were tested in the experiments. The experiments were conducted using an oil-based lubricant. The lubricant was applied to the punch, blank holder plate, die surfaces, and both surfaces of the blanks.

FEA Simulations

A rectangular cup was formed to a 50-mm height from an oblong-shaped blank. In this experiment, a flat blank holder was used, and the

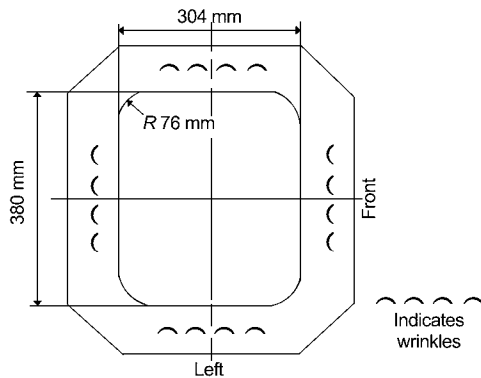
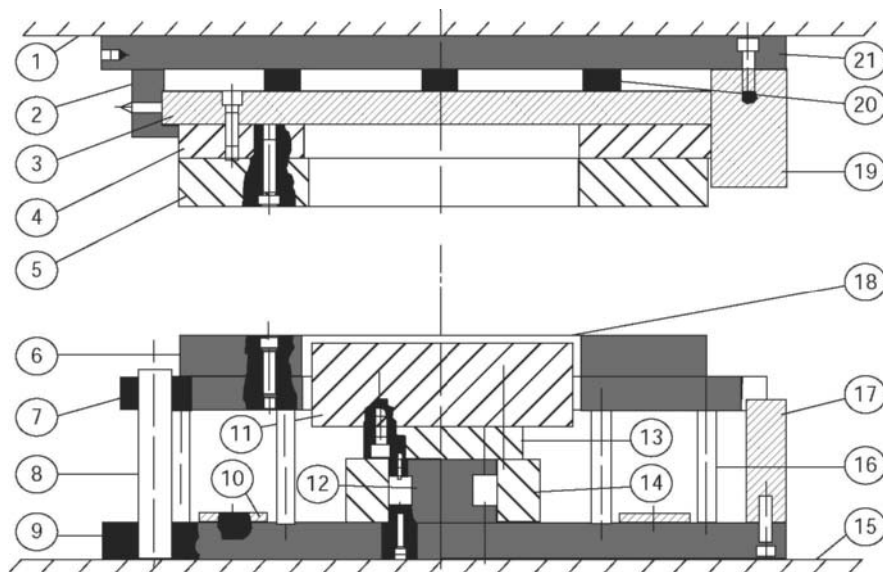


Fig. 8.27 The geometry of the deep-drawn rectangular cup.
Source: Ref 8.18

BHF was kept constant at 25 tons during the stroke.

The forming process was simulated with an FEA technique. The same process conditions from the experiments and a COF of $\mu = 0.08$ were modeled using a three dimensional FEM code developed to perform crash and metal-forming simulations. The code also used a Lagrangian explicit time integration technique and modeled sheet behavior, including membrane, bending, and shear effects. The sheet was modeled as an elastic-plastic material. The tooling was made mathematically discrete using rigid elements.

The thickness distributions predicted by the FEA simulations in three directions, diagonal, longitudinal, and transverse, are shown in Fig. 8.30. Since the nature of the deformation was



Legend

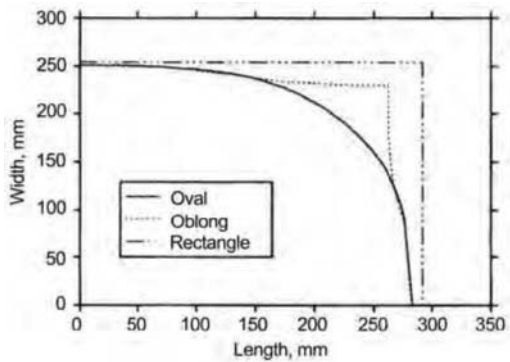
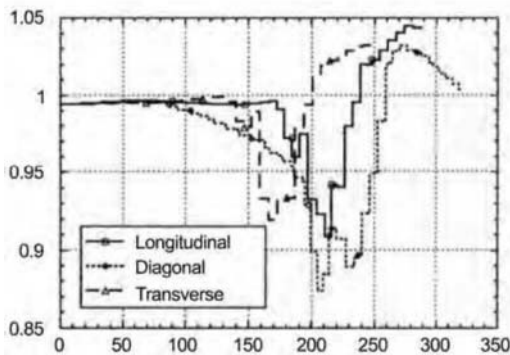
- | | |
|------------------------------|------------------------------------|
| 1 Press slide | 12 In-line load cell |
| 2 Die holder clamp | 13 Spacer |
| 3 Upper die plate | 14 Load cell locator |
| 4 Spacer | 15 Press bed |
| 5 Die ring | 16 Cushion pins (28 total) |
| 6 Rectangular blank holder | 17 Guide plate |
| 7 Blank holder support plate | 18 Formed part |
| 8 Guiding pin | 19 Die guide plate |
| 9 Lower die plate t | 20 Button load cells (eight total) |
| 10 Blank holder stopper | 21 Bolt |
| 11 Punch | |

Fig. 8.28 The tooling used to form the rectangular cup was instrumented to measure the loads and stroke during the deformation.
Source: Ref 8.18

Table 8.25 Properties of aluminum alloy AA-2008-T4

Temperature		Yield strength		Ultimate tensile strength		K		n	r
°C	°F	ksi	MPa	ksi	MPa	ksi	MPa		
-18	0	23.15	159.61	41.17	283.86	75.74	522.21	0.252	0.761
32	90	20.95	144.45	39.45	272.00	71.78	494.91	0.252	1.548
7	45	22.10	152.37	40.67	280.41	73.69	508.07	0.248	0.570

Source: Ref 8.18

**Fig. 8.29** Dimensions of the three blank shapes used in the experiments. Source: Ref 8.18**Fig. 8.30** Thickness distribution predicted by the finite element analysis simulations. Source: Ref 8.18

close to axisymmetric at the corners of the rectangular cup, additional restraining forces retarded the metal flow and caused the largest thinning to occur there. The minor strains were as high as 9% on the sides of the rectangle. These levels of minor strains and associated circumferential stresses were high enough to cause wrinkling in the flange at the sides of the rectangular cup.

To reduce forming severity at the corners and to prevent wrinkling on the sides, the metal flow around the periphery of the cup had to be made as uniform as possible. The following methods could be used for this purpose:

- The blank shape can be modified to give a smaller contact surface at the corners.
- Die surfaces can be spotted (ground) at the corners to provide more space for sheet thickening.
- Draw beads can be used on the sides of the rectangular.
- Multipoint cushions can be used to control the BHF as a function of time and location, as discussed in Chapter 13 in this book.

Wrinkling and Fracture Limits

Wrinkles usually occur on the flange at the sides of the rectangle. Since most of the BHF is concentrated on the corners where the metal thickens more, the sides of the rectangle cannot get enough pressure to restrain the metal and prevent wrinkling. Increasing the blank holder pressure at the sides of the rectangular blank using a multipoint pressure control system could improve the formability of rectangular cups.

The wrinkling amplitude and the wavelength were measured using a coordinate measuring machine. Computer code was used to find the peaks and valleys in the surface profile measurements and to calculate the wrinkling amplitudes and wavelengths. These calculations were used to establish quantitative limits for drawing quality.

To determine the formability limits, a method has to be developed to quantify both wrinkling and fracture. For this purpose, a number of cups were formed to different heights using each blank shape with various BHFs. By visual inspection, the upper and lower control limits for the wrinkling amplitude were set at 0.08 and 0.05 mm, respectively. These limits depend on the application, material, and process conditions.

The effect of blank shape on wrinkling is shown in Fig. 8.31, which plots wrinkling amplitude measurements on three cups formed to 32-mm depth under a 30-ton BHF. Because of the asymmetry in the tooling, the wrinkling amplitude measurements varied at different locations on the cup (Fig. 8.27). Wrinkling and fracture limits for rectangular cups formed from different blank shapes are shown in Fig. 8.32. These limits are determined for a wrinkling amplitude of 0.08 mm. The rectangular blanks showed higher wrinkling and fracture limits. It is clear that the blank shape affects part quality.

Wrinkling was also predicted in the process simulations using FEA. Figure 8.33 shows the deformed cup geometry with severe wrinkling as predicted by FEA simulation using a BHF of 2 tons. Fracture was predicted by means of a sudden drop in the punch force measurements

during the experiments and extensive localized stretching during the simulations.

BHF Control to Prevent Wrinkling and Fracture

A set of experiments was performed to show the effect of the BHF control on the fracture and wrinkling in deep drawing the rectangular cups. In these experiments, oblong blanks of aluminum alloy AA-2008-T4 were formed to a 50-mm depth using a water-based lubricant. Initial experiments were performed using constant BHF of 25 tons and 35 tons. With a BHF of 35 tons, fracture occurred at 41 mm. With 25 tons, minor wrinkling occurred.

Therefore, to prevent wrinkling and fracture at the same time, a BHF profile as a function of time (or stroke) was developed. In these BHF trajectories, the BHF was high initially when wrinkling was more critical. It was then reduced toward the end of the stroke to ease the metal flow and to prevent fracture.

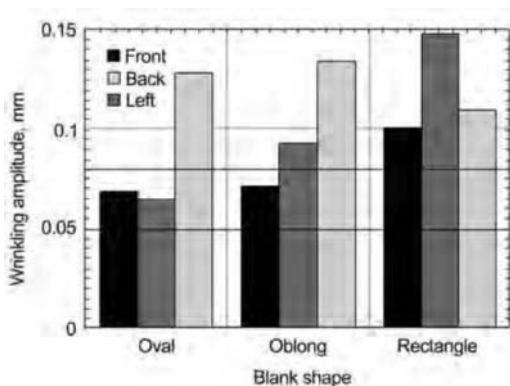


Fig. 8.31 The wrinkling amplitude measurements on three cups formed to 32-mm depth under a blank holder force of 30 tons. Source: Ref 8.18

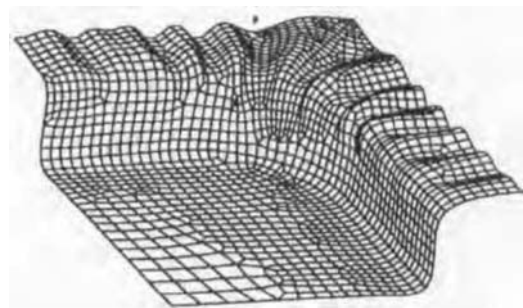


Fig. 8.33 Deformed cup geometry with severe wrinkling predicted by finite element analysis simulation using a blank holder force of 2 tons. Source: Ref 8.18

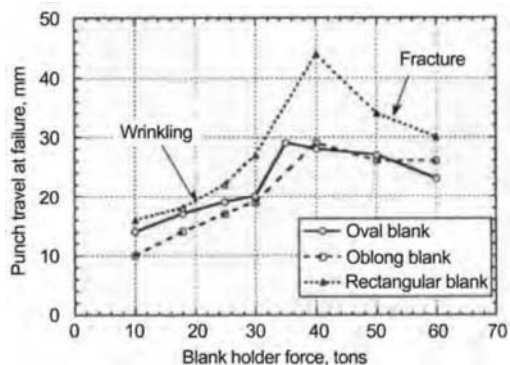


Fig. 8.32 The wrinkling and fracture limits for rectangular cups deep-drawn from different blank shapes. Source: Ref 8.18

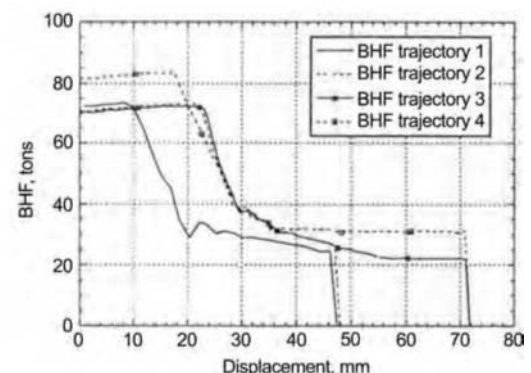


Fig. 8.34 Blank holder force (BHF) profiles used in the simulations and experiments

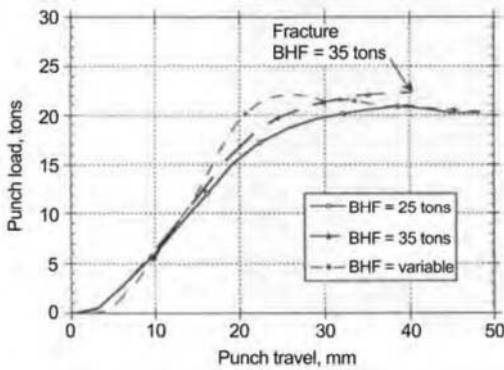


Fig. 8.35 The punch force measurements obtained with three different blank holder force values

The BHF profiles used in the simulations and in the experiments are shown in Fig. 8.34. Figure 8.35 shows the punch force measurements using three different BHF distributions: 25 tons, 35 tons, and variable (BHF trajectory 2).

Starting with a large BHF caused the punch force to increase steeply but suppressed wrinkling initiation. The BHF was reduced at a punch travel of 18 mm and was dropped down to 25 tons at a punch travel of 38 mm. The wrinkling height was significantly reduced by controlling the BHF as a function of the stroke.

REFERENCES

- 8.1 *Metalworking: Sheet Forming*, Vol 14B, *ASM Handbook*, ASM International, 2006
- 8.2 K. Lange, *Handbook of Metal Forming*, McGraw-Hill, 1985
- 8.3 B. Avitzur, *Handbook of Metal Forming Processes*, John Wiley and Sons, 1983
- 8.4 G. Eshel, M. Barash, and W. Johnson, Rule Based Modeling for Planning Axisymmetrical Deep-Drawing, *Journal of Mechanical Working Technology*, Vol 14 (No. 1), 1986, p 1–115
- 8.5 D.V. Wilson and R.D. Butler, The Role of Cup-Drawing Tests in Measuring Drawability, *Journal Institute of Metals*, Vol 90, 1961–1962, p 473–483
- 8.6 R.L. Whiteley, The Importance of Directionality in Drawing Quality Sheet Steel, *Transactions of the ASM*, Vol 52, 1960, p 154–162
- 8.7 W.F. Hosford and R.M. Caddell, *Metal Forming Mechanics and Metallurgy*, 2nd ed., Prentice Hall, 1993
- 8.8 P. Kazanowski, Forming of Aluminum Alloys, *Metalworking: Sheet Forming*, Vol 14B, *ASM Handbook*, ASM International, 2006, p 583–599
- 8.9 J. Douthett, Forming of Stainless Steel, *Metalworking: Sheet Forming*, Vol 14B, *ASM Handbook*, ASM International, 2006, p 562–582
- 8.10 W. Johnson and P.B. Mellor, *Engineering Plasticity*, Van Nostrand Reinhold, 1973
- 8.11 G. Oehler and F. Kaiser, *Blanking, Punching and Drawing Tools: Taking into Account in Particular the Latest Techniques and Tool Steels with Numerous Design and Computational Examples*, 6th ed., Springer, 1973
- 8.12 M.Y. Demeri, Deep Drawing, *Metalworking: Sheet Forming*, Vol 14B, *ASM Handbook*, ASM International, 2006, p 319–336
- 8.13 E. Siebel and H. Beisswanger, *Deep Drawing*, Munchen, Carl Hanser, 1955
- 8.14 S. Kobayashi, S.I. Oh, and T. Altan, *Metal Forming and the Finite Element Method*, Oxford University Press, 1989
- 8.15 H. Kim, J. Sung, R. Sivakumar, and T. Altan, Evaluation of Stamping Lubricants using the Deep Drawing Test, *International Journal of Machine Tools and Manufacture*, Vol 47 (No. 11), 2007, p 2120–2132
- 8.16 G. Gutscher, H. Wu, G. Ngaile, and T. Altan, Determination of Flow Stress for Sheet Metal Forming using the Viscous Pressure Bulge (VPB) Test, *Journal of Materials Processing Technology*, Vol 146, 2004, p 1–7
- 8.17 S. Keeler, Determination of Forming Limits in Automotive Stampings, *Sheet Metal Industries*, Vol. 42, 1965, p 683–691
- 8.18 M. Ahmetoglu, T.R. Brock, G. Kinzel, and T. Altan, Blank Holder Force to Eliminate Wrinkling and Fracture in Deep Drawing Rectangular Parts, *Annals of CIRP*, Vol 44 (No. 1), 1995, p. 247–225

CHAPTER 9

Principles of Sheet Forming Presses

Eren Billur, The Ohio State University

EACH SHEET FORMING PROCESS is associated, in a practical sense, with at least one type of sheet forming machine or equipment. The sheet forming equipment varies by the rate at which energy is applied to the work piece and by the ability to control the applied energy. Each machine type has distinct advantages and disadvantages, depending on the number of parts to be produced, the dimensional precision, and the alloy being formed. The introduction of a new process invariably depends on the cost-effectiveness and production rate of the equipment associated with that process. Therefore, capabilities of a forming machine are a paramount concern, so that process engineers can:

- Use existing machinery more efficiently
- Define the existing plant capacity with accuracy
- Communicate better with machine builders and at times request improved performance from the machine builder
- Develop, if necessary, in-house proprietary machines and processes not available in the machine-tool market

The most important outputs with sheet metal forming, from a practical point of view, are final part tolerances and production rate (Ref 9.1). These are affected by both machine (press) variables and process variables, as summarized in Fig. 9.1. The behavior and characteristics of the sheet forming press affect all of the following:

- Stiffness (C) and accuracy of the press (see the section “9.2 Characteristics of Presses”), which influences the “as formed” tolerances of the parts. Stiffness also affects die life.

- Strokes per minute under load (n_p) capability of a press, which influences the production rate (parts/time)
- Available machine load (L_M) and machine energy (E_M), which determine whether the press is able to perform the specific stamping operation

The die geometry and the incoming sheet material also affect the required process load (L_p) and energy (E_p). For example, the flow stress ($\bar{\sigma}$) of the material, part geometry, and tribological (friction, lubrication) conditions determine the load and energy required to perform the stamping operation. The formability (or ductility) of the incoming material also determines whether the part can be successfully formed without any fracture.

9.1 Components of Presses

The basic components of a sheet forming press (Fig. 9.2a) consist of (Ref 9.4, 9.5):

- A *frame* (1) that supports the *bolster* (2) that is a plate attached to the bed. The bolster has tapped holes, T-slots, or other means for attaching the bottom die to the press.
- A *drive* mechanism (3) that moves the *slide* (4) at a right angle to the bolster
- The *gibs* (5) that guide the reciprocating motion of the slide and ensure the parallelism of the slide to the bolster

The uppermost position of the slide is called top dead center (TDC); similarly, the lowermost position is called bottom dead center (BDC). The distance between TDC and BDC is the stroke

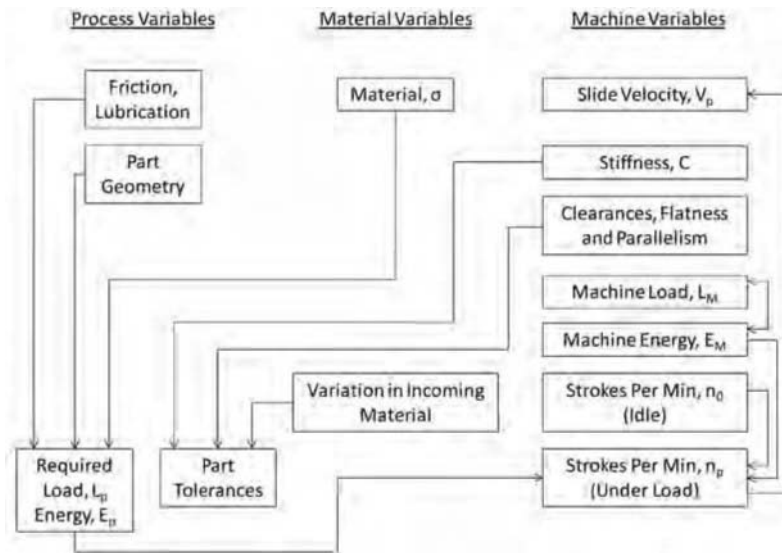


Fig. 9.1 Relationships between process and machine variables. Source: Ref 9.2

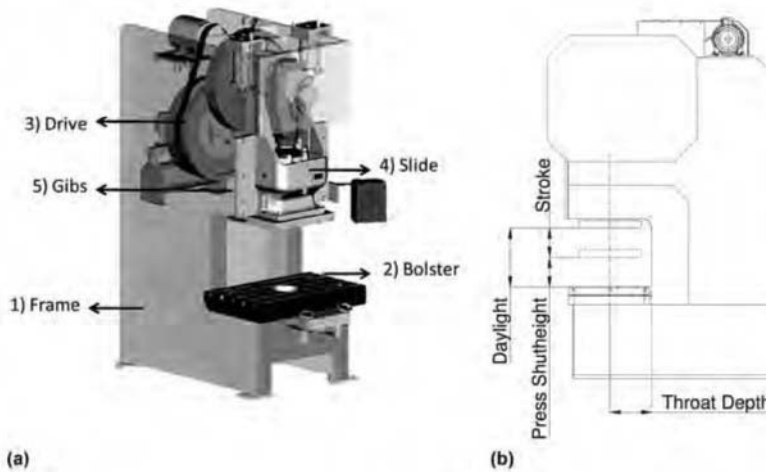


Fig. 9.2 Terminology used for (a) basic press components and (b) geometric terms. Adapted from Ref 9.3, 9.4

(s). In a mechanical press, the crank angle is measured from TDC: the crank angle is 0° at TDC and 180° at BDC. When the slide is retracted (i.e., at TDC), the distance from bolster to slide surface is called *daylight*. When the slide is moved to BDC, the distance between same components is called *press shutheight* (Fig. 9.2b) (Ref 9.4).

To carry out a sheet metal forming operation, the press has to be able to accommodate the dies and generate the necessary motion (i.e., stroke). Therefore, it is important to have sufficient die

space, bolster area, slide face area, and press shutheight. A specific forming operation (deep drawing, bending, etc.) requires a certain variation of forming load over the slide displacement (or stroke). This fact is qualitatively illustrated in Fig. 9.3, which shows the load-displacement curves for various stamping operations. The area under each curve represents the energy needed for the process (Ref 9.2).

For a given material, die geometry and lubrication (friction) conditions determine the magnitude of the forming or process load (L_p) re-

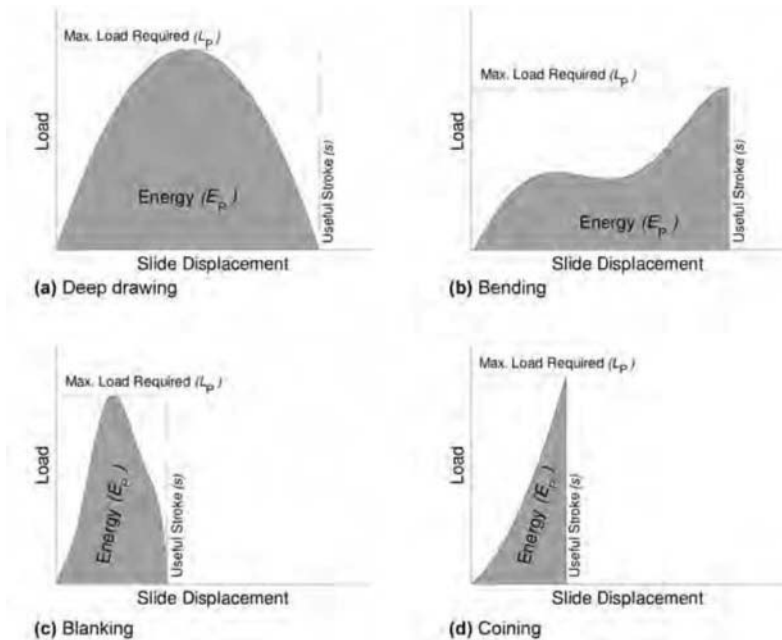


Fig. 9.3 Schematic of load-displacement curves for various sheet forming operations. Source: Ref 9.2

quired. In a forming operation, the press must be able to supply the load ($L_M \geq L_p$) and energy ($E_M \geq E_p$) required by the process during the entire stroke(s). Metal forming machines are **usually classified with respect to their capability** to supply these variables (Ref 9.6):

- **Load-Restricted Machines:** These presses are capable of supplying the nominal machine load (L_M), at any position of slide. Hydraulic presses belong to this category and are explained in more detail in Chapter 12, “Hydraulic Presses,” in this book.
- **Stroke-Restricted Machines:** These are usually mechanical presses, which are discussed in Chapter 10, “Mechanical Presses,” in this book. The kinematics of the slide motion are determined by the main drive (i.e., crank and connecting rod or pitman arm). The available machine load (L_M) is a function of stroke(s).
- **Energy-Restricted Machines:** Although not commonly used in sheet metal forming operations, screw presses with a flywheel and hammers provide a well-defined amount of energy per stroke. If the deformation requires more energy than the energy available per stroke, several strokes may be required to perform the operation (Ref 9.6).

9.2 Characteristics of Presses

In mechanical, hydraulic, screw, or servo-drive presses, the following major characteristics are important:

- Frame type
- Energy and load requirements
- Time-dependent characteristics
- Dimensional accuracy

Frame Types

Figure 9.2 shows a gap frame (also known as C-frame) press. These presses are favored because the die space is easily accessible from all sides except the rear. However, these presses are not suitable for high-accuracy production, **because they have unavoidable angular deflection** due to their asymmetric frame structure. Fitting the open side of the press with stay rods or a **bridge frame helps to reduce the angular deflection** of these presses (Fig. 9.4) that have usually relatively low force capacities (up to 2500 kN (~275 tons)) (Ref 9.1, 9.8).

Close-tolerance stampings are often made in straight-side presses. As shown in Fig. 9.5, these presses generally have larger die space and higher tonnage. Most, but not all, straight-side

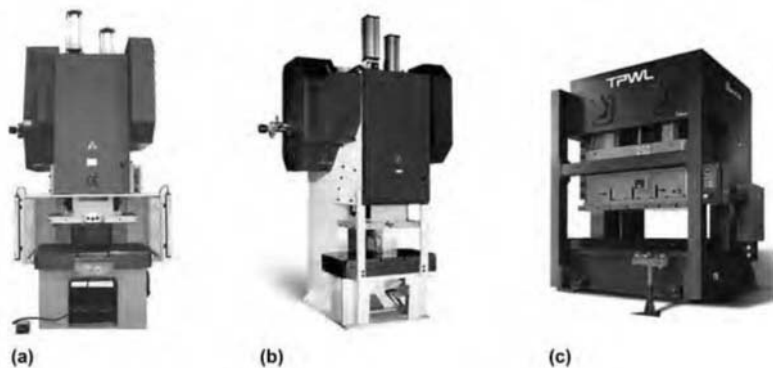


Fig. 9.4 (a) Gap frame press (b) with stay rods and (c) with bridge frame. Source: Ref 9.7

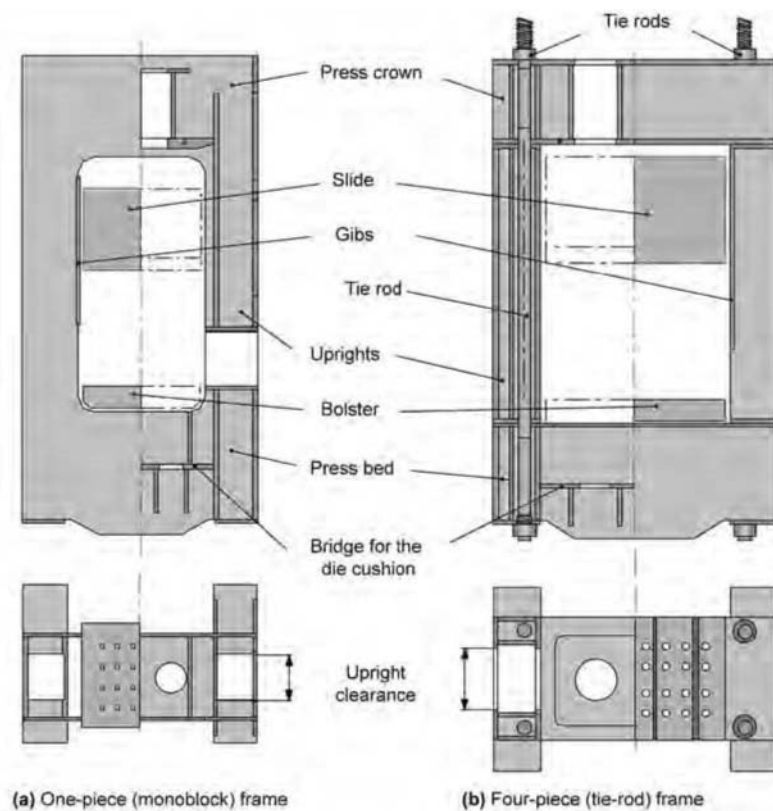


Fig. 9.5 Straight-side presses. Adapted from Ref 9.1

presses have four-piece (tie-rod) frame that comprises a bed, columns (uprights), and a crown (Fig. 9.5b). These components are held together by prestressed tie rods. This design has three advantages: (a) it is easier to transport, (b) it can withstand higher loads, and (a) in me-

chanical presses, tie rods limit potential overloading of the press (as discussed in Chapter 10, “Mechanical Presses,” in this book). If a straight-side press does not have tie rods, then it is considered to have a one-piece (monoblock) frame (Fig. 9.5a) (Ref 9.1, 9.4).

Load and Energy Requirements

Available machine load (L_M) (in tons or kN) is the load that can be applied to the forming die. In hydraulic presses, the maximum available load is available throughout the slide stroke. In mechanical presses the nominal load of a press is available only at some distance from bottom dead center (BDC).

At any time during the forming operation, the available machine load, L_M , should be larger than the load required by the process, L_p :

$$L_M \geq L_p \quad \text{Eq 9.1}$$

If this condition is not satisfied in a hydraulic press, the press will stall without completing the required deformation. In a mechanical press, the clutch may slip, and the press may stop before reaching the BDC position. Overloading of a mechanical press is further discussed in the chapter “Mechanical Presses” in this volume.

Available energy (E_M) (in ton-inch or kJ) is the energy supplied by the machine to carry out the deformation during an entire stroke. The available energy must be equal to or higher than energy required for the process (E_p) in order to be able to complete the forming operation:

$$E_M \geq E_p \quad \text{Eq 9.2}$$

If a mechanical press does not satisfy Eq 9.2, the flywheel speed will slow down to unacceptable speeds. In a hydraulic press, if Eq 9.1 is satisfied, then 9.2 is also satisfied.

Efficiency factor (η) is determined by dividing the available energy (E_M) by total input energy (E_T). Available energy, E_M , does not include the losses in electric motor (E_{EM}), friction losses in drive system and the gibs (E_F), and the losses due to elastic deflection of the machine (E_D):

$$E_T = E_M + E_{EM} + E_F + E_D \quad \text{Eq 9.3}$$

$$\eta = \frac{E_M}{E_T} \quad \text{Eq 9.4}$$

Time-Dependent Characteristics

Number of strokes per minute (n_p) is one of the most important characteristics because it determines the production rate. In a mechanical press, the number of strokes per minute is con-

trolled by crank speed (rpm). However, the number of strokes per minute under load is usually smaller than the idle crank speed ($n_p < n_0$).

Contact time under pressure (t_p) (in seconds) is the time during which the part remains in the die under the load. t_p is important in warm and hot forming, in which it affects the heat transfer and die wear; t_p is also affected by press stiffness (see the section “**Stiffness of a Press**” in this chapter).

Slide velocity under pressure (V_p) (in in./s or mm/s) is important during the deformation because it affects the friction conditions (lubrication is affected by relative speed between the die and sheet material). At elevated temperature forming, the properties of the sheet material are also affected by strain rate or slide velocity. The strain rate ($\dot{\epsilon}$) may affect the flow stress (as $\dot{\epsilon}$ increases, $\bar{\sigma}$ increases) and the formability of the sheet material.

Dimensional Accuracy

The dimensional accuracy of a stamped part is largely determined by the accuracy of the guiding of the die set and that of the press, as well as by the elastic deflection of the press and the tooling under load. Thus, the accuracy of presses has to be determined under unloaded as well as loaded conditions (Ref 9.6).

Under unloaded conditions, the relative positions of slide face and bolster are determined by:

- Clearances in the gibs
- Parallelism of slide face and bolster
- Flatness of slide face and bolster
- Perpendicularity of slide motion with respect to bolster
- Concentricity of tool holders

These characteristics are determined by the manufacturing and assembly quality of the press. Gib adjustments and guides in the die set may help to reduce some of these inaccuracies. Under loaded conditions, elastic deflections of press components cause the dies to drift. These effects are more significant in gap-frame presses and under off-center loading and are affected by the vertical and angular stiffness of the press (C).

Stiffness of a Press

The elastic behavior of a press is defined by German standard DIN 55 189 with two param-

eters of stiffness, vertical stiffness and angular stiffness, as shown in Fig. 9.6.

Vertical (linear) stiffness (C) is defined as:

$$C = \frac{L_M}{d} \quad \text{Eq 9.5}$$

Angular stiffness (C_θ) is defined as:

$$C_\theta = \frac{M}{\alpha} = \frac{L_M e}{\alpha} \quad \text{Eq 9.6}$$

L_M is the load applied by the machine, e is the eccentricity of the load, M is the tilting moment created by the eccentric load, d is the vertical deflection, and α is the angular deflection as depicted in Fig. 9.6.

The main influences of stiffness, C , on the forming process can be summarized as follows (Ref 9.14, 9.15, 9.16). Under the machine load, L_M , the press stores some elastic energy, E_D , during load buildup. This energy is smaller for a stiffer press (larger C). The deflection energy can be calculated from:

$$E_D = \frac{1}{2} d L_M = \frac{L_M^2}{2C} \quad \text{Eq 9.7}$$

Note that having smaller E_D would increase the efficiency of a press (η) (see Eq 9.3, 9.4).

The larger the stiffness, the lower the deflection of the press. Consequently, the variations in part dimensions due to changes in incoming blank thicknesses are smaller in a stiffer press.

Stiffness influences the velocity/time curve and press shutheight under load. The actual velocity/time profile under load will deviate considerably from the theoretical profile (or the

unloaded profile). As a result, the press shut-height is changed and contact time under pressure (t_p) is affected. In a stiffer press, the shut-height deviation and contact time under pressure are smaller than those of a “soft” press (Fig. 9.7).

The angular deflection, caused by either the eccentric loading or the frame’s asymmetry (i.e., gap-frame), causes tilting of the slide. If a die cushion is used in a forming process, as shown in Fig. 9.8, it is also affected by the slide tilt. This causes nonuniform blank holding pressure, which may result in variations in metal flow, wrinkling, and maximum draw depth. These effects can be reduced with (1) proper die guide design and (2) a press with higher angular stiffness (Ref 9.10, 9.11).

Measuring Press Stiffness. The stiffness of a press can be measured under static and dynamic loading conditions. Measuring static stiffness has been standardized by DIN 55 189, as shown in Fig. 9.9. To measure the vertical stiffness (C), a load (L) is applied by means of a hydraulic cylinder at the center of the press. The displacement is measured using a linear variable differential transformer or laser sensors. Similarly, to measure the angular stiffness (C_θ), a load is applied at a distance from the center of the press, and the angular deflection (α) is calculated from the difference of the height measurements (Ref 9.9, 9.13).

Static stiffness measurement does not give information about how the press will behave under real production conditions. Therefore, the concept of dynamic stiffness has been proposed, where the load is generated by the press itself. Dynamic stiffness can be measured by either of two methods (Ref 9.17, 9.18): Evaluation of

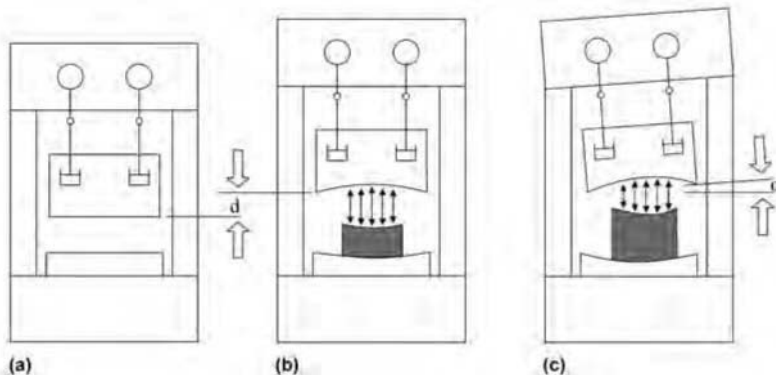


Fig. 9.6 A straight-side press (a) in unloaded condition, (b) under vertical deflection, and (c) under angular deflection. Source: Ref 9.9

press stiffness measuring the maximum deflection during upsetting, or real-time measurement of press deflection. In the former method, explained by Douglas and Altan (Ref 9.17), electrolytic copper samples of the same height but

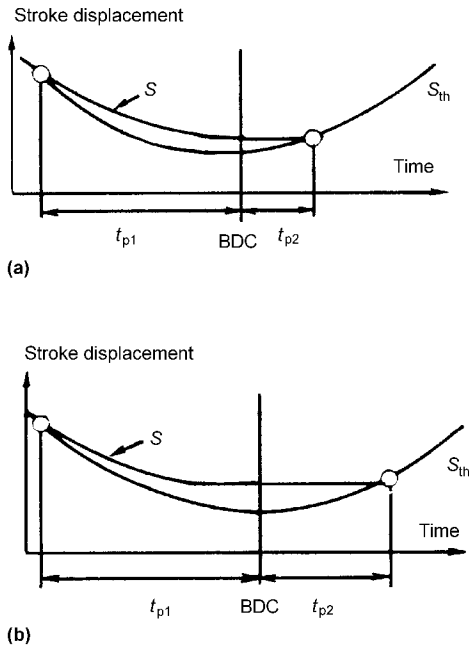


Fig. 9.7 Effect of press stiffness on contact time. (a) Stiffer press. (b) Less stiff press. As the load builds and the press deflects elastically, a stiffer press requires less time, t_{p1} , for pressure buildup and also less time, t_{p2} , for pressure release. Consequently, the total contact time under pressure ($t_p = t_{p1} + t_{p2}$) is less for a stiffer press. BDC, bottom dead center; L_{p1} and L_{p2} , loads; S_r , pressure release displacement time; S_{th} , theoretical displacement time

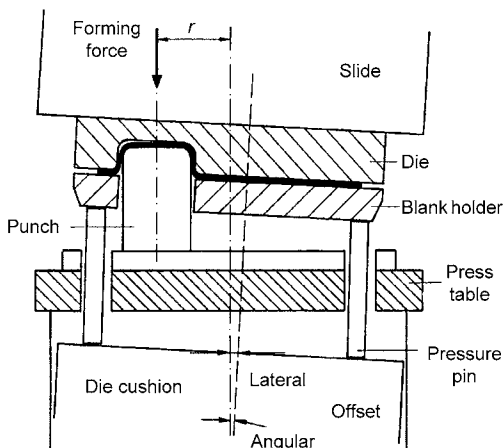


Fig. 9.8 Effect of slide tilting on die cushion. Reprinted with permission from Ref 9.10

different diameters are used. Since the diameter is changed, the upsetting forces change. In order to measure the deflection, lead samples slightly shorter than copper are placed some distance away from copper billet, as shown in Fig. 9.10(a). Differences in the dimensions of lead bars and press load are then plotted, and the slope of this curve determines the dynamic stiffness of the press (Fig. 9.10b).

With recent advances in sensor and data acquisition techniques, it is possible to track the deflection of a press in real time. Using special dies, some including wedges to create horizontal force components, several loading cases (among them concentric, eccentric, and horizontal loads) can be emulated. The measurements can be performed by laser sensors, as shown in Fig. 9.11 (Ref 9.18, 9.19).

Fig. 9.12 compares the static and dynamic stiffness of a mechanical forging press. In this particular case, the press and its frame are stiffer under dynamic conditions (Ref 9.6).

It is also possible to estimate the stiffness of a press using finite element analysis. Many press builders are optimizing the design of their frame and drive components using finite element analyses (Ref 9.20).

Other Press Accuracy Factors

Frame Type and Material. Design of the frame affects the stiffness. When stiffness is concerned, the frame types can be classified as (see Fig. 9.4, 9.5):

- gap-frame presses
- gap-frame presses with stay rod
- straight-side presses
- tie-rod frame presses

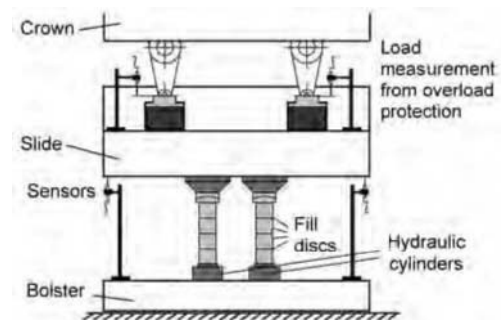


Fig. 9.9 Measurement setup as defined by DIN 55 189 to determine static vertical stiffness. Adapted from Ref 9.12

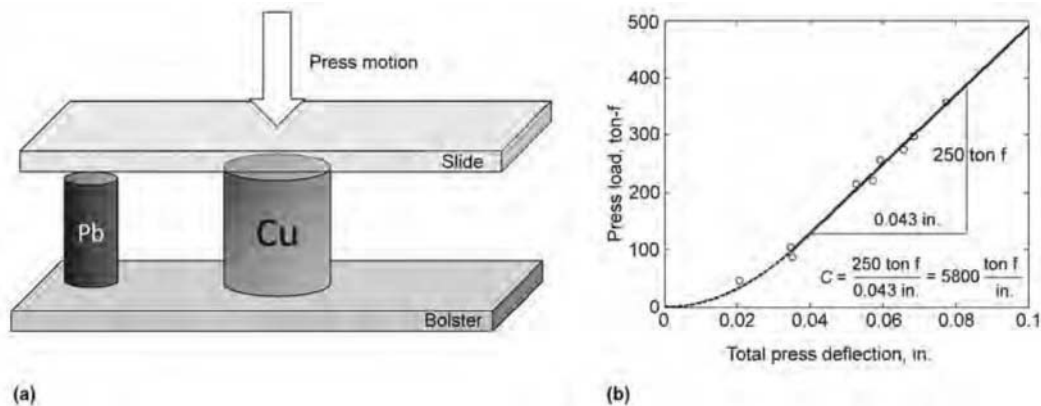


Fig. 9.10 (a) Test setup for determining dynamic stiffness; (b) dynamic stiffness measurement for a 500-ton press. Recreated after Ref 9.17

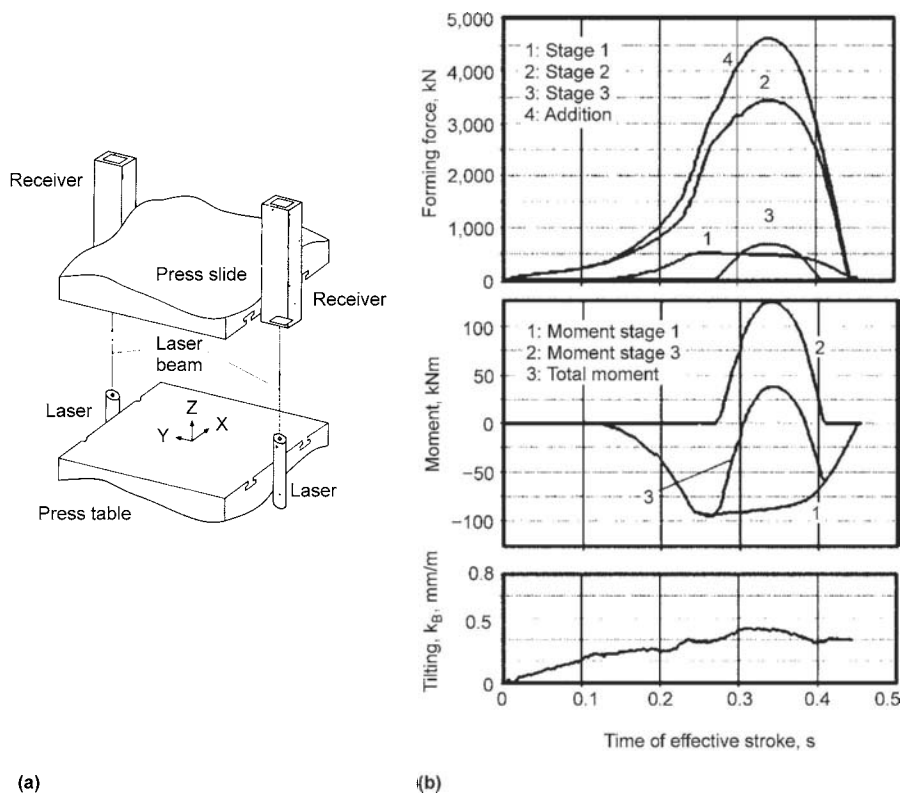


Fig. 9.11 (a) Real-time deflection measurement system; (b) real-time measurement of load, moment and tilting of the press. Reprinted with permission from Ref 9.19

In gap-frame presses, the deflection (also called gap opening) depends on the position of the center of loading. If this is closer to the front end, the moment it creates will be higher and will result in higher deflection. When properly

engineered, a stay rod (or bridge frame) could reduce the deflection of a gap-frame press by up to 60% (Ref 9.7, 9.21).

In straight-side presses, tie rods make the press stiffer up to the rated press capacity. The

prestress on the tie rod keeps crown and upright together. In the event of overloading (i.e., if the forming loads exceeds the rated press capacity), these may separate from each other (Ref 9.22).

Originally, presses had cast iron frames. Owing to progress in welding technology, today most press frames are made of fabricated steel plates welded together. Cast iron or cast steel is still favored in (a) small presses (up to 300 tons and mostly gap-frame), since it is easier to fabricate and machine one-piece frames, and (b) high-speed presses, because cast iron frames offer high damping capacity. However, due to the low elastic modulus and low strength of cast iron, larger cross sections are required in order to ensure high press stiffness. In addition, the high cost of the patterns for casting makes cast frames not cost-effective for small lot production (Ref 9.1, 9.23).

Welded steel frames have the advantage of higher elastic modulus and strength, and smaller cross sections and lighter frames are therefore possible with them. Since no pattern is needed (as in the casting process), these frames are more practical when building presses in small quantities. However, steel constructions have poor shock absorption, and stress-relieving heat treatment is required after welding. Compound designs in which welded steel and cast components are used together are also common (Ref 9.1, 9.15, 9.23).

Gib Design. The slide is guided in the press frame. In the case of off-center loads, the slide is supported by the gibs. Design of the gibs and

the clearances in the gibs are important in order to ensure that the slide face is parallel to the bolster. Figure 9.13 shows some of the common gib designs used in presses. Some designs are able to hold eccentric loads in both directions (i.e., right to left and front to back) (Ref 9.1).

In mechanical presses, the motion of the crank causes additional horizontal forces that have to be controlled by the gibs. One method to reduce the effect of these forces is to employ plunger guides, as depicted in Fig. 9.14 (Ref 9.24).

Bending of Bolster. The frame of the press is responsible for 30 to 35% of the total elastic deflection. About 20 to 25% of the frame deflection is caused by bending of the bolster (Ref 9.10). Figure 9.15(a) shows how the bolster may bend under load. Several studies have shown that, especially for large forming dies, where a high load (3,000–12,000 kN) is required, the bolster may bend with a deflection of up to 0.6 mm, as shown in Fig. 9.15(a) (Ref 9.10, 9.25). A recent study at Volkswagen also showed that even at 50% of rated capacity, the bolster exhibited about 0.5 mm (0.02 in.) deflection. Under a 20% off-center loading, with 30% load of rated capacity, the deflection was about 0.3 mm (0.01 in.), as shown in Fig. 9.15(b) (Ref 9.25).

Possible ways to avoid the effect of bolster bending are (a) cambering the tools to compensate for the bending effect (Ref 9.25), (b) adding another steel bolster and/or a die post (Ref 9.9), and (c) adding a special pressure pad allowing the pressure can be set to different values at different locations, as shown in Fig. 9.16 (Ref 9.10).

Press Speed (Strokes per Minute). Presses may operate anywhere from a few strokes per minute to several thousand strokes per minute depending on the application. Because of dynamic effects in drive, gibs, and frame deflection, as the speed of operation increases, the vibration of the press increases as well. Such vibration may affect the accuracy obtainable in the press since vibrations may cause a change in the location of bottom dead center, BDC (shut-height) or the alignment of the slide due to tilting. As the speed of the press increases, all these effects increase (Ref 9.21). Many high-speed presses have cast frames and components in order to benefit from the damping capabilities of cast steel (Ref 9.23).

Off-Center Loading. Often stamping presses are subject to off-center loading conditions during operation. The most common off-center loading conditions are described as follows.

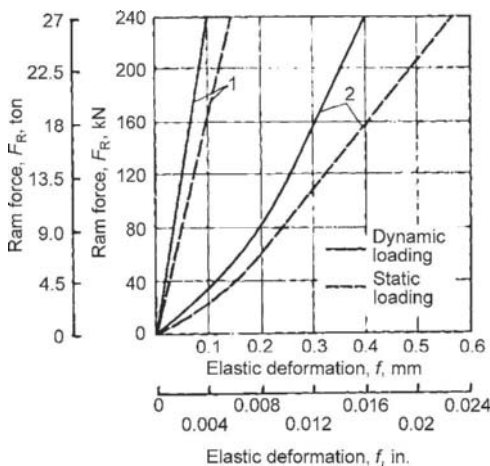


Fig. 9.12 Elastic deflection of a mechanical forging press: 1, frame deflection; 2, total deflection. Reprinted with permission from Ref 9.6

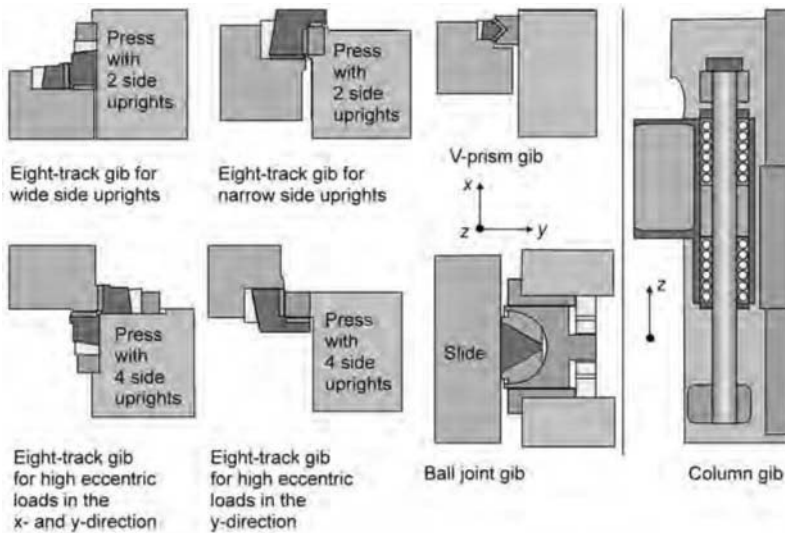


Fig. 9.13 Different gib configurations used in presses. Reprinted with permission from Ref 9.1

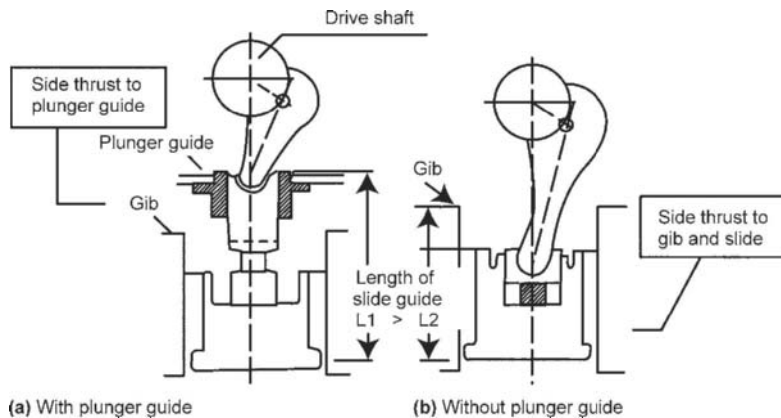


Fig. 9.14 Plunger guide design to reduce the horizontal forces caused by the crank motion. Reprinted with permission from Ref 9.24

Asymmetric Deformation in Single Operations. When forming nonsymmetric parts, the net forming force may not be aligned with the center of the press. Thus, off-center loading will create a tipping moment, which may cause slide tilting and affect the final part tolerances. This problem is also encountered in the forming of tailor-welded blanks.

Out-of-Parallel Movement. One of the accuracy characteristics under unloaded conditions is the parallelism between bolster and slide face and perpendicularity of slide motion. If these parameters are not corrected by gib adjustments, the slide/bolster parallelism will become

less accurate when off-center loads are present (Ref 9.26).

Transfer or Progressive Die Forming. Automotive parts requiring a series of operations are commonly formed under a transfer press or with the use of progressive dies under a large press with multiple forming stations. These steps may include bending, shearing, forming, and embossing, among others, which require different loads with respect to stroke position. In progressive die forming, the center of load often does not coincide with the center of the press and will not be stationary during production.

Figure 9.17 is from a study in which the

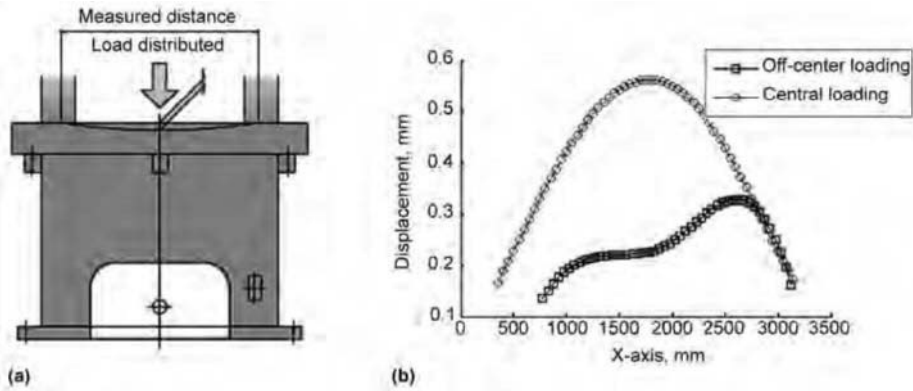


Fig. 9.15 Bending of bolster: (a) schematic; (b) experimental measurements. Reprinted with permission from Ref 9.25

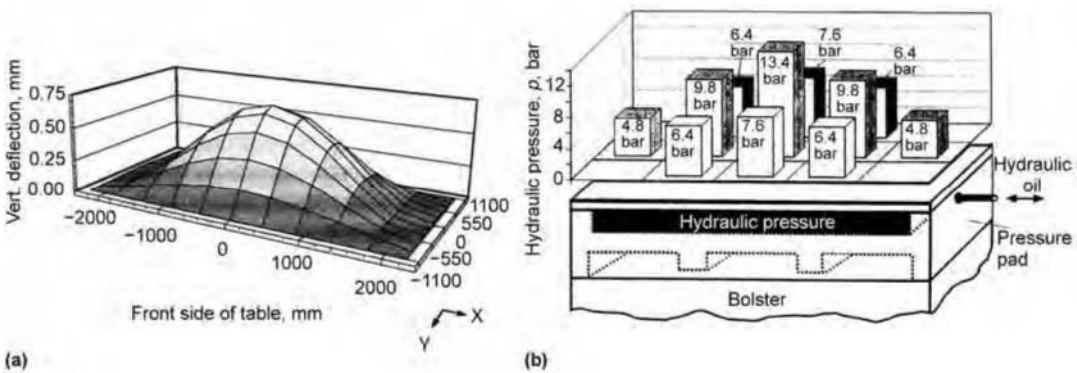


Fig. 9.16 Compensating the bolster bending: (a) measure the deflection; (b) apply pressure pad to compensate for the deflection. Reprinted with permission from Ref 9.10

forces in a progressive die are measured in each forming station. A blank is notched in the first station and the load is measured; then the cutoff is applied and the load is measured and plotted. As seen in Fig. 9.17(b), the load decomposes unevenly, causing off-center loads (Ref 9.27).

Snap-through. In blanking and shearing operations, “snap-through” can worsen the out-of-parallel movement of a press or change the BDC position of the press. In blanking operations, the press load is built gradually and elastically deflects the press and the tools. When the force generated is enough to fracture the part, the sudden release of stored elastic energy causes the press to generate reverse loads, as depicted in Fig. 9.18(a). During this stage (known as “snap-through”), the press components designed to have tensile stresses will be in compression. Figure 9.18(b) shows how elastic de-

flections due to load and snap-through alter the motion of the slide (Ref 9.28, 9.29).

As shown in Fig. 9.19, in the case of snap-through occurring under off-center conditions, tipping of the slide will be further increased. This can affect other stations of the die and cause localized wear in punches (Ref 9.24).

9.3 Quick Die Change Systems

Die change in sheet metal forming press may take hours or even shifts, if it is done manually without using special quick die-changing mechanisms. However, today, following advances in material handling technology, most stamping companies have quick die-changing systems to reduce downtime when starting to form a new part.

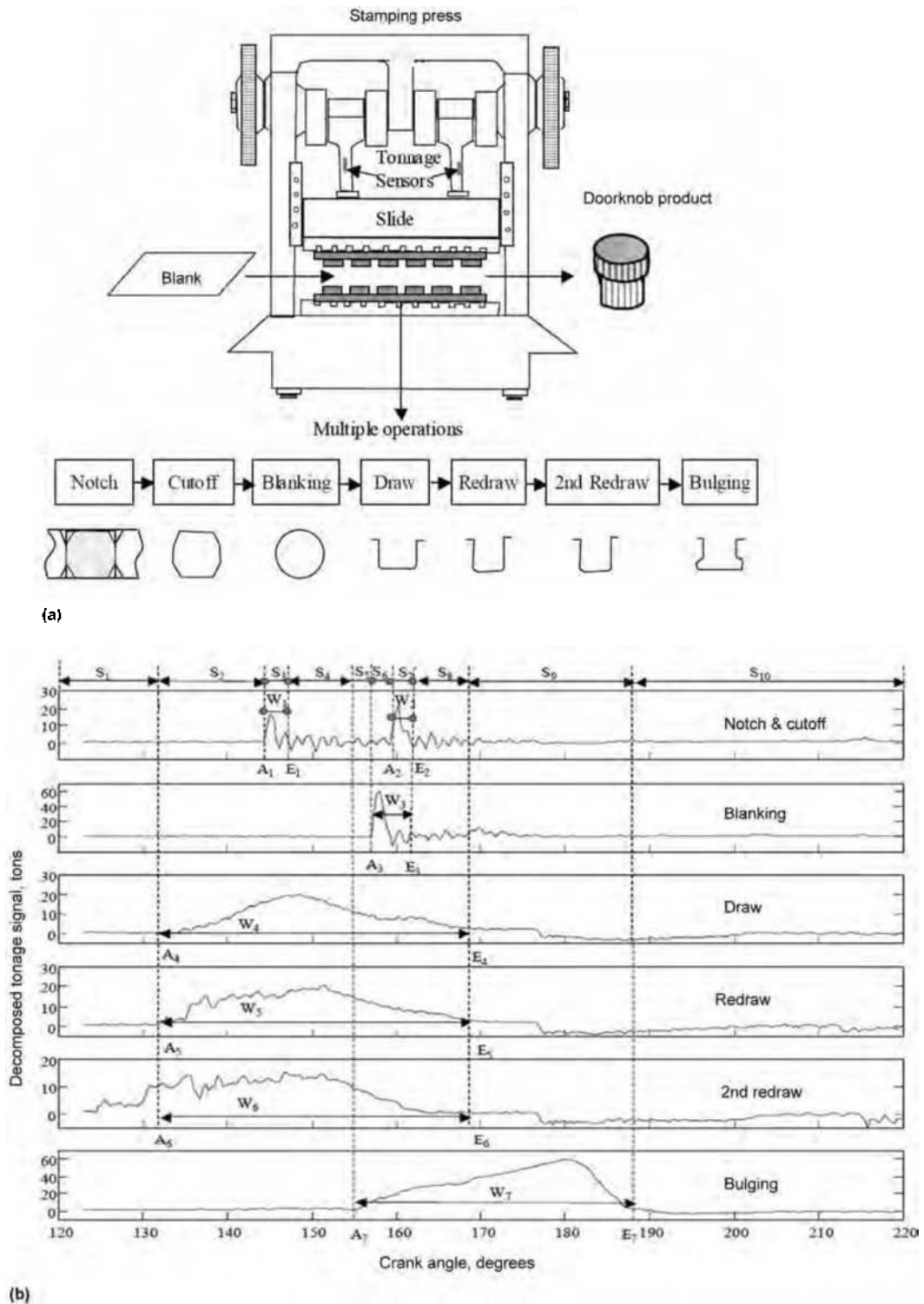


Fig. 9.17 Progressive die forming: (a) schematic of the stations; (b) load required by each station as a function of crank angle. Reprinted with permission from Ref 9.27

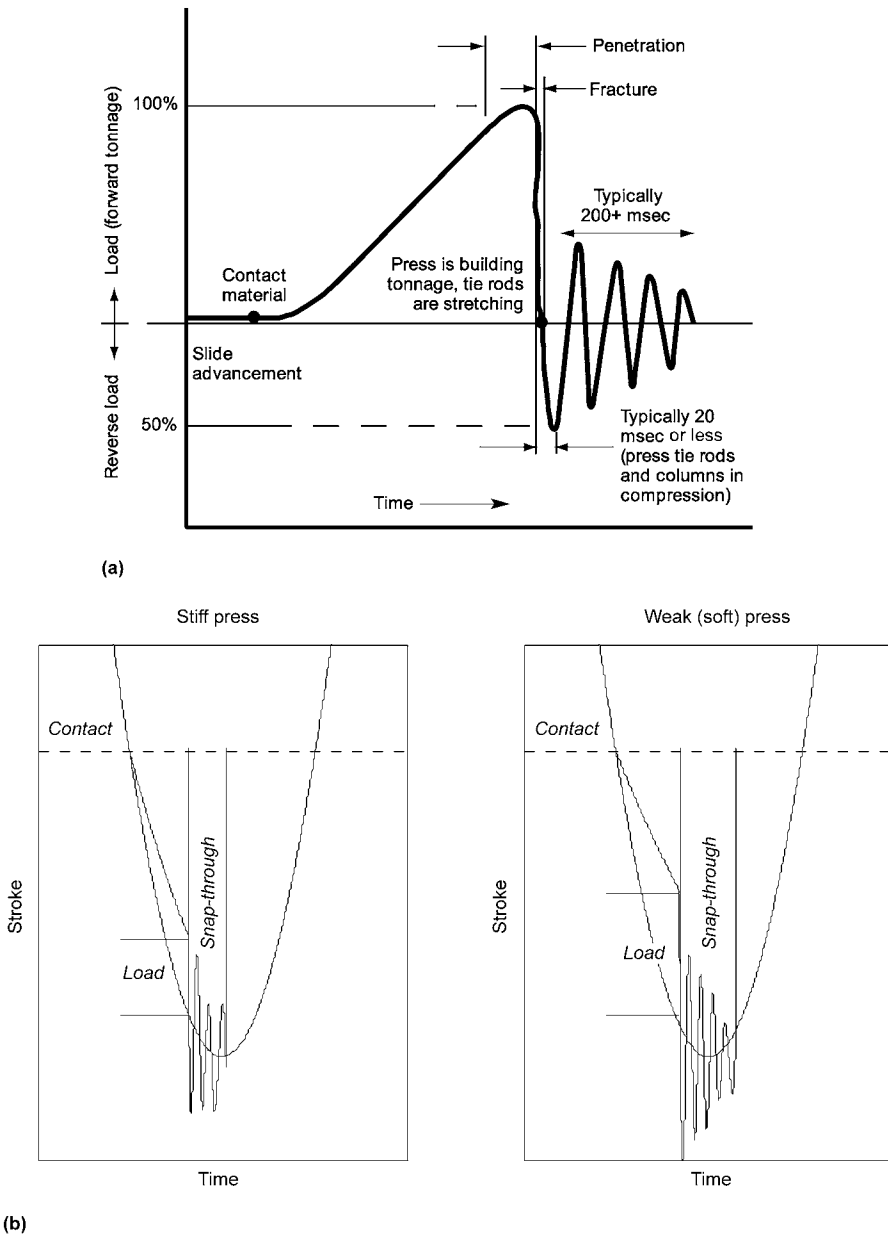


Fig. 9.18 Snap-through. (a) Load-time curve for typical blanking operation. Source: Ref 28. (b) Effect of snap-through to press motion. Recreated after Ref 9.29

A typical die-changing operation may include the following steps: (1) unclamping and (2) moving out the old die, (3) moving in and (4) centering the new die with respect to the press bed, (5) clamping the new die, and (6) setting the press (i.e., stroke, shutheight, counterbalance pressure). To speed up the die-changing

process, automation is required in the clamping and moving of dies (Ref 9.31). A typical setup for a small press is illustrated in Fig. 9.20.

Conventionally, the clamping of the lower die to the bolster and of the upper die to the slide face is done manually by springs, bolts/nuts, toggle levers, and/or wedges. Automated clamps

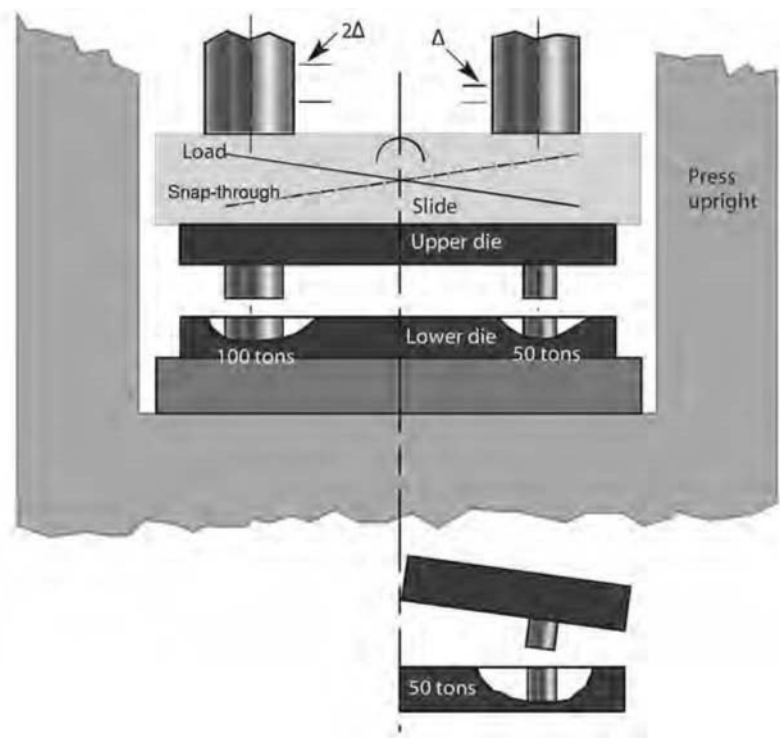


Fig. 9.19 Snap-through on a multistation die with off-center loads. Reprinted with permission from Ref 9.30

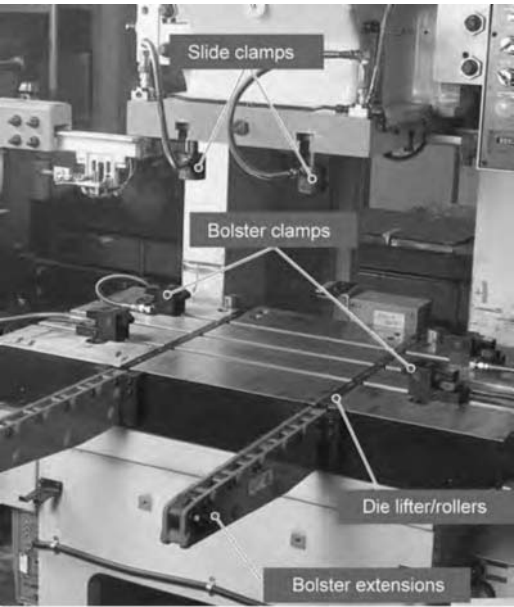


Fig. 9.20 Quick die change system installed on a small gap frame press. Source: Ref 9.32

can be electric, magnetic, or hydraulic. Different clamps are used for the upper and lower dies, since the lower dies are pushed horizontally over the bolster, whereas the slide is lowered vertically onto the upper die. Fig. 9.21 illustrates some automated clamps.

After unclamping, die lifters and die rollers are used to move out the old die. These units are placed in U- or T-channels in the bolster. Die lifters may be hydraulic, pneumatic, or mechanical. To take the die out of the press area, bolster extensions (also called prerollers) may be required. Depending on the die weight, there are several options for die lifters and bolster extensions (Ref 9.31).

When dies are to be changed in large presses, rolling mechanisms may not be adequate to handle the large weights of the dies. For large transfer presses, die carts or moving bolsters are common. These are used to move the dies out of the press area so that an overhead crane or fork-lift can be used. To utilize moving bolsters, the press table should be at ground level. When the

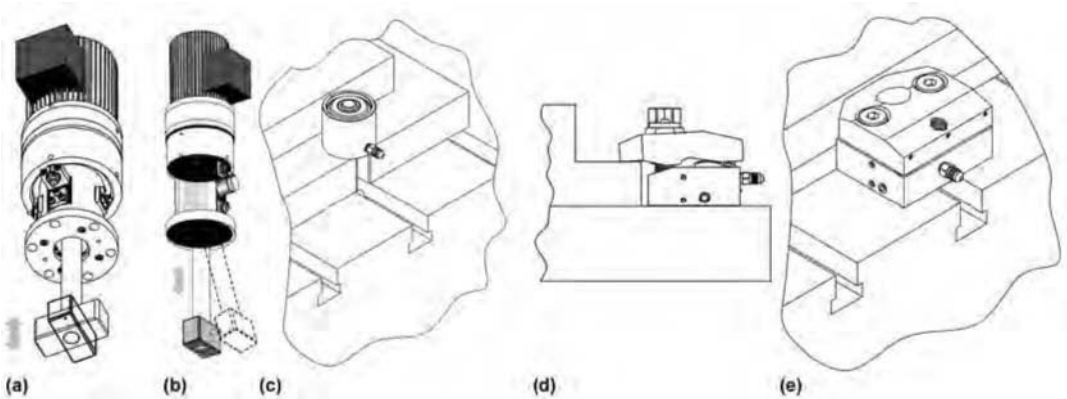


Fig. 9.21 Automated clamps: (a) electromechanical swivel and pull type, (b) electromechanical swing type, (c) hydraulic nut type, (d) and (e) hydraulic ledge type. Source: Ref 9.33, 9.34

production has to be shifted, dies and part specific transfer devices (grippers, etc.) are moved out of the press, still clamped to the first bolster. New dies and transfer equipment are clamped to the second bolster and moved into the press area. Die carts are another option for transfer presses that can be retrofitted to existing transfer press lines.

REFERENCES

- 9.1 Schuler GmbH, *Metal Forming Handbook*, Springer, 1998
- 9.2 T. Altan, F.W. Boulger, J.R. Becjer, N. Akgerman, and H.J. Henning, "Forging Equipment, Materials, and Practices," Metals and Ceramics Information Center, Battelle Columbus Laboratories, 1973
- 9.3 G. Forshall, Komatsu Power Presses Frontier II Series OBS, Product Data-sheet, 2003
- 9.4 American Society of Mechanical Engineers, "Glossary of Power Press Terms," 2008
- 9.5 P.F. Ostwald and J. Munoz, *Manufacturing Processes and Systems*, John Wiley and Sons, 1997
- 9.6 K. Lange, ed., *Handbook of Metal Forming*, McGraw-Hill, 1985
- 9.7 D.G. Stone, Achieving Straight-Side Capabilities in a Gap-Frame Press, *Fabricator*, October 2001
- 9.8 O.D. Lascoe, *Handbook of Fabrication Processes*, ASM International, 1998
- 9.9 P. Bogon, Elastische Eigenschaften von Umformmaschine und Umformwerkzeug (Elastic Properties of Forming Machines and Tools), IMAUF report 677, 2009
- 9.10 H. Wagener, New Developments in Sheet Metal Forming: Sheet Materials, Tools and Machinery, *Journal of Materials Processing Technology*, Vol 72, 1997, p 342–357
- 9.11 M. Javadi, B. Behrens, and R. Krimm, Efficient Control of Metal-Forming Machines with an Automated Load and Measurement Device, *Production Engineering*, Vol 4, 2010, p 95–100
- 9.12 P. Bogon, Elastische Eigenschaften von Umformmaschine und Umformwerkzeug (Elastic properties of forming machines and tools), IMAUF lecture, 3 October 2009
- 9.13 K. Chodnikiewicz and R. Balendra, The Calibration of Metal-Forming Presses, *Journal of Materials Processing Technology*, Vol 106, 2000, p 28–33
- 9.14 T. Altan and D.E. Nichols, Use of Standardized Copper Cylinders for Determining Load and Energy in Forging Equipment, *Journal of Engineering for Industry*, Vol 94, 1972, p 769–774
- 9.15 H. Tschatsch, *Metal Forming Practice: Processes—Machines—Tools*, Springer, 2006
- 9.16 B. Behrens, C. Brecher, M. Hork, and M. Werbs, New Standardized Procedure for the Measurement of the Static and Dynamic Properties of Forming Machines,

- Production Engineering*, Vol 1, 2007, p 31–36
- 9.17 J.R. Douglas and T. Altan, Characteristics of Forging Presses: Determination and Comparison, *Proceedings of the 13th Machine Tool Design Research Conference*, 1972
 - 9.18 A. Ghiotti and P.F. Bariani, Evaluating the Press Stiffness in Realistic Operating Conditions, *Advanced Methods in Material Forming*, 2007, Springer, p 189–198
 - 9.19 H.W. Wagener and A. Wendenburg, Analysis system: Prerequisite for Automation in Metal-Forming Technology, *Journal of Materials Processing Technology*, Vol 116, 2001, p 55–61
 - 9.20 H. Ou and C.G. Armstrong, Evaluating the Effect of Press and Die Elasticity in Forging of Aerofoil Sections using Finite Element Simulation, *Finite Elements in Analysis and Design*, Vol 42, 2006, p 856–867
 - 9.21 K. Hatsukano and T. Sano, “Dynamic Accuracy of Different Kinds of Mechanical Presses,” presented at 3rd Asia-Pacific Forum on Precision Surface Finishing and Deburring Technology (Melbourne, Australia), March 2003
 - 9.22 D.A. Smith, *Die Maintenance Handbook*, Society of Manufacturing Engineers, 2001
 - 9.23 L.A. Kren, Mechanical Presses In and Out, *Metallforming Magazine*, April 2002, p 24–37
 - 9.24 J. Landowski, Increasing Die Life and Improving Part Quality, *The Fabricator*, February 2000
 - 9.25 R. Struck, S. Kulp, B.A. Behrens, and R. Krimm, Investigation of Impacts on the Required Press Force, *Proceedings of the IDDRG 2008*, 2008, p 581–590
 - 9.26 M. Neumann and H. Hahn, Computer Simulation and Dynamic Analysis of a Mechanical Press Based on Different Engineer Models, *Mathematics and Computers in Simulation*, Vol 46, 1998, p 559–574
 - 9.27 J. Jin, Individual Station Monitoring using Press Tonnage Sensors for Multiple Operation Stamping Processes, *Journal of Manufacturing Science and Engineering*, Vol 126, 2004, p 83–90
 - 9.28 R. Miles, Combatting Snap-Through, *Metallforming Magazine*, March 2004, p 42–43
 - 9.29 T. Wenzel, Gap-Frame or Straightside? *Metallforming Magazine*, December 2003, p 38–39
 - 9.30 L.A. Kren, High-Speed Solutions to Off-Center Loading, *Metallforming Magazine*, November 2004, p 42–45
 - 9.31 L. Ellard, Quick Die Change: The Process, *Metallforming Magazine*, June 2010, p 21–23
 - 9.32 Pascal Corporation, Pascal Quick Die-Change System, Product Catalogue, QDC-01E-6, 2008
 - 9.33 Hilma-Römheld GmbH, Product Range: Die Clamping and Changing Systems, Product Catalogue, 2009
 - 9.34 PFA, Inc., Quick Die Change, Complete System Solutions, Product Catalogue, S3001 Rev A, 2008

CHAPTER 10

Mechanical Presses

Thomas Yelich, Honda
Eren Billur, The Ohio State University

MECHANICAL PRESSES use a flywheel to store energy and a slider-crank mechanism to convert rotational motion to reciprocating linear motion. Due to the slider-crank design, these presses are stroke limited; that is, the bottom **dead center (BDC) position is essentially defined** by the crank and pitman arm geometry. Because of their high stroking rate and low energy consumption, mechanical presses are the most common presses used in batch/mass production of sheet metal parts. The rated capacity (tonnage) of a mechanical press is not available throughout the stroke, only in a limited portion of it. Therefore, a good understanding of these presses is **essential in order to utilize them efficiently and avoid costly mistakes in press setup and use, such as overloading the press or the dies** (Ref 10.1).

10.1 Mechanical Press Designs

The main components of a press were described in Chapter 9, “Principles of Sheet Forming Presses,” in this book. The main difference between a hydraulic and mechanical press is the drive mechanism (see Fig. 9.2). A mechanical press drive consists of an electric motor, a flywheel, a clutch/brake, a drive shaft, a connection (also called a pitman arm or connecting rod), and a slide (ram) guided by the gibs (Fig. 10.1). Depending on the design, a press may have gear set(s) to reduce the speed and increase the torque (Ref 10.2, 10.3, 10.4).

Drive Types

Depending on the application, a mechanical press may have a simple or complex drive sys-

tem with the following common components (Ref 10.1):

- An electric motor that drives the flywheel continuously to store energy
- A slide that moves (press stroke) when the clutch is engaged and the brake is disengaged, thus transmitting torque to the crankshaft through the clutch
- A slider-crank mechanism that translates the rotational motion of the crankshaft into the linear motion of the slide.

Mechanical press drives can be classified into two types: simple drives and extended drives (Fig. 10.2). Cam-driven presses constitute a third type, but they are not widely used.

Crank and eccentric drive presses are the most commonly used mechanical presses in the industry. Extended drives are designed either to

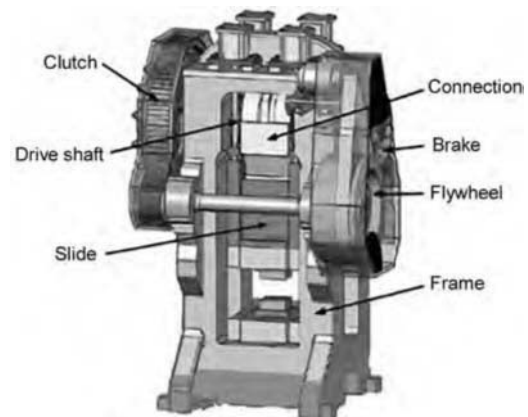


Fig. 10.1 Schematic of a mechanical press with the major components labeled. Source: Ref 10.2, 10.3

change the slide velocity (link drive presses) or to generate high press forces with small ram displacements (knuckle joint and toggle presses) (Ref 10.1).

Simple Drive Presses. The simplest drive of a mechanical press is the crank drive (sometimes called direct crank drive). This drive offers a fixed total stroke ($2r$, where r is the crank radius) and has a sinusoidal stroke-time characteristic as shown in Fig. 10.3(a). This velocity profile causes high speeds during most of the slide stroke and a decrease in the slide speed during the forming process.

Simple crank drives are modified either to alter the stroke-time characteristics or make the total stroke adjustable. One of these modifications uses noncircular gears (Fig. 10.3b). This is a relatively new technology that was patented in 2001 (Ref 10.5) and has been successfully applied to tailor the slide motion of crank presses

(Ref 10.3, 10.6). However, in the stamping industry, extended drive presses are more common for the purpose of changing the stroke-time profile.

Another modification to the simple crank drive is used in eccentric presses. In some small- and medium-size presses, the stroke can be by changing the eccentricity between the center of the connecting rod (O_1) and the axis of rotation (O_2) (Fig. 10.4). This is achieved by using two interactive eccentrics: shaft and bushing. Stroke (s) can be calculated from total eccentricity (R) as (Ref 10.3):

$$s = 2R \quad \text{Eq 10.1}$$

where (R) is a function of the eccentricity of the shaft (r), the eccentricity of the bushing (e), and the position of the bushing with respect to the

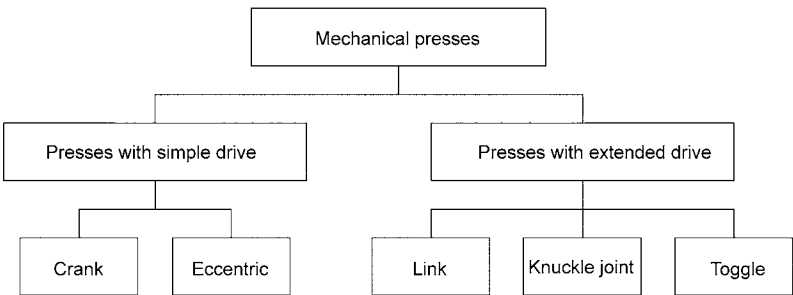


Fig. 10.2 Common drive types of mechanical presses. Adapted from Ref 10.1

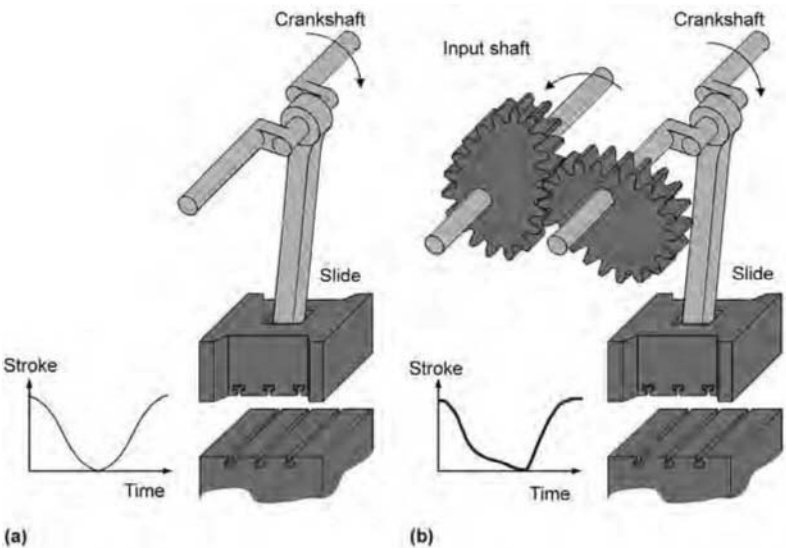


Fig. 10.3 (a) Simple crank drive, (b) slide motion can be changed with noncircular gears. Adapted from Ref 10.3

shaft. So the limits of stroke adjustment are defined by the position of bushing, as shown in Fig. 10.4:

$$s_{\min} = 2R_{\min} = 2(r - e) \quad \text{Eq 10.2}$$

$$s_{\max} = 2R_{\max} = 2(r + e) \quad \text{Eq 10.3}$$

When the stroke of a press is changed, the slide velocity, the shutheight, and the force-stroke diagram of the press change, whereas the available energy does not change. These points are further explained in the section “10.3 Other Features of Mechanical Presses” in this chapter.

Extended Drive Presses. Link drives are designed to change the stroke-time characteristics. Deep drawing is one of the operations that require modification of the slide speed. For obtaining good-quality parts in stamping, the slide velocity should be kept around 0.2 to 0.5 m/sec (0.7 to 1.6 ft/sec), depending on the material and complexity of the final geometry (Ref 10.7). It is also desirable to have a long work stroke and a constant velocity during deformation (Ref 10.1, 10.9).

It is possible to control the speed of a press by means of frequency converters so that the slide velocity does not exceed the desired value. However, this method of control will affect the production rate (parts per minute) and may drastically reduce the energy available per stroke. In a crank (or eccentric) press, it is not possible to have a constant slide speed. Moreover, in a crank press, if the stroke length is increased, the slide

velocity will increase (for constant strokes per minute).

Several “deep drawing presses” are designed to control the slide velocity during deformation. A common mechanical press design is the link press (Fig. 10.5b). As shown in Fig. 10.6, link drive presses have an almost constant slide velocity during deformation, and the velocity is lower than that of a crank press. The reduced velocity of the slide with respect to the crank angle allows longer deformation strokes and/or more strokes per minute with the same deformation speed.

Another commonly used extended drive is the “knuckle joint” drive, as shown in Fig. 10.5(c). In a knuckle joint press, the motion of the crank is transmitted through a knuckle joint to the slide. This drive is useful for coining and squeezing operations, since it has lower slide speed during deformation (Fig. 10.6) and three to four times more press force compared to a crank press of the same size. The stroke-time curve can be changed by adding a joint. The result is called a **modified knuckle joint or toggle drive**; it is commonly used for bulk forming operations and for driving the blank holder slide in double-action presses (see the section “10.2 Characteristics of Mechanical Presses,” in this chapter (Ref 10.7, 10.11).

Drive Designs

Mechanical presses can be classified according to their drive designs. In addition to the drive types and the number of useful slide mo-

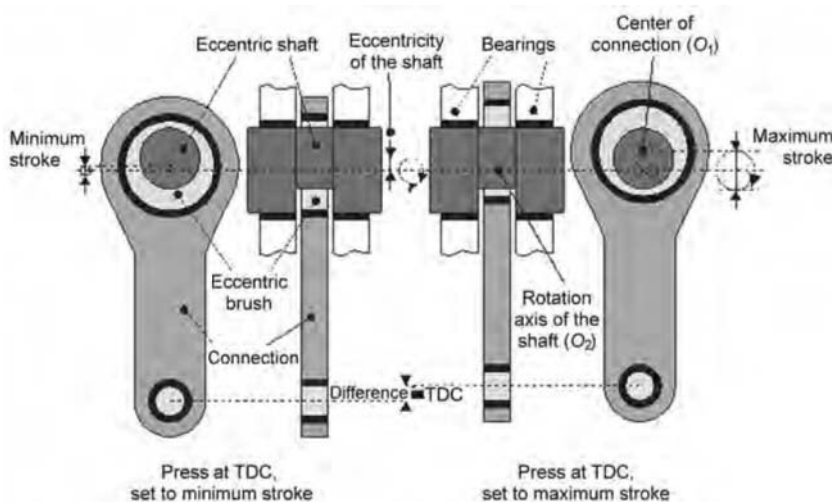


Fig. 10.4 Stroke adjustment in an eccentric press. Adapted from Ref 10.3

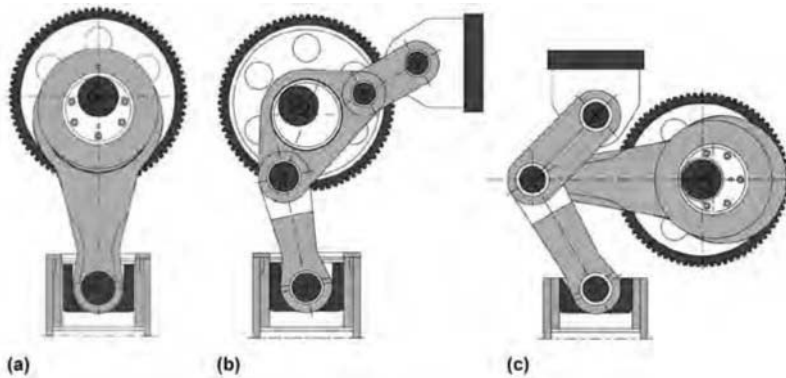


Fig. 10.5 Common drives for mechanical presses: (a) crank press, (b) link drive press, and (c) knuckle joint press. Source: Ref 10.9

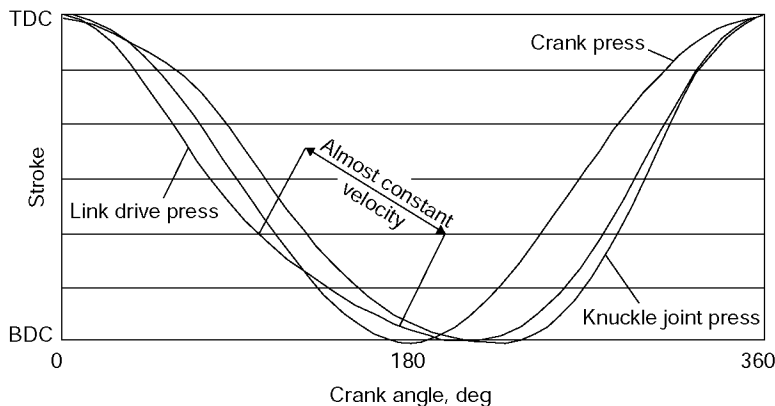


Fig. 10.6 Comparison of slide motions generated by a crank press, link drive, and knuckle joint press. BDC, bottom dead center. Source: Ref 10.10

tions, there are four other drive design parameters (Ref 10.1, 10.4):

- Gear reduction
- Location of the drive
- Number of connecting rods
- Positioning of the drive shaft

Gear Reduction. In mechanical presses, the energy stored by flywheel can be calculated as:

$$E = \frac{1}{2} I \omega^2 \quad \text{Eq 10.4}$$

where I is the angular inertia (which is equal to $\frac{1}{2}(\text{mass} \times \text{radius}^2)$ in $\text{kg}\cdot\text{m}^2$ or $\text{ton}\cdot\text{in.}^2$), and ω is the angular speed (radians per second, rad/s) of the flywheel. Therefore, to store more energy in a given flywheel, higher angular speeds are required. On the other hand, very high flywheel

speeds are rendered impractical by the capacity of the clutch and/or the brake. Depending on the energy per stroke and the strokes per minute required by the process, gear reductions may be required (Ref 10.7).

Direct drive presses (Fig. 10.7a) are used for single-station blanking and high-speed stamping of shallow parts. Since there is no gear reduction, these presses can operate relatively fast: anywhere from 90 to 1,000 strokes per minute (SPM). This design also lowers the manufacturing and maintenance costs, because there are fewer parts subject to wear. However, direct drive presses have limited energy per stroke.

To increase energy per stroke, gear reductions are used. With single gear reduction, press speeds of 35 to 150 SPM are common. These presses have more energy per stroke and are therefore more suitable for drawing and forming operations. If a press has a wide slide, which

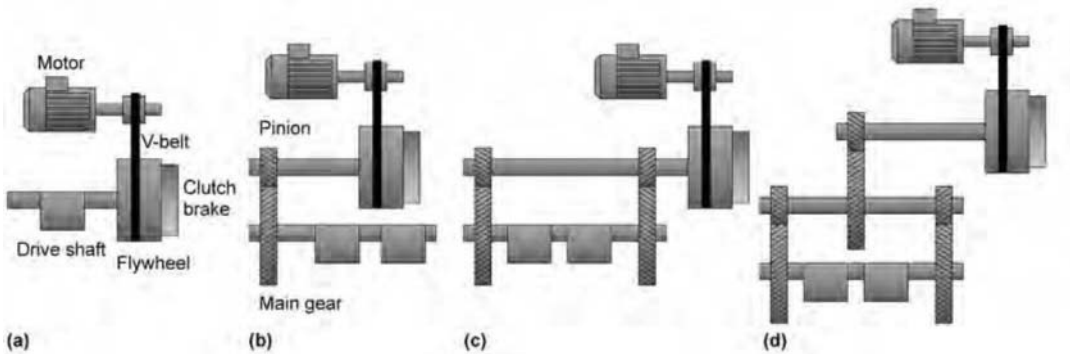


Fig. 10.7 (a) Direct drive (nongearred), (b) single gear reduction-single end drive, (c) single gear reduction-twin end drive, and (d) double gear reduction.

requires two connecting rods per driveshaft, as shown in Fig. 10.7(b), then single-end drive may result with angular misalignment in the shaft. This will cause ram tipping even in the absence of an eccentric load. Twin-end drives are therefore recommended for presses that do heavy work (Fig. 10.7c). Large transfer presses, which are used for heavy forming operations, usually employ a double gear reduction (Fig. 10.7d). These presses operate at 8 to 30 SPM (Ref 10.12).

Location of Drive. Most presses are top-drive presses: the drive mechanism is above the slide and pushes the slide down to perform the forming operation. There are also bottom-drive (also known as underdrive) presses, in which the drive mechanism is under the bed and the connecting rods are within or alongside the press uprights. The main advantages of this design, compared to top-drive presses, are that (a) a lighter frame can be used, since the frame is only guiding the slide and housing the control and auxiliary systems, (b) no tie-rods are required, and (c) presses can be installed in places with limited ceiling height. However, these presses require deeper foundations (Ref 10.2, 10.12, 10.13).

Number of Connecting Rods. In mechanical presses, the force is transmitted to the slide by connecting rods. When the slide/bolster area is large and/or high eccentric loads are expected, **single connecting rods may not be sufficient** to maintain the parallelism between the slide and the bolster (Ref 10.7). Common designs are the single-point, double-point, and four-point designs, as shown in Fig. 10.8.

Positioning of Drive Shaft(s). A single-point press has one drive shaft (crankshaft) and a four-point press has two of them. However, a

double-point press may have either one or two drive shafts, depending on the location(s) of the shaft(s). They may lay either left to right (longitudinal) or front to back (transverse or cross), as shown in Fig. 10.8. For single- and double-point presses, both designs are common; four point presses generally have transverse drive shafts (Ref 10.1).

In double-drive-shaft presses, to avoid the lateral forces, shafts have to be rotated in directions opposite to each other (Ref 10.1, 10.6).

Number of Slide Motions

A press may have one or more slides, depending on the design. Single-action presses have only one slide and therefore can create one motion and apply one force. However, in some applications, such as deep drawing, a blank holder force is required in addition to the punch force. In a single-action press, it is possible to equip the dies with springs, air or hydraulic cylinders, or high-pressure nitrogen cylinders to apply the blank holder force. The other two options are (a) to use a die cushion in a single-action press (see Chapter 13, “Cushion Systems for Sheet Metal Forming,” in this book) or (b) to use a double action press (Fig. 10.9) (Ref 10.7).

A double-action press has two slides: (1) an inner slide or drawing slide and (2) an outer slide or blank holder slide. The drive for the inner slide can be actuated by either simple crank or link drive. The outer slide may have either a cam (in early designs) or a toggle drive (Ref 10.7). In double-slide presses, even a very small (~ 0.1 mm (0.004 in)) difference in shutheight may cause an increase in blank holder force of 50 tons or more in a large press (Ref 10.15). Figure 10.10 shows the motions of both slides (Ref 10.15).

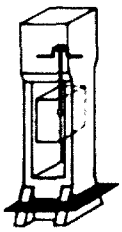
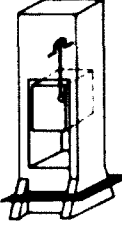
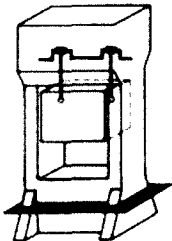
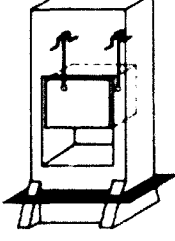
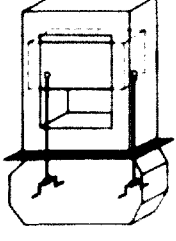
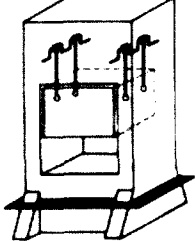
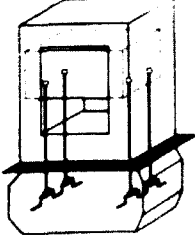
	Longitudinal		Transverse	
	Top drive	Top drive	Top drive	Bottom drive
Single point				
Double point				
Four point				

Fig. 10.8 Classification of presses with respect to: (1) number of connecting rods, (2) positioning of drive shaft(s) and (3) location of drive. Adapted from Ref 10.13

For complex drawing operations where reverse drawings are also present, a triple-action press may be needed. These presses have an additional slide that moves from bottom to top. The motion of the third slide can be independent. In triple-action presses some of the slides may be actuated with mechanical (crank, link, or knuckle joint) drives or hydraulic drives.

With advances in hydraulic control technology, a single-action press with computer numerical control (CNC) hydraulic cushions (Fig. 10.9b) can now outperform a double-action press. This design has the following advantages: (a) the blank holder force can be controlled with time, (b) if a multipoint cushion (MPC) system is employed, blank holder pressure can be changed with location and time, and (3) these presses can be less costly than a double-action press (Ref

10.16). Die cushions are discussed in detail in Chapter 13, “Cushion Systems for Sheet Metal Forming,” in this book.

10.2 Characteristics of Mechanical Presses

Load and Energy Requirements. A mechanical press has a slider-crank mechanism, shown schematically in Fig. 10.11(a).

Useful machine (press) load (L_M) can be calculated from the clutch torque (M). L_M causes a compressive force, P , on the connecting rod, according to:

$$P = \frac{L_M}{\cos \beta} \quad \text{Eq 10.5}$$

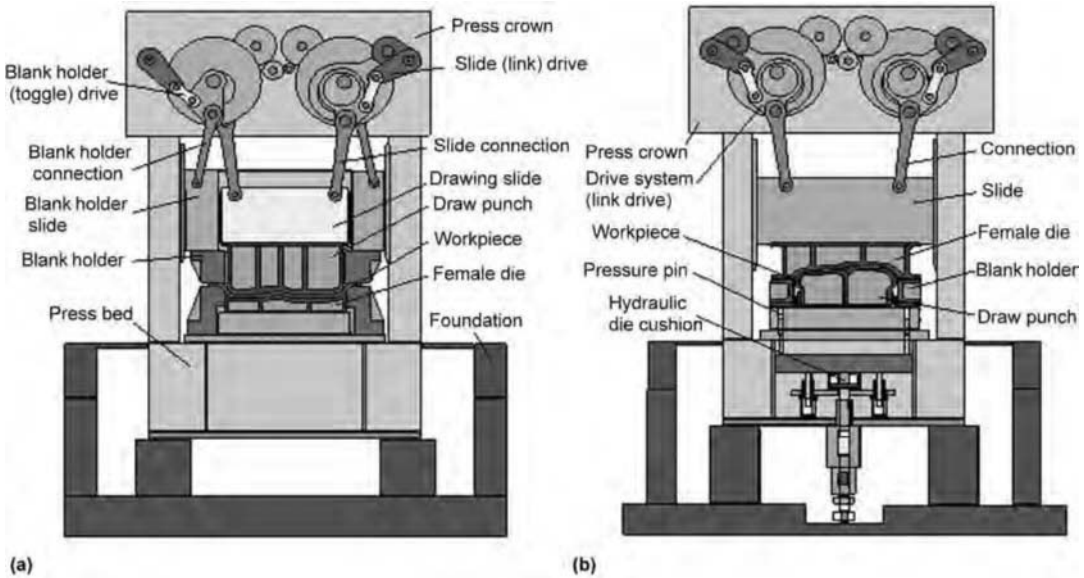


Fig. 10.9 Deep drawing operation in (a) double-action press and (b) single-action press with die cushion. Source: Ref 10.7

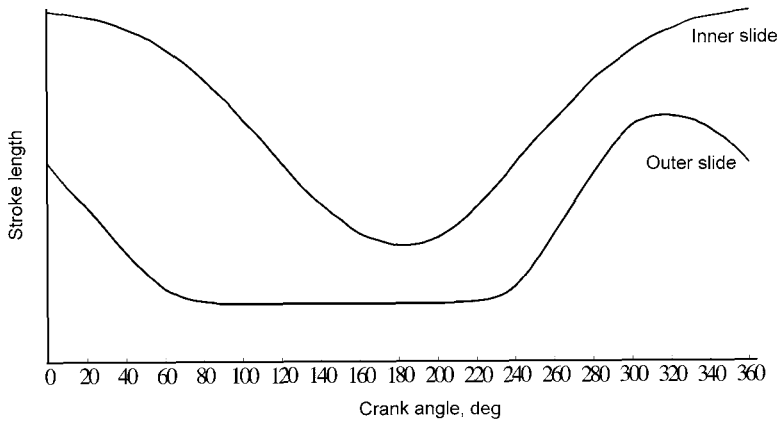


Fig. 10.10 Slide motions of a double action press. Source: Ref 10.15

This force, P , acts on the crank and has two components: tangential force (F_T) and radial force (F_R). The tangential force can be calculated from the moment equation as follows:

$$F_T = \frac{M}{r} \quad \text{Eq 10.6}$$

F_T is also given by:

$$F_T = P \sin(\alpha + \beta) \quad \text{Eq 10.7}$$

Eq 10.5, 10.6, and 10.7 are combined to find the useful press (or machine) load, (L_M), as a func-

tion of clutch torque (M), crank radius (r), and crank angle (α):

$$L_M = \frac{M}{r} \frac{\cos \beta}{\sin(\alpha + \beta)} \quad \text{Eq 10.8}$$

Generally, the connecting rod length (l) is 4 to 15 times larger than crank radius (r). This allows the assumptions $\cos \beta \cong 1$ and $\sin(\alpha + \beta) \cong \sin(\alpha)$. Then Eq 10.8 simplifies to:

$$L_M \cong \frac{M}{r} \frac{1}{\sin(\alpha)} \quad \text{Eq 10.9}$$

According to this equation, as angle α goes to 0° or to 180° (i.e., at top dead center (TDC) and BDC), the available load increases without limit. These equations show the load applicable by the mechanism. However, press components and

frame are designed for a “maximum permissible load” or nominal press capacity (in tons or kN). This is the load available in a mechanical press at a defined crank angle before BDC (α_N design angle), commonly 30° (point B in Fig. 10.12).

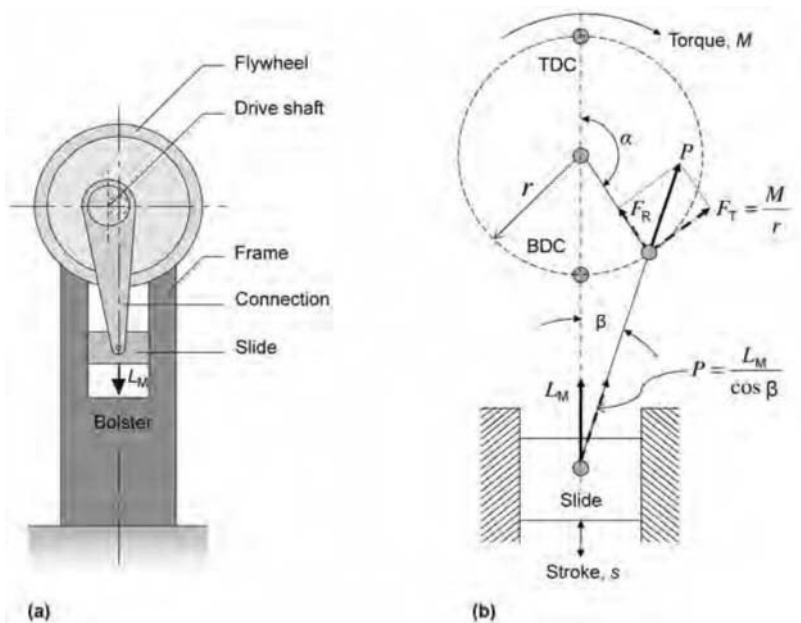


Fig. 10.11 (a) Schematic of a mechanical (crank or eccentric) press. Source: Ref 10.17. (b) Free body diagram of the drive. BDC, bottom dead center; TDC, top dead center. Source: Ref 10.18

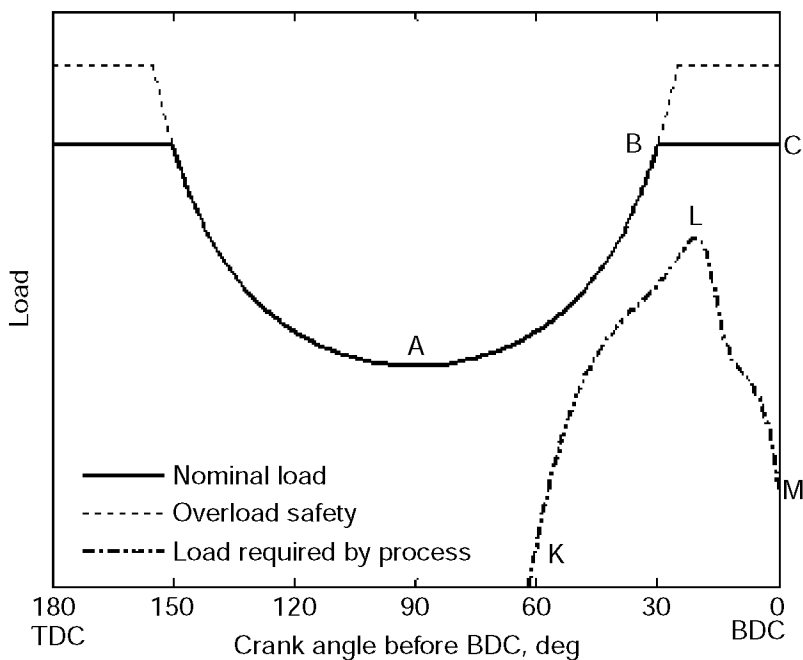


Fig. 10.12 Nominal load as a function of crank angle. BDC, bottom dead center; TDC, top dead center.

- In a mechanical press, if the load required by the forming process is smaller than the available load (*i.e.*, curve KLM in Fig. 10.12 remains below curve ABC), the process can **be carried out, provided that the flywheel** can supply the necessary energy per stroke.
- If the required load (KLM) exceeds the available load (ABC) before point B, then the friction clutch slides and the press slide stops before BDC and the flywheel continues to turn. In this case, the press can be freed by increasing the air (or hydraulic) pressure on the clutch and reversing the flywheel rotation.
- For small crank angles before BDC (the BC portion of ABC), the slide load can become larger than the nominal press load if no overload safety device is available. In this case, if the press stalls, the flywheel stops and the entire energy of the flywheel is transformed into deflection energy by straining the frame and drive mechanism. Usually the press can be freed only by burning out the tooling.

In addition to available machine load (L_M), it is important to consider the energy required by the process (E_p) and the energy available per stroke from the press (E_M). The energy in a mechanical press is stored in the flywheel according to:

$$E_{\text{stored}} = \frac{1}{2} I \omega^2 = \frac{1}{2} I \left(\frac{\pi n}{30} \right)^2 \quad \text{Eq 10.10}$$

where ω is the angular velocity in rad/s and I is the moment of inertia of the flywheel in $\text{kg}\cdot\text{m}^2$ or $\text{ton}\cdot\text{in}^2$. Depending on the unit system, the energy can be given in J (kJ) or $\text{ton}\cdot\text{in}$. To simplify Eq 10.10, angular velocity can be entered as n in rpm. Eq 10.10 gives the total energy stored in flywheel rotation. Energy available per stroke (E_M) can be calculated as:

$$E_M = \frac{1}{2} (\omega_0 - \omega_1)^2 = \frac{I}{2} \left(\frac{\pi}{30} \right)^2 (n_0 - n_1)^2 \quad \text{Eq 10.11}$$

where ω_0 is the flywheel's initial angular velocity, ω_1 is its angular velocity after deformation in rad/s, and n_0 and n_1 are the corresponding values in rpm. In continuous operations, a flywheel slowdown of 13 to 20% can be permissible; therefore, in one stroke a maximum of 25 to 35% of the flywheel energy can be consumed (Ref 10.7).

In intermittent (start-stop) operations, much more energy per stroke can be consumed, provided that the press will not be operated until the flywheel recovers its initial speed. Douglas and Altan (Ref 10.19) investigated a 500-ton mechanical forging press by upsetting copper samples with different diameters. As the diameter got larger, the energy consumed per stroke increased. They measured the time elapsed for the flywheel to recover its initial speed. This measurement could then be converted to maximum strokes per minute, as shown in Fig. 10.13.

Time-Dependent Characteristics of Presses. The movement of mechanical presses is charac-

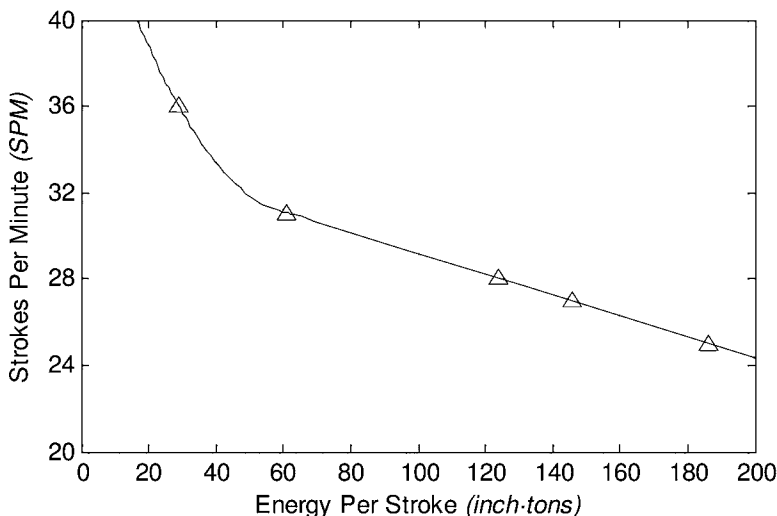


Fig. 10.13 Maximum strokes per minute versus energy available in a 500 ton mechanical press. BDC, bottom dead center; TDC, top dead center. Source: Ref 10.19

terized by slide velocity and the number of strokes per minute.

Slide Position (h) and Slide Velocity (V): For a given crank angle (α), the distance h from BDC can be estimated from:

$$h \cong r(1 - \cos \alpha) = \frac{S}{2}(1 - \cos \alpha) \quad \text{Eq 10.12}$$

where the eccentricity of the crank (r) or the stroke length (S) is also required. Slide velocity, V , can be determined by differentiation with respect to time:

$$V \cong r\omega \sin \alpha = \frac{S\pi n}{60} \sin \alpha \quad \text{Eq 10.13}$$

where ω is the angular speed of crank in rad/s and n is the corresponding value in revolution per minute (rpm). However, these values are calculated under unloaded conditions (Fig. 10.14a); loading on the press may reduce the slide speed as shown in Fig. 10.14(b).

Number of Strokes per Minute (n): This value determines the production rate. n may be governed by crank idle speed or adjusted for energy requirements per stroke (Fig. 10.14) and material handling system.

Dimensional Accuracy of Mechanical Presses. The accuracy of a press depends on stiffness (as described in detail in the chapter “Principles of Sheet Forming Presses” in this volume). For a mechanical press, the stiffness depends on the design factors:

- Drive type, orientation, and position
- Number of connecting rods
- Frame type.

Rau (Ref 10.20) investigated two mechanical presses at the same rated capacity. Assuming the **total deflection in a single connecting rod press** as 100%, the two-point mechanical press had **15% less deflection** (Table 10.1). Total deflection depends on design characteristics of a press, and sometimes a well-designed single-point mechanical press may outperform a two-point one. Fig. 10.15 summarizes stiffness data obtained from a total of 24 different presses, where one-point, two-point, and four-point mechanical presses are compared to bottom-knuckle joint drives and top-knuckle joint drives.

Four-point mechanical presses have a larger angular stiffness than other kind of mechanical presses. Some two-point presses may be vertically stiffer than four-point presses (Ref 10.21). **The number of connecting rods has a significant effect on angular stiffness**, which affects the tilting of the ram, as shown in Fig. 10.16.

Table 10.1 Contribution to vertical press deflection by various press components

	Deflection (%)	
	One-point mechanical press	Two-point mechanical press
Slide + connecting rod	30	21
Frame	33	31
Drive shaft + bearings	37	33
Total deflection	100	85

Source: Ref 10.20

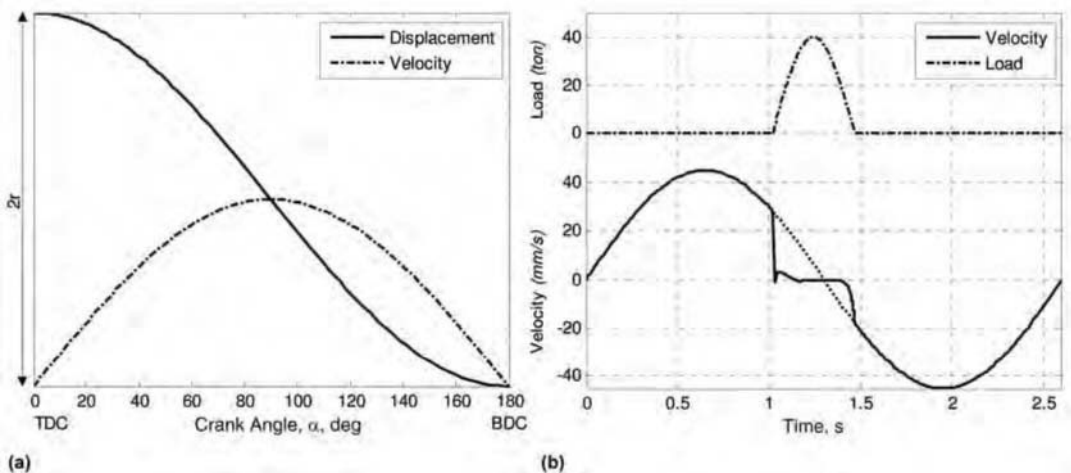


Fig. 10.14 (a) Velocity and displacement of slide during a half stroke; (b) velocity profile of a crank press under load (coining)

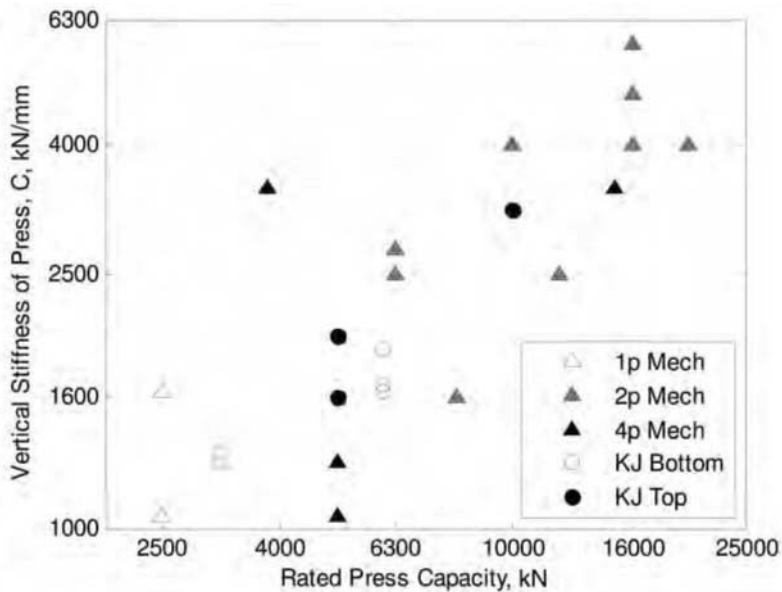


Fig. 10.15 Vertical stiffness (C) of one-point (1p Mech), two-point (2p Mech), and four-point (4p Mech) mechanical presses, bottom knuckle joint (KJ bottom) drives, and top-knuckle joint (KJ top) drives. Source: Ref 10.21

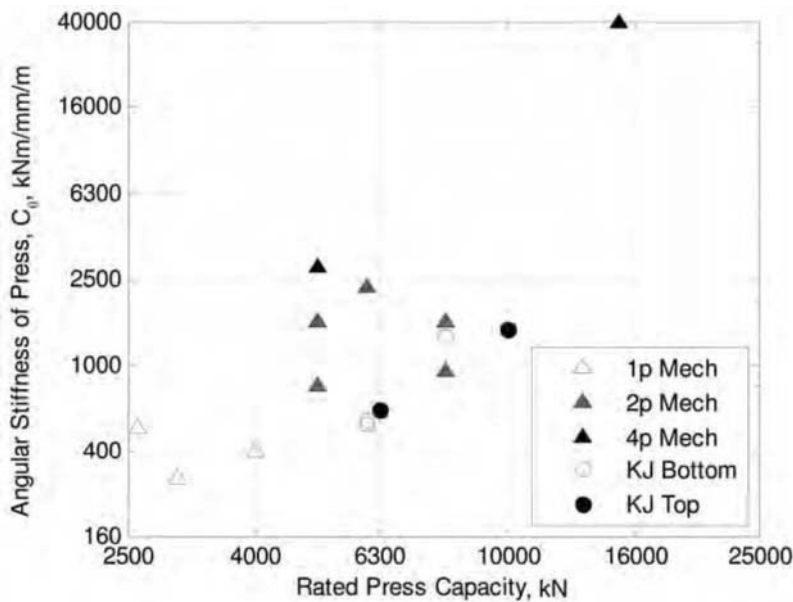


Fig. 10.16 Angular stiffness (C_θ) of one-point (1p Mech), two-point (2p Mech), and four-point (4p Mech) mechanical presses, bottom knuckle joint (KJ bottom) drives, and top-knuckle joint (KJ top) drives. Source: Ref 10.21

10.3 Other Features of Mechanical Presses

Overload Protection. As shown in Fig. 10.12, a constant-clutch torque can generate a large amount of ram force in a mechanical

press. As a result of this characteristic, mechanical presses are susceptible to overloading. Overloading can be caused by a process requiring more tonnage than rated press capacity or by inappropriate setup of the press. A properly designed die may cause overload if (a) press

shutheight is lowered, (b) foreign materials are present in the die, (c) workpiece is buckled or misfed, (d) die is worn out or have excessive galling, or (e) workpiece hardness or thickness changes.

Press components are designed to withstand the nominal press force (rated capacity). To avoid any damage to bearings, gears, clutch, frame, and other components, a press should not be loaded with more than the nominal load capacity of the press as specified by the press manufacturer. While the slide is approaching the BDC, the force starts to build up and eventually may reach the rated capacity before it travels to the BDC. If no precaution is taken, the press may not complete its stroke and may be “stuck” at the bottom of the stroke. At this point the total flywheel energy is consumed to deform the part and to elastically expand the press structure. Since the force buildup happens in fraction of a second, braking the press is not a solution. Therefore special systems are designed that (a) do not allow the slide to apply more than a preset tonnage, and (b) allow the slide to move 1/15 to 1/10 of the total stroke while the slide force is relieved.

The two most common overload protection designs are illustrated in Fig. 10.17. Mechanical overload protection systems are still found in low-tonnage presses (up to 1000 kN). These employ a brittle shear plate which needs about 130% rated capacity to break. When shear plate is broken, the slide has some free distance (s_0 in Fig. 10.17a), so that it can complete the stroke. After each incident of overload, shear plate has to be replaced with a new one.

Hydraulic overload protection devices are more popular, because (a) the press can be started after an overload without changing any plates, and (b) the press force can be limited by adjusting the hydraulic pressure. In this system, an oil pad between the slide and the connecting rod is pressurized when the force is building up. Oil pressure moves a second piston, which acts as an intensifier to the pressurized air. If the slide pressure (and therefore the oil pressure) passes a threshold value, the oil is drained back to the tank. Thus, the force applied is limited and some free movement distance is created (Ref 10.1, 10.3, 10.22).

Shutheight Adjustment. The shutheight of a press (i.e., distance from bolster to slide surface at BDC) can be adjusted in order to accomplish any of the following goals: (a) accommodate various dies with different heights, (b) compensate the change in height due to wear, grinding, or reworking, (c) accommodate a different workpiece thickness, (d) set the maximum forming force, or (e) set the shutheight after stroke adjustment (Ref 10.1, 10.3).

Shutheight is usually adjusted via screws and nuts, driven either manually or by electric motors. New presses have electronic sensors (encoders, as shown in Fig. 10.18) and controls which enable the adjustment of shutheight with 0.01 mm (0.0004 in.) accuracy. The design of a shutheight adjustment screw may be a ball screw (Fig. 10.18a) or an adjustment screw (Fig. 10.18b) Fig. 10. (Ref 10.3, 10.8). The ball-screw adjustment changes the length of the connecting rod and therefore may affect the available load to be considered (see Fig. 10.11 and Eq 10.8).

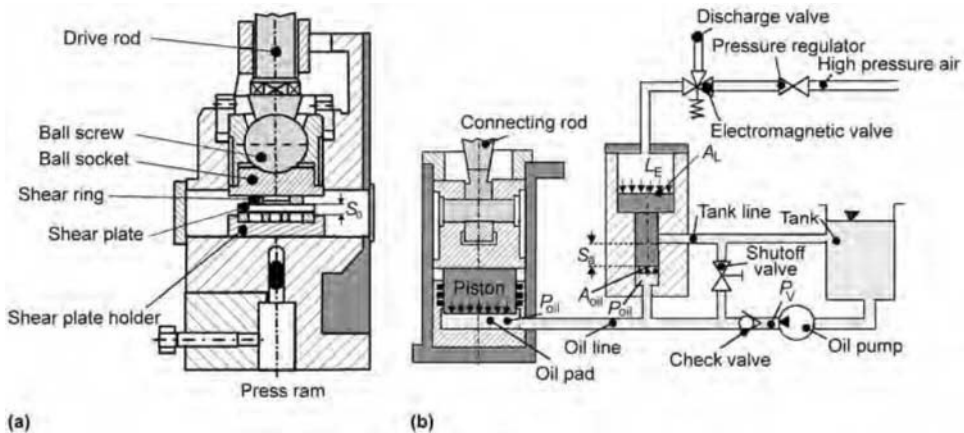


Fig. 10.17 Overload protection systems: (a) mechanical (shear plate) overload protection; (b) hydraulic overload protection. Adapted from Ref 10.3.

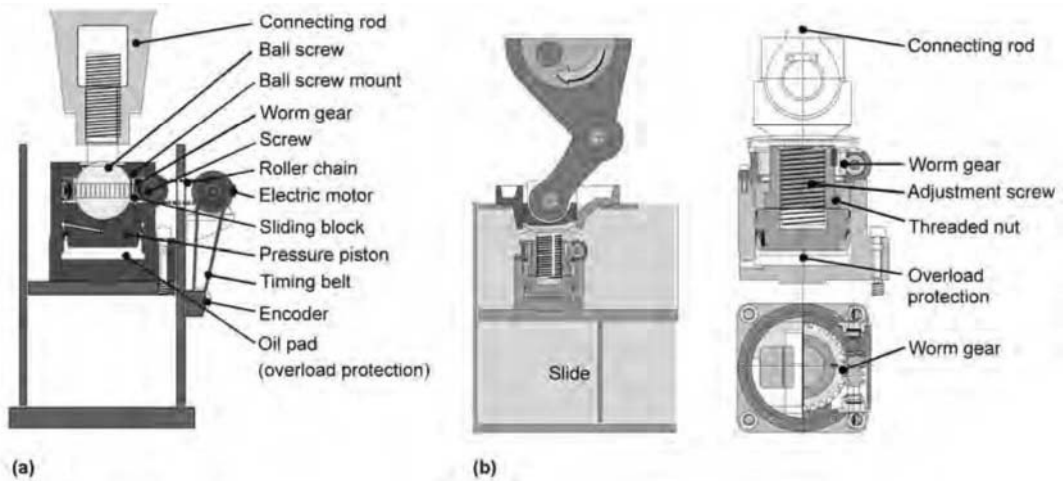


Fig. 10.18 Shutheight adjustment mechanisms: (a) ball-screw, (b) adjustment screw. Adapted from Ref 10.3

Clutch/Brake Mechanisms. The clutch is engaged to transmit the torque from the flywheel to the drive shaft, and the brake is activated to stop the press after the clutch is released. When the press is operated in single-stroke mode, the slide and other drive elements are accelerated to working speed within extremely short time periods (often 100–300 ms). Conversely, after the stroke has been completed, the press has to come to a standstill very quickly (Ref 10.7).

The clutch torque is calculated to ensure that the rated capacity (L_M) is available at the design angle (α_N). It can be calculated from:

$$M_{\text{clutch}} = L_M r \sin(\alpha_N) \quad \text{Eq 10.14}$$

If gear reduction is used in the press, then the clutch moment can be reduced, as given by the gear reduction ratio, enabling a smaller clutch to be used. In large transfer presses, clutch torque may be as large as 500,000 N·m (368,000 ft·lb). Clutch and brake may be separate units or can be combined. These units may be actuated and controlled via high-pressure air (pneumatic) or oil (hydraulic). Hydraulic units are more popular, since they can accommodate more switching frequency (i.e., engaging/releasing) and do not wear or create dust from abrasive materials (Ref 10.3, 10.7).

There are also “complete press drives” that consist of a flywheel, a clutch/brake, and a planetary gear set for reduction. These units have less angular momentum compared to a system with a spur gear set; in consequence, they can apply

more energy per stroke. Recently, a switchable gearbox has also been integrated into such a system for the purpose of adjusting the number of strokes per minute or energy per stroke or modifying the stroke-time curve (Ref 10.3).

Slide Counterbalancing. Slide counterbalances are devices compensating the weight of slide and upper die in a mechanical press. Originally, mechanical springs were employed for this purpose. These are now replaced by pneumatic cylinders (Fig. 10.19a). The counterbalancing system has two uses under static conditions: (a) when the slide is being adjusted, the weight of slide and the upper die are compensated by the cylinders, freeing the adjustment screw from the load, and (b) as presses may creep downward when they are idle for some time, a proper counterbalance can reduce the creep. However, the main uses are under dynamic conditions.

When the press slide is retracting (after BDC), the weight is suspended by the counterbalance mechanism, so that the electric motor will replace the lost flywheel energy and it is not used to lift the weight of the slide. Thus, energy can be saved (Fig. 10.19b). In addition, a counterbalance system reduces the impact on bearings and gears as well as the braking time.

Adjustment of pressure in counterbalancing cylinders is important in order for the system to perform properly. Many press builders supply information about “counterbalance cylinder pressure versus upper die weight,” but surveys show that vast majority of press users do not utilize this information. Some presses can store

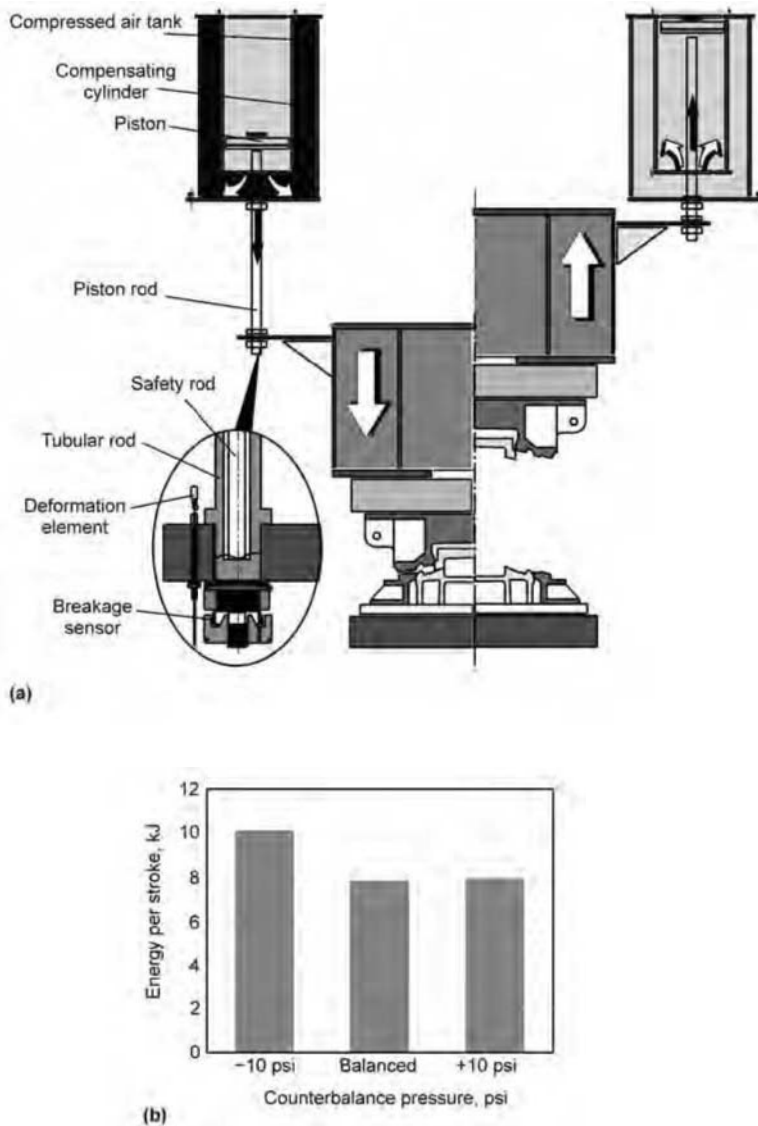


Fig. 10.19 Pneumatic slide counterbalancing. (a) Components. Source: Ref 10.7. (b) Effect of pressure setting on energy consumption for a given 1000 ton press. Source: Ref 10.23

the settings for a given die, so that whenever the die is attached to the press, the controller adjusts the pressure to the preset value for the die. There are also automatic counterbalance systems that may set the pressure either by sensing the weight of the upper die or measuring the angular velocity of the flywheel. Complex systems may have several strain gages on connecting rods and be able to set different pressures for cylinders, thus helping to reduce out-of-parallelism errors (Ref 10.7, 10.23, 10.24, 10.25).

REFERENCES

- 10.1 K. Lange, ed., *Handbook of Metal Forming*, McGraw-Hill, 1985
- 10.2 American Society of Mechanical Engineers. "Glossary of Power Press Terms," 2008
- 10.3 E. Doege and B.A. Behrens, eds., *Handbuch Umformtechnik (Metalforming Handbook)* (in German), Springer, 2010

- 10.4 H.E. Theis, ed., *Handbook of Metal-forming Processes*, Marcel Dekker, 1999
- 10.5 E. Doege, M. Hindersmann, and K. Ulrich, Antriebseinrichtung für eine Umformmaschine (Drive for a Forming Machine), European Patent EP0-786-297 B1, 2001
- 10.6 F. Würden, "Helmerding Presses," product datasheet, 2005
- 10.7 Schuler GmbH, *Metal Forming Handbook*, Springer, 1998
- 10.8 D. Boerger, "The Use of Link Motion in Mechanical Presses," AIDA Tech Bulletin 3, 2000
- 10.9 scmBLISS S.A.S., Mechanical Presses, Product Catalogue, 2006
- 10.10 Schuler AG, The Entire World of Sheet Metal Forming, Product Catalogue, 2008
- 10.11 H. Tschatsch, *Metal Forming Practise: Processes—Machines—Tools*, Springer, 2006
- 10.12 D.A. Smith, *Fundamentals of Press-working*, Society of Mechanical Engineers, 1994
- 10.13 K. Lange, ed., *Umformtechnik: Grundlagen, Bd. I: Handbuch für Industrie und Wissenschaft (Metal Forming: Fundamentals, Vol 1: Handbook for Industry and Research)* (in German), Springer, 2002
- 10.14 Z.T. Zhang, D.G. Monette, A.F. King, I.I. Bohonek, and G.A. Pitt, "Tonnage Control for a Drawing Operation in a Double-Action Press," SAE Technical Paper 1999-01-0686, 1999
- 10.15 M.E. Dingle, P.D. Hodgson, and M.J. Cardew-Hall, "Effect of Global and Local Stiffness on Blank holder Pressure in Draw Die Forming," SAE Technical Paper 2001-01-1138, 2001
- 10.16 K. Siegert, T. Altan, and T. Nakagawa, Development and Manufacture of Dies for Car Body Production, *CIRP Annals Manufacturing Technology*, Vol 46, 1997, p 535–543
- 10.17 K.H. Grote and E.K. Antonsson, eds., *Springer Handbook of Mechanical Engineering*, Springer, 2009
- 10.18 T. Altan, S.-I. Oh, and H.L. Gegel, *Metal Forming: Fundamentals and Applications*, American Society for Metals, 1983
- 10.19 J.R. Douglas and T. Altan, Characteristics of Forging Presses: Determination and Comparison, *Proceedings of the 13th Machine Tool Design and Research Conference*, 1972
- 10.20 G. Rau, A Die Forging Press with a New Drive, *Metal Forming*, July 1967, p 194–198
- 10.21 H. Wagener, New Developments in Sheet Metal Forming: Sheet Materials, Tools and Machinery, *Journal of Materials Processing Technology*, Vol 72, 1997, p 342–357.
- 10.22 S. Overly, "Hydraulic Overload Protection," AIDA Technical Bulletin 2, 2002
- 10.23 Ross Controls, Principles of Counterbalance Systems, Product Catalogue, 1999
- 10.24 W.H. Hinterman and T. Hinterman, Understanding Press Counterbalance Conditions Using Strain Technology, *Metal-forming Magazine*, June 1997
- 10.25 S. Overly, "Press Balancing Systems Pneumatic Counterbalancers," AIDA Technical Bulletin 4, 2002

CHAPTER 11

Electromechanical Servo-Drive Presses

Ajay Yadav, Caterpillar Technical Center
Serhat Kaya and Adam Groseclose, The Ohio State University

ELECTROMECHANICAL SERVO-DRIVES have been used in machine tools for several decades. Recently, several press builders, mainly in Japan and Germany, developed gap and straight-sided sheet metal forming presses that utilize the mechanical servo-drive technology. The mechanical servo-drive press offers the **flexibility of a hydraulic press (infinite ram speed and position control, availability of press force at any ram position)** with the speed and reliability of a mechanical press (Ref 11.1, 11.2). Thus, this new drive technology has considerable potential in present and future applications in blanking, bending, stamping, and coining (Ref 11.3). More than 1000 servo-drive presses are already in operation in stamping and in automotive plants all over the world. Reference 11.4 summarizes the latest developments in servo-drive presses.

In an electric servo motor, the angular position of the output shaft is determined by the duration of the current pulses provided by the controller. Thus, the output shaft can be rotated in both directions, can be stopped with precision at any given angle position, and can change speed according to the number of pulses provided per second. Modern servo-motor designs can provide constant torque over a large range of rotational speeds (rotations per minute, rpm). In a **mechanical servo press, the flywheel and the clutch** are replaced with a servo drive, with or without a linkage mechanism, as shown schematically in Fig. 11.1.

This drive offers great flexibility and accuracy in controlling the speed and position of the press slide. Thus, for a given stamping application, the press operation can be optimized to:

- Increase stroking rate and productivity
- Control the velocity of deformation during the forming stage of the stroke, which results in reduced friction and heat generation as well as improved quality and reduced scrap rate
- Reduce impact speed and noise
- Improve edge quality in blanking and shearing and increase tool life
- Reduce springback and improve part dimensions by controlling the dwell time at the BDC (bottom dead center) of the slide stroke
- Allow assembly and other secondary operations in the same press by slowing down or stopping the press slide anywhere during the slide stroke to allow for additional secondary tool motions

11.1 Servo-Press Drives versus Conventional Press Drives

For many years, stampers have known that the capability to adjust the ram speed during the ram stroke and the stroke length offers improvements in productivity and part quality (Ref 11.6). Thus, mechanical presses with linkage drives and a hydraulic press that inherently pro-

vides a programmable slide stroke have been used in many applications. The hydraulic press can develop full tonnage at any speed and at any point in the stroke. Mechanical press designs can have a variety of drive options—such as link, screw, knuckle joint, eccentric, or crank—and operate with a variable stroking rate. However, **slide motion versus stroke is fixed by the design**, although the stroke position and length can be adjusted (Ref 11.7).

As shown in Fig. 11.2, during the press stroke of a mechanical press drive, the following positions of the ram stroke versus time curve must be considered (Ref 11.7, 11.8):

- Die closing or approach from TDC (top dead center) until the upper die touches the blank
- Forming process when deformation takes place
- Die opening, when the upper die moves from BDC toward TDC

- Part transfer in automated operation or part removal and blank/perform placement into the lower die

For a high-productivity press operation, die closing should be as fast as possible, while the **forming process must be adapted to the specific part or forming operation**. During this portion of the ram stroke, it may even be desirable to have a variation in the ram speed to optimize the deformation process. The die opening portion should be as short as possible to reduce the total press cycle without causing any malfunction of the auxiliary die motions such as spring and cam actuations. Finally, the part transfer portion of the press cycle must be adjusted to **allow sufficient time for part transfer (loading and unloading)** (Ref 11.8).

In a servo-drive press, the slide motion can be adjusted to “optimize” the press cycle for different applications and part transfer require-

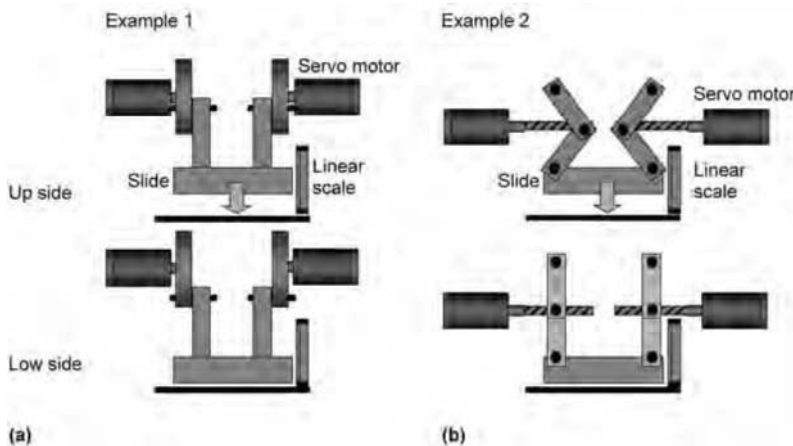


Fig. 11.1 Schematic of servo-drive press (a) without and (b) with linkage mechanism. Source: Ref 11.5

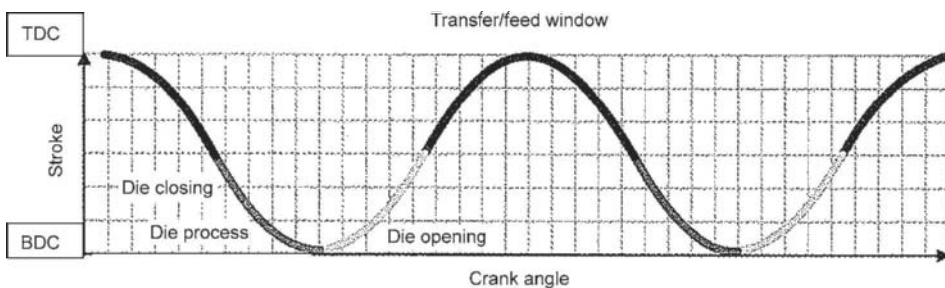


Fig. 11.2 Various portions of the slide motion in a typical mechanical press with eccentric or crank shaft drive. TDC, top dead center; BDC, bottom dead center. Source: Ref 11.7

ments. This is illustrated in Fig. 11.3 (Ref 11.9), which compares the press cycle of a servo press conceptually with that of a mechanical press. The flexible programming of the servo-drive press allows the operator to (a) obtain the “most suitable” forming velocity for the given material and forming operation, (b) dwell the slide anywhere at the desired stroke position, (c) carry out secondary operations such as painting, punching, or assembly, and (d) provide the necessary time for part transfer.

11.2 Servo-Press Drives

Servo-press drives can be classified into two main types: drive systems that use low-torque/high-speed servo motors or high-torque/low-speed servo motors.

Drives with Low-Torque/High-Speed Motors. The first-generation servo presses were built by using high-speed motors. To generate the relatively high forces that are needed in metal forming, these designs use belt, linkage, and ball screw drives to transform the rotational motion into the linear motion of a press slide, as shown in Fig. 11.1 and 11.4 (Ref 11.9).

In the design shown in Fig. 11.4(a), the rotational motion of the servo motor is transmitted to the slide using a timing belt and ball screw. The press slide is moved up and down by the reciprocating motion of the motor and ball screw. The maximum press load is available

anywhere in the stroke, but it is limited by the torque capacity of the servo motor, the diameter ratio of the belt drive, and the load-carrying capacity of the ball screw. The tilting of the press slide is detected by linear sensors and corrected by adjusting the motion of each individual motor as needed. Thus, it is possible to maintain slide/bolster parallelism under off-center loading of the press. In the linkage design shown in Fig. 11.4(b), the knuckle joint mechanism is activated by the ball screw. Thus, for a small force on the ball screw, a relatively large force is obtained on the slide. The motion of the slide is reversed by reversing the direction of the rotation of the servo motors. The linkage design can be combined with a conventional crank drive, where the reciprocating slide motion can be achieved without the reversal of the motor shaft rotation. Other linkage designs can be combined with the servo drive to obtain various force-stroke relationships (Ref 11.3). A direct-driven spindle drive press is shown in Fig. 11.5 (Ref 11.10). In this design, four servo motors drive four ball screws to activate the slide. By sensing the position of the slide at the four corners of the press, it is possible to ensure slide/bolster parallelity by controlling the output of each individual motor.

Drives with High-Torque/Low-Speed Motors. Recently, low-speed/high-torque servo motors have been developed that allow direct drive of the press eccentric or crank mechanism. Thus, there is no need for belt, linkage, or ball screw

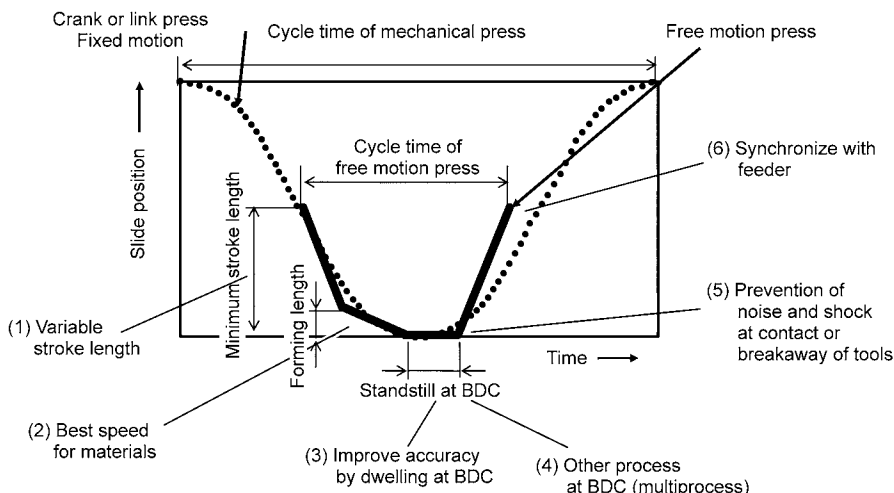


Fig. 11.3 The flexibility of slide motion in servo-drive (or free motion) presses. Source: Ref 11.9

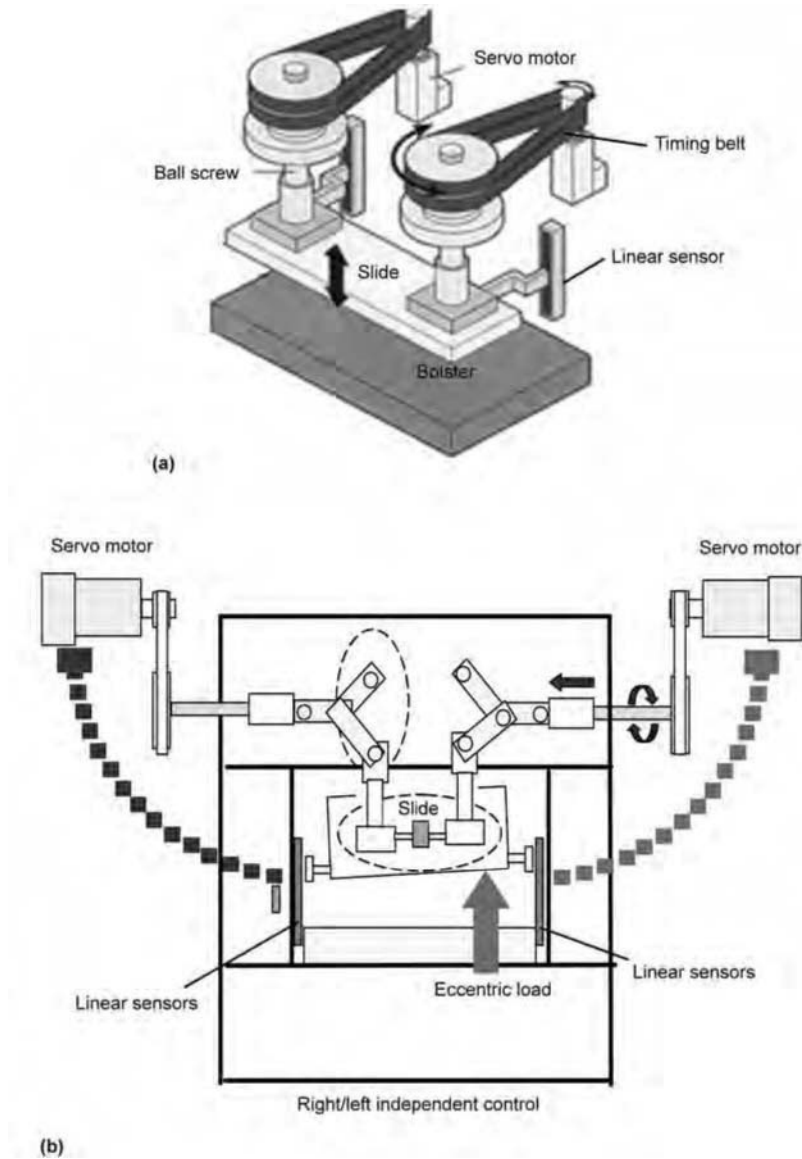


Fig. 11.4 Schematic of servo presses with high-speed/low-torque servo-motors (a) with belt and ball screw drive and (b) with ball screw and linkage drive. Source: Ref 11.9

drives. Furthermore, an existing press structure and drive system, originally designed for a mechanical slider-crank drive mechanism, can be used for servo drives. As a result, it is expected that manufacturing and maintenance costs would be reduced and the press uptime would be increased. A high-torque servo-motor, attached directly to the press drive shaft, is used extensively in the design of standard gap presses (Fig. 11.6) (Ref 11.6). Thus, the structural stiffness and well-proven gear-eccentric drive of a gap press

are maintained while only the flywheel, clutch, and main motor have been replaced with a large-capacity servo motor. For larger-tonnage straight-side presses, multiple servo motors can be used, as shown in Fig. 11.7 and 11.8 (Ref 11.12).

Mechanical press manufacturers continue to develop innovative designs using high-torque servo motors at reasonable costs and well proven press structure and drive systems. A typical mechanical press drive (Fig. 11.9) illustrates the conventional electric motor, belt drive,

flywheel, clutch-brake combination, and the drive of the eccentric gear. A servo drive, incorporated into an existing four-point linkage design of a straight-side press, is shown in Fig. 11.8.

To decrease manufacturing costs and increase reliability in the design of larger straight-side presses, up to 3000-ton capacity, compact servo modules have been developed to drive various two-point or four-point press slides (Ref 11.11). In addition to the flexibility of controlling the

slide motion, servo-drive presses also offer considerable energy savings, especially in large-capacity presses. In servo-drive presses, the installed motor power is larger than in comparable-capacity mechanical presses. However, the servo-motor power is used only when the press is operated to conduct a stamping operation (deep drawing, blanking, coining), because **there is no continuously rotating flywheel and clutch/brake mechanisms**. Furthermore, during the dynamic braking operation of the servo motors, the braking energy is fed back into the power system. It is also possible, if economically justified, to install external energy-storage capability to compensate for energy peaks and reduce the nominal power drawn from the local power supply system.

An example is given in Fig. 11.10 (Ref 11.7). In this application, power use is considered during a press cycle. Operating with the main motors (maximum output of 235 hp (175 kW) each), the energy is stored in an external energy-storage device during deceleration and then used when the press motion requires more than 235 hp. Because the stored energy (maximum of 470 hp (350 kW) based on the output of two motors) is used during peak power requirements, the power load on the facility remains nearly constant at about 70 hp (50 kW). It is suggested that the energy generated by deceleration of the slide can be stored within a capaci-

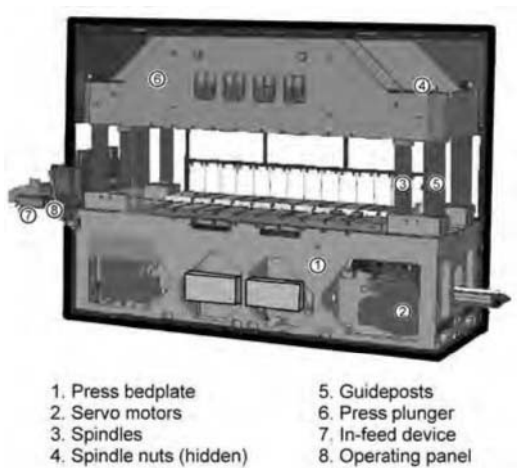


Fig. 11.5 A straight-side four-column press with four spindles directly driven by servo motors. Source: Ref 11.10

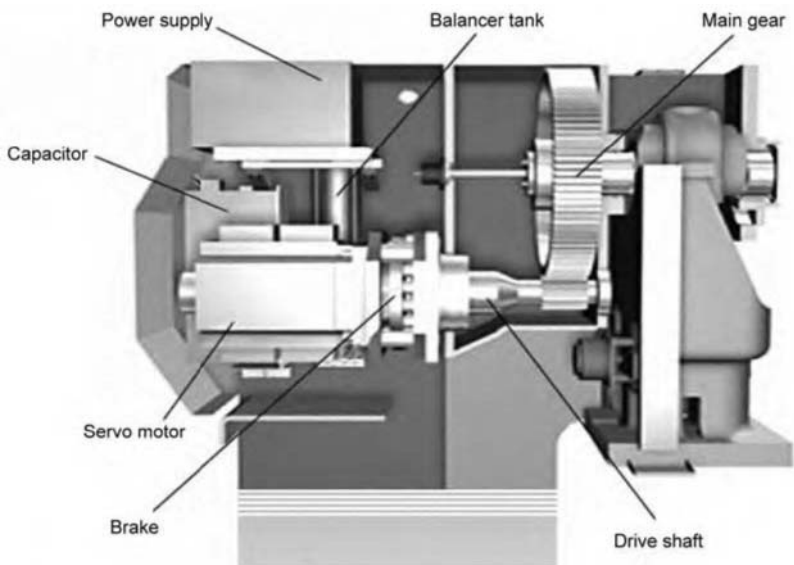


Fig. 11.6 Direct gear-driven gap press with servo drive, where the high-torque servo motor is directly coupled to press drive shaft. Source: Ref 11.6

tor or a motor/generator coupled to a rotating mass.

11.3 Applications

Servo-drive presses were initially used for blanking, coining, and stamping of small parts in gap presses. Another major initial application was in die tryout and die setup because these presses allow very precise slide motion control at very low speeds (Ref 11.10). As the industry and research groups started to explore the use of these presses, major applications emerged.



Fig. 11.7 Four identical servo motors with integrated brake system driving an eccentric shaft. Source: Ref 11.11

Noise and Die Life in Blanking. Using a hydraulic servo press, Otsu et al. (Ref 11.13) conducted experiments in blanking carbon steel, stainless steel, titanium, and copper sheets using a 15-mm (0.60-in.)-diameter punch and 50- μ m punch/die clearance. They investigated two schemes of punch motion: constant speed and variable speed (continuous “two-step blanking”), as shown in Fig. 11.11.

Figure 11.12 shows the noise levels obtained in blanking high-strength carbon steel (440 MPa (64 ksi) tensile strength, 1.2 mm (0.05 in.) thick) in the function of the stopping position of the punch, when the punch speed is 35.4 mm/s (1.39 in./s) at time for breakthrough. The noise level reduction is more significant in blanking hard materials, and the noise reduction in “two-step blanking” is due to reduction of blanking force and machine vibrations.

The burr-free blanking of Al 5052 alloy was investigated using a 60-ton servo press (Ref 11.14). The slide motion used in this study is shown in Fig. 11.13. Three steps, using a maximum slide speed of 50 mm/s (2.0 in./s), were used to obtain burr-free blanked edges in one press stroke that required a 3-s cycle time. Two die punch clearances, 5 and 10% of sheet thickness ($t = 1.5$ mm (0.06 in.)), were used with a 30-mm (1.2-in.)-diameter punch. By reducing the punch/die clearance and selecting the proper punch edge radius, it was possible to eliminate burrs with the technique used in this study.

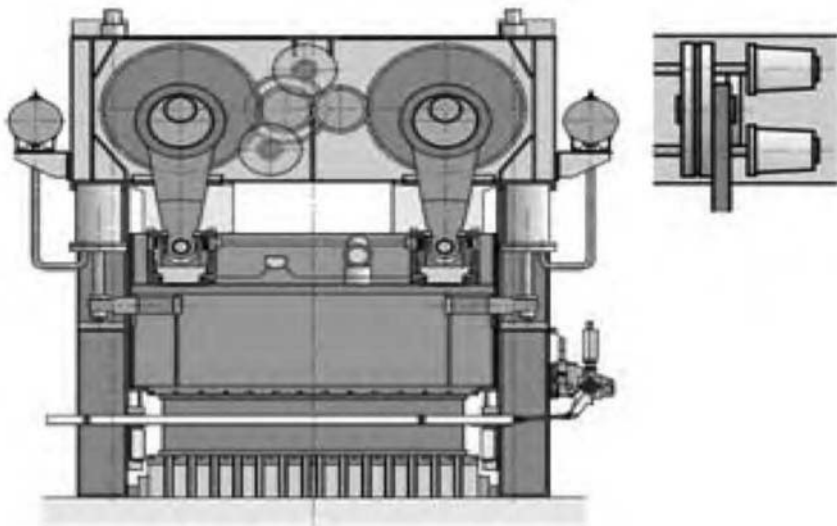


Fig. 11.8 A servo-press drive with two servo motors incorporated into a four-point straight-side press design. Source: Ref 11.12

Improvement of Die Life in Blanking.

Blanking studies were conducted using the same tools in conventional mechanical and comparable servo-drive presses (Ref 11.9). The strokes per minute (SPM) in both presses were kept approximately the same while the actual blanking velocity was reduced considerably in the servo-drive press, as shown in Table 11.1. Figure 11.14 shows the burr heights obtained in both presses after blanking several thousand parts from SPCC material. In this study, the punch used in the mechanical press needed regrinding after blanking 30,000 pieces, while in the servo press the punch needed regrinding after 100,000 blankings.

Precision Blanking. The schematic of the tooling, designed for precision blanking in a servo press, is shown in Fig. 11.15. In this process, two punches are used to complete the precision blanking operation. First, the larger punch hits the workpiece and extrudes the material slightly into the die cavity and stops before the workpiece is totally blanked (Fig. 11.16). The upper cylinder moves the punch holder plate to the right and aligns the smaller punch with the die before the final blanking operation takes place. Figure 11.17 shows the slide motion used in this process. Because of flexibility of the ram motion, the slide does not have to go

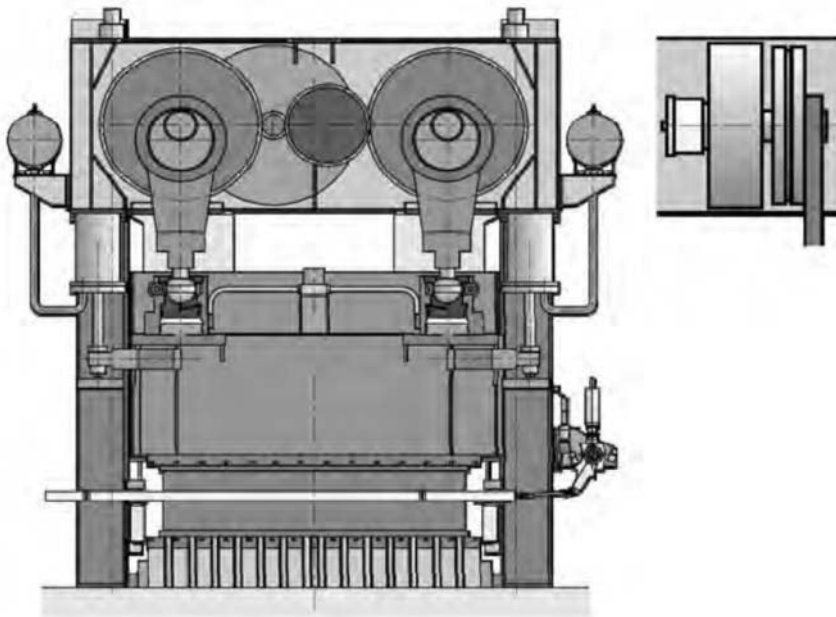


Fig. 11.9 A conventional four-point straight-side mechanical press drive. Source: Ref 11.12

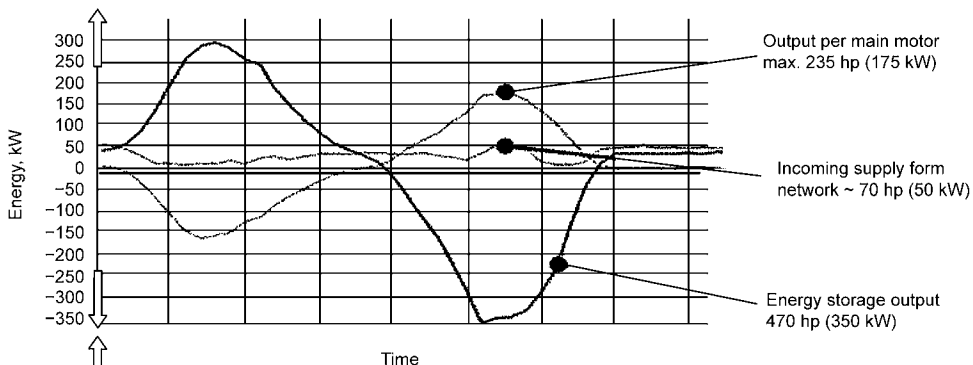


Fig. 11.10 Main motor output supplied almost entirely by energy storage. Source: Ref 11.7

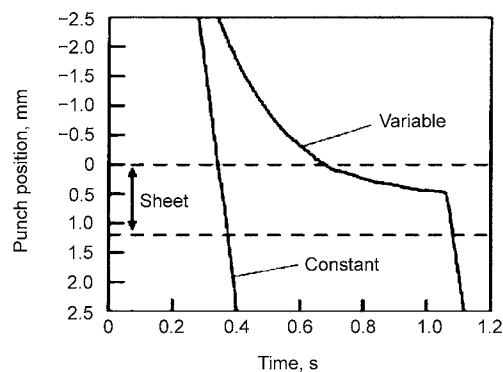


Fig. 11.11 Example punch motions of constant and variable punch speeds. Source: Ref 11.13

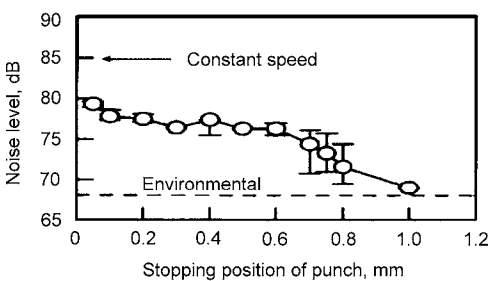


Fig. 11.12 Relation between noise level and stopping position of punch in blanking high-strength carbon steel (tensile strength = 440 MPa (64 ksi)) with variable punch speed. Source: Ref 11.13

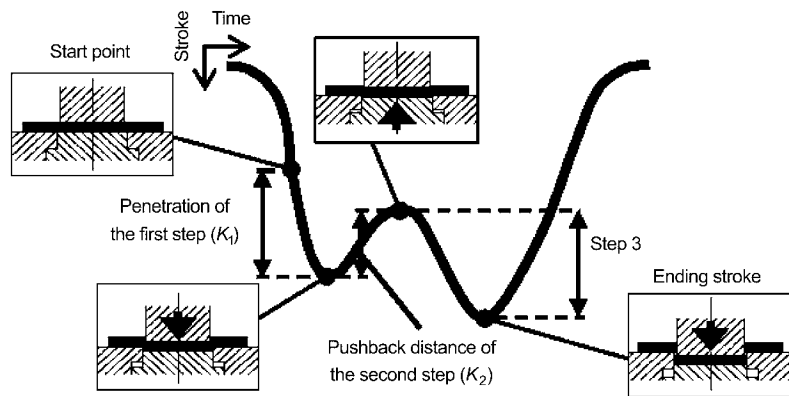


Fig. 11.13 Motion diagram of the slide of the numerical-control servo press and the corresponding blanking steps. Source: Ref 11.14

Table 11.1 Blanking velocities and strokes per minute (SPM) for servo and conventional mechanical presses

	H1F35H (servo press)	OBS35-2 (conventional mechanical press)
Strokes per minute (SPM)	68	69
Blanking velocity (mm/s)	32	86

Source: Ref 11.9

all the way back to TDC before executing the final blanking operation, thus reducing the total cycle time. The precision blanked part is shown in Fig. 11.18.

Reduction in Springback. In forming of eyeglass frames from a titanium alloy, it was necessary to reduce springback. In this application, developed by Hamamoto Technical Co.,

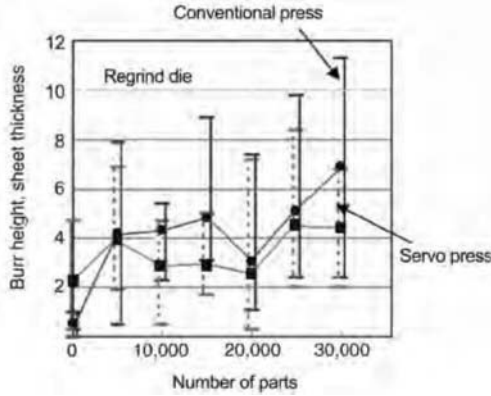


Fig. 11.14 Burr height sheet thickness ratio obtained in blanking with a servo and conventional mechanical press. Source: Ref 11.9

the springback was reduced in a single press stroke by using a multiple (three-step) motion of the slide with different BDC positions (Ref 11.9).

Warm Forming of Mg Alloy. Elevated temperature forming of Mg AZ31B alloy disks (3.0 mm (0.1 in.) diameter \times 3.0 mm thick) was conducted successfully using graphite and molybdenum disulfide lubricant with the punch and dies heated to 300 °C (572 °F) (Ref 11.9). The blank is located on a counterpunch. As the top die comes down, a center punch activated by gas pressure is pressed against the workpiece that is heated during the initial part of the slide stroke. Actual deformation starts after the workpiece reaches forging temperature. The slide motion curve, the initial blank, and the forged part are shown in Fig. 11.19.

Warm Forming of a Laptop Case. The servo-drive press is used for warm forming of difficult-to-form sheet alloys such as Mg AZ31, Al 5754, or Al 5052. The dwell that can be obtained in the slide motion allows the sheet blank to heat between the heated tool components (die, blank holder, punch). Thus, the blank is heated within the same press and tool set, elimi-

nating the need for external heating and part transfer. A general slide motion that can be used in warm forming of Al and Mg alloys is shown in Fig. 11.20 (Ref 11.16).

A laptop case from Mg AZ31-0 alloy, which can be formed only at or near 300 °C (572 °F), is shown in Fig. 11.21 (Ref 11.17). The deformation required in this part is mostly severe bending, with a small amount of drawing. The forming velocity was varied in such a way that it was slower, at about 1 mm (0.04 in.) per second, during the initial bending and faster, at about 200 mm (8 in.) per second, during the upstroke after deformation was completed.

Warm Deep Drawing of Al, Mg, and Ti Alloy Cups. In a recent study, experiments illustrated how best to use a servo-drive press in deep drawing of round cups from various alloys at temperatures between 250 and 300 °C (480 and 570 °F) (Ref 11.16). The schematic of the tooling and the open tool set are shown in Fig. 11.22 and 11.23. The blank holder and the die are heated with cartridge heaters. The punch is cooled with water circulation. The blank is placed on the heated blank holder (stage 1), the die closes and the blank is heated (stage 2), and then the part is deep drawn when the slide presses the blank holder against the air cushion pressure. Cups drawn in this tooling between 275 and 310 °C (525 and 590 °F) are shown in Fig. 11.24. The ram motion followed points 1 through 8 shown in Fig. 11.20, using the Aida Servo press shown in Fig. 11.7.

Servo Press with Three Slide Axes of Freedom. A servo press that can carry out an orbital motion has been developed recently (Ref 11.18). The slide of this 3D servo press has three axes of freedom so that orbital as well as swinging motions can be achieved using the appropriate

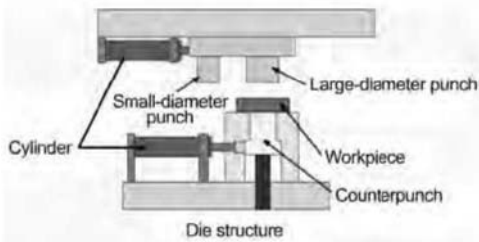


Fig. 11.15 Tooling designed for precision blanking (tool design by Todo Kogyo). Source: Ref 11.9

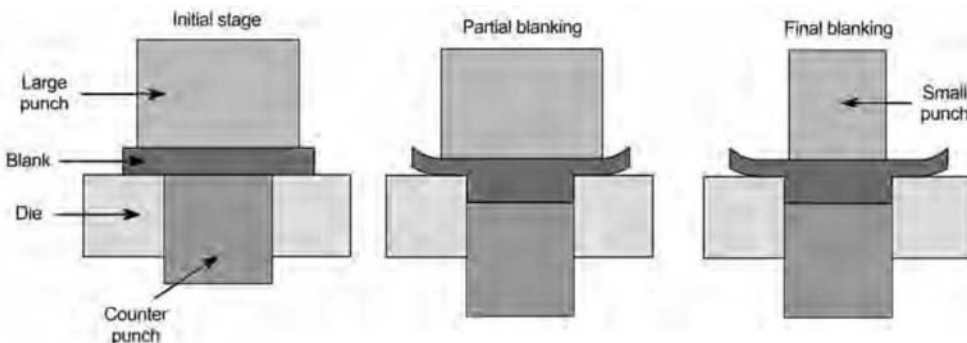


Fig. 11.16 Process sequence in precision blanking. Source: Ref 11.15

programming of the three independent servo-drive systems. Thus, it is possible to adjust the positions (TDC and BDC) as well as the stroke length of each slide corner. In orbital mode, within certain design limits, the speed of the orbital motion and the inclination angle can be controlled.

An excellent application of this novel press is illustrated in forming bearing sleeves. Conventionally, such sleeves are formed starting with a U-bent preform, using a two-step process (Fig. 11.25). The preform is first formed to a round cross section (U-O-bending) and then coined. During U-O-bending, the sharp edges of the U-preform scratch the surface of the upper die and lead to significant die wear. To avoid this die

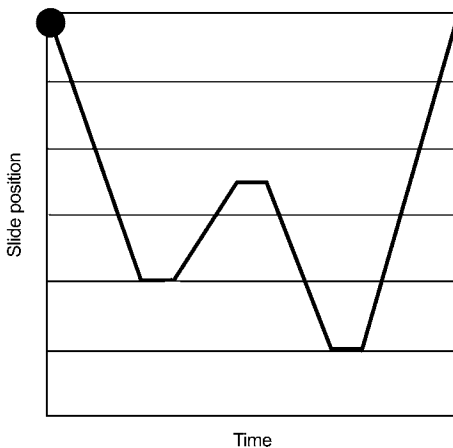


Fig. 11.17 Slide motion used for the process shown in Fig. 11.16. Source: Ref 11.9

wear problem and to improve productivity, a new process that uses the orbital/pendeling capability of the new servo press is suggested (Fig. 11.26). In the new process, preforming and finish forming operations are integrated into a single three-part tooling. A cylindrical bending punch, attached to the bottom die, can be moved vertically by the top die, using a pressure cylinder. Thus, the U-profile is formed first. At its final lower position, the cylindrical punch acts as blank holder for the preform. During the downstroke, the top die comes down with a repetitive pendeling motion to incrementally form the U-shape into the round sleeve. After the round form is reached, the top die comes down vertically to calibrate the round section. This process eliminates any significant relative motion between the sharp edges of the preform and the upper die, reducing die wear.

The 3D servo press has been further developed to conduct highly flexible forming operations. As an example, the flexibility of this press has been demonstrated by applying it to forming of internal geared wheels (Ref 11.19).

Servo-Press Applications for Large Automotive Stampings. Large servo presses have been successfully used by many major OEM car manufacturers to replace traditional mechanical transfer presses. Honda installed a 2500-ton/18-SPM (strokes per minute) Aida press in their Suzuka, Japan, plant in 2009 (Fig. 11.27), and that same year BMW installed 2500-ton/17-SPM Schuler presses in their Leipzig and Regensburg, Germany, plants (Fig. 11.28). Both BMW and Honda have plans to add another

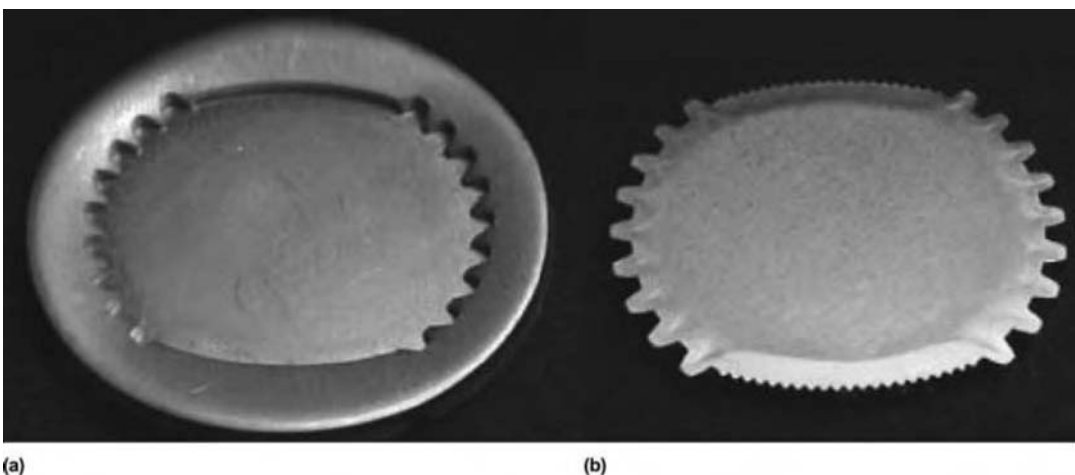
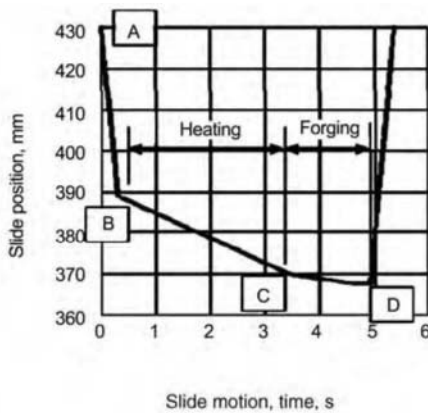


Fig. 11.18 Precision formed part (a) partially blanked and (b) finished blanked. Source: Ref 11.9



(a)



(b)

(c)

Fig. 11.19 (a) Slide motion curve, (b) initial blank, and (c) final Mg part formed in a servo-drive press. Source: Ref 11.9

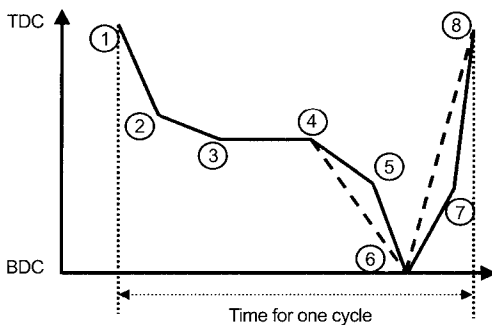


Fig. 11.20 Press slide motion used in warm forming processes. The ram motion followed points 1 through 8. TDC, top dead center; BDC, bottom dead center. Source: Ref 11.16



Fig. 11.21 Warm-formed laptop case from Mg alloy

servo-press line from Schuler and Aida, respectively.

11.4 Cushions/Die Cushions

The servo-motor drive principle has been applied to the design and control of die cushions by several press manufacturers, as well as by servo motor suppliers (Ref 11.5). The schematic of the principle of a servo-die cushion is shown in Fig. 11.29. The position of the die cushion is controlled by the pressure sensor. Thus, the operation of this cushion is similar to that of hydraulic cushions commonly used in mechanical and hydraulic presses. This design can also be incorporated on multiple-point die cushions

where each individual cushion can be controlled separately to optimize metal flow in the flange, between the die and the blank holder.

With the servo motors driving the hydraulic pumps, a precise control of the cushion pressure and motion can be achieved. Combining the cushion control with the constant velocity controls of the servo press, the pressure surge in the die cushions can be eliminated (Ref 11.22). A schematic of the independent servo-controlled cushion is shown in Fig. 11.30.

In addition, the servo die cushion can be used to regenerate energy when the cushion is pushed down by the upper die and slide, as shown in Fig. 11.31. This downward motion of the cushion causes a reversal of the flow of hydraulic fluid and hence the rotation of the hydraulic pump and servo motor. This reversal of servo-motor rotation allows for power regeneration of about 70% (Fig. 11.32).

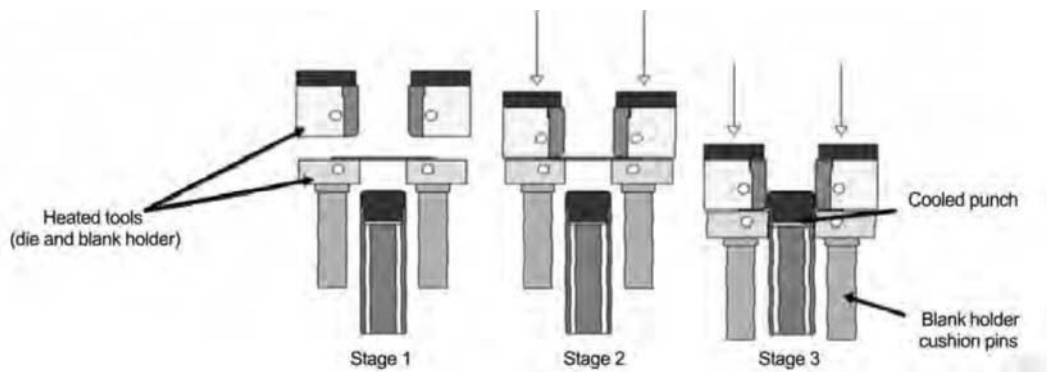


Fig. 11.22 Schematic of tooling and sequence of operations used in warm forming. Source: Ref 11.16



Fig. 11.23 Heated upper (left) and lower (right) tool sets used in the experiments. Source: Ref 11.16

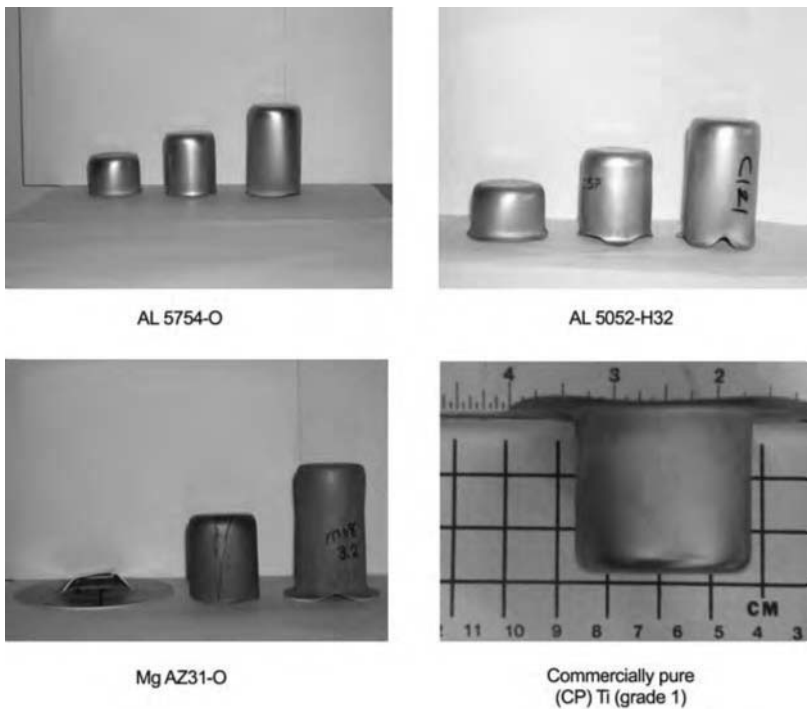


Fig. 11.24 Round cups formed in a servo-drive press with heated tooling. Source: Ref 11.16

11.5 Comparison of Mechanical and Servo Presses

The best way to illustrate the cost-effective application of modern servo-drive presses is to make actual production comparisons. In one specific case, the operation of an 1100-ton conventional crank press has been compared with that of an 1100-ton servo-drive press (Ref 11.12). Figure 11.33 illustrates the reduction of cycle time and the increase in productivity while maintaining the same slide velocity during the deformation process. Figure 11.34 illustrates the cycle time reduction by reducing the stroke length in the servo-drive press while maintaining the same slide velocity profile during deformation. In this case, the press drive is in “pendulum” mode; that is, instead of making a total revolution in one direction, the drive shaft rotates back and forth. By decreasing the tool impact speed while reducing the cycle time, it is also claimed that tool life can be improved (Fig. 11.35).

11.6 New Process Development using Servo-Press Characteristics

The servo-drive press has found a niche and various new applications in stamping technology. Research studies are being conducted to exploit the capabilities of the servo press for various forming applications (Ref 11.24).

Trapped or enclosed die forging and extrusion using different motions of the container have been investigated by Wang, Osakada, and colleagues (Ref 11.25, 11.26). They have also developed precision flashless forging of splines using an axially driven container (Ref 11.27). Cold piercing of Mg alloy billets has been accomplished using counterpressure in a servo-drive press (Ref 11.28).

Cold and warm forming of various advanced high-strength steels (AHSS) is being investigated using servo-drive presses. Tests indicated that in V-bending DP 980 steel, by increasing the reduction in thickness, t_0 ($\Delta t/t_0$) and the dwell time at BDC from 0.1 s to 0.5 s, it is pos-

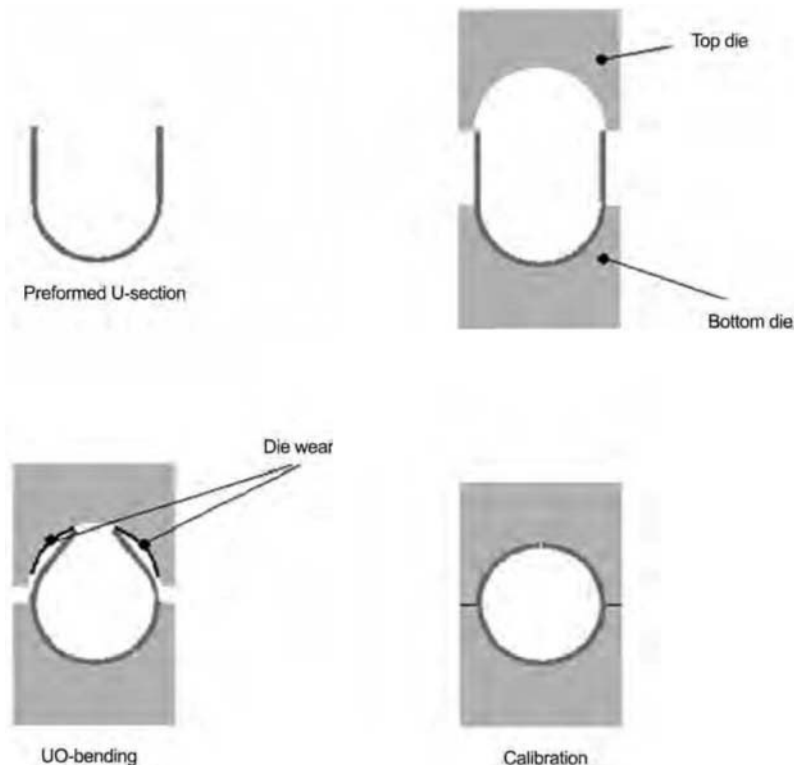


Fig. 11.25 Two-step forming process to produce bearing sleeves with the U-O bending technique. Source: Ref 11.18

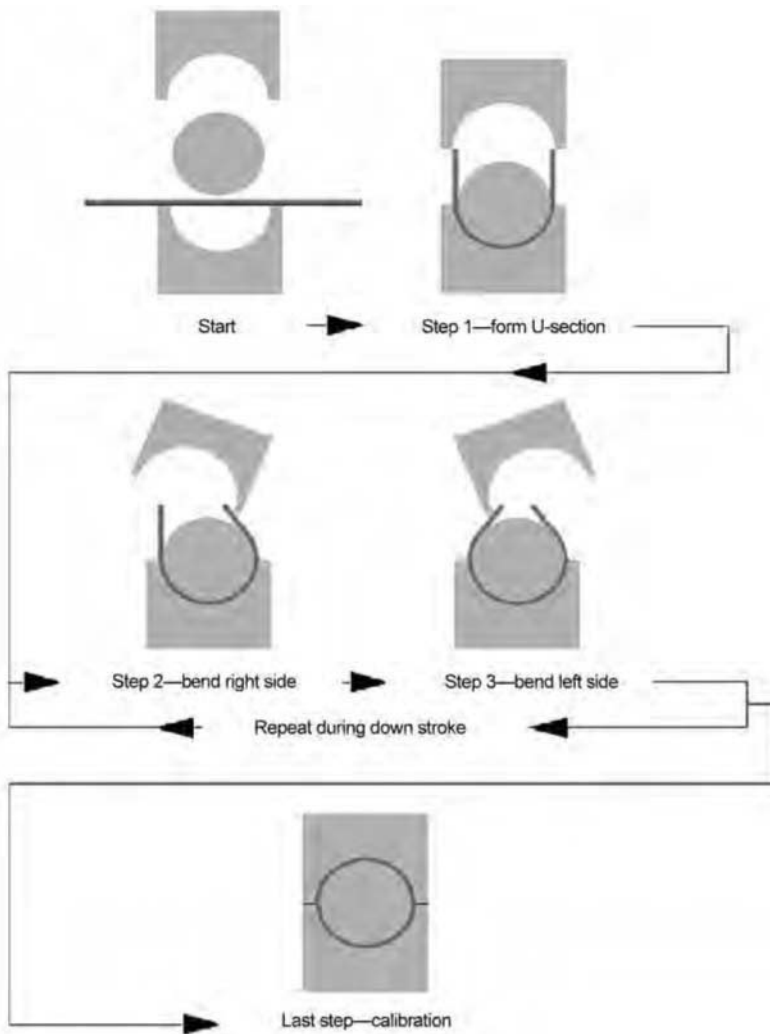


Fig. 11.26 Forming of bearing sleeves using the orbital/pendeling capability of the servo press. Source: Ref 11.18

sible to reduce springback (Ref 11.29). Using a die set equipped with electric-resistance heating located in a servo press that allows a certain amount of slide dwell, it is possible to heat an AHSS such as DP 980 up to 980 °C (1795 °F). Thus, the springback and the bending forces can be drastically reduced. Similarly, resistance heating (up to 1070 °C (1960 °F)) was combined with the servo motion control to hot shear AHSS (DP 980) to obtain sheared surfaces with reduced burr and fracture.

For deep drawing of high-strength steels (JAC270, 440, 590, 780, 980), the formability can be increased by including dwells in the forming stroke with a servo press. The stopping

of the slide at increments in the stroke (or step motion) allows for a relaxation of the stresses in the sheet, and therefore, greater deep draws to be obtained without failure (necking or cracking) (Ref 11.30).

In production settings, using a large servo-press line instead of a conventional transfer-press line to deep draw car body panels **increased the flexibility of the line to accommodate different parts**. The servo-press line allowed for optimization of forming conditions (slide stroke and velocity, and die cushions) and process conditions (part transfer) that were tailored **to the specific part being formed**. The result was better formability (increase of 50 mm (2 in.) in



Fig. 11.27 Aida servo-press line in Honda's plant in Suzuka, Japan. Source: Ref 11.20



Fig. 11.28 Schuler servo-press line in BMW's plant in Leipzig, Germany. Source: Ref 11.21

drawing depth), increased production rate (+40 to 50%), and decreased energy consumption (~32%) compared to the conventional mechanical transfer press line (Ref 11.31).

11.7 Summary

This chapter reviews some of the latest non-proprietary information available on the design and application of electromechanical servo-drive

presses. The uses of high-rpm/low-torque and low-rpm/high-torque servo motors are discussed. Various servo-press designs are reviewed. The applications of these presses and their apparent advantages are summarized.

One of the significant features of the servo-drive press is its ability to incorporate in-die operations that can, in some cases, reduce the number of needed forming steps and potentially allow forming more complex parts in one press. For example, a progressive die application, used

to produce a pen holder as a demonstration part, includes nine stations where several operations are integrated (Ref 11.10):

1. Piercing and bending
2. Bending
3. Coining
4. Hold piercing
5. Blanking of a protrusion
6. Assembly
7. Polymer injection molding
8. Inscribing
9. Quality control

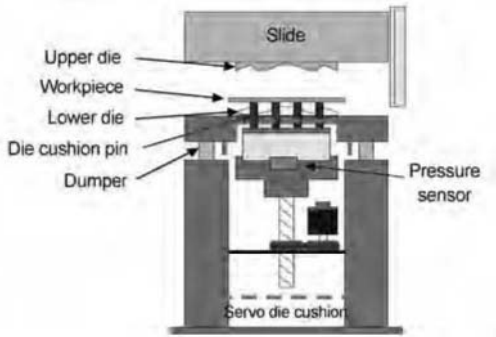


Fig. 11.29 Schematic of a simple point servo-drive die cushion. Source: Ref 11.5

Often in performing secondary operations in the die, expensive cam motions can be eliminated and replaced by electromechanical, hydraulic, or pneumatic servo activators that do not have to be synchronized with the die/slide motion (Ref 11.7). Thus, combining servo-press motion control with a novel die/tool design strategy has great potential for cost-effective application of servo-drive presses in the future, especially for:

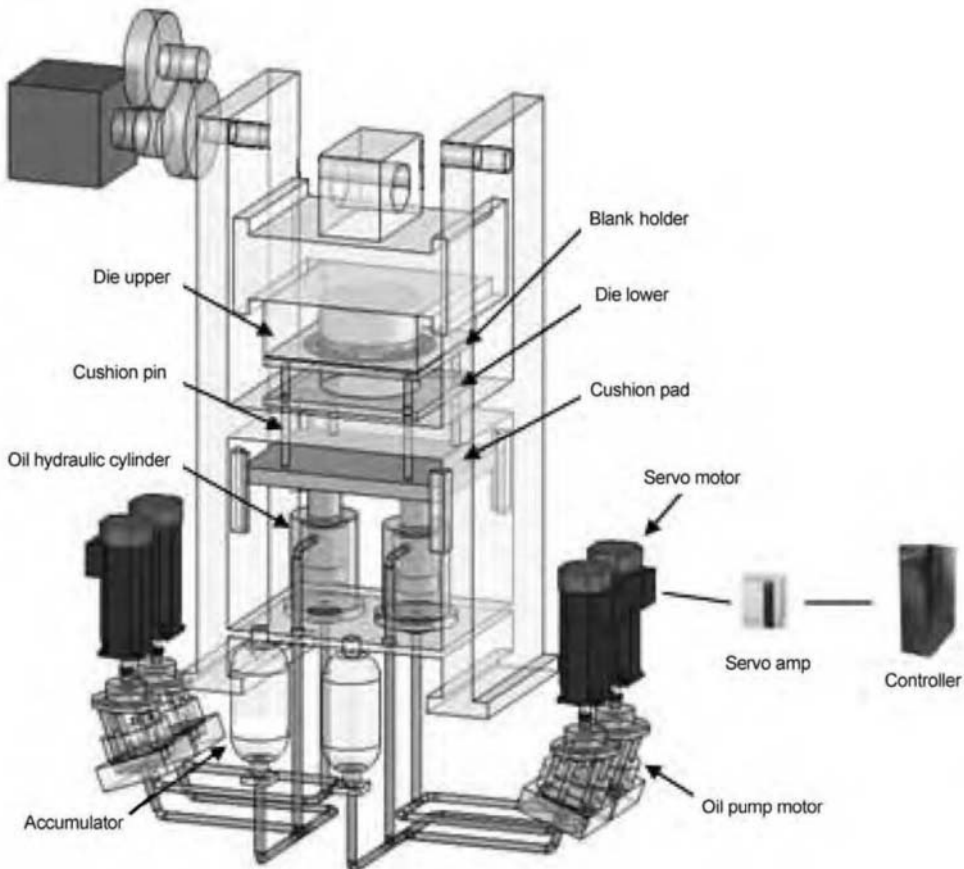


Fig. 11.30 Schematic of independent servo-drive die cushion to eliminate pressure surge. The servo-driven hydraulic die cushion transfers a large portion of the cushion energy into the electrical drive system of the press. Source: Ref 11.23

- Increasing the stroking rate to increase productivity
- Controlling the slide velocity during the forming stage to improve part quality and reduce scrap rates
- Reducing noise and increasing the quality of blanked edges in shearing and blanking
- Reducing tool wear
- Allowing for assembly and other secondary operations in the same press

One issue faced when using new technology, such as a servo press, is how to effectively use the equipment. Therefore, it is necessary to develop a methodology to determine the optimized press parameters to form a given part with high quality. The biggest advantage the

servo press has over mechanical presses is the ability to vary the velocities during forming. The velocity versus stroke curve that best forms the part (with a given shape, material, and thickness) must be determined and applied to produce quality parts with limited scrap. Studies are in progress to develop this methodology for **deep drawing through a combination of finite element analysis simulations and experiments.**

REFERENCES

- 11.1 Amino Corp., Servo Press Pages, <http://www.amino.co.jp>
- 11.2 J. Landowski, Sizing Up Servo Presses, *Stamping Journal*, April 2004, p 12–14
- 11.3 T. Nakagawa, “Servo Motor Drive Press and Market Trends in Japan,” presented at the 56th General Assembly of CIRP, Kobe, Japan, 2006
- 11.4 K. Osakada, K. Mori, T. Altan, and P. Groche, Mechanical Servo Press Technology for Metal Forming, *Annals of CIRP*, Vol 60 (No. 2), 2011, p 1
- 11.5 GE/Fanuc, “CNC Functions for Servo Press Applications,” slide presentation, 2001
- 11.6 D. Boerger, Servo Technology Meets Mechanical Presses, *Stamping Journal*, November/December 2003, p 32

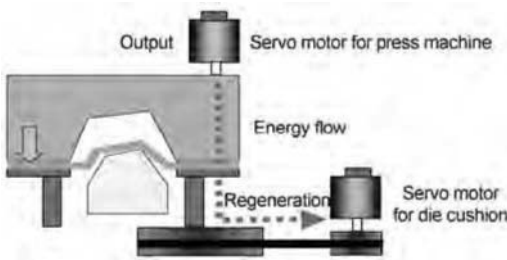


Fig. 11.31 Possible use of servo die cushion for multiple point control of blank holder force and for energy regeneration. Source: Ref 11.5

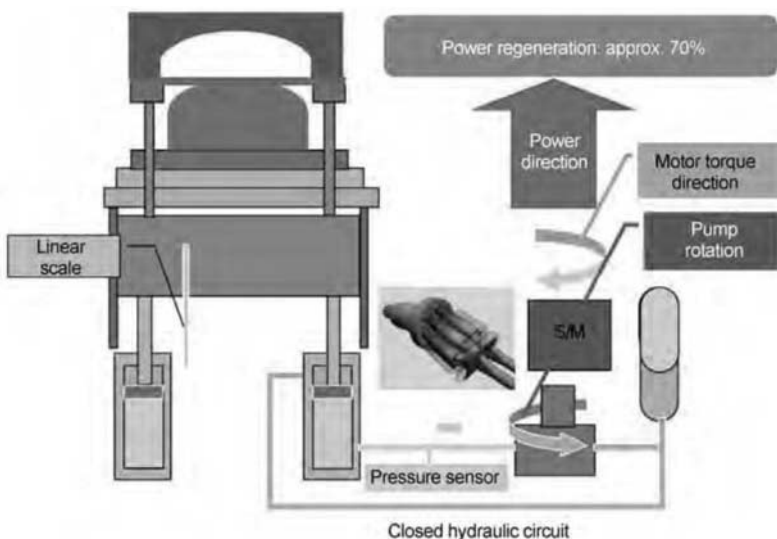


Fig. 11.32 Schematic of servo die cushion for energy regeneration. Source: Ref 11.23

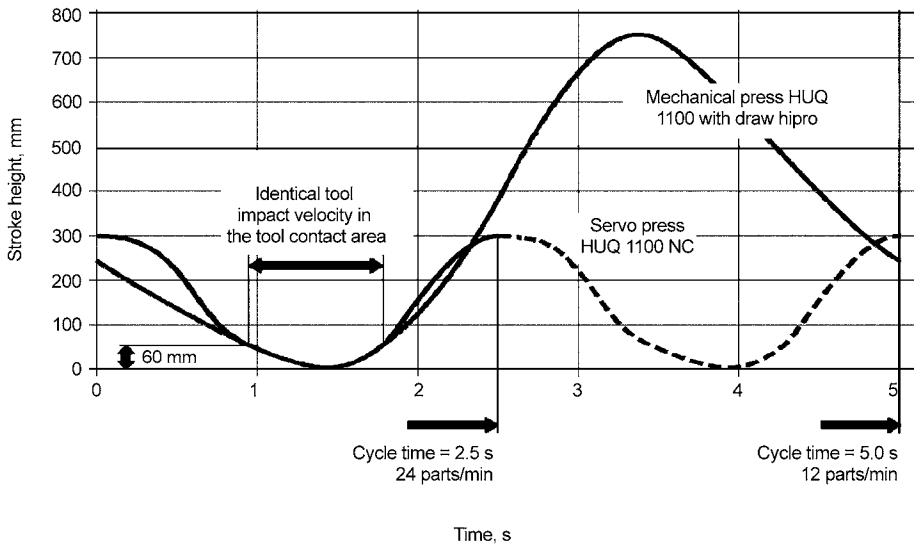


Fig. 11.33 Comparison between the slide motions of 1100-ton mechanical and servo-drive presses for identical slide velocity during forming. Source: Ref 11.12

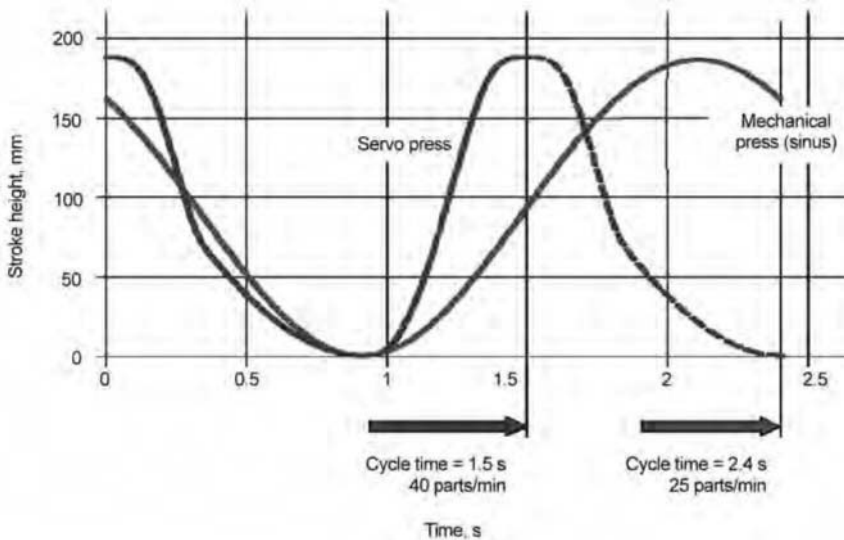


Fig. 11.34 Decrease in cycle time by reducing the stroke length and operating the servo press in “pendular” mode (progressive die stamping, 200% increase in output). Source: Ref 11.12

- | | |
|---|--|
| <p>11.7 J. Osborn and P. Stephan, Servo Press Technology—Drive Design and Performance, <i>Metallforming</i>, August 2008, p 18</p> <p>11.8 J. Roske, Raising Efficiency with Servo-Drive Presses, <i>Proceedings of the 4th Precision Forging Workshop, June 11–12, 2008, Schuler-America</i></p> | <p>11.9 K. Miyoshi, Current Trends in Free Motion Presses, <i>Proceedings of the 3rd Japan Society for Technology of Plasticity (JSTP), Int. Seminar on Precision Forming, March 2004</i></p> <p>11.10 J. Huelshorst, Merging Manufacturing Processes (MMP) (in German), <i>Proceedings of the 19th Forming Technol-</i></p> |
|---|--|

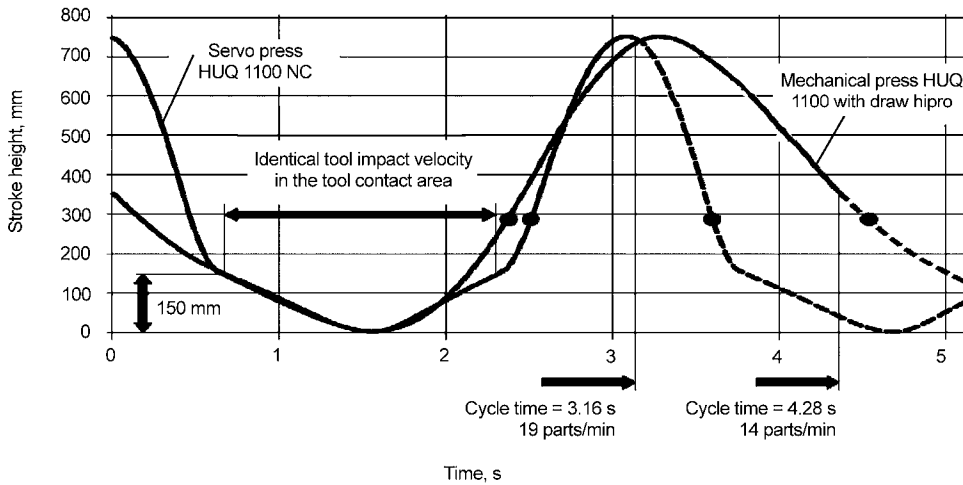


Fig. 11.35 Decrease in cycle time and impact speed using a servo press (150% increase in output). Source: Ref 11.12

- ogy Conference, 2008, Hanover, Germany, p 161
- 11.11 H. Peper, Schuler-Weingarten, A.G., personal communication, 2006
 - 11.12 T. Blum, "Servo-Drive Presses for the Next Generation Press Shop," Schuler-Weingarte, A.G. presentation, 2008
 - 11.13 M. Otsu, C. Yamagata, and K. Osakada, Reduction of Blanking Noise by Controlling Press Motion, *CIRP Annals*, Vol 52 (No. 1), 2003, p 245
 - 11.14 K. Junlopen, et al., Burr-Free Shearing using NC Servo Press Machine, *Proceedings of ICTP 2008, Korea*, p 267
 - 11.15 S. Kaya and T. Altan, Blanking Developments—Part II: Fine Blanking Process and Tool Design, *Stamping Journal*, August 2007, p 14
 - 11.16 S. Kaya, G. Spampinato, and T. Altan, An Experimental Study on Non-isothermal Deep Drawing Process using Aluminum and Magnesium Alloys, *ASME Transactions*, Vol 130, 2008
 - 11.17 Aida Engineering Ltd., Japan, personal communication, 2007
 - 11.18 P. Groche and M. Scheitza, Servo Press with a Slide of Three Axis of Motion (in German), *Werkstattstechnik*, Vol 97, 2007, p 760
 - 11.19 P. Groche, M. Scheitza, M. Kraft, and S. Schmitt, Increased Total Flexibility by 3D Servo Presses, *CIRP Annals*, Vol 59, 2010, p 267
 - 11.20 Honda Engineering USA, personal communication, 2010
 - 11.21 Schuler-Weingarten, A.G., personal communication, 2010
 - 11.22 Aida 2010, Japan, private communication
 - 11.23 K. Rothenhagen, "Servo Press Technology—Innovation, Strategy and Efficiency—New Developments in Japan and Europe," presented at IFU International Conference, Fellbach, Germany, May 2010
 - 11.24 T. Altan, S. Kaya, and J. Yadav, Servo Press Forming Applications, Parts I, II and III, *Stamping Journal*, March 2007, p ; April 2007, p ; and May 2007
 - 11.25 X. Wang, K. Osakada, and S. Hanami, Net Shape Forging Process with Axially Driven Container, *Proceedings of the 5th ICTP, Columbus, OH, 1996*, p 429
 - 11.26 K. Osakada et al., Precision Extrusion Methods with Double Axis Servo Press using Counter Pressure, *Annals of CIRP*, 2005, p 245
 - 11.27 K. Osakada, S. Wang, and S. Hanami, Precision Forging of Spline by Flashless Die Forging with Axially Driven Die, *Annals of CIRP*, 1997, p 209
 - 11.28 K. Matsumoto and K. Osakada, Precision Warm Forging of Mg Alloy 2006 with Consideration of Material Property, *Wear*, November 2006, p 20

- 11.29 K. Mori, "Application of CNC Servo Presses," slide presentation, 2008
- 11.30 H. Yamashita, H. Nakai, E. Onose, T. Higaki, and M. Sayama, "Research in Deep-Draw Forming of High-Strength Steel Sheet using a NC Servo Press Machine," presented at the International Deep Drawing Research Group, Austria, 2010
- 11.31 H. Taoka, H. Meguri, M. Azuma, H. Ikehara, M. Hashimoto, and Y. Kono, Development of the World's Fastest Servo Press Line for Manufacturing Automotive Body Panels, *Sokeizai*, Vol 50 (No. 12), 2009, www.aida-global.com/pdf/news/Honda-Deep-Draw-Servo-Press-Line.pdf

CHAPTER 12

Hydraulic Presses

Eren Billur, The Ohio State University

HYDRAULIC PRESSES generate the forming force and necessary ram motion by hydraulic cylinders. The **pressurized fluid medium drives** the piston in the cylinder, and the motion is controlled using a set of valves. A typical hydraulic circuit consists of a reservoir (tank), electric motor, pump, valves, and cylinder (Fig. 12.1). Hydraulic presses are more versatile than mechanical presses, because the force and stroke can be controlled easily. These presses are load-restricted machines; that is, their capability for carrying out a forming operation is limited mainly by the maximum available load. Hydraulic presses are used by almost every industry involved in manufacturing, because they are built in many different sizes (e.g., available load may

be from < 0.9 metric ton (< 1 ton) up to 59,000 metric tons, or 65,000 tons) with many variations and complexities (Ref 12.1, 12.2, 12.3).

The main advantages of hydraulic presses over mechanical presses include (Ref 12.3, 12.4, 12.5):

- The rated force is available throughout the stroke (may not apply to accumulator-driven presses), which makes the hydraulic presses ideal for deep drawing operations.
- **Extremely flexible slide motion allows optimizing** and automating sheet metal forming processes.
- The maximum allowable press force can be easily set to protect tooling.

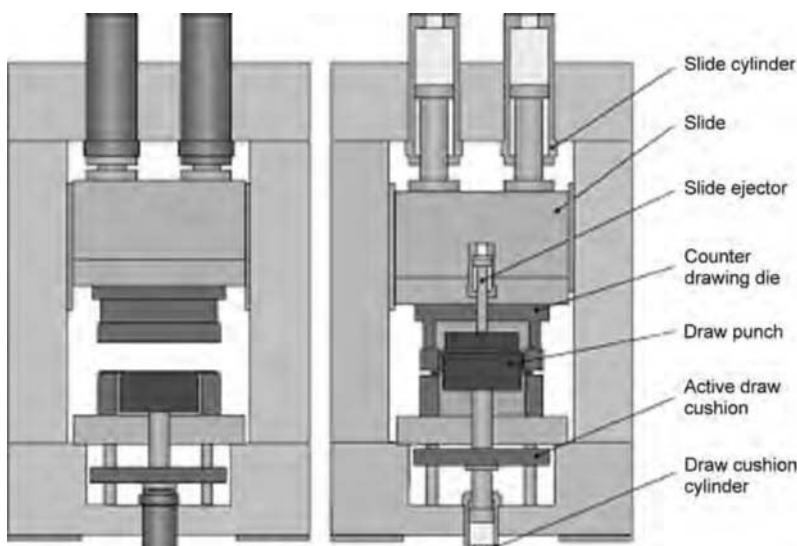


Fig. 12.1 Schematic of a hydraulic press with a draw cushion and die set, with major components labeled. Source: Ref 12.1

The disadvantages of hydraulic presses include:

- In general, lower operating speed than mechanical presses, which leads to lower production rates (parts/strokes per minute)
- Higher energy consumption
- Possible problems of leakage

12.1 Components of Hydraulic Presses

The drive system of a hydraulic press consists of a hydraulic cylinder(s) that is actuated by the hydraulic circuit. Drive systems in hydraulic presses are further discussed in the section “Drive Systems” in this chapter; first, the components in a hydraulic press are described.

Hydraulic Fluid/Pressure Medium. Hydraulic fluid is used to transfer the energy from the pump to the cylinder. In principle, any fluid can be used for this function. Early hydraulic presses had water as the pressure medium, which has several advantages, such as general availability, low cost, no risk of fire, and no messy residue in case of leakage. Despite these advantages, water has been replaced by oil and water/oil emulsions in hydraulic presses (Table

12.1), mainly because the emulsions have higher corrosion resistance and better lubricity compared with water (Ref 12.5, 12.7, 12.8).

As shown in Table 12.1, 85% of hydraulic applications employ oil as pressure medium, 10% water/oil emulsions, and the remaining 5% other synthetic fluids. In water/oil emulsions, the percentage of water content affects the lubricity and corrosion protection. As the water percentage increases (i.e., oil-in-water emulsion), the characteristics are close to water, and vice versa (Ref 12.6, 12.9).

Selection of hydraulic fluid in a press affects the stroke-time and stiffness characteristics of a press, as detailed in later sections. It is also important to note that hydraulic components such as pump and valve(s) may require certain viscosity levels for efficient operation. Seals have to be chemically compatible with the fluid used. Small to medium presses usually are run on oil, and large presses with accumulator drives commonly use water-oil emulsions (Ref 12.4, 12.8, 12.10).

Reservoir. Hydraulic fluid is stored in a reservoir (also called a tank). The reservoir should be large enough to contain the fluid used in the press. It has several openings to allow flow of hydraulic fluid and air (Fig. 12.2a):

Table 12.1 Properties of hydraulic fluids

Property	Water	Oil	Water/oil emulsions
Lubrication and wear protection	...	•	○
Corrosion/rust protection	...	•	○
Low cost	•	...	○
Kinematic viscosity at 50 °C, mm ² /s	0.55	15–70	1–70
Low compressibility (bulk modulus, κ : higher is better)	○ $\kappa \approx 2.4$ GPa ≈ 348 ksi	... $\kappa \approx 1.0 \dots 1.6$ GPa $\approx 145 \dots 232$ ksi	• $\kappa \approx 2.5 \dots 3.5$ GPa $\approx 363 \dots 508$ ksi
No flammability	•
No environmental impact	•
Usage in hydraulic applications, %	~0	85	10

Legend: •, best; ○, in-between; ..., N/A or worst. Source: Ref 12.1, 12.5, 12.6

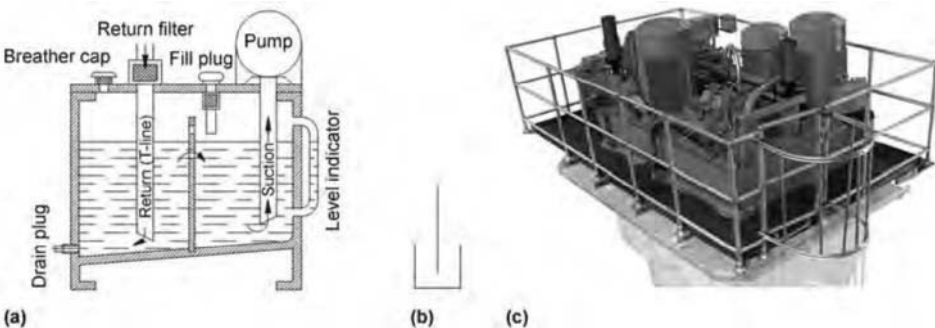


Fig. 12.2 (a) Schematic of a reservoir with attachments. Source: Ref 12.5. (b) International Organization for Standardization symbol for reservoir. Source: Ref 12.11. (c) Reservoir mounted on a press crown. Source: Ref 12.12

- Intake (suction) line, feeding the pump and therefore the circuits of hydraulic press
- Return line, which brings the used oil back
- Breather cap, which allows ventilation so that negative pressure is prevented when hydraulic fluid is pumped out
- Fill plug, to replace or add hydraulic fluid, which also houses a filter
- Drain plug, to remove deposited impurities and condensed water or remove hydraulic fluid when it has to be changed
- Level indicator

The reservoir may be divided into two sections by a plate. Return (tank) and suction lines are located in separate sections. Fluid from the return line calms at the first section (oil return chamber), where air bubbles are separated and impurities are deposited. The fluid can pass through the holes to the second section (suction chamber) and be pumped back into the system. The bottom of the reservoir is designed such that the lowest point is in the first section, and a drain plug is placed to remove impurities and condensed water near the lowest point of the reservoir (Ref 12.5, 12.13).

Depending on the press design, the reservoir may be (Ref 12.2, 12.5, 12.12):

- Mounted on the press crown to take advantage of gravity during prefill (Fig. 12.2c)

- Built in the press frame, which is common in gap-frame presses
- A unit separate from the frame (e.g., see Fig. 12.18b later in this chapter)

Hydraulic Cylinder. The hydraulic cylinder is the main component of a hydraulic press that generates force(s) and motion(s) required by the forming process. Hydraulic cylinders are used to drive the main slide, as well as additional slides in multiple-action presses, die cushions, ejectors (Fig. 12.1), and other auxiliary units, if present. Depending on the force/velocity requirements and cost considerations, several types of cylinders are used. In hydraulic presses, common cylinder types are plunger (single-acting) cylinders, differential (double-acting) cylinders, and tandem cylinders, as shown in Fig. 12.3.

Single-acting cylinders can generate force and motion in only one direction (Fig. 12.3a). They are less expensive, because there is no piston, which eliminates the need of manufacturing a piston and good surface finish in inner walls of cylinder. However, single-acting cylinders require a method of returning. If the cylinder is extending upward, such as in a die cushion or in a pushup press, gravity may retract the rod. In small shop presses, spring-return cylinders are employed (Fig. 12.3b). It is also common that a single-acting cylinder may be used parallel with other cylinders (single or double

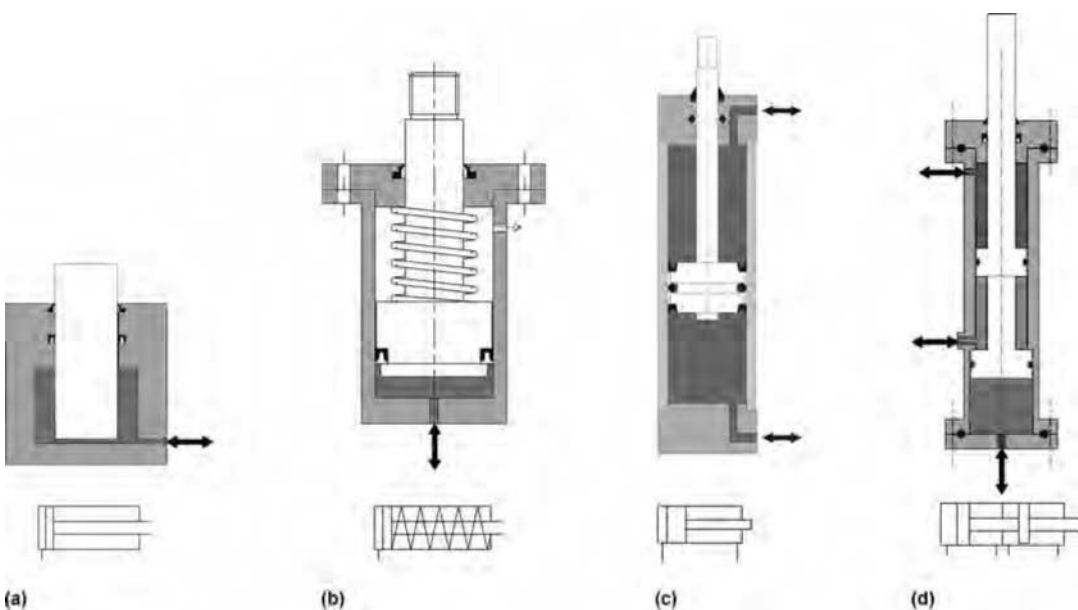


Fig. 12.3 Hydraulic cylinders used in presses and corresponding International Organization for Standardization symbols: (a) single-acting cylinder, (b) spring-return cylinder, (c) differential cylinder, and (d) tandem cylinder. Source: Ref 12.5, 12.11, 12.13, 12.14

acting) that may retract the rod when required (Ref 12.1, 12.2).

Double-acting cylinders can generate motion and force, both when extending and when retracting. In hydraulic presses, differential cylinders (Fig. 12.3c) are common. They are named *differential* because the functional (pressurized) area of the piston is not equal when the rod is extending and retracting. As a result, the rod can generate more force when extending but moves slower than when it is retracting (see Eq 12.1 and 12.2). In some applications tandem cylinders (Fig. 12.3d) may be used to generate more force while keeping the cylinder outer diameter smaller, or, with different piston sizes, a tandem cylinder can be used to create a rapid approach with low-load capacity and high-load working stroke with low speed (Ref 12.5, 12.13).

The force, F (in N or lb), generated by a hydraulic cylinder can be calculated by knowing the piston area, A (in mm^2 , or in^2), and hydraulic pressure, p (in MPa, or psi):

$$F = pA \quad \text{Eq 12.1}$$

Velocity, V (in mm/s or in./s), of the rod can be calculated by the piston area, A , and volumetric flow rate of hydraulic fluid, \dot{Q} (in mm^3/s or in^3/s):

$$V = \dot{Q} / A \quad \text{Eq 12.2}$$

Hydraulic Pumps. Hydraulic pumps transform mechanical energy (from electric motors) to hydraulic energy. In hydraulic presses, gear type and axial piston pumps are common. Gear type pumps have constant displacement per rev-

olution (commonly in cc/rev or in^3/rev). They can be either external gear type (Fig. 12.4a), where two external spur gears are used, or internal gear type, where one external gear is mated with an internal gear. The second generic type of pumps used in hydraulic presses is the axial piston type pump. These also can be in two types: bent axis type (Fig. 12.4c) or swashplate type. Axial piston pumps may be *variable displacement* per revolution, if the angle of bent axis (α in Fig. 12.4c) or angle of the swashplate can be varied (Ref 12.3, 12.5).

Hydraulic Lines. In a hydraulic press, flexible hoses or hard pipes can be used to transfer the hydraulic fluid. These are also called hydraulic lines. There are five main types of hydraulic lines in a press:

- **Suction line:** the line between the reservoir and the inlet of the pump (see Fig. 12.2a). Usually a filter is located in this line, so that only filtered oil is pumped into the system.
- **Pressure line (P):** the line between the control valve's P-port and pump outlet. This line has the highest pressure, because it is the one just after the pump.
- **Work lines (A, B, etc.):** lines connected to the cylinder's different ports. If A is retracting the cylinder, then B could be extending it.
- **Return (tank) line (T):** the line carrying the fluid back to the tank (reservoir). When a double-acting cylinder is retracting, for example, the oil in the second chamber should be flowing to the tank, through the T-line.
- **Leakage line (L):** the line that returns the leaked oil from valves, pumps, and/or other hydraulic attachments to the tank. This line carries much less flow than the T-line.

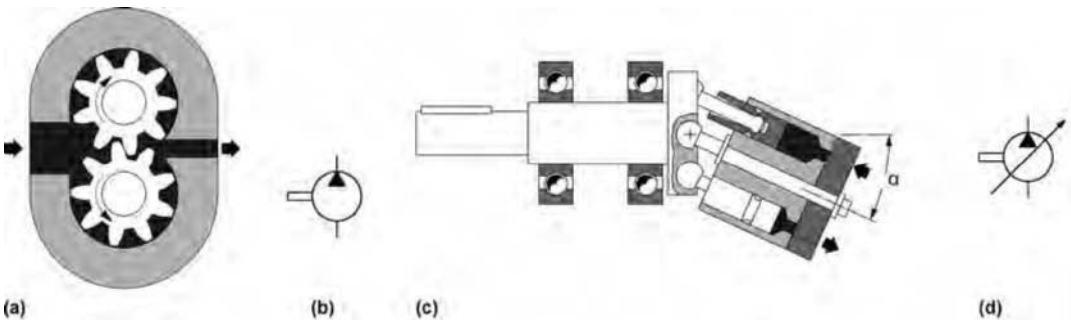


Fig. 12.4 Hydraulic pumps commonly used in presses: (a) external gear pump, (b) International Organization for Standardization symbol for constant-displacement pump, (c) bent axis axial piston pump, and (d) International Organization for Standardization symbol for variable-displacement pumps. Source: Ref 12.5

Hydraulic Valves. Valves are used to control and regulate (a) the direction of the flow (i.e., to move the slide of a press upward or downward), (b) the pressure (i.e., force generated by the slide), and/or (c) the flow rate and consequently flow velocity (i.e., velocity of the slide) (Ref 12.15).

One of the simplest hydraulic valves, employed to ensure that the fluid is flowing only along one direction, is called “check valve” (also known as a *nonreturn valve*). In a typical check valve, a metal ball is seated on a tapered channel (Fig. 12.5b) and is pushed by a compressed spring. When the fluid flows in the free-

flow direction, the fluid pushes the spring and opens the gap and therefore can flow. However, when the fluid is flowing in the *incorrect* direction, the spring will push the ball and block the fluid flow (Ref 12.13, 12.15).

Directional control valves (DCVs) are used to control the fluid flow to the actuator. In a hydraulic press, DCVs are used to control the direction of motion of slides, cushion pins, ejectors, and other auxiliary units. DCVs are named by the number of ports (lines for inlet/outlet, e.g., A, B, T, and P) and number of positions the spool can move. Fig. 12.6 shows a four-port DCV, where the leakage line (L) is not counted

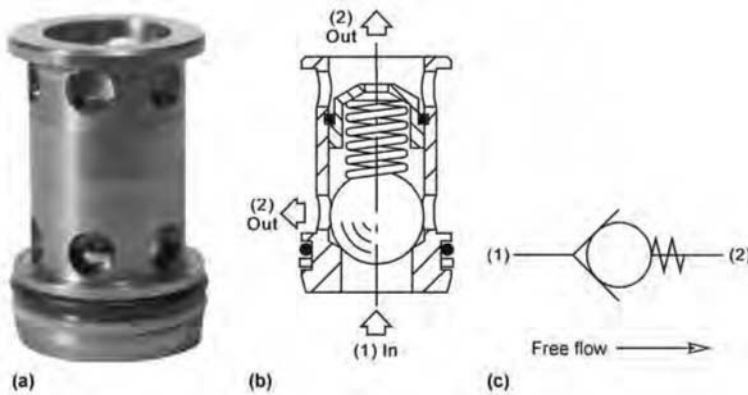


Fig. 12.5 Inline check valve: (a) photo, (b) schematic, and (c) International Organization for Standardization symbol. Source: Ref 12.16

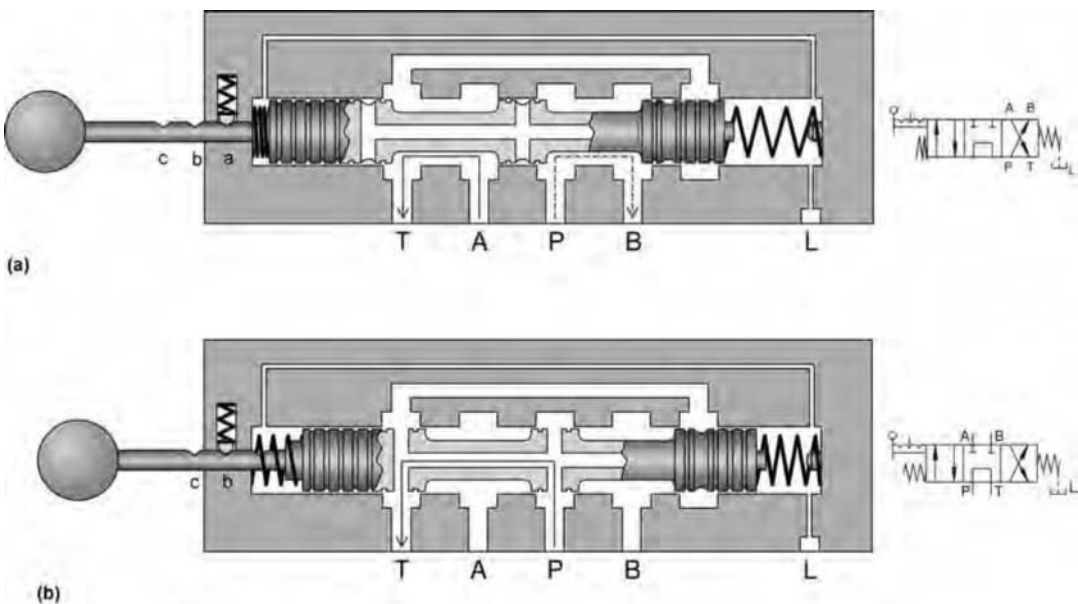


Fig. 12.6 Operating of a 4/3 directional control valve: (a) pressurized fluid flowing to port B, and (b) pressurized fluid directed back to the reservoir. Source: Ref 12.13

as a port. This DCV has three positions, a, b, and c. This particular DCV is called a 4/3 valve. In position a, pressurized fluid is flowing to port B (Fig. 12.6a), and in position c (not shown), it is flowing to port A. This may be extending and retracting of a cylinder. In position b, the pressurized fluid is directed back to the reservoir (Fig. 12.6b) while the cylinder is at a standstill (Ref 12.13, 12.15).

The maximum force in a hydraulic press can be easily set and controlled. This is done by pressure valves. There are two main classes of pressure valves: pressure relief valves and pressure regulators. A pressure relief valve senses the incoming pressure (inlet, P-line), whereas a pressure regulator senses the output pressure (outlet, A-line). In the pressure relief valve, an adjustable compression spring presses a sealing element to its seat. When the force is generated by the pressure in the P-line ($F = p_1 A_1$), the valve opens and flow is directed to the tank. However, resistance in the return line (tank line, T) may act on surface A_2 (an additional $F = p_2 A_2$), which must be considered. In the pressure regulator, Fig. 12.7b, a similar principle is employed with an adjustable compression spring. However, a piston is used where the outlet line (A-line) is acting on one side of the piston, Fig. 12.7b(i). When the outlet pressure is higher than the adjusted level, the valve moves

and closes the throttle gap (Fig. 12.7b(ii)), thus reducing the outlet pressure (Ref 12.13).

The last set of valves are flow control valves. As the name suggests, these are used to regulate (reduce) the flow rate within a line. As explained in the section “Hydraulic Cylinder” above, the flow rate (Q) is directly proportional to the velocity of the cylinders. The flow rate can be controlled by flow control valves or flow-regulating valves. Flow control valves can be of a restrictor or of an orifice type in order to create a resistance to the flow. Flow-regulating valves, on the other hand, can be adjustable, similar to the faucets in a kitchen sink (Ref 12.13, 12.15).

All of the valves explained here are actuated manually, mechanically, or by other means. For example, a check valve is actuated by pressure in one direction and by the mechanical spring in the other. In modern presses, most of the control is done by solenoid or servo valves, which are controlled through the programmable logic controllers. It is also common to see mechanical actuation, such as hand levers, in small presses (Ref 12.1, 12.17).

Servo-actuated valves have a feedback loop and a controller that drives a torque motor to actuate the valve. These allow a very accurate control of the spool. A DCV (e.g., Fig. 12.6) can be servo actuated, where the spool can be moved incrementally and act as a restrictor for

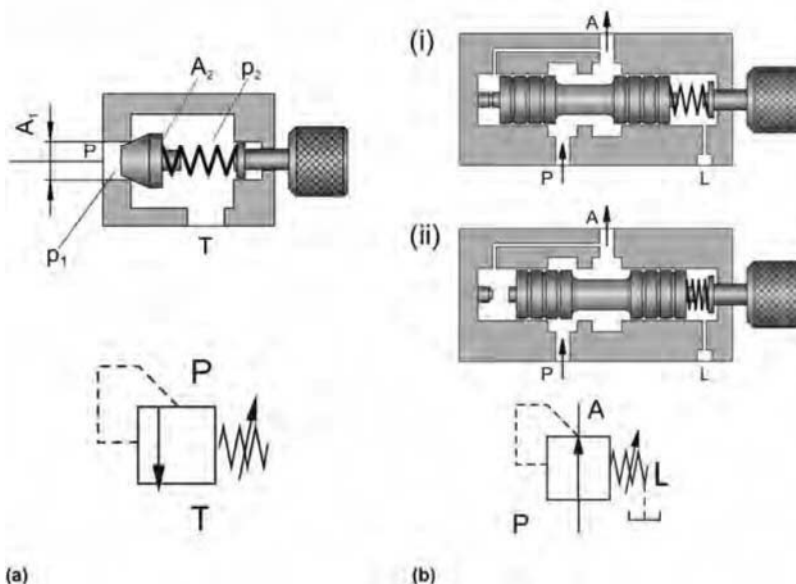


Fig. 12.7 (a) Pressure relief valve and (b) two-way pressure regulator. Source: Ref 12.13

A and/or B lines. Such valves are called *proportional directional valves* or sometimes abbreviated as *servo valves* (Ref 12.18). Table 12.2 lists the different types of valve actuation and their International Organization for Standardization (ISO) symbols.

Intensifier. A hydraulic intensifier is used when very high pressure is required that cannot be supplied by the pumps. The device consists of two pistons that have different areas (Fig. 12.8), which may be in the order of 1:2 to 1:20. Hydraulic fluid from the tank is first filled in the small piston chamber (the high-pressure chamber) and then pumped in to the large piston chamber (low pressure). The low pressure moves the piston assembly and, because of the surface ratio, compresses the oil in the high-pressure chamber (Ref 12.16, 12.19).

Intensifiers are commonly used in hydro-forming presses to increase the pressure of forming fluid, and in very small hydraulic presses operated by air pressure.

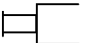
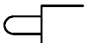

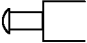


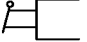
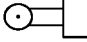
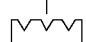
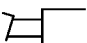


Accumulator. Hydraulic pumps can deliver a certain volume flow (\dot{Q}) depending on their design and rpm of the motor. However, it is

common (especially for large hydraulic presses) that a press may require high flow rates for short time periods. In this case, to conserve energy, a smaller pump is installed with an accumulator. When the press is idle, the pump fills the accumulator, and when high flow rate is required, the fluid is provided by the accumulator (Ref 12.5).

The main task of an accumulator is to keep a volume of hydraulic fluid under pressure and to release it to the circuit when necessary. To keep the liquid under pressure, often pressurized gas is used. This might be done by a bladder separating the gas and liquid media (Fig. 12.9a, b), a diaphragm (Fig. 12.9c), or a rodless piston where one end is subject to gas pressure and the other one to the hydraulic fluid (Fig. 12.9d) (Ref 12.5, 12.15).

Accumulators may also be used to keep the pressure in the cylinder for a long time. When clamping a workpiece (i.e., in hydroforming applications or during quenching in hot stamping processes), the pump is not required to generate pressure. Possible leakages can be compensated by the accumulator (Ref 12.5).

Table 12.2 ISO symbols for actuation of valves

Manual		Mechanical		Others	
	Manual, general		Stem/key		Pressure
	Pushbutton		Spring		Solenoid
	Lever		Roller		Detent
	Pedal		Roller, idle return		Servo

Source: Ref 12.11, 12.18

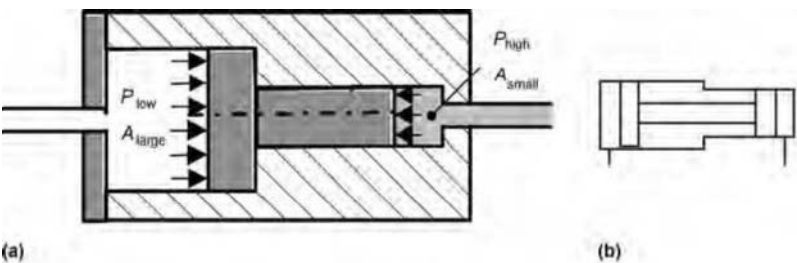


Fig. 12.8 Hydraulic intensifier. (a) Schematic. Source: Ref 12.3. (b) International Organization for Standardization symbol. Source: Ref 12.13

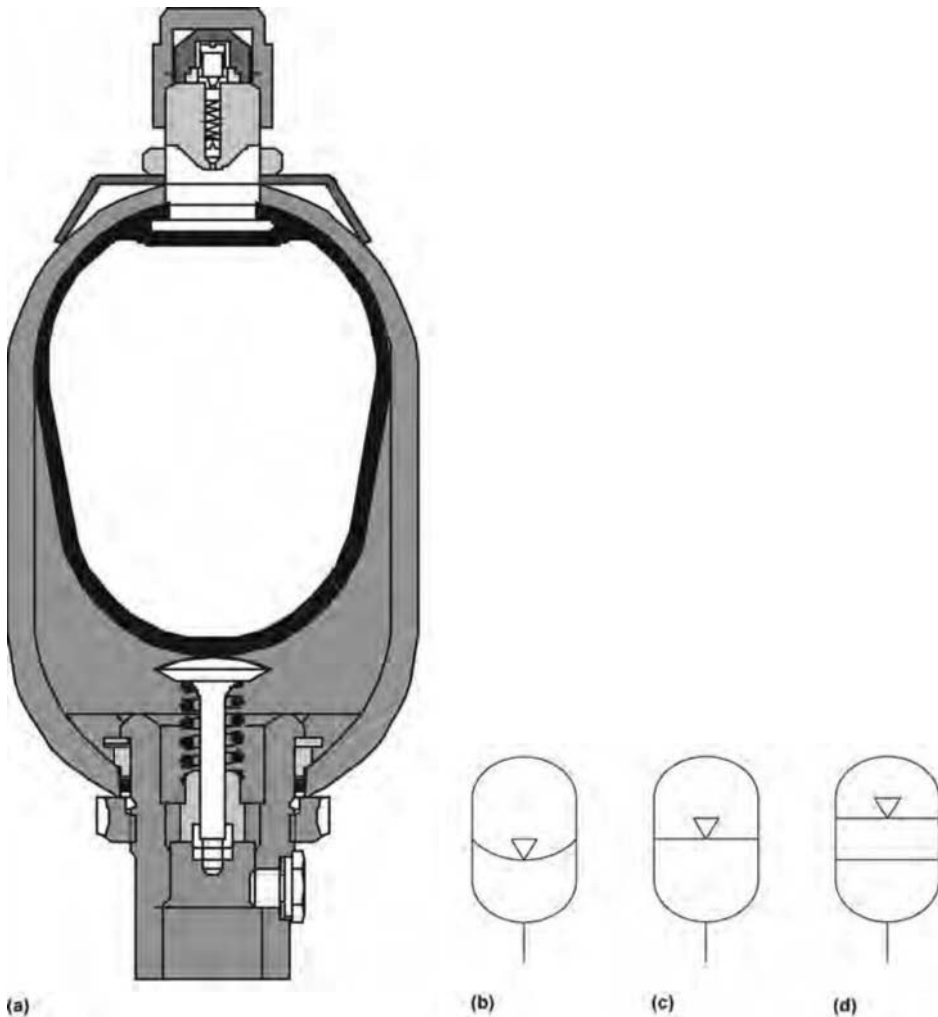


Fig. 12.9 (a) Schematic view of a bladder-type accumulator. Source: Ref 12.5. (b)-(d) International Organization for Standardization symbols for accumulators: (b) bladder type, (c) diaphragm type, and (d) piston type. Source: Ref 12.20

12.2 Drive Systems

As the forming/blanking process is performed, force builds up and increases the pressure in the cylinder (as $F = pA$). The hydraulic drive should be designed such that, under this pressure, the pump or accumulator should still be able to maintain the required volume flow. To achieve these goals, several drive systems have been designed for hydraulic presses. As the technology of pumps, valves, motors, and control systems evolves, new designs that are more energy efficient are becoming available.

In a hydraulic press, the forming cycle can generally be divided into three portions:

- High-speed approach (closure), with almost no force
- Forming, where the forces are highest but speeds can be modest
- Return, where the slide has to return to the uppermost point as fast as possible

It may be also possible that a dwell can be required order to (a) heat the workpiece before a warm forming process, (b) quench the part after a hot stamping process, (c) do secondary operations such as tapping, and so on, or (d) reduce springback.

High-speed approach and return portions do not require high forces but have to be completed

in short time periods in order to increase the total output (i.e., parts per minute). During these periods, the flow rate may exceed the supply by the pump. In this case, a prefill valve may be used. This is a large valve that connects the cylinder directly to the reservoir. Prefill can be done either by gravity (if the reservoir is attached to the crown of the press) or by using a small cylinder and pump to move the slide and create vacuum in the large cylinder to achieve prefill (Ref 12.2).

Direct Drive. Direct drive (also known as pump drive) in a hydraulic press refers to a hydraulic circuit where the high-pressure fluid is supplied only by pump(s) (Fig. 12.10). The pump(s) deliver a certain flow rate (\dot{Q}) to the system, and as external forces resist to the mo-

tion of the cylinder, pressure is built up. Direct drives are designed for the highest load and flow rate; therefore, the nominal load is always available. However, this also causes the pump(s) and motor(s) to be selected for the highest power requirement (Ref 12.1, 12.8).

Direct-driven hydraulic presses can be more energy efficient than accumulator-driven presses because the pump supplies only the required amount of pressure. Several versions of direct drives are available for hydraulic presses. The selection of the drive system is a trade-off between the initial investment and energy efficiency (Ref 12.1, 12.8, 12.22):

- *Constant-rpm electric motor and constant-displacement pump*, where the pump deliv-

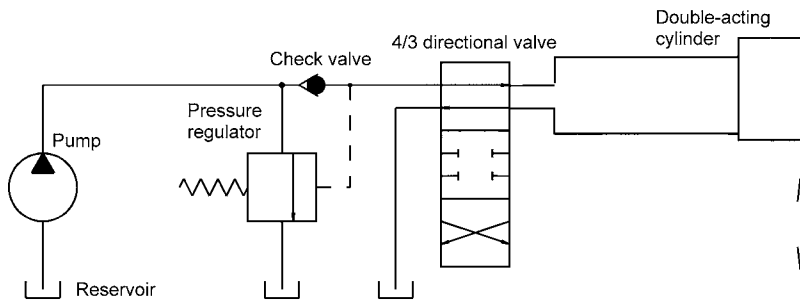


Fig. 12.10 Direct-drive circuit for a hydraulic press. Source: Ref 12.21

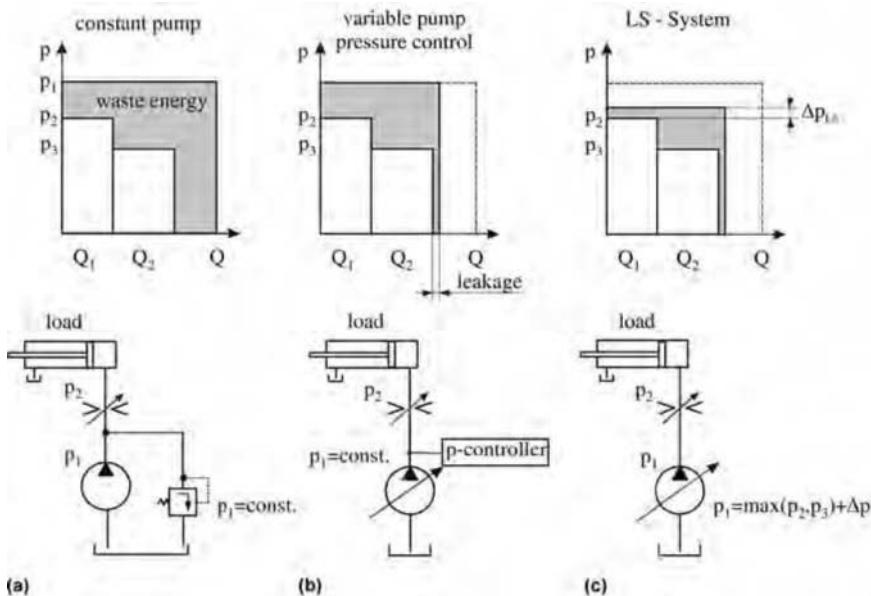


Fig. 12.11 Direct drives and their energy efficiencies: (a) constant-rpm electric motor and constant-displacement pump, (b) constant-rpm electric motor and variable-displacement pump, and (c) variable-rpm electric motor and constant-displacement pump. p , pressure. Source: Ref 12.22

ers constant flow rate (\dot{Q}) at a set pressure (p) (Fig. 12.11a). The system is simple to build and maintain. However, it has the lowest efficiency with the lowest initial cost. Waste energy would be converted to heat. Additional cooling devices may be required.

- *Constant-rpm electric motor and variable-displacement pump*, where the pump delivers a constant pressure but at a variable flow rate (use of axial piston pumps with bending axis control or swashplate) (Fig. 12.11b). This alternative offers better efficiency than a constant-rpm electric motor with constant-displacement pump, but it has higher initial cost due to the variable-displacement pump.
- *Variable-rpm electric motor and constant-displacement pump*, where the rpm of the motor is controlled such that the flow rate and the pressure required by the process can be supplied (Fig. 12.11c). This circuit can be ~30% more energy efficient than the other two techniques; however, it has higher initial costs due to the complex controls and load sensing systems (Ref 12.22, 12.23).

It is also possible to combine a number of motors and pumps and to operate them at several stages. For example, a high-rpm motor with constant-displacement pump may be used for high-speed closure/return cycles. It is also possible to use several pumps with constant flow rates and control the speed by either switching the pumps off or running them idle (Ref 12.8).

Accumulator Drive. In an accumulator-drive press (Fig. 12.12), the pumps are used to pressurize the accumulator(s). When hydraulic fluid is required at high pressure and flow rate, it can be supplied by the accumulator(s) within

a very short time. By the next cycle, pump(s) have to pressurize the accumulator(s) back. Accumulators are used to store energy, similar to the flywheel in a mechanical press or capacitance in servo-drive presses. Accumulator-drive presses are favored if the press has long idle periods between cycles, or very large press capacities are required, on the order of 9,000 to 45,000 metric tons (10,000 to 50,000 tons) (Ref 12.1, 12.24).

Accumulator drives have the advantage of downsizing the motor(s) and pump(s) in the system. Thus, they reduce the initial investment. However, the pumps have to operate against the full work pressure of the accumulators even though the nominal force may not be used at all times. To control the velocity of the press, a flow-regulating valve can be used, where the excessive hydraulic energy will be wasted and converted into heat energy (Ref 12.1, 12.8).

Accumulator-drive presses used in sheet metal forming are large deep drawing presses, tryout presses, and fine blanking presses. A comparison of direct-drive presses and accumulator-drive presses is given in Table 12.3 (Ref 12.2, 12.12, 12.25).

12.3 Characteristics of Hydraulic Presses

Load and Energy. Hydraulic presses are load-restricted presses. Regardless of the drive type (direct or accumulator), the maximum pressure (p_{\max} , in MPa/bar, or psi) would limit the nominal load (L_M , in kN, or lb) that the machine can exert on the dies:

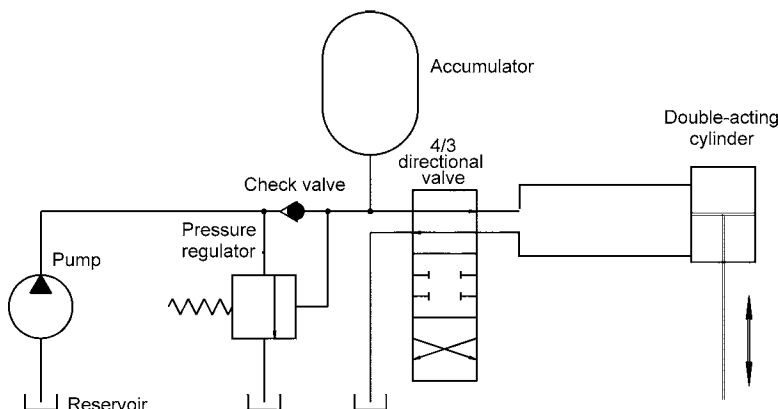


Fig. 12.12 Accumulator-drive circuit for a hydraulic press. Source: Ref 12.21

$$L_M = p_{\max} A_{\text{piston}}$$
Eq 12.4

where A_{piston} is the area (mm², or in.²) of the piston under pressure.

Energy per stroke in an accumulator-driven press is directly proportional to the energy capacity of the accumulators. Usually, during the stroke, 10 to 15% pressure drop is allowed. On the other hand, with the direct-drive presses, energy per stroke is limited by the maximum load and stroke:

$$E_M = L_m s_{\max}$$
Eq 12.5

where E_M is the energy per stroke by the machine (in kJ, or ton-in.), L_M is the maximum load

(in kN, or in.), and s_{\max} is the maximum stroke (in m or in.) (Ref 12.4, 12.8).

Usually hydraulic presses are not as energy efficient as mechanical presses. As shown in Fig. 12.13, a mechanical press is about 30% more energy efficient and may produce more parts per minute. Therefore, energy requirement per part of a mechanical press is much lower than that of a hydraulic press. However, a hydraulic press can exert the nominal force all over the stroke (speaking of a direct-driven hydraulic press) and therefore may apply much higher energy per stroke (Ref 12.1).

Stroke. The maximum stroke of a hydraulic press is limited only by the design of the cylinder. However, it is possible to use only a small portion of the available stroke of the press, unlike in mechanical presses. This allows hydrau-

Table 12.3 Comparison of direct-drive and accumulator-drive presses

	Direct drive	Accumulator drive
Hydraulic fluid	Oil	Oil/water emulsions
Press speed	Determined by the installed pump and motor Flow-regulating valves may be applied	Determined by flow-regulating valves
Power requirement	Not constant Will make peaks as the press needs more power	Almost constant, smooth over time (similar to mechanical presses)
Energy per stroke	Unlimited Nominal force is available throughout the entire stroke	Limited by the capacity of the accumulator(s)
Pressure/Force	Equal to the force required by the process Maximum force can be limited by use of pressure valves	Accumulators have to operate always at the full capacity

Source: Ref 12.1, 12.8

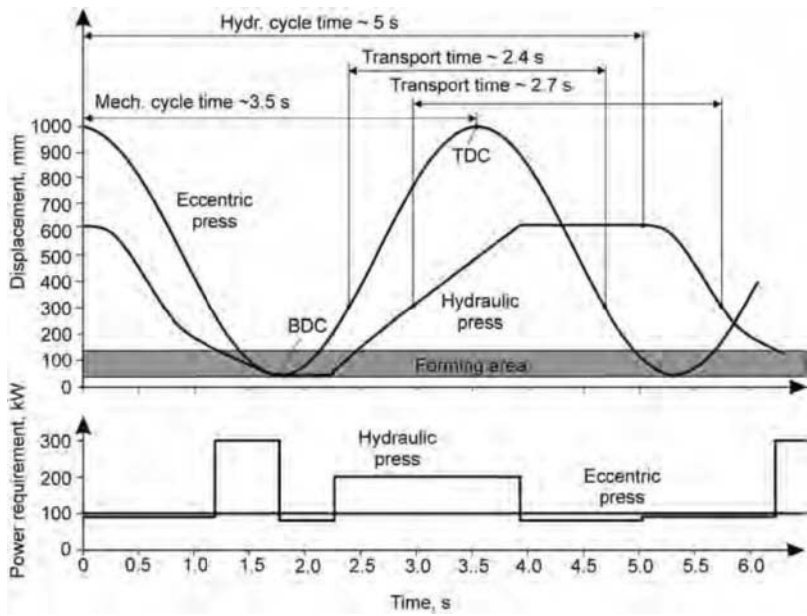


Fig. 12.13 Stroke time and energy time for a hydraulic press and an equivalent mechanical press. BDC, bottom dead center; TDC, top dead center. Source: Ref 12.1

lic presses to be more flexible than mechanical or eccentric presses, and allows faster cycle times, because the slide is moved only in the portion that is necessary to form the part.

Provided that the forming/cutting forces fluctuate within certain limits (because of deviation in thickness, material, friction, etc.), dimensional accuracy of the final part is repeatable only if the hydraulic press has repeatable strokes. Generally, limit switches are employed to set the end of stroke. The slide's downward motion is reversed when the switch is triggered. Depending on the slide speed and load, the slide may pass this switchover point by a few millimeters (Ref 12.1, 12.8).

If close tolerances are required in production with hydraulic presses, positive stops in combination with a hydraulic damping system may be utilized, as shown in Fig. 12.14. Positive stops ensure that the press stops at the same point in every hit, similar to bottom dead center (BDC) in mechanical presses, thus minimizing the variation. Damping systems are needed when blanking in a hydraulic press (Ref 12.1, 12.3).

Time-Dependent Characteristics. In a hydraulic press, each cycle consists of different phases that together add up to the total cycle time. In general, each cycle is defined by fast approach, forming, and fast return phases (Fig. 12.15).

Low-force/high-speed approach stroke and high-force/low-speed forming stroke can be achieved by:

- Using a tandem cylinder (as in Fig. 12.3d), where a small area piston is used for fast ap-

proach and a large area piston is used for the forming process

- Using a tandem pump (more than one pump attached to same electric motor), where one pump would be delivering very high flow rate at low pressure and the other low flow rate at high pressure
- Using several cylinders in parallel (Fig. 12.16)
- Using a prefill valve (Fig. 12.17)

When several cylinders are used in parallel, it is possible to use a combination of them to speed up the press when excess force is not required. In Fig. 12.16, a hydraulic press with three identical cylinders is shown.

A prefill valve may be used to accelerate the fast approach and return phases. During these phases, the fluid flow rate (Q in liters per minute or gallons per minute) may well exceed what can be supplied by a pump. In this case, a prefill valve is used, which is connecting the head of the cylinder directly to the reservoir. The prefill valve is opened when the slide is in the fast approach stroke, and the fluid flows either by gravity or suction created by the main cylinder as the slide is pushed down by small cylinders (Fig. 12.17a). During the forming stroke, high pressures have to be developed, so the prefill valve is closed (Fig. 12.17b). When the slide is in fast return stroke, the prefill valve is opened, so a large amount of fluid can flow back to reservoir (Fig. 12.17c) (Ref 12.2).

A hydraulic press's displacement-time curve also depends on:

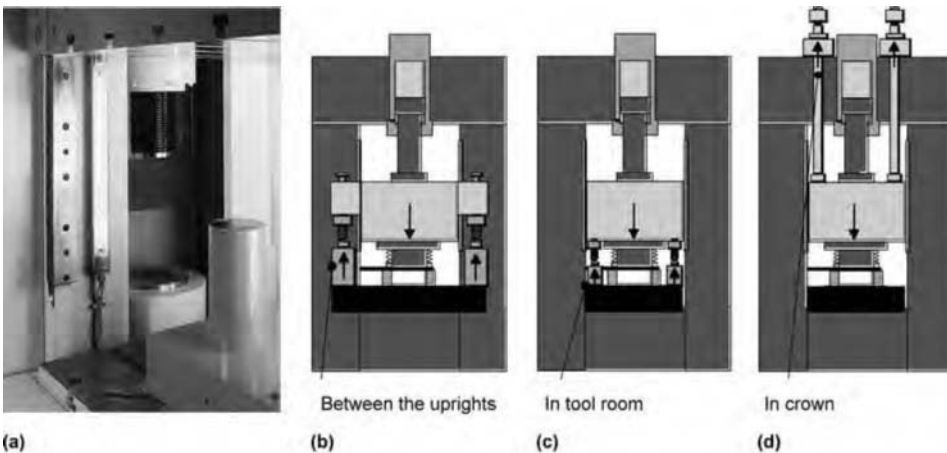


Fig. 12.14 Stroke-limiting and damping devices: (a) and (b) between the uprights, (c) in tool room, and (d) in crown. Source: Ref 12.1, 12.3

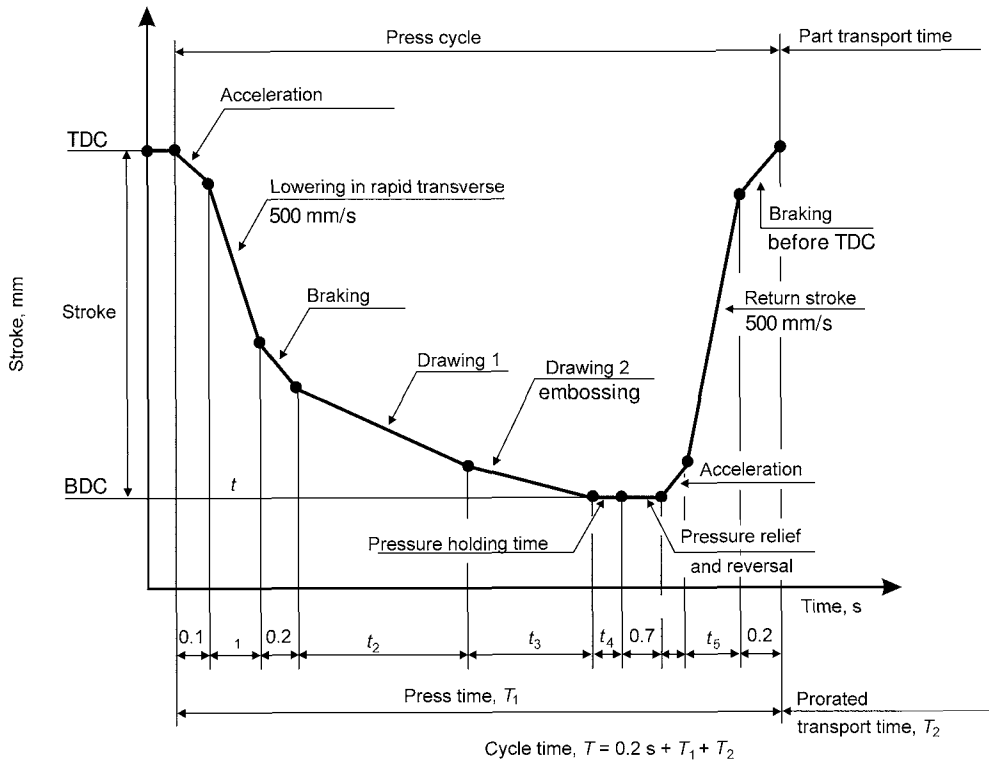


Fig. 12.15 Displacement-time curve of a hydraulic press. BDC, bottom dead center; TDC, top dead center. Source: Ref 12.1

- Fluid type, because this changes the compressibility of the fluid and thus affect speed under pressure and contact time under pressure (Ref 12.8)
- Response time of the valves, which will affect the transition time between phases (i.e., pressure relief and reversal in Fig. 12.15) (Ref 12.28).

Characteristic Data for Accuracy. Stiffness and therefore accuracy of a hydraulic press depend on (a) the frame and gib design, (b) number of hydraulic cylinders, (c) the hydraulic fluid used in the circuit, and (d) presence and effectiveness of a parallelism control system.

As explained in earlier chapters, the stiffness of a press is directly related with the frame and gib designs. A gap frame press (Fig. 12.18a) has very low angular stiffness compared to other frame types. Number of hydraulic cylinders also affects the stiffness of press as well as parallelism of the slide.

However, in hydraulic presses, one of the key components that defines the accuracy is the hy-

draulic fluid itself. All fluids are compressible, and their bulk modulus is much smaller than metals. Hydraulic fluid in the cylinder acts as a spring as it is compressed under pressure:

$$C_F = \frac{\kappa L_M}{sp} \quad \text{Eq 12.6}$$

where C_F is the stiffness of the fluid column (in kN/mm, or ton/in.), κ is the bulk modulus of the fluid (in GPa, or psi), L_M is the load generated by the press (in kN, or ton), s is the stroke (i.e., distance traveled by the slide from uppermost point in mm, or in.) and p is pressure in the cylinder (in MPa, or psi).

Thus, the stiffness of a hydraulic press is determined by the compressibility of the hydraulic fluid and the elastic deformation of the frame and drive system. The former causes the high contact time under pressure and is directly proportional to the bulk modulus of the fluid. Therefore, the stiffness characteristic of a hydraulic press may change with time, as the temperature of the fluid may rise with time. Javadi

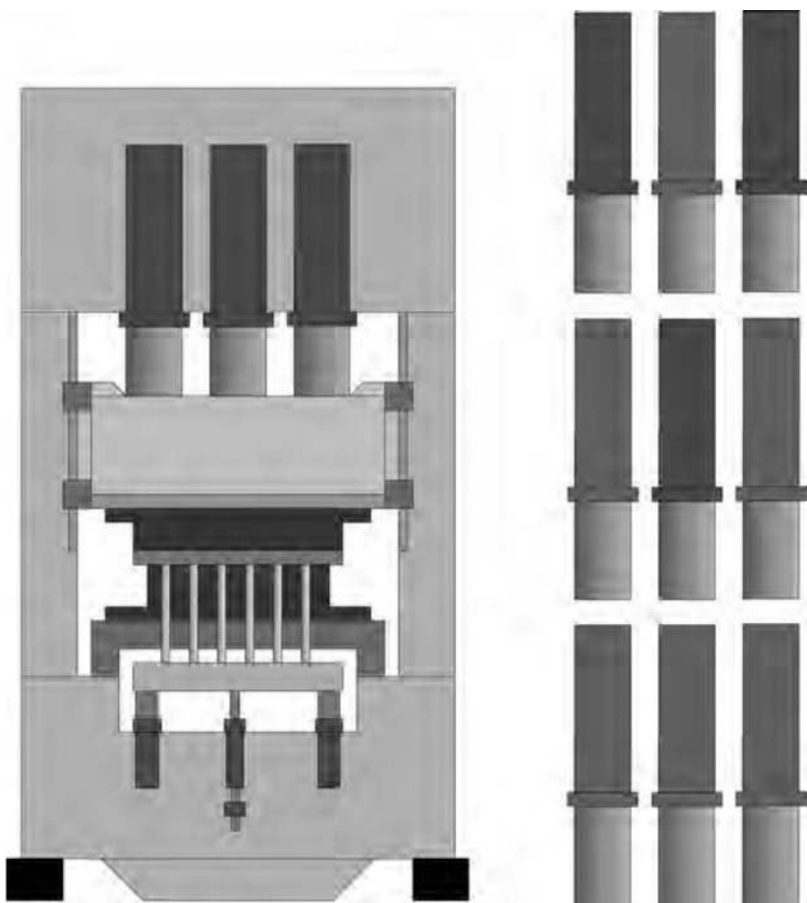


Fig. 12.16 Selective activation of cylinders in a press with three identical cylinders. Source: Ref 12.26

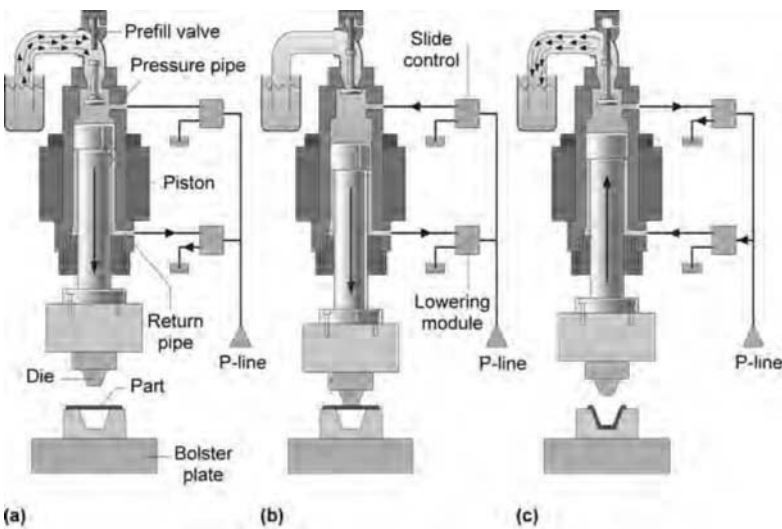


Fig. 12.17 Use of prefill valve in hydraulic press: (a) the prefill valve is opened when the slide is in the fast approach stroke, (b) the prefill valve is closed during the forming stroke, and (c) the prefill valve is opened when the slide is in fast return stroke. Source: Ref 12.27

et al. (Ref 12.29) has shown that the initial tilt of a hydraulic press and its tilt stiffness may change after a few hours of operation.

In applications where off-center loads are present and the accuracy is important, hydraulic presses either are required to be stiffer or can be built with a parallelism control system. A parallelism control system consists of multiple cylinders with position feedback and a servo controller. Depending on the application and economics, there are mainly two types of control systems: with and without applied force (Ref 12.1, 12.4).

In the system with applied force (Fig. 12.19a), cylinders are installed on the corners of the slide and are pushed with a constant pressure (therefore applies force). When deviation is sensed, the pressure is increased on the leading side and is decreased on the other side by servo valves. The sum of applied force (i.e., $F_2 + F_3$) is always constant. The press has to generate more force than required by the forming process; **therefore, this method is not energy efficient.** However, by employing this system, a parallelism (between slide and bolster plate) of 0.05 to 0.2 mm/m (0.002 to 0.008 in./ft) can be achieved (Ref 12.1, 12.26).

In the second system, an average pressure is applied to two cylinders that are connected to each other by means of diagonal pipe connections. If an off-center force is exerted on the

slide, the slide tilt is sensed and the servo valve is triggered. The control system increases the pressure on the underside of the cylinder acting on the leading side, due to the diagonal connection on the opposite cylinder. At the same time, the pressure in the other two chambers is reduced. A moment has been generated by force couple (i.e., $F_1 = -F_2$), so that the sum of forces **is neutral.** This system can be more energy efficient because it is not generating any force resisting the slide motion. However, the parallelism by this system is limited to 0.6 to 0.8 mm/m (0.02 to 0.03 in./ft) (Ref 12.1).

12.4 Hydraulic Press Designs

The frame of the press is the main structure that carries all the forces generated by the press and has to provide guidance of the slide. Similar to other presses, hydraulic presses can also be built in gap frame (also known as C-frame or open frame; Fig. 12.18a) or straight side (closed frame; Fig. 12.18c). Hydraulic presses are also built in a special frame type, where the frame itself is a number of columns (depending on the design, generally two or four columns are used) that are both holding the bolster plate and guiding the slide. This is named as column-type frame, as illustrated in Fig. 12.18(b).

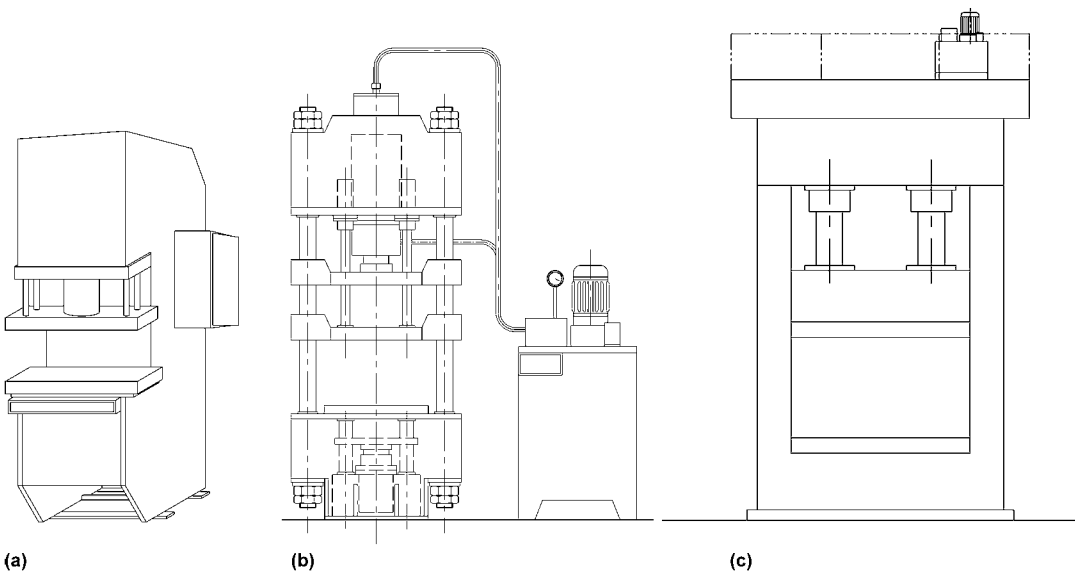


Fig. 12.18 Hydraulic press frames: (a) gap frame, (b) column type, and (c) straight side. Source: Ref 12.14

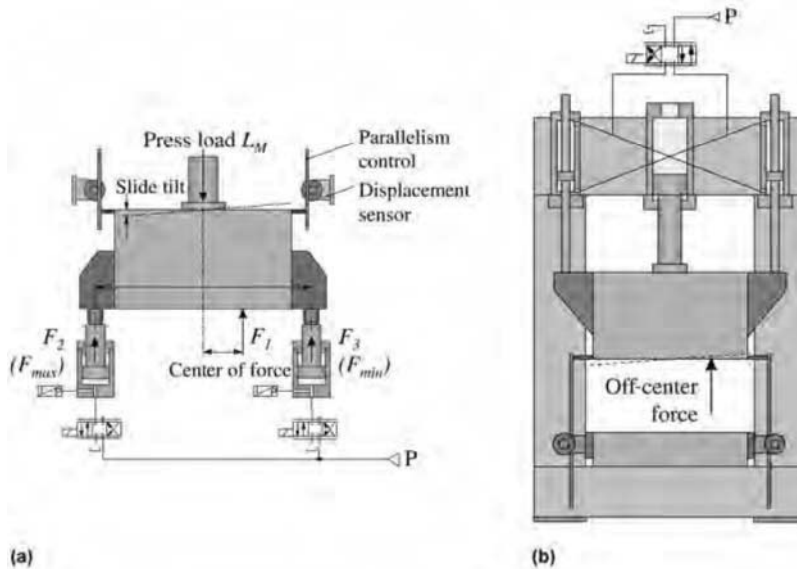


Fig. 12.19 Parallelism control systems: (a) with applied force and (b) without applied force. Source: Ref 12.1

Hydraulic Presses by Function

Hydraulic presses are very versatile compared to mechanical presses. It is also much easier to develop double/triple action, compared to mechanical presses with complex toggle drives. For this reason, they are used in many different applications.

Deep Drawing Press. In deep drawing operations, the slide is pushing against the cushion. To do this, some energy is spent in cushion (E_{cushion}), and then that amount of energy is spent in slide to overcome the cushion force and additional energy to form the part ($E_{\text{slide}} = E_{\text{cushion}} + E_{\text{forming}}$). Thus, the overall energy would be an addition of both. To make a deep drawing press more efficient, it can be equipped with eco-cushions (Fig. 12.20). In this cushion system, cushion cylinders are connected to secondary cylinders that move the slide, so as the blank holder force increases, the same amount of force moves the slide down. By this method, it is possible to downsize the total electric capacity for the press by ~30%. More important, as the energy efficiency is increased, the hydraulic fluid does not generate as much heat as a deep draw press without eco-cushion. The cooling system can be downsized drastically (Ref 12.3, 12.26).

Fine Blanking Presses. Fine blanking is a precision blanking process, where the cut edge is very smooth. A typical fine blanking press is required to:

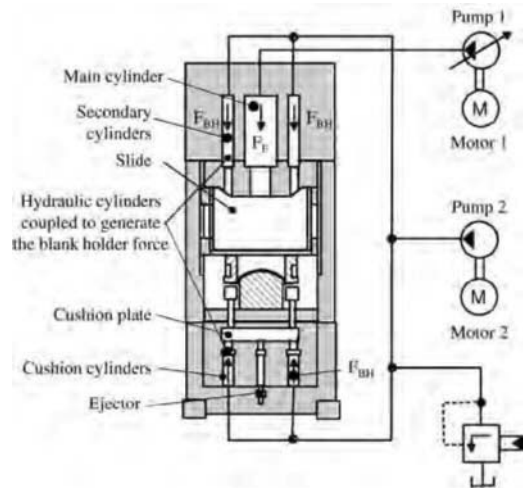


Fig. 12.20 A deep drawing press with eco-cushion. Source: Ref 12.3

- Generate three forces: (a) the blanking force, (b) the ring indenter (V-ring) force, and (c) the counterforce
- Rigidify the frame with precise guides
- Control ram movement
- Have a tool safety system
- Have automation systems (for quick die change, part/slug removal, etc.)

Small presses (up to 2500 kN, or 275 tons) are generally built with a bottom-drive knuckle

joint mechanism for the main slide (i.e., blanking force is generated by the mechanism), and two hydraulic cylinders are used to generate the other two forces (the V-ring force and the counterforce). Larger presses (up to 14,000 kN, or 1540 tons) are generally built with all three actions hydraulic (as in Fig. 12.21) and are driven by an accumulator drive (Ref 12.1, 12.2).

Another important advantage of fully hydraulic fine blanking presses is that they can be built with a “die-independent pressure-sensing system.” The system can sense even a very small increase in the counterforce cylinder pressure and therefore can detect if any foreign object was left in the die (which is possible because slugs/parts from previous strokes may have been left in the die area). If the system detects no foreign objects, then it activates the high-pressure accumulator to initiate the main (blanking) slide movement.

Hydroforming Presses. Hydroforming is a sheet metal or tube forming process where the workpiece is formed under high pressure of fluid. There are several types of hydroforming processes, mainly:

- *Sheet hydroforming with punch* (SHF-P, also known as hydromechanical deep drawing),

where the sheet metal is clamped between a pot and a blank holder. The deformation is carried out by the punch.

- *Sheet hydroforming with die* (SHF-D), where the blank is clamped and the deformation is carried out by pumping high-pressure oil into the pot
- *Tube hydroforming* (THF), where a tube is clamped between upper and lower dies and pressurized for the deformation

For SHF-P, a double-action press is required for clamping and forming (moving the punch). Often a second hydraulic unit is used to control the pressure inside the pot (Fig. 12.22a). For SHF-D and THF, the press is required only to clamp the upper and lower tools. The deformation is done by high-pressure fluid (Fig. 12.22b), which is on the order of 200 MPa (30 ksi) or even more and is supplied by an intensifier.

Both in SHF-D and THF applications, very high pressure is generated in the tool. Therefore, high clamping forces are required to keep the upper and lower tools in position. Typically a column-type or straight-side conventional hydraulic press can be used for hydroforming. The upper die can be attached to the slide, and the press could generate the clamping force (Fig.

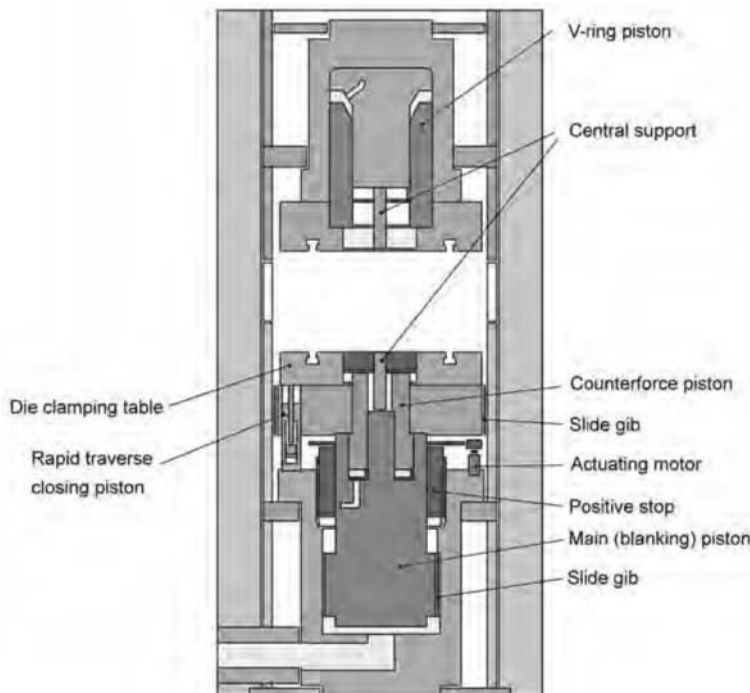


Fig. 12.21 Hydraulic fine blanking press. Source: Ref 12.1

12.23a). However, such systems are not preferred for mass production applications because a long stroke cylinder cannot generate the necessary high clamping forces, and clamping time would take a long time. To avoid such disadvantages, hydraulic clamping presses are designed where the upper tool is stationary and lower tool is attached to a short stroke cylinder (Fig. 12.23b). In THF applications, a long stroke is required to load/unload the workpiece. For this purpose, hydromechanical clamping presses (Fig. 12.23c) were designed where a long stroke cylinder with low force closes the tools. Furthermore, this main cylinder may perform some preforming operations. After the die closes, spacer cylinders are moved between the slide and the frame, and then the short stroke clamping cylinder is activated (Ref 12.1, 12.23, 12.33).

Tryout Presses. Operation of a large press line may cost several thousand dollars per hour.

Therefore, when a new die set is to be put in production, it might be more economical to try it out in a so-called tryout press (Fig. 12.24) to minimize the die setup time on the production line. If any reworking is required for flawless production, this should be done at the tryout stage (also known as die spotting). A tryout press can be mechanical or hydraulic and should be able to emulate the speed characteristics and behavior of die cushion in the real production line. Hydraulic presses are often preferred because they are more cost efficient and offer high energy capacity and controllable slide motion. These presses are often equipped with moving bolsters, quick die change systems, and rotating slide plate to make reworks and die changes easier and faster (Ref 12.1, 12.25).

To be able to simulate high slide velocities of production press, most hydraulic tryout presses are accumulator driven. A problem, however,

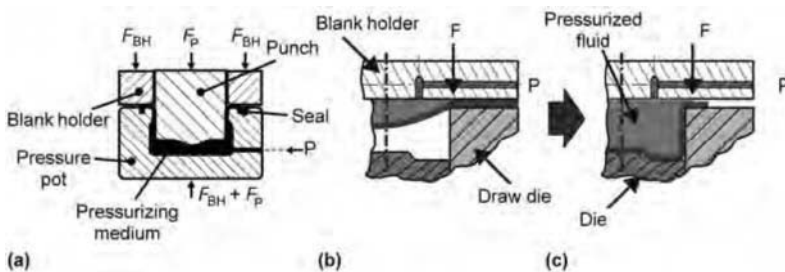


Fig. 12.22 Sheet hydroforming scenarios: (a) sheet hydroforming with punch. Source: Ref 30. (b) and (c) initial and final phases of sheet hydroforming with die. Source: Ref 12.31

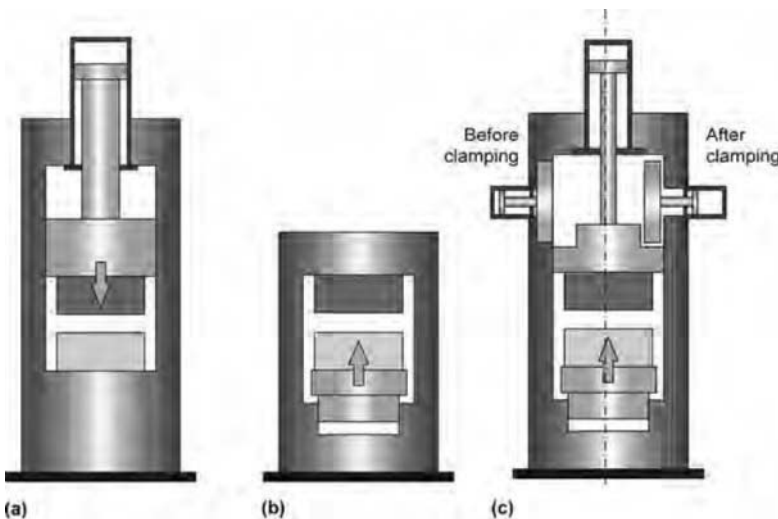


Fig. 12.23 Presses for hydroforming: (a) conventional hydraulic press, (b) hydraulic clamping press, and (c) hydromechanical clamping press. Source: Ref 12.19



Fig. 12.24 A tryout press with moving bolster and rotating slide plate to allow quick reworking of the dies.
Source: Ref 12.1

with the tryout presses is that the elastic deflection of the press cannot be emulated in these presses, unless a controlled parallelism system is installed. In such presses, the parallelism system is set such that it can tilt the slide to emulate the conditions in production press (Ref 12.25).

Presses for Warm Forming and Hot Stamping. Warm forming (i.e., forming materials at elevated temperature without changing the microstructure) and hot stamping (i.e., forming special alloy steels at elevated temperature and quenching within the die to form martensitic microstructure) require the press to be able to control the speed, because the material is strain rate dependent at elevated temperatures, and to control the dwell when needed. In warm forming, dwell is used to heat the workpiece, and in hot stamping dwell is needed for quenching. A conventional double-action hydraulic press or a single action hydraulic press with cushion can be used for these operations.

In hot stamping applications, fast forming stroke is followed by a long quenching (dwell) cycle that makes this application a good candidate for an accumulator-driven hydraulic press. In a selected application described by Karlsson (Ref 12.34), the quenching time was 11 s, and depending on the drive, the forming cycle was either 1 or 3 s. Considering the total time (12 instead of 14 s), about a 16% increase in output was achieved (Fig. 12.25). Another recent ap-

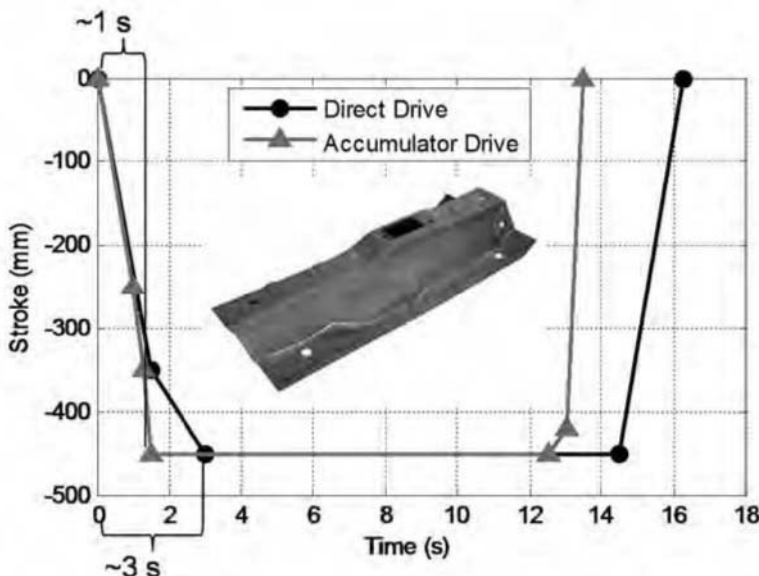


Fig. 12.25 Hot stamping cycle time of a direct-driven and accumulator-driven hydraulic press. Source: Ref 12.34

plication is to use flywheels so that when the press is idle at quenching stage the energy can be stored to flywheels. When the press needs high energy in forming or return cycles, energy can be drawn from the flywheels. Approximately 50% energy could be saved by using fly-wheel hydraulic presses (Ref 12.35).

REFERENCES

- 12.1 Schuler GmbH, *Metal Forming Handbook*, Springer, 1998
- 12.2 H.E. Theis, ed., *Handbook of Metal-forming Processes*, Marcel Dekker, 1999
- 12.3 E. Doege and B.A. Behrens, eds., *Handbuch Umformtechnik (Metallforming Handbook)* (in German), Springer, 2010
- 12.4 H. Tschatsch, *Metal Forming Practise: Processes—Machines—Tools*, Springer, 2006
- 12.5 M. Römer, “Mechatronics—Module 3: Fluidics,” MINOS Module, Technical University of Chemnitz, 2007
- 12.6 E. Trostmann, *Water Hydraulics Control Technology*, Marcel Dekker, 1996
- 12.7 C. Wick, J.T. Benedict, and R.F. Veilleux, *Tool and Manufacturing Engineers Handbook*, Vol 2, *Forming*, 4th ed., Society for Mining, Metallurgy, and Exploration, 1984
- 12.8 K. Lange, ed., *Handbook of Metal Forming*, McGraw-Hill, 1985
- 12.9 Moog Inc., “Radial Piston Pump RKP-II,” rev. 3.1, 2010
- 12.10 Rexroth, A.G., “Hydraulic Fluids Based on Mineral Oil and Related Hydrocarbons,” RE90220/10:08, 2008
- 12.11 International Organization for Standardization, “DIN 1219, Fluid Power Systems and Components—Graphic Symbol and Circuit Diagrams,” 1996
- 12.12 LASCO Umformtechnik GmbH, Hydraulic Deep Drawing Presses, Product Catalogue, August 2005
- 12.13 D. Merkle, B. Schrader, and M. Thomes, *Hydraulics*, 2nd ed., Festo Didactic GmbH, 1998
- 12.14 Q.S. Khan, *Introduction to Hydraulic Presses*, Tanveer, 2010
- 12.15 K.K. Tan and A.S. Putra, *Drives and Control for Industrial Automation*, Springer, 2011
- 12.16 Parker Hannifin Corp., Hydraulic Cartridge Systems, Product Catalogue, HY15-3502/USA,EU, 2010.
- 12.17 Y. Osokin and S. Kozlov, Hydraulic Press with Two-Lever Control, *Russian Engineering Research*, Vol 30, 2010, p 276–277
- 12.18 Rexroth, A.G., “4/3 Servo Directional Control Valve with Mechanical Position Feedback,” RE29564-XN-102-B2, 2010
- 12.19 Rexroth, A.G., Fluid Forming, Product Catalogue, RE09348/10.04, 2004
- 12.20 Festo Didactic GmbH. “Hydraulic Symbols,” 2006
- 12.21 A. Akers, M. Gassman, and R.J. Smith, *Hydraulic Power System Analysis*, CRC Press, 2006
- 12.22 D. Lovrec, M. Kastrevc, and S. Ulaga, Electro-hydraulic Load Sensing with a Speed-Controlled Hydraulic Supply System on Forming-Machines, *International Journal of Advanced Manufacturing Technology*, Vol 41, 2009, p 1066–1075
- 12.23 Parker Hannifin Corp., Energy Saving Solutions, Product Catalogue, HY02-8052/UK, 2009
- 12.24 T. Altan, G. Ngaile, and G. Shen, *Cold and Hot Forging: Fundamentals and Applications*, ASM International, 2004
- 12.25 U. Konnerth, A Hydraulic High-Speed Tryout Press for the Simulation of Mechanical Forming Processes, *Journal of Materials Processing Technology*, Vol 111, 2001, p 159–163
- 12.26 F.X. Kürzinger, New Concepts for Hydraulic Production Press, *New Developments in Sheet Metal Forming*, 2000
- 12.27 K.H. Grote and E.K. Antonsson, eds., *Springer Handbook of Mechanical Engineering*, Springer, 2009
- 12.28 Schuler SMG GmbH, Hydraulic Press Lines, Product Catalogue, 205E-102008-WSP-1000, 2008
- 12.29 M. Javadi, B. Behrens, and R. Krimm, Efficient Control of Metal-Forming Machines with an Automated Load and Measurement Device, *Production Engineering*, Vol 4, 2010, p 95–100
- 12.30 M. Aust, Modified Hydromechanical Deep Drawing, *Hydroforming of Tubes, Extrusions, and Sheet Metals*, 2001
- 12.31 M. Kleiner and W. Homberg, New 100,000kN Press for Sheet Metal Hy-

- droforming, *Hydroforming of Tubes, Extrusions and Sheet Metals*, 2001
- 12.32 K. Siegert and M. Aust, A Survey of Presses for Hydroforming Tubes, Extrusions, *Tube and Pipe Journal*, September 2003
- 12.33 C. Hartl, Research and Advances in Fundamentals and Industrial Applications of Hydroforming, *Journal of Materials Processing Technology*, Vol 167, 2005, p 383–392
- 12.34 J. Karlsson, “Press Requirements,” presented at AP&T Advanced Hot Stamping Seminar, Detroit, MI, September 2010
- 12.35 R. Hund, Continuous Improvement of Hot Forming Technology, *Proceedings of 3rd International Conference on Hot Sheet Metal Forming of High-Performance Steel, Kassel, Germany, July 13–17 (2011)*, p 189–200

CHAPTER 13

Cushion Systems for Sheet Metal Forming

Hari Palaniswamy, Altair Engineering, Inc.
Lars Penter, Technical University of Dresden

IN DEEP DRAWING, the sheet metal blank is subjected to restraining force at its periphery by the blank holder while it is forced to flow into the die cavity by the punch (as discussed in Chapter 8, “Deep Drawing of Round and Rectangular Cups,” in this book). The quality of a formed part is determined by the amount of material drawn into the die cavity. An excess material flow will cause wrinkling; insufficient material flow will cause tearing or fracture (Fig. 13.1).

Blank holder force (BHF) plays a key role in controlling material flow. When estimated correctly, BHF provided by the press cushion system can prevent wrinkling and tearing in the formed part (Ref 13.1). In some cases a custom-built cushion system in the tooling provides the necessary force for the blank holder. Presses used for deep drawing could be either single ac-

tion or double action (in some cases triple action) and have either mechanical or hydraulic drives. Accordingly, the cushion construction and its characteristics differ (Fig. 13.2).

13.1 Blank Holder Systems in Double-Action Presses

Double-action presses have two slides, inner and outer, which operate independently in the same direction. In deep drawing, the motions of the inner and outer slides have to be synchronized.

An example of a deep drawing tooling mounted on a double-action press is shown in Fig. 13.3(a). The die sits on the press bed, the blank holder is attached to the outer slide, and the punch is attached on the inner slide. At the start, the blank is placed on the die cavity. The inner slide and the outer slide move together. The blank holder attached to the outer slide first contacts the sheet and wraps it against the die by applying the preset BHF. At this time the punch is slightly offset from the sheet (Fig. 13.3b).

Figure 13.3(c) represents the drawing process, in which the punch moves down and forms the sheet against the die cavity. During the process, the blank holder continues to be in contact with the blank and applies the preset BHF. Figure 13.3(d) represents the end of the process, when the inner slide retracts, followed by outer slide, to the initial position.

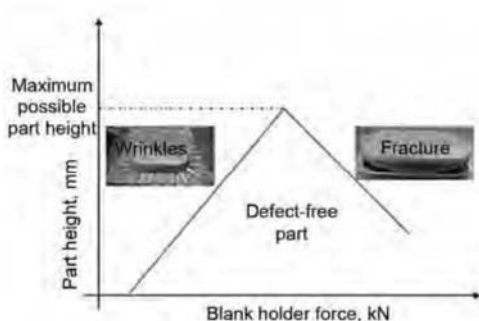


Fig. 13.1 Potential failure modes in deep drawing that are influenced by blank holder force

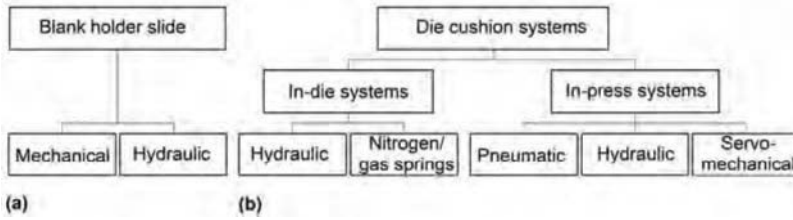


Fig. 13.2 Overview of blank holder force generating systems in sheet forming presses: (a) double-action and (b) single-action presses

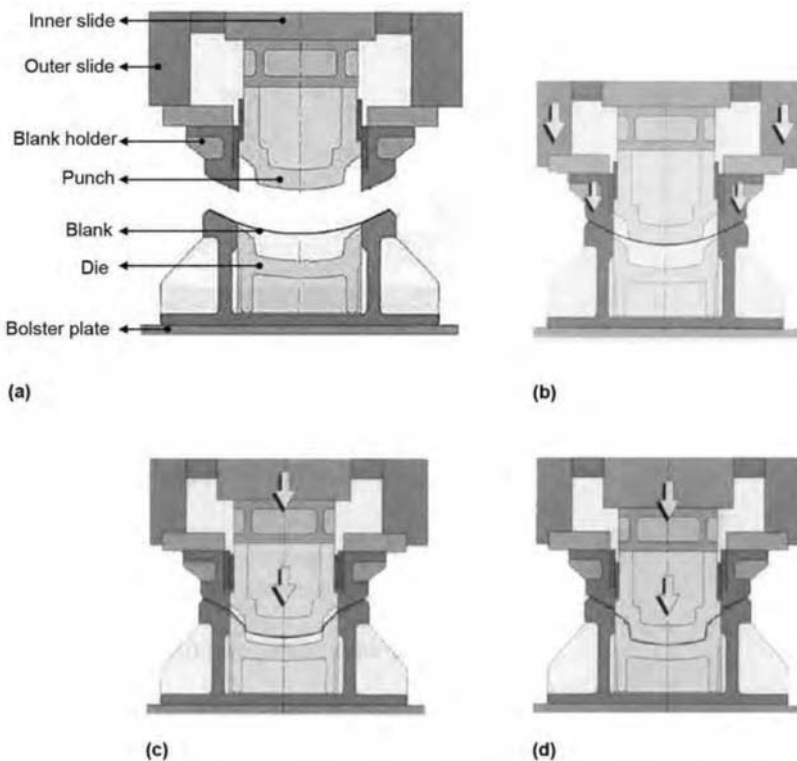


Fig. 13.3 Schematic of double-action deep drawing die: (a), initial setup (b), closing the tool (c), forming the part, and (d) end of drawing. Source: Ref 13.2

Mechanical Presses. The displacement characteristics of both the inner and the outer slides are substantially different during a single cycle of the forming operation. Therefore, different but synchronized mechanical linkage mechanisms are used to move the inner and outer slides.

Displacement of Inner and Outer Slide. Figure 13.4 shows the displacement versus crank angle characteristics for both inner and outer slides of a double-action press. The outer slide, which holds the blank holder, reaches bottom

dead center (BDC) at a crank angle of 80° and remains there until 220° . While resting at BDC, the blank holder clamps the blank against the die and applies the BHF. At the same time, the punch forms the part into the die cavity (Ref 13.3).

Forces Exerted by the Outer and Inner Slide. During forming, the outer slide applies a BHF, determined by the die and blank holder geometry as well as by the slide setting. During the forming process, the forces acting on the punch and the die change with stroke, depending on the part geometry, sheet thickness, material, and

so forth. The punch reaches its maximum value at the end of the forming process, when the part corners are coined to obtain the desired part geometry. The process forces cause the die, punch, linkage mechanism, and press frame to deflect elastically. The deflection causes an increasing gap between blank holder and die as it changes the position of BDC of the press. As a result, the BHF, applied by the outer slide, decreases with increasing forming force (Fig. 13.5). In some cases the BHF may decrease up to 40%, depending on the punch force. The deflections of the press and the tool are proportional to the press stiffness. The decrease in BHF can be reduced by the press and slide design (Ref 13.3, 13.4). The inability to control the BHF accurately is one of the main disadvantages of conventional double-action presses used in deep drawing operations. Furthermore, stamped parts need to be turned upside down in a separate forming station before successive operations can be performed (Ref 13.5).

Adjustment of the Blank Holder. In modern double-action mechanical presses, the decrease in BHF during deep drawing operations may be corrected by the short-stroke hydraulic cylinders located between the linkage mechanism and the outer slide (Fig. 13.6). The hydraulic cylinders are connected to an accumulator. During the forming process, the deflection of the press system by higher forming forces results in small retraction of the drive link, which in turn decreases the applied BHF. The negligible link displacement due to elastic deflection is compensated by the fluid pressure from the accumulator, thereby providing the specified BHF (Fig. 13.6) (Ref 13.6).

Hydraulic Presses. Hydraulic presses are discussed in detail in Chapter 12, "Hydraulic Presses," in this book. In double-action designs, independent pressure cylinders actuate inner and outer slides. The cylinders that apply the BHF are independently controlled and compensate for the elastic deflections of the dies and

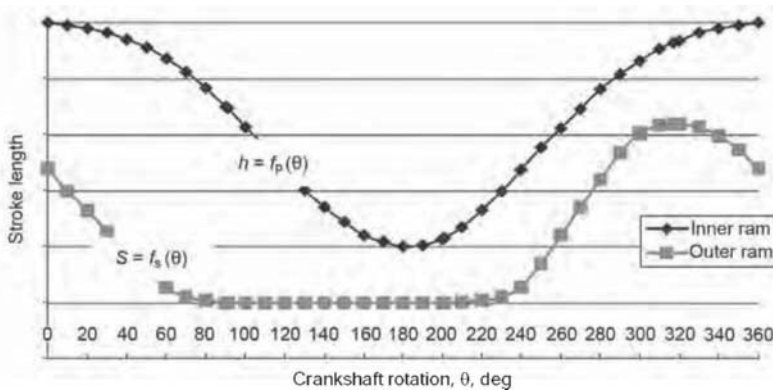


Fig. 13.4 Stroke length (or displacement) in inches (or mm) versus crank angle (or crankshaft rotation) in a double-action press with slider crank mechanisms for inner slide (h) and six-bar linkage for outer slide (s). Source: Ref 13.3

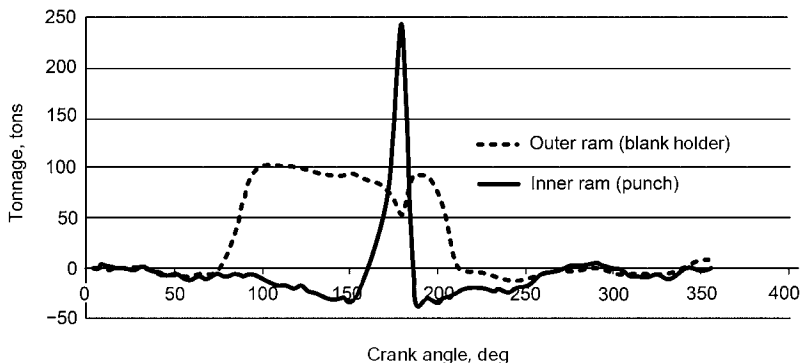


Fig. 13.5 Force characteristics of a mechanical double-action press. Source: Ref 13.3

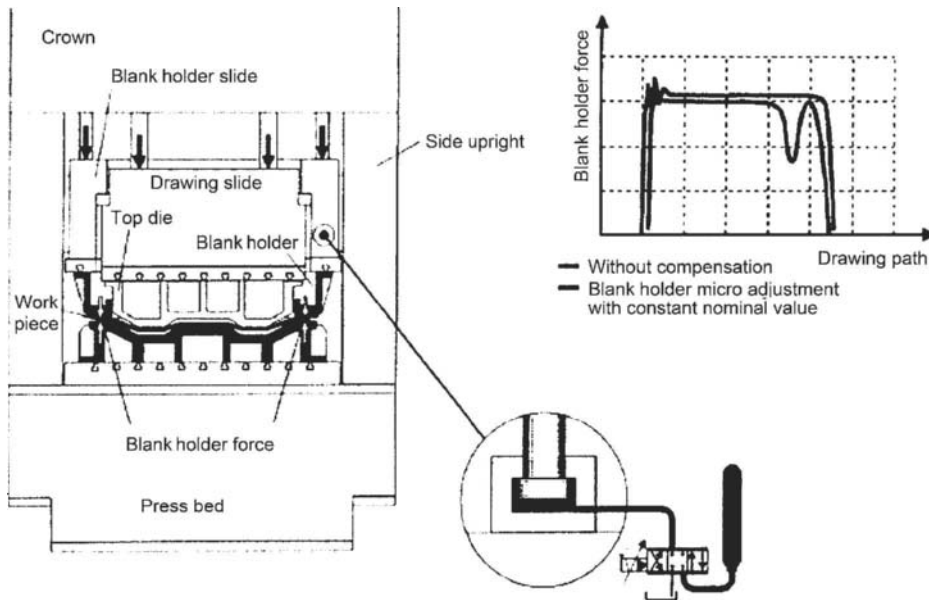


Fig. 13.6 Schematic of the blank holder force adjustment and its effect on the blank holder force. Source: Ref 13.6

blank holder. Thus, the double-action hydraulic press overcomes the deficiencies of a double-action mechanical press and is better suited for deep drawing applications.

13.2 Single-Action Presses with Cushion System

In single-action presses, the die cavity is attached to the slide. The punch sits stationary on the press bed. The blank holder is supported by the die cushion system, which provides the BHF. Most commonly, the BHF is generated by one or more pneumatic or hydraulic cylinders and is transmitted via the pressure box (also referred to as the cushion table) and cushion pins to the blank holder. The die cushion system is located in the press bed (Fig. 13.7).

At the start, the blank holder sits in the upper position with the blank placed on it (Fig. 13.7, right). The ram comes down and holds the blank between the blank holder and the die cavity. As the ram proceeds farther down against the resistance offered by the die cushion, the punch touches the sheet and forms it against the die cavity (Fig. 13.7, left). During the return part of the stroke, the die retracts, the die cushion moves up, and the blank holder strips the formed part from the punch.

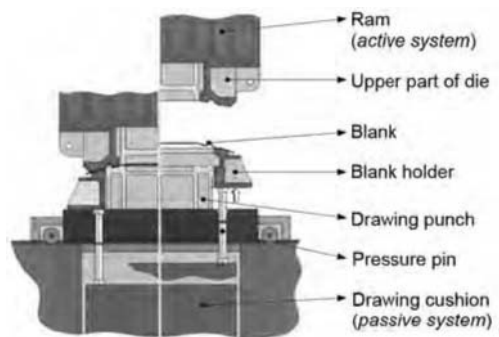


Fig. 13.7 Schematic of single-action deep drawing operation. Source: Ref 13.2

Pneumatic Cushions

In pneumatic cushion systems, the BHF is generated by moving a piston against compressed air in an enclosed cylinder (Fig. 13.8). Pneumatic cylinders are seldom used in modern presses because the maximum pressure in such a system is limited to 16 bar (240 psi) and a very large piston area is needed to generate the required force (Ref 13.7). Furthermore, it is relatively difficult to control a pneumatic cushion because the air is very compressible.

In pneumatic cushion systems, the piston of a pneumatic cylinder is always under pressure.

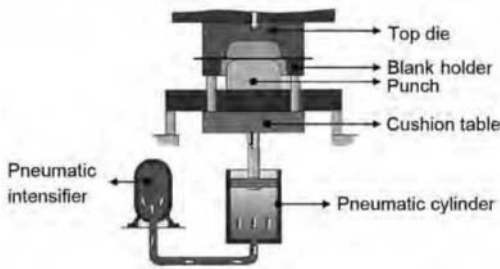


Fig. 13.8 Principle of pneumatic cushions. Source: Ref 13.2

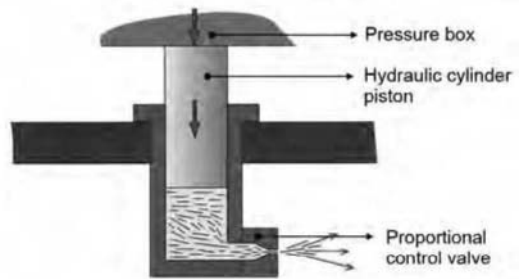


Fig. 13.9 Principle of hydraulic cushions. Source: Ref 13.2

Therefore, the required BHF is applied instantaneously when the die establishes contact with the blank holder. As a result, depending upon the ram speed, the initial impact of the ram on the blank holder/pneumatic cylinder piston causes the BHF to oscillate. Oscillations of BHF reduce tool life and can also damage the surface of the formed part. In order to diminish the influence of the BHF oscillation on the forming process, the lead travel of the blank holder is increased, so that the punch starts forming the part after the BHF oscillations are dampened (Ref 13.8).

Hydraulic Cushions

In hydraulic cushion systems, the required BHF is generated by the oil pressure. The BHF can be controlled by controlling the oil flow from the cushion cylinder with a proportional valve (Fig. 13.9). The energy generated during blank holding is dissipated as heat in the hydraulic cushion system.

A typical hydraulic cushion system with two cylinders in a single-action press is shown in Fig. 13.10. The blank holder (labeled 5) is supported by the cushion pins (6 and 7), which sit on the pressure box (8). The pressure box slides up and down during the forming process and is guided (10). The downward motion of the pressure box/cushion cylinder is controlled by the displacement piston (11), which is attached to the pressure box and slides inside the displacement cylinder (13) that provides the applied BHF. The pressure inside the displacement cylinder is controlled by the fluid flow from the cylinder, which is regulated by valve on the hydraulic control block (14). In Fig. 13.10, two displacement cylinders equally share the applied BHF and control the motion of the blank holder during the forward stroke. The return motion of the pressure box is controlled by the

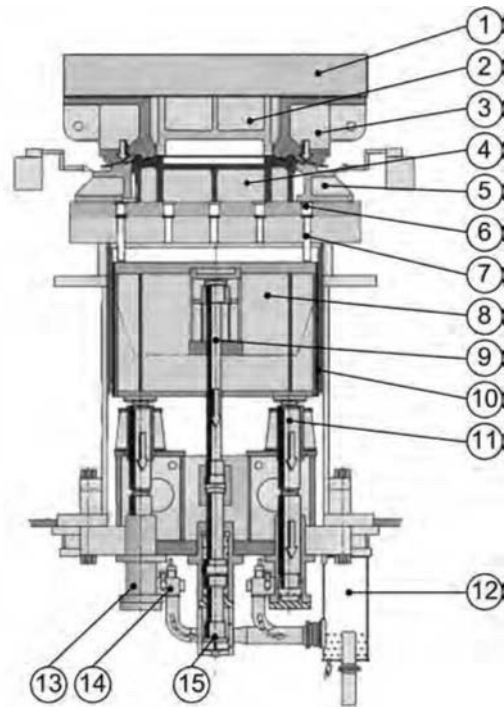


Fig. 13.10 Components of the hydraulic cushion system: 1, ram; 2, ejector; 3, upper die; 4, punch; 5, blank holder; 6, pressure pins in die; 7, pressure pins in drawing cushion; 8, pressure box; 9, lifting piston rod; 10, die cushion guide; 11, displacement piston; 12, overflow tank; 13, displacement cylinder; 14, hydraulic control block; 15, mechanical stroke limitation. Source: Ref 13.2

lifting piston rod (9), which slides inside the lifting cylinder, while the displacement cylinder passively follows the pressure box during the return stroke. The lifting piston rod has a mechanical stroke limitation (15), which limits both forward and return strokes of the entire cushion system.

Force Characteristics of Hydraulic Cushions. The pressure in a hydraulic cylinder is generated by compressing the hydraulic fluid in

the cylinder; it is controlled by regulating the fluid flow from the cylinder. When the cushion is inactive prior to contact with the die, the pressure in the cylinder is defined by the weight of the cushion system. When the blank holder comes into contact with the die, the cushion cylinders start to build up the pressure. Because of the compressibility of the hydraulic fluid, there is a slight delay before the required blank holder pressure is built up. The high velocity impact of the die on the stationary blank holder causes a pressure overshoot in the die cushion cylinders and the BHF. The BHF can be changed with stroke during the forming process. However, the rate of this change is limited by the inherent inertia of the hydraulic system. Nevertheless, most hydraulic cushion systems have sufficiently fast response time to operate successfully in a mechanical press.

Preacceleration and Delayed Return Motion. The impact of the moving die on the stationary cushion results in higher forces, may disturb the lubricant film on the blank, and reduces the life of the blank holder and the cushion. In order to prevent these consequences, modern die cushions can be preaccelerated to minimize or even eliminate the relative velocity between the blank holder and the die during the initial contact. In such a system, the cushion begins to travel downward before the die establishes contact with the blank (Fig. 13.11). Reducing the relative velocity between the moving

die and the stationary blank holder also reduces the impact forces.

In modern cushion systems, the return motion of the die cushion is activated by a lifting piston rod (labeled 9 in Fig. 13.10). After the forming operation, the return motion of the die cushion is delayed at the BDC to avoid back-to-back contact of the blank holder with the formed part (Fig. 13.11).

Energy Recovery from the Hydraulic Cushion. During the forming process, the energy used to apply the BHF by compressing the hydraulic fluid is released as heat in the hydraulic system. This heat release results in wasted energy and heating of the hydraulic oil, requiring oil cooling systems. In order to prevent this problem, modern hydraulic cushions are designed to reuse the generated energy in the press drive system. In mechanical and servo-drive presses, the cushion energy can be saved by using hydraulic motors that drive small generators (see Fig. 11.30 in Chapter 11, “Electromechanical Servo-Drive Presses,” in this book).

In a hydraulic press application, additional compensation cylinders on the slide are aligned with each cushion cylinder. Each cushion cylinder and its corresponding compensation cylinder are hydraulically connected with a servo valve and an accumulator (Fig. 13.12). During the rapid advance of the slide, before it comes into contact with the blank holder, the compensating cylinder and slide cylinders are filled

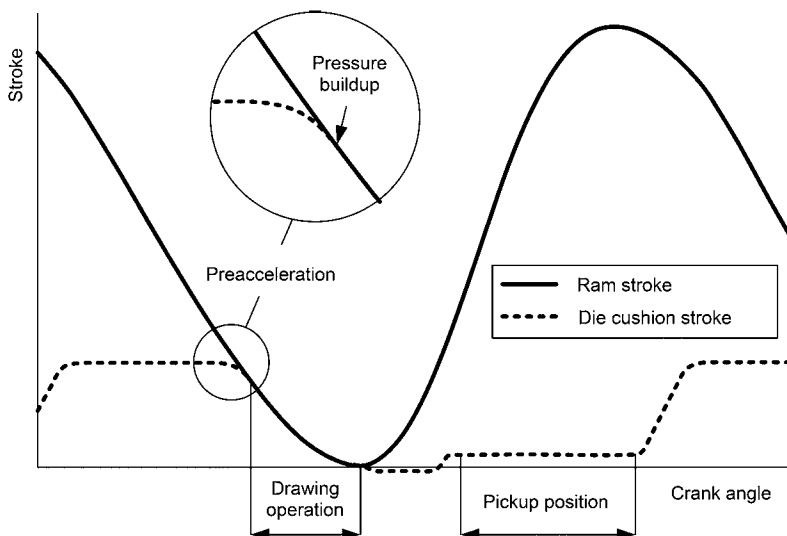


Fig. 13.11 Example ram displacement and cushion displacement over crank angle of a mechanical press with preaccelerated die cushion. Source: based on Ref 13.9

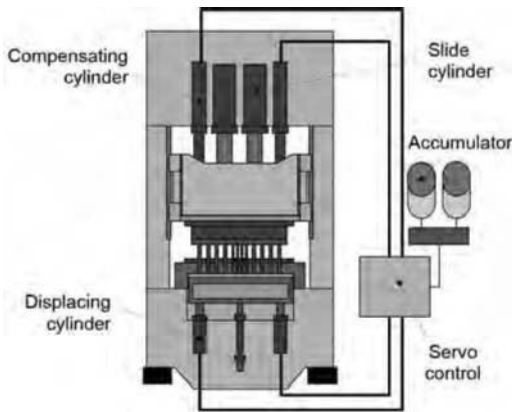


Fig. 13.12 Schematic of an energy-saving cushion in a single-action hydraulic press. Source: Ref 13.10

with hydraulic fluid from the tank using a prefill valve. Once the die touches the blank holder, the prefill valve is closed for both the compensating and slide cylinder. The pressure in the slide cylinder is generated by either an accumulator or a pump-driven system. The compensation cylinders are connected to the hydraulic line from the corresponding cushion cylinder, and the pressure required to apply the necessary force is initially generated by additional fluid from the accumulator through a servo valve. During further motion of the slide, the fluid displaced from the cushion cylinder is fed directly to the compensation cylinder, thereby adding capacity to the slide; energy used to apply the BHF is thus not wasted but recovered.

Factors Affecting Force Flow in Cushion Systems

In a single-action press, part of the force applied by the die is transmitted through the sheet to the blank holder and from the blank holder through the cushion pins to the pressure box. The pressure box is supported by one or more cylinders, which generate the BHF on the sheet (Fig. 13.13).

Since all machine parts are more or less elastic, the elastic deformation of the parts involved in the force flow affects the BHF distribution on the sheet, often at an unacceptable level (Ref 13.11). Various factors have an impact on the deformation of the cushion system:

- Variation in the height of the cushion pins
- Slide tilting due to off-center loading
- Deflection of the cushion table/pressure box due to off-center loading

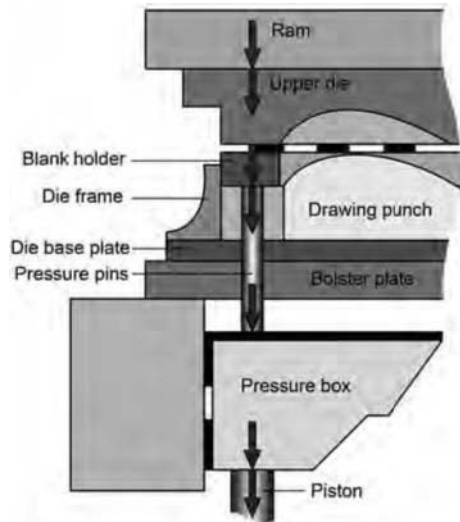


Fig. 13.13 Typical force flow diagram of a single-action press with in-press die cushion system. Source: Ref 13.2

Variation in Pin Heights. Cushion pins transmit force between blank holder and the pressure box. If there are differences in pin heights, then only the taller pins establish contact with both the blank holder and pressure box. Thus, only the taller pins transmit the applied force, while the shorter pins sit on the pressure box surface without coming into contact with the blank holder (Fig. 13.14). This leads to high contact pressure at the sheet-die interface near taller pins and negligible or no contact pressure at sheet-die interface near shorter pins. This nonuniform pressure distribution can result in an undesired pressure distribution in the blank holder, which may in turn cause unpredictable fracture or wrinkling in the deep drawn part. Studies have shown that the force transmitted by individual pins is very sensitive to pin height and the total applied BHF. With higher BHF, forces transmitted by taller pins result in local deflection, causing smaller pins to come into contact with the blank holder. As a result, the forces transmitted by the pins were more uniform compared to force transmitted by individual pins at lower BHF (Ref 13.11). The wear and tear of the pins due to continuous usage also affects the deflections in the blank holder. The use and maintenance of cushion pins are therefore important in controlling part quality in deep drawing with hydraulic cushions.

Slide Tilting Due to Off-Center Loading. Off-center loading during deep drawing may

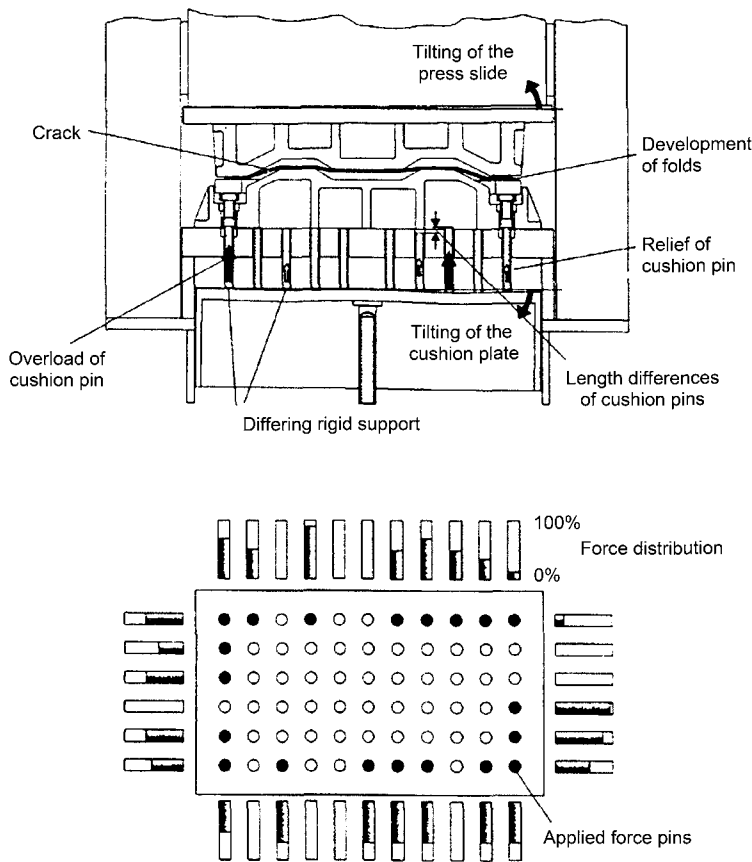


Fig. 13.14 Effect of variation of pin height on the force transmitted by individual pins. Source: Ref 13.6

occur because of the shape of the formed part, resulting in tilting of the slide. Off-center loading is more common in a single-slide transfer press where several dies that perform different operations are attached to the same slide. Each operation requires maximum load at different instants during stroke, and ram tilting may result. This slide tilting may cause loss of contact between the sheet and blank holder at certain locations and may give higher contact pressure at other locations. As a result, the force distribution on the cushion pins also changes, causing tilting of the pressure box/cushion table (Fig. 13.15) (Ref 13.5, 13.11).

Deflection of Pressure Box. The majority of pressure boxes built in stamping presses are supported by four cushion cylinders in the corners, which provide the cushion force. However, depending on the part geometry, the location of the cushion pins on the pressure box

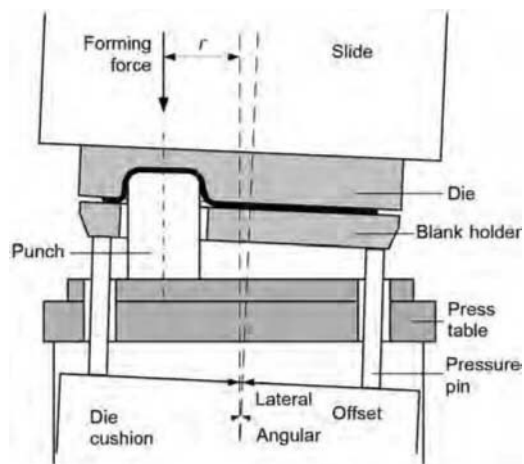


Fig. 13.15 Schematic of ram and blank holder tilting in single-action press due to off-center loading. Source: Ref 13.5

varies and may not be symmetric. Hence the loading on the pressure box also will not be symmetric, and the box may be deflected (Fig. 13.16).

Compensation for Pin Height Variation and Slide Tilting. Reference 13.6 used hydraulic cylinders to compensate for pin height variations. Reference 13.13 used servo-motor-driven, height-adjustable cushion pins with load cells mounted on the pressure box. This system compensates for the variation of the height in cushion

pins and adjusts the height of pins such that the forces transmitted by the pins are all equal. These measures, developed to compensate for the height variations in cushion pins, help to improve process control in deep drawing, but they add additional complexity and costs to the cushion designs.

13.3 Multipoint Cushion (MPC) Systems

In deep drawing large body parts, metal flow into the die cavity is nonuniform. Therefore, BHF that varies by location on the blank holder can control metal flow and part quality more accurately. For this reason, modern cushion systems include multipoint control capabilities.

In-Press Systems

Designs of multipoint cushion systems can be broadly classified into two types: (a) cushion systems that transmit the cylinder force through the pressure box and cushion pins to the blank holder, and (b) cushion systems that directly apply the cylinder force to the blank holder. In type (a), more cylinders are added to the pressure box to provide the BHF. Each cylinder is independently controlled and can apply a different force, thereby achieving the variation of force in space. The number of cylinders added to apply force on the pressure box ranges from four to eight (Fig. 13.17).

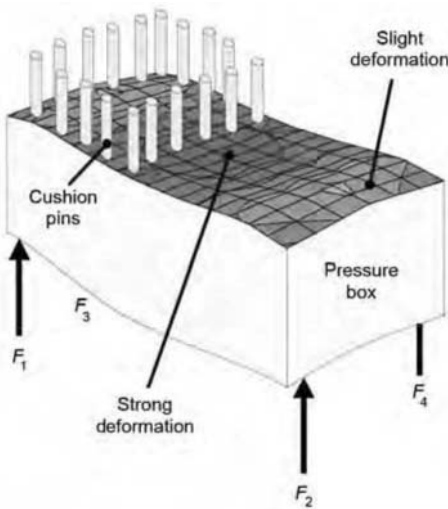


Fig. 13.16 Schematic of deflection of the pressure box due to nonuniform loading of the cushion pins.
Source: Ref 13.12

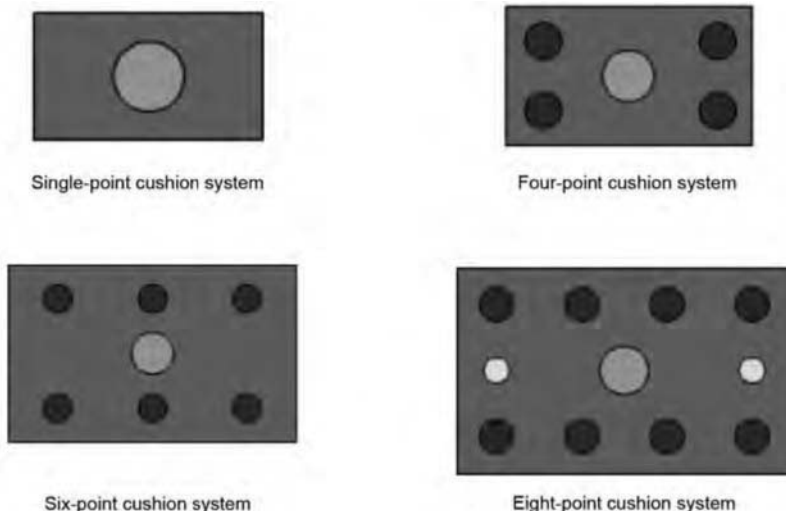


Fig. 13.17 Layout of single-point, four-point, six-point, and eight-point cushion system built in the press. Source: Ref 13.2

In type (b), the cushion cylinders directly apply the BHF to the blank holder in the absence of pressure box and cushion pins (Fig. 13.18). Each cylinder is independently controlled so that the BHF can vary with location.

One of the most successful applications of an MPC system worldwide is in the deep drawing of stainless steel sinks. In this application, the material flow is regulated precisely (Fig. 13.19). In order to provide accurate performance even

under highly eccentric loads, the ram is clamped against hard stops and the BHF is applied by short-stroke cylinders.

In the manufacturing of stainless steel sinks, high surface quality, especially in the flange area, is required; that is, no visible wrinkles are allowed (Ref 13.11). In general, the flange areas on the long sides tend to wrinkle because of blank holder pressure reduction caused by sheet thickening in the flange corners. The stability of the bridge area is very sensitive; no material can be fed into the cavity from this region. Therefore, the blank holder pressure has to be very high in this area to prevent material flow (Fig. 13.20).

In-Die Systems

Pressure distributions similar to the one shown in Fig. 13.20 can also be achieved by using an electronic shimming that is built into the die (Ref 13.14). This application uses a plate approximately 3 in. thick with built-in membranes that transfer the hydraulic pressure to the appropriate areas of the blank holder. Other in-die systems use hydraulic or nitrogen cylinders, located in the die shoe.

Systems with Hydraulic Cylinders. Single-action and double-action hydraulic cylinders can be mounted on the die shoe and used as cushion cylinders to apply the BHF. Hengelhaupt et al. (Ref 13.15) from Institut für Umfor-



Fig. 13.18 Schematic of the cushion system built in the die. Source: Ref 13.15

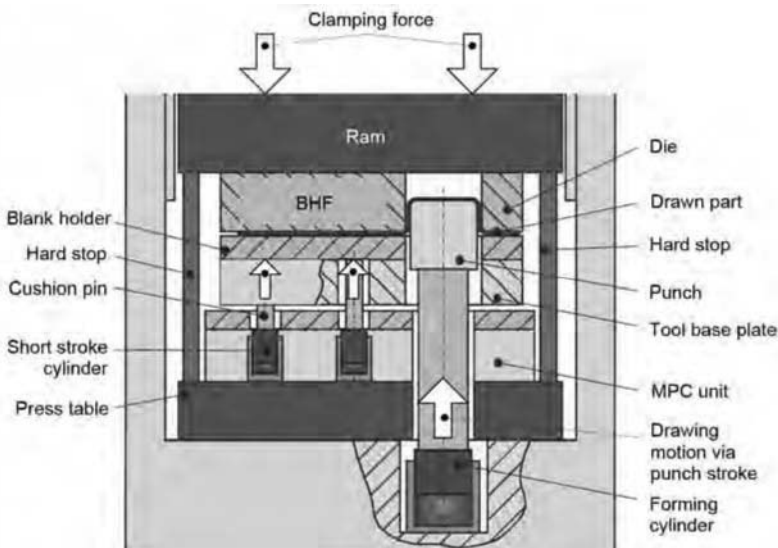


Fig. 13.19 Deep drawing of stainless steel sinks with multipoint cushion (MPC) technology. BHF, blank holder force. Source: Ref 13.11

mtechnik at Universität (IFU) Stuttgart in cooperation with Moog Inc. and HYDAC, as part of the research project USCAR, developed a hydraulic built-in die cushion system for part geometry (Fig.13.18). The system has 10 hydraulic cylinders. Each cylinder is independently controlled and can generate a BHF varying with stroke. The system can be operated in both mechanical and hydraulic presses. Preacceleration and delayed return functions are achieved by double-action cylinders. This research unit has a closed-loop control to adjust the BHF automatically based on punch force and wrinkles in the flange area of the stamping. This unit illustrates the principles of commercially available MPCs.

A similar system was built for practical-part geometry (GM inner lift gate) with 26 independently controlled hydraulic cylinders, as part of

the same research program (Ref 13.16). The Engineering Research Center for Net Shape Manufacturing at The Ohio State University developed a hydraulic built-in die cushion system that uses an accumulator as hydraulic power source (Fig.13.21). This system also illustrates the design principles of modular MPC systems, which are used in many commercial presses. The hydraulic cushion cylinder is connected to the accumulator by a servo valve, a check valve, and a relief valve. During forming, as the cylinder is moving downward, the servo valve controls the fluid flow from the hydraulic cylinder to the accumulator, thereby maintaining the desired pressure in the hydraulic cylinder to provide the BHF. The spool position in the servo valve is computer controlled based on the measured line pressure and the stroke of the slide. Thus, the user can define a force-stroke profile.

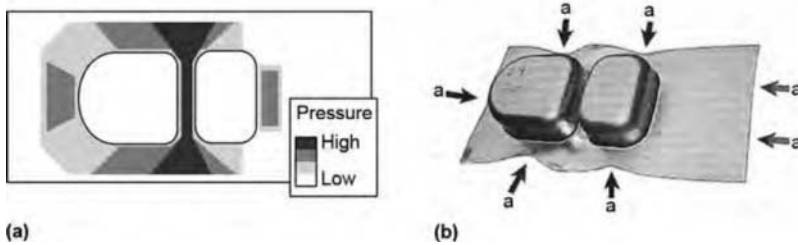


Fig. 13.20 Schematic of (a) blank holder pressure distribution and (b) stainless steel sinks produced using MPC technology. Source: Ref 13.11

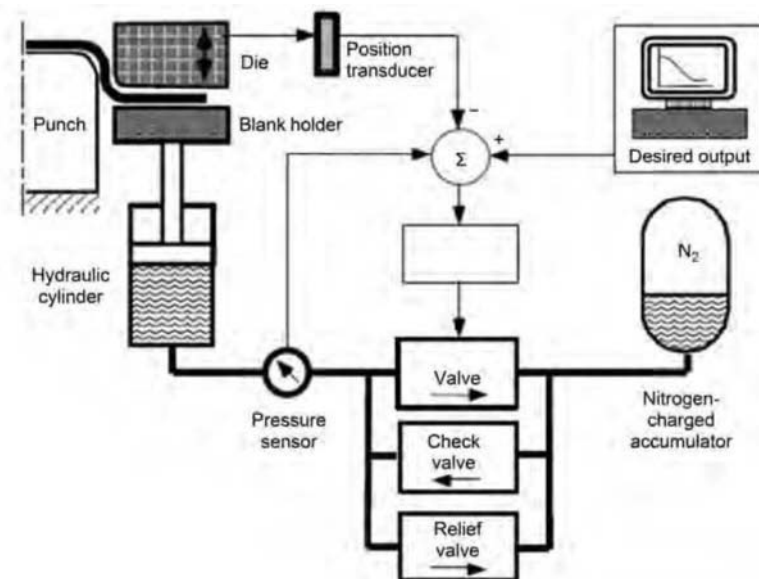


Fig. 13.21 Schematic of hydraulic built-in die cushion system using an accumulator as power source, developed at the Engineering Research Center for Net Shape Manufacturing. Source: Ref 13.17

During the return stroke, the fluid from the accumulator is used to fill the cylinder and lift the blank holder back to the top dead center (Ref 13.18).

A Force Modulator System supplied by Metalforming Controls Corporation (Ref 13.19) consists of hydraulic cylinders connected with a common manifold, which is provided by a hydraulic power source (pump, tank, and accumulator). The tonnage of each cylinder can be controlled and can vary with stroke. The entire unit rests in a lower die shoe. The hydraulic cylinders provide preacceleration to avoid initial impact, and bottom delay to avoid pad bounce as in press cushions (Ref 13.20).

Systems with Nitrogen Cylinders. The principle of nitrogen cylinder cushions is similar to pneumatic cushions, except that instead of compressed air, compressed nitrogen gas is used as a pressurizing medium. The design of nitrogen cylinders is such that the cylinder force does not increase significantly with the piston displacement (Fig. 13.22). Furthermore, nitrogen cylinders offer high load density and allow compact packaging in the die. They are therefore preferred to mechanical springs.

The three most common designs of nitrogen cylinders used in cushions are (a) one-chamber design, (b) two-chamber design, and (c) modified two-chamber design.

The one-chamber system consists of the piston sliding against the compressed nitrogen gas in the cylinder (Fig. 13.23a). During the downward motion, the piston is guided in the cylinder,

and the area above the piston is exposed to atmosphere. Since the gas is trapped in the cylinder, the pressure increases, and this increase leads to an increasing force-stroke curve. The pressure inside the cylinder can increase by as much as 70% of the initial cylinder pressure. One-chamber systems are commonly used for short-stroke applications (Ref 13.23).

Two-chamber systems consist of a piston that compresses nitrogen gas in a cylinder as in a single-chamber design (Fig. 13.23b). However, during the downstroke, the volume above the piston is filled with nitrogen gas from the lower chamber. The gas flows through the valves in the piston head. The gas flow reduces the compression of the gas and the buildup in pressure beyond the charge pressure. Thus, the force applied by the cylinder is relatively constant, with a maximum increase of 10 to 20%. Two-chamber systems are commonly used for large-stroke applications. In the modified two-chamber design, valves at the top and bottom of the cylinder allow the gas to flow in and out of the chamber above and below the piston during the downward motion. However, there is no valve in the piston head to connect the two chambers, so it is possible to maintain two different pressures at either side of the piston.

The use of nitrogen cylinders as a cushion system can be broadly classified into two types: (a) autonomous (Fig. 13.24a) and (b) system installation (Fig. 13.24b). Autonomous systems consist of independent nitrogen cylinders that are not attached to an external circuit. System

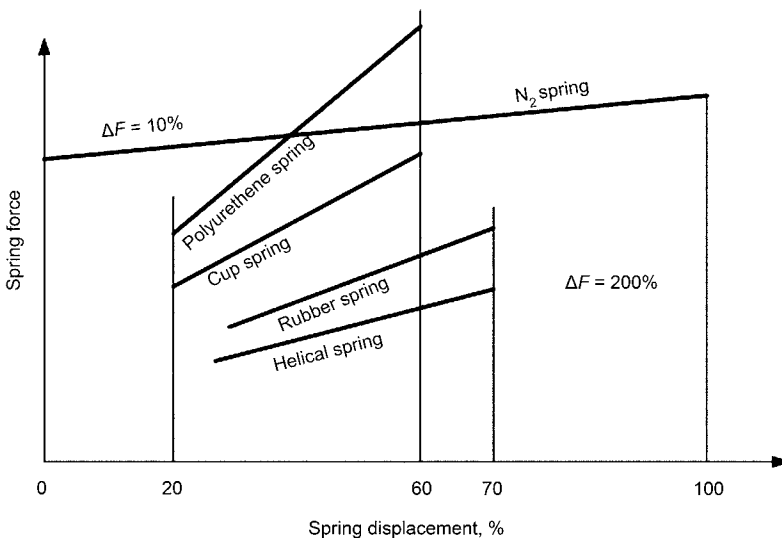


Fig. 13.22 Force characteristics of nitrogen springs compared to other springs. Source: Ref 13.21

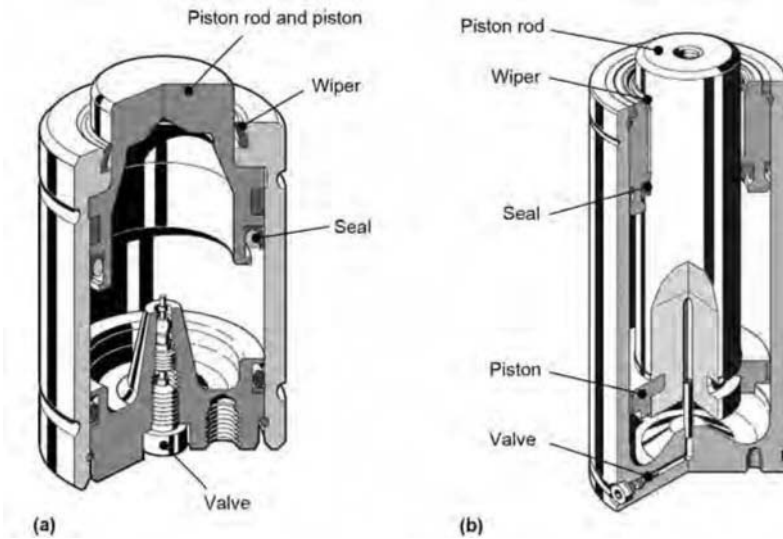


Fig. 13.23 Schematic of (a) one-chamber nitrogen cylinder and (b) two-chamber system. Source: Ref 13.22

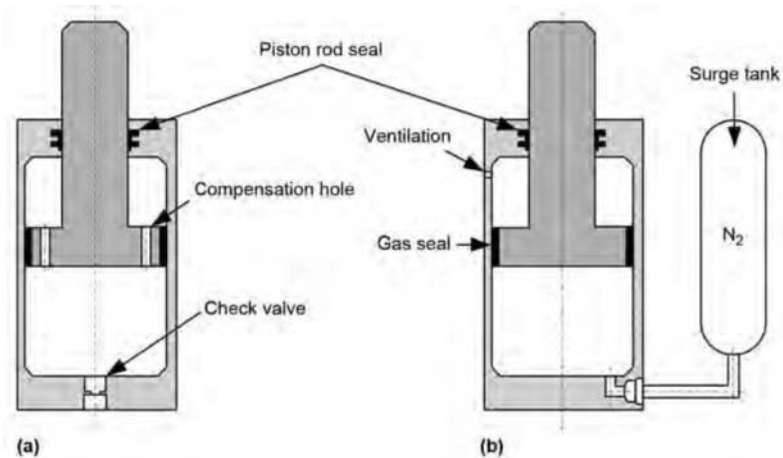


Fig. 13.24 Schematic of common types of nitrogen cylinder installed as cushions: (a) autonomous gas spring and (b) gas spring system cylinder. Source: Ref 13.13.

installations are characterized by nitrogen cylinders that are attached to a surge tank; gas flows from the cylinder to the tank during the piston's downstroke.

In a self-contained gas spring, each autonomous nitrogen cylinder is charged independently to the desired pressure and bolted onto the lower die shoe. The cylinders operate independently from each other.

In hosed systems, the autonomous cylinders are connected by a hose to a control valve that allows the cylinders to be charged and discharged simultaneously. The same pressure is maintained in all hosed cylinders (Ref 13.23).

In a manifold system, nitrogen cylinders are attached to a metal plate that has a large-diameter metal hose connecting all the cylinders and acting as an accumulator (Fig. 13.25) (Ref 13.24). The metal plate has a control panel that allows charging and discharging of all the cylinders simultaneously. The presence of accumulator-like features reduces the increase in the pressure during the downward stroke to a maximum of 10 to 20%, depending on the forming velocity (Ref 13.23).

In controllable nitrogen cylinders, it is possible to reduce the cylinder pressure with the piston stroke (Fig. 13.26). During the downstroke,

the nitrogen gas in the bottom chamber is forced to pass through a flow control valve and a two-way flow valve to reach the top chamber. Initially the flow control valve is closed leading to a pressure increase. Once the valve is opened, the force decreases drastically as the pressure in the bottom chamber decreases due to the gas flow into the top chamber, where the gas exerts an opposite force on the piston head. Replacing the flow-controlled valve with a servo valve and a closed-loop control system enables nitrogen cylinders to follow user-defined force-stroke curves (Ref 13.21, 13.23).

Preacceleration to avoid initial die impact can be achieved with nitrogen cylinders, equipped with hydraulic timing cylinders (Fig. 13.27). The nitrogen cylinder attached to the blank holder is connected to the timing cylinder via a hydraulic circuit. The cross-sectional area of the timing cylinder is less than the cross-sectional area of the nitrogen cylinder. During the downstroke, the slide first comes into contact with the timing cylinder pin and compresses the hydraulic fluid from the timing cylinder to the top

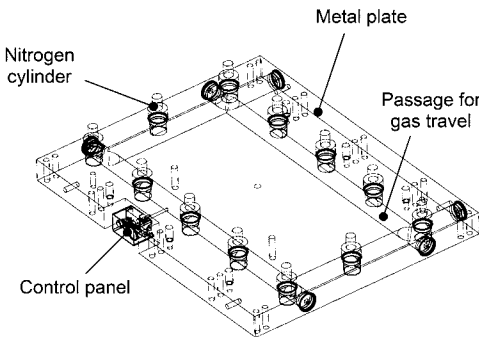


Fig. 13.25 Schematic of manifold system installation. Source: Ref 13.24

chamber of the nitrogen cylinder. Because of the differential pressure in the nitrogen cylinder chambers, the piston tends to move down, resulting in downward motion of the blank holder. The relative velocity between slide and blank holder depends on the amount of fluid flow from the timing cylinder, the cross sectional areas of the timing cylinder, and the nitrogen cylinder. Since the cross section of the hydraulic cylinder is smaller than that of the nitrogen cylinder, the blank holder moves more slowly than the slide. Generally, the blank holder moves down with 80% of the slide's velocity. As soon as the blank holder touches the die, the BHF is applied by the compressed nitrogen gas in the bottom cylinder chamber (Ref 13.24).

Delay at BDC to avoid pad bounce can be achieved by using a delay circuit and additional cylinders (Fig. 13.28). The nitrogen cylinder is connected to a so-called prime cylinder and a timing cylinder via two different hydraulic circuits (Ref 13.24).

During the downstroke, valve A is open, allowing fluid flow from the prime cylinder into the top chamber of the delay cylinder. Since valve B is closed, the fluid in the timing cylinder is compressed by the nitrogen gas in the

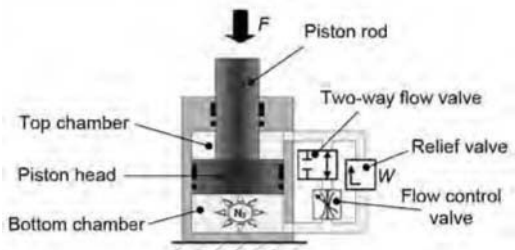


Fig. 13.26 Schematic of the controllable gas spring. Source: Ref 13.23

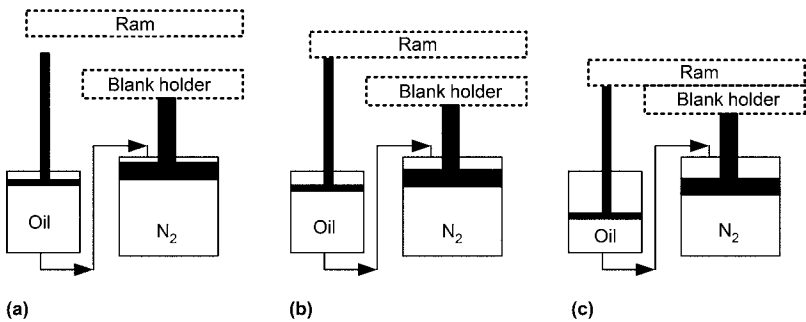


Fig. 13.27 Preacceleration of the blank holder using nitrogen cylinders: (a) initial setup; (b) preacceleration; (c) ram catches blank holder. Source: Ref 13.24

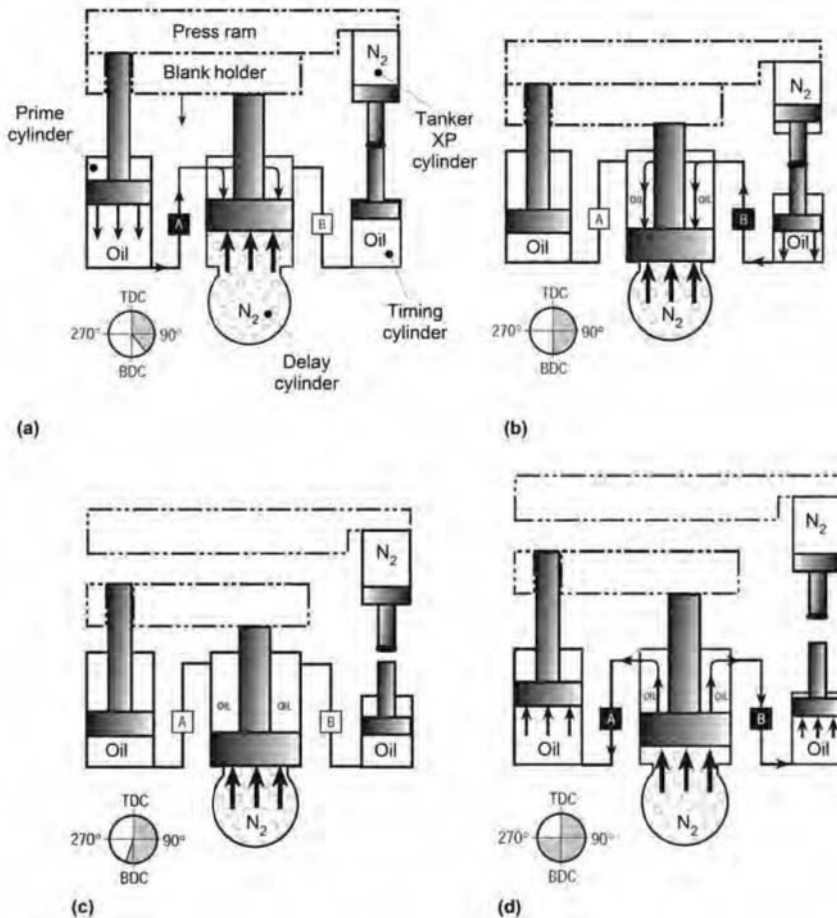


Fig. 13.28 Working sequence of the delay circuit: (a) downstroke, (b) compression of the fluid in the timing cylinder, (c) blank holder retained at bottom dead center (BDC), and (d) main cylinder retracts to original position; top dead center (TDC). Source: Ref 13.24

Tanker XP cylinder (Fig. 13.28a). Toward the end of the stroke, valve B is opened and valve A is closed. The high-pressurized fluid from the timing cylinder fills the top chamber of the delay cylinder and locks the piston down (Fig. 13.28b). The blank holder is retained at the BDC as both valves A and B are closed (Fig. 13.28c). After a defined time delay both valves are opened, allowing the main cylinder to retract to its original position (Fig. 13.28d) (Ref 13.24). Similar designs that allow a delay at BDC are available by various manufacturers of nitrogen cylinders (Ref 13.24, 13.25).

Application of Nitrogen Cylinders in MPC Systems. Built-in cushion systems have nitrogen cylinders or hydraulic cylinders that are attached to the lower die shoe and apply force on the blank holder. The cylinders are usually connected to a power source, and therefore, the

pressure in all the cylinder remains the same. However, each cylinder can always be connected to an independent power source, allowing the BHF to be varied between consecutive cylinders and resulting in an MPC system. Having an independent power source for each cylinder significantly increases the auxiliary units that come with each cylinder and therefore cannot be packed into the lower die shoe. Auxiliary units are placed next to the press and are connected to the tool (Ref 13.26, 13.27).

Programming of MPC Systems

Implementing an MPC system in presses or tools allows varying the BHF with location and stroke. However, this capability is underutilized in current production because it is difficult to estimate the BHF that should be applied by each

cushion cylinder; and conventional steel sheets can be formed with the existing method that involves using a BHF that is uniform on the blank holder and constant in stroke.

Increasing complexity of the parts and increasing use of lightweight materials with low formability require the use of MPC capabilities to better control the material flow and expand the process window. Successful application of an MPC system to form complex parts demands a methodology to predict the BHF for each cushion cylinder before the first part is stamped. In practice, the required BHF to form a part is usually estimated by trial and error based on the experience of the die maker and the press operator. This approach is feasible for single-point cushions, since only one force variable needs to be determined. However, in MPC systems, there are as many variables as the number of independent cushion cylinders that can be controlled. Thus, the trial-and-error approach is ineffective and time-consuming. The determination of the individual BHF on each cushion cylinder is best determined by finite element (FE) simulations in the process design stage. The Engineering Research Center for Net Shape Manufacturing, as part of an USCAR project, developed an optimization methodology coupled with commercial finite element codes to estimate the BHF for individual cylinders in MPC systems (Fig. 13.28, 13.29) (Ref 13.1).

The estimation of an optimum BHF for MPC systems is formulated as an optimization problem with the BHF as the design variable and with minimization of the risk of failure by tearing in the part as a design objective. The constraints are the wrinkles in the formed part that need to be avoided. This optimization problem cannot be solved analytically. Therefore, optimization techniques coupled with FE simulations were used. The objective function and the

constraint functions for the optimization were calculated from the results of FE forming analysis. This methodology was applied to estimate the BHF variable in space and constant in stroke to form a full size-automotive panel (inner lift-gate) from three different materials using the 26-point hydraulic cushion built as part of the USCAR project. An example of a BHF profile estimated by the developed methodology for A6111-T4 material is shown in Fig. 13.30.

Forces for only 15 pins are calculated since the part geometry is symmetric and the same force was used for pins at symmetric positions. The same method was used to form this part from three different materials (Al6111-T4, 1 mm thick; bake-hardened steel BH210, 0.8 mm thick; DP600, 0.8 mm thick) using the same die by changing only the BHF, illustrating the enhancement in the robustness of the process by using MPC systems. The force applied by each cylinder for each sheet material was different and estimated by the developed routine (Ref 13.1).

REFERENCES

- 13.1 H. Palaniswamy and T. Altan, Programming Multipoint Cushion Systems—Progress and Future Work, *New Developments in Sheet Metal Forming*, IMFU, 2006
- 13.2 Muller Weingarten AG (now part of Schuler Group - www.schulergroup.com) Basic Principles of Drawing Technology, *Technology Journal*, 1999, www.Müller-weingarten.de/English/Technology
- 13.3 M.E. Dingle, P.D. Hodgson, and M.J. Cardew-Hall, Analysis of the Elastic Behavior of the Press Systems in Draw Die Forming, *Innovations in Processing*

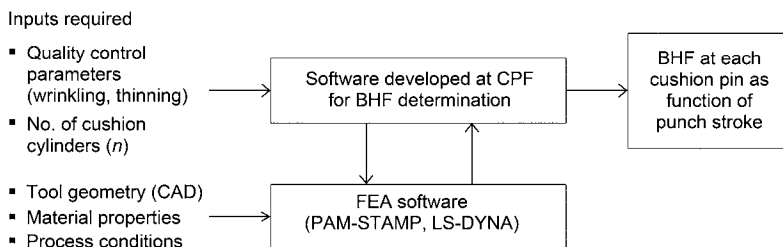


Fig. 13.29 Flow chart of program to estimate optimum blank holder force (BHF) required to program multipoint cushions; computer-assisted design (CAD); Center for Precision Forming (CPF); finite element analysis (FEA).

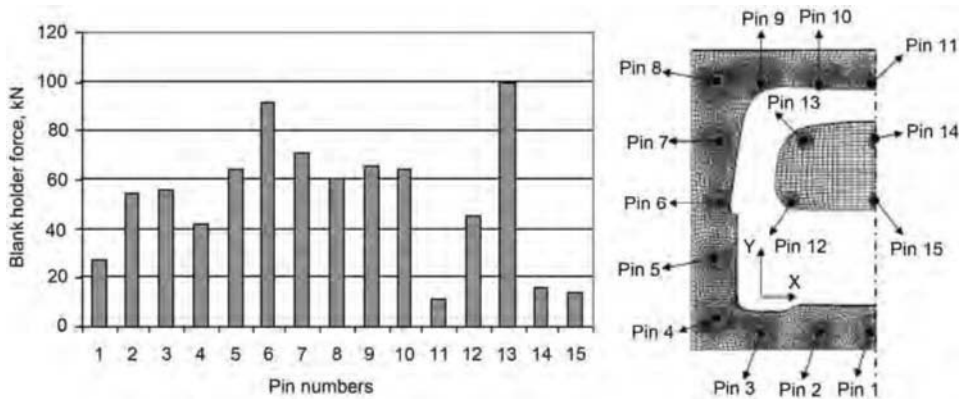


Fig. 13.30 Optimum blank holder force variable in space and constant in time (predicted by optimization for forming the lift gate part from aluminum alloy A6111-T4 of 1 mm thickness)

- and *Manufacturing of Sheet Materials*, 2001
- 13.4 H. Hoffmann, *Comparative Studies in Hydraulic and Pneumatic Drawing Devices*, DGM Informations GmbH, 1991
- 13.5 H.W. Wagener, New Developments in Sheet Metal Forming: Sheet Materials, Tools and Machinery, *Journal of Materials Processing Technology*, Vol 72, 1997, p 342–357
- 13.6 K. Kirii, M. Shinabe, Y. Hirabayashi, and M. Akiyama, “Binding Force Control of Uni-pressure Cushion in Automobile Stamping,” SAE paper 950916, 1995
- 13.7 H. Cherek and C.P. Neumann, *Die Cushions on Hydraulic and Mechanical Presses*, DGM Informations GmbH, 1991
- 13.8 Schuler, *Metal Forming Handbook*, Springer, 1998
- 13.9 *Modulares hydraulischer Tischkissen*, Schuler GmbH, 2007
- 13.10 F.X. Kürzinger, New Concepts for Hydraulic Production Press, *New Developments in Sheet Metal Forming*, IFU, Technical University Stuttgart, 2000
- 13.11 K.-J. Pahl, New Developments in Multi-point Die-Cushion Technology, *Journal of Material Processing Technology*, Vol 71, 1997, p 168–173
- 13.12 J. Hohnhaus and D. Schollhammer, Holistic View of the Press-Die System for the Production of Automotive Parts, *New Developments in Sheet Metal Forming*, IFU, Technical University Stuttgart, 2000
- 13.13 K. Siegert, M. Haussermann, D. Haller, S. Wagner, and M. Ziegler, Tendencies in Presses and Dies for Sheet Metal Forming Process, *Journal of Materials Processing Technology*, Vol 98, 2000, p 259–264
- 13.14 Hydraulic, www.hydraulic.com
- 13.15 J. Hengelhaupt, M. Vulcan, F. Darm, P. Ganz, and R. Schweizer, Robust Deep Drawing Process of Extensive Car Body Panels, *New Developments in Sheet Metal Forming*, IFU, Technical University Stuttgart, 2006
- 13.16 M. Demeri, Application of Flexible Binder Technology for Stamping of Light Weight Panels, *New Developments in Sheet Metal Forming*, IFU, Technical University Stuttgart, 2006
- 13.17 L. Schulkin, J. Rowan, T. Altan, and G. Kinzel, Experimenting with Flexible Blank Holder Force Control, *Stamping Journal*, July 12, 2001
- 13.18 L. Schulkin, J. Rowan, T. Altan, and G. Kinzel, Experimenting with Flexible Blank Holder Force Control, *Stamping Journal*, 2000, p 36–41
- 13.19 Metalforming Controls Corporation, www.mfcontrols.com
- 13.20 T. Altan, Using Binder Force Control, Force Modulation to Improve Part Quality, *Stamping Efficiency*, *Stamping Journal*, July/August 2003, p 44
- 13.21 K. Siegert and D. Haller, Controllable Nitrogen Gas Spring Systems, *Production Engineering*, Vol 8 (No. 1), 2001, p 63–67

- 13.22 Nitrogen Gas Cylinders, Fibro Product Catalogue, FIBRO, 2010
- 13.23 D. Haller, Controllable Nitrogen Gas Spring Systems for Stamping Applications, *New Developments in Sheet Metal Forming*, IFU, Technical University Stuttgart, 2000
- 13.24 Nitrogen Cylinders, Hyson Product Catalogue, 2007
- 13.25 Controllable Gas Springs, Kaller Product Catalogue, 2010
- 13.26 K. Siegert, Research and Development in Sheet Metal Forming at the Institute for Metal Forming Technology of the University of Stuttgart, *New Developments in Sheet Metal Forming*, IFU, Technical University Stuttgart, 2004
- 13.27 S. Rittmeier, "Systemunterstützte Umformung," Ph.D. dissertation, Technical University of Dresden, Cuvillier, 2007

Abbreviations and Symbols

q_d	die angle	CDV	critical damage value
q_p	punch tip angle	C.L.	curvilinear length
A	area, geometric contact area, instantaneous cross-sectional area	CMM	coordinate measuring machine
		CNC	computer numerical controlled
		COF	coefficient of friction
A_a	apparent contact area	CP	complex-phase, commercially pure
A_{BH}	area of the blank under the blankholder	CPF	Center for Precision Forming
A_f	cross-sectional area at fracture	CQ	commercial quality
A_p	cross-sectional area of the punch	CR	cold rolled
A_{piston}	area of piston	CVD	chemical vapor deposition
A_r, A_s	area reduction, real contact area	d	punch stroke, diameter, diameter of mandrel, vertical deflection, dimpling
A_s	area of the cut surface		
A_0	original cross-sectional area	d_b	blank diameter, diameter of blankholder
ac	alternating current	d_c	diameter of die cavity
AHSS	advanced high-strength steel	d_d, D_d	die diameter, punch-die clearance
AISI	American Iron and Steel Institute	d_f	diameter of flanged hole after flanging
AKDQ	aluminum-killed drawing quality	$d_{F,max}$	outside diameter of flange when drawing load is maximum
AS	adaptive simulation	d_h	diameter of pierced hole
ASAME	Automated Strain Analysis and Measurement Environment	d_m	diameter of the cup wall at max- imum drawing force
b	width of die opening	d_p, D_p	punch diameter, external cup diameter at maximum drawing force
BA	bend allowance	d_s	punch stroke
bcc	body-centered cubic	d_0	initial diameter, blank diameter
BD	bend deduction	d_1	inner cup diameter
BDC	bottom dead center	de	infinitesimal engineering strain
BEF	Bauschinger effect factor	dl	differential change of length
BH	bake hardening, bake hardenable	dt	infinitesimal time
BHF	blankholder force	$d\epsilon$	infinitesimal natural strain
BHP	blankholder pressure	$d\epsilon_{xy}$	infinitesimal shear angle change
c	Cowper-Symonds coefficient	D	diameter, sag
c	empirical factor, width of warp	D_{cp}	depth of crack penetration
c_d	speed of sound	D_F	mandrel diameter
c_p	heat capacity		
C	die clearance, stiffness		
C_F	compression force, stiffness of the fluid column		
C_θ	angular stiffness		
CAD	computer-aided design		
CAM	computer-aided manufacturing		

D_p	punch diameter	F_R	ring force, radial force
D_0	diameter of initial blank	F_S	blanking force
dc	direct current	F_T	tangential force
DCV	directional control valve	F_V	vertical force
DDS	deep-drawing steel	fcc	face-centered cubic
DIN	German Industry Standard	F	index to define material flow
DP	dual phase	FE	finite element
DQ	drawing quality	FEA	finite-element analysis
DQSK	drawing quality, special killed	FEM	finite-element method, finite- element modeling
DR	dent resistant, draw ratio	FLC	forming limit curve
DS	drawing steel	FLD	forming limit diagram
e	engineering strain, endpoint of tool motion, eccentricity of the load	FRF	flexible roll forming
e_t	total elongation	h	clearance, depth of cup, slide position
e_u	uniform elongation	h_{conv}	convective heat-transfer coefficient
E	Young's modulus, elastic modulus, energy of deformation	h_d	bulge or dome height
E^*	Young's modulus in plane strain	h_{eff}	effective heat-transfer coefficient
E_{cushion}	cushion energy	h_o	original height
E_D	elastic deflection	$h(P)$	contact heat-transfer coefficient
E_{EM}	electric motor energy	h_{rad}	radiation heat-transfer coefficient
E_F	friction energy	H	height, surface hardness
E_{forming}	forming energy	H_e	heat-transfer coefficient with air
E_M	machine energy	H_t	heat-transfer coefficient
E_p	process energy	HCO	hem curved outboard
E_{slide}	slide energy	HDGA	hot dip galvanized
E_T	total energy	HDGI	hot dip galvanized
EA	evolutionary algorithm	HE	hole expansion
E-coating	electrocathodic coating	HER	hole expansion ratio
EDDS	extra-deep- drawing steel	HF	hot forming
EDDS+	extra-deep-drawing steel plus	HR	hot rolled
EL	elongation	HRB	Rockwell B hardness
EMF	electromagnetic forming	HRC	Rockwell C hardness
EP	extreme pressure	HSLA	high-strength, low-alloy
ERC/NSM	Engineering Research Center for Net Shape Manufacturing	HSPR	hydro-self-pierce riveting
ET	extreme temperature	HSS	high-strength steel
f	friction factor	HV	Vickers hardness
f^*	modified friction factor	I	moment of inertia, angular inertia, identity sensor
f_b, F_b	blankholder force	IE	Erichsen index
f_r	feed rate	IF	interstitial free
F	force, applied load	IFU	Institut für Umform- technik (Institute of Forming Technology)
F_b	bending force	ISF	incremental sheet forming
F_{BH}	blankholder force	ISM	inside of metal
F_c	clamping force, clamping load	ISO	International Organization for Standardization
F_d	deformation force	IUL	Institut für Umformtechnik und Leichtbau (Institute of Forming Technology and Lightweight Construction)
$F_{d,\text{max}}$	maximum punch force	J	deviatoric stress invariant
$F_{\text{draw,max}}$	maximum drawing force	k	empirical constant
F_f	friction force		
F_G	counterforce		
F_H	horizontal force		
F_N	normal force		
F_P	punch force		

k	stripping constant, heat conductivity, shear strength, bend allowance	p_1	internal pressure
k_f	flow stress	p_{\max}	maximum pressure
K	springback ratio, strength coefficient, wear coefficient, shear flow stress	P	penetration, pressure, compression load, normal load, deformation power
K-B	Keeler-Breizer equation	P_b	blankholder pressure
KSIF	kinematic incremental sheet forming	P_e	interface pressure
l	distance, length, roll spacing	P_f	fluid pressure
l_F	total elongation at fracture	P_i	instantaneous pressure
l_o, l_0	original length	PPG	pulsed power generator
l_U	uniform elongation	PTFE	polytetrafluoroethylene
l_1	final length	PVD	physical vapor deposition
L	length, sliding distance, load	\dot{Q}	flow rate
L_d	draw-in length	QPF	quick plastic forming
L_{hem}	hem length	r	bending radius, tube radius, mean radius, instantaneous radius, plastic or normal anisotropy, plastic strain ratio or Lankford coefficient, eccentricity of the crank
L_M	machine load	r_{avg}	average strain ratio
L_{\min}	dimensions of smallest element	r_c	die cavity radius
L_o, L_0	initial length	r_d, r_D	die radius, die corner radius
L_p	process load	r_f	die fillet radius
L_{st}	stripping force	r_m	weighted average of strain ratios
LDH	limiting dome height	r_o	outer radius
LDR	limiting draw ratio	r_p	punch corner radius
LED	light-emitting diode	r_R	die corner radius
LVDT	linear variable differential transformer	r_z	radius of curvature in the longitudinal direction
m	friction factor	r_0	parallel to the rolling direction
m	friction shear factor, strain-rate sensitivity	r_{45}	diagonal to the rolling direction
m_r	modified shear factor	r_{90}	transverse to the rolling direction
M	index describing the shape of the yield loci	r_θ	bulge radius, radius of curvature in the hoop direction
M	bending moment, tilting moment, torque	r_{θ_0}	tube radius prior to deformation
MPC	multipoint cushion	\bar{r}, \bar{R}	normal anisotropy
MS	martensitic steels	Δr	planar anisotropy
n	strain-hardening coefficient, strain exponent, speed of crank in revolutions per minute, number of strokes per minute	R	rake, radius, bending radius, bend die radius, instantaneous outside radius, stress ratio, total eccentricity
n_p	number of strokes per minute under load	R_c	radius of die ring
n_0	number of strokes per minute when idle	R_d	die radius, bulge radius
OBI	open-back inclinable press	R_i	initial radius, inner bending radius
OD	outside diameter	R_m	mean bending radius, tensile strength
OEM	original equipment manufacturer	R_{\min}	minimum bend radius
OSM	outside of metal	R_n	neutral radius
p	Cowper-Symonds coefficient	R_o	outer bending radius
p	pressure, normal pressure, hydraulic pressure, magnetic pressure	R_p	punch radius, punch tip radius
p_{BH}	blankholder pressure	RD	rolling direction
		RT	room temperature

s	instantaneous sheet flange thickness, stroke, recoil	TRIP	transformation-induced plasticity
s_h	flange height	TS	tensile strength
s_{ij}	deviatoric stress state	TSA	thickness strain analysis
s_{\max}	maximum stroke	TW	tendency of wrinkling
s_0	initial sheet thickness, wall thickness, blank thickness	TWIP	twinning-induced plasticity
s_1	instantaneous sheet wall thickness	u	instantaneous material point velocity in the x -direction
S	strength, arc length of inner curve, yield stress, microstructure, stroke length, slide	u_D	punch-die clearance
S_r	pressure release displacement time	U_d	constant speed
S_s	shear strength	U_D	die clearance
S_{th}	theoretical displacement time	UHS	ultra-high speed
S_u	ultimate tensile strength	UHSS	ultrahigh-strength steel
SB	stretch bend	UTS	ultimate tensile strength
SDT	strip drawing test	v	distribution of tool motion, sliding velocity
SF	self-feeding	\dot{v}	instantaneous material point velocity in the y -direction
SHF-D	sheet hydroforming with die	v_p	punch velocity
SHF-P	sheet hydroforming with punch	V	velocity, volume
SMA	simplified modeling approach	V_p	slide velocity under pressure
SPIF	single-point incremental forming	V_{punch}	punch velocity
spm, SPM	strokes per minute	V_ϕ	angle distribution
SPR	self-piercing riveting	VPB	viscous pressure bulge
SQ	surface quality, structural quality	w	width, depth of warp
SS	structural steel	\dot{w}	instantaneous material point velocity in the z -direction
t	thickness, sheet thickness, time	W	width, V-die opening, worn volume
t_d	thickness at apex of bulge	W_d, W_D	die opening width
t_o, t_0	initial thickness	W_o	original width
t_p	time under pressure	y	distance
t_γ	austenitization time	Y	yield strength
T	thickness, sheet thickness, tension stress, temperature, applied torque	YS	yield strength
T_e	temperature of environment	z_b, Z_b	burr zone
T_f	temperature at forming	z_f, Z_f	fracture/rupture zone
T_F	tension load, tension force, final thickness	z_r, Z_r	rollover zone
T_i	initial temperature	z_s, Z_s	shear zone
T_O	original thickness	α	angle, measured angle, bending angle, crank angle, angular deflection, thermal expansion, heat-transfer coefficient, stress ratio, cone angle, real contact area ratio
T_{punch}	punch temperature	α_d	die angle
T_t	tool temperature	α_N	design angle
T_u	temperature of contact plates	α_p	punch tip angle
T_y	tension required for yield	β	camera angle, spinning ratio, depressor angle
T_γ	austenitization temperature	γ	clearance angle
T_0	initial temperature	Δr	planar anisotropy
TCT	twist compression test	ε	strain, true or natural strain
TD	transverse direction, thermal diffusion	$\dot{\varepsilon}$	strain rate
TDC	top dead center	ε_b	bending strain
THF	tube hydroforming	ε_e	elastic strain
TPIF	two-point incremental forming	ε_{el}	elastic strain
TRB	tailored rolled blanks		

$\varepsilon_{e,0}$	elastic limit	ρ_e	elastic radius of curvature
ε_o	initial strain	ρ_0	radius of curvature
ε_{pl}	plastic strain	σ	stress, flow stress, true normal stress
ε_r	strain in radial direction	σ_b	yield stress in balanced biaxial state
ε_t	total strain, strain in thickness direction, strain in tangential direction	σ_{CY}	compressive yield strength
ε_w	width strain	σ_e	engineering stress
ε_z	strain in axial direction	σ_f	flow stress
ε_0	prestrain	σ_m	stress quantity, mean stress
ε_θ	strain in the hoop direction	σ_n	normal stress
ε_ϕ	strain in the longitudinal direction	σ_{oc}	compression yield stress
$\bar{\varepsilon}$	equivalent strain, effective strain	σ_r	rupture stress, stress in radial direction
$\bar{\varepsilon}^P$	plastic strain	σ_t	stress in tangential direction
$\bar{\dot{\varepsilon}}$	equivalent strain rate, effective strain rate, von Mises equivalent plastic strain	σ_{UTS}	ultimate tensile strength
η	lubricant viscosity, deformation efficiency, efficiency factor	σ_Y	yield strength
θ	bending angle, punch angle, crankshaft rotation, temperature	σ_z	longitudinal stress, stress in axial direction
θ'	final bend angle	σ_0	initial yield stress
θ_p	half bending angle	σ	hoop stress
θ_s	springback angle	$\bar{\sigma}$	flow stress, instantaneous yield stress
θ_1	half angle (under load)	τ	shear stress, frictional shear stress
θ_2	half angle (unloaded)	τ_a	average shear stress at contacting asperity peaks
$\theta\theta$	hoop stress	τ_b	average shear stress at lubricant pockets
$\theta\phi$	axial stress	τ_f, τ_f	frictional shear stress
$\Delta\theta$	springback angle	τ_s	shear stress
κ	bulk modulus	ϕ	bend angle, logarithmic strain
λ	hole expansion ratio, roughness parameter	ω	angular speed or velocity
μ	coefficient of friction	2-D	two-dimensional
μ_m	mean coefficient of friction	3-D	three-dimensional
ν	Poisson's ratio		

APPENDIX A

Flow Stress Curves

Soumya Subramonian and Nimet Kardes, The Ohio State University

VISCOUS PRESSURE BULGE TESTS were conducted at The Ohio State University's Center for Precision Forming (CPF), formerly Engineering Research Center for Net Shape Manufacturing (ERC/NSM), in order to obtain the flow stress characteristics of various sheet materials, such as steels, stainless steels, and aluminum and magnesium alloys. These flow curves are better suited for analysis of forming operations when compared with flow stress obtained from tensile tests. This appendix presents mainly biaxial flow curves for different materials. For some of the sheet materials, flow stress curves obtained from tensile tests were also provided. Table A.1 lists materials that have been tested at CPF using the biaxial bulge test.

REFERENCES

- A.1 E. Doege and K. Dröder, Sheet Metal Forming of Magnesium Wrought Alloys—Formability and Process Technology, *Journal of Materials Processing Technology*, Vol 115, 2001, p 14–19
- A.2 S. Kaya and T. Altan, Warm Forming of Al and Mg: Part II, Determination of Magnesium Sheet Properties at Elevated Temperatures, *Stamping Journal*, 2006, p 32

Table A.1 Summary of flow stress data of various sheet materials

Figure	Material	Thickness	Source of data/CPF report no.
Steel			
Fig. A.1	St14	1 mm	CPF-4.2b/06/01
Fig. A.2	St1403	1 mm	CPF-4.2b/07/01
Fig. A.3	AISI 1018	2.13 mm	CPF-2.3/06/06
Fig. A.4	AKDQ	0.83 mm	CPF-2.1/06/01
Fig. A.5	1050	...	Viscous pressure bulge test conducted May 2005
Fig. A.6	DP 590	1.24 mm	CPF-2.3/07/02
	DP 600	1 mm	CPF-2.3/07/02
	DP 780	1 mm	CPF-2.3/07/02
	TRIP 780	1 mm	CPF-2.3/07/02
	DP 980	1 mm	CPF-2.3/07/02
	AKDQ	0.72 mm	CPF-2.3/07/02
Fig. A.7	DR 120	1 mm	CPF-2.1/06/02
Fig. A.8	DP 500	...	Viscous pressure bulge test conducted April 2008
	BH 210	...	Viscous pressure bulge test conducted April 2008
Fig. A.9	DP 600	...	CPF-1.4/07/03
Fig. A.10	DP 600	1 mm	CPF-2.1/09/01
Fig. A.11	DP 780	1 mm	CPF-2.1/09/01
Fig. A.12	DP 780-CR	1 mm	CPF-2.1/09/01
Fig. A.13	DP 780-HY	1 mm	CPF-2.1/09/01
Fig. A.14	TRIP 780	1 mm	CPF-2.1/09/01

(continued)

Table A.1 (continued)

Figure	Material	Thickness	Source of data/CPF report no.
Steel			
Fig. A.15	Bare DP 980 Y-type X	1.4 mm	CPF-5.1/09/01
	Bare DP 780 T-Si type	1.2 mm	CPF-5.1/09/01
	GA DP 780 T-Al type	1.2 mm	CPF-5.1/09/01
	GA DP 780 Y-type U	1.2 mm	CPF-5.1/09/01
	GA DP 780 Y-type V	1.2 mm	CPF-5.1/09/01
Fig. A.16	DQS-270F GA-phosphate coated	0.75 mm	CPF-2.5/09/01-a
	DQS-270D GA-phosphate coated	0.75 mm	CPF-2.5/09/01-a
Stainless steel			
Fig. A.17	SS 201	0.25 mm	ERC/NSM-08-R-01
	SS 301	0.25 mm	ERC/NSM-08-R-01
Fig. A.18	SS 304	1 mm	CPF-1.1/06/03
Aluminum alloys			
Fig. A.19	AA 6111	1.04 mm	CPF-2.1/06/01
Fig. A.20	AA 5754-O	1.3 mm	CPF-1.1/08/04
Fig. A.21	AA 5754-O	1.01 mm	CPF-1.1/08/04
Fig. A.22	Aluminum X626-T4P	0.95 mm	CPF-2.5/09/01-a
Magnesium alloys			
Fig. A.23	AZ31B	1 mm	(Ref A.1)
Fig. A.24	AZ31B-O	1.2 mm	CPF 1.1/06/01
			Temperature: room temperature to 225 °C
			Strain rate: 0.025 to 0.25 1/s
Various sheet materials			
Fig. A.25	AMS 5504	...	Test conducted May 2005
	AZ31B	...	Test conducted May 2005
	AKDQ	...	Test conducted May 2005
	SS 409	...	Test conducted May 2005
	HSS	...	Test conducted May 2005
	AA 5754-O	1.3 mm	CPF-2.1/07/01
	DP 600	0.6 mm	CPF-2.1/07/01
	DDS	0.77 mm	CPF-2.1/07/01

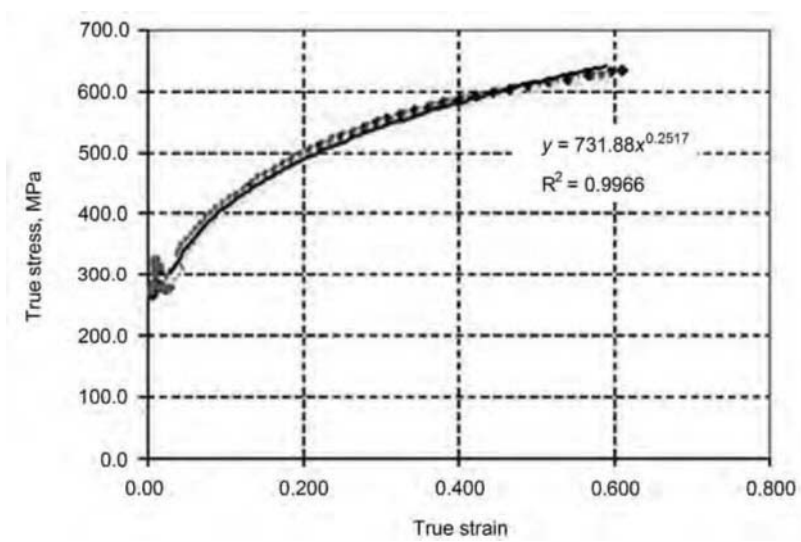


Fig. A.1 Flow stress of St14 (DC04) sheet material of thickness 1 mm estimated by viscous pressure bulge test

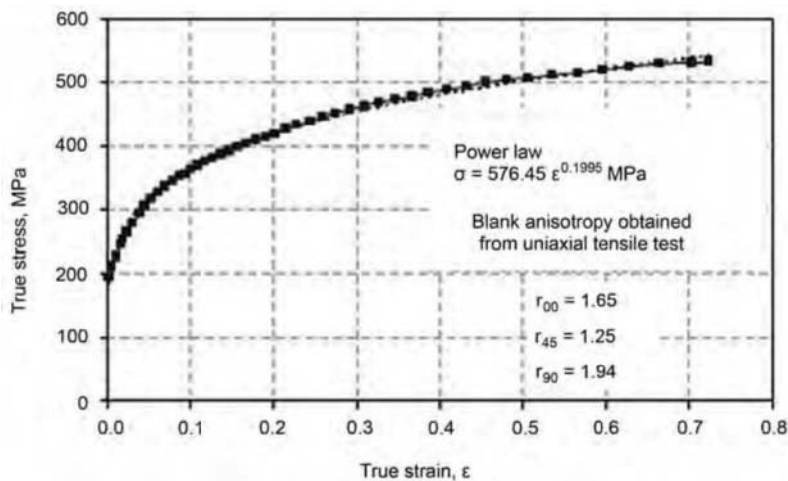


Fig. A.2 Flow stress of St1403 sheet material (1 mm) estimated by viscous pressure bulge test. Uniaxial tensile tests were conducted to obtain the anisotropy coefficients (r_0 , r_{45} , r_{90}). Experimental strain range, bulge test: 0 to 0.72

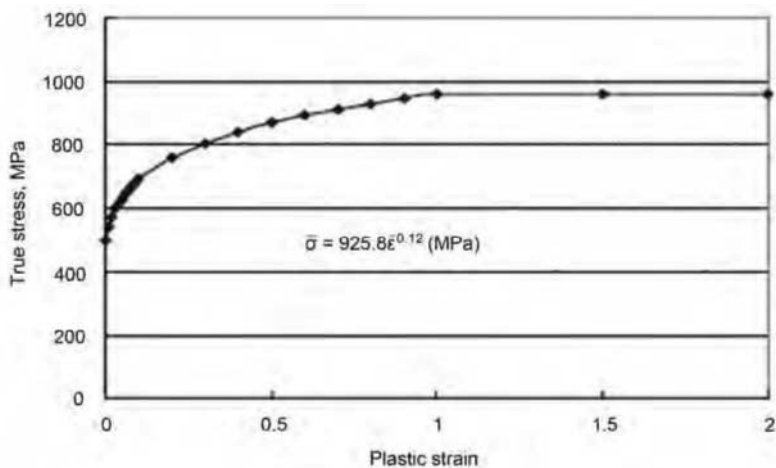


Fig. A.3 Flow stress of AISI 1018 sheet (2.13 mm) obtained by viscous pressure bulge test. Experimental strain range, bulge test: 0 to 1

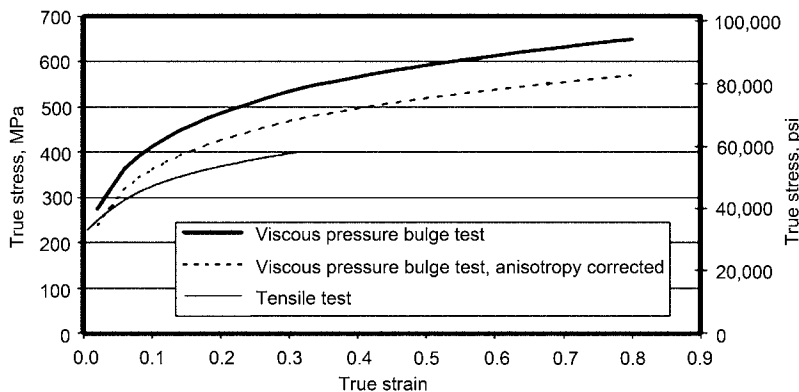


Fig. A.4 Flow stress of AKDQ steel sheet (0.83 mm) obtained by viscous pressure bulge test and uniaxial tensile test. Experimental strain range, tensile test: 0 to 0.32; bulge test: 0.25 to 0.8

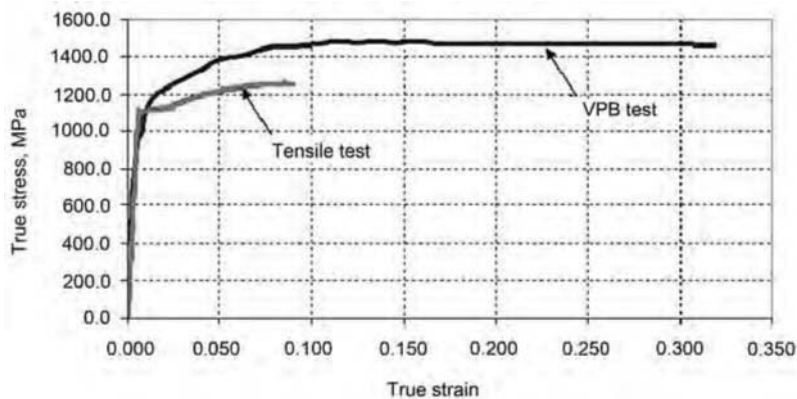


Fig. A.5 Flow stress of 1050 sheet obtained by viscous pressure bulge (VPB) test and tensile test. Experimental strain range, tensile test: 0 to 0.058; bulge test: 0 to 0.32

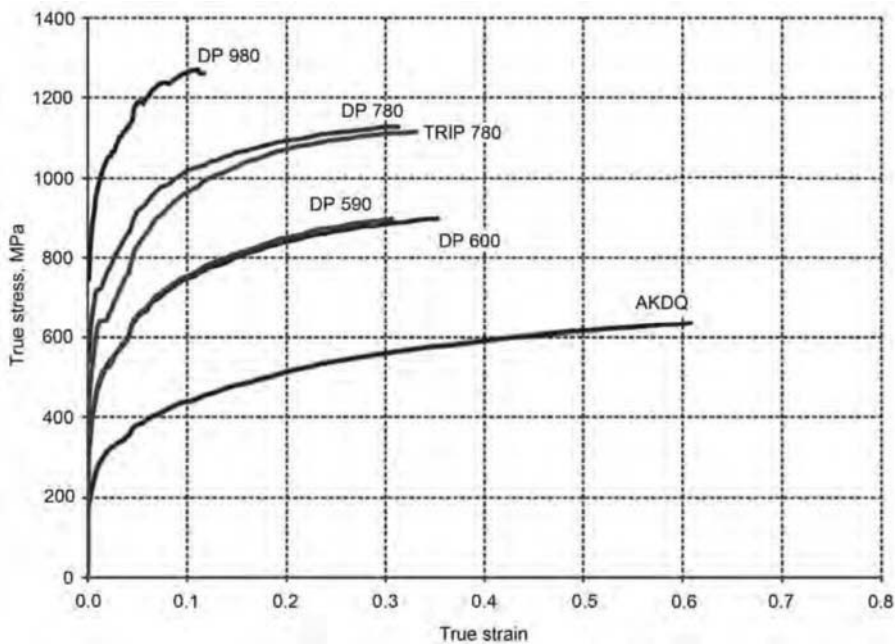


Fig. A.6 Flow stress of different sheet materials obtained by viscous pressure bulge test. The sheet material thicknesses were, for AKDQ, 0.72 mm; DP 600, 1 mm; DP 590, 1.24 mm; DP 980, 1 mm; DP 780, 1 mm; and TRIP 780, 1 mm. Experimental strain range, bulge test, DP 980: 0 to 0.12; DP 780: 0 to 0.32; TRIP 780: 0 to 0.34; DP 590: 0 to 0.31; DP 600: 0 to 0.35; AKDQ: 0 to 0.61

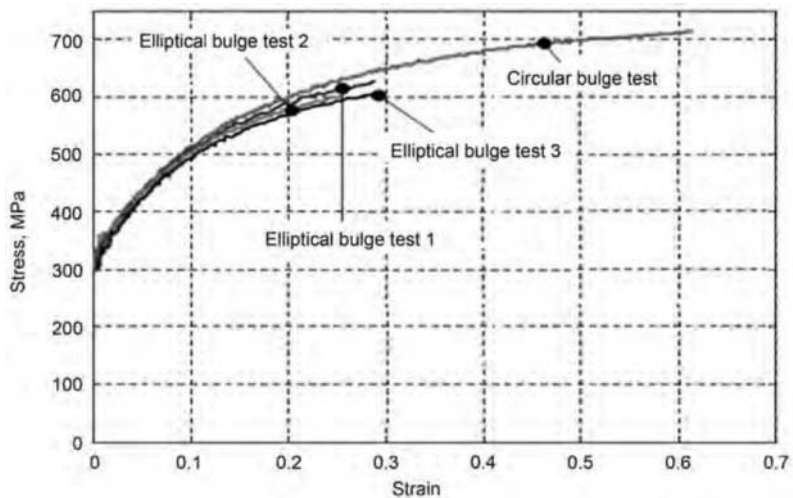


Fig. A.7 Flow stress of DR 120 (1 mm) obtained by circular and elliptical viscous pressure bulge tests. Experimental strain range, circular bulge test: 0 to 0.62

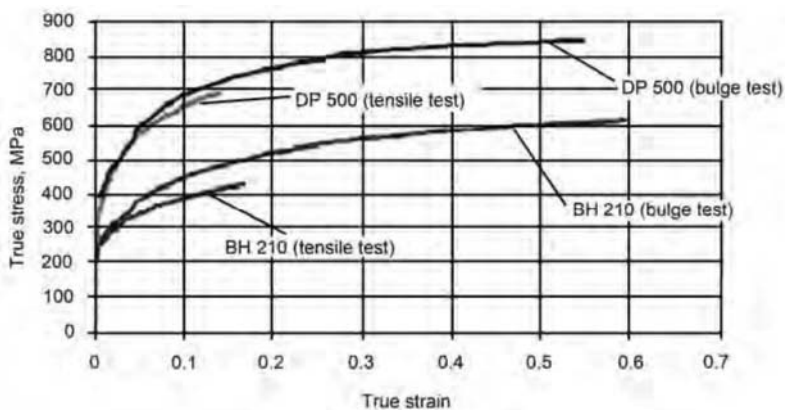


Fig. A.8 Flow stress obtained by viscous pressure bulge test and uniaxial tensile test for both DP 500 and BH 210 Experimental strain range, DP 500 tensile: 0 to 0.14; DP 500 bulge: 0 to 0.55; BH 210 tensile: 0 to 0.17; BH 210 bulge: 0 to 0.6.

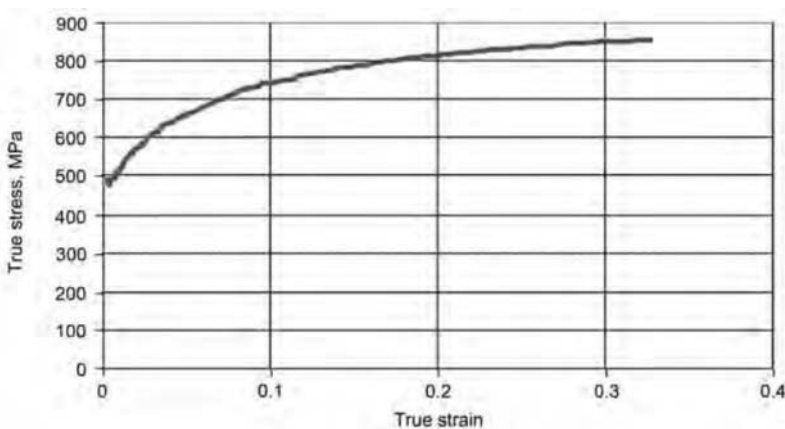


Fig. A.9 Flow stress of DP 600 obtained by viscous pressure bulge test. Experimental strain range, bulge test: 0 to 0.33

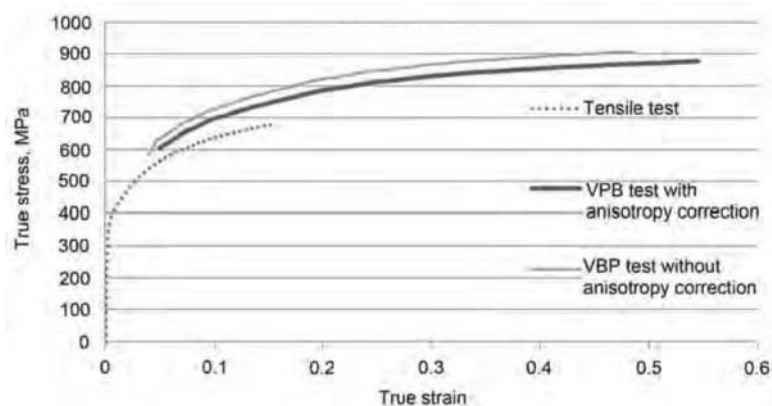


Fig. A.10 Flow stress of DP 600 (1 mm) determined by tensile test and viscous pressure bulge test. Experimental strain range, tensile test: 0 to 0.15; bulge test without anisotropy correction: 0.04 to 0.49; bulge test with anisotropy correction: 0.05 to 0.55

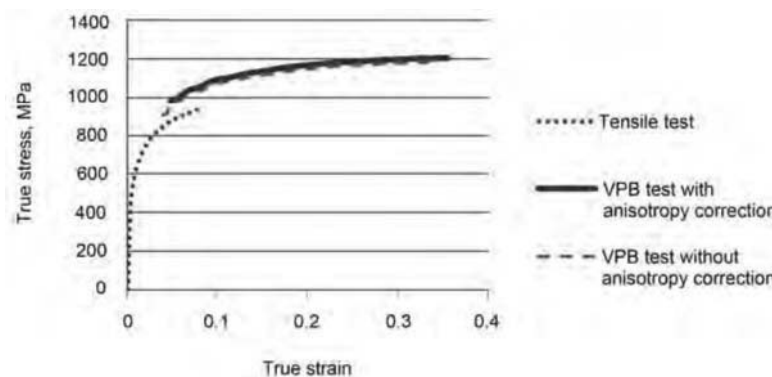


Fig. A.11 Flow stress of DP 780 (1 mm) determined by tensile test and viscous pressure bulge (VPB) test. Experimental strain range, tensile test: 0 to 0.09; bulge test without anisotropy correction: 0.04 to 0.33; bulge test with anisotropy correction: 0.05 to 0.36

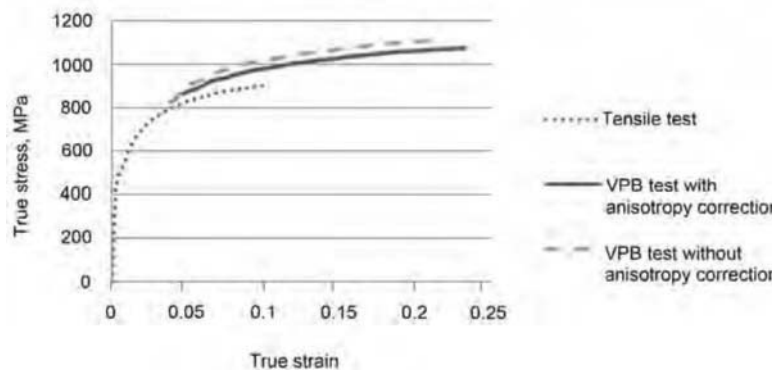


Fig. A.12 Flow stress of DP 780-CR (1 mm) determined by tensile test and viscous pressure bulge (VPB) test. Experimental strain range, tensile test: 0 to 0.1; bulge test without anisotropy correction: 0.04 to 0.22; bulge test with anisotropy correction: 0.05 to 0.24

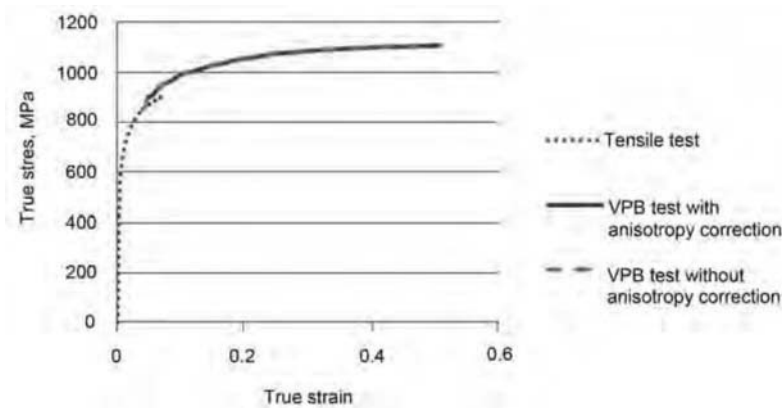


Fig. A.13 Flow stress of DP 780-HY (1 mm) determined by tensile test and viscous pressure bulge (VPB) test. Experimental strain range, tensile test: 0 to 0.75; bulge test without anisotropy correction: 0.04 to 0.45; bulge test with anisotropy correction: 0.05 to 0.5

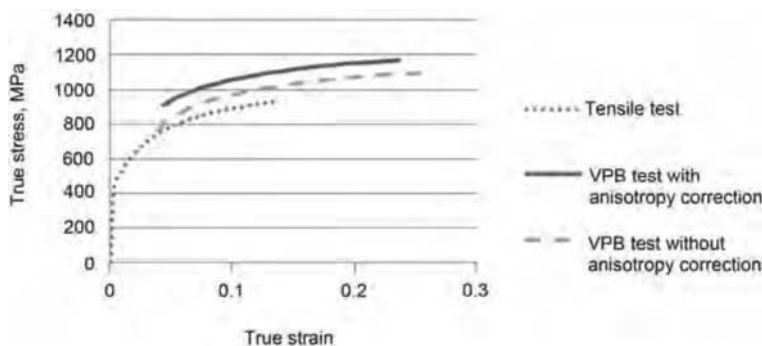


Fig. A.14 Flow stress of TRIP 780 (1 mm) determined by tensile test and viscous pressure bulge (VPB) test. Experimental strain range, tensile test: 0 to 0.14; bulge test without anisotropy correction: 0.04 to 0.26; bulge test with anisotropy correction: 0.05 to 0.25

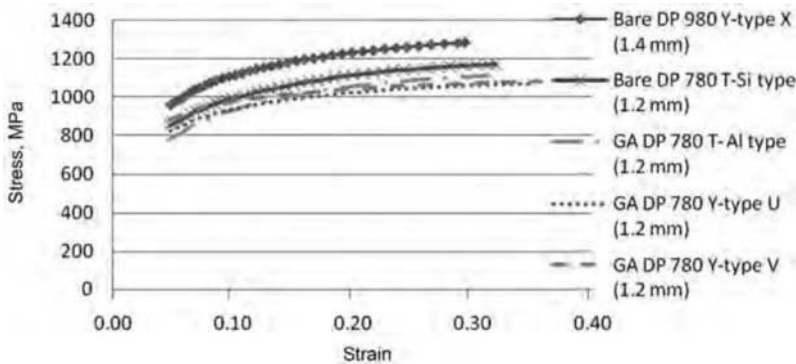


Fig. A.15 Flow stress of five advanced high strength steel (AHSS) sheet materials obtained by viscous pressure bulge test. Experimental strain range, bulge test, DP 980: 0.05 to 0.3; bare DP 780: 0.05 to 0.33; DP 780 T-Al type: 0.05 to 0.31; DP 780 Y-type U: 0.05 to 0.35; DP 780 Y-type V: 0.05 to 0.36

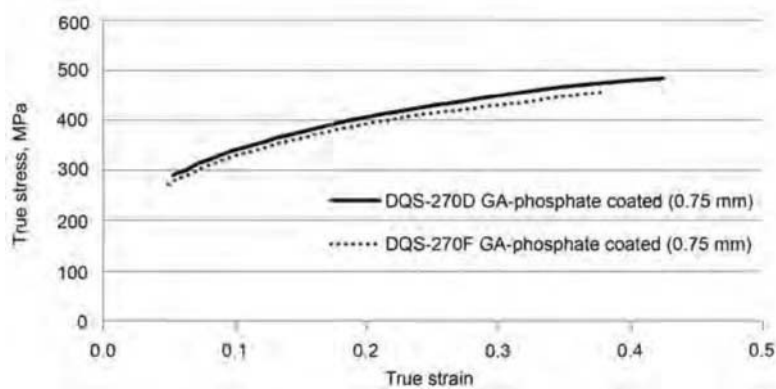


Fig. A.16 Flow stress curves of DQS (0.75 mm) obtained by viscous pressure bulge test. Experimental strain range, bulge test, DQS-270D: 0.05 to 0.44; DQS-270F: 0.05 to 0.37

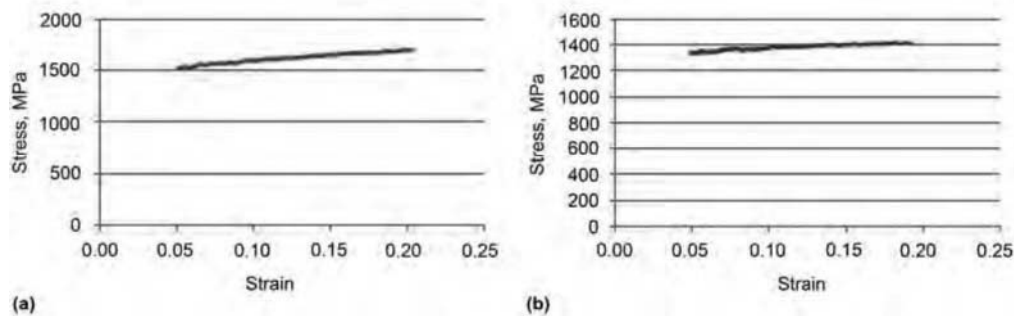


Fig. A.17 Flow stress of (a) SS 301 and (b) SS 201 (0.25 mm) obtained by viscous pressure bulge test. Experimental strain range, bulge test, SS 301: 0.05 to 0.2; SS 201: 0.05 to 0.19

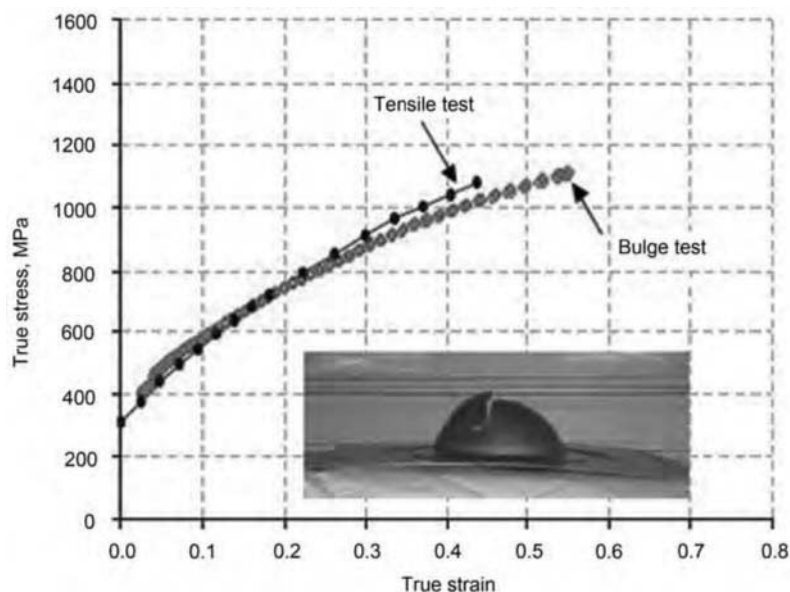


Fig. A.18 Flow stress of SS 304 (1 mm) obtained by viscous pressure bulge test and tensile test. Experimental strain range, tensile test: 0 to 0.44; bulge test: 0.03 to 0.56

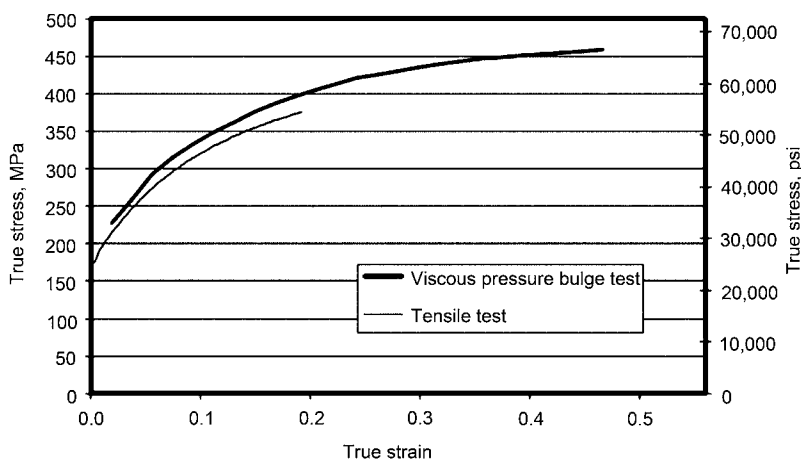


Fig. A.19 Flow stress of AA 6111 (1.04 mm) obtained by tensile test and viscous pressure bulge test. Experimental strain range, tensile test: 0 to 0.19; bulge test: 0.03 to 0.46

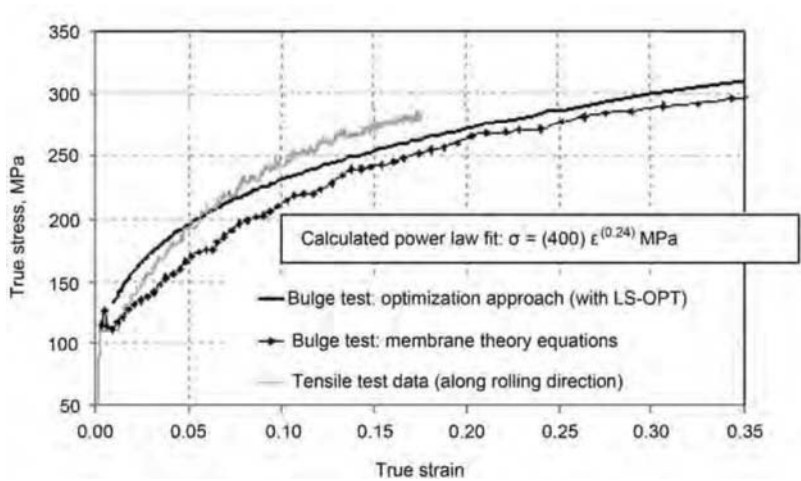


Fig. A.20 Flow stress of AA 5754-O (1.3 mm) obtained by tensile test, bulge test, and the LS-OPT graphical optimization tool, a new optimization methodology developed at the ERC/NSM. Experimental strain range, tensile test: 0 to 0.157; bulge test, membrane theory: 0.01 to 0.35; bulge test, optimization: plotted using the power law equation

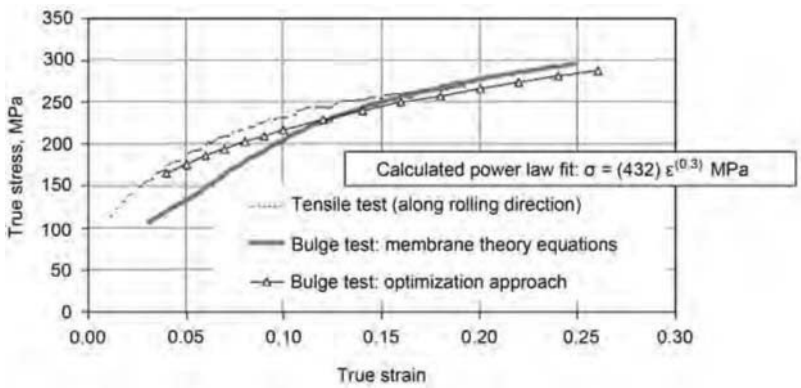


Fig. A.21 Flow stress of AA 5754-O (1.01 mm) obtained by tensile test, bulge test, and the LS-OPT graphical optimization tool, a new optimization methodology developed at the Engineering Research Center for Net Shape Manufacturing. Experimental strain range, tensile test: 0 to 0.159; bulge test, membrane theory: 0.03 to 0.25; bulge test, optimization: plotted using the power law equation

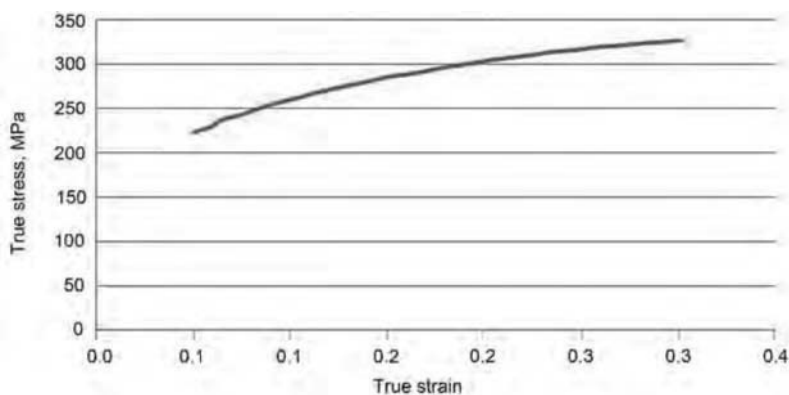


Fig. A.22 Flow stress of aluminum X626 obtained by viscous pressure bulge test. Experimental strain range, bulge test: 0.1 to 0.31

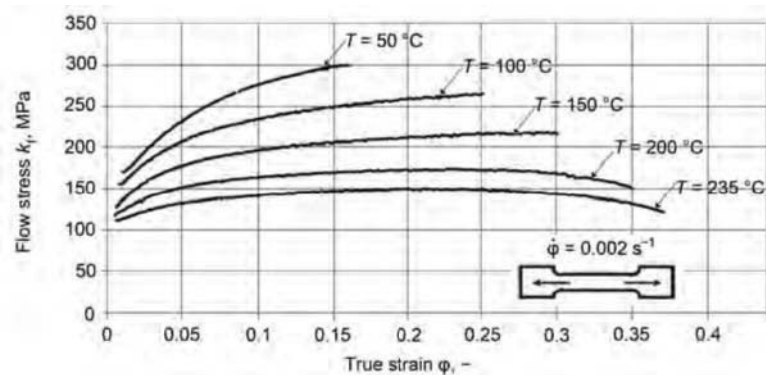


Fig. A.23 Results of tensile tests: variation of flow stress and strain with forming temperature T . Source: Ref A.1

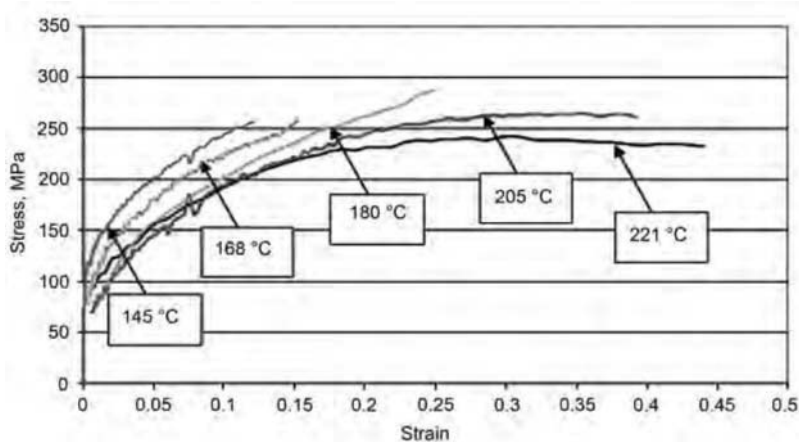


Fig. A.24 Flow stress of AZ31B-O (1.2 mm) obtained by hydraulic bulge test at a strain rate of approximately 0.25 1/s and in a temperature range of 145 to 221 °C. Experimental strain range, at 145°C: 0 to 0.12; 168 °C: 0 to 0.16; 180 °C: 0.02 to 0. Source: Ref A.2

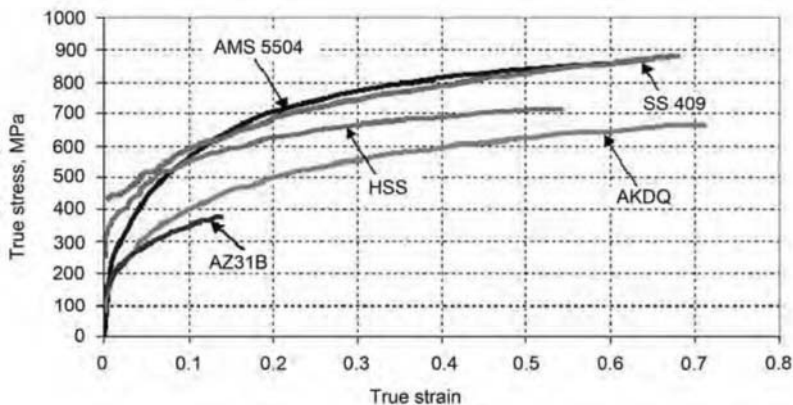


Fig. A.25 Flow stress data of various materials by viscous pressure bulge test. Experimental strain range, for AMS 5504: 0 to 0.6; SS 409: 0 to 0.68; HSS: 0 to 0.54; AKDQ: 0 to 0.72; AZ31B: 0 to 0.14

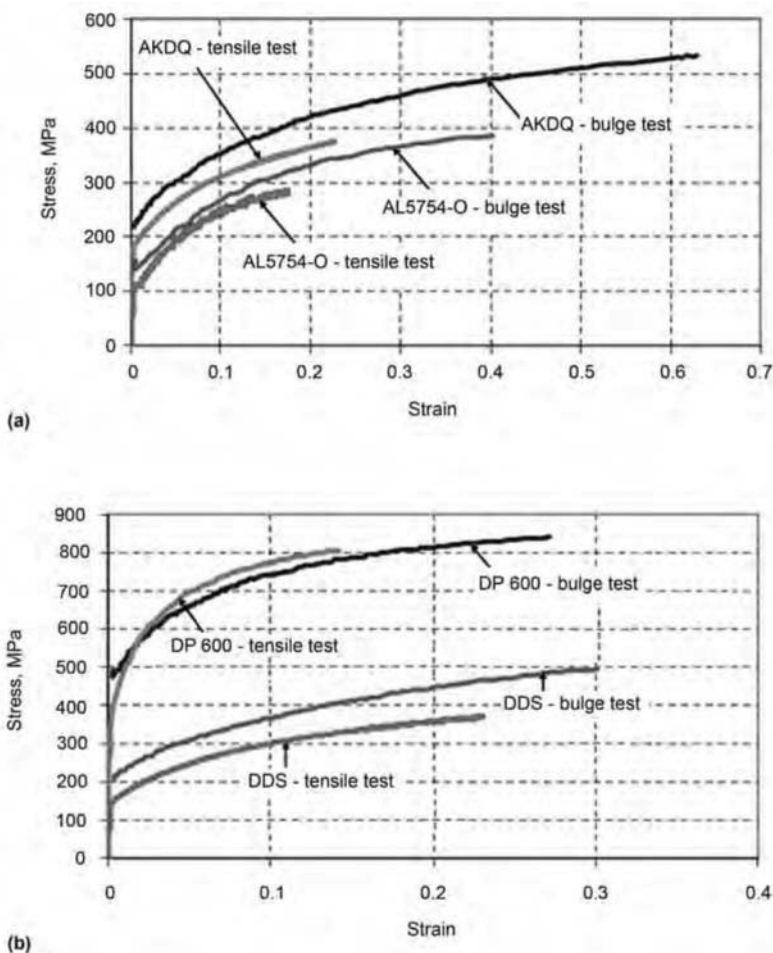


Fig. A.26 Comparison of flow stress curves obtained by viscous pressure bulge test and tensile test (a) for AKDQ steel (0.83 mm) and AA 5754-O (1.3 mm) and (b) for DP 600 (0.6 mm) and DDS (0.77 mm). Experimental strain range, for AKDQ, tensile: 0 to 0.24; AKDQ, bulge: 0 to 0.64; AA 5754-O, tensile: 0 to 0.18; AA 5754-O, bulge: 0 to 0.4; DP 600, tensile: 0 to 0.14; DP 600, bulge: 0 to 0.27; DDS, tensile: 0 to 0.23; DDS, bulge: 0 to 0.3

INDEX

Index Terms

Links

3D servo press	169–170	
bearing sleeves	170	174(F)
U-O bending technique	173(F)	

A

accumulator		
bladder-type	188(F)	
hydraulic cushions	208–209(F)	
in-die systems	213	
rodless piston	187	
accumulator drive	197	
accumulator-drive presses	190(F)	191(T)
adapter. <i>See</i> die post		
adapter (lower)	233	
adhesives	233	
advance. <i>See</i> progression		
advanced high-strength steels (AHSSs)	73	
cold/warm forming	173	
springback, reducing	174	
aerial cam	233	
aerospace industry		
aluminum alloys	82	
bulging	20	
creep forming	19	
expanding	21	
fluid bladder forming	17	

Index Terms

Links

aerospace industry (<i>Cont.</i>)			
joggling	14		
linear stretch forming	19		
shear forming	23		
spinning	22		
age forming	20(F)		
application	19		
equipment	19		
materials	19		
overview	19		
age hardening	84	85	
AHSS steel	49–50	73	173
	174	227(F)	
Aida servo-press line	175(F)		
aids. <i>See</i> cast; skin			
air bend die	233		
air bending	11(F)		
air cushion	233		
air draw	233		
air pin. <i>See</i> pressure pin			
air spring. <i>See</i> pneumatic spring			
aircraft industry			
aluminum alloys	82		
coining	24		
creep forming	19		
drop hammer forming	18		
expanding	21		
linear stretch forming	19		
roll bending	12		
spinning	22		
air-hardening steel	233		
airless spraying	92		
AISI 1008 CR steel	98		
AISI 5115	100		

Index Terms

Links

AKDQ steel

flow stress curves	75(F)	223(F)	224(F)
	231(F)		
hydraulic bulge test	43(F)		
pressure time measurement	43(F)		
tensile data	36(F)		
true stress-strain curves	35		

alloy

233

alloy steels

brake bending	11
bulging	20
coining	23
deep drawing	15
dimpling	21
drop hammer forming	18
fluid bladder forming	17
hemming	11
ironing	23
joggling	14
Marform process	18
nosing	24
roll bending	12
roll forming	11
sheet hydroforming with die	17
sheet hydroforming with punch	16
spinning	22

aluminum

aluminum-zinc alloy coatings	78
coatings	78
coining	23
creep	19
ironing	23

Index Terms

Links

aluminum alloys		
aerospace industry	82	
age forming	19	
age hardening	84	85
aircraft industry	82	
ANSI number system	82	
applications	86	
automotive body sheets	83(T)	
automotive industry	82	
automotive structural parts	83(T)	
Barlat 1996 yield criterion	64(F)	
Barlat and Lian yield criterion	63	
brake bending	11	
bulging	20	
classification of	82	
coining	23	
deep drawing	15	
designations	82–84	
die quench forming	20	
dimpling	21	
drop hammer forming	18	
electromagnetic forming	22	
expanding	21	
explosive forming	22	
flow stress	85	
fluid bladder forming	17	
heat treatment (<i>see</i> aluminum alloys, heat treatment of)		
ironing	23	
joggling	14	
linear stretch forming	19	
Marform process	18	
nosing	24	
overview	82	
punch corner radius	110	

Index Terms

Links

aluminum alloys (*Cont.*)

quick plastic forming	86
roll bending	12
roll forming	11
shear forming	23
sheet hydroforming with die	17
sheet hydroforming with punch	16
spinning	22
strain-hardened products	84
stretch forming	19
T tempers	84
temper designations	84
tempers	82–84
wrought alloys, naming scheme	84

aluminum alloys, heat treatment of

age hardening	85
flow stress	85
overview	84
quenching	85
solution heat treatment	84
warm forming	85–86

aluminum alloys, specific types

5000 series, formability of	85(F)		
6022-T4	64(F)		
A6111-T4	218	219(F)	
AA-2008-T4	126–127		
AA5754-O	85(F)		
Al 5052	167(F)	169	
Al 5083	86		
Al 5754	35	36(F)	169

aluminum-killed steels	73	78	
------------------------	----	----	--

American Society for Testing Materials	33		
--	----	--	--

angle steel. *See* prehem steel

angular deflection	131		
--------------------	-----	--	--

Index Terms

Links

angular stiffness	133	134	154
	155(F)	193	
anisotropic yield criteria			
Barlat 1996 yield criterion	63	64(F)	
Barlat and Lian yield criterion	62–63(F)		
Hill's 1948 yield criterion	59–61(F)		
Hill's 1990 yield criterion	61–62		
overview	58–59		
anisotropy	233		
<i>See also</i> plastic anisotropy			
deep drawing	109		
normal anisotropy	36		
planar anisotropy	36–37		
sheet orientations relative to normal and planar aniso-			
tropy	37(F)		
tensile test	36–37		
true stress-strain curve of Al 1100-O	37(F)		
annealing	233		
ANSI number system	82		
ANSYS	115		
anvil steel	233		
appliance industry			
expanding	21		
spinning	22		
arbor press	233		
area reduction	34–35		
artificial aging	85		
ASTM A1011 DS type B	115(T)		
austenitic alloys	79		
austenitic stainless steels			
formability of	80–81		
martensite	80–81		
overview	80		
warm forming	80–81		

Index Terms

Links

AUTOFORM	115	
automated clamps	141–142	143(F)
automatic counterbalance systems	158	
automatic press	233	
automatic press stop	233	
automotive industry		
AHSS steel	73	
Al 5083	86	
aluminum alloys	82	
bake-hardening steels	76	
bulging	20	
coining	24	
deep drawing using hard dies	15	
expanding	21	
ferritic stainless steels	82	
fluid bladder forming	17	
hemming	11	
hot stamping	18	
large stampings	170–171	175(F)
linear stretch forming	19	
sheet hydroforming with die	17	
sheet steels	73	
spinning	22	
stamping operation	96	
stretch forming	19	
tube hydroforming	20–21	
type 409	82	
axisymmetric drawing	233	

B

back stress	67	68	69
	70		
back-off. <i>See</i> relief			
backstroke force	101		

Index Terms

Links

back-ups	233		
<i>See also</i> details			
bake hardening	76		
bake-hardenable (BH) steel	75	76	225(F)
bake-hardening (BH) steels	76		
balancing pins. <i>See</i> equalizer pins			
ball seat	233		
barber shop	233		
barbering	233		
Barlat 1996 yield criterion	64(F)		
Barlat and Lian yield criterion	62–63		
aluminum alloys	63		
Bishop Hill model	62		
Logan and Hosford yield criterion	62–63		
Logan and Hosford yield surface	62(F)		
plastic strain ratio, influence of	63(F)		
Barlat YLD89	64(F)		
Bauschinger effect	8	66	67(F)
kinematic hardening	69(F)		
Yoshida-Uemori model	69–70		
bead	234		
<i>See also</i> factor			
beaded flange	234		
bearing sleeves	170	173(F)	174(F)
bellmouth	234		
bend angle	234		
bend radius	234		
bendability	45–46	234(F)	
defined		46	
of several steels	46(F)		
bending. <i>See also</i> bending stress			
air bending	11(F)		
brake bending	11		
defined	234		

Index Terms

Links

bending. *See also* bending stress (*Cont.*)

die bending	11(F)
edge bending	11(F)
hemming	11
roll bending	11–12(F)
roll forming	11
tube bending	12–13(F)

bending brake 234

bending dies 234

bending rolls 234

bending stress 234

beryllium

 dimpling 21

 spinning 22

beryllium alloys

 brake bending 11

 joggling 14

BH210 218

biaxial bulge test 115 221

biaxial flow curves 221

biaxial strain 120

biaxial viscous pressure bulge (VPB) test 75

binder 234

See also blank holder; draw ring

binder area. *See* blank holder

binder force. *See* blank holder force (BHF)

binder ring. *See* blank holder

bird bath. *See* low spot

Bishop Hill model 62

bladesteel. *See* low spot

blank

 deformation zones 107

Index Terms

Links

blank (*Cont.*)

slab method 112–114(F)

tribological tests (warm and hot stamping) 99

warm deep drawing 169

blank development 234

blank fatness 8

blank holder

cup drawing test 99–100

cushion systems 203–218(F) 219(F)

cushions/die cushions 171 177(F)

deep drawing 15 16(F)

deep drawing press 196

deep drawing, round and rectangular cups 105–127(F,T)

deep drawing tests 95

defined 234

double-action presses 149

draw beads 9(F)

drawability 47

extended drive presses 147

hydraulic cushions 207(F)

hydroforming presses 197

Marform process 17 18(F)

pin height variation 209

schematic 235(F)

servo press with three slide axes of freedom 170

single-action presses 150

single-action presses, with cushion system 206

warm deep drawing 169

wave forming 81

blank holder force (BHF)

allowable 112(F)

cup drawing test 99

deep drawing 8 105 111–112

deep drawing press 196

Index Terms

Links

blank holder force (BHF) (*Cont.*)

deep drawing tests	95		
defined	234		
FEA simulations	124		
hydraulic cushions	207	208	
in-die systems	212		
mechanical presses	205		
MPC systems	218		
optimal blank holder force/time profile	112(F)		
pin height variation	209		
pneumatic cushions	206–207		
potential failure modes in deep drawing	203(F)		
rectangular cups, deep drawing	118–119		
wrinkling	121		
blank holder pressure	234		
blank preparation			
blanking/piercing	15		
shearing	15		
sheet leveling/roll straightening	14–15(F)		
blanking	15(F)		
<i>See also</i> shearing			
burr height sheet thickness ratio	168(F)		
damping systems	192		
defined	235		
direct drive presses	148		
noise and die life in	166		
example punch motions	168(F)		
high-strength carbon steel	168(F)		
motion diagram of the slide	168(F)		
overview	15		
precision blanking	167–168(F,T)	169(F)	170(F)
tribological tests	100		
velocities and SPM	168(T)		

Index Terms

Links

blanks

22MnB5 blanks	99		
case study—prediction of punch force and BHF	123	126	
circular	47	49	
deep drawing	105		
drawability	47		
driving	49		
FEA simulations	123		
Marciniak test	49		
material characterization	8		
Nakajima test	49		
shearing	15		
sheet forming	3		
sheet metal forming as a system	6		
stretch forming	19		
tailor-welded blanks	138		
tribological tests, warm and hot stamping	99		
BMW, Schuler servo-press line	170–171	175(F)	
body-centered cubic (bcc) crystal structure	79		
bologna. <i>See</i> kidney			
bolster	129	137	139(F)
bolster area	130		
bolster extensions	142		
bolster plate	235		
bolsters, moving	142–143		
boron	18	77	98
boss	235		
<i>See also</i> adapter (lower)			
bottom dead center (BDC)	129–130	133	145
bottoming	24(F)		
bottoming bending	235		
bottoming blocks	235		
<i>See also</i> stop blocks			
bottoming in brake bending	4		

Index Terms

Links

bottoming stamp	235		
bottoming the die. <i>See</i> homing the die			
boundary lubrication	90(F)		
box cam	235		
box heels. <i>See</i> heel block			
brake bending			
application	11		
equipment	11		
materials	11		
process variations	11		
breakage	235		
breakage on trim. <i>See</i> clearance			
breathing	235		
bubble die	235		
buckling			
defined	235		
rectangular cups	119		
bulge test			
A5754-O	44(F)		
AA 5754-O	229(F)		
AA 6111	229(F)		
AA5754-O	85(F)		
AHSS	227(F)		
AKDQ	75(F)	223(F)	224(F)
DP 590	224(F)		
DP 600	44(F)	76(F)	225(F)
	226(F)		
DP 780	224(F)	226(F)	
DP 780-CR	226(F)		
DP 980	224(F)		
DQS	228(F)		
flow stress, determining	41	42	43(F)
Hill's 1948 yield criterion	60–61		
1050 sheet	224(F)		

Index Terms

Links

bulge test (*Cont.*)

SS 201	228(F)	
SS 301	228(F)	
SS 304	80(F)	228(F)
SS304	45	
test specimens	42(F)	
TRIP 780	224(F)	227(F)
X626	230(F)	

bulging

applications	20
defined	235
equipment	20
materials	20
overview	20
process variations	20

bulk deformation (massive forming) processes

characteristics of	3
description of	3

bumper-actuated die. *See* free-shoe die

burr	235
burring	235
bushing. <i>See</i> guide pin bushing	
buster	235
button	235
bypass	235

C

cam	235
<i>See also</i> cam slide; specific cams	
cam action	235
cam driver	235
cam press	235
cam slide	235
camber	235

Index Terms

Links

cam-driven press	145	
canning	235	
<i>See also</i> elastic instabilities		
carbon alloys	21	
carbon steels		
brake bending	11	
bulging	20	
coining	23	
deep drawing	15	
defined	236	
drop hammer forming	18	
fluid bladder forming	17	
hemming	11	
ironing	23	
Marform process	18	
nosing	24	
roll bending	12	
roll forming	11	
sheet hydroforming with die	17	
sheet hydroforming with punch	16	
spinning	22	
carburizing	236	
carburr	236	
carrier strip	236	
<i>See also</i> skeleton; web		
Cartesian coordinate system	31	
case	236	
case hardening	236	
cast	236	
center drill	236	
Center for Precision Forming (CPF)	218(F)	221
C-frame press	131	236
chain slots	236	
chair	236	

Index Terms

Links

chamfer	236		
charge-coupled device cameras	49		
check valve	185(F)	186	213
Chicago screw	236		
chlorinated paraffin oil	100	101	
chlorine, in lubricants	92		
chopoff. <i>See</i> cutoff			
chord modulus	236		
chromium	78	79	84
chute	236		
circle grid	236		
circle grid analysis	237		
circle grid patterns	236(F)		
circular-cup deep-drawing process	47(F)		
clamping force	197–198(F)		
clamps	141–142		
classes of milled pockets	237		
clearance	237		
<i>See also</i> breakage; die clearance			
clinch die. <i>See</i> nutter die			
clinch nut die. <i>See</i> nutter die			
closed hem. <i>See</i> flattened hem; hems			
clutch/brake mechanisms	157		
coated sheet steel coatings			
aluminum coatings	78		
aluminum-zinc alloy coatings	78		
phosphate coatings	78		
prepainted sheets	79		
terne coatings	78–79		
zinc coatings	78		
coated sheet steels			
application	78		
application methods	78		
coatings (<i>see</i> coated sheet steel coatings)			

Index Terms

Links

coated sheet steels (*Cont.*)

equipment	78
lubrication	78
overview	78
tooling	78

cobalt-base superalloys

brake bending	11
dimpling	21
joggling	14
roll forming	11
spinning	22

coefficient of friction (COF)

friction and lubrication	89
laboratory-scale tribological tests	94

coin straightening

237

coining

24(F)

applications	24
bottoming	24(F)
bottoming in brake bending	4
defined	237
equipment	23
as a hybrid forming process	4
knuckle joint press	147
materials	23
overview	23–24
process variations	24

cold developing

237

cold forging. *See* cold working

cold forming. *See* cold working

cold heading

237

cold piercing

173

cold working

3

5–6

80

82

237

cold-rolled sheet

237

Index Terms

Links

column press	237		
combination die. <i>See</i> compound die			
combined drill and countersink. <i>See</i> center drill			
commercially pure titanium	19		
commercial-quality (CQ) steel	77		
compound die	237		
compressive strength	237		
compressive stress	237		
computer numerical control (CNC) hydraulic cushions	150	152(F)	
computer-assisted design (CAD)	114	115	218(F)
concave perimeter contour	237		
concave surface contour	237		
<i>See also</i> OSM			
construction hole	237		
continuous casting	74		
contour forming. <i>See</i> roll forming; stretch forming; tangent bending			
contouring	237		
control factors	237		
conventional draw die. <i>See</i> draw die			
convex perimeter contour	237		
convex surface contour	237		
<i>See also</i> OSM			
cookie cutter die. <i>See</i> steel rule die			
cookware industries	17		
coordinating hole. <i>See</i> construction hole			
copper	135		
low-carbon sheet steels	77		
shear forming	23		
corn cob. <i>See</i> roughing cutter			
corrosion control	91	92–93	

Index Terms

Links

corrosion resistance			
ferritic stainless steels	82		
phosphate coatings	78		
terne coatings	78–79		
22Cr duplex stainless steel	82		
type 304 stainless steel	82		
corrugating	237		
corrugations	237		
Coulomb’s friction model	90–91		
Coulomb’s law	9	95	
counterbalance. <i>See</i> slide counterbalances			
counterbalance pressure. <i>See</i> slide counterbalance pressure			
(counterbalance pressure)			
counterbore	238		
counterboring	238		
countersink	238		
crank angle	130	140(F)	
crank drive press	145	146	
crank press	238		
crankshafts	145	149	205(F)
<i>See also</i> drive shafts			
creep	238		
<i>See also</i> yield			
creep forming	20(F)		
applications	19		
equipment	19		
materials	19		
overview	19		
process variations	19		
crimping	238		
<i>See also</i> corrugating			
critical temperatures	238		
cross-over	238		

Index Terms

Links

crown	238	
<i>See also</i> hydraulic presses; mechanical presses		
cup and cone fracture	238	
cup drawing. <i>See</i> deep drawing		
cup fracture	238	
cupping	238	
cupping test	238	
<i>See also</i> cup fracture; Erichsen test; Olsen ductility test		
cups. <i>See also</i> deep drawing, round and rectangular cups; rectangular cups, deep drawing		
aluminum alloys	86	169
deep drawing tests	96	
defined	238	
drawability	47	
drawing test	99–100	101(F)
earing	37	39(F)
Erichsen cup test	44	
hybrid forming processes	4	
ironing	23	
ironing tests	97–98	
lubrication	95	96
magnesium alloys	169	
rectangular (<i>see</i> deep drawing, round and rectangular cups; rectangular cups, deep drawing)		
round cups	172(F)	
<i>(see also</i> deep drawing, round and rectangular cups)		
spinning	22	
SS304	81	82(F)
titanium alloys	169	
curling	238	
cushion pin. <i>See</i> pressure pin		

Index Terms

Links

cushion pins	209
pin height variation, effect of	210(F)
cushion systems	
BHF	203(F)
blank holder force generating systems	204(F)
double-action presses	
double-action deep drawing die	204(F)
mechanical presses	204–205
overview	203
hydraulic presses	205–206
multipoint cushion (MPC) systems (<i>see</i> multipoint cushion (MPC) systems)	
overview	203
potential failure modes	203(F)
single-action presses (<i>see</i> single-action presses, with cushion system)	
cushions	171
for energy regeneration	177(F)
independent servo-drive die cushion	176(F)
for multiple point control of BHF	177(F)
simple point servo-drive die cushion	176(F)
cut-and-carry method	238
cutoff	238
<i>See also</i> blank	
cutting land. <i>See</i> die life	
cylindrical coordinate system	31(F)

D

date of run. <i>See</i> run stamps		
daylight	130	238
<i>See also</i> shutheight		

Index Terms

Links

deep drawing		
applications	15	
COFs, values for	111	
defined	238–239	
deformation (<i>see</i> deep drawing, deformation during)		
deformation zones	106(F)	
die radius	109–110(F)	
drawing operations	16(F)	
drop hammer forming	18	
equipment	15	
fluid bladder forming	17(F)	
hot stamping	18	19(F)
Marform process	17–18(F)	
materials	15	
potential failure modes influenced by BHF	203(F)	
process variations	15	
rectangular cups (<i>see</i> rectangular cups, deep drawing)		
schematic	105(F)	
sheet hydroforming with die	17	
sheet hydroforming with punch	15–17(F)	
states of stress	53(F)	
tool geometry	108(F)	
using hard dies	15	
deep drawing, deformation during		
anisotropy, effect of	109	
COFs, values for	111	
deformation zones	106(F)	
blank	107	
blank holder	107	
die radius	107	
out-of-plane deformation	107	
overview	105–107(F)	
puckering	107	
thickness variation along cup wall	107(F)	

Index Terms

Links

deep drawing, deformation during (*Cont.*)

thinning and thickening of cup	107(F)	
zone A-C	107	
zone C-D	106(F)	107
zone D-E	106(F)	107
zone E-F	106(F)	107
zone F-G	106(F)	107

equipment and tooling

blank holder	111–112(F)
drawing speeds	111(T)
example optimal blank holder force/time profile	112(F)
ram speed	111
symbols used in the analysis of cup drawing	113(F)

FEM 114–118(F,T)

formability

overview	108
strain hardening, effect of	109
strength coefficient, K , effect of	108–109

friction, effect of 110–111

geometric parameters

die radius	109–110
empirical equations for die clearance	111(T)
ironing process	110(F)
punch force/punch stroke diagram	111(F)
punch-die radius	110

LDR 108(T)

overview 105–107

parameters affecting

equipment and tooling	108
geometry	108(F)
interface conditions	108
material properties	108
overview	108

punch force, prediction of 114

Index Terms

Links

deep drawing, deformation during (<i>Cont.</i>)		
slab method	112–114(F)	
in position III	114(F)	
in position I-II and stress state position II	113(F)	
Tresca yield criterion	113	
strains, prediction of	114	
stresses, prediction of	112–114	
deep drawing, round and rectangular cups. <i>See also</i> rectangular cups, deep drawing		
BHF	105	
blank holder	105	
blanks	105	
deep drawn cups	106(F)	
deformation during		
(<i>see</i> deep drawing, deformation during)		
deformation zones	106(F)	
flange	105	
friction	105	
overview	105	
schematic	105(F)	
symbols used in the analysis of cup drawing	113(F)	
wrinkling	105	
deep drawing tests	95–96(F)	
deflection	154	239
gap frame press	136	
DEFORM	115	
deformation		
homogeneous deformation of a block	65(F)	
power and energy of	65	
deformation curve. <i>See</i> stress-strain diagram		
deformation limit, (<i>see also</i> limiting drawing ratio (LDR))	239	
delayed necking	81	
Demarest process	239	
dent-resistant (DR) steel	75	225(F)

Index Terms

Links

design process	6		
details	239		
developed blank	239		
deviatoric stress	55(F)		
deviatoric stress state	55(F)		
die	3	239	
die aid. <i>See</i> cast; skin			
die assembly	239		
die bending	11(F)		
die block	239		
die button. <i>See</i> button			
die carts	142–143		
die cavity	239		
die clearance	239		
<i>See also</i> breakage			
die cushions			
defined	239		
for energy regeneration	177(F)		
hydraulic cushions	208		
independent servo-drive die cushion	176(F)		
mechanical presses	149		
for multiple point control of BHF	177(F)		
simple point servo-drive die cushion	176(F)		
stiffness of a press	135(F)		
die geometry	17	108	109
	111	129	130
die height	239		
die holder	239		
die hooks. <i>See</i> turnover			
die impression	239		
die life	239		
die lifters	142		
die line	239		

Index Terms

Links

die lubricant	239		
<i>See also</i> lubricant			
die maker's friend or helper. <i>See</i> profile grinder			
die match	239		
die pad	239		
die post	239		
<i>See also</i> adapter (lower)			
die proof (cast)	239		
die quench forming			
application	20		
die quench die	20(F)		
equipment	20		
materials	20		
overview	19–20		
process variations	20		
die radius	107	109–110(F)	239
die rollers	142		
die sections. <i>See</i> details			
die set	239–240		
die shoes	240		
die space	130	240	
die stamping	240		
die temperature	9		
die-independent pressure-sensing system	197		
diemaker's friend or helper. <i>See</i> profile grinder			
differential, defined	183		
differential change of length	28		
differential cylinders	183	184	216
dimpling			
applications	21		
defined	240		
equipment	21		

Index Terms

Links

dimpling (<i>Cont.</i>)		
materials	21	
overview	21	
process variations	21	
ram-coin dimpling	22(F)	
DIN 55 189	134	135(F)
dings	240	
direct crank drive	146	
direct drive presses	149(F)	
direct drives (hydraulic presses)	189(F)	
constant-rpm electric motor and		
constant-displacement pump	189–190(F)	
constant-rpm electric motor		
and variable-displacement pump	189(F)	190
energy efficiencies	189(F)	
overview	189	
variable-rpm electric motor and		
constant-displacement pump	189(F)	190
direct extrusion. <i>See</i> extrusion		
direct-driven spindle drive press	163	165(F)
directional control valves (DCVs)	186–187	
4/3 directional control valve	185(F)	
distortion. <i>See</i> extrusion		
dog leg cam. <i>See</i> aerial cam		
dog-leg driver	240	
dope	240	
double-action die	240	
double-action mechanical press	240	
<i>See also</i> slide		
dowel	240	
dowel puller. <i>See</i> slide hammer		

Index Terms

Links

DP steels			
DP 590	97–98		
DP 600	35	36(F)	44(F)
	70	76(F)	96
	218		
DP 980	173–174		
FLCs	50	51(F)	
Draft	240		
draw bead	240		
draw bead schematic	240(F)		
draw bead test	94(F)		
draw beads	8	9(F)	47
	119	125	240
draw die	240		
draw line. <i>See</i> impact line			
draw marks	240		
draw pad. <i>See</i> blank holder			
draw plate	240–241		
draw radius	241		
draw ring	241		
draw stock	241		
drawability	240		
circular-cup deep-drawing process	47(F)		
defined	47		
LDR	47	48(F)	
tooling to evaluate the drawability			
of the sheet materials	47(F)		
drawing	240		
drawing compound	240		
<i>See also</i> die lubricant			
drawing quality (DQ) materials	74		
drawing quality special killed (DQSK)	74		
drawing steel (DS)	75	76(F)	77
drawing-quality special-killed (DGSK) steel	74	77	

Index Terms

Links

drive	129		
drive shafts			
clutch/brake mechanisms	157		
drive designs	145	148	
positioning	149	150(F)	
servo press drives	164	165(F)	173
vertical press deflection	154(T)		
driver. <i>See</i> cam driver			
drop hammer forming			
applications	18		
equipment	18		
materials	18		
overview	18(F)		
process variations	18		
ductility	241		
duplex stainless steels			
formability	79		
22Cr duplex stainless steel	82		
dutchman	241		
dwell			
AHSS	173–174		
defined	241		
drive systems	188		
electromechanical servo-drive presses	163		
high-strength steels, deep drawing of	174		
hot stamping	199		
laptop case, warm forming	169		
warm forming	199		
dwell cam	241		
<i>See also</i> filler cam			

Index Terms

Links

E

earing

anisotropy	36	
in cup drawing	109(F)	
defined	241(F)	
planar anisotropy	109	
sheet metal drawn cup	39(F)	109(F)

Eberly screw. *See* Chicago screw

eccentric	241		
eccentric gear	241		
eccentric press	145	146–147(F)	241
eco-cushions	196(F)		
edge bending	11(F)		
edge rolling. <i>See</i> edging			
edge stretching limits	47–48		
hole expansion test	48(F)		
%HE	48		
edger	241		
edging	241		
effective draw	241		
effective strain	65–66		
effective strain rate	39	65–66	
effective stress	65		
ejecting	241		
ejector	242		
ejector rod	242		
elastic deformation	242		
elastic instabilities	242		
elastic limit	242		
<i>See also</i> proportional limit			
elastic modulus	34	137	
elastic strain	27	53	
elasticity	242		

Index Terms

Links

electric servo motor	161		
electro-deposition	92		
electromagnetic forming	23(F)		
applications	22		
defined	242		
equipment	22		
materials	22		
overview	21–22		
process variations	22		
electromechanical servo-drive presses			
Aida servo-press line	175(F)		
applications	166–171(F)	172(F)	173(F)
	174(F)	175(F)	
Al alloy cups, warm deep drawing	171	172(F)	
bearing sleeves	170	173(F)	174(F)
blanking, noise and die life in	166–168(F)		
die life, improving	167	168(F,T)	
laptop case, warm forming	169	171(F)	
large automotive stampings	170–171	175(F)	
Mg alloy cups, warm deep drawing	171	172(F)	
Mg alloy, warm forming	169	171(F)	
precision blanking	167–168	169(F)	170(F)
press slide motion	171(F)		
servo press with three slide axes of freedom	169–170		
springback reduction	168–169		
Ti alloy cups, warm deep drawing	171	172(F)	
conventional press drives, versus	161–163		
cushions/die cushions	171		
for energy regeneration	177(F)		
independent servo-drive die cushion	176(F)		
for multiple point control of BHF	177(F)		
simple point servo-drive die cushion	176(F)		

Index Terms

Links

electromechanical servo-drive presses (*Cont.*)

drives with high-torque/low-speed motors	163–166		
conventional four-point straight-side			
mechanical press drive	167(F)		
direct gear-driven gap press	165(F)		
four-point straight-side press design	166(F)		
main motor output	167(F)		
straight-side press with multiple servo motors	166(F)		
drives with low-torque/high-speed motors	163	164(F)	
direct-driven spindle drive press	163	165(F)	
straight-side four-column press	165(F)		
energy savings	165–166	167(F)	
flexibility of slide motion	163(F)		
mechanical and servo presses, comparison	173		
cycle time reduction	178(F)		
slide motions comparison	178(F)		
new process development	173–175		
overview	161		
schematic	162(F)		
Schuler servo-press line	175(F)		
slide motion	162–163(F)		
elephant ears	242		
emboss	242		
embossing	242		
embossing die	242		
enameling steels	75	77	
enclosed die forging	173		
energy-restricted machines	13	1	
Engineering Research Center for Net Shape Manufacturing	73	213(F)	218
engineering strain	27	28	29
	34	35	
engineering stress	34	35	
engineering stress-strain curves	33–34(F)		

Index Terms

Links

environmental factors			
in forming process	10		
in manufacturing processes	2		
equalizer pins	242		
equivalent strain rate	32		
equivalent stress	65		
Erichsen cup test	44–45(F)		
Erichsen index (IE)	44–45		
Erichsen test	242		
expanding	21(F)		
applications	21		
materials	21		
overview	21		
explosive forming	242		
<i>See also</i> high-energy-rate forming			
applications	22		
confined system for	23(F)		
equipment	22		
materials	22		
overview	22		
extended drive presses	145–146	147	148(F)
extensometer	33		
extractor	242		
extra-deep-drawing steel (EDDS)	75	77	
extra-deep-drawing steel plus (EDDS+)	75	77	
extreme pressure (EP) additives	92		
extreme temperature (ET) additives	92		
extruding	242		
extrusion	242		
eye bolt	242		
eyeglass frames	168		
eyeleting	242		

Index Terms

Links

F

face-centered cubic (fcc) crystal structure	79
factor	242
feed. <i>See</i> progression	
ferritic stainless steels	
advantages of	80
automotive industry	82
corrosion resistance	82
ferritic types, formability of	82
formability	79
400 hundred series	82
overview	82
fill slide. <i>See</i> filler cam	
filler cam	242
fillet	242
final hem contact path	242
final hem dwell	242
final hem face geometry	243
<i>See also</i> hemming	
final hem force	243
final hem springback	243(F)
final hem steel	243
fine blanking	
accumulator-drive presses	190
blank preparation	15
die-independent pressure-sensing system	197
hydraulic fine-blanking press	197(F)
presses	196–197(F)
tribological tests	100
fine blanking presses	190
accumulator drive	197

Index Terms

Links

fine blanking presses (*Cont.*)

blanking force 197

die-independent pressure-sensing system 197

hydraulic fine-blanking press 197(F)

finish 243

finish form 243

See also restrike

finite element (FE) simulation-based inverse technique 42–43

finite element (FE) simulations 60 218

finite element method (FEM). *See also* restrike

overview 114–115

process variables

effect of BHF 118 122(T)

effect of blank diameter 117 120(T) 121(F)

effect of blank thickness 117 119(T) 120(F)

effect of COF (μ) 117–118 121(T) 122(F)

effect of strain-hardening coefficient (n) 116 118(T) 119(F)

effect of strength coefficient (K) 116 117(T) 118(F)

effects of tool geometry and friction 117

overview 115–116

tool geometry 116(F)

punch force, prediction of 115 117(F)

round cup drawing, FE model of

ASTM A1011 DS type B 115(T)

overview 115

process parameters 115(T)

quarter finite element model 115(F)

tool geometry 116(F)

stress and strain, prediction of 115 116(F)

flange

deep drawability 8

deep drawing 95 105

defined 243

die cushions 171

Index Terms

Links

flange (*Cont.*)

dimpling	21	
earring	37	
expanding	21	
hemming	11	
hole flanging	14(F)	
in-die systems	213	
Marform process	18	
material characterization	8	
overview	13(F)	
perimeters	97	
punch force	114	
rectangular cups, deep drawing	105–127(F,T)	
spinning	22	
stainless steel sinks	212	
stamping lubricants	94(F)	
flange breakline	243(F)	
flange breakline radius	243(F)	
flange die	243(F)	
flange relief	243(F)	
flange steel		244
flange stripper	244	
flange wrinkling	119	
flanging		
applications	14	
equipment	13	
hole flanging	14	
joggling	14(F)	
materials	13	
overview	13–14	
process variations	13	
shrink flanging	13(F)	
stretch flanging	13(F)	
types of	13(F)	

Index Terms

Links

flanging springback	244(F)	
flash	244	
flat surface contour	244(F)	
flattened hem	244	
flattening	244	
flattening dies	244	
flex roll	244	
flex rolling	244	
floating die	244	
floating form punch	244	
flow control valves	186	
flow criterion	56	
flow curve equations	39	
flow lines	244	
flow rules	63–64	
Levy-Mises flow rule	64	
strain increments based on the Levy-Mises flow rule	65(F)	
flow stress	85	
<i>See also</i> flow stress curves		
AA5754-O	85(F)	
AZ31B-O	87(F)	
FEM	114	
formability	108	
friction and lubrication	9	
Hill's 1948 yield criterion	60	61
isotropic hardening law	66	
material characterization	6	7
orange peel	119	
plastic deformation	38–44(F,T)	
punch force, prediction of	114	
round cup drawing	117	
sheet forming presses	129	
slide velocity under pressure (V_p)	133	

Index Terms

Links

flow stress (*Cont.*)

strain rate	87		
stresses, prediction of	113		
Tresca yield criterion	56	57	
type 304 stainless steel	80(F)		

flow stress curves. *See also* flow stress curves (Center for Precision Forming)

Center for Precision Forming (CPF)	221		
flow curve equations	39		
flow stress	38–39		
low-carbon sheet steels	75		
normal stress components	37		
shear stress components	37–38		
sheet metal drawn cup	39(F)		
strain	39		
stress, nine components of	39(F)		
stress components	37–38		
work hardening	39		

flow stress curves (Center for Precision Forming)

AA5754-O	229(F)	231(F)	
AA6111	229(F)		
AISI1018sheet	223(F)		
AKDQ	223(F)	224(F)	231(F)
AMS 5504	231(F)		
AZ31B	231(F)		
AZ31B-O	230(F)		
BH 210	225(F)		
DDS	231(F)		
DP 500	225(F)		
DP 590	224(F)		
DP 600	224(F)	225(F)	226(F)
	231(F)		
DP 780	224(F)	226(F)	227(F)
DP 780 T-Al type	227(F)		

Index Terms

Links

flow stress curves (Center for Precision Forming) (*Cont.*)

DP 780 Y-type U	227(F)	
DP 780-CR	226(F)	
DP 780-HY	227(F)	
DP 980	224(F)	227(F)
DQS-270D	228(F)	
DQS-270F	228(F)	
DR 120	225(F)	
flow stress data of various sheet materials	221–222(T)	
HSS	231(F)	
1050 sheet	224(F)	
SS 201228(F)		
SS 301228(F)		
SS 304228(F)		
SS 409231(F)		
St14 (DC04) sheet material	222(F)	
St1403 sheet material	223(F)	
tensile tests results	230(F)	
TRIP 780	224(F)	227(F)
X626 aluminum	230(F)	
flow stress, determining		
flow curve equations	40(F)	
hydraulic bulge test	41–44(F,T)	
methods	40(T)	
overview	39	
stress-strain conditions for necking in simple tension	41(F)	
tensile test	39–41(F,T)	
flow-regulating valves	186	
fluid bladder (diaphragm) forming		
applications	17	
equipment	17	
fluid bladder and diaphragm process	17(F)	

Index Terms

Links

fluid bladder (diaphragm) forming (<i>Cont.</i>)			
material	17		
overview	17		
process variations	17		
fluid forming	244		
<i>See also</i> rubber-pad forming			
fluid-cell process	244		
<i>See also</i> fluid forming; rubber-pad forming			
flush	245		
flying cam. <i>See</i> aerial cam			
flying cutoff device	245		
flying shear	245		
flywheels			
available energy (E_M)	133		
energy savings advantage	200		
energy-restricted machines	131		
hot stamping	200		
hydraulic presses	200		
mechanical presses	145–158(F,T)		
mechanical servo press	161	164	165
foil	245		
follow die	245		
force flow (cushion systems)			
BHF	209		
cushion pins	209		
deformation	209		
overview	209		
pin height variation	209		
pin height variation and slide tilting	211		
pressure box	209		
pressure box, deflection of	210–211(F)		
single-action press with in-press die cushion system	209(F)		
slide tilting, off-center loading	209–210		

Index Terms

Links

force-elongation curve	34(F)	
forging	245	
form block	245	
form die	245	
formability		
bendability	45–46(F)	
combined bending/stretching limits	46–47	
defined	245	
drawability	47(F)	48(F)
edge stretching limits	47–48(F)	
overview	44	
stretch bend (SB) test	47(F)	
stretchability	44–45(F)	46(F)
forming	245	
forming die	245	
forming limit curves (FLCs). <i>See also</i> forming limit dia- gram		
AHSS steel	49–50	
determination of	49–50	
experimental FLCs with the Keeler-Brazier equation	51(F)	
factors affecting		
sheet thickness	50	
strain path/deformation history	50–51	
test conditions	50	
and grid analysis used to calculate strains	49(F)	
HSS steel	49	
limiting dome height test	50(F)	
Marciniak test	49	51(F)
mild steel	49	
Nakajima test	49	50(F)
overview	48–4	9
forming limit diagram	245(F)	
forward extrusion. <i>See</i> extrusion		

Index Terms

Links

fracture. *See also* splits

aluminum alloys	86		
area reduction	34		
bending	45		
bending and stretching limits	47		
binder forces	8		
cushion systems	203		
deep drawing, round and rectangular cups	105–127(F,T)		
design process	6		
drawability	47		
Erichsen cup test	44		
FLCs	50		
formability	129		
hole expansion test	48		
LDH test	45	50(F)	94
lubricants	95	96	
pin height variation	209		
rectangular cups	118	119–120	123(F)
shearing	15		
snap-through	139	141(F)	
tooling setup	8		
total elongation	34–35(F)		

fracture strain. *See* maximum elongation

frames

C-frame	195
column-type frame	195(F)
sheet forming presses	129
special frame type	195
straight-side frame	195(F)

free flow direction 185

free-shoe die 245

French cut. *See* pitch notch

French hook 245

French notch. *See* pitch notch

Index Terms

Links

frequency converters	147	
friction. <i>See also</i> friction and lubrication		
blank holder	105	
deep drawing	110–111	
deep drawing, round and rectangular cups	105–122(F,T)	
drawability	47	
efficiency factor (η)	133	
electromechanical servo-drive presses	161	
Erichsen cup test	45	
FLCs	50	
flow stress	38	
hydraulic bulge test	45	
hydraulic presses	192	
LDH test	45	
Marciniak test	49	51(F)
sheet forming presses	129	130
sheet metal forming operations	9–17(F,T)	
slide velocity under pressure (V_p)	133	
stainless steels	79	
friction and lubrication		
Coulomb's friction model	90–91	
factors affecting	89(F)	
lubricants	91–94	
lubrication mechanisms	89–90	
boundary lubrication	90(F)	
contact pressure and frictional shear stress	91(F)	
dry condition	90	
hydrodynamic lubrication	90(F)	
mixed-layer lubrication	90(F)	
Stribeck curve	90(F)	
modified shear friction models	91	
overview	89	

Index Terms

Links

friction and lubrication (*Cont.*)

Reynolds equation	91	
shear friction model	90	91
tribological tests (<i>see</i> tribological tests (lubricants))		
Wanheim and Bay general friction model	91	
furniture manufacturing	13	

G

gage	246	
gage pin	246	
galling. <i>See also</i> scoring		
tribological tests (punching)	101	
gang-die	246	
gap frame. <i>See</i> C-frame press		
gap opening	136	
gap-frame press	132(F)	246
<i>See also</i> C-frame press		
angular deflection	134	135(F)
defined	246	
deflection	136	
dimensional accuracy	133	
frames	137	
press accuracy	136	
quick die change systems	142(F)	
reservoir location	183	
gas cylinder	246	
geometric terms	130(F)	
geometry		
dry condition	90	
engineering stress-strain curves	34	
extended drive presses	147	
flow stress	38	
formability	44	
hydraulic built-in die cushion system	212(F)	213

Index Terms

Links

geometry (*Cont.*)

manufacturing processes	1–2	3	4
mechanical presses	145	204–205	
MPC systems	218		
practical-part geometry	213		
pressure box	210		
rectangular cups	119	120	121
	122	124(F)	126(F)
round cup drawing, FE model of	115		
sheet metal forming operations	5–17(F,T)		
gib design	137	138(F)	
gibs	129	133	137
	246		
grid analysis	246		
growing	246		
growing (grow)	246(F)		
Guerin process	246		
guide pin	246		
guide pin bushing	246		
guide post. <i>See</i> guide pin			
guide post bushing. <i>See</i> guide pin bushing			

H

hammer steel. <i>See</i> hem steel			
handling core	246		
handling hook. <i>See</i> turnover			
handling ring	246		
hardening anisotropy	8		
hardening laws			
Bauschinger effect	69(F)		
isotropic hardening law	66–67(F)		
kinematic hardening law	67–68(F)	69(F)	
mixed hardening law	68–69		

Index Terms

Links

hardening laws (*Cont.*)

nonlinear hardening models 69

overview 66

strain-hardening behavior 66

Yoshida-Uemori model 69–70(F)

Hartmann lines. *See* Luders lines

heat treatable 84

heel block 246

heel plate 246

heel post 246

hem curved outboard 246 247(F)

hem deflection 247(F)

See also recoil

hem die 243(F) 247

hem die plus 247

See also creep

hem edge roll 247(F)

hem flange split 247(F)

hem length 247(F)

hem steel 248

hemming 248(F)

application 11

defined 247

equipment 11

flattened hem 12(F)

materials 11

modified flat hem 12(F)

open hem 12(F)

overview 11

process variations 11

radius flat hem 12(F)

rope hem 12(F)

teardrop hem 12(F)

hemming die 248

Index Terms

Links

hem-out	248(F)		
hems	248(F)		
herf	248		
high collar lock washer	248		
high-energy-rate forming	248		
<i>See also</i> electromagnetic forming; explosive forming			
higher-strength steel sheets	77		
high-strength low-alloy (HSLA) steels	73	75	76–77
high-temperature alloys			
deep drawing	15		
explosive forming	22		
Hill's 1948 yield criterion			
anisotropy constants, effect of	61(F)		
FE simulations	60		
first anomalous behavior	60–61		
overview	59–60		
plastic strain ratio and yield stress	64(F)		
second anomalous behavior	61		
Hill's 1990 yield criterion	61–62		
hoist ring. <i>See</i> swivel ring			
hold down. <i>See</i> blank holder			
hold-down	248		
hold-down plate	248		
hole expansion test	48		
%HE versus ultimate tensile strength	48(F)		
schematic	48(F)		
hole flanging. <i>See also</i> extruding			
applications	14		
defined	248		
equipment	14		
materials	14		
overview	14		
process variations	14		

Index Terms

Links

Hollomon's (power) law	35–36	39	40
	41		
homing the die	248–249		
homogeneous (uniform) deformation	27(F)		
case 1: tension	28		
case 2: compression	28		
elastic deformation	27		
elastic strain	27–28		
engineering strain	27		
engineering strain/true strain, comparison	28(T)		
homogeneous strain	27		
overview	27–28		
plastic strain	27–28		
Honda	170–171	175(F)	
hone	249		
<i>See also</i> superior hone			
hone bucket	249		
Hooke's law	35–36		
horizontal cam. <i>See</i> straight cam			
horn	249		
hot developing	249		
hot flat drawing test	98–99(F)		
hot shear	249		
hot stamping			
applications	18		
dwell	199		
equipment	18		
flywheels	200		
materials	18		
overview	18		
principles of	19(F)		
quenching	199–200		
tribological tests	98–99		
hot stretch forming	87		

Index Terms

Links

HSLA steels			
cold forming	76		
hot forming	77		
springback	77		
HSS steel	48(F)	49–50	51(F)
hybrid forming processes			
coining	4		
description of	3–4		
hydraulic bulge test			
AKDQ sheet material, pressure-time measurement	43(F)		
AZ31B-O, flow stress	230(F)		
AZ31B-O, true stress/true strain curve	87(F)		
dome height for different sheet materials	46(F)		
dome height for sheet material SS304	46(F)		
FE simulation-based inverse technique	42–43		
flow stress, determining	40(T)	41–44(F)	
flow stress, iterative procedure to estimate	43(F)		
flow stress obtained from tensile test and bulge test	44(F)		
infinitesimal element, schematic of	42(F)		
schematic	41(F)		
stretchability	45		
test specimens	42(F)		
hydraulic cushions			
blank holder	207(F)	208	
compensation cylinders	208–209(F)		
components	207(F)		
delayed return motion	208		
energy recovery	208–209		
energy-saving cushion	209(F)		
force characteristics	207–208		
overview	207		
preacceleration	208(F)		
principle of	207(F)		

Index Terms

Links

hydraulic cylinders	183–184(F)	
differential cylinders	183(F)	184
single-acting cylinders	183–184(F)	
tandem cylinders	183(F)	
hydraulic damping system	192	
hydraulic fluids		
properties of	182(T)	
seals	182	
selection of	182	
hydraulic lines	184	
hydraulic press brake	249	
hydraulic presses	191(T)	195(F)
advantages of	181	
BHF	196	205–206
characteristics of		
characteristic data for accuracy	193	195
cylinders, selective activation of	194(F)	
displacement-time curve	193(F)	
energy efficiency	191(F)	
frames	195(F)	
load	190–191	
parallelism control system	195	
prefill valve	194(F)	
slide tilt	195	
stiffness	193	195
stroke	191–192	
time-dependent characteristics	192–193	
components		
accumulator	187	188(F)
hydraulic cylinders	183–184(F)	
hydraulic fluid/pressure medium	182	
hydraulic lines	184	
hydraulic pumps	184(F)	
hydraulic valves	185–187(F,T)	

Index Terms

Links

hydraulic presses (*Cont.*)

intensifier	187(F)
overview	182
reservoir	182–183(F)
seals	182
cushion systems	205–206
deep drawing press	196(F)
defined	249
disadvantages of	182
drive systems	
accumulator drive	190(F)
direct drive (pump drive)	189–190
direct drives	189–190(F)
direct-drive presses versus	
accumulator-drive presses	191(T)
energy efficiencies	189(F)
overview	188–189
eco-cushions	196(F)
fine blanking presses	196–197(F)
frames	195(F)
by function	196–200(F)
gap frame press	195(F)
hot stamping	199–200
hot stamping cycle time	199(F)
hydraulic fluids	182(T)
hydroforming presses	197–198(F)
initial tilt	195
load-restricted machines	131
overview	181–182
schematic	181(F)
tilt stiffness	195
tryout presses	198–199(F)
warm forming	199

Index Terms

Links

hydraulic pumps	184(F)	
bent axis type	184(F)	
external gear type	184(F)	
internal gear type	184	
swashplate type	184(F)	
variable displacement per revolution	184	
hydraulic shear	249	
hydraulic valves	185–187(F,T)	
check valve	185(F)	186
DCVs	185–186(F)	
flow control valves	186	
flow-regulating valves	186	
ISO symbols for actuation of valves	187(T)	
pressure valves	186(F)	
proportional directional valves (servo valves)	187	
servo-actuated valves	186–187	
solenoid valves	186	
hydraulic-mechanical press brake	249	
hydrodynamic lubrication	90(F)	
hydroforming. <i>See also</i> hydroforming presses; sheet hydro-		
forming		
accumulators	187	
deep drawing	15	
intensifiers	187	
Marform process	18	
hydroforming presses		
sheet hydroforming scenarios	198(F)	
SHF-D	197–198	
SHF-P	197	
THF	197–198	
Types	198(F)	
hydromechanical deep drawing. <i>See</i> sheet hydroforming		
with punch (SHF-P)		
hydrostatic stress	55	

Index Terms

Links

hydrostatic stress state	55
HyperMesh	115
Hyson cylinder. <i>See</i> gas cylinder	

I

IDEAS	114	115
impact line	249	
inching	249	
inclinable press	249	
incline cam	249	
inclusion-shape-controlled steels	75	77
incremental forming		
shear forming	23	24(F)
spinning	22	23(F)
infinitesimal shear angle	30	
infinitesimal true strains and strain rates	29–31	
cylindrical coordinate system	31(F)	
infinitesimal shear angle	30	
three-dimensional deformation	31	
two-dimensional deformation	29–30	
undeformed/deformed infinitesimal material element	29(F)	
initial tilt	195	
inner panel bleed through. <i>See</i> inner panel read through		
inner panel burr	249(F)	
inner panel read through	249	
inner panel thickness	249(F)	
insert	249	
<i>See also</i> window		
inside of metal outer panel	249	
inside of metal/flange length	249	
Institut für Umformtechnik at Universität (IFU) Stuttgart	212–213(F)	
intensifier (hydraulic)	187(F)	
International Organization for Standardization (ISO)	187(T)	

Index Terms

Links

interstitial-free (IF) steels	76	77	78
invariants	54	55	
inverted die	249		
iron hand	250		
<i>See also</i> extractor			
iron-base superalloys			
brake bending	11		
dimpling	21		
joggling	14		
roll forming	11		
spinning	22		
ironing	24(F)	250	
applications	23		
equipment	23		
materials	23		
overview	23		
ironing tests	96–98(F)		
ISM	250		
isoplot	250		
isotropic hardening law	66–67		
Bauschinger effect	66	67(F)	
von Mises yield criterion	66	67(F)	
isotropic yield criteria	56–58(F)		

J

J hook	250
<i>See also</i> turnover	
jig borer	250
jog. <i>See</i> inching	
joggle	250
joggling	
applications	14

Index Terms

Links

juggling (*Cont.*)

equipment	14
materials	14
overview	14

K

Keeler-Brazier equation	49–50	51(F)
keeper	250	
Kellering. <i>See</i> contouring		
Kellering aid	250	
Kelly screws. <i>See</i> Chicago screw		
key	250	
kicker. <i>See</i> ejector		
kidney	250	
killed steels	73–74	78
kinematic hardening law		
back stress	67	
Prager's kinematic hardening rule	67	68(F)
Ziegler's kinematic hardening rule	67–68(F)	69(F)
Kirk site	250	
kiss off	250	
knockout	250	
<i>See also</i> ejector		
knockout mark	250	
knockout pin	250	
knuckle joint press	146	147

L

lancing	250
land	250
<i>See also</i> die life	
Lankford coefficient	37
lap. <i>See</i> superior hone	

Index Terms

Links

laser beam cutting	250		
laser sensors	134	135	136(F)
lead	135		
lead hit	250		
lead shear. <i>See</i> lead hit			
leader pin. <i>See</i> guide pin			
leader pins. <i>See</i> guide pin			
leveler lines	250		
leveling	8	250	
<i>See also</i> roller leveling; stretcher leveling			
leveling blocks	250		
Levy-Mises flow rule	64	65(F)	
lifter	250		
liftout	250		
limit switch	192	251	
limiting dome height	250–251		
limiting dome height (LDH) test	45	94(F)	
forming limit curves	50(F)		
limiting dome height tooling	45(F)		
stretchability results of different steels	45(F)		
limiting draw ratio (LDR)	251		
<i>See also</i> deformation limit			
AHSS	48(F)		
for common materials	108(T)		
deep drawing, deformation during	108		
die radius	108(F)		
drawability	47		
mild steel	48(F)		
line dies	251		
linear stretch forming	20(F)		
applications	19		
equipment	19		

Index Terms

Links

linear stretch forming (<i>Cont.</i>)		
materials	19	
overview	19	
process variations	19	
linear variable differential transformer	134	
link drive press	146	147
load	190–191	
load-displacement curves	131(F)	
load-restricted machines	131	
locating pin. <i>See</i> gage pin; pilot		
locator	251	
<i>See also</i> jig borer		
lock bead	251	
lock spleen. <i>See</i> locking bead		
locking bead	251	
Logan and Hosford yield criterion	62–63(F)	
loose hem. <i>See</i> open hem (radius flat)		
low profile screw	251	
low spot	251	
low-carbon sheet steels		
biaxial VPB test	75	
cold rolled steel sheet forming features	75(T)	
composition ranges and limits	74(T)	
flow stress curves	75	
formability		
effect of composition on	77	
effect of microstructure on	77–78	
effect of steelmaking methods on	77–78	
forming characteristics		
CQ steel	77	
DGSK	77	
DS	77	
enameling steels	77	
higher-strength steel sheets	77	

Index Terms

Links

low-carbon sheet steels (*Cont.*)

inclusion-shape-controlled steels	77
interstitial-free steels	77
structural steels	77
forming grades	74
grade designations	75
mechanical properties	74(T)
mechanical properties determined using tensile test	75(T)
modified low-carbon steel sheet	75–77
overview	73–74
properties	74–75
in stamping	74(T)
uniaxial tensile test	75

low-carbon steel sheet (modified)

BH steels	76
IF steels	76
overview	75–76

low-carbon steels

1008	83(F)	98
linear stretch forming	19	
stretch forming	19	

lower dies

6

lower yield point

266

See also yield point

LS-DYNA

115

lubricant

die temperature effect on	9
impact speed effect on	9

lubricants. *See also* friction and lubrication

additives

chlorine	92
EP additives	92
ET additives	92
overview	92

Index Terms

Links

lubricants. *See also* friction and lubrication

additives (*Cont.*)

phosphorus 92

sulfur 92

temperature-activated EP additives 92

application

airless spraying 92

drip method 92

electro-deposition 92

mops 92

roll coating 92

sponges 92

case study—prediction of punch force and BHF 123

chlorinated paraffin oil 101

cleanliness 93

corrosion control 92–93

nonchlorinated paraffin oils 101

overview 91–92

plain mineral oil 101

post-metal forming operations 93

prelubricants, compatibility with 93

removal methods 93

selecting 91–92

stamping processes compared 93(F)

types

dry-film lubricants 92

oils 92

semisynthetics 92

soluble oils 92

synthetics 92

water-free dry-film lubricants 92

water-soluble dry-film lubricants 92

washer oils, compatibility with 93

Luders bands. *See* Luders lines

Index Terms

Links

Luders lines 251

M

magnesium alloys

AZ31-0 169 171(F)

AZ31B 169

AZ31B-O 87(F) 230(F)

billets, cold piercing 173

designations 86

formability of 87

hot stretch forming 87

overview 86

properties 86(T)

springback 87

strain rate 87

warm forming 169 171(F)

magnetic pulse forming. *See* electromagnetic forming

mahogany stick. *See* spotting stick

manganese 75 84

manganese boron steel (22MnB5) 18 98 99
100

manufacturing processes

characteristics of

environmental factors 2

geometry 1–2

production rate 2

tolerances 2

classification of

forming 1

joining 1

material removal 1

material treatment 1

primary shaping 1

overview 1

Index Terms

Links

map	251		
Marciniak test	49	51(F)	
Marform process	15	16	17–18(F)
Marforming process	17(F)	251	
applications	18		
die closed	18(F)		
die open	18(F)		
equipment	18		
material	18		
overview	17–18		
process variations	18		
marriage gap	251(F)		
martensite	18	80–81	
martensitic stainless steel	79		
master	251		
<i>See also</i> adapter (lower)			
master adapter. <i>See</i> adapter (lower)			
master plug. <i>See</i> adapter (lower)			
match	251		
mating flange area	251(F)		
mating surface	251(F)		
maximum depth of draw. <i>See</i> effective draw			
maximum draw. <i>See</i> effective draw			
maximum elongation	251		
maximum permissible load	152–153(F)		
maximum strength. <i>See</i> ultimate strength			
maximum strokes per minute	153(F)		
mechanical press brake	251		
mechanical presses			
angular stiffness	155(F)		
automatic counterbalance systems	157	158(F)	
BHF	205		
cam-driven press	145		
classification of	150(F)		

Index Terms

Links

mechanical presses (*Cont.*)

clutch/brake mechanisms	157	
common drives	148(F)	
complete press drives	157	
crank drive press	145	146
crankshafts	149	
deep drawing operation, double action press	151(F)	
deep drawing operation, single action press	151(F)	
defined	251	
deflection	154	
die cushions	149	
dimensional accuracy	154–155	
direct crank drive	146	
direct drive presses	149(F)	
displacement characteristics		
adjustment of the blank holder	205	
blank holder force adjustment	206(F)	
displacement of inner and outer slide	204	205(F)
forces exerted by the outer and inner slide	204–205	
mechanical double-action press	205(F)	
double-action press, slide motions	151(F)	
drive designs		
connecting rods, number of	149	
direct drive presses	148	
double gear reduction	149	
drive location	149	
drive shaft, positioning of	149	
gear reduction	148–149	
high-speed stamping	148	
overview	147–148	
twin-end drives	149	
drive types	145–147(F)	148(F)
eccentric press	145	146–147(F)
energy requirements	153	

Index Terms

Links

mechanical presses (*Cont.*)

extended drive presses	145–146	147	148(F)
gibs	137		
knuckle joint press	146	147	
link drive press	146	147	
load requirements	150–153		
maximum strokes per minute	153(F)		
nominal load as a function of crank angle	152(F)		
overload protection	155–156		
overload protection systems	156(F)		
overview	145		
pneumatic slide counterbalancing	158(F)		
schematic	145(F)	152(F)	
shutheight adjustment	156		
shutheight adjustment mechanisms	157(F)		
simple crank drive	146(F)		
simple drive presses	146–147		
slide counterbalancing	157–158		
slide motion, crank press	148(F)		
slide motion, knuckle joint press	148(F)		
slide motion, link drive press	148(F)		
slide motions	149–150		
stiffness of a press	154		
switchable gearbox	157		
time-dependent characteristics	153–154		
toggle press	146	147	
velocity and displacement of slide	154(F)		
vertical press deflection	154(T)		
vertical stiffness	155(F)		
mechanical working	252		
metal clearance	252		

Index Terms

Links

metal forming processes. *See also* manufacturing processes

classification of

bulk deformation processes 3

hybrid forming processes 3

sheet metal forming processes 3

in manufacturing 2–3

metalworking. *See* forming

midget mill. *See* carburr

mild steel 48(F) 49

mill 252

mill edge 252

mill finish 252

mill product 252

mill scale 252

mixed hardening law

back stress 68

Bauschinger effect 68

Prager's kinematic model 69

mixed-layer lubrication 90(F)

model 252

modified cup drawing test 98 99–100

modified flat hem 248(F) 252

modified shear friction model 91

modulus of elasticity 252

Mohr's circle

Hill's 1990 yield criterion 62

for in-plane stresses 56(F)

Tresca yield criterion 56

in uniaxial tensile and compression tests 57(F)

molds 1

See also die

Index Terms

Links

molybdenum alloys		
brake bending	11	
joggling	14	
roll forming	11	
spinning	22	
mops	92	
multiple. <i>See</i> bladesteel		
multiple die	252	
multiple punching. <i>See</i> perforating		
multiple-slide press	252	
<i>See also</i> slide		
multipoint cushion (MPC) systems		
FE simulations	218	
in-die systems		
BHF	212	
hydraulic built-in die cushion system	212	213(F)
with hydraulic cylinders	212–214(F)	
nitrogen cylinder systems	214–217(F)	
overview	212(F)	
practical part geometry (GM inner lift gate)	213	
in-press systems	211–212	
cushion system built in the die	212(F)	
stainless steel sinks	212(F)	
single-point cushion system	211(F)	
four-point cushion system	211(F)	
six-point cushion system	211(F)	
eight-point cushion system	211(F)	
nitrogen cylinders, application of	217	
overview	211	
programming		
BHF	217–218(F)	

Index Terms

Links

multipoint cushion (MPC) systems (*Cont.*)

CAD 218(F)

CPF 218(F)

FEA 218(F)

optimum BHF 218

multitooth cutter. *See* roughing cutter

m-value. *See* strain-rate sensitivity (*m*-value)

N

Nakajima test 49 50(F)

necking

area reduction 35

austenitic steels 81

defined 252

FLCs 49

flow stress 38

high-strength steels 174

Hill's 1948 yield criterion 60 61(F)

homogeneous deformation 27

hydraulic bulge test 42(F) 43

Nakajima test 49

stress-strain conditions 41(F)

tensile test 39 40 41

Tresca yield criterion 56

true stress-strain curves 35

UTS 34

nest 8 252

nesting 252

nickel-base superalloys

brake bending 11

dimpling 21

joggling 14

roll forming 11

spinning 22

Index Terms

Links

niobium alloys		
joggling	14	
roll forming	11	
spinning	22	
nitro-dyne cylinder. <i>See</i> gas cylinder		
nitrogen cylinder systems	214–217	
autonomous system	214	215
BDC, delay at	216	217(F)
controllable nitrogen cylinders	215–216(F)	
cylinder force	214	
delay circuit	216–217(F)	
force characteristics of nitrogen springs	214(F)	
hosed systems	215	
manifold system	215	216(F)
modified two-chamber system	214	
nitrogen cylinder installed as cushions	215(F)	
nitrogen cylinders, application of	217	
one-chamber nitrogen cylinder	215(F)	
one-chamber system	214	215(F)
preacceleration	216(F)	
prime cylinder	216	
self-contained gas spring	215	216(F)
system installations	214–215	
timing cylinder	216	
two-chamber system	214	215(F)
nitrogen die cylinder. <i>See</i> gas cylinder		
no stock movement	253	
nominal strength. <i>See</i> ultimate strength		
nonchlorinated paraffin oils	100	
nonlinear hardening models	69	
nonreturn valve	185	
normal anisotropy	36	252(F)

Index Terms

Links

normal stress		
Barlat and Lian yield criterion	62	
components	37	
deep drawing	54	
defined	54	
deviatoric stress state	55	
flow stress curves	37–38	
friction and lubrication/tool work interface	9	
Hill’s 1948 yield criterion	59	
Tresca yield criterion	56	
true stress-strain curves	35	
volumetric stress	54–55	
normalizing	252	
nosing	24(F)	
applications	24	
equipment	24	
materials	24	
overview	24	
process variations	24	
notching	253	
nuclear reactors	12	
number of strokes per minute (n_p)	154	
nutter die	253	
n -value		
aluminum alloys	85	
austenitic steels	80	
defined	253	
ferritic stainless steels	82	
punch force/punch stroke curves	119(F)	
stainless steels	79	80(F)
strain hardening	109	

Index Terms

Links

O

OBI. *See* open-back inclinable press

off-center loading

asymmetric deformation in single operations 138

out-of-parallel movement 138

ram and blank holder tilting 210(F)

slide tilting 209–210(F)

transfer or progressive die forming 138–139 140(F)

oil canning 119 253

See also canning; elastic instabilities

Olsen ductility test 253

one-piece (monoblock) frame 132

open hem (radius flat) 253(F)

open-back inclinable press 253

See also inclinable press

orange peel 119 253

ordinary steel. *See* carbon steels

ordnance

deep drawing using hard dies 22

ironing 23

nosing 24

spinning 22

Orowan shear friction model 91

oscillating die 253

OSM 253

outer panel thickness 253

outer ram (binder) load 253

out-of-plane deformation 107

outside of metal flange length 253(F)

outside of metal outer panel 253(F)

overbending 253(F)

overcrown 253(F)

Index Terms

Links

overhanging press	253(F)
<i>See also</i> C-frame press	
overload protection systems	155–156(F)
hydraulic	156
mechanical	156

P

pad	254
pad bounce	216
pad drivers	254
pad retainer pins	254
pad window. <i>See</i> window	
PAMSTAMP	115
parallelism control system	195
parallelism system	199
parting	254
pedestal. <i>See also</i> punch riser; riser	
percent hole expansion (%HE)	48(F)
percent strain safety	254
percent total elongation	254
percent uniform elongation	254
perforating	254
<i>See also</i> piercing	
perforator	254
<i>See also</i> punch	
permanent set	254
petroleum industries	22
petroleum-based oils	92
phosphate coatings	78
phosphorus	
low-carbon sheet steels	77
in lubricants	92
SQ steels	75
pick-&-place	254

Index Terms

Links

pickoff	254	
pickup	254	
<i>See also</i> galling; scoring		
pierce block	254	
pierce button.	<i>See</i> button	
pierce dies.	<i>See</i> clearance	
pierce punch	254	
<i>See also</i> perforator; punch		
piercing	254	
piercing die	254	
piggy back cam	254	
pilot	254	
pinch trimming	254	
Piobert lines.	<i>See</i> Luders lines	
pitch.	<i>See</i> progression	
pitch notch	254	
plain carbon steel.	<i>See</i> carbon steels	
plain mineral oil	101	
planar anisotropy	36–37	254(F)
plane-strain	254	
plastic anisotropy	254–255	
<i>See also</i> normal anisotropy		
in sheet forming	8	
plastic deformation, defined	53	
plastic deformation—flow stress, anisotropy, and form-		
ability		
anisotropy (<i>see</i> anisotropy)		
FLCs (<i>see</i> forming limit curves (FLCs))		
flow stress	38–39	
<i>(see also</i> flow stress curves)		
flow stress, determining (<i>see</i> flow stress, determining)		
formability (<i>see</i> formability)		
overview	33	
tensile test (<i>see</i> tensile test)		

Index Terms

Links

plastic deformation—state of stress, yield criteria flow rule, and hardening rules		
anisotropic yield criteria (<i>see</i> anisotropic yield criteria)		
deep drawing process	53(F)	
deformation, power and energy of	64–65	
effective strain	65–66	
effective strain rate	65–66	
flow rules	63–64	65(F)
hardening laws (<i>see</i> hardening laws)		
homogeneous deformation of a block	65(F)	
isotropic yield criteria (flow criteria) (<i>see</i> isotropic yield criteria)		
overview	53	
state of stress (<i>see</i> stress)		
plastic deformation—strain and strain rate		
defined		255
equivalent strain rate	32	
homogeneous (uniform) deformation	27–28(F,T)	29(F)
infinitesimal true strains and strain rates	29–31(F)	
overview	27	
principle strains	31–32(F)	
slip	29	
strain paths	32	
twinning	29	
volume constancy	29(F)	
plastic flow	255	
<i>See also</i> yield		
plastic hit	255	
plastic strain		
Barlat and Lian yield criterion	63	
equivalent strain rate and equivalent strain	32	
flow rules	64	
hardening laws	66	
homogeneous deformation	27	

Index Terms

Links

plastic strain (<i>Cont.</i>)		
hydraulic bulge test	44	
isotropic hardening law	66	
kinematic hardening law	67	
low-carbon sheet steels	74	
mixed hardening law	68–69	
plastic strain ratio (<i>r</i> -value)		
anisotropy	37	
Barlat 1996 yield criterion	63	64(F)
Barlat and Lian yield criterion	62	63(F)
DS	77	
ferritic stainless steels	82	
Hill's 1948 yield criterion	60	62
low-carbon steels	74(T)	
plastic working	255	
plasticity	255	
plastic-strain ratio (<i>r</i> -value)	255	
platen. <i>See</i> press slide		
plunger. <i>See</i> press slide		
plunger guides	137	138(F)
pneumatic cushion system	206–207	
pneumatic cushions	206–207	
BHF	206–207	
pneumatic cylinders	206	
principle of	207(F)	
pneumatic cylinders	157	158(F)
pneumatic slide counterbalancing	158(F)	
pneumatic spring	255	
pogo stick	255	
point of origin	255	
<i>See also</i> construction hole		
polishing bob or cone	255	
<i>See also</i> sanding bob		
positive stops	192	

Index Terms

Links

power generation	22		
Prager's kinematic hardening rule	67	68(F)	
preacceleration	208(F)	213	214
	216	216(F)	
precipitation hardened stainless steels	79		
precision blanking	167–168		
precision formed part	170(F)		
process sequence	169(F)		
slide motion process	170(F)		
tooling	169(F)		
velocities and SPM	168(T)		
precision flashless forging of splines	173		
prefill valve	192	194(F)	
preformed part	255		
preheating	255		
prehem contact path	255(F)		
prehem face geometry	255(F)		
prehem flange angle	255(F)		
prehem force	255		
prehem springback	255		
prehem steel	256		
prehemming	11		
prepainted sheets	79		
prerollers	142		
press bed	256		
press brake	256		
<i>See also</i> bending brake			
press capacity	256		
press forming	256		
press hemmer	256		
press load	256		
press ram. <i>See</i> press slide			
press shutheight	130	134	

Index Terms

Links

press slide	256	
<i>See also</i> slide		
press speed (strokes per minute)	137	
press stiffness		
contact time, effect on	135(F)	
contact time under pressure (t_p)	133–134	
die cushion, effect of slide tilting on	135(F)	
measuring	134–135(F)	
stiffness of a press	133–134	
straight-side press	134(F)	
pressure box	209	210–211(F)
pressure pad read through	256(F)	
pressure pin	256	
pressure plate	256	
pressure regulators	186	
pressure relief valve	186(F)	
pressure valves		
pressure regulators	186	
pressure relief valve	186(F)	
two-way pressure regulator	186(F)	
prestrain	256(F)	
principle strains	31–32	
principle directions	31–32	
principle strain directions	31(F)	
principle strain rates	31	
principle stress	54	
production rate		
environmental factors	10	
forming processes	3	
frequency converters	147	
hydraulic presses	182	
lubricants	92	
manufacturing processes	2	
number of strokes per minute (n_p)	133	154

Index Terms

Links

production rate (<i>Cont.</i>)			
servo-press line	174		
sheet forming presses	129		
stroking rate	8		
tooling	8		
Pro-E	114		
profile grinder	256		
profiling	256		
progression	256		
progressive die	256		
progressive forming	256		
project number	256		
<i>See also</i> service order number			
Proof	256		
<i>See also</i> die proof (cast)			
proof load	256		
proof stress. <i>See</i> yield point			
proportional limit	257		
<i>See also</i> elastic limit			
puckering	123(F)	257	
<i>See also</i> buckling			
deformation zones	107		
rectangular cups, deep drawing	119		
punch			
cushion systems	203–213(F)		
deep drawing, round and rectangular cups	105–127(F,T)		
deep drawing tests	95	96(F)	
defined	257		
description of	3		
electromechanical servo-drive presses	166–170(F,T)	171(F)	172(F)
	173(F)	174(F)	
FLCs	50		
formability	45–48(F)		
hot stamping	99		

Index Terms

Links

punch (<i>Cont.</i>)			
ironing tests	97		
LDH test	45	94	
Marciniak test	49		
Nakajima test	49		
sheet metal forming operations	6–23(F,T)		
SHF-D	197		
SHF-P	197	198(F)	
stainless steels	81		
tribological tests, punching and blanking	100–101(F)	102(F)	
punch corner radius	110		
punch die clearance	110		
punch force			
cup drawing test	99		
deep drawing	114		
prediction of	114		
punch line	257		
punch radius	257		
punch riser	257		
punch shoe	257		
punch speed	8–9	166	168(F)
punch stroke			
bending	47		
BHF	112		
deep drawability	8		
prediction of	115–118(F,T)		
punch force/punch stroke curves	119(F,T)	120(F,T)	121(F,T)
	122(F,T)		
punch force/punch stroke diagram	110	111(F)	
punch-die radius	110		
punching	100–101	257	
punchout. <i>See also</i> blank; slug			
punch-to-die clearance. <i>See</i> die clearance			

Index Terms

Links

Q

quenching

aluminum alloys 85

hot stamping 199–200

quick die change systems

advantage of 139

automated clamps 141–142 143(F)

bolster extensions 142

clamping 141–142

clamps 141–142

die carts 142–143

die lifters 142

die rollers 142

gap frame press 142(F)

moving bolsters 142–143

steps 141–142

T-channels 142

U-channels 142

unclamping 141

quick plastic forming 86

R

rabbit ear 257

radial draw forming 257

radial drawing. *See* deep drawing

radius flat hem. *See* open hem (radius flat)

ram. *See* press slide

ram speed 111 161 162
207

ram tilting 209–210(F)

ready hemmer 257

recoil 257(F)

recoil line. *See* impact line

Index Terms

Links

rectangular cups, deep drawing

BHF 118–119

case study—prediction of punch force and BHF

AA-2008-T4 125(T)

BHF profiles 126(F)

deformed cup geometry 126(F)

FEA simulations 123–125

fracture limits 126(F)

geometry 124(F)

lubrication 123

material 122–123

overview 121–122

press 122

punch force measurements 127(F)

thickness distribution predicted 125(F)

three blank shapes, dimensions of 125(F)

three dimensional FEM code 124

tooling 122 124(F)

wrinkling 125–126

wrinkling amplitude measurements 126(F)

wrinkling and fracture, BHF control 126–127

wrinkling and fracture limits 126(F)

example 123(F)

flange 118–119

fracture in 123(F)

major defects in

fracture 118 119–120 123(F)

overview 119

thinning 120

wrinkling 120–121 123(F)

overview 118–119

redrawing 257

reduction 257

reduction in area 257

Index Terms

Links

register	257
relief	257
relief valve	213
relieving. <i>See</i> stress relief	
reservoir	182–183
hydraulic press frames	195(F)
schematic	182(F)
reset	257
residual stress	257
restrike	257
restriking	257
reverse drawing	257–258
reverse flange	258
reverse redrawing	258
Reynolds equation	91
rib	258
rider pin. <i>See</i> guide pin	
rider pin bushing. <i>See</i> guide pin bushing	
rimmed (or capped) ingot cast steel	73
ring. <i>See</i> blank holder	
riser	258
<i>See also</i> adapter (lower); punch riser	
riser block	258
rod	258
rodless piston	187
roll bending	12(F)
applications	12
defined	258
equipment	12
materials	12
process variations	12
roll coating	92
roll flattening	258
roll forging	258

Index Terms

Links

roll forming	258	
application	11	
contour roll forming	12(F)	
equipment	11	
materials	11	
overview	11	
process variation	11	
roll straightener	258	
roll straightening		
applications	15	
defined	258	
equipment	14	
overview	14–15(F)	
process variations	15	
roller leveler breaks	258	
roller leveling	258	
rope	258	
rope hem	248(F)	258
rose bud	258	
rotary file. <i>See</i> carburr		
rotary shear	258	
rough blank	258	
roughing cutter	258	
round cup deep drawing test	94	96(F)
round cups. <i>See</i> deep drawing,		
round and rectangular cups		
rubber duck	258	
rubber screws. <i>See</i> Chicago screw		
rubber-pad forming	258	
<i>See also</i> Marforming process		
run marker. <i>See</i> run stamps		
run numbers. <i>See</i> run stamps		
run stamps	259	
running clearance	259	

Index Terms

Links

S

safety	10	
safety pin	259	
sag. <i>See</i> hem deflection		
sanding bob	259	
sausage. <i>See</i> kidney		
saxophone	259	
scaling	259	
<i>See also</i> spotting stick		
scanning electron microscopy (SEM)	101	
Schuler servo-press line	175(F)	
scoring	259	
scrap	259	
scrap cutter	259	
scrap strip. <i>See</i> skeleton		
screw press	259	
seals	182	
secant modulus	259	
<i>See also</i> modulus of elasticity		
sections. <i>See</i> details		
segment die. <i>See</i> split die		
self-contained gas spring	215	
self-hardening steel. <i>See</i> air-hardening steel		
service order number	259	
servo-actuated valves		
hydraulic cushions	208	209(F)
in-die systems	213	
shadow. <i>See</i> low spot		
shaving	259	
shear	259	

Index Terms

Links

shear forming	24(F)	
applications	23	
equipment	23	
materials	23	
overview	23	
process variations	23	
shear friction model	90	91
shear knives	259	
shear strength	259	
shear stress	54	259
shear stress components	37–38	
shearing. <i>See also</i> blanking		
applications	15	
defined	259	
electromechanical servo-drive presses	161	
equipment	15	
hydrostatic stress state	55	
materials	15	
overview	15	
principle directions	31	
process variations	15	
progressive die forming	138	
shear friction model	91	
snap-through	139	
tribological tests, punching and blanking	100	
shedder	259	
sheet	259–260	
sheet forming. <i>See also</i> forming		
characteristics of	3	
defined	260	
description of	3	

Index Terms

Links

sheet forming, materials for	73		
aluminum alloys (<i>see</i> aluminum alloys)			
coated sheet steels (<i>see</i> coated sheet steels)			
low-carbon sheet steels (<i>see</i> low-carbon sheet steels)			
magnesium alloys (<i>see</i> magnesium alloys)			
stainless steels (<i>see</i> stainless steels)			
sheet forming presses			
bolster, bending of	137	139(F)	
bolster area	130		
C-frame press	131		
components	129–131		
bolster	129		
drive	129		
frame	129		
geometric terms	130(F)		
gibs	129		
slide	129		
terminology	130(F)		
crank angle	130		
daylight	130		
die space	130		
dimensional accuracy	133		
energy-restricted machines	131		
finite element analysis	135		
frame types	131–132(F)	136–137	
gap frame press	131	132(F)	136
gib configurations used in presses	138(F)		
gib design	137		
load and energy requirements			
available energy (E_M)	133		
available machine load (L_M)	133		
efficiency factor (η)	133		
load-displacement curves	131(F)		
load-restricted machines	131		

Index Terms

Links

sheet forming presses (*Cont.*)

off-center loading	137–139	140(F)	
one-piece (monoblock) frame	132		
overview	129		
plunger guides	137	138(F)	
press shutheight	130		
press speed (strokes per minute)	137		
process and machine variables	130(F)		
quick die change systems	139	141–143(F)	
slide displacement	130		
slide face area	130		
snap-through	139	141(F)	142(F)
stiffness of a press	133–134		
contact time, effect on	135(F)		
die cushion, effect of slide tilting on	135(F)		
DIN 55 189	134	135(F)	
measuring	134–135(F)		
mechanical forging press	137(F)		
real-time deflection measurement system	136(F)		
straight-side press	134(F)		
test setup for determining dynamic stiffness	136(F)		
straight-side press	131–132(F)	136–137	
stroke	130		
stroke-restricted machines	131		
tie rods	132	136–137	
time dependent characteristics			
contact time under pressure (t_p)	133		
number of strokes per minute (n_p)	133		
slide velocity under pressure (V_p)	133		
welded steel frames	137		
sheet hydroforming			
with die	17(F)		

Index Terms

Links

sheet hydroforming (*Cont.*)

fluid bladder forming	17		
scenarios	198(F)		
SHF-D	197		
SHF-P	15–17(F)	197	
sheet hydroforming with die (SHF-D)	17(F)	197–198	
application	17		
equipment	17		
materials	17		
overview	17		
process variations	17		
sheet hydroforming with punch (SHF-P)	16(F)	197	
applications	17		
equipment	16		
materials	16		
overview	15–16		
process variations	16		
sheet leveling/roll straightening			
applications	15		
equipment	14		
overview	14		
process variations	15		
roll straightening	15(F)		
sheet materials			
anisotropy	36		
bending and stretching limits	45–46(F)		
deep drawing, round and rectangular cups	109		
dome height	46(F)		
drawability	47(F)		
flanging	13		
flow curves for	6–7		
flow stress	39–44(F,T)		
flow stress curves	221–222(T)	224(T)	227(T)
Hill's 1948 yield criterion	59		

Index Terms

Links

sheet materials (*Cont.*)

hole flanging	14
hot stamping	98
hydraulic bulge test	45
low-carbon sheet steels	73
plastic anisotropy	8
sheet forming	73
strain path/deformation history	51
TCT	94
Yoshida-Uemori model	70

sheet metal forming

bending (<i>see</i> bending)		
blank preparation	14–15(F)	
coining	23–24(F)	
deep drawing (<i>see</i> deep drawing)		
design process steps	6	
draw beads	8(F)	
flanging (<i>see</i> flanging)		
geometries, classification of	10–11	
hybrid forming processes	23–24f	
incremental forming (<i>see</i> incremental forming)		
ironing	23	24(F)
overview	5	
process components	6(F)	
process variables	5–6	
processes	10(T)	
stretch forming (<i>see</i> stretch forming)		
as a system		
deformation, mechanics of	9–10	
deformation zone	9–10	
environmental factors	10	
equipment	8–9	
material characterization	6–8	
mechanical properties	10	

Index Terms

Links

sheet metal forming (*Cont.*)

overview 6

product geometry 10

safety 10

tooling 8–9

tool/workpiece interface, friction and lubrication at 9

system approach 7(F)

variables in 7(T)

workability 7

shim 260

shimmy cam 260

shock lines 9

shoe 260

shooting plastic. *See* plastic hit

shoulder screw 260

shrink flanging 13(F)

shute. *See* chute

shutheight. *See also* press shutheight

adjustment 156 157(F)

defined 8 260

double-action presses 149

effect of 8

mechanical presses 15

press stiffness 134

press stroke 147

press strokes 137

quick die change systems 141

shutheight adjustment 156–157(F)

shutheight adjustment mechanisms 157(F)

silicon 77 84

single-action die 260

Index Terms

Links

single-action presses. <i>See also</i> single-action presses, with cushion system		
blank holder force generating systems	204(F)	
deep drawing	151(F)	
defined	260	
slide motions	149	150
single-action presses, with cushion system		
blank holder	206	
force flow	209–211(F)	
hydraulic cushions	207–209(F)	
overview	206–207(F)	
pneumatic cushions	206–207(F)	
single-action deep drawing operation	206(F)	
sizing	260	
<i>See also</i> restriking		
skeleton	260	
skid lines	260	
skid marks. <i>See</i> draw marks		
skin	260	
slab method	112–114(F)	
sled runner	260	
slide	129	260
<i>See also</i> cam slide; press slide		
slide adjustment	260	
slide counterbalance pressure (counterbalance pressure)	260	
slide counterbalances	157	
slide displacement	130	
slide face area	130	
slide hammer	260	
slide position	154	
slide tilting	209–210(F)	
slide velocity	154	
slip	29	
slitting	260	

Index Terms

Links

slug	260		
<i>See also</i> bladesteel			
slug trails	260		
snap-through	139	141(F)	142(F)
solenoid or servo valves	186		
solution heat treatment	84	85	
spalling	260		
spank. <i>See</i> restrike			
spares. <i>See</i> back-ups			
spear punching	260–261		
<i>See also</i> extruding			
spearing. <i>See</i> extruding; spear punching			
spider	261		
spinning			
applications	22		
defined	261		
before deformation/end of deformation	23(F)		
equipment	22		
materials	22		
overview	22		
process variations	22		
spleen. <i>See</i> draw bead; factor			
splines	173		
split die	261		
splits	261		
sponges	92		
spool	261		
spot face	261		
spotting	261		
spotting aid. <i>See</i> cast; skin			
spotting rack. <i>See</i> cast; skin			
spotting scale	261		
spotting stick	261		
<i>See also</i> scaling			

Index Terms

Links

spring can	261	
spring plate	261	
springback. <i>See also</i> buckling		
defined	261	
HSLA steels	77	
magnesium alloys	87	
predictions	66–67	70
reason for	53	
reducing	174	
reduction in	168–169	
squeeze block	261	
squeezing operations	147	
SS304 cups	81	82(F)
stack up	261(F)	
stainless steel sinks	212(F)	213(F)
stainless steels		
austenitic steels (<i>see</i> austenitic stainless steels)		
chromium	79	
expanding	21	
ferritic stainless steels	82	83(F)
flow stress at room temperature for type 304 stainless		
steel	80(F)	
H-version	80	
linear stretch forming	19	
martensitic stainless steel	79	
overview	79–80	
precipitation hardened stainless steels	79	
properties	79(T)	
punch corner radius	110	
stretch forming	19	
suitability of stainless steels for various methods of		
forming	81(T)	

Index Terms

Links

stainless steels (*Cont.*)

work-hardening qualities

type 301 83(F)

type 409 83(F)

type 430 83(F)

stainless steels, specific types

type 301 80

type 304 45 46(F) 80(F)

81 82(F)

type 304L 80

type 305 80

type 316 82

type 316L 82

type 409 82

type 430 82

staking 261

stamp 261

stamping

accumulators 187

direct drive presses 148

electromechanical servo-drive presses 161 165 166

extended drive presses 146 147

FLCs 48–51(F)

in-die systems 213

large automotive stampings 170–171 175(F)

LDH test 94

load-displacement curves 130 131(F)

low-carbon sheet steels 73 74(T)

lubricants 92–99(F) 100(F) 101(F)

new process development 173

off-center loading 137

Index Terms

Links

stamping (<i>Cont.</i>)			
pressure box	210		
quick die change systems	139		
sheet forming presses	129		
straight-side press	131–132(F)		
stamping flange angle	261(F)		
stamping presses	137–139	140(F)	210
stamping processes			
electromechanical servo-drive presses	161		
extended drive presses	146		
high-speed stamping	148		
stampings	131	170–171	175(F)
standoff blocks. <i>See</i> leveling blocks			
stand-off blocks. <i>See</i> leveling blocks			
standoff blocks. <i>See</i> stop blocks			
stand-off blocks. <i>See</i> stop blocks			
starting ring. <i>See</i> prehem steel			
starting steel. <i>See</i> prehem steel			
steel rule die	261		
steels. <i>See also</i> details			
explosive forming	22		
shear forming	23		
stiffness. <i>See</i> bending stress			
stitch and run die	261–262		
stock guide	262		
stock strip. <i>See</i> skeleton			
stone	262		
stool	262		
<i>See also</i> adapter (lower); die post			
stop, automatic	262		
stop blocks	262		
stop pin	262		
storage blocks	262		
straight cam	262		

Index Terms

Links

straight carbon steel. *See* carbon steels

straightener rolls. *See* roll straightener

straight-side press	131–132(F)	134(F)	136–137
	164	165	262

strain

anisotropy, effect of	109
-----------------------	-----

defined	39	262
---------	----	-----

deformation zones	106(F)	107
-------------------	--------	-----

FEM	114	115
-----	-----	-----

laboratory-scale tribological tests	95
-------------------------------------	----

metal forming processes	2
-------------------------	---

plastic deformation—flow stress

anisotropy, and form-ability	33–51(F,T)
------------------------------	------------

plastic deformation—state of

stress, yield criteria flow

rule, and hardening rules	53–70(F)
---------------------------	----------

plastic deformation—strain and strain rate	27–32(F,T)
--	------------

sheet forming, materials for	74–87(F,T)
------------------------------	------------

sheet metal forming operations	6–10(F,T)
--------------------------------	-----------

thinning	120
----------	-----

strain aging	74	76	262
--------------	----	----	-----

strain hardening

behavior	66
----------	----

deep drawing	109
--------------	-----

defined	262
---------	-----

deformation zones	107
-------------------	-----

effect of	109
-----------	-----

FLCs	49
------	----

flow stress	39
-------------	----

hardening laws	66
----------------	----

isotropic hardening law	66
-------------------------	----

kinematic hardening law	67
-------------------------	----

LDR	108
-----	-----

plastic deformation	33–42(F,T)
---------------------	------------

Index Terms

Links

strain hardening (<i>Cont.</i>)			
stainless steels	79(T)	82	83(F)
stress-strain relationships	36		
Yoshida-Uemori model	69		
strain hardening coefficient, n			
deep drawing	108		
formability	108		
round cup drawing, FE model of	115(T)	116	118(T)
tensile test	41		
strain paths			
FLCs	49	50	
Nakajima Test	49		
principle strain directions	31–32		
strain path/deformation history	50–51(F)		
thinning	120		
variables in sheet metal forming	7(T)		
strain rate	27–32		
austenitic steels	80		
AZ31B-O	87(F)	230	
deformation	10		
design process	6		
FEM	114		
ferritic stainless steels	82		
flow curve equations	39		
flow stress	38		
magnesium alloys	87		
material characterization	6		
metal forming processes	2		
product geometry and properties	10		
quick plastic forming	86		
slide velocity under pressure (V_p)	133		
warm forming	199		
strain-hardening behavior	66	67	

Index Terms

Links

strain-hardening coefficient. <i>See</i> strain-hardening exponent (<i>n</i> -value)		
strain-hardening exponent (<i>n</i> -value)	262	
strain-rate sensitivity (<i>m</i> -value)	262	
strains		
deep drawing	114	
prediction of	114	
strength coefficient, <i>K</i>	40(F)	108–109
stress		
back stress	67	
deep drawing	112–114	
defined	262	
deviatoric stress	55(F)	
general state of	53–54	
hydrostatic stress	55	
normal stress	54	
principal stresses	54	
shear stress	54	
states of stress	53(F)	
stress components	54(F)	
true stress values	35	
volumetric stress	54–55	
stress and strain, prediction of	115	116(F)
stress cracking	262	
stress raisers	262	
stress relief	262	
stress-strain curve. <i>See</i> stress-strain diagram		
stress-strain diagram	262	
stress-strain relationships	35–36(T)	37(T)
stretch bend (SB) test	47	
height of failure versus <i>r</i> -to- <i>t</i> ratio	47(F)	
schematic	47(F)	
stretch drawing. <i>See</i> deep drawing		
stretch flanging	13(F)	

Index Terms

Links

stretch former	263		
stretch forming	19(F)		
age forming	19	20(F)	
asymmetric parts	18–19		
applications	19		
equipment	19		
materials	19		
bulging	20	21(F)	
creep forming	19	20(F)	
defined	263		
die quench forming	19–20(F)		
dimpling	21	22(F)	
electromagnetic forming	21–22	23(F)	
expanding	21	22(F)	
explosive forming	22	23(F)	
linear stretch forming	19	20(F)	
tube hydroforming	20–21(F)		
stretchability			
defined	44		
Erichsen cup test	44–45(F)		
hydraulic bulge test	45	46(F)	
LDH test	45(F)		
stretcher leveling	262		
stretcher straightening	263		
stretcher strains	119	263	
<i>See also</i> Luders lines			
stretching	263		
Stribeck curve	90(F)		
striker. <i>See</i> sled runner			
striking surface	263		
strip	263		
strip drawing (SDT) test	94(F)	95	96(F)
strip reduction setup	95(F)		
strip reduction test	94(F)		

Index Terms

Links

stripper	263		
stripper bolts. <i>See</i> shoulder screw			
stripper insert. <i>See</i> window			
stripper plates	263		
stripper punch	263		
<i>See also</i> ejector rod; knockout			
stripping	263		
stroke	130	191–192	263
stroke-restricted machines	131		
strokes per minute (SPM)	148	149	
stroking rate	8		
structural steel (SS)	75	77	
structural-quality (SQ) steels	75–76		
carbon contents	76		
cold rolled	76		
hot rolled	75–76		
submarines	12		
sulfur			
low-carbon sheet steels	77		
in lubricants	92		
sump	263		
<i>See also</i> spot face			
superior hone	263		
superplasticity	263		
support plate	263		
surface distortion	263		
surge tank	263		
swift cup test	263		
Swift's law	39		
switchable gearbox	157		
swivel ring	263		

Index Terms

Links

T

T tempers	84	
tailor-welded blanks	138	
tangent bending	263	
tangent modulus	263	
<i>See also</i> modulus of elasticity		
T-channels	142	
teardrop hem	264(F)	
tears. <i>See</i> splits		
temperature-activated EP additives	92	
tempering	264	
tempers		
aluminum alloys	82–84	
T tempers	84	
tensile strength	264	
tensile stress	264	
tensile test		
anisotropy	36–37(F)	38(F)
area reduction	34–35	
definitions of width and thickness strains	38(F)	
elastic modulus	34	
engineering stress-strain curves	33–34(F)	
extensometer	33	
fixture used in test	34(F)	
flow curve equations	37(T)	
flow stress, determining	39–41(F,T)	
force-elongation curve	34(F)	
material properties list	38(T)	
overview	33	
stress-strain relationships	35–36(T)	
tensile data		
engineering stress-strain curves	36(F)	
force-elongation curves	36(F)	

Index Terms

Links

tensile test (*Cont.*)

true stress-strain curves	36(F)	
test device	33	34(F)
test specimen	33(F)	
total elongation	34	
true stress-strain curves	35	36(F)
uniform elongation	34	
UTS	34(F)	
yield strength	34	35(F)
tension	264	
terne coatings	78–79	
test coupon	264	
thickness strain analysis (TSA)	264	
thinning	120	
third action	264	
three-dimensional deformation	31	
three-point bending	264	
<i>See also</i> V-bend die		
throat (gap)	264	
throw	264	
<i>See also</i> crank press; eccentric press		
tie rods		
defined	264	
sheet forming presses	132	
straight-side press	136–137	
tilt stiffness	195	
tilting of the ram	154	155(F)
titanium		
creep	19	
low-carbon sheet steels	77	
titanium alloys		
age forming	19	
brake bending	11	
coining	23	

Index Terms

Links

titanium alloys (*Cont.*)

deep drawing	15		
die quench forming	20		
dimpling	21		
drop hammer forming	18		
eyeglass frames	168		
ironing	23		
joggling	14		
nosing	24		
roll bending	12		
roll forming	11		
shear forming	23		
spinning	22		
stretch forming	19		
toggle draw die. <i>See</i> double-action die			
toggle drawing press	264		
toggle press	146	147	264
tolerances			
deformed products	10		
final part	129	138	
hydraulic presses	192		
manufacturing processes	2		
tool geometry	9	108(F)	115(T)
	116(T)	117	117(T)
tool order number. <i>See also</i> project number; service order number			
top dead center (TDC)	129–130		
torsion	264		
torsional stress	264		
total elongation			
aluminum alloys, warm forming	86		
defined	34(F)	264	
material properties in metal forming	38(T)		
percent total elongation	254		

Index Terms

Links

transfer die	264		
transfer pin. <i>See</i> pressure pin			
transfer press	265		
transformation temperatures. <i>See</i> critical temperatures			
trapped die forging	173		
Tresca yield criterion			
Barlat and Lian yield criterion	62		
Mohr's circle	56(F)		
overview	56–57		
slab method	113		
in three-dimensional stress space	57(F)		
in two-dimensional stress space	57(F)		
von Mises, comparison	58	59(F)	
tribological tests (blanking)	100		
tribological tests (lubricants)			
contact pressure and frictional shear stress	91(F)		
evaluation of lubricants			
BHF	95		
COF	94	95(F)	
Coulomb's law	95		
deep drawing tests	95–96(F)		
draw bead test	94(F)		
flange perimeters and punch forces	97	97(F)	
ironing tests	96–98(F)		
laboratory-scale tribological tests	94–95(F)		
LDH test	94(F)		
load-stroke curves	96	97(F)	
round cup deep drawing test	94	96(F)	
SDT	94(F)	95	96(F)
sidewall thinning distributions	98(F)		
strip reduction setup	95(F)		
strip reduction test	94(F)		
TCT	94	95(F)	

Index Terms

Links

tribological tests (lubricants) (*Cont.*)

factors affecting	89(F)
fine blanking	100
Stribeck curve	90(F)

tribological tests (punching)

punching	100–101
SEM	101

tribological tests (warm and hot stamping)

aluminum	98	
aluminum alloys	98	
BHF	99	
boron alloys	98	
COF, μ_3 , as a function of the blank temperature	98–99	102(F)
cup drawing test	101(F)	
effect of die pressure on mean coefficient of friction	100(F)	
effect of furnace temperature on mean coefficient of friction	100(F)	
effect of scale thickness on mean coefficient of friction	101(F)	
evolution of COF	102(F)	
hot flat drawing test	98–99(F)	
ironing tests	98	
load-stroke curves	98(F)	
modified cup drawing test	98	99–100
punch force	99	
tribosimulator	99(F)	
tribosimulator	99(F)	
trim edge	265(F)	
trimming	265	
TRIP 780	224(F)	227(F)
TRIP steels	50	51(F)
triple-action press	265	
true stress	35	
true stress-strain curves	35	36(F)
tryout	265	

Index Terms

Links

tryout presses	190	198–199(F)
tube bending		
mandrels	13	
overview	12–13(F)	
tube hydroforming (THF). <i>See also</i> tube bending		
applications	20–21(F)	
equipment	20	
hydroforming presses	197–198	
materials	20	
overview	20–21(F)	
process variations	20	
tungsten		
dimpling	21	
spinning	22	
turnover	265	
<i>See also</i> turnover device		
turnover device	265	
twinning	29	
twist compression test (TCT)	94	95(F)
two-dimensional deformation	29–30(F)	31–32(F)

U

u-bend die	265		
U-channels	142		
ultimate strength	265		
<i>See also</i> tensile strength			
ultimate tensile strength (UTS)	34(F)	89(F)	
ultrasonic gage	265		
undercut. <i>See</i> relief			
underdrive press	265		
uniaxial tensile test	75		
uniform elongation	34(F)	35	40
	86		
Unigraphics	114		

Index Terms

Links

U-O bending technique	173(F)		
upper dies	6		
upper yield point	266		
<i>See also</i> yield point			
USCAR	212(F)	213	
V			
variable displacement	184		
Variotherm thermal imaging camera	99		
V-bend die	265		
velocity of final hem steel	265		
vent	265		
vent mark	265		
vertical stiffness	134	135(F)	155(F)
viscous pressure bulge (VPB) test	73	75	224(F)
	226(F)	227(F)	
<i>See also</i> hydraulic bulge test			
Volkswagen	137		
volume constancy	29		
volumetric stress	54–55		
von Mises criterion of plastic flow	9		
von Mises equivalent plastic strain	32		
von Mises yield criterion	57–58		
Barlat and Lian yield criterion	62		
isotropic hardening law	66	67(F)	
plastic strain ratio and yield stress	64(F)		
Prager's kinematic hardening rule	68(F)		
strain increments based on the Levy-Mises flow rule	65(F)		
in three-dimensional stress space	58(F)		
Tresca criteria, comparison	58	59(F)	
in two-dimensional stress space	58(F)		

Index Terms

Links

W

walking cam. *See* aerial cam

Wanheim and Bay general friction model 91

warm deep drawing

Al alloy cups 171 172(F)

Mg alloy cups 171 172(F)

Ti alloy cups 171 172(F)

warm forming

aluminum alloys 85–86

austenitic stainless steels 80–81

hydraulic presses 199

laptop case 169 171(F)

Mg alloys 169 171(F)

warp 265(F)

washer oils 93

wear plates 266

web 266

welded steel frames 137

welding 137

window 266

wiping steel. *See* flange steel

work hardening. *See also* strain hardening

defined 39

flow stress 39

work hardening exponent. *See also* *n*-value

workability 7

See also formability

wrap forming. *See* stretch forming

wring fit 266

wrinkling 120–121 123(F)

See also buckling

Index Terms

Links

wrinkling (*Cont.*)

BHF	111–112	118	121
BHF control	126–127(F)		
case study—prediction of punch force and BHF	125–126		
cushion systems	203		
deep drawing	105		
defined	266		
deformation zones	107		
die radius	110		
FEA simulations	125		
formability	73		
limits	125–126(F)		
pin height variation	209		
press stiffness	134		
rectangular cups	119		
rectangular cups, deep drawing	123(F)		
sheet metal forming	6	7	8
wrought alloys, naming scheme	84		

Y

yield	266		
yield criteria. <i>See also</i> flow rules			
defined		56	
FEM	114		
isotropic hardening law	66		
isotropic yield criteria	56–63(F)		
kinematic hardening law	67		
mixed hardening law	68		
yield point			
defined	266		
magnesium alloys	87		
yield point elongation	266(F)		

Index Terms

Links

yield strength		
austenitic steels	80	
engineering stress-strain curves	34	35(F)
flow stress	85(F)	
low-carbon sheet steels	73–77(F,T)	
magnesium alloys	86	
metal forming processes	3	
stainless steels	79	
yield stress. <i>See also</i> flow stress		
Barlat 1996 yield criterion	63	64(F)
Barlat and Lian yield criterion	62	63
flow rules	63	
Hill's 1948 yield criterion	59–60	61
Hill's 1990 yield criterion	61–62	
isotropic yield criteria	56	
kinematic hardening law	67	
metal forming processes	2	
mixed hardening law	69	
Tresca yield criterion	56	57
Yoshida-Uemori model	69	
Yoshida-Uemori model	69–70	
Bauschinger effect	69	
bounding surface	70(F)	
hardening behavior	70	
unloading modulus	70	
yield surface	70(F)	
Young's modulus	34	
<i>See also</i> elastic modulus		

Index Terms

Links

Z

Ziegler's kinematic hardening rule	67–68(F)	69(F)
zinc		
coatings	78	
drawing speed	111(T)	
magnesium alloys	86	
TCT	94	
wrought alloys	84	
zinc powdering	96	